

Neuronal correlates of goal-directed sensorimotor transformation in sensory, motor and higher-order cortical areas

Présentée le 26 mai 2023

Faculté des sciences de la vie
Laboratoire de traitement sensoriel
Programme doctoral en neurosciences

pour l'obtention du grade de Docteur ès Sciences

par

Anastasiia ORYSHCHUK

Acceptée sur proposition du jury

Prof. P. P. Ramdya, président du jury
Prof. C. Petersen, directeur de thèse
Prof. F. Helmchen, rapporteur
Prof. A. Lak, rapporteur
Prof. M. Mathis, rapporteuse

Acknowledgments

I would like to begin by expressing my deepest gratitude to my supervisor Prof. Carl Petersen, for granting me the opportunity to pursue my Ph.D. thesis in the laboratory of sensory processing and for his invaluable guidance. I extend my heartfelt gratitude to Dr. Sylvain Crochet for his precious supervision and guidance throughout my Ph.D. I am grateful to both of them for their unwavering support and attentiveness, especially in the harsh circumstances of my Ph.D. Their enthusiasm for understanding the mammalian brain has consistently inspired me and will undoubtedly continue to serve as a driving force for my future scientific endeavors.

I would like to extend a special thank you to my teacher, mentor, and best friend, Vahid Esmaeili. His expertise and guidance in electrophysiology have been instrumental in shaping me into a skilled scientist.

I am grateful to all of my lab members for being such fantastic colleagues and for stimulating discussions during lab meetings. We have grown together scientifically and learned a lot from one another. I also cherish the fun times we shared over the years and retreats.

I want to thank my co-authors for their collaboration and effort in writing the three amazing articles that are included in this manuscript.

To my big family and friends, I am thankful for your unwavering support and encouragement throughout my Ph.D. journey. I would like to express my deepest gratitude to my lovely mom, dad, and brother for being the reason that I am a successful person. Your love and solace have been my constant inspiration.

I owe a debt of gratitude to my fiancé, Dr. Sebastien Tourbier, for his constant encouragement and the biggest contribution to my happiness. You are the backbone of my success and I am so grateful to have you in my life!

Lastly, I would like to express my profound gratitude to my thesis committee members, Prof. Mackenzie Mathis, Prof. Armin Lak, Prof. Fritjof Helmchen, and Prof. Pavan Ramdya, for agreeing to serve on my Ph.D. thesis committee.

Abstract

An important function of the brain is to interpret incoming sensory information from the outside world to guide adaptive behavior. Understanding how and where sensory information is transformed into motor commands in a context- and learning-dependent manner is a key question in neuroscience. Which cortical areas are responsible for sensory perception, decision-making, and motor execution is still a matter of discussion. During my Ph.D. I attempted to disentangle the coding of sensory versus decision and motor information by neurons in different brain regions along the transformation path of whisker sensory stimuli to licking motor output during goal-directed behaviors in mice. To address this question I combined electrophysiological recording of a large population of neurons across multiple brain areas with fine monitoring of behavior and movements, as well as time-resolved optogenetic manipulations.

I first explored the sequence of cortical activity involved in transforming a brief whisker stimulus into delayed licking in mice. With coauthors, we discovered two crucial features related to activity evoked by whisker deflection. Firstly, an enhanced excitation of the secondary whisker motor cortex suggested its important role in connecting whisker sensory processing to lick motor planning. Secondly, a transient reduction of activity in the orofacial sensorimotor cortex helped to suppress premature licking. During the delay period, we observed widespread cortical activity that largely correlated with anticipatory movements. However, when accounting for these movements, we identified sustained activity in the frontal cortex that was essential for licking in the response period. Our results highlight key cortical nodes involved in motor planning. We next categorized neurons as regular or fast spiking, which I confirmed with optotagging method. We investigated how their activity changes before and after mice learn a task. We observed opposite changes in the whisker-evoked activity of regular versus fast spiking neurons in primary and secondary whisker motor cortices, but similar changes in primary and secondary orofacial motor cortices. Hence, altered excitation and inhibition in local circuits, combined with changes in long-range synaptic inputs may underlie delayed sensory-to-motor transformation.

Finally, I recorded and systematically compared the neuronal activity of the cortical sensory input area (primary somatosensory cortex), a presumably decision area (medial prefrontal cortex), and the motor output area (tongue and jaw primary motor cortex) in the psychophysical whisker detection task. We have uncovered that the representation of sensory information, decision-making, and motor action is not a discrete function of each individual brain region, but rather distributed and encoded across all three regions. We proposed that the decision to lick after the whisker stimulus is a gradual process that involves the flow of information from wS1 to mPFC and tjM1. Importantly, we also observed that signal processing failures can occur at

any level of this information flow. These findings highlight the complexity and distributed nature of the neural processes underlying decision-making and sensorimotor transformation.

In this thesis, I have presented various findings that add to the existing knowledge and shed light on the neural circuits and computations involved in sensorimotor transformation in the mammalian brain.

Keywords: sensorimotor transformation, whisker detection task, delayed-response, licking, decision, barrel cortex, medial prefrontal cortex, tongue-jaw motor cortex, electrophysiology, optogenetics

Résumé

Une fonction importante du cerveau est d'interpréter les informations sensorielles venant du monde extérieur pour guider le comportement de manière adaptée. Comprendre comment, et où, les informations sensorielles sont transformées en commandes motrices en fonction du contexte et de l'apprentissage est une question clé en neurosciences. Quelles zones corticales sont responsables de la perception sensorielle, de la prise de décision et de l'exécution motrice est encore sujet à discussion. Pendant mon doctorat, j'ai tenté de démystifier le codage des informations sensorielles, motrices et décisionnelles par les neurones de différentes aires corticales au cours de la transformation d'entrées sensorielles appliquées aux vibrisses, en sortie motrice par l'action de lécher pour obtenir une récompense, chez la souris. Pour cela, j'ai combiné des enregistrements électrophysiologiques de grandes populations de neurones dans plusieurs zones corticales avec une surveillance fine du comportement et des mouvements orofaciaux, ainsi que des manipulations optogénétiques à haute-résolution temporelle.

J'ai d'abord collaboré à une étude dans laquelle nous avons exploré la séquence d'activité corticale impliquée dans la transformation d'un bref stimulus d'une vibrisse en l'action de lécher avec un délai chez la souris. Nous avons découvert deux caractéristiques essentielles liées à l'activité évoquée par la stimulation de la vibrisse. Premièrement, une excitation accrue du cortex moteur secondaire des vibrisses qui indique son rôle important dans la connexion du traitement sensoriel des vibrisses à la planification motrice. Deuxièmement, une réduction transitoire de l'activité neuronale dans le cortex moteur orofacial primaire impliquée dans la suppression de léchage prématuré. Au cours de la période de délais entre la stimulation sensorielle et la réponse motrice, nous avons observé une activité corticale généralisée largement corrélée aux mouvements d'anticipation. Cependant, lors de la prise en compte de ces mouvements, nous avons identifié une activité soutenue dans le cortex frontal qui était essentielle pour l'exécution motrice pendant la période de réponse. Nos résultats mettent ainsi en évidence les principaux nœuds corticaux impliqués dans la planification motrice. Nous avons ensuite divisé les neurones en fonction de la durée de leurs potentiels d'action en neurones présumés excitateurs et neurones présumés inhibiteurs. J'ai validé cette classification avec la méthode de marquage optogénétique. Nous avons étudié comment leur activité change avant et après que les souris aient appris la tâche de détection sensorielle avec délais. Nous avons observé des changements opposés dans l'activité évoquée par la stimulation de la vibrisse pour les neurones présumés excitateurs et ceux présumés inhibiteurs dans les cortex moteurs primaires et secondaires des vibrisses, mais des changements similaires dans les cortex moteurs orofaciaux primaires et secondaires. Par conséquent, une modification de la balance excitation / inhibition dans les circuits

locaux, combinées à des modifications de la communication synaptique entre aires corticales, peuvent sous-tendre l'apprentissage de la transformation sensorimotrice avec délai.

Finalement, j'ai enregistré et comparé systématiquement l'activité neuronale de la zone d'entrée sensorielle corticale (le cortex somatosensoriel primaire, S1), d'une zone impliquée dans la prise de décision (le cortex préfrontal médian, CPFm) et d'une zone impliquée dans l'exécution motrice (le cortex moteur orofacial primaire, M1-Or) dans une tâche psychophysique de détection sensorielle. Nous avons découvert que la représentation des informations sensorielles, de la prise de décision et de l'action motrice n'est pas une fonction discrète de chaque région cérébrale individuelle, mais est plutôt distribuée et codée dans les trois régions. Nous avons proposé que la décision de lécher après le stimulus de la vibrisse est un processus graduel qui implique un flux d'information de S1 vers CPFm et M1-Or. Par ailleurs, nous avons également observé que des défaillances dans la transformation sensorimotrice peuvent survenir à n'importe quel niveau de ce flux d'informations. Ces résultats mettent en évidence la complexité et la nature distribuée des processus neuronaux sous-jacents à la prise de décision et à la transformation sensorimotrice.

Dans cette thèse, j'ai présenté diverses découvertes qui s'ajoutent aux connaissances existantes et éclairent les circuits neuronaux et les processus impliqués dans la transformation sensorimotrice dans le cerveau des mammifères.

Mots-clés: transformation sensorimotrice, tâche de détection sensorielle, réponse avec délai, léchage, décision, cortex somatosensoriel, cortex préfrontal médial, cortex moteur primaire, électrophysiologie, optogénétique

List of figures and tables

Image 0.1. Artificial intelligence chatbot definition regarding sensorimotor transformation (<https://chat.openai.com>).

Image 0.2. Funny facts regarding sensorimotor transformation given by artificial intelligence chatbot GPT (<https://chat.openai.com>).

Figure 1.1. Analyzing psychophysical data with signal detection theory.

Figure 1.2. Psychometric - neurometric comparison.

Figure 1.3. Translation of sensory input to a perceptual decision.

Figure 1.4. Whisker-based tactile detection task.

Figure 1.5. Sequential propagation of neuronal responses evoked by whisker stimulation.

Figure 1.6. Learning-driven changes of the whisker stimulus processing.

Figure 1.7. Mouse whisker somatosensory system.

Figure 1.8. Parallel pathways that bring whisker sensory information to the cortex were revealed through AAV-mediated anterograde trans-synaptic gene expression.

Figure 1.9. Spatiotemporal dynamic of the sensory response in the mouse barrel cortex.

Figure 1.10. Functional and structural organization of barrel cortex.

Figure 1.11. Membrane potential of wS1 causally correlates with mice behavioral responses.

Figure 1.12. Optogenetic inhibition revealed the involvement of several cortical regions during an object location discrimination task.

Figure 1.13. Different strategies identified the tongue-jaw primary motor cortex (tjM1).

Figure 1.14. Different roles of ALM and tjM1 in sensorimotor behaviors.

Figure 1.15. Brain circuits controlling goal-directed licking.

Figure 1.16. Mouse prefrontal module is on the top of the cortical hierarchy.

Figure 1.17. Connectivity of mouse vmPFC.

Figure 2.1. Learning a whisker detection task with a delayed response changes licking patterns and orofacial movements.

Figure 2.2. Wide-field imaging reveals global changes in cortical processing.

Figure 2.3. Task epoch-specific processing across single neurons.

Figure 2.4. Active suppression of orofacial sensorimotor areas.

Figure 2.5. Conversion of a sensory signal into a motor plan.

Figure 2.6. Delay processing beyond preparatory movement.

Figure 2.7. Spatiotemporal causal map of behavioral impact.

Figure 2.8. Task-epoch specific involvement of cortical regions.

Figure 2.9. Whisker training changes behavioral patterns.

Figure 2.10. Wide-field imaging in different trial types.

Figure 2.11. Control experiment in tdTomato mice.

Figure 2.12. Silicon probe locations, average activity patterns across probes and firing differences in Hit vs Miss trials in different areas.

Figure 2.13. Unsupervised neuronal clustering.

Figure 2.14. Critical early delay processing.

Figure 2.15. Orofacial movements in Quiet trials and Poisson encoding model.

Figure 2.16. Spatiotemporal effect of different regions on premature licking and movements.

Figure 3.1. Multi-area recordings during delayed whisker detection task and assignment of RS and FS units to cortical sub-divisions.

Figure 3.2. FS neurons had similar but larger task-modulation compared to RS neurons in the same region.

Figure 3.3. Fast propagation of sensory responses across cell classes and cortical regions.

Figure 3.4. Fast whisker responses in FS neurons of sensory areas.

Figure 3.5. Distinct frontal projections of wS1 and wS2.

Figure 3.6. Learning differently modulated sensory responses of RS and FS neurons in wM1 and wM2 areas.

Figure 3.7. FS neuronal responses in tJM1 and ALM changed similarly to RS neurons.

Figure 3.8. Diverse changes of putative excitation-inhibition balance in different cortical regions across learning.

Figure 3.9. Anatomical localization of neurons.

Figure 3.10. Distribution of spike width in different cortical areas.

Figure 3.11. Baseline firing rates of RS and FS neurons.

Figure 3.12. Opto-tagging GABAergic neurons in VGAT-ChR2 mice.

Figure 3.13. FS neurons remain at baseline level during correct rejection trials.

Figure 3.14. Sequential activation of cortical regions upon whisker stimulation.

Figure 3.15. Early sensory response map across different probes.

Figure 3.16. Faster and larger sensory response in FS neurons across all layers of wS1 and wS2.

Figure 3.17. Layer-specific quantification of RS and FS neuronal responses during the secondary late response in wS1 and wS2 across learning.

Figure 3.18. Layer-specific quantification of RS and FS neurons in wM1 across learning.

Figure 3.19. Layer-specific quantification of RS and FS neuronal activity in wM2 across learning.

Figure 3.20. Inter-areal functional connectivity.

Figure 3.21. Layer-specific quantification of RS and FS neurons in tjM1 across learning.

Figure 3.22. Suppression of activity in tjM1 during response window in no-lick trials of Expert mice.

Figure 3.23. Layer-specific quantification of RS and FS neuronal activity in ALM.

Figure 3.24. Preparatory neuronal activity in ALM is decreased, but remains significant in quiet trials devoid of movements.

Figure 4.1. A psychometric whisker-based tactile detection task involving wS1, mPFC, and tjM1.

Figure 4.2. Cortical activity patterns during task execution.

Figure 4.3. Graded evoked responses in Hit trials in all three regions.

Figure 4.4. Purely sensory-evoked response in the absence of licking in R+ mice.

Figure 4.5. Purely motor-related activity in the absence of sensory stimulus.

Figure 4.6. Motor and sensory-evoked activity in Hit trials.

Figure 4.7. Decision-related information is encoded in all three regions.

Figure 4.8. Decision “gated” neurons are mostly found in mPFC.

Figure 4.9. Multiple decision points in the sensorimotor transformation.

Figure 4.10. Calibration of the magnetic whisker stimulus.

Figure 4.11. Anatomical localization and registration of the recording probes.

Figure 4.12. Bayesian information criteria curve for the number of clusters.

Figure 4.13. High-density extracellular recordings in mice exposed to the non-rewarded whisker stimuli.

Figure 4.14. Neuronal clusters of interest.

Figure 4.15. Evoked whisker and jaw movements.

Figure 4.16. Purely sensory-evoked responses in R- mice.

Figure 4.17. Decoding of sensory stimulus and licking in R+ and R- mice.

Figure 4.18. Purely motor activity in R- mice.

Figure 4.19. Jaw-phase correlation and encoding in R+ and R- mice.

Table 4.1. Optoinhibition: average lick probability (P_{Lick}) and statistical differences (Wilcoxon signed-rank test with Bonferroni correction) (Figure 4.1E)

Table 4.2. Mean and SEM of the delta firing rate of early (0-0.2 s) sensory-evoked responses during Hit and Spontaneous lick trials for the different stimulus amplitudes (Figure. 4.3E).

Table 4.3. *P*-values obtained from multiple comparison tests of the delta firing rate for different stimulus amplitudes (Figure. 4.3 E).

Table 4.4. *P*-values obtained from multiple comparison tests of the mean Pearson correlation coefficient different stimulus amplitudes (Figure. 4.3 F).

Table 4.5. *P*-values obtained from multiple comparison tests of the mean Pearson correlation coefficient different stimulus amplitudes (Figure.4.4 E).

Table 4.6. *P* values for Multiple Comparison Test between reaction times for different amplitudes (Figure 4.6A).

Table 4.7. Quantification of delta firing rate (Figure 4.6F).

Table 4.8. Multiple comparison Kruskal-Wallis test to identify significant differences between mean delta firing rates for different stimulus amplitudes (Figure 4.6F)

Table 4.9. *P*-values obtained from multiple comparison tests of the mean Pearson correlation coefficient different stimulus amplitudes (4.6 G).

Table 4.10. Distribution of decision neurons across areas and layers (Fig.4.8 D).

Table 4.11. *P*-values obtained from multiple comparison tests of the mean Pearson correlation coefficient different stimulus amplitudes (Figure. 4.16F).

Table 4.12. Mean and SD accuracy for real and shuffle data when decoding Spontaneous licks versus Correct rejection trials (related to Figure 4.18C).

Table 4.13. Proportion of cells with significant jaw-phase correlation, whisker-phase correlation, and jaw-phase correlation but no whisker-phase correlation (Figure 4.19D).

Figure 5.1. Pathways underlying transformation of whisker stimulus into a goal-directed licking.

Content

Acknowledgments	3
Abstract	5
Résumé	7
List of figures and tables.....	9
Content.....	15
Chapter 1 Introduction.....	19
Opening remarks: definition of sensorimotor transformation by AI (artificial intelligence)	19
1.1 Sensorimotor transformation	22
1.1.1 Psychophysical approach to study sensorimotor transformation	24
1.1.2 Relationship between neurometric and psychometric data in sensory perception and decision-making	26
1.1.3 Sensorimotor transformation occurs across a large network of cortical areas	28
1.1.4 Transformation of mouse whisker stimulus into licking motor output during goal-directed behaviour	31
1.2 Sensory processing of tactile whisker stimuli	36
1.2.1 Mouse whisker system	36
1.2.2 Structural and functional organization of barrel cortex.....	39
1.2.3 wS1/wS2 as a starting point of sensory processing in the cortex during tactile detection task.....	42
1.3 Licking as a motor command.....	47
1.3.1 Cortical control of licking.....	47
1.3.2 Identification of the anterior lateral motor area (ALM).....	47
1.3.3 Identification and role of Tongue-Jaw Primary Motor Cortex (tjM1)	49
1.3.4 Motor planning and execution	51
1.4 Perceptual decision-making	54
1.4.1 The importance of the prefrontal cortex in perceptual decision-making.....	56
1.4.2 Anatomical and functional organization of the mouse PFC	58
1.4.3 Functions and neuronal correlates of mouse prefrontal cortex (PFC) in goal-directed sensorimotor transformation.....	60
1.5 Aim of the Ph.D. Thesis.	65
Chapter 2 Rapid suppression and sustained activation of distinct cortical regions for a delayed sensory-triggered motor response.....	67
2.1 Abstract	68
2.2 Introduction.....	68
2.3 Results	69

2.3.1	Behavioral changes accompanying delayed-response task learning	69
2.3.2	Emergence of cortical activation and deactivation patterns through whisker training	70
2.3.3	Distinct modification of early and late whisker processing in single neurons	74
2.3.4	Active suppression of orofacial sensorimotor areas	78
2.3.5	Routing of whisker information to the frontal cortex.....	79
2.3.6	Focalized delay period activity in the frontal cortex	83
2.3.7	Temporally-specific causal contributions of different cortical regions.....	86
2.4	Discussion	90
2.4.1	Essential cortical delay period activity in ALM	90
2.4.2	A putative corticocortical signaling pathway linking sensory to the motor cortex through learning.....	91
2.4.3	Lick and No-Lick signals in tJM1.....	92
2.5	Methods	94
2.5.1	Experimental model and subject details	94
2.5.2	Experimental design	94
2.5.3	Implantation of metal headpost.....	95
2.5.4	Skull preparation and craniotomies	95
2.5.5	Behavioral paradigm	96
2.5.6	Quantification of orofacial movements	97
2.5.7	Wide-field calcium imaging	98
2.5.8	Electrophysiological recording	98
2.5.9	Optogenetic manipulations.....	99
2.5.10	Histology and localization of electrode/optical fiber tracks	100
2.5.11	Wide-field imaging data	101
2.5.12	Electrophysiology data	102
2.5.13	Assessing Expert/Novice and Hit/Miss differences	102
2.5.14	Receiver Operating Characteristic (ROC) analysis	102
2.5.15	Clustering neuronal responses	103
2.5.16	Single neuron whisker-evoked response latency	105
2.5.17	GLM encoding model	105
2.5.18	Assessing optogenetic manipulation impact.....	107
2.5.19	Quantifying involvement index	107
2.5.20	Statistics.....	108
Chapter 3	Learning-Related Congruent and Incongruent Changes of Excitation and Inhibition in Distinct Cortical Areas	121
3.1	Abstract	122

3.2	Introduction.....	122
3.3	Results	124
3.3.1	Localisation and classification of cortical neurons	124
3.3.2	Strong task-modulation of fast-spiking neurons	128
3.3.3	Rapid excitation of FS neurons	128
3.3.4	Fast sensory processing in wS1 and wS2.....	130
3.3.5	Parallel anatomical pathways from wS1 and wS2 to wM1 and wM2	132
3.3.6	Changes in fast sensory processing in wM1 and wM2.....	133
3.3.7	Neuronal activity in tongue and jaw-related motor cortices	137
3.3.8	Changes in excitation and inhibition across learning	141
3.4	Discussion	143
3.5	Materials and Methods	146
3.5.1	Behavioral paradigm and electrophysiological recordings	146
3.5.2	Optogenetic tagging of GABAergic neurons.....	147
3.5.3	Anatomical analysis of axonal projections from wS1 and wS2 to frontal cortex.....	147
3.5.4	Data analysis and statistics.....	148
3.5.5	Inter-areal functional connectivity measures	149
3.5.6	Quantifying learning modulation index.....	151
3.5.7	Statistics.....	151
Chapter 4	Representation of sensory, motor and decision information in sensory, motor and medial prefrontal cortices of mice	177
4.1	Summary.....	178
4.2	Introduction.....	178
4.3	Results	182
4.3.1	wS1, mPFC and tJM1 are necessary for the execution of a psychophysical whisker detection task in mice	182
4.3.2	Patterns of cortical activity across cortical areas	186
4.3.3	Graded responses to the whisker stimulus during Hit trials in all three areas	187
4.3.4	Purely sensory responses in the absence of licking are mostly restricted to neurons in wS1	193
4.3.5	Purely motor response in the absence of sensory stimulus is broadly distributed	194
4.3.6	Motor and sensory information in Hit trials.....	197
4.3.7	Decision encoding	200
4.3.8	Multiple decision points in the sensorimotor transformation.....	209
4.4	Discussion	211
4.4.1	Early Hit Miss difference in wS1 contributes to the perception	211
4.4.2	Widespread movement-related activity	212

4.4.3	Multiple decision points along the sensorimotor transformation	213
4.4.4	Role of mPFC in sensorimotor transformation	215
4.5	Conclusion	216
4.6	Methods	218
4.6.1	Experimental model and subject details	218
4.6.2	Implantation of metal headpost.....	218
4.6.3	Skull preparation and craniotomies	219
4.6.4	Behavioral paradigm	219
4.6.5	Electrophysiological recordings.....	222
4.6.6	Optogenetic manipulations	222
4.6.7	Histology and localization of electrode/optical fiber tracks	223
4.6.8	Behavioral data analysis	223
4.6.9	Quantification of orofacial movements	224
4.6.10	Electrophysiology data	225
4.6.11	Receiver Operating Characteristic (ROC) analysis	226
4.6.12	Clustering neuronal responses	227
4.6.13	Decoding of behavioral variables	228
4.6.14	Pearson correlations.....	229
4.6.15	Phase-modulation analysis.....	229
4.6.16	Analysis of paired recordings	230
4.6.17	Statistics.....	231
Chapter 5	Conclusions and Future Perspectives.....	247
5.1	Role of primary sensory cortex in goal-directed sensorimotor transformation	249
5.3	Cortical control of planning and executing licking as a motor output	256
5.3	Role of the frontal cortex (PFC) in goal-directed behavior	259
5.4	Neuronal circuits for the transformation of whisker stimulus into a goal-directed licking	263
5.5	Closing remarks	266
	References.....	269
	List of abbreviations	288
	Curriculum vitae	291

Chapter 1 Introduction

Opening remarks: definition of sensorimotor transformation by AI (artificial intelligence)



Hello! What is sensorimotor transformation?



Sensorimotor transformation refers to the process by which sensory information is used to guide motor actions. It involves the integration of sensory signals from various modalities (such as vision, touch, and hearing) with motor commands to produce appropriate actions in response to the environment.



During sensorimotor transformation, the brain must perform several complex operations, including decoding sensory information, computing the spatial and temporal characteristics of the sensory input, and generating motor commands to produce a specific behavior. This process is essential for a wide range of motor behaviors, from simple reflexes to complex movements, such as reaching for an object or driving a car.

In summary, sensorimotor transformation is the process of integrating sensory information with motor commands to produce appropriate behaviors.



From where did you take that information? Can you provide the reference, please.



As an AI language model, my knowledge comes from a large dataset of texts, including scientific articles, books, and other sources. In the case of the definition of sensorimotor transformation, my training data includes many scientific articles from fields such as neuroscience, psychology, and robotics, which describe and analyze the concept.



Image 0.1. Artificial intelligence chatbot definition regarding sensorimotor transformation (<https://chat.openai.com>).

We are currently living in a period of rapid digital transformation, during which the progress of science and artificial intelligence is on the rise and accelerating. I would

like to start the introduction of my thesis with the definition of sensorimotor transformation given by the artificial intelligence language model called ChatGPT, created by OpenAI (<https://chat.openai.com>) (Image 0.1). In the 21st century, humanity has been known to follow various trends, some of which are quite bizarre, such as those created by social media. While I was working on my Ph.D. thesis, there was a sudden surge in interest in AI chatbots that were made available to everyone.

At one point, I was struggling with writer's block and turned to Chat GPT for inspiration. Although the tool provided a highly accurate answer to my query (Image 1) about sensorimotor transformation, it wasn't the best fit for writing my thesis due to certain copywriting issues (Thorp 2023). Here I state that the chat GPT during my thesis writing was used solely for the inspiration to write this little introduction remarks. Nevertheless, I still considered this technological advancement in digital communication to be a significant topic to document in this manuscript as several scientific papers have already listed ChatGPT as a co-author (Else 2023; O'Connor and ChatGPT 2023; Stokel-Walker 2023).

Here, I add a short explanation to future generations who might read my Ph.D. thesis and wonder what is ChatGPT. ChatGPT (GPT is an acronym for "generative pre-trained transformer") is a chatbot powered by artificial intelligence, created by OpenAI, and released in November 2022. It was built upon OpenAI's GPT-3 suite of large language models and has undergone fine-tuning through a combination of supervised and reinforcement learning techniques. Upon its initial release, ChatGPT quickly gained recognition for its ability to provide detailed and articulate responses across a wide range of knowledge domains. However, its accuracy in terms of factual information has been noted as a significant limitation (Dahmen et al. 2023).



Tell me a funny fact about sensorimotor transformation?



While sensorimotor transformation is a complex and important process for many animals and robots, it can also be the cause of some amusing and even embarrassing situations for humans.



For example, have you ever reached for a glass of water, only to miss it and knock it over instead? This type of error can happen because the brain is constantly computing and updating the spatial relationships between objects in the environment and the body's movements. Sometimes, however, these calculations can go awry, leading to mistakes such as misjudging the distance to an object or misaligning the hand with the object's position.

Another funny example of sensorimotor transformation is the so-called "phantom limb" phenomenon, in which an amputee continues to experience sensations or even pain in a limb that is no longer there. This occurs because the brain's sensorimotor system is still "wired" to expect signals from the missing limb, leading to a kind of sensory "confusion" that can be both frustrating and amusing.

While these examples may seem humorous, they also highlight the incredible complexity and adaptability of the human brain, which is capable of performing precise sensorimotor transformations in a wide range of contexts, from the mundane to the extraordinary.

Image 0.2. Funny facts regarding sensorimotor transformation given by artificial intelligence chatbot GPT (<https://chat.openai.com>).

While my thesis is not about artificial intelligence but about sensorimotor transformation, here is a "funny" fact about sensorimotor transformation given by chatGPT (Image 0.2).

Even though I can not understand this sense of humor I think the examples provided above highlight the importance of sensorimotor transformation as a vital process in life for all living beings starting from amoeba (Schaeffer 1917) and the medicinal leech (Kristan et al. 2005a) to humans (Emken et al. 2007; Schlicht and Schrater 2007; Creem-Regehr 2009).

1.1 Sensorimotor transformation

Sensorimotor transformation is an essential process that enables organisms to interact with their environment. Therefore, interpreting incoming sensory information and generating appropriate motor responses is one of the most important functions of the nervous system to control the behavior of an animal. Even in animals with small and less complex nervous systems, like the medicinal leech, simple tactile stimulation might elicit different behavioral responses such as local bending, crawling, or swimming depending on the context (Kristan et al. 2005b). In more complex organisms, sensorimotor transformation is essential for a wide range of behaviors, such as moving through a complex environment and navigation (Harvey et al. 2012; Havenith et al. 2018), locating and processing the food (Whishaw et al. 2017), avoiding predators (Ferrero et al. 2011), and interacting with conspecifics (Wills et al. 1983). At every moment, the brain receives an enormous amount of sensory information simultaneously from different sensory organs. The sensorimotor transformation process involves integrating this information received from multiple sensory modalities, such as vision, hearing, touch, smell, and even echolocation to generate appropriate motor responses. For instance, a bat flying through a forest must process echolocation and visual information about the position of trees, branches, and other obstacles, as well as auditory cues, such as the sound of the prey, to navigate through the environment. The bat's sensorimotor system must interpret these sensory signals and generate motor commands that control its flight path, speed, and altitude (Bar et al. 2015).

Another nice example of sensorimotor transformation where sensory input (the tap on the knee) is translated into a motor command (the kick) is the knee-jerk reflex, a simple reflex action (Lazar 2022). When a doctor taps a patient's knee with a hammer, sensory receptors in the leg send a signal to the spinal cord, triggering a motor response that causes the leg to kick. Hence sensorimotor transformation can be of different complexity like in the example of the complex behavior of the flying bat or the simplicity of the knee-jerk reflex.

How the brain chooses what appropriate action to perform in response to a given stimulus, depends on multiple factors including experience, context, arousal state, or satiety. Sensorimotor transformation is also critical for learning and memory (Valyear 2016; Huda et al. 2019; Esmaeili et al. 2020). Through repeated exposure to sensory stimuli or motor adaptation (Mathis et al. 2017) organisms can refine their motor responses to better suit their environment. This allows organisms to adapt to changes in their surroundings and develop more efficient and effective behaviors.

The process by which sensory information is translated into motor commands in the brain is known as *sensorimotor transformation*, and can be broken down into three main steps:

- the processing of the sensory stimulus;
- perceptual decision-making;
- the execution of the motor command.

In a mammalian nervous system in the context of complex behaviors this process involves a chain of sensory neurons that receive sensory information and send it to primary sensory brain regions, after in the brain sensory information is transformed into motor signals and primary motor regions through motor neurons that innervate muscles will control the execution of movements. Sensory regions in the brain could be identified by stimulating sensory organs and recording neuronal activity in the brain. For example, in a classical study from Hubel and Wiesel, the authors measured the neuronal firing in the visual cortex of cats in response to visual stimuli (Hubel and Wiesel 1962). Inversely, by stimulating different regions in the brain and identifying corresponding evoked movement of the body one can identify motor areas (Fritsch and Hitzig 1870; Woodworth and Sherrington 1904; Penfield 1953; Georgopoulos et al. 1992; Mayrhofer et al. 2019). Almost 100 years before Hubel and Wiesel, in 1870, Eduard Hitzig and Gustav Fritsch were able to evoke movement through the electrical stimulation of specific parts of the cerebral cortex of dogs.

However, often it becomes hard to separate between what is 'sensory' and what is 'motor'. There are several important features of the sensory signal that researchers consider: they are time-locked to stimulus onset (Crochet and Petersen 2006), graded by stimulus amplitude (Britten et al. 1992; Romo and de Lafuente 2013; Takahashi et al. 2016), present irrespective of the behavioral outcome and transient (Sachidhanandam et al. 2013a). Motor signals, on the other hand, are time-locked to the reaction time, dependent on the behavioral outcome (Britten et al. 1992; de Lafuente and Romo 2006), may encode specific movement directions (Mayrhofer et al. 2019a; Xu et al. 2022), and show ramp-like features until the motor response time (Roitman and Shadlen 2002; Chen et al. 2017). Multiple brain regions are involved in the transformation of sensory stimulus into a motor signal. These processes are governed by orchestrated neuronal activity and information flow between many different brain regions (Romo and de Lafuente 2013; Siegel et al. 2015; Steinmetz et al. 2019; Esmaeili et al. 2020; Francis et al. 2022) and are strongly influenced by motivation, context, learning, and brain states (Crochet et al. 2019; Huda et al. 2019).

In summary, sensorimotor transformation is vital for all organisms, from simple reflexes to complex behaviors. It enables organisms to interact with their environment, navigate through complex spaces, and learn from experience. Without this critical process, organisms would be unable to survive and thrive in their surroundings.

1.1.1 Psychophysical approach to study sensorimotor transformation

Perception is the process by which we acquire information about the environment through our sensory systems (Goldstein and Brockmole 2017). Our understanding of perception has progressed by combining a variety of techniques since the rise of experimental psychology in the 19th Century. One of the methods that were developed in that period by Gustav Fechner was Psychophysics. Fechner described it as a study of the relationship between the physical properties of a stimulus and the perception of that stimulus. In his manuscript “*Elements of Psychophysics*” he defined it as “*an exact science of the fundamental relations of dependency between body and mind*” (Fechner 1948). Psychophysical methods benefit our understanding of the limits of sensory systems and measurement of the absolute perceptual threshold (i.e. the minimal intensity of a stimulus that can be detected). Fechner, during his work, developed several experimental protocols with the ultimate goal of finding the tiniest intensity of a sensory stimulus that can be detected by the subject.

One of the primary goals of psychophysics is to measure the relationship between physical stimuli and the behavioral responses they evoke. This allows to measure the threshold of detection for a given stimulus, as well as the sensitivity of the sensory system to changes in stimulus intensity or quality (Carandini and Churchland 2013). Psychophysics is widely used in the study of neural coding, as researchers seek to understand how sensory information is encoded and decoded by the brain (O'Connor, Peron, et al. 2010a; Romo and de Lafuente 2013a; Takahashi et al. 2016a, 2020a; Lacefield et al. 2019a; Lak et al. 2020a). Modern psychophysics has developed a substantial number of experimental designs routinely used in humans, primates, and, increasingly, rodents, to study how perceptual decisions depend on sensory input. The data resulting from these experiments are typically analyzed with a paradigm called *Signal Detection Theory (SDT)* (Ingleby 1967; DeCarlo 1998) that quantifies the response of an observer to the presentation of a signal in the presence of noise. SDT stands on the assumption that a subject's behavioral performance results from the population activity of a pool of decision neurons. The neural activity of this pool of neurons on each trial is drawn from one of two distributions: *signal* (represented by stimulus trials) and *noise* (represented by no-stimulus trials). The behavioral outcome (decision) relies on a threshold between these two distributions (Bruce et al. 2003).

To adapt this paradigm to rodents, scientists often use *go/no-go* experimental designs that can be quickly learned by animals and are well adapted for studies in both freely-moving and head-restrained animals. In *go/no-go* tasks, the animal is required to respond – by pressing a lever or licking a reward spout – only when the *go* stimulus is presented and not to respond when the *no-go* stimulus is presented. *Go* and *no-go* trials are randomly interleaved. The trials can then be classified in 4 categories depending on which stimulus is presented and the behavioral response: *Hit* when the animal responds on a *go* trial, *Miss* when the animal does not respond on a *go* trial,

False-alarm when the animal responds on a *no-go* trial and *Correct rejection* when the animal does not respond on a *no-go* trial (Fig. 1.1A). A well-trained animal would have a high *Hit* rate and a low *False-alarm* rate. Another task often used in rodents and is closely related to *go/no-go* tasks, is the detection task where the “*no-go*” trials are replaced by the absence of any stimulus which are referred to as *Catch trials*: the animal learns to respond only on *Stimulus* (“*go*”) trials but not on *Catch* (“*no-go*”) trials – both trial types being randomly interleaved across a session (Eimer 1993; Gomez et al. 2007).

During *go/no-go* tasks, stimuli of different intensities (strength) can be presented and the animal has to report the detection of the target stimulus, or a given feature of the stimulus. As the stimulus strength increases, the number of correct responses (*Hit* and *Correct rejection*) increases as well. The pattern of detection can be fitted with a *sigmoidal function* that is also called a *psychometric curve* (Fig. 1.1B). An ideal psychometric curve would range from 0% detection for the weakest stimuli to 100% detection for the strongest stimuli, and can be described by two parameters: its middle point and its slope. The middle point of the curve is the stimulus intensity that corresponds to 50% of detection – the stimulus was detected in half of the trials and not in the other half. It is the statistical mean of the cumulative probability curve and is also referred to as the *detection threshold*. A change in the detection threshold for a sensory stimulus is indicated by a shift of the psychometric function along the abscissa (stimulus strength). Another parameter commonly used to describe the psychometric function is its slope. The slope of the psychometric function corresponds to the statistical variance of the cumulative probability curve and indicates the underlying variability in the behavior. Performance with bigger variability has a shallower slope whereas less variability of the performance results in a steeper slope (Stüttgen et al. 2011; Carandini and Churchland 2013).

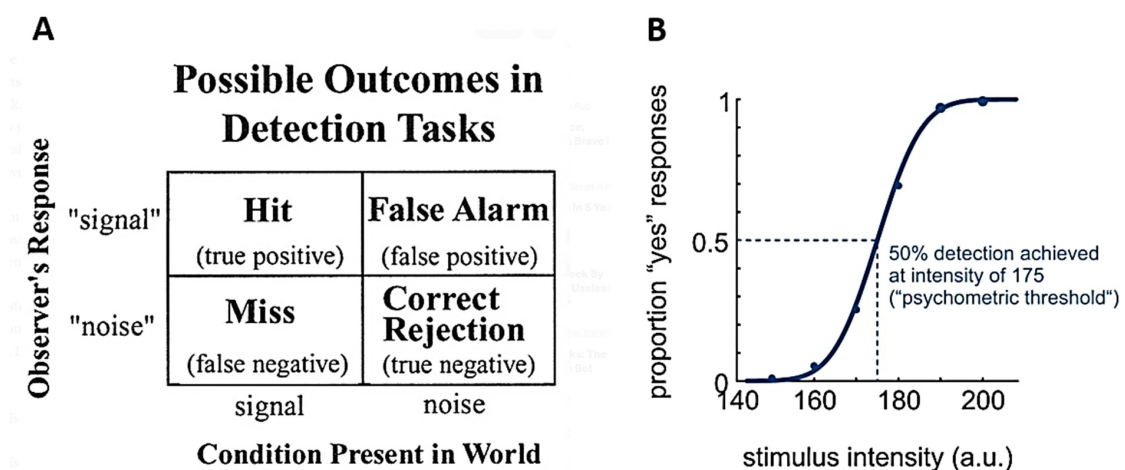


Figure 1.1. Analyzing psychophysical data with signal detection theory.

(A) Possible trial outcomes in go/no-go tasks according to Signal Detection Theory (adapted from (Boothe 2021)).

(B) Typical psychometric detection curves were obtained by plotting the proportion of Yes responses (Hit rate) as a function of the stimulus intensity. The psychometric threshold is defined as the stimulus intensity that corresponds to 50% of detection (adapted from (Stüttgen et al. 2011)).

1.1.2 Relationship between neurometric and psychometric data in sensory perception and decision-making

Studying only the behavioral outcome is not enough to address the link between neuronal activity and sensory perception. Coming back to the 19th century, Fechner distinguished between what he called “*outer psychophysics*”, the relationship between physical stimuli and sensation, and “*inner psychophysics*”, the relationship between (neuro-) physiological activity and sensation. By developing experimental psychology methods Fechner succeeded with *outer psychophysics* but due to technological limitations, it was challenging to pursue the direct investigation of inner psychophysics (Burt 1960). The study of the correlation between neural activity and perception has changed dramatically with the progress of electrophysiology in the awake-behaving monkey preparation (Britten et al. 1992). The clearest answers about the relationship between neural activity and perception can be achieved by recording from an appropriate sensory area while a subject is performing a rigorously controlled detection or discrimination task. This experimental approach allows for the simultaneous assessment of psychophysical measurements, by analyzing the behavioral data, and of neuronal activity, by measuring the spike rate of single cortical neurons in sensory areas (Newsome et al. 1989; Mountcastle et al. 1990). The ultimate goal of those studies was to evaluate the relationship between neural activity and perception, hence they were centered on the psychometric neurometric comparison (Parker and Newsome 1998). In one of the pioneering studies, authors compared the ability of psychophysical observers and single cortical neurons to discriminate weak motion. All data were obtained from monkeys trained to perform a direction discrimination task near the psychophysical threshold. The results revealed that the sensitivity of most recorded neurons was very similar to the psychophysical sensitivity of the animal perceptual report. Moreover, responses of single neurons provided a good account of both the absolute psychophysical threshold and the shape of the psychometric function (Kenneth et al., 1992). For a long time, the gold standard for the investigation of the relationship between the brain and behavior has been the head-fixed awake behaving primate preparation. But recently, the head-fixed preparation has been adapted for rodents and is now widely used to study sensory tactile perception.

The relationship between neurometric and psychometric data can be studied by applying Signal Detection Theory. The psychometric function represents the behavioral detection outcome described by a cumulative probability curve, starting

from 0% to 100% detection depending on the stimulus intensity. The neurometric function represents the neural codes based on spike rate or spike counts in response to stimuli of different intensities. Studies in anesthetized rats presented with different textures to their whiskers (Arabzadeh et al., 2006), compared the information contents of “spike count” coding versus “temporal pattern” coding and found that the analysis of spike patterns allowed better discriminability of textures than the analysis of spike counts. However, a more reliable approach to tackle this question is to combine neural recordings with a behavioral task, as has been done by Hernández in the primate tactile system (Hernández et al., 2010). Similarly, to what was found in the whisker system, the temporal patterns of spikes in the primate’s primary somatosensory cortex provided more information about the frequency of a vibrotactile signal than the simple spike count model. However, neurometric discriminability based on spike count yielded a good match with the psychometric data.

The models of neuronal responses described previously rely on single-unit activity, however, information in the mammalian brain is represented by the activity of neuronal populations. Moreover, in nature, animals have to detect stimuli that occur randomly in time. Stüttgen and Schwarz investigated the ability of rat barrel cortex neurons to detect weak and transient whisker deflections occurring without any preceding cues. They concluded that neuronal sensitivity degraded under stimulus uncertainty such that it is highly unlikely that single neurons can provide the basis for perception. However, modeling the sensitivity of neuronal pools on basis of spike timing showed that the subject’s perception could be based on the occurrence of coincident spikes from several neurons (Fig. 1.2) (Stüttgen and Schwarz, 2008).

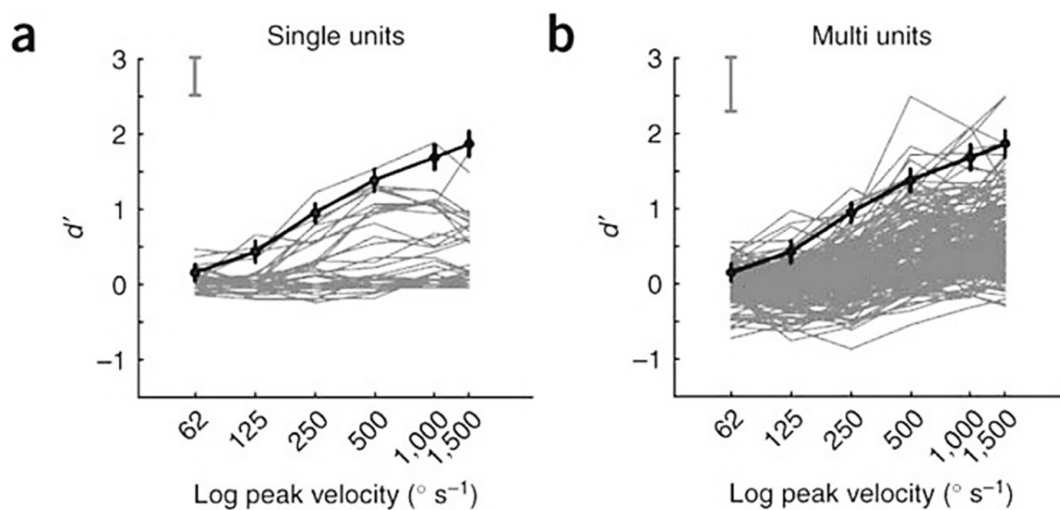


Figure 1.2. Psychometric - neurometric comparison.

(A) Sensitivity of single units in barrel cortex as a function of the logarithm of stimulus velocity expressed as d' (thin gray lines). The bold line represents mean psychometric performance.

(B) Same as **a** but for multi-units. The psychometric function acts as an upper bound for the neurometric precision of barrel cortex neurons.

(adapted from (Stüttgen and Schwarz 2008))

The comparison of psychometric and neurometric functions is a valuable tool for separating sensory processing from decision-making in the brain. By examining the responses of neurons or brain regions, researchers can determine whether they encode pure sensory information or are involved in decision-making processes. When examining pure sensory information, the neurometric functions should be similar regardless of whether the subject responds correctly (Hit) or not (Miss) to the stimulus. This indicates that the neuron or brain area is solely responsible for processing sensory information and is not influenced by decision-making processes. Conversely, when examining decision-making processes, the neurometric functions should differ depending on the subject's behavioral response. This suggests that the neuron or brain area is involved in the decision-making process and is influenced by the subject's behavioral report. By comparing psychometric and neurometric functions, researchers can gain insights into the complex processes that underlie sensory processing and decision-making in the brain.

1.1.3 Sensorimotor transformation occurs across a large network of cortical areas

Many studies in system neuroscience using different sensory systems, different animal models, and different behavioral tasks have described a large and distributed network of brain regions that are involved in the execution of goal-directed behaviors. However, what remains controversial in the literature is whether each brain area would execute very specific computation – as an example, primary sensory cortical areas would generate a neural representation of the sensory stimulus and forward it to higher-order frontal regions where a decision would be made and transferred to motor regions for the execution of the motor command – or the transformation of sensory signal into motor output is a gradual and distributed process. In the latter case, one would expect sensory-, decision- and motor-related neuronal representations in multiple cortical regions including sensory, higher-order, and motor areas. In this chapter, I will review key papers that support one, another, or a mixture of these hypotheses.

One of the simplest sensorimotor transformations that can be studied in a laboratory is the sensory detection task. In this experimental paradigm, the subject is simply asked to report the perception of a given sensory stimulus by a simple motor

response. The use of well-controlled sensory stimuli allows for addressing the question of the perception of the near-threshold stimuli that are detected by the subject in 50% of the cases. In the detection task precise control in both magnitude and time over the input stimulation that would lead to a decision, makes the study of perceptual decision-making experimentally tractable.

Following this idea, Romo and Lafuente trained monkeys to respond to a vibrotactile stimulus of varying intensity applied to the fingertip by pressing a button. They recorded the neuronal activity from the primary somatosensory (S1) and the motor cortices as the monkeys performed the task. They investigated neuronal information coding by correlating the neuronal activity with the amplitude of the vibrotactile stimulus applied to the fingertip, or with the perceptual report of the monkey. First, they observed that the evoked neuronal activity in the primary somatosensory cortex (S1), but not in the medial premotor cortex (PMC), was scaled as a function of the stimulus amplitudes, suggesting that S1 encoded the physical nature of the sensory stimulus. Second, they observed that neuronal activity during Hit trials (correct report) and Miss trials (absence of report) for the near-threshold stimulus was very similar in the S1 but very different in the PMC. This suggests that the neuronal activity in PMC, but not in S1, covaried with the subject perceptual choice (Fig. 1.3A). They concluded that the functional role of primary sensory cortices in goal-directed perceptual detection tasks may be mostly to generate a neural representation of the sensory stimuli, whereas higher cortical areas use this information to make the decision (de Lafuente and Romo 2005).

In another study, Romo and Lafuente recorded neuronal activity across several brain regions while monkeys reported the presence or absence of mechanical stimulation of varying amplitudes. Similarly, to the previous study, they found that the neuronal activity in S1 linearly correlated with the strength of the sensory stimuli and showed little predictive capacity regarding the monkey outcomes. Moreover, they demonstrated that the sensory stimulus engaged multiple areas of the cerebral cortex with sensory-evoked responses propagating through sensory areas, premotor and motor areas, up to higher-order frontal areas. To test the role of distinct recorded areas in the processing of sensory stimuli, they measured how normalized neuronal firing rate was modulated by the stimulus amplitude using linear regression analysis. As a result, they observed the highest slope of the linear fit for the S1 and small slopes close to zero for higher-order areas, indicating that higher-order areas do not encode stimulus amplitude with the same fidelity as the early somatosensory cortex. As information travels to higher-order areas it progressively shows a higher correlation to the perception, memory, and decision of the monkey (Fig. 1.3B) (Romo and de Lafuente 2013). Similar serial information flow in perceptual decision tasks has also been observed and described in other sensory systems in primates, such as visual (Gold and Shadlen 2002; Bisley and Goldberg 2006). The work of Gilbert and Li has

shown that sensory processing in the primary visual cortex (V1) can be modulated by top-down influences. They trained monkeys to perform a task that required them to discriminate the orientation of a line. The researchers found that the activity of neurons in V1 was modulated by the task demands, with greater activity observed when the monkeys were performing a more difficult version of the task. This suggests that top-down attentional influences can modulate the processing of sensory information in V1 (Gilbert and Li 2013). Similarly, in Roelfsema's study, monkeys were trained to trace a line with their eyes while ignoring distracting lines. The researchers found that the activity of neurons in V1 was modulated by the context of the task, with greater activity observed when the monkeys were tracing the target line compared to when they were ignoring it. Showing that task demands also can modulate the processing of sensory information in V1 in a context-dependent manner (Roelfsema et al. 1998). Context-dependent processing in primary sensory cortices could thus be important.

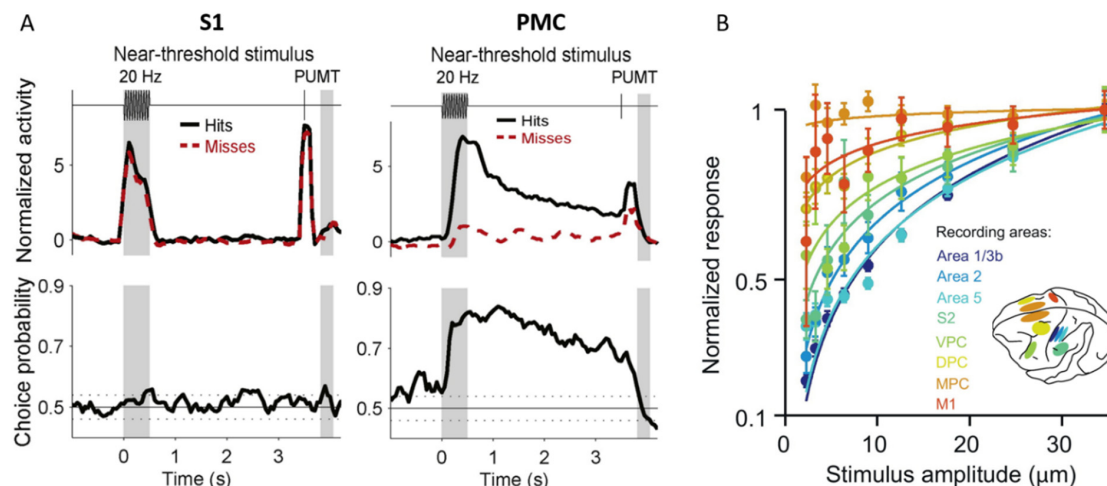


Figure 1.3. Translation of sensory input to a perceptual decision.

(A) Top averaged normalized neuronal population activity recorded from the primary somatosensory area (S1) and the primary motor cortex (PMC) during Hit (black) and Miss (red) trials for near-threshold stimulus amplitude while a monkey performed a vibrotactile detection task. (Wide grey bar indicates the time of vibrotactile stimulation period, PU – withdrawal of the stimulator that served as a go cue for the monkey to push the buttons, MT – response window where the monkey should push one of the two buttons. The bottom panels show the choice probability index.

(B) Mean normalized population firing rates as a function of the stimulus amplitude. Curves are the linear fits to the data, color-coded according to the recorded area as annotated in the insert.

(adapted from (Romo and de Lafuente 2013))

Another study in non-human primates identified multiple cortical areas that could be involved in the execution of a tactile delayed comparison task in which rhesus monkeys were required to compare the frequency of the vibration of two stimuli – f_1 and f_2 – separated by a time delay. For the majority of the neurons recorded in the S1,

the firing rate increased monotonically with increasing stimulus frequencies. As no decision can be assigned to the first stimulus (f1) in this experiment, the neuronal representation during the first stimulus is less affected by the later decision or motor-related signals. During the presentation of f1, a sensory-related signal was observed in all areas including the PMC. During the presentation of the second (f2) stimulus, the response of neurons in S1 was modulated mainly by the frequency of f2 while in the secondary somatosensory, premotor, and prefrontal cortical areas, neurons encoded not simply the frequency of f2 but its relative value compared to f1. This series of studies led to the conclusion that sensory, memory, and decision-related signals are represented in multiple brain areas including the dorsolateral prefrontal cortex, but no single area can be identified as the unique site that implements the sensory-to-motor transformation (Romo and Salinas 2003).

Similarly, in mice, several studies have reported the recruitment of multiple cortical regions during the execution of simple sensory detection or discrimination tasks (Goard et al. 2016; Le Merre et al. 2018a; Gallero-Salas et al. 2021a). The cortical areas recruited extend far beyond sensory and motor regions, to associative and higher-order areas including the medial prefrontal cortex or the dorsal hippocampus and posterior parietal cortex (Pennartz et al. 2011a; Euston et al. 2012a; Pinto and Dan 2015a; Goard et al. 2016; Le Merre et al. 2018a; Gallero-Salas et al. 2021a).

In conclusion, the literature remains divided on whether specific computations are performed by each brain region or if the transformation of sensory signals to motor output is a gradual and distributed process. Nevertheless, it is evident that sensorimotor transformation involves intricate neuronal activity and information exchange among various brain regions. Despite several proposed hypotheses in this regard, the process continues to be an active area of research and debate within the neuroscience community.

1.1.4 Transformation of mouse whisker stimulus into licking motor output during goal-directed behaviour

In order to identify the neuronal circuits that are recruited and necessary for sensorimotor transformations, it is crucial to monitor the activity of well-defined neuronal populations, as well as to manipulate the neuronal activity in a precise and controlled manner. This has become possible in mice through the use of advanced technologies such as high-density silicon probe recordings which allow to simultaneously record a big population of single neurons with high temporal precision, and optogenetics, which allows selective control of the activity of specific brain regions or even neurons with light. By combining these techniques with behavioral assays,

researchers can gain a more complete understanding of the neural circuits involved in sensorimotor transformations.

Mice are an ideal model organism for studying the neuronal circuits responsible for sensorimotor transformation due to their genetic tractability, which allows for easy manipulation and study of their genetic makeup. The mouse genome and the structure of its nervous system are very similar to those of humans, which will likely help the future generalization of knowledge gained from mice studies.

A well-studied sensorimotor transformation in mice is the association of a whisker stimulus with the action of licking for reward, which is an important example of how the brain integrates sensory information with motor output to produce adaptive behaviors. In this chapter, I will describe what is currently known about the cortical circuits involved in this goal-directed sensorimotor transformation of the whisker sensation into licking in the mouse. One of the simplest but well-controlled paradigms in mice is a whisker detection task in which head-restrained mice are trained to associate a brief whisker stimulus to the action of licking to obtain a water reward (Fig. 1.4) (Sachidhanandam et al. 2013a).

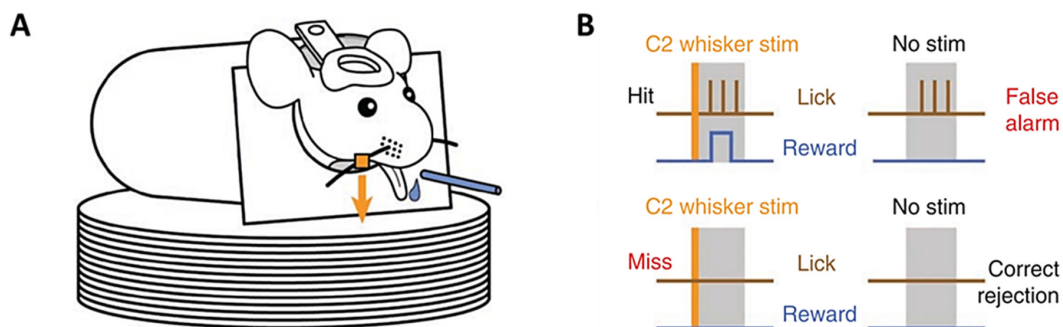


Figure 1.4. Whisker-based tactile detection task.

(A) Experimental setup: a metal particle is attached to the right C2 whisker of the water-restricted, head-restrained mouse on the top of a magnetic coil. The mouse must lick the reward spout shortly (< 1 s) after the brief (1 ms) whisker stimulation to obtain water.

(B) During each behavioral session, trials with (Stim) and without (No stim) whisker stimulation were randomly delivered. In total, four trial types were considered: **Hit** trial (rewarded) if the mouse licked after the whisker stimulus within the 1 s response window; **Miss** trial (not rewarded) if the mouse didn't lick after whisker stimulation; **False alarm** trial if mouse licked and **Correct rejection** if the mouse did not lick during the response window in No stim trials (not rewarded).

(adapted from (Sachidhanandam et al. 2013))

In this task, mice have to detect and interpret a whisker stimulus and execute licking as a perceptual report. From multiple studies, we know that wS1 and the secondary whisker somatosensory cortex (wS2) are likely to be the starting input areas

for the processing of the whisker sensory information in the cortex. However, the precise computations occurring in these areas are still debated. There is consistent evidence that wS1 encodes the physical nature of the stimulation, similar to visual primary sensory areas. But, there are conflicting results about whether or not wS1/wS2 also encodes decision variables. I will cover this question in more detail in the following chapter.

wS1 is densely and reciprocally connected to a motor cortical area, the whisker primary motor cortex (wM1), implicated in the initiation and control of whisker movements. The neuronal activity in the whisker motor cortex (wM1) is correlated to whisker movements (Hill et al. 2011; Sreenivasan, Esmaeili, et al. 2016). Intracellular stimulation of single cells in the motor cortex can evoke small but significant whisker movements (Brecht et al. 2004). Optogenetic activation of the whisker motor cortex elicits whisker protraction whereas opto-inhibition strongly reduces whisker movements (Sreenivasan, Esmaeili, et al. 2016; Auffret et al. 2018). In the whisker-based detection task, the motor output is a licking action of the mouse. And although wM1 receives direct inputs from wS1, wM1 does not control licking and, in fact, is not necessary for the execution of the whisker-based detection task (Le Merre et al. 2018). In a recent study from our laboratory, we have identified another region of the motor cortex controlling tongue and jaw movements that we refer to as the tongue/jaw primary motor cortex (tjM1). Neurons in this region have high selectivity for the direction of the licking and its stimulation-caused movements of the jaw and the tongue. (Mayrhofer et al. 2019; Xu et al. 2022). Cortical control of licking and the detailed function of tjM1 will be also covered in the next chapters. Thus tjM1 is a likely endpoint for the sensorimotor transformation in which a brief whisker deflection is converted into goal-directed licking in order to obtain the reward. However, although tjM1 receives direct sensory inputs from the tongue/jaw primary sensory cortex, it does not receive a major input from wS1. Therefore, the transformation of the whisker sensory information into a motor command likely transits through other cortical or subcortical areas.

Now the question is how the sensory information flows from wS1/wS2 to the tjM1 and which brain regions are likely to contribute to the execution and learning of this goal-directed behavior. A recent study from our laboratory demonstrated that in a simple whisker-based detection task, sensory-driven neuronal activity rapidly spread across multiple cortical areas. Le Merre et al. recorded the local field potential of multiple brain regions across the learning of the detection task. They observed sensory-evoked responses starting in whisker primary and secondary somatosensory cortices (wS1/wS2), which rapidly spread to the whisker primary motor cortex (wM1), and reached the medial prefrontal cortex and dorsal hippocampus with short latencies (Fig. 1.5A) (Le Merre et al. 2018).

Another advance in studying the sequential flow of excitation of cortical areas came from voltage-sensitive dye imaging of the dorsal neocortex during the simple whisker detection task. Consistently, sensory-evoked responses originated in wS1/wS2 following the whisker stimulation in both Hit (correct detection) and Miss (absence of detection) trials. Later, activity propagated frontally causing depolarisation of a large part of the frontal cortical surface including wM2, tJM1, and tJM2/ALM with larger excitation in Hit trials compared to Miss trials (Fig. 1.5B) (Kyriakatos et al. 2017; Aruljothi et al. 2020). In addition, the study of Steinmetz et al. using a combination of extracellular recordings and wide-field calcium imaging also demonstrated sequential activation of different brain regions. The authors observed an activation pattern, where different regions of the brain were activated in a specific order during the decision-making process. Specifically, they found that sensory regions of the brain were activated first, followed by regions involved in decision-making and planning, and finally, regions involved in motor control and execution (Steinmetz et al. 2019).

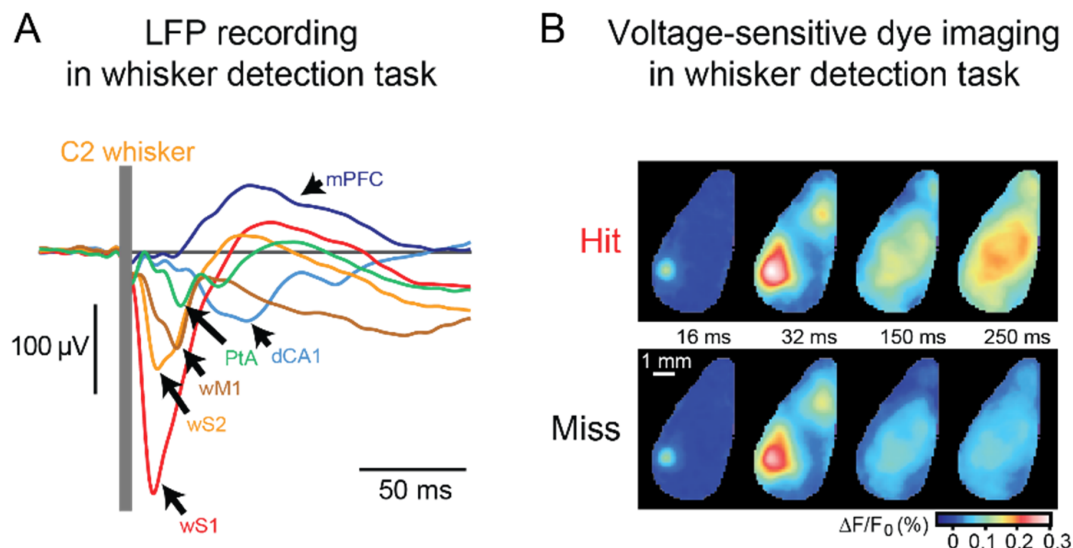


Figure 1.5. Sequential propagation of neuronal responses evoked by whisker stimulation.

(A) Local field potential recordings revealed sequential activation of wS1, wS2, wM1, the parietal association area (PtA), the dorsal part of the CA1 region of the hippocampus (dCA1) and the medial prefrontal cortex (mPFC) (adapted from (Le Merre et al. 2018)).

(B) Voltage-sensitive dye imaging demonstrated wide depolarization of frontal (motor) regions in Hit trials compared to Miss trials (adapted from (Kyriakatos et al. 2017)).

The sensory-to-motor coupling required for task execution is not instantaneous and is learned over time by experiencing whisker stimulation followed by licking that leads to a reward. Le Merre et al. demonstrated that the medial prefrontal cortex (mPFC) and dorsal part of the CA1 region (dCA1) were recruited through the learning of the detection task and might thus contribute to rule learning (Fig. 1.6A) (Le Merre et

al. 2018). These regions might help route the information in a context-dependent manner to the whisker secondary motor cortex (wM2) (Esmaeili et al. 2020). wM2 is a cortical region located in the frontal cortex of mice, and it receives inputs from both sensory and motor areas of the brain. wM2 is involved in a wide range of behaviors, including movement initiation and planning, sensory processing, and decision-making, hence, it may play a key role in integrating sensory information with motor output, allowing mice to respond quickly and adaptively to changing environmental cues (Barthas and Kwan 2017). The whisker-evoked sensory signal from wM2 might be transmitted further to ALM/tjM2 and then to tjM1 to drive licking (Esmaeili et al. 2020a). ALM region in mice is a critical brain area involved in the control of motor movements, as well as in learning and decision-making processes related to motor behavior (Komiyama et al. 2010; Guo et al. 2014; Chen et al. 2017; Svoboda and Li 2018). ALM has been also implicated in the planning of voluntary movements for complex motor sequences (Xu et al. 2022). Whereas, tjM1 appears to be more important for the cortical control of tongue and jaw movements by integrating sensory information from tjS1/tjS2 and motor planning signals from tjM2/ALM. Then, tjM1 and tjM2/ALM PT (pyramidal tract) neurons, which have cell bodies in deep cortical layers, project to central pattern generators in the brainstem which in turn control licking (Travers et al. 1997).

While it is evident that several regions of the brain contribute to the translation of whisker stimuli into purposeful licking, the specific neural pathways and plasticity mechanisms that connect these regions are yet to be fully elucidated. Further research is needed to gain a comprehensive understanding of the intricate neural circuits that enable goal-directed licking in response to whisker stimulation.

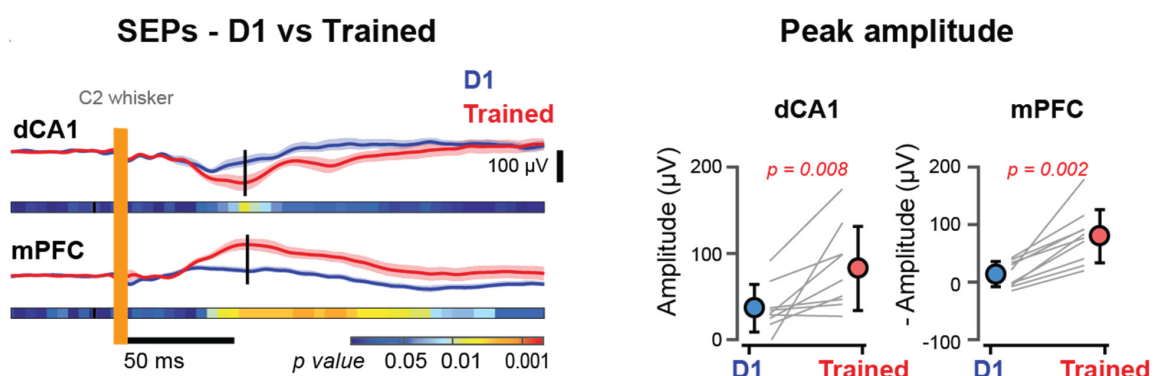


Figure 1.6. Learning-driven changes of the whisker stimulus processing.

Left, Grand-average whisker sensory-evoked potentials (SEPs) were recorded in the same mice in dCA1 and mPFC regions during the first training day of the whisker detection task (D1, blue) and once trained in the task (Trained, red). *Right*, the peak amplitude of the sensory-evoked potential for D1 and Trained sessions (adapted from Le Merre et al. 2018).

1.2 Sensory processing of tactile whisker stimuli

1.2.1 Mouse whisker system

Mice are primarily nocturnal animals. They live in narrow underground tunnels and strongly rely on tactile information sampled with their whiskers to sense their environment (Vincent 1912; Ahl 1986; Brecht et al. 1997). Rodents use their whiskers to recognize and locate objects in space and guide their locomotion through an active process called 'whisking'. Whisker-based touch represents the major input information, particularly for the space surrounding the head, that allows mice to navigate in dark tunnels (Vincent 1912; Ahl 1986). Common modes of whisking include "exploratory" whisking, which is bilateral symmetric movements with high amplitude, and frequency of around 10-20 Hz for mice, and lower-amplitude "foveal" whisking (Berg and Kleinfeld 2003). Rodents also exhibit asymmetric and irregular whisking during some object recognition tasks. Different whisker-based behavioral paradigms were adopted for head-fixed mice that can allow good control of whisking through tracking with a high-speed camera (Crochet and Petersen 2006; O'Connor, Peron, et al. 2010).

Whiskers are thin tapered rods that are anchored to the skin by follicles with mechanosensory receptors at their base. Each of the follicles is innervated by a branch of about 200 sensory neurons of the trigeminal ganglion. Deflection of a whisker opens mechano-gated ion channels at the base of the follicle converting the mechanical energy into action potentials that propagate through the trigeminal nerve emerging from the trigeminal ganglion (Tg). A given trigeminal neuron only fires action potentials to deflection of one specific whisker. These sensory neurons make excitatory glutamatergic synapses in the principal trigeminal nucleus of the brainstem (Pr5) and spinal trigeminal nucleus (Sp5). From the brainstem sensory information is sent to the somatosensory thalamus, where a second glutamatergic synapse excites thalamocortical neurons which project to the primary somatosensory cortex (Fig. 1.7A) (Petersen 2007; Diamond et al. 2008).

A very peculiar feature of the whisker system is its somatotopic organization. Whisker follicles have a well-defined topography on the snout of the rodent (Fig. 1.7B) that is highly conserved throughout the synaptic pathway up to the primary somatosensory cortex: in the brainstem, neurons in the principal trigeminal nucleus are organized into somatotopically arranged "barrelettes" that correspond to and receive strong input from a specific whisker (Deschênes et al. 2003). Subsequently, the thalamic ventral posterior medial (VPM) nucleus is also somatotopically laid out into anatomical units termed "barreloids" (Van Der Loos 1976). The axons of VPM neurons within individual barreloids project to the primary somatosensory cortex forming discrete clusters in layer 4 – the "barrels" – which form the basis of the "barrel" map

(Woolsey and Van der Loos 1970). The layout of the barrels in the somatosensory cortex repeats the layout of the whiskers on the snout of mice and rats. These clear anatomical maps at each level of the ascending pathway suggest a 'whisker-to-barrel' connection (Petersen 2007).

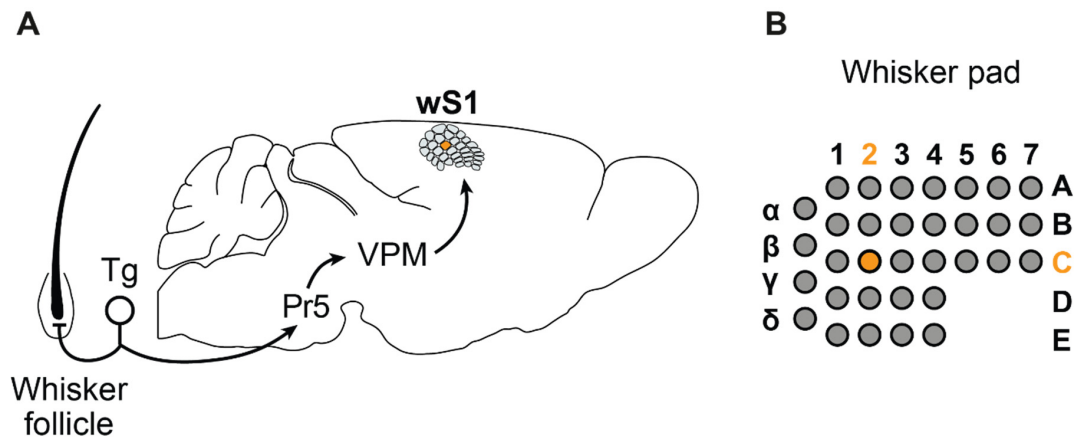


Figure 1.7. Mouse whisker somatosensory system.

(A) Schematic representation of the pathway. The deflection of a whisker evokes action potentials in sensory neurons of the trigeminal ganglion, which release glutamate at a first synapse in the brainstem (Pr5). The brainstem neurons send sensory information to the thalamus (VPM), where a second glutamatergic synapse excites thalamocortical neurons projecting to the primary somatosensory barrel cortex (wS1).

(B) The grid-wise layout of the whisker pad (only macro whiskers shown). Each whisker is identified by a combination of its row (letters A to E from dorsal to ventral) and its arc (numbers 1 to 7 from caudal to rostral), with α, β, γ, and δ straddlers between rows.

(adapted from Esmaeili et al. 2020))

Recent anatomical studies using viral tracing techniques described two parallel pathways that bring whisker tactile information to the cortex. Two distinct trigemino-thalamocortical inputs to primary and secondary mouse whisker somatosensory cortices were imaged. Through the Lemniscal pathway whisker sensory information is relayed to trigeminal ganglion Pr5, which is further transferred to the first-order ventral posteromedial nucleus (VPM-FO), which neurons mainly project to layer 4 of wS1. Through the Paralemniscal pathway, whisker sensory information is relayed to trigeminal ganglion Sp5i, which is further transferred to the first-order thalamic medial posterior nucleus (POM-FO), which neurons mainly project to layer 4 of wS2. First-order (FO) thalamic nuclei bring sensory information mainly to layer 4 of sensory cortices. A higher-order subdivision of POM (POM-HO) does not receive ascending

sensory input from the brainstem and innervates layers 1 and 5A of both wS1 and wS2 (Fig. 1.8) (El Boustani 2020).

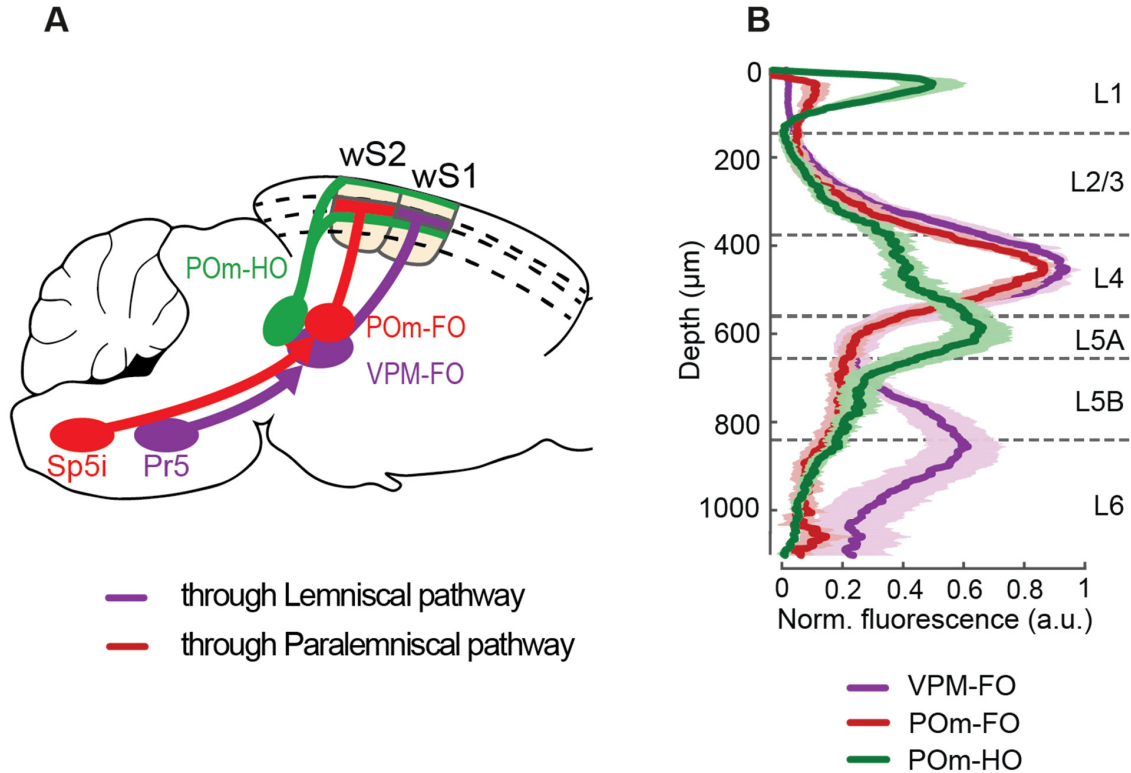


Figure 1.8. Parallel pathways that bring whisker sensory information to the cortex were revealed through AAV-mediated anterograde trans-synaptic gene expression.

- (A) Schematic of the different somatosensory trigemino-thalamocortical circuits.
 (B) Normalized fluorescent expression of axonal projections in wS1/wS2 from different thalamic nuclei.
 (adapted from (El-Boustani et al. 2020))

While the somatotopy is largely conserved throughout the sensory pathway, from the brainstem to the primary whisker somatosensory cortex (wS1), the sensory processing in each station appears to be strikingly different. Arabzadeh et al. recorded simultaneously first-order sensory neurons (trigeminal ganglion) and neurons in the whisker area of the cerebral cortex of anesthetized rats during the presentation of different textures to a single whisker. This approach allowed a direct comparison of the activity of different stations along the sensory pathway. Several coding properties of first-order and cortical neurons were described: (i) first-order neurons fired a greater number of spikes during texture presentation than during free-whisking (artificial whisking); (ii) first-order neurons fired in a highly reproducible manner across trials; (iii)

sensory cortex neurons also fired at higher rates for texture presentation than free-whisking; but (iv) sensory cortex neurons fired in a less reproducible manner across trials (Arabzadeh et al. 2005).

1.2.2 Structural and functional organization of barrel cortex

In 1955 Mountcastle discovered the cortical column and described it as a discrete structure, aligned in radial columns of the somatosensory cortex and perpendicular to the brain surface spanning the layers, which contains cells responsive to only a single modality (Mountcastle et al. 1955). These radial columns in wS1 are also called barrels. It was shown both in anesthetized and awake animals that each barrel receives the strongest input from its “principal” whisker and a blurred signal from surrounding whiskers. Brecht and Sakmann (Brecht and Sakmann 2002) mapped receptive fields for brief whisker deflections in anesthetized rats. Using *in vivo* whole-cell recordings they measured evoked postsynaptic potentials of different cell types in layer IV of the primary somatosensory cortex induced by principal whisker deflection. They found that the deflection of a single whisker is represented in multiple barrels and septa. However, the sensory-evoked response appears with a shorter latency in the barrel that corresponds to its principal whisker and then propagates to surrounding barrels. Accordingly, in the principal barrel, the response to the surrounding whiskers' deflection was delayed and significantly decreased depending on the distance to the principal whisker. The authors concluded that barrel cells represent dynamically the deflection of a single whisker with high temporal and spatial acuity (Petersen and Sakmann 2000; Brecht and Sakmann 2002).

The above-described functional organization of cortical barrels is well supported by the structural organization of the microcircuit within the individual barrels. As described above the sensory information from a single whisker deflection reaches the primary somatosensory cortex through two thalamic nuclei: the ventral posterior medial nucleus (VPM) and posteromedial nucleus (Pom). VPM axons innervate primarily the cortical layer 4 and, to a lesser extent, layer 3, through glutamatergic synapses. Thalamocortical PoM neurons also project to cortical layer 1 and layer 5A, making dense glutamatergic innervation. In the mouse, each layer 4 barrel is composed of a central region of high-density neuropil that contains the clustered VPM axonal arborizations and is surrounded by a cell-dense wall of layer 4 neurons that orient their dendritic arborizations into the corresponding specific barrel. In addition, cell reconstruction showed that dendritic and axonal arborizations of excitatory spiny stellate barrel cells were mostly restricted to the borders of the barrel column. In this way, the thalamic input arriving to a single layer 4 barrel remains confined to that barrel

for the initial step of cortical processing. Whereas, dendrites and axons of septum cells mostly extend across barrel borders (Brecht and Sakmann 2002; Petersen et al. 2003).

The excitatory layer 4 axons synapse onto layer 2/3 neurons of the same barrel column (Lefort et al. 2009). Strong evidence for functional cortical columns defined by the horizontal extent of the layer 4 barrels was shown using the glutamate uncaging technique by Shepherd et al. (Shepherd et al. 2003), revealing a strictly columnar input to layer 2/3 from layer 4. Thus, within the cortical microcircuit, the signal is initially propagated in a strictly columnar fashion. That was confirmed by studies using voltage-sensitive dye (VSD) imaging.

A Voltage-Sensitive Dye Imaging

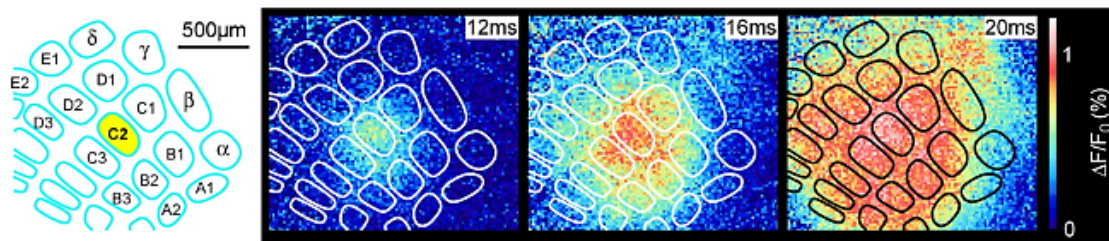


Figure 1.9. Spatiotemporal dynamic of the sensory response in the mouse barrel cortex.

Voltage-sensitive dyes (VSD) can be used to map the spatiotemporal dynamics of the sensory response at millisecond temporal resolution and with a spatial resolution of $\sim 50 \mu\text{m}$. *Left*: barrel map indicating the location of the C2 barrel column (yellow). *Right*: the time-dependent spreading of the subthreshold electrical activity in layer 2/3 of the barrel cortex imaged with VSD. A brief deflection of the C2 whisker evokes an early localized depolarization limited to the C2 barrel column (12 ms). Over the next milliseconds, the depolarization spreads across the barrel field (adapted from (Ferezou et al. 2007a)).

Figure 1.9 displays the activation of a single cortical column following a single-whisker deflection in VSD imaging. In vivo, the sensory response subsequently propagates across the entire barrel map in the next tens of milliseconds. The lateral propagation of the sensory signal is supported by the anatomical organization of cortical layer 2/3. In layer 2/3, the excitatory pyramidal neurons that have their soma located above a barrel send their axons projecting through the barrel. Whereas the excitatory pyramidal neurons that have their soma located above the septum project through the septum between barrels. Barrel-related cells have shorter sensory-evoked response latency and higher amplitude than septum-related cells. Axonal arbors of barrel-related cells project horizontally into several surrounding whisker barrel columns, making glutamatergic synapses, suggesting that they are the major anatomical substrate for the sensory-evoked signal propagation to surrounding barrels (Brecht et al. 2003). Recent studies also revealed that deep layers (border of layers 5 and 6) receive sensory-evoked responses through primary thalamocortical axons and

further propagate them through their extensive horizontally projecting axons (Egger et al. 2020). In addition, layer 2/3 pyramidal neurons innervate layers 5 and 6, which makes complex synaptic integration receiving direct thalamic input along with excitatory input from layers 4 and other pyramidal neurons in the infragranular layers (Lefort et al. 2009; Petersen and Crochet 2013) (Fig. 1.10).

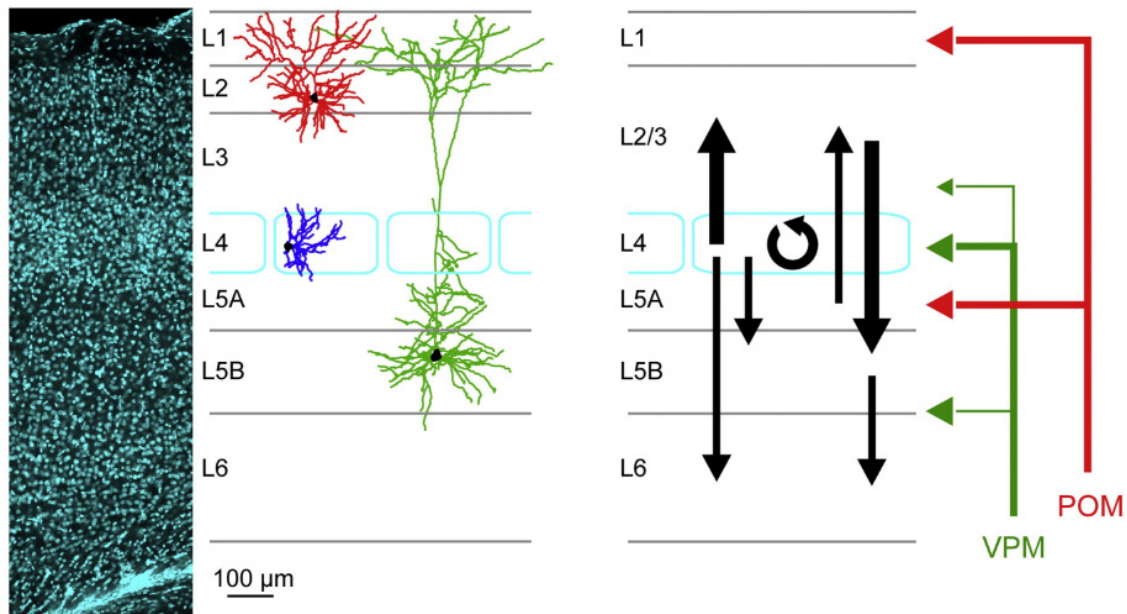


Figure 1.10. Functional and structural organization of barrel cortex.

Left: A confocal image of DAPI-stained nuclei (cyan) at a single focal plane through the C2 barrel column. *Middle:* schematic representation of the cortical layers (barrels within L4 in cyan) with examples of typical dendritic morphologies of excitatory cortical neurons (in red, an L2 neuron; in blue, a spiny stellate L4 cell; in green, an L5B pyramidal neuron). *Right:* schematic representation of the main excitatory connections between cortical layers within a barrel column (black), as well as the main thalamic inputs to the barrel cortex from the ventral posteromedial nucleus (VPM, green) and the posteromedial nucleus (POM, red) (adapted from (Petersen and Crochet, 2013)).

The rodent's primary somatosensory cortex, like any other cortical area, is spontaneously active even in the absence of any sensory inputs. During quiet wakefulness, cortical neurons display large amplitude, low-frequency membrane potential fluctuations that are highly synchronous between nearby neurons (Crochet & Petersen, 2006; Poulet & Petersen, 2008). During active motor behavior, the cortical neurons slightly depolarize and display small amplitude, fast membrane potential fluctuations that are less synchronized locally. This profound state change, occurring during spontaneous motor activity also affects sensory processing. Typically, sensory-evoked responses are reduced during active behaviors in the primary somatosensory cortex and propagate less to other cortical areas (Crochet and Petersen 2006;

Ferezou et al. 2007; Poulet and Petersen 2008). Thus, brain states have an important impact on sensory processing and may account for part of the trial-by-trial variability of the cortical sensory-evoked responses. The trial-by-trial variability of cortical responses to identical, well-controlled, stimuli is a key feature of cortical processing and an important question to address to understand how sensory information is transformed into goal-directed behaviors. This variability is partly driven by the interaction between sensory signals and the ongoing spontaneous cortical activity and may have a significant impact on animals' performance in sensory detection or discrimination tasks.

1.2.3 wS1/wS2 as a starting point of sensory processing in the cortex during tactile detection task

The neural basis of tactile sensory perception was studied in depth during the recent decade, however, there is no consensus on the exact mechanistic model. There is a general agreement that primary and secondary somatosensory areas serve as a starting point for processing tactile sensory information in the cortex during tactile detection task. This idea is supported by various substitution experiments, where instead of training the subject to respond to an external stimulus, researchers have directly stimulated the primary sensory cortex. Weak electrical (Butovas and Schwarz 2007) or optogenetic (Huber et al. 2008; Musall et al. 2014) activation of the barrel cortex is sufficient to generate a behavioral response and it is possible to train rodents to detect such stimuli. Moreover, in animals trained to detect or discriminate tactile stimuli, the substitution of the peripheral stimulus by direct cortical stimulation led to a similar behavioral performance (Romo et al. 1998; Sachidhanandam et al. 2013). In 1998 Romo et al. substituted a second sensory stimulus by current injected from the microelectrode to a primary sensory cortex in monkeys trained to discriminate two flutter stimuli delivered on their fingertips. The conclusion was that neural code underlying the sensation of tactile stimulation in wS1 can be finely manipulated, to the extent that the behavioral reports caused by natural stimuli or brain stimulation were indistinguishable (Romo et al. 1998). More recently, Sachidhanandam et al. used an optogenetic technique to stimulate excitatory neurons in the C2 barrel column of Emx1-Cre mice expressing channelrhodopsin-2 (ChR2). After training the mice to detect whisker stimuli, optogenetic excitation of the wS1 was found to substitute for whisker stimulation, resulting in a high mice performance (Sachidhanandam et al. 2013). Conversely, mice trained to detect wS1 optogenetic stimulation also licked immediately in response to the first presentation of a whisker deflection (Sachidhanandam et al. 2013). Thus the direct stimulation of wS1 can directly substitute to the whisker stimulus and suggest that neural activity in the wS1 is causally related to sensory perception and drives downstream circuits involved in the sensorimotor transformation.

Nevertheless, one might argue that wS1 activation can provide another source of activity for stimulus detection, and potentially the animal will detect the activity in the barrel cortex as an extra source of information. Therefore, the direct activation of a given area cannot certainly prove its necessity.

Another classical strategy to prove the involvement of a brain structure in a given function is the use of lesions or inactivation with optogenetics or pharmacology. The important difference between these methods is the duration of wS1 inactivation and whether inactivation is reversible or permanent. And that is where the results of wS1 inactivations have different consequences on behavioral performance. A classic study by Hutson and Masterton postulates that stimulus detection won't be impaired after a permanent lesion of the barrel cortex (Hutson and Masterton 1986). But more recent studies disagreed: transient inactivation of wS1 through Muscimol application impaired detection of multi-whisker stimuli and caused the reduction of the animal report (Miyashita and Feldman, 2012). Overall, different laboratories using pharmacological or optogenetic silencing of wS1 have found that wS1 is necessary for the execution of both whisker discrimination and detection tasks (Miyashita and Feldman 2013; Sachidhanandam et al. 2013; Kwon et al. 2016; Takahashi et al. 2016; Yang et al. 2016; Le Merre et al. 2018). Hence one possible explanation was that during permanent lesions of wS1 cortical circuit reorganization could occur therefore mice still were able to perform the task. However study from Hong et al. demonstrated that shortly after the lesion of wS1 mice were able to perform whisker detection task with a decent accuracy arguing that circuit reorganization or plasticity wouldn't have time to occur (Hong et al. 2018). Importantly they also demonstrated that brief optogenetic inhibition decreased the mice performance. This constellation of findings – impairment through transient but not permanent inactivation can possibly be explained by involvement of wS1 in the execution of the whisker detection task during normally functional intact brain, which might not be a case after the permanent injury.

Classical studies in monkeys and rats demonstrated that the primary somatosensory cortex encodes physical features of the stimuli for example the amplitude of the vibrotactile stimulation (Romo and de Lafuente 2013). Both amplitude and frequency of the whisker deflection modulate the activity of wS1 neurons (Stüttgen and Schwarz 2008). The experimental design in which the subject is required to detect different ranges or amplitudes of the stimulation is widely used to study perceptual mechanisms. These studies rely on correlating recorded neuronal activity to the relative change of the stimulation or the perceptual report of the subject. A similar approach was followed by Takahashi et al., who provided evidence that perception of the sensory stimuli depends on dendritic mechanisms in wS1. This mechanism was explained by the apical amplification hypothesis derived from conducting Ca^{2+} imaging of dendrites in Layer 2/3 barrel cortex in mice performing a psychophysical whisker detection task. They demonstrated that the activity of the apical dendrites of

pyramidal neurons in wS1 correlated with the mouse perceptual report for near-threshold whisker stimulation. Moreover, the reduction or the amplification of the dendritic activity using pharmacological or optogenetic approaches respectively decreased or increased the probability of the mouse detecting the stimulus (Takahashi et al. 2016).

Another step towards understanding the neuronal correlates of perception in wS1 came from the work of Sachidhanandam *et al.*. The authors carried out whole-cell membrane potential recordings of layer 2/3 pyramidal cells in mice performing a whisker detection task. They reported a biphasic response evoked by the whisker stimulus composed of an early, fast depolarization spanning the first 50 ms, which amplitude was independent of mice perceptual report (Hit vs Miss); and a late depolarization between 50 to 400 ms that was correlated with the behavioral report (Fig. 1.11A). Temporally precise optogenetic inhibition of wS1 indicated that both early and late sensory evoked responses causally contributed to perception and behavioral reports (Fig. 1.11B) (Sachidhanandam et al. 2013). This initial finding that the early sensory-evoked response in wS1 does not correlate with behavioral report whereas the late response does, has been corroborated by similar findings using VSD imaging or local field potential recordings in a similar task. It is also in good agreement with other studies in the visual cortex of human and non-human primates showing a late secondary evoked activity that correlates with perception (Supèr et al. 2001; Cul et al. 2007), and suggests that perception (the conscious processing of sensory information) involves long-range cortico-cortical reverberatory activity that follows the initial thalamic-driven sensory-evoked activity in primary sensory areas (Dehaene and Changeux 2011).

Following wS1 activation, the sensory activity rapidly spreads to wS2 and wM1 (Ferezou et al. 2007; Le Merre et al. 2018) which are the two main cortical downstream targets of wS1 neurons (Aronoff et al. 2010; Yamashita et al. 2013). wS1 has important direct, and reciprocal, axonal connections with wS2 and wM1. In a previous study from our laboratory, Yamashita *et al.*, have investigated projection-specific responses to whisker stimuli during the whisker-detection task using 2-photon targeted whole-cell patch-clamp recording of retrogradely labeled wS1→wS2 projecting (S2-p) and wS1→M1 (M1-p) projecting neurons. Both neuronal populations had similar membrane potential responses right after the whisker stimulus (early sensory-evoked response), whereas S2-p neurons were significantly more depolarised during the late response than M1-p neurons in Hit trials. Comparison between Hit and Miss trials revealed that late depolarization of S2-p neurons was correlated with the mouse perceptual decision but that was not the case for M1-p neurons (Fig. 1.11C). The lack of decision-related activity in M1-p neurons was further supported by the fact that optogenetic inactivation of wM1 during the detection task did not decrease the mice stimulus detection probability, whereas inactivation of wS2 significantly decreased stimulus detection

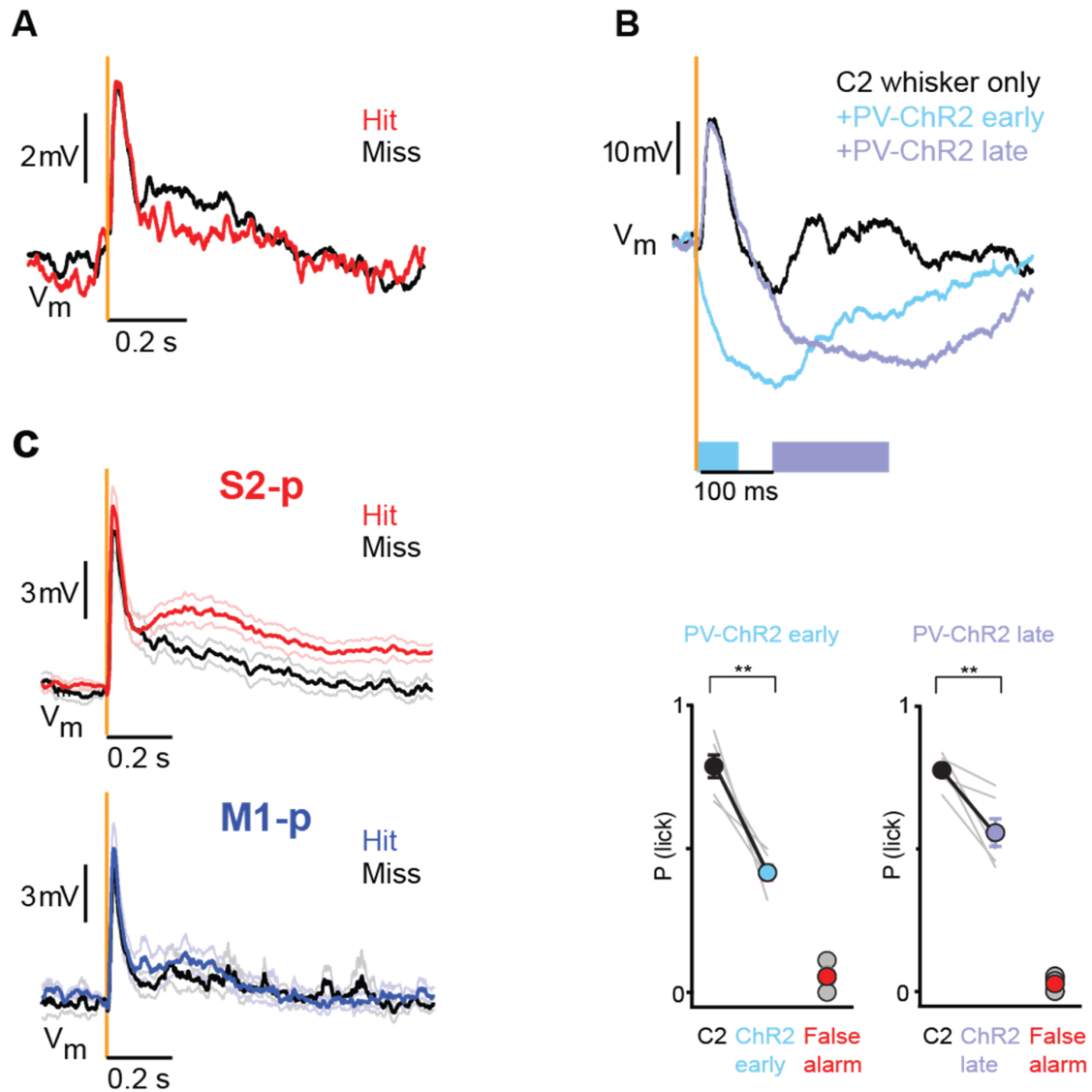


Figure 1.11. Membrane potential of wS1 causally correlates with mice behavioral responses.

(A) Grand-average membrane potential (V_m) recordings from 19 layer 2/3 barrel cortex neurons in response to the whisker stimulus recorded in mice performing a whisker-detection task. Comparison between Hit trials (black) and Miss trials (red) revealed late choice-related activity (adapted from (Sachidhanandam et al. 2013)).

(B) Temporally precise silencing of wS1 through optogenetic activation of parvalbumin-expressing (PV) GABAergic interneurons in PV-ChR2 mice. *Top*: averaged V_m in control (no light, black) trials and during early light stimulation (light blue) or late light stimulation (violet), abolishing the early and late evoked response, respectively. *Bottom*: optogenetic silencing during both early and late phases decreased stimulus detection probability (P Lick) (adapted from (Sachidhanandam et al. 2013)).

(C) Targeted whole-cell V_m recordings of two distinct projection-specific neuronal populations in layer 2/3 of wS1. wS1→wS2 projecting neurons (S2-p) had differential responses during Hit (red) and Miss (black) trials. wS1→wM1 projecting neurons (M1-p) had very similar responses during Hit (blue) and Miss (black) trials (adapted from (Yamashita and Petersen 2016)).

probability (Le Merre et al. 2018). This led to the conclusion that during the whisker detection task, relevant touch sensory information from wS1 is routed to wS2 (Yamashita et al. 2013).

The activity of projection-specific neurons in wS1 was also described in mice performing a whisker-based texture-discrimination or object localization task, using 2-photon functional Ca²⁺ imaging. During a texture discrimination task, more S2-p neurons showed more Hit vs. CR discrimination power than M1-p neurons, whereas, during an object localization task, M1-p neurons exhibited more discrimination power. In addition, S2-p neurons could discriminate better the texture during the discrimination task than M1-p neurons, and M1-p were better at discriminating object location than S2-p neurons in the object localization task (Chen et al. 2016). The authors suggested that S1 neurons adapt to tasks by adjusting information routing through their projection pathways. Importantly these results showed the functional heterogeneity and behavior-dependence of L2/3 neuronal population representations (Helmchen et al. 2018).

The importance of the interaction between wS1 and wS2 for perceptual decisions in whisker-based detection tasks has been further supported by the work of O'Connor's group. In mice performing a whisker-detection task, they observed a prominent decision-related activity (Hit vs Miss) in wS1 that could not be explained by a difference in sensory input from the thalamus. They found that S2-p neurons in wS1 showed stronger decision-related activity compared to neurons that do not project to wS2. Comparing the evoked activity in wS1 and wS2, they found that wS1 better encoded the stimulus whereas wS2 neurons encoded better the mouse decision. Finally, the activity of wS2 axons in wS1 also strongly encoded mice decisions (Yang et al. 2016; Kwon et al. 2016). Thus, the authors proposed that whisker stimulus-evoked activity propagates in a feedback loop between S1 and S2 during the formation of a perceptual choice.

In conclusion, the sensory perception of whisker detection tasks requires both wS1 and wS2 brain regions. The early activity in the wS1 brain region is not necessarily related to the behavioral response of the individual. This activity is likely driven by bottom-up sensory inputs that originate in the thalamus, meaning that it is a direct response to the sensory input rather than a cognitive or decision-making process. Therefore, this early activity in wS1 may not directly influence the animal's behavior or perception of the sensory information. Instead, it is suggested that the transformation of sensory input into perception occurs through a feedforward loop between wS1 and wS2, which is reinforced through feedback connections. This loop may strengthen synaptic connections between these regions, allowing for learning and improved sensory perception over time (Crochet et al. 2019). Overall, these findings contribute to our understanding of the complex neural processes involved in sensory perception and highlight the importance of the reciprocal connectivity between different brain regions.

1.3 Licking as a motor command

1.3.1 Cortical control of licking

Licking in mice is a highly stereotypical rhythmic motor pattern aimed to consume liquid, and consists of rhythmic bouts of tongue protractions and retraction at ~7 Hz (Travers et al. 1997; Komiyama et al. 2010a). Licking is a widely used motor output as a read-out of the percept of the mouse in sensory decision-making tasks. It is particularly used in head-restrained behavioral tasks. Recent progress in behavioral video filming and machine learning algorithms allows careful monitoring and tracking of facial movements of mice, including jaw opening and tongue protrusion, with near millisecond time-precision (Mathis et al. 2018), making possible the investigation of fine correlations between neuronal activity and movement kinematics.

Initiation of licking was shown to be driven by cortical activity whereas rhythmic licking is driven by brain stem nuclei, which act as central pattern generators (CPGs). These CPGs are presumably under control from descending inputs from the motor cortex (Travers et al. 1997). Cortical pyramidal tract (PT) neurons, with their cell bodies in deep layers, were shown to be important for voluntary movement initiation and execution. PT neurons project to the thalamus, and also have a direct projection to brainstem premotor nuclei and spinal cord that innervate motor neurons for tongue and jaw muscle control (Guo et al. 2014; Rojas-Piloni et al. 2017; Baker et al. 2018; Economo et al. 2018).

Over the last decade, two cortical areas have been identified with an important role in the control of licking: the anterior lateral motor cortex (ALM) was first identified based on the effect of cortical microstimulation and projection to licking-related brainstem regions (Komiyama et al. 2010); the primary tongue and jaw primary motor cortex (tjM1) was also identified as a cortical area receiving direct synaptic inputs from the tongue-jaw primary somatosensory cortex (tjS1), as well as based on the effect of cortical stimulation and inactivation (Mayrhofer et al. 2019). In the next chapters, we will review evidence suggesting that ALM might be primarily involved in motor planning, whereas tjM1 might be more directly responsible for motor execution.

1.3.2 Identification of the anterior lateral motor area (ALM)

Using optical and electrical microstimulation, the initial study by Komiyama et al. (Komiyama et al. 2010), identified ALM as an area in which stimulation reliably evoked movement of the tongue, jaw, and lips. ALM had cortical coordinates centered to 2.0 mm lateral and 2.4 mm anterior to bregma. In the same study, the authors used

trans-synaptic retrograde labeling with the pseudorabies virus to label the cortical areas that could be involved in the control of licking. They injected the pseudorabies virus directly into the tongue and a few days after they identified clusters of neurons in layer 5 bilaterally in the motor cortex. The reported coordinates of the hot spot projection were 1.2 mm lateral and 0.3 mm anterior to bregma; therefore, they referred to this cortical region as the posterior-medial motor cortex (PMM). Interestingly, no labeled cells were found in the ALM, and optostimulation of PMM caused movements of whiskers and forelimbs, but not the tongue or the jaw. However, pharmacological inactivation of both ALM and PMM regions strongly suppressed licking during an odor-detection task.

A subsequent study from the same laboratory used a two-alternative forced-choice task with delay to investigate the respective contribution of different cortical areas in different phases of the sensorimotor transformation (Guo et al., 2014). The task consisted in a sample period during which mice had to actively sample an object and discriminate its location with a single whisker. Depending on the object location (caudal or rostral), the mouse will have to lick a water spout on the right or on the left, respectively, after a delay, to obtain a reward. Following the sample period, the object was removed from the whisker path and the mouse had to withhold licking during a delay period and remember which spout to lick. At the end of the delay period, an auditory tone signaled that the mouse could respond by licking. The authors performed systematic focal optogenetic inactivation mapping of the dorsal cortex during different tasks epochs (Fig. 1.12A). By doing this, they found that wS1 and wS2 activity was necessary for the correct detection of the object position during the sampling period, whereas inactivation of a large frontal region impaired the mouse's performance during the delay period (Fig. 1.12). This frontal region included ALM, but not PMM.

Following this study, many other studies (Chen et al. 2017; Guo et al. 2017; Economo et al. 2018; Gao et al. 2018) from the same group have focused on the neuronal activity in ALM in the same task. They showed that neuronal activity in ALM ramped up during the delay period and was very selective for the direction of licking (lick right or left). They identified two populations of PT cells in layer 5 of ALM, one was projecting to the thalamus, and the other to the medulla and brainstem. By recording the neuronal activity of these two types of PT neurons in ALM during the object location discrimination task with a delay, they found that thalamus-projecting neurons were important for maintaining the persistent preparatory movement activity. They increased the firing rate starting from the moment of stimulus presentation and remained active during the delay, encoding the upcoming movement direction. Whereas the second type of PT neurons projecting to the medulla was presumably involved in movement execution. These neurons showed varied activity with some being locked to movement initiation, others persistently firing until the termination of licking bouts, and others being locked to movement termination (Economo et al. 2018).

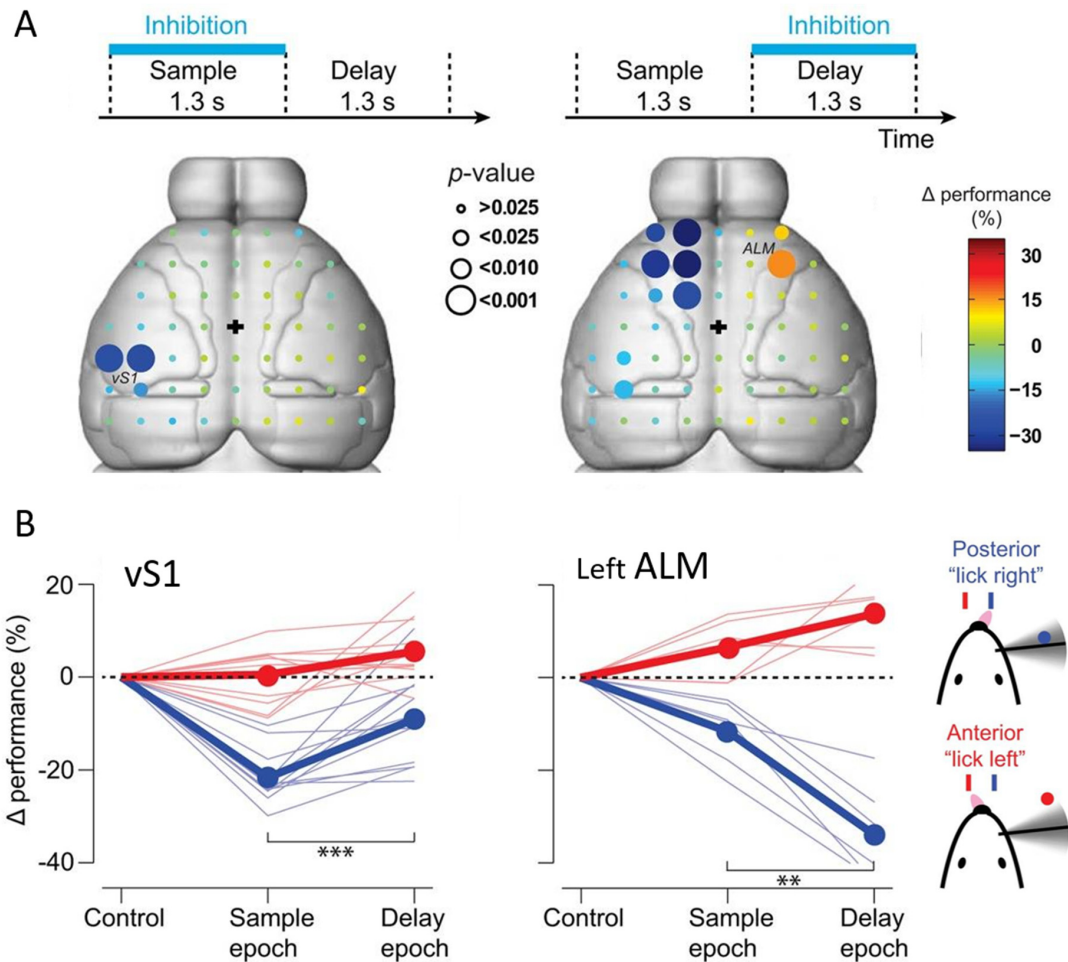


Figure 1.12. Optogenetic inhibition revealed the involvement of several cortical regions during an Object Location Discrimination Task.

(A) Effect of photoinhibition applied to a grid of 55 cortical regions during the *Sample* and *Delay* epochs. The color of the circle indicates the behavioral effect size, and its size corresponds to the p -value.

(B) Effects of photoinhibition of vS1 (*left*) and left ALM (*right*) for "lick right" (blue) and "lick left" (red) trials during the *Sample* and *Delay* epochs.

(adapted from (Guo et al. 2014))

1.3.3 Identification and role of Tongue-Jaw Primary Motor Cortex (tjM1)

Following the idea that the primary motor cortex requires direct sensory information from the corresponding body part to execute specific movements, one can identify primary motor regions based on the projection they receive from the primary somatosensory cortex. In agreement, wM1 has been identified as the region of the motor cortex that receives direct synaptic inputs from wS1 (Sreenivasan, Esmaili, et

al. 2016; Yamashita and Petersen 2016; Yamashita et al. 2018; Esmaeili et al. 2020; Liu et al. 2022). Similarly, our laboratory has defined tjM1 anatomically as the frontal region receiving input from the tongue and jaw representations in the primary somatosensory cortex (tjS1). Viral tracing identified direct long-range axonal projections from tjS1 to tjM1 that are likely to transmit touch and proprioceptive information to tjM1 (Fig. 1.13A) (Luo et al. 2019; Mayrhofer et al. 2019). Other studies have shown that the orofacial primary motor area (including tjM1) receives additional cortical input from other brain regions including orofacial S1/S2 and the anterolateral part of the secondary motor area (Luo et al. 2019).

Functional wide-field imaging demonstrated that passive mechanical stimulation of the tongue and the jaw first evoked a focal increase of the calcium signal in the tjS1 region that later spread and appeared as a localized spot in the tjM1 region (Fig. 1.13B) (Mayrhofer et al. 2019). This sensory information appears to be of immediate importance for sensory-guided movements of the tongue (Xu et al. 2022). Cortical motor maps of orofacial movements constructed using focal optogenetic stimulation in awake mice showed that stimulation of the tjM1 region evoked an opening of the jaw (Figure 1.13 C). Anatomy, functional imaging, and motor mapping converged to a cortical region centered around ~2.5 mm lateral and ~1.7 mm anterior to bregma, thus more lateral and posterior than ALM (Mayrhofer et al. 2019).

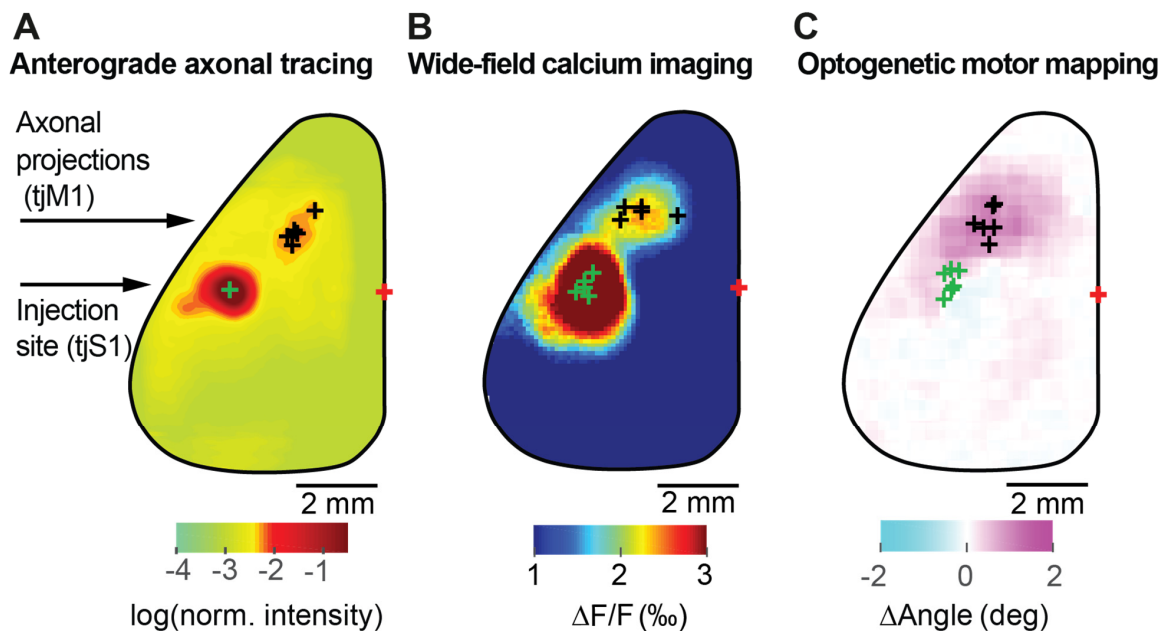


Figure 1.13. Different strategies identified the Tongue-Jaw Primary Motor Cortex (tjM1).

(A) Anterograde axonal tracing: mean fluorescence intensity map from viral injections in tjS1 region (green cross) showing axonal projections in a localized region of the motor cortex (tjM1, black crosses are the centers of the anterior spot for each mouse).

(B) Wide-field functional calcium imaging: mean change in fluorescence ($\Delta F/F_0$) evoked 100-200 ms after the stimulation of the tongue in Thy1-GCaMP6f mice. Green crosses show the early activation region (0-100 ms) for individual mice corresponding to tjS1. Black crosses show the frontal secondary spot (100-200 ms) for individual mice corresponding to tjM1.

(C) Optogenetic motor mapping: the dorsal cortex was stimulated with a blue laser in a grid-like manner. Evoked orofacial movements were monitored using high-speed video filming. Black crosses show the region evoking tongue-jaw movements for individual mice. Green crosses show the center of the intrinsic optical signal evoked by tongue-jaw sensory stimulation for individual mice.

(Adapted from (Mayrhofer et al. 2019))

1.3.4 Motor planning and execution

To disentangle the respective roles of tjM1 and ALM in the control of licking, Mayrhofer *et al.* performed focal optogenetic inactivations of the two areas in mice performing two tasks. The first one is a multisensory detection task (Fig. 1.14A). Mice were trained to lick a water spout in response to whisker or auditory stimuli that were randomly interleaved. In this task, the mice always had to perform the same motor action in response to the two sensory stimuli, without delay. The same mice were afterward trained in a multi-motor task, in which they were instructed to lick in response to a whisker stimulus, either to a left or to a right water spout in alternating blocks of trials (Fig. 1.14B). Interestingly, the inactivation of tjM1 and ALM had different effects depending on the task performed: when mice were performing the simple sensory-detection task, inactivation of tjM1 during the response window strongly impaired licking whereas inactivation of ALM had only a minor effect. However, when mice had to alternate between licking left and right in response to the whisker stimulus, inactivation of both tjM1 and ALM during the response window similarly impaired mice performance, reducing correct licking to the contralateral side and increasing incorrect licking to the ipsilateral side (Mayrhofer et al. 2019) (Fig. 1.14).

Studying a behavioral task where mice had to execute more complex licking patterns permitted to differentiate further the activity of neurons anatomically located in ALM and tjM1. Xu *et al.* investigated the cortical control of flexible and context-dependent motor sequences by training mice to execute a sequence of directional licking following an arc in order to collect a reward. During the task execution, they recorded and manipulated the neuronal activity of the motor regions ALM (also called by the authors a ‘tongue premotor cortex’) and tjM1, and the sensory area tjS1. Electrophysiological recordings revealed that the tjS1 and tjM1 encoded and controlled tongue kinematics at the level of individual lick bouts, encoding well the amplitude and angle of the tongue protrusion. Whereas, the ALM encoded the upcoming lick angle but also the sequence identity (from left-to-right or right-to-left) and the relative sequence time (Xu et al. 2022). Neurons in the ALM region also encoded reward or reward expectations by increasing their firing rate closer to the end of the sequence, when the mouse was expecting to receive a drop of water (Xu et al. 2022).

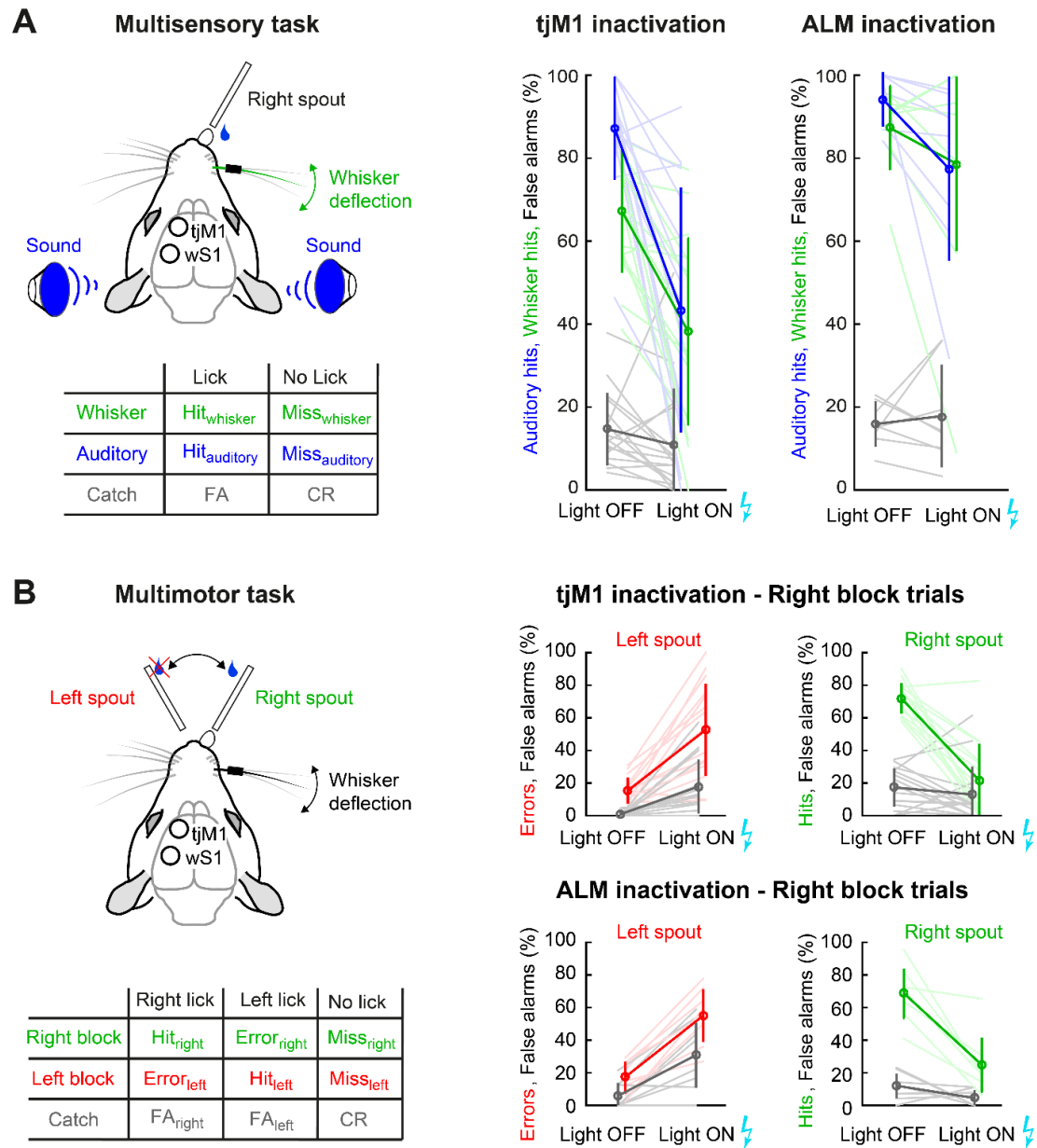


Figure 1.14. Different Roles of ALM and tjM1 in Sensorimotor Behaviors.

(A) On the left is a schematic of a multisensory detection task. Mice were rewarded by licking a spout after a whisker deflection or an auditory tone. On the right, is the behavioral effect of tjM1 and ALM inactivation.

(B) On the left is a schematic of a multi-motor detection task. Mice were trained to lick a spout on the right or left in response to whisker deflection. Reward location was changed every 50 trials between the right and left spouts. On the right, is the behavioral effect of tjM1 and ALM inactivation during the trials with either left rewarded spout or right.

(Adapted from (Mayrhofer et al. 2019))

Another evidence for ALM being more important for motor planning and tjM1 more involved in direct licking control comes from the delayed-response whisker detection task. In this task, mice needed to withhold licking during a delay period following the whisker stimulus and execute it only after an auditory go-cue. Interestingly in Hit trials where mice successfully repress from licking during the delay period, tjM1 showed a transient inhibition immediately after the whisker stimulus that was not present in trials with premature licking after whisker stimulation (Early licks). In contrast, ALM neurons increased their firing rate following the whisker stimulation in both Hit and Early Lick trials. ALM neurons, but not tjM1 neurons, showed prominent ramping activity during the delay devoid of orofacial movements (quiet trials) (Chapter 2 (Esmaeili et al. 2021)).

Based on anatomical tracing studies (Stanek et al. 2014; Luo et al. 2019) and previously described functional studies, the voluntary control of licking could be achieved through the following pathway: tjM1 would control licking movement via long-range axons to premotor nuclei of the brainstem which in turn innervate the motor nuclei controlling the tongue and jaw muscles: respectively, the hypoglossal motor nucleus (Hg) and the trigeminal motor nucleus (Mo5) (Fig. 1.15). The tjM1 area would integrate information from tjS1 providing sensory feedback and allowing fine adjustment of the movement kinematic (licking angle and amplitude), as well as inputs from the secondary tongue and jaw motor area (tjM2) /ALM region important for the planning of the movements (Esmaeili et al. 2020).

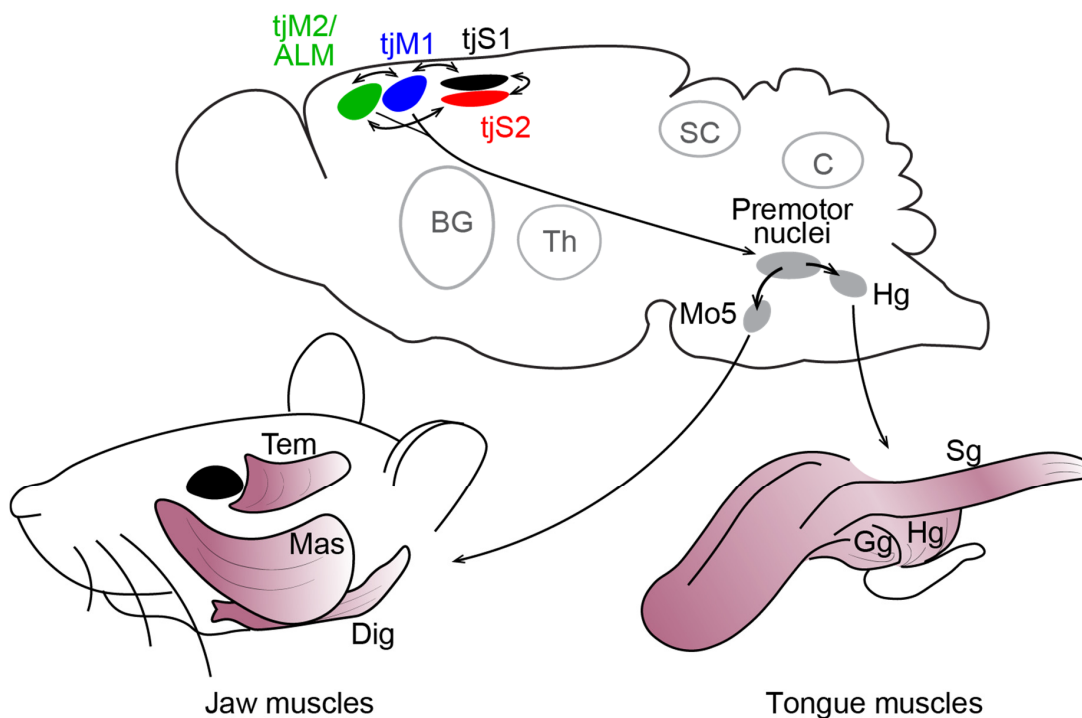


Figure 1.15. Brain circuits controlling goal-directed licking.

tjM1 integrate inputs arriving from tjM2/ALM and tjS1 and possibly other cortical areas. → Then tjM1 sends a motor command to the premotor nuclei of the brainstem. → These premotor nuclei in turn project to motor neurons in hypoglossal (Hg) and trigeminal motor nucleus (Mo5) which control the muscles of the tongue and the jaw. Muscles for the jaw closing: Mas and temporalis (Tem). Muscles for the jaw opening: digastric (Dig). Muscles for tongue protrusion Gg and muscles for tongue retraction, hyoglossus (Hg), and styloglossus (Sg) (adapted from (Esmaeili et al. 2020)).

1.4 Perceptual decision-making

So far, we have identified the sensory areas wS1 and wS2 as likely starting points of a cortical circuit for the transformation of a whisker sensory stimulus into the action of licking in whisker-sensory detection or discrimination tasks. These two areas appear to play an important role in the detection and perception of the whisker sensory stimulus. At the other end of the sensorimotor transformation, we have identified two motor areas, ALM and tjM1 that are likely responsible for the planning and execution of the sensory-driven action of licking. An important question that remains now, is where is the decision of licking in response to the whisker stimulus being made. In the following chapters, we will review pieces of evidence showing that the medial prefrontal cortex might be an important area for perceptual decision-making.

Perceptual decisions involve converting incoming sensory information into discrete, categorical variables. The process of decision-making is not fully understood, but there are many theories about the computation and neuronal mechanisms involved. Research has revealed that decision-making is a complex process that involves the integration of information from multiple brain regions, including the sensory cortices, prefrontal cortex, and parietal cortex, and is influenced by both cognitive and emotional factors. Additionally, recent studies suggest that decision-making is a dynamic process that changes over time based on prior knowledge, context, and feedback from the environment.

While studying sensorimotor transformation and decision making one has to carefully consider task design and choice of the sensory stimuli. Some sensory stimuli in order to be perceived have to be presented over time, for example, frequency discrimination (Recanzone et al. 1991), auditory clicks counting (Brunton et al. 2013; Raposo et al. 2014; Hanks et al. 2015), or random dot motion direction discrimination (Shadlen and Newsome 2001). In such tasks, animals are presented with noisy sensory evidence that is accumulated over time to reach a categorical decision. In the random dot motion discrimination task the monkeys are trained to decide whether the direction of motion of the dot-stimulus is towards one or another choice target. At the end of the trial, the monkeys have to report their decision by making an eye movement to the appropriate target. Shadlen and Newsome through extracellular recordings revealed neural correlates of evidence accumulation in several cortical areas: lateral

intraparietal area (LIP) of the posterior parietal cortex (PPC) and the frontal eye field (FEF) division of the prefrontal cortex (PFC). The authors identified single FEF and LIP neurons which average firing rate showed ramp-like increase in activity during stimulus presentation. Importantly, this activity developed faster on 'easy' (i.e., with high evidence for one alternative) trials, but rose slower on 'hard' trials (with an ambiguous sensory evidence) in which subjects responses were slower (Shadlen and Newsome 2001).

This framework of sensory evidence integration was adapted from primates to rodents with either passively received evidence or actively generated by the sensorimotor system (Maravall 2019; Zuo and Diamond 2019a, 2019b). In the task when rats whisk on a surface to identify the texture, they typically carry out several touches to select a rewarded port. The rat takes a decision when the accumulated amount of whisker evidence for the rewarded texture reaches a threshold (Zuo and Diamond 2019b). Authors demonstrated that S1 encoded information of individual touches but the decision was presumably computed downstream of S1 through the integration of sensory evidence transmitted by S1 (Zuo and Diamond 2019a). Similarly, when the relevant sensory information is distributed across time during stimulus presentation and no instantaneous event provides the adequate signal, then decision-making requires a longer-timescale integrative process that does not occur in the somatosensory cortex, where time constants are short (Fassihi et al. 2017).

However, by using prolonged stimuli that evolve over time the subject reaches its decision at the same time as the stimulus is presented, hence, sensory information overlaps with decision information. In the case of tasks with active stimulus discovery (whisking to detect the texture), there is one more extra dimension of movements and there should be a simultaneous representation of sensory, decision and motor signals in the brain. In the case of my project, I was interested in separating these bits of information and wanted to study the sequence of events. And one of the possible ways to do it would be to present the subject with a very brief sensory stimulus (a few milliseconds) (Sachidhanandam et al. 2013). If the sensory stimuli are very brief in time one can also assume that: (1) pure sensory information should be transiently encoded by neurons; (2) the decision will be more time-locked to the stimulus onset rather than in case of prolonged stimulus presentation. Another advantage of using brief sensory stimuli is the reduction of complexity, there is no sensory evidence integration process and the subject has to make its decision based on a short bit of information available. In addition, it has been demonstrated that when a single, temporally discrete event must be detected, the somatosensory cortex might participate in evolving cascade of responses in multiple cortical regions (Ferezou et al. 2007; Le Merre et al. 2018). Therefore in this study, we have decided to use brief whisker stimuli and to try to understand the mechanism underlying the mice's decision to execute a lick in response to the brief whisker stimulus in order to receive a reward.

1.4.1 The importance of the prefrontal cortex in perceptual decision-making

Multiple studies in humans, monkeys, and rodents have revealed the importance of the prefrontal cortex (PFC) in perceptual decision-making, describing its involvement in sensory processing, sensory integration, value estimation, tracking of the trial outcome, rule learning, or other processes which help guiding the appropriate action (Miller 2000; Amodio and Frith 2006).

Studies from non-human primates and rodents brought a mechanistic understanding of the neuronal functions, neuronal classes, and computation in PFC. Neurons in the prefrontal cortex (PFC) are important in the organization of goal-directed behavior and encode different types of information from all stages of the perception–action cycle. In non-human primates, PFC neurons have been found to be activated by stimuli from different sensory modalities. For example, PFC cells respond selectively to both tones and colors according to the task rule (Fuster et al. 2000), suggesting that PFC neurons represent behaviorally meaningful cross-modal associations. The activity of PFC neurons has also been found to covariate with the choice of the subject as well as the sensory information. Mante et al. (2013) and Siegel et al. (2015), demonstrated that both sensory and choice information is present in PFC during a sensorimotor decision. By modeling population dynamics of PFC neurons, they proposed that flexible sensorimotor choices develop in the prefrontal cortex from the integration of sensory and task information (Mante et al. 2013; Siegel et al. 2015).

To be able to achieve all these functions PFC must have access to internal and external information regarding the present state, have information about future goals and motives, and have access to representations about previous experiences. These functions can be accomplished and explained through dense interconnectivity to other cortical and subcortical areas. Hubel and Wiesel (Hubel and Wiesel 1962) and Rockland and Pandya (Rockland and Pandya 1979) theorized the importance of connectivity in determining brain functions. Recent studies have used these theories as a framework to identify the functional hierarchy of cortical regions based on their connectivity. In humans, the advancement of neuroimaging integrated with network science has paved the way for creating intricate wiring diagrams, known as connectomes, of the human brain. These computational analyses of connectivity, based on the data from magnetic resonance imaging (fMRI), have led to the identification of the human prefrontal cortex as a region with extremely high connectivity (Hub regions) that likely integrates diverse information (Haber et al. 2022). Alternatively, anatomical tracing studies have formed the foundation for mapping the direct, one-synapse connectivity from the cells of origin, through axonal pathways, to synaptic endpoints. The Allen Institute for Brain Science has recently traced the output of almost all regions of the mouse isocortex and thalamus and found the prefrontal module to have the highest hierarchical index, meaning it had the most feedback

projections. The prefrontal module was shown to be at the top of the mouse cortical hierarchy (Fig. 1.16) (Harris et al. 2019).

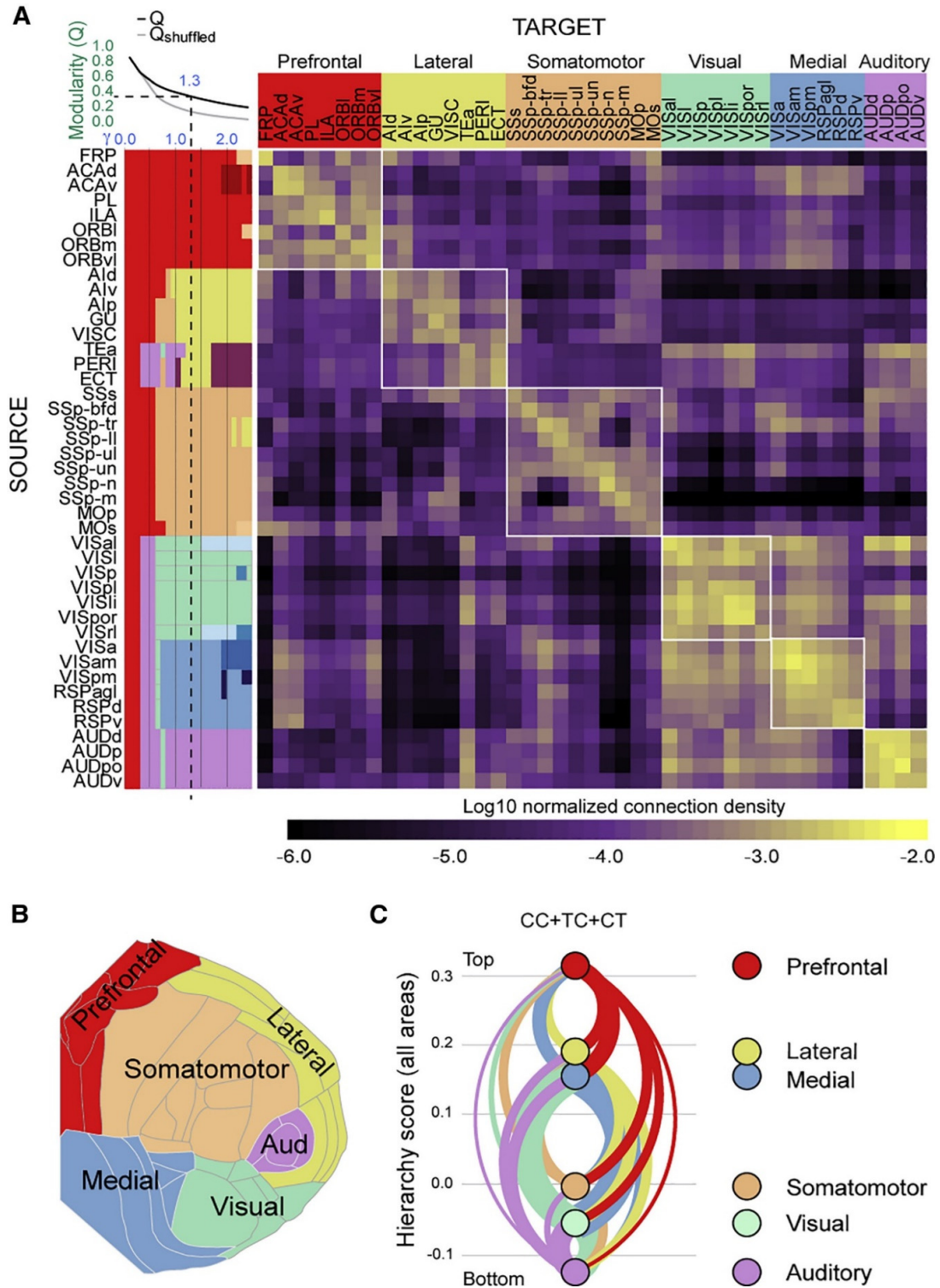


Figure 1.16. The mouse prefrontal module is at the top of the cortical hierarchy.

(A) Cortical projections matrix that displays normalized connection densities between 43 cortical areas. Top left corner: the modularity metrics for the isocortical areas (Q) and a shuffled network (Qshuffled) are plotted for each γ level, where γ is the spatial resolution parameter. Colors to the left of each row indicate community structure (module affiliation), which were determined independently for each value of γ . Columns are colored by the six modules identified at $\gamma = 1.3$ (dashed line).

(B) Cortical regions on the flat cortical map were colored by module affiliation from (A).

(C) Network diagram of interconnections of all cortical areas shown in (A). The output from the six cortical modules is indicated by curved lines (color-coded according to the module's color). The thick lines represent the sum of connection densities from (A), outputs (left), and inputs (right). Nodes are positioned along a single axis based on respective hierarchical scores. CC, corticocortical projection neurons; TC, thalamocortical projection neurons; CT, corticothalamic projection neurons.

(adapted from (Harris et al. 2019))

1.4.2 Anatomical and functional organization of the mouse PFC

The mouse PFC is traditionally parcellated into specific subregions based on their cytoarchitectural criteria. But a more functionally-relevant alternative to cytoarchitectural subdivisions of the brain would probably be based on afferent and efferent connectivity patterns. Historically PFC was described as a region targeted by the medial dorsal thalamus (MD), but nowadays this identification is questionable. Whole-brain connectivity mapping has consistently identified shared and tight connectivity of the PFC subregions and defined three prefrontal subdivisions, which differed by the density of their afferent and efferent connections. The connectivity of these subdivisions largely overlapped but differed quantitatively:

- the dorsomedial PFC (dmPFC). Includes ARA annotations (Allen atlas) of the secondary motor cortex (Mos, which includes wM2 and ALM, mentioned before) and Anterior cingulate cortex (ACA)
- ventromedial PFC (vmPFC). Includes prelimbic (PL) and infralimbic (IL) areas
- ventrolateral PFC (vlPFC). Includes the medial, ventro-lateral, and lateral divisions of the orbitofrontal cortex (ORBm, ORBvl, and ORBI)

The dmPFC subdivision is of particular interest because it is reciprocally connected with sensory and motor cortical regions. The dmPFC has distinguishably dense connections with the primary and supplemental somatosensory areas (SSp and SSs) (Sreenivasan, Esmaeili, et al. 2016b; Barthas and Kwan 2017) and the primary motor area (Mop) (Sreenivasan, Kyriakatos, et al. 2016; Barthas and Kwan 2017), visual areas (VIS), the retrosplenial area (RSP), and the primary auditory cortex (AUD) (Nelson et al. 2013; Zhang et al. 2016). Anatomical connectivity is well supported by functional studies showing auditory and whisker somatosensory responses in Mos (Chen et al. 2017). The dmPFC also projects to the striatum, in particular its rostro-dorsal part, where its axons colocalize with axons coming from visual, auditory, and

somatosensory cortical areas (Hintiryan et al. 2016; Ährlund-Richter et al. 2019; Le Merre et al. 2021).

The vmPFC is densely targeted by the basolateral amygdalar nucleus (BLA) and the CA1 part of the hippocampus (which only partially projects to dmPFC (ACA)). vmPFC is also reciprocally connected with the midbrain ventral tegmental area (VTA) (Beier et al. 2015). It also projects to ventro-medial part of the striatum, in particular to the nucleus accumbens, as well as to the dorsal raphe nucleus (DRN) and lateral habenula (LHb) (Ährlund-Richter et al. 2019; Le Merre et al. 2021) (Fig. 1.17).

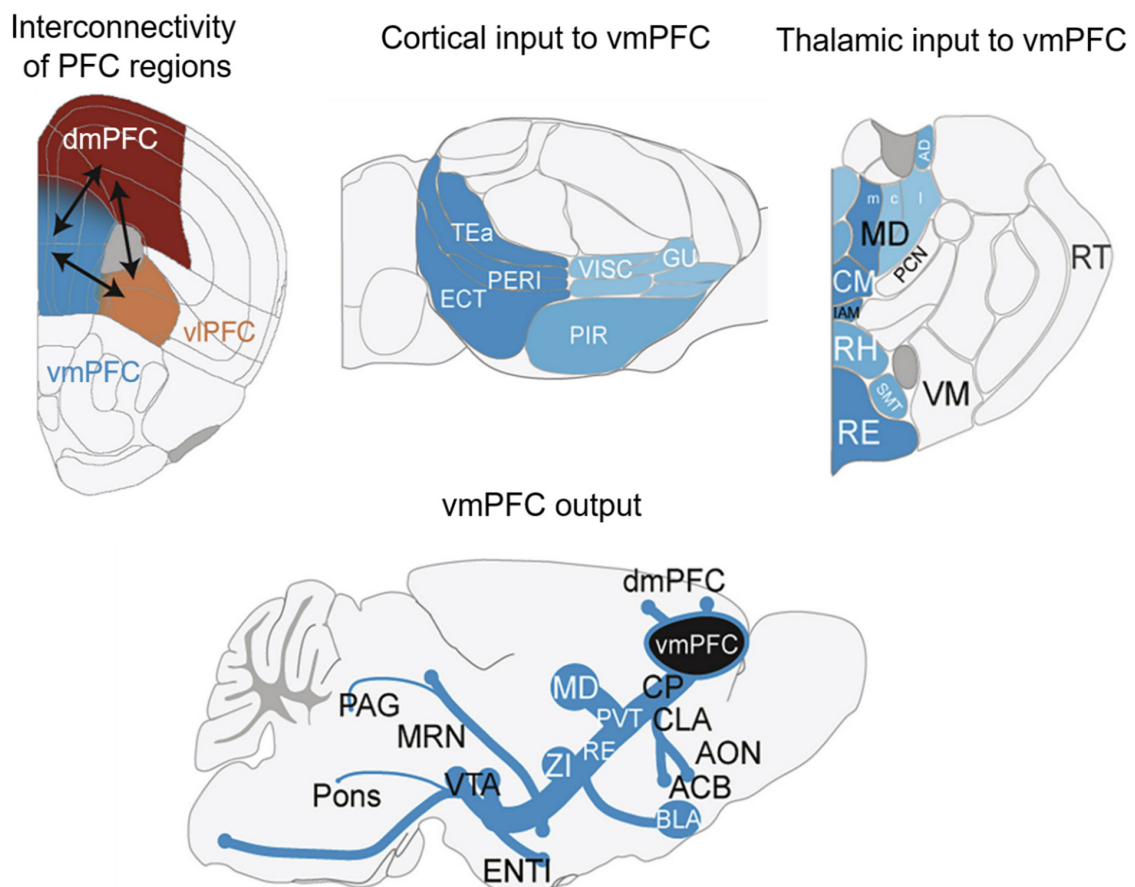


Figure 1.17. Connectivity of mouse vmPFC.

Interconnectivity of PFC regions. The dorsomedial prefrontal cortex (dmPFC), ventromedial prefrontal cortex (vmPFC), and ventrolateral prefrontal cortex (vlPFC) are three regions of the mouse prefrontal cortex (PFC) that are largely reciprocally connected in the mouse brain.

Cortical input to vmPFC: Temporal association cortex (area TeA); Perirhinal cortex (PERI); Ectorhinal cortex (ECT), Visceral cortex (VISC); Piriform cortex (PIR), Gustatory cortex (GU)

Thalamic input to vmPFC: Mediodorsal thalamic nucleus (MD), which includes the following subregions: Anterodorsal thalamic nucleus (AD), Central medial thalamic nucleus (CM), Interanteromedial thalamic nucleus (IAM); Medial dorsal nucleus of the thalamus (m); Central lateral

nucleus of the thalamus (c); Intergeniculate leaflet of the thalamus (I); Rhomboid nucleus of the thalamus (RH); Submedial thalamic nucleus (SMT); Reticular nucleus of the thalamus (RE). The mediodorsal thalamic nucleus is particularly important for its connectivity with the prefrontal cortex, and its subregions AD, CM, and IAM have been shown to provide important inputs to the vmPFC. Other thalamic regions on this list also play important roles in regulating cognitive and emotional processes, and their connectivity with the vmPFC is an area of active research.

The cortical output of vmPFC: the dorsomedial prefrontal cortex (dmPFC); the ventrolateral prefrontal cortex (vlPFC); the caudoputamen (CP); the claustrum (CLA); the anterior olfactory nucleus (AON); the nucleus accumbens (ACB); the paraventricular thalamic nucleus (PVT); the mediodorsal thalamic nucleus (MD); the reticular nucleus of the thalamus (RE); the zona incerta (ZI); the ventral tegmental area (VTA); the median raphe nucleus (MRN); the periaqueductal gray (PAG); the pons (Pons); the entorhinal cortex (ENTI).

(adapted from (Le Merre, Ährlund-Richter, and Carlén 2021))

The vlPFC subdivision is peculiar in its combination of sensory and limbic input but, at the same time, lacks motor input. Cortical inputs that send sensory information to vlPFC come from the primary somatosensory areas (SSp), visual areas (VIS), the primary auditory cortex (AUD), anterior olfactory nucleus (AON), piriform cortex (PIR), gustatory cortex (GU), and visceral cortex (VISC) (Aronoff et al. 2010a; Mori et al. 2013; Winkowski et al. 2018; Le Merre et al. 2021a). Another input pathway comes from the thalamus, specifically the mediodorsal thalamus (MDT) (Kuramoto et al. 2017). Other inputs to the vlPFC come from the amygdala (Mátyás et al. 2014), and the rostroventral part of the caudate putamen (CP) (Hunnicutt et al. 2016). However, much fewer studies investigated the functions and connectivities of the mouse vlPFC subdivision than the two other subdivisions.

If we think of three subdivisions of PFC together they receive projections from almost all brain regions, such as the isocortex (Fig. 1.16A), hippocampal formation, thalamus, hypothalamus, cerebral nuclei, cortical subplate, and olfactory areas. In total PFC is targeted by the highest number of cortical and subcortical regions (Harris et al. 2019; Ährlund-Richter et al. 2019). The PFC has a wider projection to different brain regions than other cortical regions, and has the greatest reciprocal connectivity, making it well-positioned to coordinate various neuronal processes.

1.4.3 Functions and neuronal correlates of mouse prefrontal cortex (PFC) in goal-directed sensorimotor transformation

The functions of the PFC have been extensively studied and are thought to involve the representation and production of purposeful sequences of actions. The mouse is currently the dominant mammalian animal model used to study brain functions, which are determined through experiments that link neuronal activity to behavior, often with the help of perturbation experiments. A research synthesis of 100 recent publications (from 2011 to 2020) was conducted to provide an overview of the

latest work on the functions of the mouse PFC, with a focus on *in vivo* perturbation experiments. The authors also extensively discuss the complexity of the current mouse PFC nomenclature, and discrepancies in the anatomical delineations of different subregions that introduce some confusion in the attribution of a functional role to the different subregions of PFC (Le Merre et al. 2021). Here I will review the papers that are most relevant in the context of goal-directed sensorimotor transformation, focusing on the vmPFC, which we will simply term mPFC.

Although mPFC is believed to guide behavior by integrating different rules in complex tasks, inactivation experiments have shown its necessity for the execution of even simple sensory detection (Le Merre et al. 2018) or discrimination tasks in mice (Pinto and Dan 2015; Otis et al. 2017; Lak et al. 2020). Similar to dlPFC monkey studies, mPFC neurons in rodents display a large variety of task-related activity: they respond to the relevant sensory cues, the subject's motor output, and action outcomes (Pinto and Dan 2015; Lak et al. 2020; Kim et al. 2021; Lui et al. 2021; Francis et al. 2022). The major advantage of using mice as an animal model is their genetic tractability which allows monitoring the activity of specific cell types and projection neurons. Neurons of different cortical layers receive different inputs and project to distinct target areas, and their local circuit interconnections play a crucial role in information processing. This approach is highly important in the case of mPFC, where neurons often show multiplexed encoding properties. Pinto et al (Pinto and Dan 2015) studied the neuronal activity of genetically distinct cell types in mPFC during a simple Go/NoGo task. In this study, the start of the trial was signaled by a light flash and followed by either a target (17 kHz) or a non-target (9 kHz) auditory cue. After the auditory stimulus presentation, the animal's lick response was rewarded if the target signal was presented and was punished by an air puff if the non-target signal was presented. In this experiment, pyramidal neurons formed a heterogeneous population, and their functional responses varied across layers. These neurons exhibited both excitatory and inhibitory responses following a relevant sensory cue. However, inhibitory interneurons signaled different task-related events. The activity of most somatostatin (SST) positive neurons was correlated to licking behavior, whereas the activity of vasoactive intestinal peptide (VIP) positive neurons was strongly modulated by the action outcome. Parvalbumin (PV) positive neurons were the least selective, and they were the only class with robust responses to the sensory stimuli (Pinto and Dan 2015).

The heterogeneity of mPFC pyramidal cell responses might in part be ascribed to their dorsoventral location (i.e., prelimbic vs. infralimbic areas) (Euston et al. 2012). One hypothesis proposes an antagonist role for the prelimbic (PL) and infralimbic (IL) regions of the mPFC: the PL would be involved in behavioral execution – “go” signal – whereas the IL would be involved in behavioral suppression – “stop” signal. That would be particularly the case during extinction in fear conditioning studies (Peters et al.

2009). However, other recent works have failed to find any clear difference in the neuronal activity of PL vs IL in encoding “go” vs. “stop” signals (Moorman and Aston-Jones 2015a). Another potential source of heterogeneity in the response of mPFC neurons could be accounted by their projection targets (Euston et al. 2012). A recent study has addressed this question by monitoring the activity of mPFC neurons identified by their projections to two major mPFC targets: the nucleus accumbens (NA) and the paraventricular nucleus of the thalamus (PVT). The two neuronal populations were labeled by injecting retrograde cholera toxins conjugated with two different fluorophores into the ventral striatum and paraventricular nucleus of the thalamus. After labeling, they observed two distinct and nonoverlapping populations of neurons in mPFC that reside in different layers. The authors further measured the activity of these two populations by injecting retrograde virus to NA and PVT to express the calcium indicator GCaMP6s in a projection-specific manner. Using two-photon microscopy, they found that responses in corticostriatal neurons were tuned to reward-predictive cues. During the learning of the task, a larger proportion of corticostriatal neurons developed an excitatory response (increased activity) to the reward-predictive cue, whereas corticothalamic neurons developed mostly inhibitory responses to the reward prediction cue (Otis et al. 2017).

A very recent study (Lui et al. 2021a) challenged and tested the assumption that dividing neuron populations based on transcriptomic criteria will help decipher the correspondence between transcriptomic versus projection types, at least in PFC. They suggested that projection patterns can only be predicted to a limited extent by transcriptomic data in adult neurons. Interestingly they showed that neither molecularly homogeneous groups of neurons nor projection-specific groups of neurons do encode exclusively given task signals. They observed a diversity of information in the population and individual cells, including cells that fulfill criteria of mixed selectivity, even within a specific projection type, within a cortical layer, and within a transcriptomic type. Different cell types came into action in different behavioral tasks and at the same time, the same cell types or projection neurons represented different experimental and behavioral variables in various behaviors. An interesting observation of particular relevance for our topic of interest was that periaqueductal gray (PAG) projecting mPFC neurons encoded the sensory cue (specific odor), and even more of these neurons encoded sensory stimulus-driven choice of the mouse during a two-alternative choice task. But the same neurons did not encode choice when it was predetermined by prior knowledge of the mouse regarding the reward side. This second uncued task, where the mouse had to collect the reward on the left or on the right in blocks of 20 trials, revealed a new population of mPFC neurons encoding reward context even 1s before the reward availability (Lui et al. 2021). Anticipatory coding of upcoming rewards by individual mPFC neurons was also observed by recording membrane potential in mice performing behaviors in which the sensory stimulus predicted rewards with different

delays and with different probabilities. It should be noted however that the anticipatory activity of mPFC neurons was correlated to anticipatory licking (Kim et al. 2021). Thus motor-related activity could contribute importantly to the activity of mPFC neurons.

Another important function of the mPFC is to form associations between external stimuli and their internal representations. Goal-directed behaviors require making predictions and building up knowledge about external events and actions that are likely to lead to the achievement of the objective (for example, to stop your car when the traffic light turn red to avoid an accident, or to lick the water spout following a whisker deflection to obtain a reward). Prefrontal neuron activity does show this type of learned associative relationships and conjunctive tuning between sensory stimuli, voluntary actions, and rewards (Miller 2000). Acquired by experience, the response of mPFC neurons develops during learning only for behaviorally relevant sensory stimuli, in contrast, mPFC neurons do not respond to non-rewarded stimuli (Pinto and Dan 2015; Otis et al. 2017; Le Merre et al. 2018). The presence of sensory-evoked response in mPFC after learning could suggest that mPFC encodes reward predictive cues (Otis et al. 2017). The learning/reward-dependent aspect of mPFC functions is possibly mediated by strong reward-related information coming from dopaminergic signals arising from the ventral-tegmental area (VTA) (Moorman and Aston-Jones 2015; Popescu et al. 2016).

In a recent study, Lak *et al.* (Lak et al. 2020) proposed that the learning of the association between the sensory stimulus and the reward depends on the predicted value of the trial outcome, signaled by mPFC neurons. They designed a psychometric visual discrimination task where they alternated the reward size in blocks of trials. Many mPFC neurons reflected the predicted value of the choice during the trial pre-outcome activity (aligned to action). Interestingly, during correct trials, the response of mPFC neurons was scaled both as a function of the stimulus contrast and according to the future reward size, suggesting coding of the confidence-dependent predicted value of the trial outcome (Lak et al. 2020).

Importantly, mPFC neurons not only tend to respond only to behaviorally relevant sensory stimuli, but their response depends also strongly upon the behavioral response or decision. In mice executing a whisker-detection task, mPFC response is strongly reduced in Miss trials, compared to Hit trials (Le Merre et al. 2018). This, together with the strong decrease in performance during inactivation, suggests an important role of mPFC in decision-making.

To summarise the mPFC has been shown to play an important role in the transformation of sensory information into an appropriate motor response in goal-directed behaviors in mice. Neurons in the mPFC can exhibit differential activity depending on the value of available options and the animal's choice. In particular, the mPFC has been implicated in the ability of mice to use information about past

experiences to guide their behavior toward achieving future goals. The important regions of the mPFC in this context are the prelimbic cortex (PL) and the infralimbic cortex (IL), which are critical for updating and encoding information about reward expectations during goal-directed behavior. Optogenetic perturbation experiments have also suggested that the prelimbic (PL) and the infralimbic (IL) regions of the mPFC may be involved in the formation and maintenance of goal-directed behavior. Overall, the mPFC appears to play a key role in the cognitive processes that underlie goal-directed behavior in mice, including encoding of reward value, context-dependent memory, and decision-making. However, it should be noted that many studies investigating the activity of mPFC neurons during goal-directed behaviors did not carefully take into account task-evoked movement-related activity. In many tasks, sensory, decision, and motor activity are tightly correlated and/or overlap in time. Thus a better understanding of mPFC activity would require to better take motor activity into consideration.

1.5 Aim of the Ph.D. Thesis.

The neuronal circuits supporting even simple sensorimotor transformations remain poorly defined. In particular, which cortical areas are responsible for sensory perception, decision-making, and motor execution is still a matter of discussion. This is largely due to the fact that these processes are encoded in complex neuronal population dynamics distributed across many distant brain areas, and until recently it was simply not technically possible to access this level of complexity.

Over the last few years, new technological advances have made it possible by combining the recording of a large population of neurons across multiple brain areas with fine monitoring of behavior, as well as the manipulation of neuronal activity in specific brain regions using optogenetics. During my Ph.D. I have tried to use these recently developed tools to better understand a mechanism of sensorimotor transformation in mice performing goal-directed behavior. More specifically to disentangle the coding of sensory information versus decision and motor information by neurons in different brain regions along the transformation path of whisker sensory stimuli to licking motor output during goal-directed behaviors.

An important question that we tried to address is what information is encoded by mPFC neurons. Previous studies from our and other laboratories have pointed to the specific activity of mPFC neurons for behaviorally relevant sensory events and suggested that this activity developed with learning. However, many of those previous studies lacked careful monitoring of task-related movement, making difficult a final interpretation of what is encoded in mPFC activity. We, therefore, tried to disentangle the sensory, decision, and motor-related information in the activity of mPFC neurons, and also compared the activity with other cortical areas involved in the sensorimotor transformation.

One way to do it would be to physically separate in time periods when the mouse receives the sensory stimulus and periods when it is instructed to lick for reward by introducing a delay between them, and this was the approach we took first. Another way would be to use a method of psychophysics and to vary the sensory stimuli, hence the sensory coding would be indicated by a high correlation between neuronal activity and the strength of the stimulations, and the decision coding would be indicated by a high correlation between neuronal activity and mouse performance.

In the first study, described in Chapter 2 (Esmaeili et al., 2021), we designed a whisker detection task with a delayed response and applied a generalized linear model (GLM) approach to take better account for the motor component of the neuronal activity. This task would allow us to study and manipulate neuronal activity in different periods of the trial: sensory epochs, delay epochs, and response epochs. The delay period would be important to address the question of decision-making and movement

planning, whereas, during the response epoch, we would study the coding of the movement execution.

The goal of the second study, described in Chapter 3 (Esmaeili et al., 2022), was to complement the analysis of the previous study, which was done on the regular spiking neurons (RSU), by now looking at the activity and contribution of fast spiking units (FSU) to coding of task variables through the learning of the delay detection task. The important first aim was to revise and define the method for RSU/FSU categorization based on action potential waveforms and to validate the method using an optotagging approach. The second aim was to look at the session with simultaneous recordings and to address the functional connectivity and firing correlations between them.

In the last study (Chapter 4; Oryshchuk et al., manuscript in preparation), we more specifically addressed the coding of the pure sensory and pure motor information, and how this coding is changed and shaped by goal-directed behavior when a sensory stimulus is now driving the motor output through perceptual decisions. The important goal was to design the psychophysical detection task which will allow to deliver sensory stimuli in the physiological range of the mouse perception. We chose this approach because of several reasons: (1) contrary to the strong whisker stimulation that was used in the delay task, we would find a near-threshold whisker stimulus that would allow as better address the question of the decision made by a mouse on a single trial; (2) by applying different amplitudes of the stimulation we can understand the pure sensory coding in the absence of licking; (3) from the previous study we appreciated the difficulty of the mouse to suppress the licking during a delay period that resulted in a long training, hence combining the notion of stimulus ambiguity with the delay response would result in extremely long training of mice. Hence there would be no delay in the psychophysical detection task and we would account for the motor component of the neuronal activity using different computational approaches and careful monitoring of behavior.

In summary, the aim of the thesis was to gain a better understanding of the neuronal circuits supporting sensorimotor transformations and to identify the cortical areas responsible for sensory perception, decision-making, and motor execution in mice. In this study, we revealed causal contributions of the primary somatosensory cortex (wS1), medial prefrontal cortex (mPFC), and primary motor cortex (tjM1) to the transformation of whisker sensory stimuli to the goal-directed licking, and proposed a hypothesis on how the decision to execute an action is taken during psychophysical detection task in mice. Our results provide new insights into the sensory-motor transformation process and offer a promising direction for further research into the cognitive aspects of decision-making.

Chapter 2 Rapid suppression and sustained activation of distinct cortical regions for a delayed sensory-triggered motor response

The text and figures of this chapter are reproduced from the following published journal article:

Vahid Esmaeili¹, Keita Tamura¹, Samuel P. Muscinelli, Alireza Modirshanechi, Marta Boscaglia, Ashley B. Lee, Anastasiia Oryshchuk, Georgios Foustoukos, Yanqi Liu, Sylvain Crochet, Wulfram Gerstner, and Carl C.H. Petersen. 2021

1: These authors contributed equally

“Rapid Suppression and Sustained Activation of Distinct Cortical Regions for a Delayed Sensory-Triggered Motor Response.”

Neuron 109 (13): 2183-2201.e9.

<https://doi.org/10.1016/j.neuron.2021.05.005>.

My contribution to this paper:

I performed histological slicing, mounting, and imaging of the brain slices for the verification of the probes after electrophysiological recordings.

I performed a part of movement analysis (tracking of body parts in time) for the optogenetic experiments and electrophysiology.

Assisted in multiple optogenetic and electrophysiology experiments, and mice training.

Actively participated in all discussions and edited the manuscript.

2.1 Abstract

The neuronal mechanisms generating a delayed motor response initiated by a sensory cue remain elusive. Here, we tracked the precise sequence of cortical activity in mice transforming a brief whisker stimulus into delayed licking using wide-field calcium imaging, multi-region high-density electrophysiology, and time-resolved optogenetic manipulation. Rapid activity evoked by whisker deflection acquired two prominent features for task performance: i) an enhanced excitation of the secondary whisker motor cortex, suggesting its important role connecting whisker sensory processing to lick motor planning, and ii) a transient reduction of activity in the orofacial sensorimotor cortex, which contributed to suppressing premature licking. Subsequent widespread cortical activity during the delay period largely correlated with anticipatory movements, but when these were accounted for, a focal sustained activity remained in the frontal cortex, which was causally essential for licking in the response period. Our results demonstrate key cortical nodes for motor plan generation and timely execution in delayed goal-directed licking.

2.2 Introduction

Incoming sensory information is processed in a learning- and context-dependent manner to direct behavior. Timely execution of appropriate action requires motor planning, in particular when the movement triggered by a sensory cue needs to be delayed. In this situation, the motor plan must persist throughout the delay period while the immediate execution of the motor response needs to be suppressed. Delayed-response paradigms are often used to study the neuronal circuits of sensorimotor transformation because they allow to temporally isolate the neuronal activity that bridges sensation and action. In such paradigms, prominent delay period activity has been reported in many cortical areas (Fuster and Alexander 1971; Tanji and Evarts 1976; Funahashi et al. 1989; Guo et al. 2014; Li et al. 2015; Chen et al. 2017; Fassihi et al. 2017; Makino et al. 2017; Gilad et al. 2018; Chabrol et al. 2019; Esmaeili and Diamond 2019). In particular, a previous study in mice identified delay period activity in the anterolateral motor (ALM) cortex, which causally contributed to a lick motor plan (Guo et al., 2014). The persistent delay period activity in ALM is driven through a recurrent thalamocortical loop (Guo et al., 2017), and is further supported by cerebellar interactions (Chabrol et al., 2019; Gao et al., 2018). The circuit mechanisms maintaining the persistent activity in ALM are therefore beginning to be understood. However, less is known about the circuits that initiate such persistent activity, and how task learning shapes such circuits. In addition, how the persistent neuronal activity is related to body movements which animals often exhibit during delay periods needs to be carefully considered (Musall et al. 2019; Steinmetz et al. 2019; Stringer et al. 2019).

Similarly, the neuronal circuits contributing to withholding a premature motor response during the delay are poorly understood. To dissect this process, it would be crucial to examine how neuronal activity flows across brain areas as sensory information is transformed into goal-directed motor plans (de Lafuente and Romo, 2006), and to investigate how the underlying sensory and motor circuits become connected through reward-based learning (Esmaeili et al., 2020).

Here, we address these questions in head-restrained mice performing a whisker-detection task with delayed licking to report perceived stimuli. In our task, a brief and well-defined sensory input is rapidly transformed into a decision and mice need to withhold the response until the end of the delay period. Through a unified and comprehensive approach, we detail the spatiotemporal map of causal cortical processing which emerges across learning. We found that following the fast sensory-evoked response in somatosensory cortex (Petersen, 2019), the activity in orofacial sensorimotor cortex (Mayrhofer et al., 2019) was rapidly and transiently suppressed, which contributed causally to withholding premature licking. The subsequent rapid sequential excitation of frontal cortical regions and their changes across task learning revealed that the secondary whisker motor cortex (wM2) likely plays a key role in linking whisker sensation to motor planning. We also found that the global activation of the dorsal cortex during the delay period could be largely ascribed to preparatory movements that develop with learning, except for a localized neuronal activity in ALM (Komiyama et al., 2010), consistent with previous studies (Chen et al., 2017; Guo et al., 2014). Our results, therefore, point to task epoch-specific contributions of distinct cortical regions to whisker-triggered planning of goal-directed licking and timely execution of planned lick responses.

2.3 Results

2.3.1 Behavioral changes accompanying delayed-response task learning

We designed a Go/No-Go learning paradigm where head-restrained mice learned to lick in response to a whisker stimulus after a one second delay period (Figure 2.1A-C). To precisely track the sequence of cortical responses, we used a single, short (10 ms) deflection of the right C2 whisker. The trial start was indicated by a 200 ms light flash, followed 1 s later by the whisker stimulus in 50% of the trials (referred to as Go trials); after a subsequent 1 s delay, a 200 ms auditory tone signaled the beginning of a 1 s response window. Licking during the response window, in Go trials, was rewarded with a drop of water, whereas licking before the auditory tone (early lick) led to abortion of the trial and time-out punishment (Figure 2.1B). To study

essential neuronal circuit changes specific to the coupling of the whisker stimulus with the licking response, a two-phase learning paradigm was implemented: i) Pretraining, and ii) Whisker training (Figure 2.1C). Pretraining included trials with visual and auditory cues only, and licking during the response window was rewarded, while licking before the auditory cue aborted the trial. Novice mice only went through the Pretraining, which established the general task structure. Expert mice followed an additional Whisker training phase, during which they learned the final task structure (Figures 2.1B-C and 2.9A).

Novice and Expert mice were recorded in the same final task condition, but performed differently. While, Novice mice licked in both Go and No-Go trials, Expert mice had learned to lick preferentially in Go trials (Figures 2.1D and 2.9A; mean \pm SEM, Novice: Hit=70.6 \pm 3%, False-alarm=71.1 \pm 2.7%, $p=0.85$, $n=15$ mice; Expert: Hit=67 \pm 1.5%, False-alarm=19.7 \pm 1.6%, $p<0.001$, $n=25$ mice; Wilcoxon signed-rank test). Expert mice made more frequent premature early licks in Go-trials compared to Novice mice (Figures 2.1D; mean \pm SEM, Novice=12.5 \pm 2.7%, Expert= 25.1 \pm 3.3%, $p=0.02$; Wilcoxon rank-sum test) and most of their early licks happened toward the end of the delay period, reflecting predictive licking. Considering trials with licking during the response window, Expert mice showed longer reaction times in No-Go trials (False-alarm) compared to Go trials (Hit) (Figure 2.9B; mean \pm SEM, Novice: Hit=298.5 \pm 21.2 ms, False-alarm=292.7 \pm 21.4 ms, $p=0.14$; Expert: Hit=297.8 \pm 16.7 ms, False-alarm=380.3 \pm 16.3 ms, $p<0.01$; Wilcoxon signed-rank test). These results indicate that Expert mice used whisker information and learned to produce delayed licking. After Whisker training, mice also adopted new movement strategies (Figures 2.1E-F and 2.9C-D). In Hit trials, Expert mice compared to Novice mice decreased whisker movement before whisker stimulus, possibly to improve the detection of brief whisker stimuli in the receptive mode of perception (Diamond and Arabzadeh 2013; Kyriakatos et al. 2017). The tongue and jaw movements in the delay period after the whisker stimulus increased in Hit trials of Expert mice compared to Novice mice, reflecting preparation for licking. These anticipatory movements were absent in Miss and Correct-rejection trials (Figure 2.9C), and thus correlated with the perceptual response. These patterns were similar comparing mice used for electrophysiology and imaging (Figures 2.1F and 2.9D).

2.3.2 Emergence of cortical activation and deactivation patterns through whisker training

The delay-task enables the investigation of different aspects of neuronal computations underlying reward-based behavior including: sensory processing, motor planning and motor execution in well-isolated time windows. As a first step, we mapped the large-scale dynamics of cortical activity using wide-field calcium imaging at a high

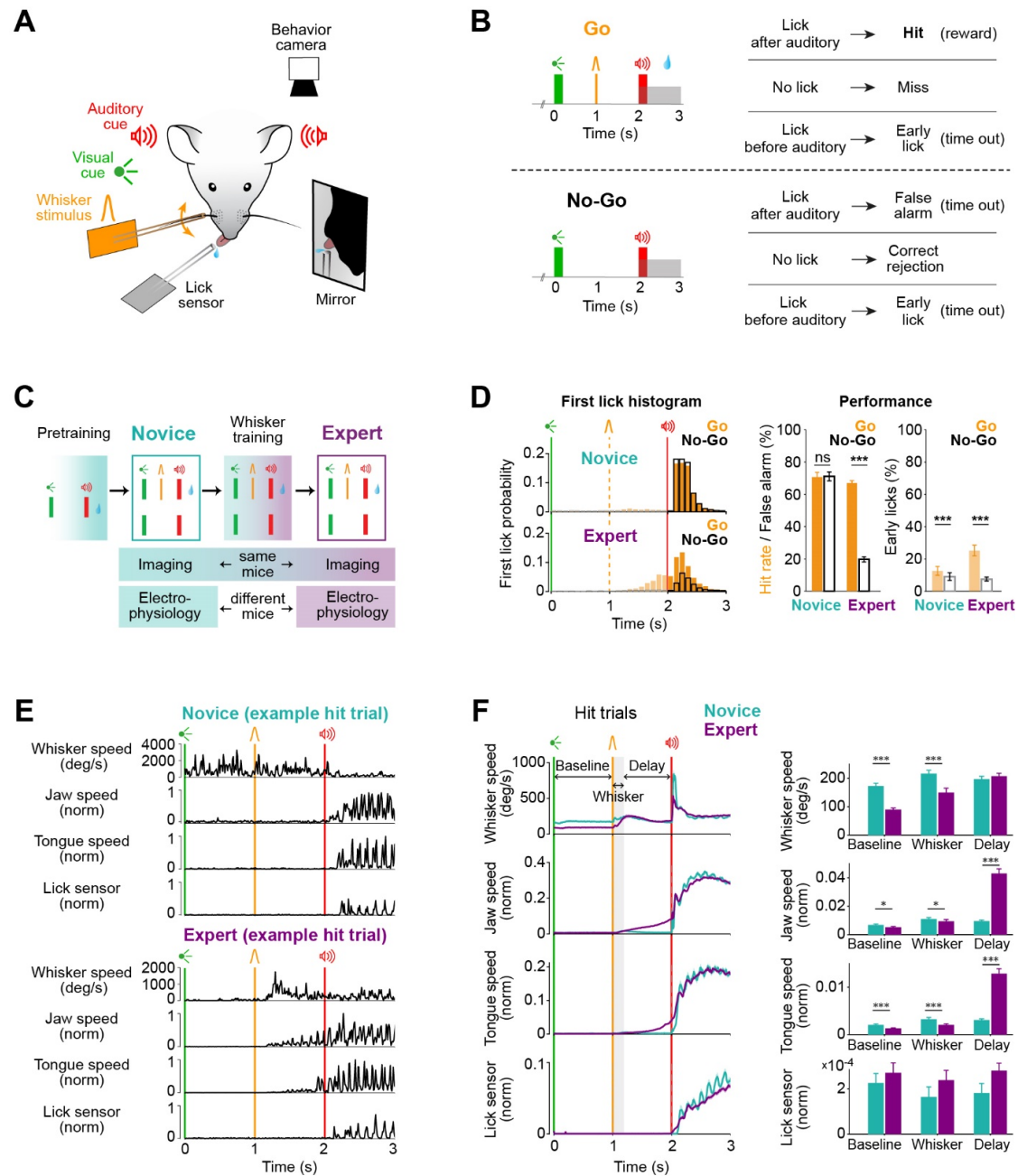


Figure 2.1. Learning a whisker detection task with a delayed response changes licking patterns and orofacial movements.

(A and B) Delayed whisker detection task. A, Behavioral setup. Sensory stimuli were delivered to head-restrained mice and licking and orofacial movements were monitored using a piezoelectric lick sensor and a behavior camera. B, Task structure and trial outcomes in Go and No-Go trials.

(C) Learning paradigm. All mice went through visual-auditory Pretraining, where all licks after the auditory cue were rewarded. Expert mice went through Whisker training where final task structure was used as in panel B. Neural data were obtained using the final task design in Novice mice and Expert mice, before and after Whisker training respectively. The same mice were imaged during Novice and Expert stages, while different mice were used for electrophysiological recordings.

(D) Task performance. *Left*, first lick time histogram was similar in Go vs No-Go trials in Novice mice, but differed in Expert mice. Early licks (licks between visual cue and auditory cue) are shown with light colors. *Middle*, Novice mice licked equally in Go and No-Go trials, whereas Expert mice licked preferentially in Go trials (quantified as mean \pm SEM across all completed trials; Novice, $n=15$ mice; Expert, $n=25$ mice). *Right*, both groups of mice made more early licks in Go compared to No-Go trials. *** indicates $p<0.001$ according to Wilcoxon signed-rank test.

(E and F) Orofacial movements. E, Example trials from Novice (*top*) and Expert (*bottom*) mice: extracted angular speed of left C2-whisker, and normalized jaw and tongue speed together with the lick sensor signal are plotted along the trial time-course. F, Average movement (mean \pm SEM) traces (*left*) and bar plots comparing Novice and Expert movements in 3 different windows (*right*). Expert mice reduced all movements during Baseline and Whisker time windows, while they increased tongue and jaw movements during the Delay. Asterisks represent statistical comparison of movement between Novice and Expert mice in: Baseline (0-1 s), Whisker (1-1.2 s), and Delay (1.2-2 s) time windows (Wilcoxon rank-sum test, false discovery rate (FDR) corrected, ***: $p<0.001$, *: $p<0.05$). Only mice used for electrophysiology (8 Novice and 18 Expert mice) are plotted.

temporal resolution (100 frames per second) (Figures 2.2, 2.10 and 2.11). In transgenic mice expressing a fluorescent calcium indicator in pyramidal neurons (RCaMP mice) (Bethge et al. 2017), functional images of the left dorsal cortex were obtained through an intact skull preparation, and registered to the Allen Mouse Brain Common Coordinate Framework (Figures 2.2A-B) (Lein et al. 2007; Wang et al. 2020).

To examine the changes in cortical processing upon learning, we compared the activity in the same mice ($n=7$) before (Novice, 62 sessions) and after (Expert, 82 sessions) whisker training (Figures 2.2C for Hit trials and 2.10A for Correct-rejection trials). The visual cue evoked responses in the primary visual (Vis) and surrounding areas (Wang and Burkhalter 2007; Andermann et al. 2011; Marshel et al. 2011), which decreased after whisker training (Figures 2.2C and 2.10A; subtraction between Novice and Expert mice images; Wilcoxon rank-sum test, $p<0.05$; for details, see Methods). Stimulation of the C2 whisker evoked two focal responses, in the primary and secondary whisker somatosensory areas (wS1, wS2), both in Novice and Expert mice (Figure 2.2C). Immediately after, activity transiently decreased in orofacial areas including the primary tongue/jaw sensory and motor areas (tjS1, tjM1), followed by a widespread gradual increase toward the auditory cue initiating in the primary and secondary motor areas for whisker (wM1, wM2) and tongue/jaw (tjM1, ALM), as well as posterior parietal cortex (PPC) and limb/trunk areas. These positive and negative responses during the delay period were selective to Hit trials of Expert mice (Figures 2.2C, 2.10B-C). We further quantified response selectivity of different cortical regions for Hit and Correct-rejection trials by comparing their trial-by-trial activity based on ROC analysis (Figure 2.2D; see Methods). Across all cortical regions tested, selectivity was significantly enhanced in Expert compared to Novice mice during the delay period and response window ($p<0.05$; non-parametric permutation test). Therefore, important learning-induced global changes of information processing emerged during the delay period.

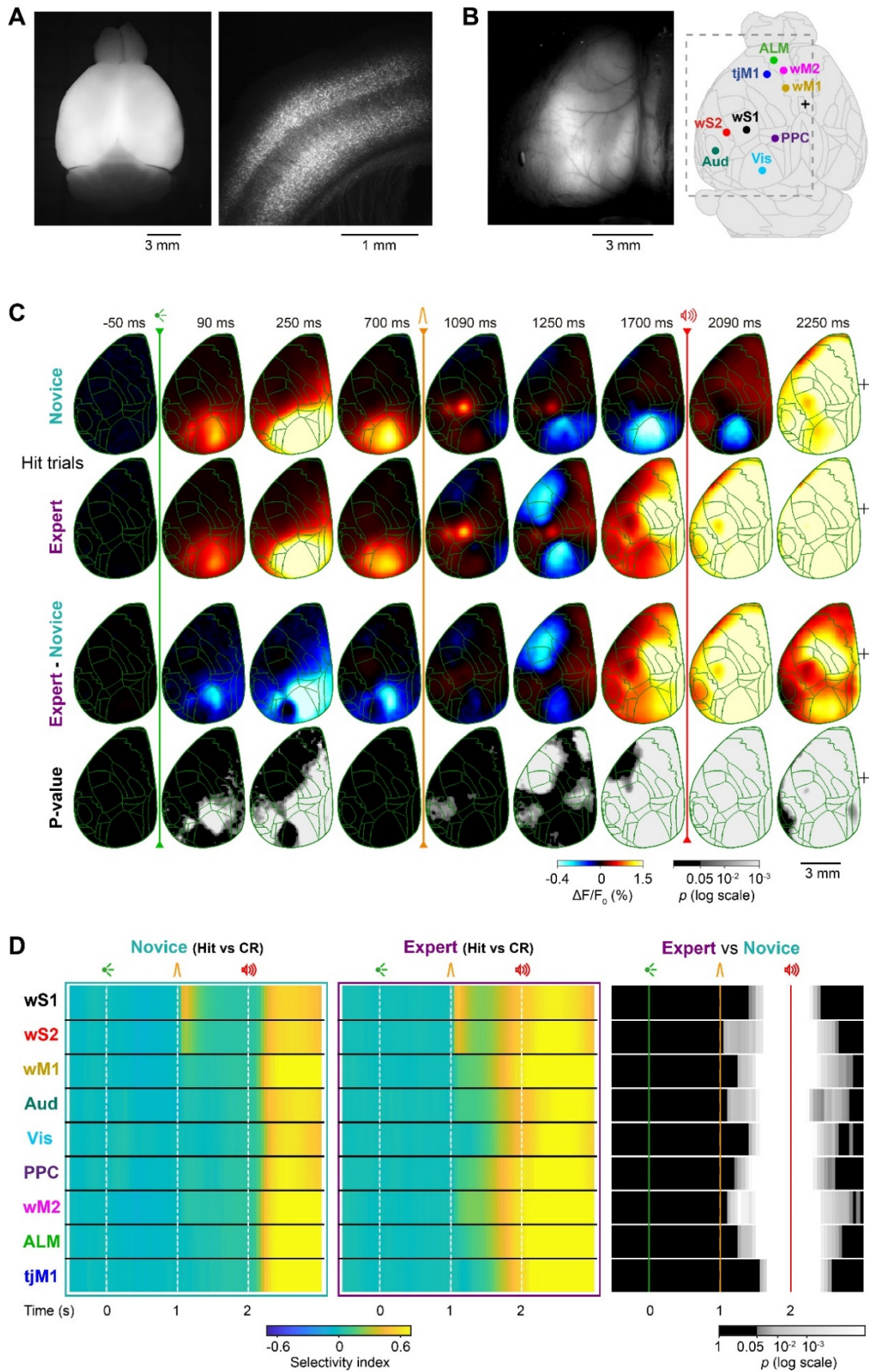


Figure 2.2. Wide-field imaging reveals global changes in cortical processing.

(A and B) Wide-field calcium imaging in Emx1-RCaMP mice. A, Fluorescence images of an ex vivo fixed brain in dorsal view (left) and a coronal section of somatosensory area (right) showing RCaMP expression in pyramidal neurons in deep and superficial layers. B, In vivo fluorescence image of the tilted (24 degrees) left dorsal hemisphere through a transparent, intact skull preparation (left). In vivo images were registered to the Allen Mouse Brain Atlas (right). Cortical areas targeted for electrophysiological experiments are indicated: wS1, primary whisker somatosensory cortex; wS2, secondary whisker somatosensory cortex; wM1, primary whisker motor cortex; wM2, secondary whisker motor cortex; Aud, auditory area; Vis, visual area; PPC, posterior parietal cortex; tJM1, primary tongue and jaw motor cortex; ALM, anterior lateral motor area.

(C) Grand-average time-course of global cortical activity in Hit trials for Novice vs Expert mice. Each frame shows $\Delta F/F_0$ without temporal smoothing (10 ms/frame). For each pixel, baseline activity in a 50 ms window before visual cue onset was subtracted. Mean calcium activity of 62 Novice and 82 Expert sessions from 7 mice, Novice and Expert difference, and the statistical significance of the difference (p-value of Wilcoxon rank-sum test, FDR-corrected, $p < 0.05$) are plotted from top to bottom. Green traces, anatomical borders based on Allen Mouse Brain Atlas. Black '+' indicates bregma.

(D) Selectivity index in Novice and Expert mice. For each brain region, selectivity between Hit versus Correct-rejection trials was determined in non-overlapping 50 ms bins based on the area under the ROC curve. Mean selectivity of each area in 62 Novice and 82 Expert sessions from 7 mice, and the statistical significance of the difference (p-value of non-parametric permutation test, FDR-corrected, $p < 0.05$) is plotted. ROI size, 3 x 3 pixels.

To control for hemodynamic effects of the wide-field fluorescence signal (Makino et al. 2017), we also imaged transgenic mice expressing an activity-independent red fluorescent protein, tdTomato, which has excitation and emission spectra similar to RCaMP (Figure 2.11; 57 sessions from 7 Expert mice). We imaged RCaMP and tdTomato mice at the same baseline fluorescence intensity (Figure 2.11E; $p = 0.80$, Wilcoxon rank-sum test, $n = 7$ RCaMP mice and $n = 7$ tdTomato mice) by adjusting illumination light power and using identical excitation and emission filters. The tdTomato control mice showed significantly smaller task-related changes in fluorescence than the RCaMP mice (Figure 2.11A-D; subtraction between RCaMP and tdTomato mice images; Wilcoxon rank-sum test, $p < 0.05$). In the visual cortex of both RCaMP and tdTomato mice, negative intrinsic signals were evoked around 1 s after the visual stimulus. However, the short whisker stimulation evoked a rapid positive sensory response only in RCaMP mice, and no clear response was evoked in tdTomato mice (Figure 2.11F). On the other hand, some positive intrinsic optical signals were evoked in the midline and frontal regions of tdTomato mice, but the amplitude of these signals was significantly smaller than for RCaMP mice (Wilcoxon rank-sum test, $p < 0.05$). These results suggest that the spatiotemporal patterns of fluorescence signals in RCaMP mice largely reflected the calcium activity of the cortex.

2.3.3 Distinct modification of early and late whisker processing in single neurons

To further investigate learning- and task-related cortical dynamics with higher temporal and spatial resolution, we carried out high-density extracellular recordings

(Buzsáki 2004) from 12 brain regions, with guidance from wide-field calcium imaging (Figures 2.2 and 2.10), optical intrinsic imaging and previous literature (Harvey et al. 2012; Guo et al. 2014; Sippy et al. 2015; Sreenivasan, Kyriakatos, et al. 2016; Kyriakatos et al. 2017; Le Merre et al. 2018; Esmaeili and Diamond 2019; Mayrhofer et al. 2019) including: Vis, wS1, wS2, wM1, wM2, tjM1, ALM, PPC, auditory cortex (Aud), the dorsolateral region of striatum innervated by wS1 (DLS), medial prefrontal cortex (mPFC) and the dorsal part of hippocampal area CA1 (dCA1) (Figures 2.3A and 2.12A-C). Two areas were recorded simultaneously during any given session. The precise anatomical location of the recording probes was determined by 3D reconstruction of the probes' tracks using whole-brain two-photon tomography and registration to the Allen atlas (Figures 2.3A and 2.12A-C; for details, see Methods) (Lein et al. 2007; Wang et al. 2020). In total, 4,415 neurons - classified as regular spiking units (RSUs) based on their spike waveform - were recorded in 22 Expert mice, and 1,604 RSUs in 8 Novice mice.

Single neurons encoded different task aspects such as whisker sensory processing, lick preparation, and lick execution (Figure 2.3B). Assuming that neurons with similar firing dynamics perform similar processing, it is informative to identify those temporal patterns and investigate whether a single pattern is confined or distributed across the brain. We, therefore, performed unsupervised clustering of neurons according to their temporal firing pattern in different trial types (Hit, Miss, Correct-rejection, and False-alarm) by pooling neurons from different brain regions of both Novice and Expert mice (Figures 2.3C and 2.13; see Methods). Gaussian mixture model (GMM) clustering (Figure 2.13A-B) yielded 24 clusters of neurons, among which 20 were modulated in at least one of the task epochs (Nordhausen 2009). By sorting task-modulated clusters by their onset latency and labeling them based on their task epoch-related response, we analyzed the distribution of clusters across areas along a functional axis (Figure 2.3C-D). Clusters composed predominantly of neurons from Expert mice were particularly modulated during the Delay period (Clusters 5, 6, and 7) and the Response window (Clusters 14, 15, and 17), and were mainly distributed across different motor-related areas (Figure 2.3D). Next, we calculated a “distribution index” which quantifies the within-area versus between-area composition of clusters (Figures 2.3D and 2.13C; for details, see Methods). The distribution index was small for Visual and Whisker clusters, indicating a localized distribution of those clusters in specific brain regions. On the other hand, the distribution index was large in the majority of Response clusters, indicating a broad distribution of those clusters across brain areas. Across learning, prominent activity patterns remained similar in wS1, wS2, and Vis areas, while it changed in all other regions (Figure 2.13D).

To reveal spatial changes in neuronal firing following whisker training, we calculated the average time-dependent firing rate for all recording probes (Figure 2.12D) and for the 12 anatomically defined areas (Figure 2.3E). The visual cue evoked

responses localized in Vis and PPC of Novice and Expert mice. Following the auditory cue, excitation rapidly covered all recorded regions in both mice groups. Major changes following whisker training appeared in the delay period between the whisker and auditory stimuli. Similar to deactivation patterns of the orofacial cortex revealed by wide-field imaging (Figure 2.2C), tjM1 showed a transient suppression of firing after whisker stimulation in Expert mice. The whisker stimulus also evoked a widespread excitation across whisker sensorimotor areas (wS1, wS2, wM1, wM2), as well as PPC, DLS, and ALM with different latencies. The initial excitation was significantly enhanced in wM2 and ALM (non-parametric permutation test, $p < 0.05$). Firing rates of all areas in Novice mice returned to baseline levels shortly after whisker stimulation, whereas in Expert mice wS2, PPC, DLS, wM2, ALM and tjM1 neurons showed increased activity in different parts of the delay. PPC neuronal firing remained elevated only during the first part of the delay period, returning to baseline before the auditory cue, while the activity of wM2, DLS, and tjM1 neurons ramped up towards the lick onset. Average neuronal firing in ALM remained elevated throughout the entire delay period. These results suggest that the whisker training enhanced the initial distributed processing of the whisker stimulus, and formed the memory of a licking motor plan among higher-order areas of whisker and tongue/jaw motor cortices, while introducing a transient inhibitory response in tjM1.

We further investigated what was encoded in the acquired neural activity by considering other trial types. First, we found that the pronounced delay period activity during Hit trials was absent in Miss trials, and thus correlated with percept (Figure 2.12E-F). Second, we quantified the selectivity of single neurons for whisker detection and delayed licking by comparing their trial-by-trial spiking activity in Hit and Correct-rejection trials based on ROC analysis (Figure 2.3F; see Methods). We found that a significantly larger percentage of neurons became selectively recruited during the delay period in many areas of the Expert mice, suggesting the possible involvement of widespread cortical networks in the acquisition of motor planning for delayed licking ($p < 0.05$; non-parametric permutation test).

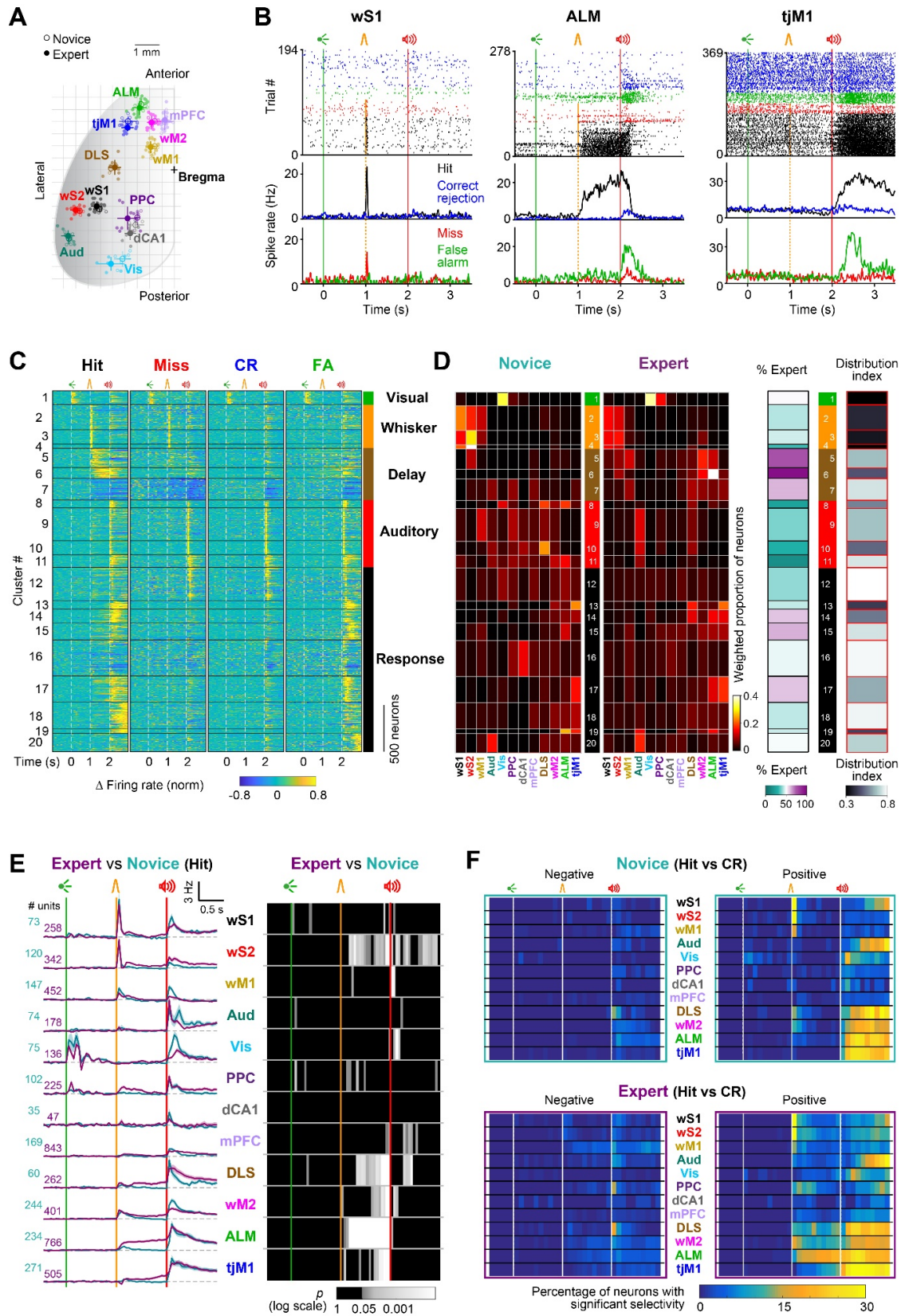


Figure 2.3. Task epoch-specific processing across single neurons.

(A) Reconstructed location of silicon probes registered to the Allen Mouse Brain Atlas in 2D dorsal view in Expert (filled circles) and Novice (open circles). Probes assigned to each anatomical region are shown with different colors and their average coordinates (mean \pm SEM) are indicated with larger circles and whiskers. Abbreviations: Medial prefrontal cortex, mPFC; dorsal hippocampal CA1, dCA1; dorsolateral striatum, DLS; other regions as defined in Figure 2B.

(B) Example neurons from Expert mice. Raster plots and peristimulus time histograms (PSTHs) for three representative units in wS1, ALM, and tjM1 encoding whisker, delay and licking, respectively. Trials are grouped and colored based on trial outcome.

(C) Unsupervised neuronal clustering. Activity maps of all single units from Novice and Expert mice clustered based on their trial-type average normalized firing rate. Black horizontal lines separate different clusters. Labels on the right, indicate the task epoch where the response onset was observed on cluster average response. Only task-modulated clusters (20/24) are shown.

(D) Composition of clusters. Left, Weighted proportion of neurons within each cluster belonging to different brain regions in Novice and Expert mice. Right, Percentage of neurons in each cluster from Novice and Expert mice, and distribution index. To calculate the distribution index for each cluster, the probability distribution of the area composition was compared to a uniform distribution and an index between 0 (localized in one area) to 1 (uniformly distributed) was defined. Values are corrected for different sample sizes in different areas and mouse groups.

(E) Population firing rate in Hit trials. Left, Baseline-subtracted mean firing rate (mean \pm SEM) in each region is superimposed for Expert (purple) and Novice (cyan) mice. Right, p-value map of Expert vs Novice mice comparison in 50-ms non-overlapping windows (non-parametric permutation test, FDR-corrected).

(F) Proportion of neurons with significant selectivity index in Novice and Expert mice. For individual neurons, selectivity between Hit vs Correct-rejection trials was determined in 100 ms non-overlapping windows based on the area under the ROC curve. The percentage of neurons with significant negative (left) or positive (right) selectivity in each region is shown across time in Novice (top) and Expert (bottom) mice. The significance of selectivity was determined using non-parametric permutation tests ($p < 0.05$).

2.3.4 Active suppression of orofacial sensorimotor areas

In the delay period, Expert mice showed a transient suppression in broad orofacial sensorimotor cortices selectively in Hit trials (Figures 2.2, 2.3, 2.10, and 2.12). The suppression of activity in this region coincided with the onset of the whisker-evoked excitation in adjacent secondary motor cortices including ALM (Figure 2.4A). This inhibition could contribute to suppressing immediate licking in response to the whisker stimulus. To test this hypothesis, we first compared trials in which mice successfully withheld licking until the end of the delay period (Hit), with trials in which mice made premature licking following the whisker stimulus (Early licks). We found that tjM1 activity was significantly suppressed in Hit compared to Early lick trials (Figure 2.4B), in both calcium imaging signals (tjM1: $p = 0.040$; Wilcoxon signed-rank test) and neuronal firing rate (tjM1: $p = 0.017$; non-parametric permutation test). Next, to evaluate the causal role of tjM1 in the suppression of premature licking, we optogenetically manipulated tjM1 activity during task execution (Figure 2.4C). Activation of tjM1 in transgenic mice expressing ChR2 in excitatory neurons (Emx1-ChR2) increased the fraction of Early licks (Figure 2.4C; $n = 19$ sessions in 6 Expert mice, Light-off versus Light trials, No-Go trials: $p = 4.27 \times 10^{-4}$, Go trials: $p = 1.94 \times 10^{-3}$; Wilcoxon signed-rank

test). Conversely, the inactivation of tJM1 in transgenic mice expressing ChR2 in GABAergic inhibitory neurons (VGAT-ChR2) (Guo et al., 2014) significantly reduced premature licking (Figure 4C; 32 sessions in 9 mice, Light-off versus Light trials, Go trials: Whisker: $p=0.018$, Delay: $p=2 \times 10^{-6}$; Wilcoxon signed-rank test). The opposite effect of these optogenetic manipulations indicates that the behavioral changes are not visually-induced by the stimulation light. Altogether, these results suggest that the tJM1 suppression acquired in Expert mice plays an important role in delaying the lick response.

To further investigate the relationship between the reduction of cortical activity and movement suppression, we compared neural activity after the auditory cue between Correct-rejection and Miss trials, as they likely reflect distinct origins of a “no-lick” response (Figure 2.4D). We found that the calcium signal in orofacial sensorimotor cortices showed significantly stronger suppression in Correct-rejection trials compared to Miss trials (Figure 2.4D; $p<0.05$; Wilcoxon signed-rank test). Consistently, the spiking activity in tJM1 during the response window revealed a stronger inhibition in Correct-rejection trials (Figure 2.4D, $p=0.005$; non-parametric permutation test). Moreover, in the same behavioral epoch, a larger proportion of neurons in tJM1 were negatively modulated in Correct-rejection trials (Figure 2.4D; $p<0.05$; non-parametric permutation test). These results highlight the correlation and causality between the deactivation of the orofacial sensorimotor cortex and the active suppression of licking.

2.3.5 Routing of whisker information to the frontal cortex

The brief whisker stimulation allowed us to follow the sequence of evoked responses across cortical regions. Frame-by-frame analysis of high-speed calcium imaging data and high-resolution quantification of spiking activity showed that the whisker stimulus evoked the earliest responses in wS1; activity then spread to wS2, wM1, wM2, and finally reached ALM (Figures 2.5A and 2.14A-C). This earliest sequence of excitation, as well as the deactivation of tJM1/S1, was significantly enhanced across learning by whisker training (Figure 5A, Wilcoxon rank-sum test, $p<0.05$). This sequential activation and deactivation were diminished when mice failed to lick (Miss trials) (Figure 2.14D-E; Wilcoxon signed-rank test, $p<0.05$), supporting its involvement in whisker-detection and delayed-licking (see also Figure 2.4).

To test whether the sequential activation of cortical areas occurs in single trials, we examined whether the variability of the response latency in wS1 propagates to downstream areas in the imaging data. We divided the data into *Slow* and *Fast* trials

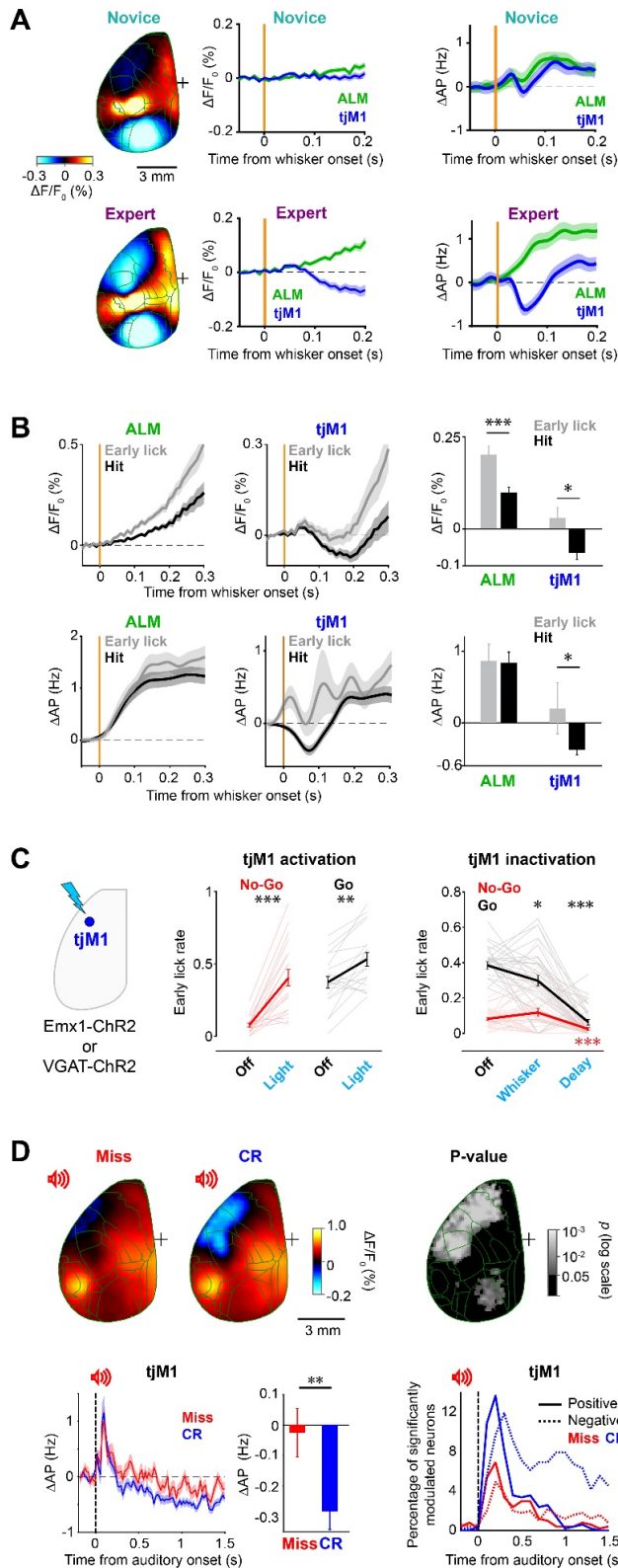


Figure 2.4. Active suppression of orofacial sensorimotor areas.

(A) Transient suppression of tJM1 in Hit trials of Expert mice. Grand average wide-field image (170 ms after whisker onset) of Novice (n=62 sessions, *upper left*) and Expert (n=82 sessions, *lower left*) sessions from 7 mice, calcium traces (*middle*, mean \pm SEM) and firing rates (*right*, mean \pm SEM) in tJM1 and ALM after whisker stimulus. For the calcium signal, the mean during 50-ms period before whisker stimulation is subtracted, and for spiking data, the mean during 200 ms before whisker onset is subtracted.

(B) tJM1 suppression during delayed licking in Expert mice. *Top*, calcium traces averaged (mean \pm SEM) across Hit and Early lick trials in ALM (*left*) and tJM1 (*middle*), and comparison of signal amplitude in the suppression window (*right*, 160-210 ms after whisker stimulus; n=82 sessions from 7 mice; ALM: $p=2.93 \times 10^{-4}$, tJM1: $p=0.040$; Wilcoxon signed-rank test, FDR-corrected). Mean signal during 50 ms period before whisker onset is subtracted. *Bottom*, average spiking activity (mean \pm SEM) in Hit vs Early lick trials in ALM (*left*) and tJM1 (*middle*) and comparison in the suppression window (*right*, 50-100 ms; ALM: n= 766 neurons, $p=0.466$, tJM1: 377 neurons, $p=0.017$, non-parametric permutation test, FDR-corrected). Mean spike rate during 200 ms before whisker stimulus is subtracted. Trials with first lick latency ranging from 300 ms to 1000 ms after whisker stimulus onset were selected for Early lick trials.

(C) Causal contribution of tJM1 activity to delayed licking. *Left*, Optogenetic activation and inactivation of tJM1 were performed in Emx1-ChR2 and VGAT-ChR2 transgenic mice, respectively. *Middle*, Fraction of early lick trials in Go and No-Go conditions upon tJM1 activation and no light control trials (n=19 sessions in 6 Expert mice; Light-off versus Light trials, No-Go trials: $p=4.27 \times 10^{-4}$, Go trials: $p=1.94 \times 10^{-3}$; Wilcoxon signed-rank test, FDR-corrected). *Right*, Fraction of early licks in Go and No-Go trials upon tJM1 inactivation during Whisker or Delay epochs (n=32 sessions in 9 Expert mice; Light-off versus Light trials, No-Go trials: Whisker: $p=0.239$, Delay: $p=1.2 \times 10^{-4}$; Go trials: Whisker: $p=0.018$, Delay: $p=2 \times 10^{-6}$; Wilcoxon signed-rank test, FDR-corrected).

test, FDR-corrected). Thick lines show mean \pm SEM; lighter lines show individual sessions. For details see Methods.

(D) Movement suppression in no-lick trials. *Top*, wide-field images 250 ms after auditory cue in Miss (*left*) and Correct-rejection (*middle*) trials, and *p*-value of comparison (*right*; $n=82$ Expert sessions from 7 mice; *p*-value of Wilcoxon signed-rank test, FDR-corrected). Mean signal during 50 ms period before auditory onset is subtracted. *Bottom*, baseline-subtracted (200 ms prior to auditory cue) average firing rate (mean \pm SEM) of tJM1 neurons in Miss vs Correct-rejection trials (*left*) and the comparison of mean tJM1 spike rate during response window (200-1000 ms window after auditory cue; $n=377$ neurons; $p=0.005$, non-parametric permutation test); percentage of neurons with positive (solid lines) and negative (dotted lines) modulation in Miss (red) and Correct-rejections (blue) trials during the response period compared to baseline (*right*) ($p<0.05$; non-parametric permutation test, FDR-corrected).

based on the latency of the whisker-evoked response in wS1 (Figure 2.5B), and analyzed the latencies in other areas where single-trial analysis of whisker-evoked response latency was feasible (wS2, wM1, and wM2). The latencies of those areas were significantly longer in *Slow* trials (wS1: $p=2.2 \times 10^{-8}$, wS2: $p=1.1 \times 10^{-7}$, wM1: $p=2 \times 10^{-9}$, wM2: $p=3.3 \times 10^{-4}$; Wilcoxon signed-rank test), further suggesting a chain of activation from wS1 to the other regions.

We also analyzed the change in response latency in single neuron data between Novice and Expert mice. For neurons with significant firing rate modulation in the 200 ms window following the whisker stimulus compared to the 200 ms before the whisker stimulus ($p<0.05$, non-parametric permutation test), latency was calculated as the half-maximum (minimum for suppressed neurons) whisker-evoked response (see Methods). The latency of the whisker-evoked response in wM2 was shorter following whisker training, whereas that of wM1 was longer (Figure 5C, wM1: $p=0.008$, wM2: $p=0.041$, Wilcoxon rank-sum test). Moreover, among all areas recorded, wM2 showed the earliest significant increase in firing upon whisker training (Figure 2.5D, Novice vs Expert: $p=0.015$, non-parametric permutation test), as well as the earliest significant difference comparing Hit and Miss trials (Figure 2.5E, Hit vs Miss: $p=0.010$, non-parametric permutation test).

The neuronal clustering revealed 3 main patterns of activity during the delay period (Figures 2.3C and 2.5F): i) a fast and transient increase in neuronal activity following the whisker stimulus (Clusters 2-4) that was mostly represented in wS1 and wS2 of both Novice and Expert mice; ii) a slow ramping activity (Cluster 6) that was mostly represented in ALM but only in Expert mice; and iii) the activity of Cluster 5 rose and peaked after Clusters 2-4, but before Cluster 6, and slowly decayed along the delay period, thus bridging the activities of Clusters 2-4 and Cluster 6. Interestingly, Cluster 5 was most prevalent in wM2 of Expert mice, as well as contributing importantly to activity in wS2, wM, and ALM (Figures 2.3C-D and 2.5F).

Altogether (Figure 2.5C-F), these results highlight the possible role of wM2 as a potential node to bridge sensory processing to motor planning perhaps helping to relay whisker sensory information from wS1/wS2 to ALM.

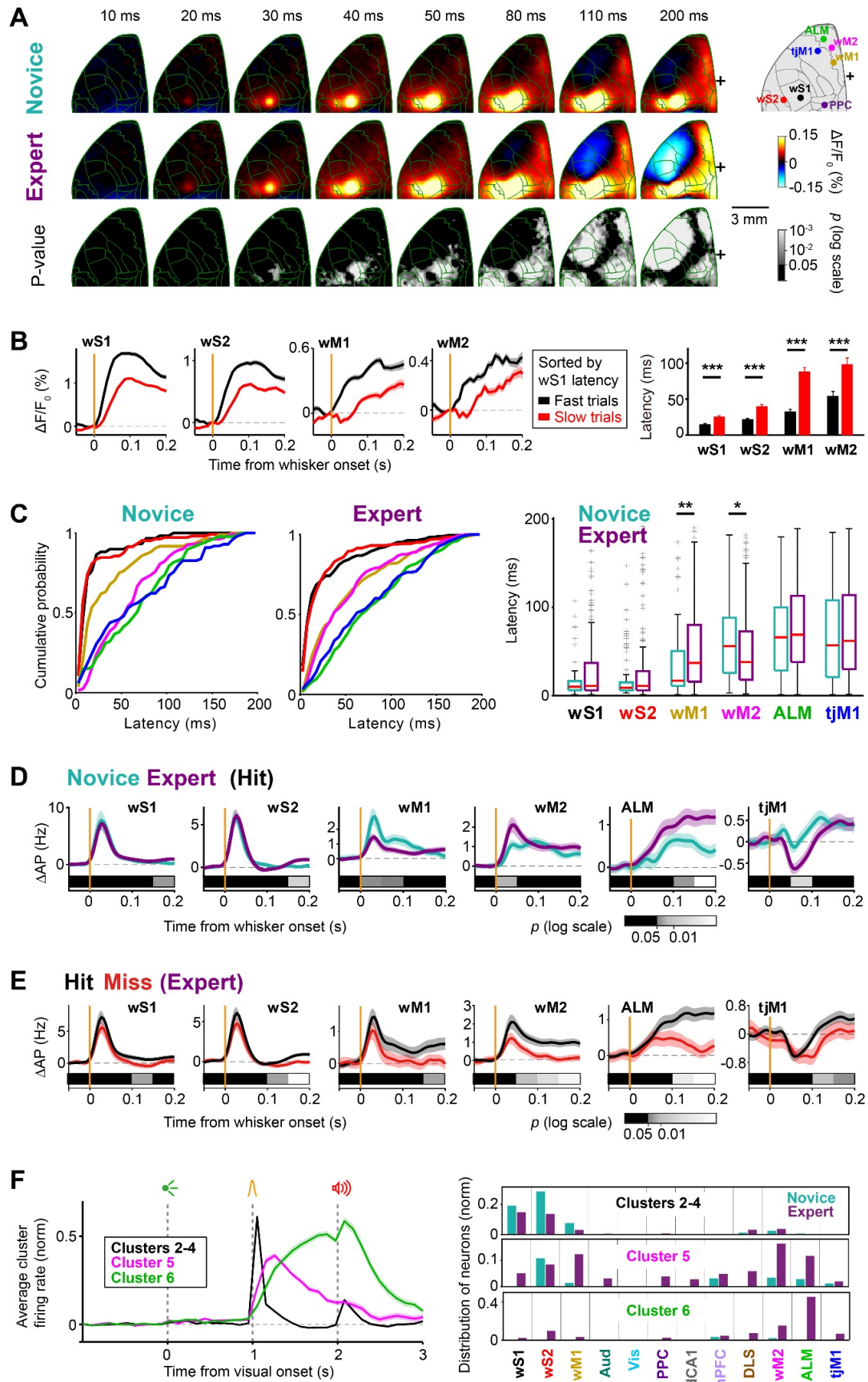


Figure 2.5. Conversion of a sensory signal into a motor plan.

(A) Wide-field signal after whisker stimulus in Novice and Expert mice in Hit trials. Each frame shows the instantaneous calcium activity (10 ms/frame). Mean signal during the 50 ms period before whisker onset is subtracted. From top to bottom, average calcium signal of 62 Novice and 82 Expert sessions from 7 mice, and the statistical significance of the difference (p -value of Wilcoxon rank-sum test, FDR-corrected).

(B) Propagation of whisker-evoked response latency to downstream regions in Expert mice (82 sessions, 7 mice). *Left*: Calcium traces (mean \pm SEM) in different regions were grouped based on single-trial response latencies in wS1. *Right*: Latencies of whisker-evoked calcium response (mean \pm SEM) in Fast and Slow trials (wS1: $p=2.2 \times 10^{-8}$, wS2: $p=1.1 \times 10^{-7}$, wM1: $p=2 \times 10^{-9}$, wM2: $p=3.3 \times 10^{-4}$; Wilcoxon signed-rank test, FDR-corrected).

(C) Latency of the whisker-evoked spiking response. Cumulative distribution of single neuron latencies for key cortical areas in Novice (*left*) and Expert (*middle*) mice. Distribution of latencies across different areas and their change across learning (*right*). Boxplots indicate median and interquartile range. Only neurons with significant modulation in the 200 ms window following whisker stimulus compared to a 200 ms window prior to the whisker stimulus are included ($p < 0.05$, non-parametric permutation test). Latency was defined at the half maximum (minimum for suppressed neurons) response within the 200 ms window.

(D) Early whisker-evoked spiking activity in Hit trials. Baseline-subtracted (200 ms prior to whisker onset) mean \pm SEM firing rate across critical cortical areas in Expert and Novice mice are overlaid. Gray horizontal bars represent the p -value of Novice/Expert comparison in 50 ms consecutive windows (non-parametric permutation test, FDR-corrected).

(E) Spiking activity in Hit vs Miss trials. Baseline-subtracted (200 ms prior to whisker onset) mean \pm SEM firing rate across critical cortical areas in Hit and Miss trials of Expert mice are overlaid. Gray horizontal bars represent the p -value of Hit/Miss comparison in 50 ms consecutive windows (non-parametric permutation test, FDR-corrected).

(F) Whisker and Delay responsive neuronal clusters, related to Figure 3C-D. *Left*, Average normalized firing rate (mean \pm SEM) of Whisker (Clusters 2, 3, and 4) and two distinct Delay clusters (Clusters 5 and 6). *Right*, Proportion of neurons within each cluster belonging to different brain regions and groups of mice, related to Figure 3D.

2.3.6 Focalized delay period activity in the frontal cortex

The most prominent cortical change after whisker training was the emergence of widespread delay period activity (Figures 2.2 and 2.3). In the late delay period, Expert mice showed uninstructed, anticipatory movements of whisker, jaw, and tongue (Figures 2.1E-F and 2.9C-D), which could be broadly correlated with activity across the brain (Musall et al., 2019; Steinmetz et al., 2019). To identify neural activities more directly related to task execution, we leveraged trial-by-trial variability of the neuronal activity and anticipatory movements (Figure 2.6).

First, we separated neural activities by selecting trials in which mice did not make jaw movements during the delay period (Quiet trials) (Figures 2.6A-B, S7A; see Methods). When only Quiet trials were considered, the increased calcium activity during the delay became more localized to ALM (Figure 2.6A). This focal activation emerged across learning (Wilcoxon rank-sum test, $p < 0.05$). Electrophysiology data

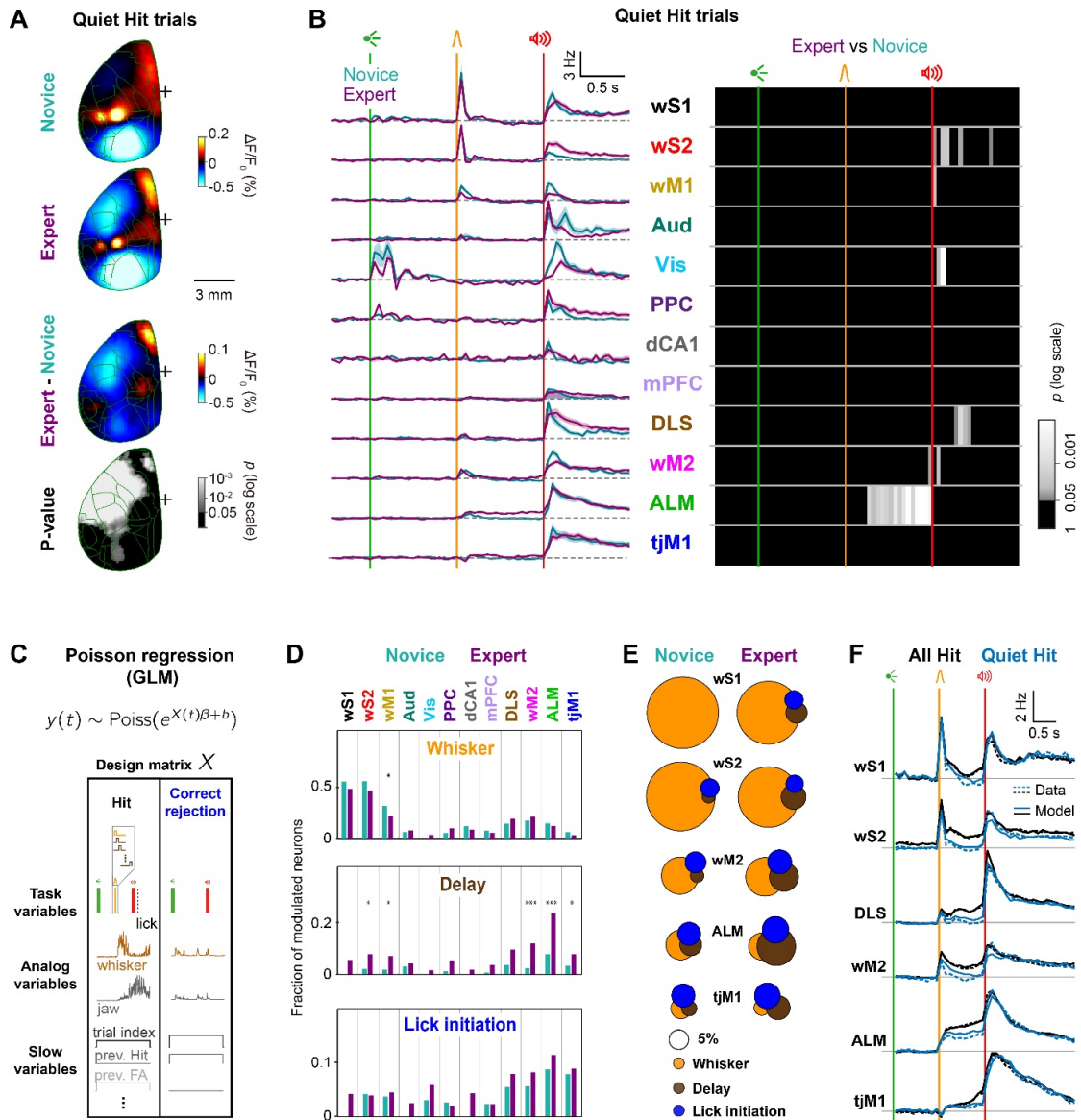


Figure 2.6. Delay processing beyond preparatory movement.

(A and B) Focalized delay activity in Quiet Hit trials. Imaging and neuronal data were averaged across selected Quiet trials with no preparatory jaw movements during the delay period (see Methods). A, Mean wide-field calcium signal in a 50 ms window during the delay period (270 to 320 ms after whisker onset) subtracted by the mean during the 50 ms period before whisker onset. From top to bottom, mean calcium signal of 62 Novice and 82 Expert sessions from 7 mice, their difference, and the statistical significance of the difference (p -value of Wilcoxon rank-sum test, FDR-corrected). B, Mean \pm SEM firing rate in Expert and Novice mice (*left*) and p -value map of Expert/Novice comparison in 50 ms non-overlapping windows (non-parametric permutation test, FDR-corrected) (*right*).

(C-F) Poisson encoding model capturing trial-by-trial neuronal variability. C, Schematic of the Poisson encoding model. Concatenated spike trains from Hit and Correct-rejection trials ($y_{(t)}$) were fitted using a Poisson regression model (GLM). The design matrix ($X_{(t)}$) included different types of task-related and movement variables (see Methods). D, Fraction of neurons significantly encoding Whisker (*top*), Delay (*middle*) and Lick initiation (*bottom*) ($p < 0.05$, likelihood ratio test, See Methods) in different regions. Asterisks represent significant change comparing the fraction of Novice and Expert neurons

(proportion test, ***: $p < 0.001$, *: $p < 0.05$). E, Venn diagrams showing the amount of overlap among neuronal populations in different regions significantly encoding Whisker, Delay and Lick initiation variables. The sizes of the circles are proportional to the fraction of significantly modulated neurons. F, Comparison of empirical (Data, dotted lines) and reconstructed (Model, solid lines) PSTHs for Quiet (blue) and all (black) trials in Expert mice.

also demonstrated a consistent localization of the neuronal delay period activity (Figure 2.6B). In Quiet Hit trials, only ALM population firing remained elevated throughout the delay period and was clearly enhanced by whisker training. In the other regions, the whisker-evoked firing during the delay period returned to baseline, just as in Novice mice. Thus, selecting Quiet trials demonstrated that the essential processing in the cortex during the delay period is localized in a focal frontal region that includes ALM.

Assessing the impact of movements considering only Quiet trials highlighted the unique activity pattern of ALM during the delay period. However, Quiet Hits represented a minority of all Hit trials in Expert mice ($42 \pm 2\%$; mean \pm SEM). Trials with movements during the delay period may carry richer information about how neuronal activity drives behavior. Therefore, to capture neuronal encoding during single trials, we used a generalized linear model (GLM) (Nelder and Wedderburn 1972) to fit a Poisson encoding model to spiking data of individual neurons including all correct trials (Park et al. 2014) (Figures 2.6C-F and 2.15B-F; see Methods). Three types of model predictors were included (Figure 2.6C): discrete task events (e.g. sequential boxcars time-locked to sensory stimuli and first lick onset); analog movement signals (whisker, tongue and jaw speed); and slow variables capturing motivational factors (e.g. current trial number) and trial history (e.g. outcome of the previous trial). We assessed fit quality using predictor-spike mutual information and selected only the neurons with a good quality of fit for the rest of analysis (Cover and Thomas 1991a; Gerstner et al. 2014a) (Figure 2.15C; see Methods). The contribution of each model variable to the neuron's spiking activity was tested by re-fitting the data after excluding the variable of interest (reduced model) and comparing the fit quality to the model including all variables (full model), using a likelihood ratio test (Figures 2.6D and 2.15D) (Buse 1982).

Whisker-related sensorimotor areas (wS1, wS2, wM1 and wM2) had the largest proportion of neurons significantly modulated by whisker stimulus in the first 100 ms, in both Novice and Expert mice (Figures 2.6D and 2.15E). The fraction of Whisker encoding neurons decreased across whisker training in wM1 ($p = 0.029$). In contrast, Delay encoding neurons - that were significantly modulated between 100 ms and 1 s after the whisker stimulus (Figures 2.6D and 2.15E) - were mainly found in ALM, but also in wM2, which was strikingly enhanced by whisker training ($p = 5 \times 10^{-5}$). Some neurons in wM2, ALM, tJM1 and DLS were found to be significantly modulated during the 200 ms prior to the lick onset, before and after whisker training (Figures 2.6D and

2.15E), reflecting the licking initiation signal in these areas beyond those captured by orofacial movements or sound onset predictors in the model.

We next asked to what extent the same neurons encode different task variables. To address this question, we quantified the degree of overlap across populations of Whisker, Delay and Lick initiation encoding neurons in the key areas of interest and visualized it using Venn diagrams (Figure 2.6E). We found that enhanced Delay and Lick initiation encoding populations were largely non-overlapping. Finally, we asked whether our encoding model, fitted using all trials, can reproduce neuronal activity in Quiet trials (Figures 2.6F and 2.15F). Model-reconstructed PSTHs after removing movement-related regressors confirmed that neurons in ALM kept their firing throughout the delay period, while the firing in other areas returned to baseline, in agreement with the empirical data. This result supports the model's validity and highlights the prominence of ALM for motor planning.

2.3.7 Temporally-specific causal contributions of different cortical regions

Imaging and electrophysiology data suggested multiple phases of neural processing for whisker detection, motor planning, and delayed licking. To examine the causal contribution of cortical regions in each of these phases, we performed spatiotemporally-selective optogenetic inactivation in transgenic mice expressing ChR2 in GABAergic neurons (n=9 VGAT-ChR2 mice). We applied blue light pulses to each brain region through an optical fiber randomly in one-third of the trials, occurring in one of the four temporal windows (Figure 2.7A): Baseline (from visual cue onset to 100 ms before whisker stimulus onset), Whisker (from 100 ms before to 200 ms after whisker stimulus onset), Delay (from 200 ms to 1000 ms after whisker stimulus onset), or Response (from 0 ms to 1100 ms after auditory cue onset).

Inactivation in different time windows provided spatiotemporal maps of the behavioral impact (Figures 2.7B-C and 2.16). During the Baseline window, a significant decrease in Hit rate occurred after the inactivation of Vis, dCA1, and mPFC (Light-off versus Light, Vis: $p=0.031$, dCA1: $p=0.016$, mPFC: $p=0.031$; Wilcoxon signed-rank test). During the Whisker window, a significant decrease in Hit rate occurred in every region tested with the strongest impact in wS2 (Light-off versus Light, $p=0.016$; Wilcoxon signed-rank test). During the Delay period, the inactivation of ALM and mPFC produced a strong reduction in Hit rate (Light-off versus Light, ALM: $p=0.016$, mPFC: $p=0.016$; Wilcoxon signed-rank test). Finally, during the Response window, when the licking behavior had to be executed, inactivation of tongue-related tJM1 and ALM, but also whisker-related wM2, impaired behavior by decreasing both Hit and False-alarm rate (Light-off versus Light, tJM1: $p=0.016$, ALM: $p=0.016$, wM2: $p=0.016$; Wilcoxon

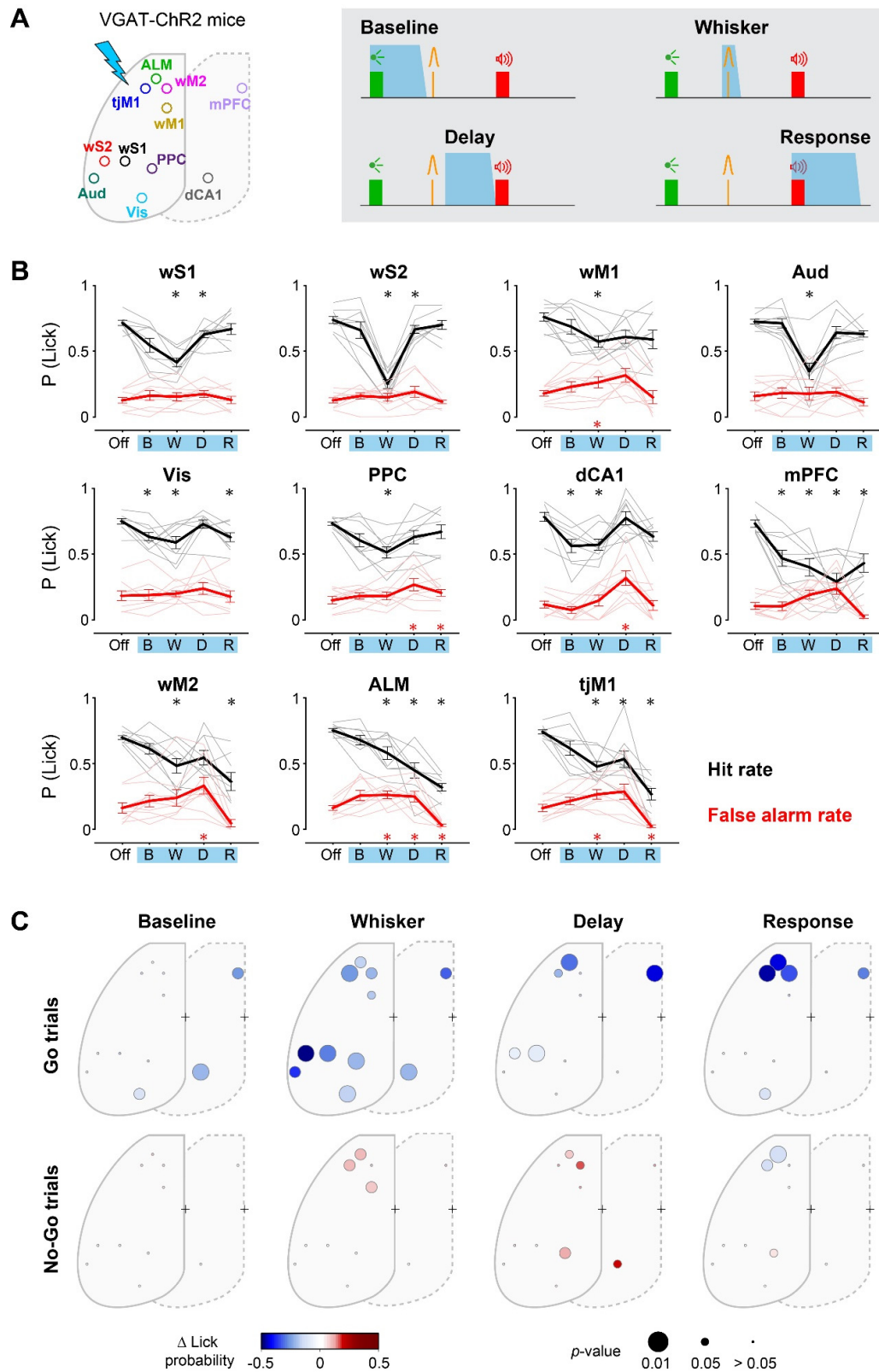


Figure 2.7. Spatiotemporal causal map of behavioral impact.

(A) Spatiotemporally specific optogenetic inactivation in VGAT-ChR2 transgenic mice. Blue shaded areas represent inactivation windows across the trial-timeline.

(B) Behavioral impact of optogenetic inactivation across time windows for each brain region (mean \pm SEM). For each area, Hit rate (black) and False-alarm rate (red) are plotted for Light-off (Off), Baseline (B), Whisker (W), Delay (D) and Response (R) windows. Asterisks represent significant difference comparing Hit (black) or False-alarm (red) in light trials vs light-off trials (n=9 mice; *, $p < 0.05$; Wilcoxon signed-rank test, Bonferroni correction for multiple comparison).

(C) Spatiotemporal map of behavioral impact of focal inactivation in Go (*top*) and No-Go trials (*bottom*). Circles represent different cortical regions labeled on the schematic in Panel A; color shows change in Lick probability and circle size shows the p -value of the significance test comparing light trials vs light-off trials (n=9 mice, Wilcoxon signed-rank test, Bonferroni correction for multiple comparison).

signed-rank test), supporting the causal involvement of the lick initiation-encoding of wM2 neurons (Figure 2.6D). The differential impact of inactivating nearby cortical regions is consistent with the high spatiotemporal specificity of our optogenetic manipulations. Inactivation during the Whisker and Delay periods also broadly reduced the fraction of premature licking and reduced preparatory movements, with spatiotemporal specificities relatively similar to those observed in Hit rate changes (Figure 2.16). Thus, spatiotemporal mapping of causal impacts suggests that critical whisker processing is initially distributed across diverse cortical regions, and then converges in frontal regions for planning lick motor output, in agreement with neural activity.

To directly compare the obtained causal maps with observed neural correlations, we quantified the difference in firing rate between Hit versus Correct-rejection and the change in Hit rate upon optogenetic inactivation, for each brain area and time window (Figure 2.8A). If a brain region is critically involved in task execution, neural activity in that area would code behavioral decision (large Hit-Correct rejection difference), and its inactivation would cause behavioral impairments (strong decrease in Hit rate). This is further quantified by an involvement index as the product of the two terms described above (Figure 2.8B). The involvement index during the Whisker period was largest in wS2 and wS1 (mean \pm SEM, wS2: 0.7 ± 0.11 , $p < 0.01$, wS1: 0.58 ± 0.11 , $p < 0.05$; non-parametric permutation test versus other areas) highlighting these areas as the main nodes of whisker sensory processing. During the Delay period, ALM had the largest involvement index (mean \pm SEM, ALM: 0.48 ± 0.09 , $p < 0.001$; non-parametric permutation test versus other areas). Although, mPFC inactivation during the delay provoked the largest reductions in hit rate, there was little change in neuronal activity in this area, resulting in small involvement values. The most critical areas in the Response window were tjM1 and ALM (mean \pm SEM, tjM1: 1.16 ± 0.15 , $p < 3 \times 10^{-5}$, ALM: 0.76 ± 0.09 , $p < 0.05$; non-parametric permutation test versus other areas). This reflects the prominent role of tjM1 in licking execution. Interestingly, wM2 had a moderate but significant involvement index in all three time-windows, supporting its possible role in bridging sensory processing and motor execution.

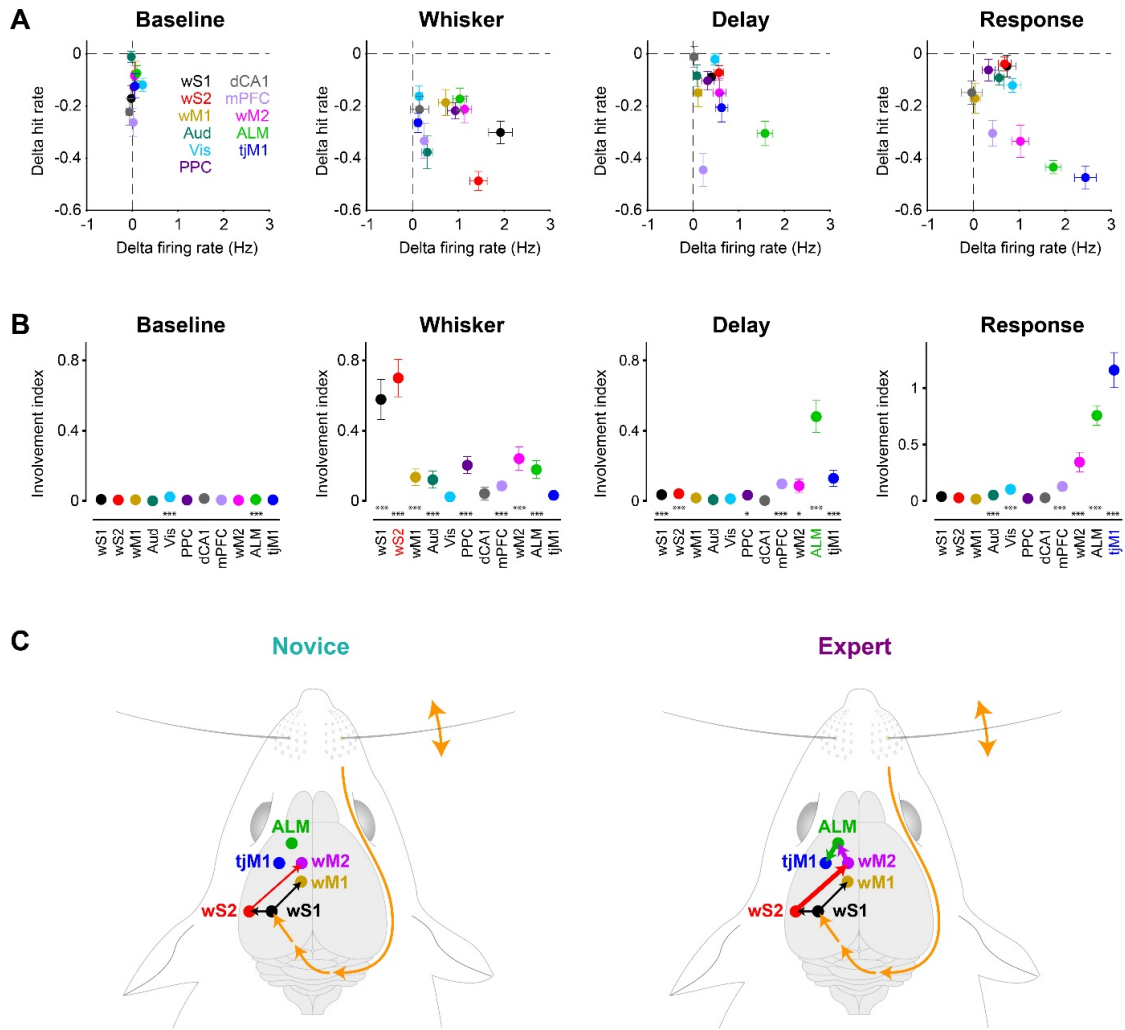


Figure 2.8. Task-epoch specific involvement of cortical regions.

(A) Trial specific neural firing versus the behavioral impact of inactivation. Firing rate difference in Hit vs Correct-rejection trials ($n=22$, Expert mice) in each time window is plotted against the change in hit rate upon optogenetic inactivation ($n=9$, VGAT-ChR2 mice). Temporal windows are defined similarly to Figure 7. Circles represent mean values in different areas; horizontal and vertical error bars show SEM.

(B) A causal involvement index was defined as the region- and epoch-specific absolute value of the difference in firing rate comparing Hit and Correct-rejection trials ($n=22$, Expert mice) multiplied by the change in hit rate induced by optogenetic inactivation ($n=9$, VGAT-ChR2 mice). Error bars are obtained from bootstrap (see Methods) and represent standard deviation (bootstrap standard error). Asterisks represent significance level (*, $p<0.05$; ***, $p<0.001$; non-parametric permutation test, Bonferroni correction for multiple comparison).

(C) Proposed cortical circuits connecting whisker somatosensory cortex to tongue/jaw motor cortex upon task learning.

2.4 Discussion

We found converging evidence for the temporally distinct involvement of diverse cortical regions in delayed sensorimotor transformation using an array of complementary technical approaches. Our analyses of the learning-induced changes in causal neural activity revealed three key findings further discussed below: i) widespread neuronal delay-period activity was dominated by preparatory movements, but essential causal neuronal delay-period activity was predominantly localized to ALM; ii) sequential activation of cortical regions wS1, wS2, wM2, and ALM suggests the possible contribution of a corticocortical pathway for whisker sensory information to reach ALM, with wM2 showing the earliest increase in sensory-evoked response across learning; and iii) suppression of orofacial sensorimotor cortex in the early delay period, likely contributing to inhibition of premature licking.

2.4.1 Essential cortical delay period activity in ALM

Broad regions of the cortex showed elevated activity in Expert mice during the delay period in Hit trials (Figures 2.2 and 2.3), correlating with preparatory movements (Figures 2.1 and 2.6). These results are thus in good agreement with widespread motor-related cortical activity (Musall et al., 2019; Steinmetz et al., 2019; Stringer et al., 2019). When we analyzed only trials free from the delay period preparatory movements, wide-field imaging, and electrophysiology demonstrated a localized excitatory activity in a small region of the secondary motor cortex including ALM (Figure 2.6A-B). Inactivation of ALM during the delay period was highly effective in reducing hit rates in the subsequent Response period (Figure 2.7). Essential causal neuronal delay period activity, therefore, appears to be predominantly localized to ALM (Figure 2.8A-B), in good agreement with previous closely-related tasks (Guo et al. 2014; Li et al. 2015).

By accounting for movement contributions using linear regression analysis of trial-by-trial variability, we found that most delay period-responsive neurons were indeed localized in ALM, but that the fraction of delay encoding neurons was also significantly enhanced by learning in wS2, wM1, wM2, and tjM1 (Figure 2.6C-E). Furthermore, during the delay period, the inactivation of several cortical areas including not only ALM but also wS1, wS2, mPFC, and tjM1 significantly reduced hit rates (Figure 2.7). Indeed, causal contributions to the Delay period measured by the Involvement Index were also significant in wS1, wS2, PPC, mPFC, wM2, and tjM1, as well as ALM. In addition to the strongest causal involvement found for ALM, these causal impacts observed in broader cortical areas during the delay period might in part result from reduced preparatory movements induced by inactivation (Figure 2.16B-C). The

preparatory movements, which were most prominent in Hit trials of Expert mice, may thus contribute a form of embodied sensorimotor memory in which ongoing movements might help maintain a plan for delayed licking (Mayrhofer et al., 2019).

During the Delay period, mPFC inactivation had the largest impact on the hit rate across the tested areas (Figure 2.7). However, we did not find robust sustained activity in mPFC during this window for maintenance of the motor plan. Interestingly, mPFC inactivation during all task epochs (including baseline) impaired behavior. One possibility is that the observed behavioral effect relates to the representation of task rules (Durstewitz et al. 2010), behavioral strategy (Powell and Redish 2016), or motivation (Popescu et al. 2016).

2.4.2 A putative corticocortical signaling pathway linking sensory to the motor cortex through learning

Our measurements at high spatiotemporal resolution revealed a rapid sequential activation of cortical areas evoked by whisker-deflection, ultimately reaching ALM in Hit trials of Expert mice. The earliest cortical response to whisker stimulus occurred in wS1 and wS2, which changed relatively little after whisker training (Figures 2.2, 2.3, and 2.5). This initial processing was essential as shown by optogenetic inactivation (Figure 2.7), and therefore wS1 and wS2 appear to form the cortical starting points for task execution, in agreement with previous studies of whisker detection tasks without a delay period (Miyashita and Feldman 2013; Sachidhanandam et al. 2013; Kwon et al. 2016; Yang et al. 2016; Kyriakatos et al. 2017; Le Merre et al. 2018).

Sensory cortical areas project directly and strongly to the frontal cortex through parallel pathways, with wS1 innervating wM1, and wS2 innervating wM2 (Ferezou et al. 2007; Mao et al. 2011; Oh et al. 2014; Sreenivasan et al. 2017). Whisker-deflection evoked rapid sensory responses in these downstream motor regions. Interestingly, the sensory response in wM2 showed the earliest significant increase in whisker-evoked firing and a decrease in response latency across learning (Figure 2.5C-D), whereas a decrease in amplitude and increase in latency was found in wM1. Neuronal activity in wM2 also showed the earliest choice-related activity when comparing Hit and Miss trials (Figure 2.5E). Thus, wM2 might serve as a key node in the corticocortical network to begin the process of converting a whisker sensory stimulus into longer-lasting preparatory neuronal activity. Shortly after wM2 activation, ALM, an important premotor area for control of licking (Guo et al., 2014; Li et al., 2015; Mayrhofer et al., 2019), started to increase firing (Figure 2.5). Through cortico-cortical connectivity (Luo et al. 2019), activity in wM2 could contribute directly to exciting its neighbor region ALM, which manifested the most prominent delay period activity through whisker training

(Figures 2.3 and 2.6), consistent with previous studies (Chen et al., 2017; Li et al., 2015).

Our results suggest a hypothesis for a minimal cortical network connecting whisker sensory coding to preparatory neuronal activity for motor planning: a pathway $wS1 \rightarrow wS2 \rightarrow wM2 \rightarrow ALM$ could be the main stream of signal processing (Figure 2.8C). Some of the most prominent whisker-related changes through whisker training occurred in $wM2$ and ALM , and it is possible that reward-related potentiation of synaptic transmission between $wS2 \rightarrow wM2$ and $wM2 \rightarrow ALM$ could underlie important aspects of the present learning paradigm. All of these cortical areas are likely to be connected through reciprocal excitatory long-range axonal projections, which could give rise to recurrent excitation helping to prolong firing rates of neurons in relevant brain regions during the delay period of Hit trials. Interestingly, in a related whisker detection task without a delay period, enhanced reciprocal signaling between $wS1$ and $wS2$ has already been proposed to play an important role (Kwon et al. 2016; Yamashita and Petersen 2016). It is also important to note that a large number of subcortical structures are also likely to be involved in task learning and performance including the thalamus (Guo et al. 2017; El-Boustani et al. 2020), basal ganglia (Sippy et al., 2015) and cerebellum (Gao et al. 2018; Chabrol et al. 2019).

2.4.3 Lick and No-Lick signals in $tjM1$

In Expert mice, we found that the whisker stimulus evoked a sharp deactivation broadly across the orofacial sensorimotor cortex, including $tjM1$, an area thought to be involved in the initiation and control of licking (Mayrhofer et al., 2019). In contrast, $tjM1$ neurons were activated soon after whisker deflection in a previous study of a detection task without a delay period before licking (Mayrhofer et al., 2019). One interesting possibility is thus that the deactivation in $tjM1$ develops through the learning of a task where suppression of immediate licking is demanded. In support of this hypothesis, here, we found that premature early licking during the delay period was accompanied by reduced suppression of $tjM1$ (Figure 2.4B), and that activation of $tjM1$ increased early licks whereas inactivation of $tjM1$ reduced early licks (Figure 2.4C). We furthermore found that $tjM1$ activity was suppressed after the auditory cue in Correct-rejection trials where mice are supposed to suppress licking, compared to Miss trials where mice failed to lick, suggesting that the reduction of activity in the orofacial cortex reflects active response inhibition (Figure 2.4D). Finally, the inactivation of $tjM1$ in the Response window evoked the strongest decrease in hit rates further supporting the causal involvement of this area in the control of licking (Figure 2.7).

Previous studies in human subjects have suggested the importance of inhibitory mechanisms for preventing actions from being emitted inappropriately (Chikazoe et al.

2009; Duque et al. 2017). Parallel suppression and activation during a delay period might be a common principle of response preparation preserved across species (Cohen et al. 2010). Here, we reveal causal contributions of inhibitory and excitatory cortical delay period activity in a precisely-defined task, and, as a hypothesis, we put forward a specific corticocortical circuit that could contribute to task learning and execution, requiring future further experimental testing.

2.5 Methods

2.5.1 Experimental model and subject details

All procedures were approved by Swiss Federal Veterinary Office (License number VD-1628) and were conducted in accordance with the Swiss guidelines for the use of research animals. For calcium imaging, we produced RCaMP mice by crossing Emx1-IRES-Cre mice [B6.129S2-Emx1^{<tm1(cre)Kj>}/J, JAX: 005628] (Gorski et al. 2002), CaMK2-tTA mice [B6.Cg-Tg(Camk2a-tTA)1Mmay/DboJ, JAX: 007004] (Mayford et al. 1996), and TITL-R-CaMP mice [TIGRE1.0-RCaMP, B6.Cg-Igs7^{<tm143.1(tetO-RCaMP1.07)Hze>}/J, JAX: 030217, kind gift from Fritjof Helmchen (University of Zurich)] (Bethge et al. 2017). For control imaging, we produced tdTomato mice by crossing VIP-IRES-Cre mice [STOCK Vip^{<tm1(cre)Zjh>}/J, JAX: 010908] (Taniguchi, He, Wu, Kim, Paik, Sugino, Kvitsiani, Fu, et al. 2011) and LSL-tdTomato mice [B6.Cg-Gt(ROSA)26Sor^{<tm9(CAG-tdTomato)Hze>}/J, JAX: 007909] (Madisen et al. 2010). For optogenetic activation, we produced Emx1-ChR2 mice by crossing Emx1-IRES-Cre mice, LSL-ChR2(H134R)-EYFP mice [B6;129S-Gt(ROSA)26Sor^{<tm32(CAG-COP4*H134R/EYFP)Hze>}/J] (Madisen et al. 2012) and RCaMP mice. For optogenetic inactivation, we used VGAT-ChR2 mice [B6.Cg-Tg(Slc32a1-COP4*H134R/EYFP)8Gfng/J, JAX: 014548] (Zhao et al., 2011). For electrophysiological recording, we used C57BL/6 wild type mice, and VGAT-ChR2 mice, as well as A2A-Cre mice [B6.FVB(Cg)-Tg(Adora2a-cre)KG139Gsat/Mmucd, MMRRC: 036158] (Gong et al. 2007) crossed with LSL-tdTomato mice. Adult male and female mice were at least 6 weeks old at the time of head-post implantation (see below). Mice were kept in a reverse light/dark cycle (light 7 p.m. to 7 a.m.), in ventilated cages at a temperature of 22 ± 2°C with food available ad libitum. Water was restricted to 1 ml a day during behavioral training with at least 2 days of free access to water in the cage every 2 weeks. All mice were weighed and inspected daily during behavioral training.

2.5.2 Experimental design

This study did not involve randomization or blinding. We did not estimate sample-size before carrying out the study. However, the sample-size in this study is comparable with those used in related studies (Harvey et al. 2012; Guo et al. 2014a; Allen et al. 2017; Hattori et al. 2019; Pinto et al. 2019; MacDowell and Buschman 2020).

2.5.3 Implantation of metal headpost

Mice were deeply anesthetized with isoflurane (3% with O₂) and then were maintained under anesthesia using a mixture of ketamine and xylazine injected intraperitoneally (ketamine: 125 mg/kg, xylazine: 10 mg/kg). Carprofen was injected intraperitoneally (100 µl at 0.5 mg/ml) for analgesia before the start of surgery. Body temperature was kept at 37°C throughout the surgery with a heating pad. An ocular ointment (VITA-POS, Pharma Medica AG, Switzerland) was applied over the eyes to prevent them from drying. As a local analgesic, a mix of lidocaine and bupivacaine was injected below the scalp before any surgical intervention. A povidone-iodine solution (Betadine, Mundipharma Medical Company, Bermuda) was used for skin disinfection. To expose the skull, a part of the scalp was removed with surgical scissors. The periosteal tissue was removed with cotton buds and a scalpel blade. After disinfection with Betadine and rinsing with Ringer solution, the skull was dried well with cotton buds. A thin layer of super glue (Loctite super glue 401, Henkel, Germany) was then applied across the dorsal part of the skull and a custom-made head fixation implant was glued to the right hemisphere without a tilt and parallel to the midline. A second thin layer of the glue was applied homogeneously on the left hemisphere. After the glue had dried, the head implant was further secured with self-curing denture acrylic (Paladur, Kulzer, Germany; Ortho-Jet, LANG, USA). For electrophysiological recordings a chamber was made by building a wall with denture acrylic along the edge of the bone covering the left hemisphere. Particular care was taken to ensure that the left hemisphere of the dorsal cortex was free of denture acrylic and only covered by super glue for optical access. This intact, transparent skull preparation was used to perform wide-field calcium imaging as well as intrinsic optical signal imaging (IOS) experiments. Mice were returned to their home cages and ibuprofen (Algifor Dolo Junior, VERFORA SA, Switzerland) was added to the drinking water for three days after surgery.

2.5.4 Skull preparation and craniotomies

For wide-field calcium imaging and optogenetic activation, an intact transparent skull was used as described above. For electrophysiological recordings, up to 10 small craniotomies were made over the regions of interest using a dental drill under isoflurane anesthesia (2-3% in O₂). The craniotomies were protected using a silicon elastomer (Kwik-Cast, World Precision Instruments, Sarasota, FL, USA). Regions of interest were selected based on the hotspots of activity from wide-field calcium imaging experiments, and functionally relevant areas based on previous studies (Esmaeili and Diamond, 2019; Guo et al., 2014; Harvey et al., 2012; Le Merre et al., 2018; Mayrhofer et al., 2019; Sachidhanandam et al., 2013; Sippy et al., 2015; Sreenivasan et al., 2016) and IOS imaging (Lefort et al. 2009). IOS was performed under isoflurane anesthesia

(1-1.5% with O₂) to map the C2-whisker representation in the primary and secondary whisker somatosensory cortex (wS1 and wS2), as well as the auditory area (Aud). A piezoelectric actuator was used to vibrate the right C2 whisker, or to generate rattle sounds. An increase in absorption of red light (625 nm) upon sensory stimulation indicated the functional location of the corresponding sensory cortex. For the other regions stereotaxic coordinates relative to bregma were used: primary and secondary whisker motor cortices (wM1: AP 1.0 mm; Lat 1.0 mm and wM2: AP 2.0 mm; Lat 1.0 mm), primary and secondary tongue/jaw motor cortices (tjM1: AP 2.0 mm; Lat 2.0 mm and ALM: AP 2.5 mm; Lat 1.5 mm), visual cortex (Vis: AP -3.8 mm; Lat 2.5 mm), posterior parietal cortex (PPC: AP -2 mm; Lat 1.75 mm), medial prefrontal cortex (mPFC: AP 2 mm; Lat 0.5 mm), dorsal part of the CA1 region of the hippocampus (dCA1: AP -2.7 mm; Lat 2.0 mm) and dorsolateral striatum (DLS: AP 0.0 mm; Lat 3.5 mm). For optogenetic inactivation experiments, the bone over the regions of interest was thinned and a thin layer of superglue was applied to protect the skull for stable optical access over days. For the inactivation of mPFC and dCA1 a small craniotomy was made for the insertion of an optical fiber or an optrode.

2.5.5 Behavioral paradigm

A total of 55 mice were examined in the delayed whisker detection task including 9 RCaMP, 24 wild-type or negative, 6 Emx1-ChR2, 9 VGAT-ChR2 and 7 tdTomato mice. During the behavioral experiments, all whiskers were trimmed except for the C2 whiskers on both sides, and the mice were water restricted to 1 ml of water/day. Mice were trained daily with one session/day and their weight and general health status were carefully monitored using a score sheet. Both groups of mice (Expert and Novice) went through a Pretraining phase which consisted of trials with visual and auditory cues (without any whisker stimulus) (Figure 2.1C). Mice were rewarded by licking a spout, placed on their right side, in a 1-second response window after the auditory cue onset. Trials were separated 6-8 seconds and started after a quiet period of 2-3 seconds in which mice did not lick the spout. Each trial consisted of a visual cue (200 ms, green LED) and an auditory cue (200 ms, 10 kHz tone of 9 dB added on top of the continuous background white noise of 80 dB). The stimuli were separated with a delay period which gradually was increased to 2 seconds over Pretraining days. Licking before the response period (Early lick) aborted the trial and introduced a 3-5 second timeout. After 3-6 days of Pretraining, mice learned to lick the spout by detecting the auditory cue and to suppress early licking.

The wide-field imaging and electrophysiological recordings from the Novice group of mice was performed when mice finished the Pretraining phase and were introduced to the whisker delay task (Figure 2.1C). In this phase, a whisker stimulus (10 ms cosine

100 Hz pulse through a glass tube attached to a piezoelectric driver) was delivered to the right C2 whisker 1 second after the visual cue onset in half of the trials. Importantly, the reward was available only in trials with the whisker stimulus (Go trials), and time-out punishment (together with an auditory buzz tone) was given when mice licked in trials without the whisker stimulus (No-Go trials) (Figure 2.1B). Thus, mice were requested to use the whisker stimulus to change their lick/no-lick behavior. Since the whisker stimulus was weak, Novice mice continued licking in most of Go and No-Go trials irrespective of the whisker stimulus and did not show any sign of whisker learning (Figure 2.1D and 2.9B).

The Expert mice entered a Whisker-training phase of 2-29 days during which a stronger whisker stimulus (larger amplitude and/or train of pulses) and shorter delays (for some mice) was introduced (Figure 2.9A). As the mice learned to lick correctly, the whisker stimulus amplitude was gradually returned to a smaller amplitude and delay was extended to 1 second, eventually matching the conditions in Novice mice. Expert mice decreased licking in No-Go trials but increased their premature early licks after the whisker stimulus, as monitored by the piezoelectric lick sensor (Figure 2.1D, see below). Behavioral hardware control and data collection were carried out using data acquisition boards (National Instruments, USA) and custom-written Matlab codes (MathWorks).

2.5.6 Quantification of orofacial movements

Contacts of the tongue with the reward spout were detected by a piezo-electric sensor. Continuous movements of the left C2 whisker, tongue and jaw were filmed by a high-speed camera (CL 600 X 2/M, Optronis, Germany; 200 or 500 Hz frame rate, 0.5- or 1 ms exposure, and 512x512-pixel resolution) under blue light or infrared illumination. Movements of each body part were tracked using custom-written Matlab codes. For the imaging sessions, arc regions-of-interest were defined around the basal points for both the whisker and jaw (Mayrhofer et al., 2019). Crossing points on these arcs were detected for the whisker (the pixels with the minimum intensity) and the jaw (pixels with the maximum slope of intensity). A vector was then defined for each pair of basal point and the cross point, and the absolute angle was calculated for each vector with respect to the midline. For the electrophysiology sessions, whisker angular position was quantified in a similar manner while movements of tongue and jaw were quantified as the changes in mean image intensity within rectangular regions-of-interest (ROI) defined separately on the tracks of tongue and jaw. These signals were then normalized to the area covered by tongue and jaw ROIs. Absolute derivatives of orofacial time series (whisker/jaw/tongue speed) were calculated to derive angular whisker speed and normalized tongue/jaw speed.

2.5.7 Wide-field calcium imaging

Mice were mounted with a 24-degree tilt along the rostro-caudal axis. The red fluorescent calcium indicator R-CaMP1.07 or the red fluorescent protein tdTomato were excited with 563-nm light (567-nm LED, SP-01-L1, Luxeon, Canada; 563/9-nm band pass filter, 563/9 BrightLine HC, Semrock, USA) and red emission light was detected through a band pass filter (645/110 ET Bandpass, Semrock). A dichroic mirror (Beamsplitter T 588 LPXR, Chroma, USA) was used to separate excitation and emission light. Through a face-to-face tandem objective (Nikkor 50 mm f/1.2, Nikon, Japan; 50 mm video lens, Navitar, USA) connected to a 16-bit monochromatic sCMOS camera (ORCA FLASH4.0v3, Hamamatsu Photonics, Japan), images of the left dorsal hemisphere were acquired with a resolution of 256x320-pixels (4x4 binning) aligned in rostro-caudal axis at a frame rate of 100 Hz (10 ms exposure). Behavioral task and imaging were synchronized by triggering the acquisition of each image frame by digital pulses sent by the computer for behavioral task control. For each trial, 600 frames (6 seconds) of images were acquired from 1 second before the visual cue onset to 3 seconds after the auditory cue onset. To control for calcium-independent changes in cortical fluorescence (Makino et al. 2017), we imaged transgenic mice expressing tdTomato in vasoactive intestinal peptide-expressing neurons (tdTomato mice) by using the same optical filters as the imaging of RCaMP. tdTomato had excitation and emission spectra similar to RCaMP, and the illumination condition was adjusted so that tdTomato mice and RCaMP mice had comparable fluorescence intensity.

2.5.8 Electrophysiological recording

Extracellular spikes were recorded using single-shank silicon probes (A1x32-Poly2-10mm-50 s-177, NeuroNexus, MI, USA) with 32 recording sites covering 775 μm of the cortical depth. In each session two probes were inserted in two different brain targets acutely. Probes were coated with Dil (1,1'-Diocetadecyl-3,3,3',3'-Tetramethylindocarbocyanine Perchlorate, Invitrogen, USA) for post-hoc recovery of the recording location (see below). The neural data were filtered between 0.3 Hz and 7.5 kHz and amplified using a digital headstage (CerePlex™ M32, Blackrock Microsystems, UT, USA). The headstage digitized the data with a sampling frequency of 30 kHz. The digitized signal was transferred to our data acquisition system (CerePlex™ Direct, Blackrock Microsystems, UT, USA) and stored on an internal HDD of the host PC for offline analysis.

2.5.9 Optogenetic manipulations

Optogenetic activation of tJM1 was performed in 6 Expert Emx1-ChR2 mice with the same transparent skull preparation and 24-deg tilt as the wide-field imaging. 473-nm laser beam (S1FC473MM, Thorlabs) was steered on the cortex by a pair of Galvo mirrors (GVS202, Thorlabs) (Mayrhofer et al., 2019) connected to the wide-field imaging system via a short-pass beam splitter (F38-496SG, Semrock). In a random half of Go and No-Go trials, a single brief laser pulse (duration, 2 ms; diameter, ~ 400 μ m; power, 1.5, 3, 4.5, 6, or 9 mW, randomly selected) was delivered to the tJM1 (2.6 mm lateral and 1.8 mm anterior to the bregma in 24-deg tilt) (Mayrhofer et al., 2019) at 1050 ms after the visual stimulus onset, at which time the neuronal firing in tJM1 showed the maximal suppression in Hit trials. In the other half of trials, the laser pulse with the same parameters was delivered to the edge of the implant as a control stimulation so that mice could not discriminate tJM1-stimulated and non-stimulated trials by visual cues. Both spontaneous and optogenetically evoked Early licks led to trial abortion with time-out, thus preventing any reinforcement of Early licks.

Optogenetic inactivations were performed in 9 Expert VGAT-ChR2 mice. An ambient blue masking light was used in the training sessions as well as testing days. Testing sessions started when mice reached Expert levels of performance ($d\text{-prime} > 1$). All the areas of interest were examined in each mouse by inactivating one area per session. The order for the areas was randomized across mice, but inactivations of deep areas (mPFC and dCA1) were performed last. Three sessions per superficial area were performed in each mouse, followed by one session for each deep area. An optic fiber (400 μ m; NA = 0.39, Thorlabs) coupled to a 470 nm high power LED (M470F3, Thorlabs, USA) was positioned in contact to the thinned bone for superficial areas or inserted above the left dCA1 at a depth of 1000 μ m below the pia. In a subset of mice, dCA1 inactivation was performed using an optrode (silicon probe with an attached optical fiber: 100 μ m; NA = 0.22, A1x32-Poly3-10mm-50 s-177-OA32, NeuroNexus, MI, USA). A similar optrode was used for all mPFC inactivations by inserting the tip of the fiber at a depth of 1700 μ m, just above the prelimbic area of mPFC. The optrodes were connected to a blue Laser (MBL-F-473/200mW, GMP SA, Switzerland).

Light trials were randomly interleaved with light-off control trials and made up 1/3 of Go and No-Go trials. On light trials, a 100 Hz (40 Hz with laser) train of blue light pulses (50-65% duty cycle, mean power 8-10 mW) was applied in one of the 4 possible windows: *Baseline* (from visual cue onset to 800 ms after), *Whisker* (from 100 ms before the whisker onset to 100 ms after), *Delay* (from 200 ms after the whisker onset to 900 ms after) and *Response* (from auditory cue onset to 1000 ms after). All light windows were terminated by an additional 100 ms ramping down to prevent rebound excitation. In total, 21,293 light trials were tested in 9 mice, 11 areas and 4 trial epochs. On average, for each area and trial epoch, 60.7 ± 6.6 (mean \pm SD) light trials were

delivered for superficial areas in each mouse across 3 sessions; for deep areas (i.e. mPFC and dCA1), 22.4 ± 4 light trials were examined in one session.

2.5.10 Histology and localization of electrode/optical fiber tracks

At the end of experiments mice were perfused with phosphate buffered saline (PBS) followed by 4% paraformaldehyde (PFA, Electron Microscopy Science, USA) in PBS. The brain was post-fixed overnight at room temperature. Expression of RCaMP was observed by epifluorescence microscope in serial 100- μ m coronal sections cut by a conventional vibratome (VT 1000S; Leica, Wetzlar, Germany). The Dil track of silicon probes were identified with either two-photon tomography (Mayrhofer et al., 2019) or conventional histological analysis. For three-dimensional imaging with two photon tomography, we embedded the brains in 3-5 % oxidized agarose (Type-I agarose, Merck KGaA, Germany) and covalently cross-linked the brain to the agarose by incubating overnight at 4 °C in 0.5 – 1 % sodium borohydride (NaBH_4 , Merck KGaA, Germany) in 0.05 M sodium borate buffer. We imaged the brains in a custom-made two-photon serial microscope, which was controlled using Matlab-based software (ScanImage 2017b, Vidrio Technologies, USA) and BakingTray (<https://github.com/BaselLaserMouse/BakingTray>, version master: 2019/05/20, extension for serial sectioning) (Han et al. 2018a). The setup consists of a two-photon microscope coupled with a vibratome (VT1000S, Leica, Germany) and a high-precision X/Y/Z stage (X/Y: V-580; Z: L-310, Physik Instrumente, Germany). The thickness of a physical slice was set to be 50 μ m for the entire brain and we acquired optical sections at 25 μ m using a high-precision piezo objective scanner (PIFOC P-725, Physik Instrumente, Germany) in two channels (green channel: 500 – 550 nm, ET525/50, Chroma, USA; red channel: 580 – 630 nm, ET605/70, Chroma, USA). Each section was imaged by 7 % overlapping 1025x1025- μ m tiles. A 16x water immersion objective lens (LWD 16x/0.80W; MRP07220, Nikon, Japan), with a resolution of 1 μ m in X and Y and measured axial point spread function of ~ 5 μ m full width at half maximum. After image acquisition, the raw images were stitched using a Matlab-based software (StitchIt, <https://github.com/BaselLaserMouse/StitchIt>). The stitched images were then down-sampled by a factor of 25 in X and Y obtaining a voxel size of 25 x 25 x 25 μ m, using a Matlab-based software (MaSIV, <https://github.com/alexanderbrown/masiv>) to match the Allen Mouse Common Coordinate Framework version 3 (Wang et al., 2020). We used a Matlab-based software (ARA tools, https://github.com/SainsburyWellcomeCentre/ara_tools) (Han et al. 2018a) to register brain volumes and probe locations to the Allen mouse brain atlas. For some brains with Dil tracks, 100 μ m-thick serial sections were cut on a conventional vibratome. The slices were then mounted and imaged under a fluorescence microscope (Leica DM5500). Matlab-based software (Allen CCF tools, <https://github.com/cortex->

[lab/allenCCF](#)) was used to register brain slices and probe locations to Allen mouse brain atlas (Shamash et al. 2018a).

2.5.11 Wide-field imaging data

Sessions in which the difference between the Hit rate and False-alarm rate was larger than 0.1 (for Novice) and smaller than 0.2 (for Expert) were excluded from further analysis. In total, 62 Novice sessions and 82 Expert sessions from 7 RCaMP mice, and 57 Expert sessions from 7 tdTomato mice were used for analysis. Acquired images were down-sampled to 77x96 pixels (111 μm /pixel). For each trial, we calculated the normalized signal intensity of each pixel as $\Delta F/F_0 = (F - F_0)/F_0$, where F is the intensity of a pixel in each frame, and F_0 is the mean intensity of that pixel during the 1 second baseline period before the onset of the visual cue. In each imaging session, mean $\Delta F/F_0$ images for different trial outcomes (Hit, Miss, False-alarm and Correct-rejection trials) were calculated by averaging all trials in each trial type, or by averaging “Quiet” trials in which mean jaw speed during the 1-second delay period after the whisker stimulus did not exceed 4 times of the mean absolute deviation of the jaw speed (angle) during the 1-second baseline period in each trial. Images from different mice were aligned according to the functionally-identified C2-barrel (RCaMP mice) (Mayrhofer et al., 2019) and the cerebellar tentorium (RCaMP and tdTomato mice), and smoothed by spatial gaussian filter (sigma = 1 pixel, 111 μm). Those trial-averaged images in each session were used as individual samples for statistical analysis. To test statistical differences in the pixel values, Wilcoxon rank-sum test (Expert vs Novice and RCaMP vs tdTomato) or Wilcoxon signed-rank test (Hit vs Miss and Miss vs Correct-rejection) was performed in each pixel, and p -value was corrected for multiple comparison by false-discovery rate, FDR (Benjamini and Hochberg 1995). The corrected p -values were log-scaled ($-\log_{10}P$) to create spatial p -value maps. Borders between anatomical areas were drawn on the functional images (Vanni et al. 2017) by using Allen Mouse Common Coordinate Framework version 3 (CCF) (Lein et al. 2007; Wang et al. 2020a) and ARA tools (Han et al., 2018; MacDowell and Buschman, 2020; Musall et al., 2019; Pinto et al., 2019). First, we defined the three-dimensional location of bregma in 25- μm resolution Allen CCF by considering brain structures in the stereotaxic atlas (Paxinos and Franklin, 2019), and the thickness of skull (325 μm) (Soleimanzad et al. 2017). Second, the atlas was rotated by 24 degrees along the rostro-caudal axis. Third, anatomical borders were projected onto the horizontal plane to make a 24-deg tilted border map. Then, the border map was linearly scaled and horizontally shifted to match the functional images of RCaMP mice according to the C2-barrel, bregma, and the anteromedial end of the left hemisphere.

2.5.12 Electrophysiology data

Spiking activity on each probe was detected and sorted into different clusters using Klusta, an open source spike sorting software suited for dense multielectrode recordings (Rossant et al. 2016). After an automated clustering step, clusters were manually inspected and refined. Single units were categorized as regular spiking (RSU) or fast-spiking neurons based on the duration of the spike waveform, and, in this study, we specifically focus on the putative excitatory RSUs (spike peak-to-baseline > 0.34 ms, 4415 units in 22 Expert and 1604 units in 8 Novice mice). Activity maps in Figure 2.12D and 2.14B were computed by averaging the trial-aligned peristimulus time histograms of all excitatory units recorded on the same probe.

2.5.13 Assessing Expert/Novice and Hit/Miss differences

Statistical difference between mean firing rates of Expert vs Novice (Figures 2.3E and 2.5D) and Hit vs Miss (Figures 2.5E, 2.12E and 2.12F) in each area was identified using non-parametric permutation tests in 50-ms bins and p -values were corrected by FDR.

2.5.14 Receiver Operating Characteristic (ROC) analysis

To quantify the selectivity of ROI calcium traces for Go vs No-Go trials we built ROC curves comparing the distribution of calcium activity in bins of 50 ms including only correct trials (Hit and Correct-rejection). Selectivity index was defined by scaling and shifting the area under the ROC curve (AUC) between -1 and 1:

$$Selectivity\ index = 2(AUC - 0.5),$$

where positive selectivity reflects higher activity in Hits and vice versa (Figure 2.2D). Similarly, to quantify the selectivity of single units for Go vs No-Go trials we built ROC curves comparing distribution of spiking activity in bins of 100 ms including only correct trials (Hit and Correct-rejection). The area under the ROC curve was then compared to a baseline distribution (5 bins of 100 ms before visual cue onset) to examine the significance of selectivity beyond baseline fluctuations. Non-parametric permutation tests were performed and p -values were corrected by FDR and percentage of neurons with significant positive or negative selectivity in each area were identified ($p < 0.05$, FDR-corrected, Figure 2.3F).

2.5.15 Clustering neuronal responses

For clustering the neuronal response patterns, RSUs from both Novice and Expert mice (1) with more than 200 spikes throughout the recording, and (2) with more than 5 trials for each trial-type (i.e. Hit, Miss, CR and FA) were included in the analysis ($n=5405$ out of 6019 RSUs). For each neuron and each trial type, time varying PSTHs (100 ms bin size) were computed over a 4-s window starting from 1 s before the visual cue and lasting until 1 second after the auditory cue. PSTHs from different trial types were baseline subtracted, normalized to the range of values across all bins (of all 4 trial types) and then concatenated resulting in an activity matrix $X \in \mathbb{R}^{5405 \times 160}$ whose row i corresponds to the concatenated normalized firing rate of the neuron i across different trial types (Figure 2.13A). Other normalization methods such as z-scoring resulted in similar clustering outcomes. To reduce the existing redundancy between firing rate time bins, we used Principal Component Analysis (PCA) and linearly projected firing rate vectors on a low-dimensional space. We applied PCA on the centered version of X (i.e. $x_i - \bar{x}_i$) and found 14 significant components (permutation test with Bonferroni correction for controlling family-wise error rate by 0.05) (Macosko et al. 2015). The weight of different components was equalized by normalizing the data resulting in unity variance for different components ($X' \in \mathbb{R}^{5405 \times 14}$).

Next, we employed spectral embedding on the data to detect non-convex and more complex clusters (von Luxburg 2007; Abbe 2018). To do so, we computed the similarity matrix $S \in \mathbb{R}^{5405 \times 5405}$ whose element at row i and column j measures the similarity between x_i' and x_j' as

$$s_{ij} = \exp \frac{-||x_i' - x_j'||_2^2}{2\sigma^2} \in [0,1],$$

where σ is a free parameter determining how local similarity is measured in the feature space. We tuned σ by putting the average of similarity values equal to 0.5 (the tuned value for σ is 0.0987). Then, we computed the normalized Laplacian matrix as

$$L = I - D^{-0.5} W D^{-0.5},$$

where I is the identity matrix, and D is the diagonal degree matrix defined as

$\text{diag} \left(\left\{ \sum_{k=1}^{5405} s_{ik} \right\}_{i=1}^{5405} \right)$. The transformed features are rather abstract and computed as the eigenvectors of L . It should be noted that the new feature space is non-linearly transformed version of the PCA-space which is itself a linearly transformed version of the original firing rate space. Such a transformation is believed to naturally separate data points which are clustered together (Abbe, 2017; Von Luxburg, 2007). Using the elbow method on the eigenvalues of matrix L (i.e. finding the sharp transition in the derivative of sorted eigenvalues), we considered (after excluding the very 1st eigenvector) the first 13 eigenvectors of matrix L as representative features which yielded matrix $\tilde{X} \in \mathbb{R}^{5405 \times 13}$.

Finally, neurons were clustered based on the resulting matrix \tilde{X} using a Gaussian Mixture Model (GMM). The algorithm considers that underlying distribution of data is a mixture of K Gaussians with means $\{\mu_1, \dots, \mu_k\}$, diagonal covariance matrices $\{\Sigma_1, \dots, \Sigma_k\}$, and weights $\{p_1, \dots, p_k\}$. For a given K , we estimated the parameters of this mixture model by using expected maximization (EM) algorithm (5000 repetitions and 1000 iterations). The number of clusters was then selected ($K = 24$) by minimizing the Bayesian information criterion (BIC) (Engelhard et al. 2019). (Figure 2.13B). Using the fitted parameters, we assigned a cluster index $c_i \in \{1, \dots, 24\}$ to each neuron corresponding to the Gaussian distribution to which it belongs with the highest probability. The output of the GMM step was the vector $C \in \{1, \dots, 24\}^{5405}$ containing the cluster indices of neurons. Task-modulated clusters (20/24) were sorted by their onset latency and were labeled based on their task epoch-related response (Figure 2.3C).

To study to what extent neurons from different brain regions and Novice and Expert mice contribute to the composition of clusters we took 3 steps. First, we quantified the distribution of neurons of each cluster across different brain regions in Novice and Expert mice (Figures 2.3D, 2.5F, and 2.13C). To account for the differences in the total number of neurons belonging to each group and brain region, weighted proportions were considered. Next, to identify the patterns which are more prevalent after whisker training, we quantified the percentage of neurons in each cluster that belong to Expert mice (Figure 2.3D). Similarly, in computing this percentage, weighted proportions were considered to correct for the difference in sample sizes ($n=3960$ neurons from Expert, $n=1445$ neurons from Novice). Finally, we defined a “distribution index” which quantifies the spread of each cluster among different brain regions (Figure 2.3D). For this purpose, we measured the total-variation distance between the weighted distribution of neurons of each cluster across 12 brain regions and the uniform distribution:

$$TV_c = \frac{1}{2} \sum_a \left| p_{c,a} - \frac{1}{12} \right|,$$

Where $p_{c,a}$ is the weighted proportion of neurons in cluster c belonging to area a . Note that $p_{c,a}$ is normalized with respect to areas, i.e., $\sum_a p_{c,a} = 1$. The distance TV_c takes 0 as its minimum value when the neurons of cluster c are uniformly distributed in all areas, and takes $\frac{11}{12}$ as its maximum value when all neurons of cluster c

belong to a single brain area. To scale this value between zero and one, for each cluster c we defined a distribution index (D_c) as:

$$D_c = 1 - \frac{12}{11} TV_c \in [0, 1],$$

where $D_c = 1$ indicates that cluster c is uniformly distributed among areas, and $D_c = 0$ indicates that cluster c is concentrated in a single brain region.

To characterize changes across learning of the delay task in each area, we computed separately in Novice and Expert mice, the activity pattern of the two most representative clusters (i.e. clusters with the highest number of neurons among all clusters) by averaging the activity among neurons belonging to the pair of area and cluster. The two most representative clusters are labeled as 1st and 2nd rank (Figure 2.13D).

2.5.16 Single neuron whisker-evoked response latency

To quantify the latency of whisker-evoked sensory response in spiking activity of single neurons (Figure 2.5C), we limited the analysis to the first 200-ms window following the whisker stimulus. We first examined whether each neuron was modulated (positively or negatively) in the 200-ms window following the whisker stimulus compared to a 200-ms window prior to the whisker onset. For responsive neurons ($p < 0.05$, non-parametric permutation test), latency - calculated on the temporally smoothed PSTHs (1 ms non-overlapping binned PSTH filtered with a Gaussian kernel with $\sigma = 10$ ms) - was defined as the time where the neural activity reached half maximum (half minimum for suppressed neurons) within the 200-ms window. Only responsive neurons are included in the cumulative distributions and boxplots in Figure 2.5C.

2.5.17 GLM encoding model

We used Poisson regression to fit an encoding model (generalized linear model, GLM) to predict the spiking activity of each individual neuron given behavioral data (Nelder and Wedderburn 1972; Park et al. 2014). For each session, we concatenated all correct trials (Hit and Correct-rejection) and then split the data to perform five-fold cross-validation. In Poisson regression, one aims at predicting the spike count $y(t)$ in a time bin t according to the formula:

$$y(t) \sim \text{Poisson}(e^{X(t) \cdot \beta}),$$

i.e. assuming that the spike counts are sampled from a Poisson distribution with rate that depends on the design matrix $X(t)$ and on the weight vector β . In our case, y was constructed by binning the spikes in 100-ms bins. The weights β were fit by maximizing the likelihood with Ridge regularization for each fold, and then averaged across the five folds. The parameter that controls the strength of the regularization was determined separately for each neuron using evidence optimization (Cunningham et al. 2007; Park et al. 2014).

The design matrix was constructed by including three types of variables: “event” variables, associated to task-related events; “analog” variables, associated to real-valued behavioral measures from videography; and “slow” variables, which were constant during one trial but could vary over the course of one session. Event variables included the visual cue onset, the whisker stimulus onset, the auditory cue onset and the onset of the first lick. The exact time of lick onset was determined from the high-speed video using a custom algorithm. To assess the delayed effect of such task-related variables, each of these event-like variables was associated with a set of ten 100-ms wide and unit height boxcar basis functions, spanning in total one second after each event. The first-lick variable was associated with two additional boxcar functions covering 0.2 seconds prior to the lick onset, to capture lick-specific preparatory neuronal activity. Analog variables included in the design matrix were the whisker, tongue and jaw speed. These quantities were first extracted from the high-speed videos using custom code and then averaged in 100-ms bins. Among the slow variables, we included the trial index, i.e. a variable that at each trial k took a constant value equal to k/k_{total} , where k_{total} is the total number of trials in a session. This variable could capture shifts in a neuron baseline activity due to slow effects across the session such as changes in satiety and motivation. Finally, we included three binary variables that took value one only if the previous trial was an early lick, a False-alarm or a Hit trial, to capture the effect of the previous trial outcome on the subsequent trial. In total, our design matrix had 50 columns, corresponding to the number of free parameters of the model.

To assess the significance of each variable in the design matrix, we fitted a new GLM model obtained by removing the variable of interest (reduced model) from the full model. If for a certain neuron the reduced model fitted the data significantly worse than the full model ($p < 0.05$, according to a likelihood ratio test (Buse 1982)), then that neuron was considered significantly modulated by the removed variable. The reduced model was fitted independently for each fold, using the same data splitting used for the full model. In the likelihood ratio test, the test statistics are given by

$$2\log\left(\frac{L_{full}}{L_{reduced}}\right), \text{ where } L_{full} \text{ and } L_{reduced} \text{ are the full and reduced model}$$

likelihood respectively. These statistics were computed for each fold and then averaged to obtain an average statistic, from which the final p -value was computed (Buse, 1982). Note that in the presence of correlations among variables, this approach is stringent in that it tends to underestimate the significance of different variables. To separately assess the effect of the onset of event-like variables from their delayed effects, we quantified their significance independently by separately removing the first two basis functions or remaining eight basis functions (Visual, Auditory and Lick). For the whisker variable, since it was very brief in time (10 ms), we removed either the first or the remaining nine bins (referred to as ‘Whisker’ and ‘Delay’ respectively in Figure

2.6D, and 2.6E). To assess the significance of the modulation due to lick-preparatory neuronal activity we separately removed the two basis functions that preceded the lick onset (referred to as 'Lick initiation' in Figure 2.6D, and 2.6E). Spatial weight maps for selected model variables (Figure 2.15E) were built by first averaging the weights over the time course of the variable, i.e. by averaging over the weights of the boxcar basis functions. Next, for each neuron these weights were projected on the reconstructed anatomical location in 2D, and were then averaged across all neurons with a certain spatial bin (50x50 μm). The resulting spatial weight map was smoothed using a 2D Gaussian kernel (sigma=150 μm). All the GLM analysis was performed in Matlab using a combination of existing and custom-written code.

2.5.18 Assessing optogenetic manipulation impact

We measured the impact of optogenetic activation in tjM1 by counting early licks evoked during the delay period. Sessions with a difference between Hit rate and False alarm rate smaller than 0.2 were excluded from the analysis. The early lick rates with the strongest optogenetic stimulation (9 mW) were calculated in each session to test statistical difference between light-off and light trials.

To quantify the impact of optogenetic inactivation we compared mouse averaged performance (n=9; Hit rate, False alarm rate and Early lick rate) for different light windows (i.e. Baseline, Whisker, Delay, Response) to light-off control trials. *P*-values were corrected for multiple comparison (i.e. 4 windows) using Bonferroni correction.

To assess the effect of inactivation on movements, we quantified the change in light versus no-light trials by defining a movement modulation index as:

$$\text{Movement modulation index} = \frac{\text{Movement}_{\text{light}} - \text{Movement}_{\text{notlight}}}{\text{Movement}_{\text{light}} + \text{Movement}_{\text{notlight}}},$$

for different orofacial movements (whisker, jaw and tongue speed) and lick spout reading with the piezo sensor (Figure 2.16).

2.5.19 Quantifying involvement index

The involvement index was defined by combining the neuronal correlates and behavioral impact of optogenetic inactivation. For each pair of area and temporal window of interest, we built two distributions of bootstrap estimation of the mean, separately for neuronal correlates and inactivation impact, by bootstrapping 1000 times. The neuronal correlates were quantified as the mean firing rate difference in Hit vs Correct-rejection trials across all neurons recorded from 22 Expert mice. The inactivation impact was quantified as the mean change in Hit rate across 9 VGAT-

ChR2 mice. The distribution of involvement index was calculated as the product distribution of the two bootstrap distributions.

2.5.20 Statistics

Data are represented as mean \pm SEM unless otherwise noted. The Wilcoxon signed-rank test was used to assess significance in paired comparisons; and the Wilcoxon rank-sum test was used for unpaired comparisons (Matlab implementations). Analysis of spiking activity, selectivity of calcium signals and involvement index was performed using a non-parametric permutation test. The statistical tests used and n numbers are reported explicitly in the main text or figure legends. *P*-values are corrected for multiple comparisons and methods are indicated in figure legends.

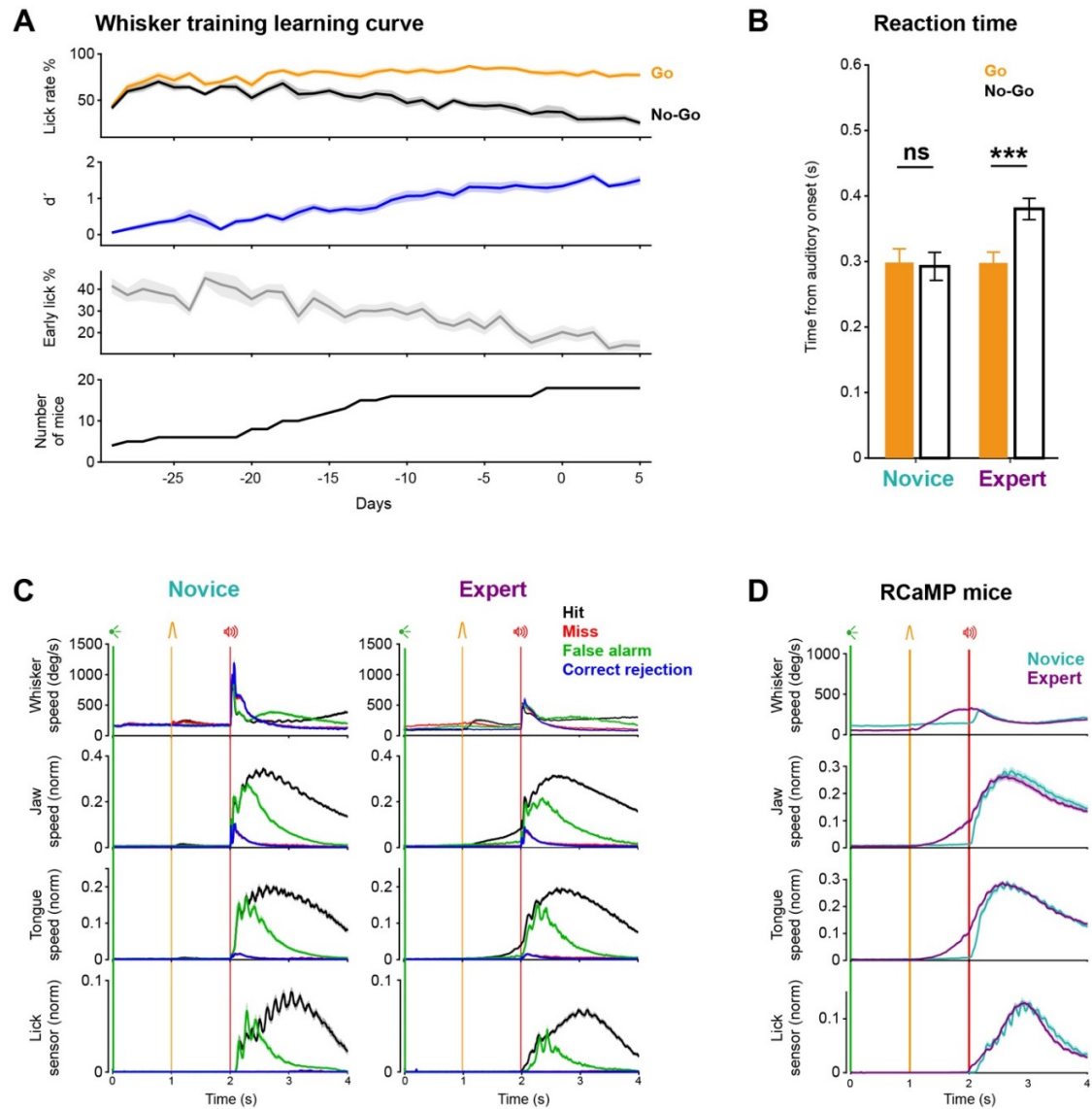


Figure 2.9. Whisker training changes behavioral patterns, Related to Figure 2.1.

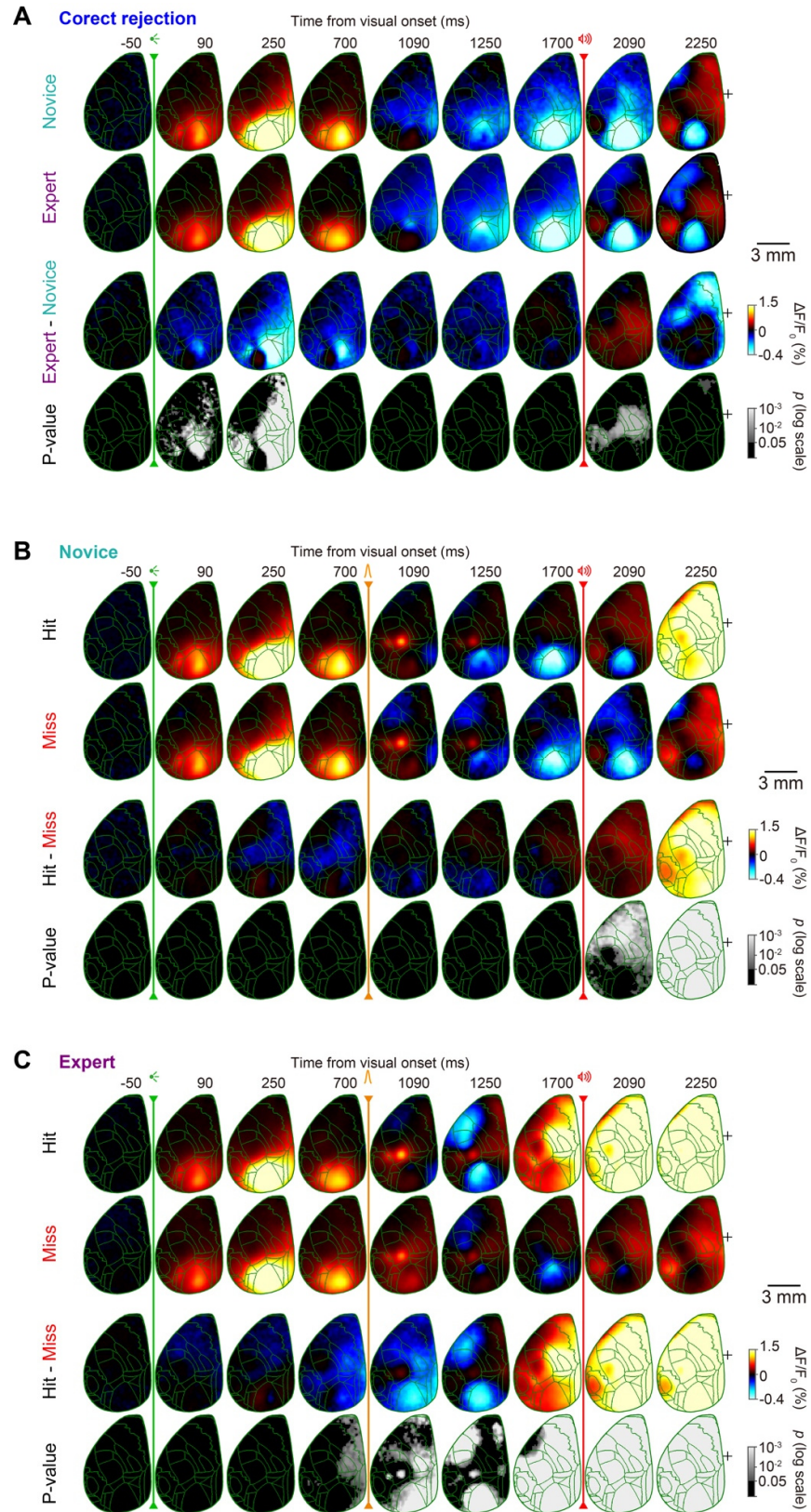


Figure 2.10 Wide-field imaging in different trial types, Related to Figure 2.2.

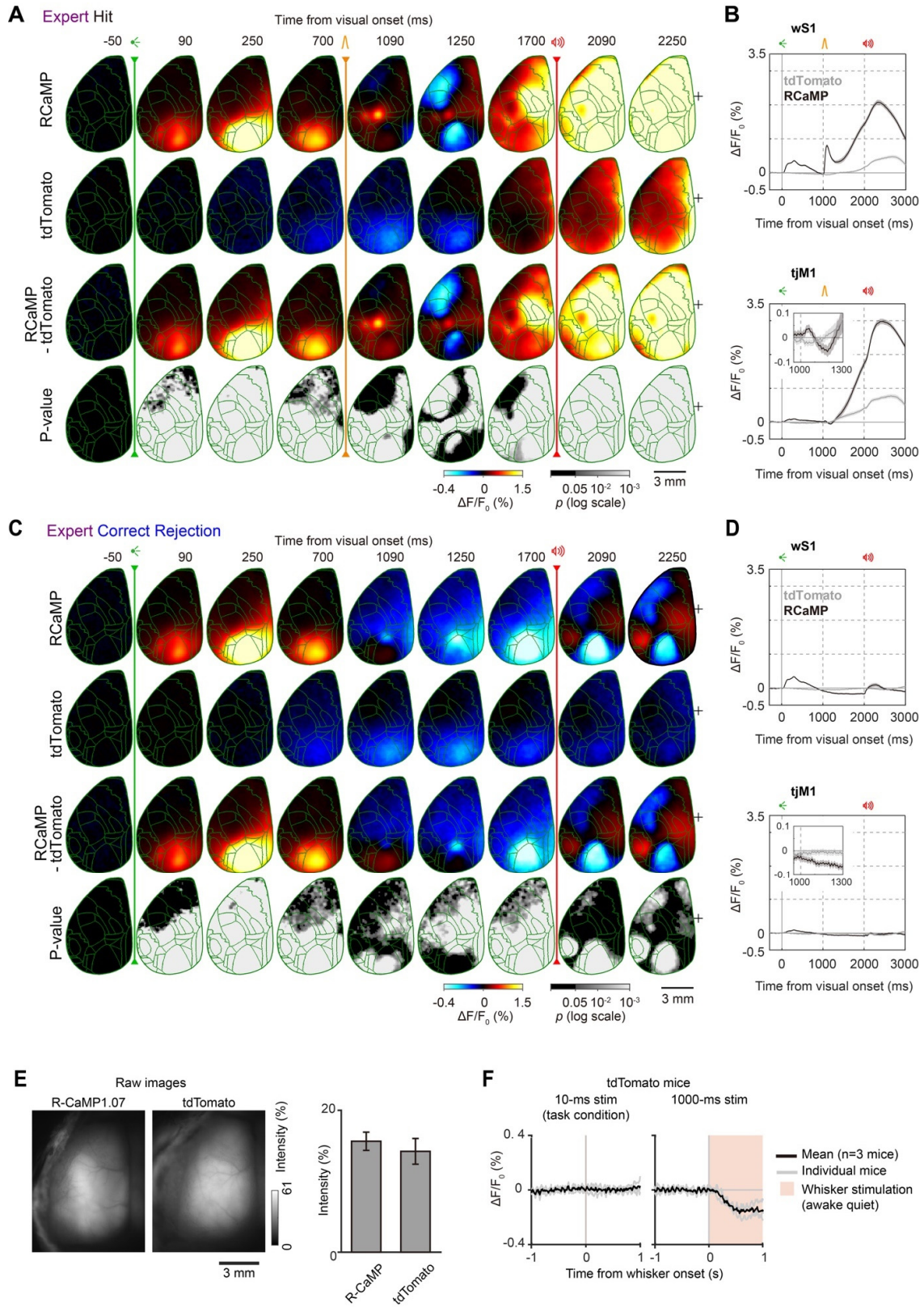


Figure 2.11. Control experiment in tdTomato mice, Related to Figure 2.2.

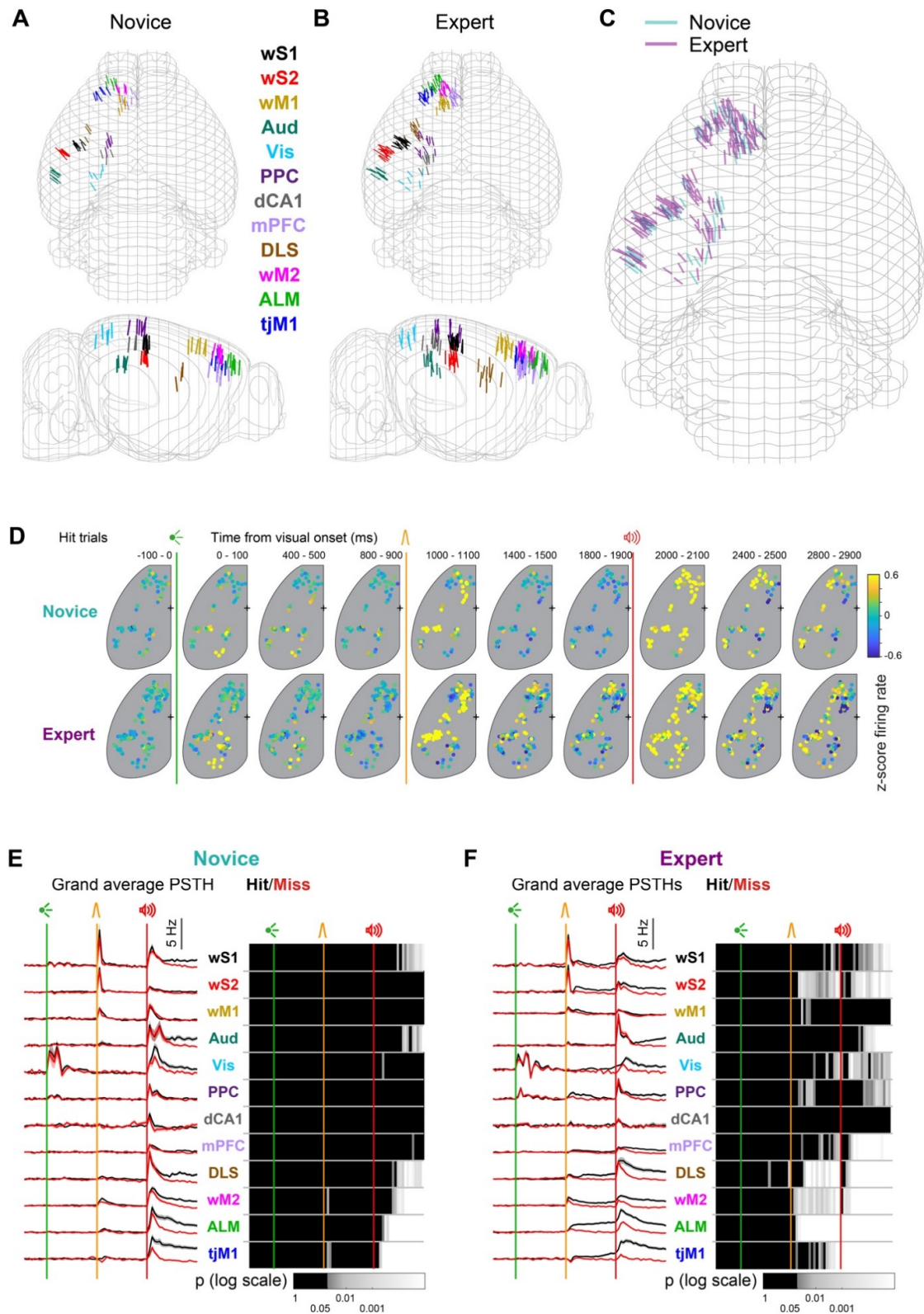


Figure 2.12. Silicon probe locations, average activity patterns across probes and firing differences in Hit vs Miss trials in different areas, Related to Figure 2.3.

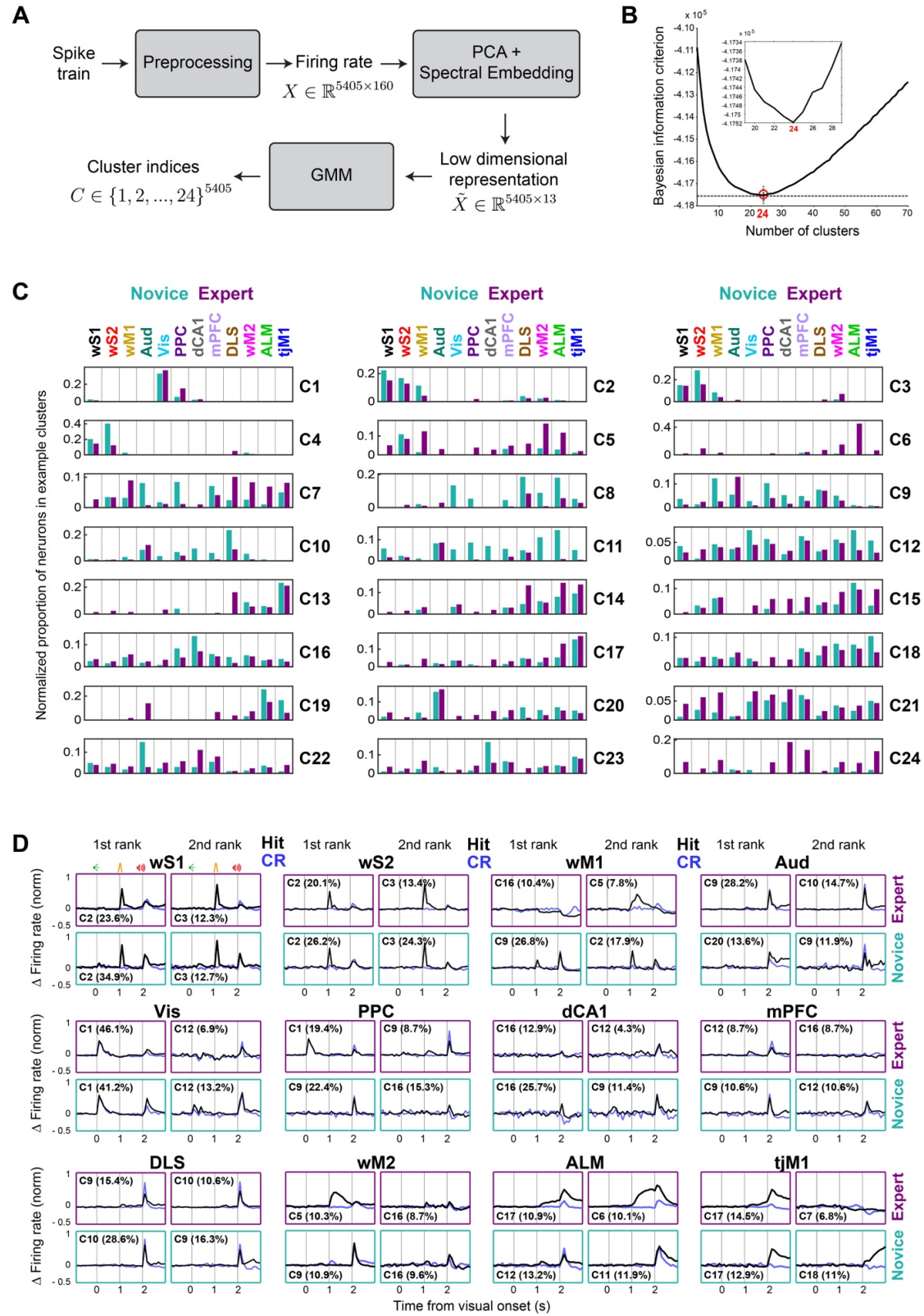


Figure 2.13. Unsupervised neuronal clustering, Related to Figures 2.3 and 2.5.

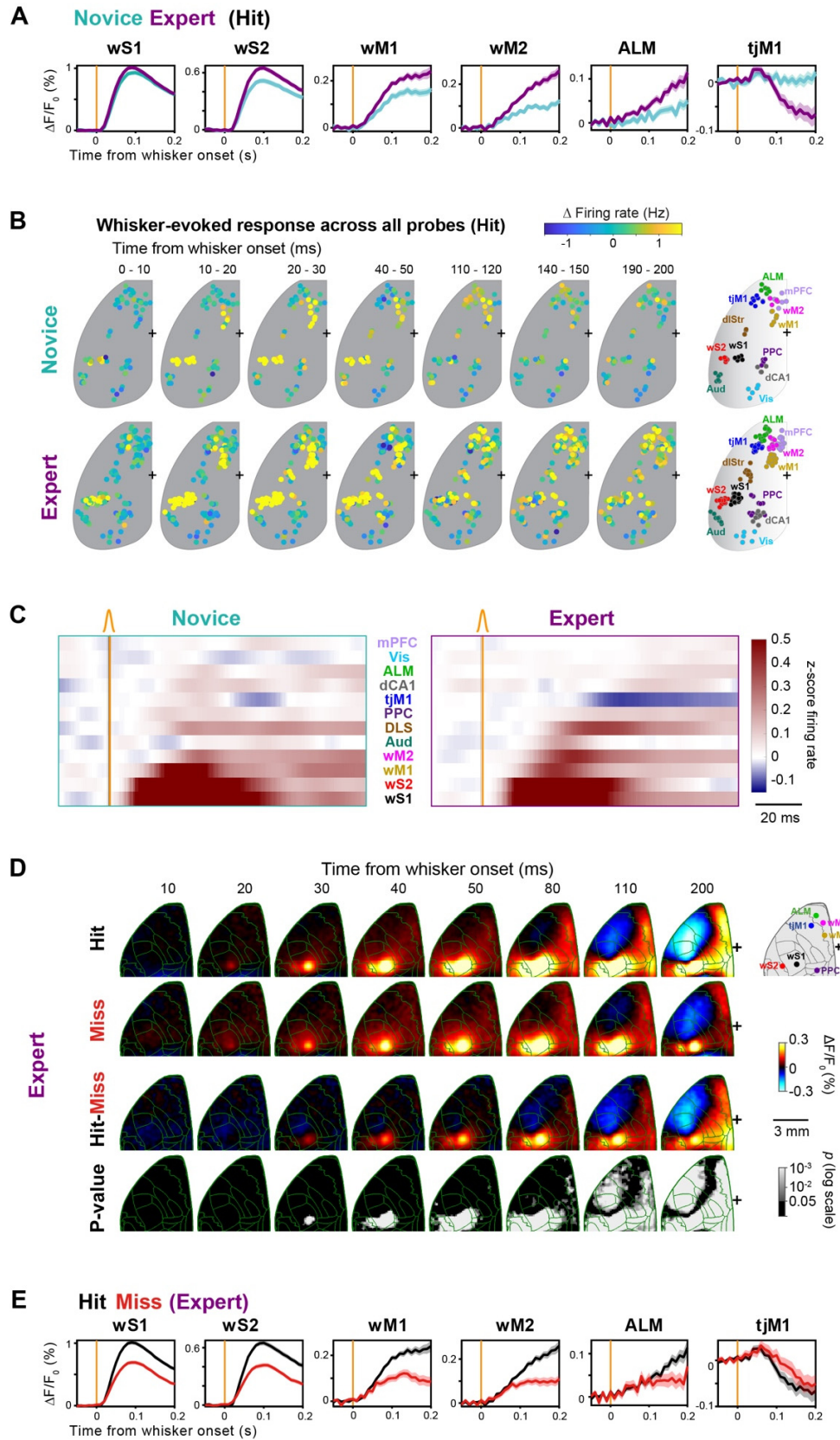


Figure 2.14. Critical early delay processing, Related to Figure 2.5.

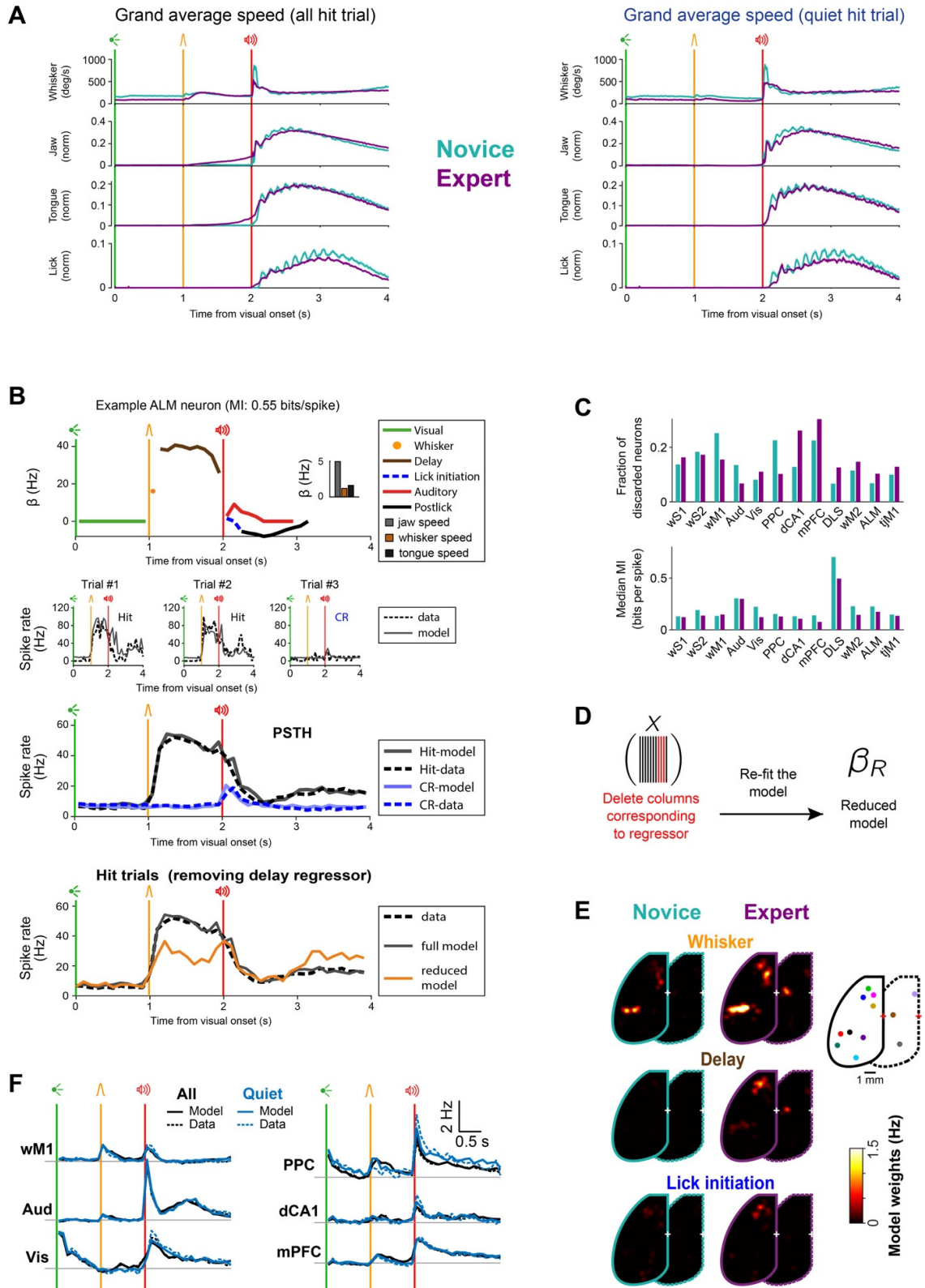


Figure 2.15. Orofacial movements in Quiet trials and Poisson encoding model, Related to Figure 2.6.

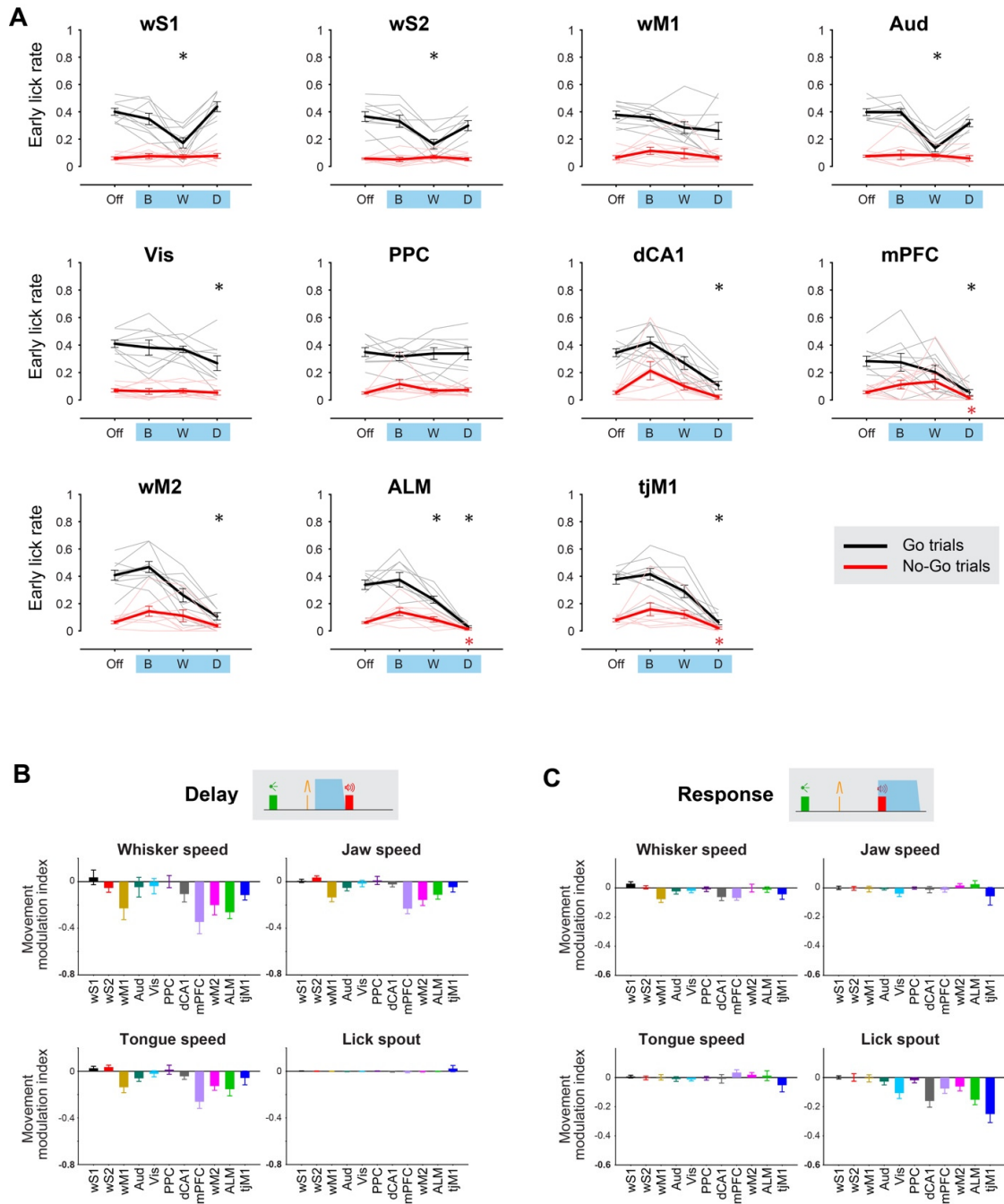


Figure 2.16. Spatiotemporal effect of different regions on premature licking and movements, Related to Figure 2.7.

Figure 2.9. Whisker training changes behavioral patterns, Related to Figure 2.1.

(A) Time courses of behavioral performance across whisker training. From top to bottom: Lick rate (i.e. the probability of licking in the Response window) in Go and No-Go trials, discriminability of Go and No-Go trials (d'), percentage of early licks (licks between visual and auditory cues), and number of mice in each day are plotted along training days relative to the start of neuronal recording (day=0). Only mice used for electrophysiology are shown here ($n=18$ mice).

(B) Changes in licking behavior. Reaction time (first lick time relative to auditory cue onset time) in completed trials. Reaction times were shorter in Go (Hit, orange) compared to No-Go (False-alarm, black) trials in Expert ($p<0.01$, $n=25$; Wilcoxon signed-rank test), but not in Novice mice ($p=0.14$, $n=15$). Mice used for electrophysiology and imaging are included.

(C) Orofacial movements in different trial types. Average movement across mice (mean \pm SEM). Novice mice ($n=8$) showed similar levels of movements across different trial types until auditory cue whereas Expert mice ($n=18$) increased movements of tongue and jaw toward the auditory cue selectively in Hit trials. Only mice used for electrophysiology are included.

(D) Orofacial movements in Hit trials for Novice and Expert RCaMP mice ($n=7$). Same configuration as Figure 1F, left.

Figure 2.10. Wide-field imaging in different trial types, Related to Figure 2.2

(A) Time-course of global cortical activity in Correct-rejection trials for Novice vs Expert mice. Each frame shows instantaneous $\Delta F/F_0$ without averaging (10 ms/frame). For each pixel, baseline activity in a 50 ms window before visual cue onset was subtracted. Mean calcium activity of 62 Novice and 82 Expert sessions from 7 mice, Novice and Expert difference, and the statistical significance of the difference (p -value of Wilcoxon rank-sum test, FDR-corrected) are plotted from *top* to *bottom*. Green traces, anatomical borders based on Allen Mouse Brain Atlas. Black '+' indicates bregma.

(B-C) Time-course of global cortical activity in Novice (B) and Expert (C) mice comparing Hit vs Miss trials. Same configuration as panel A. Mean calcium activity of 62 Novice and 82 Expert sessions from 7 mice. Hit, Miss, Hit-Miss difference, and the statistical significance of the difference (p -value of Wilcoxon signed-rank test, FDR-corrected) are plotted from *top* to *bottom*.

Figure 2.11. Control experiment in tdTomato mice, Related to Figure 2.2

(A-D) Time-course of cortical fluorescence in control mice expressing a red fluorescence protein tdTomato during Hit (A-B) and Correct-rejection (C-D) trials, compared with RCaMP mice.

A and C, each frame shows instantaneous $\Delta F/F_0$ without averaging (10 ms/frame). For each pixel, baseline activity in a 50 ms window before visual cue onset was subtracted. RCaMP (mean of 82 Expert sessions from 7 mice) and tdTomato (mean of 57 sessions from 7 Expert mice), RCaMP-tdTomato difference, and the statistical significance of the difference (p -value of Wilcoxon rank-sum test, FDR-corrected) are plotted from *top* to *bottom*. Green traces, anatomical borders based on Allen Mouse Brain Atlas. Black '+' indicates bregma. Note slow and spatially diffuse signals related to hemodynamics in tdTomato mice. After subtraction of the tdTomato data, RCaMP mice still show similar patterns of cortical responses.

B and D, fluorescence traces (mean \pm SEM) in wS1 (*top*) and tJM1 (*bottom*). ROI size, 7 x 7 pixels. Inset in tJM1 shows enlarged traces right after the whisker onset.

(E) Representative raw fluorescence images of a RCaMP mouse and a tdTomato mouse obtained during wide-field imaging (*left*). There was no statistical difference in the raw intensity between two mouse lines in the imaging conditions for each line ($n=7$ RCaMP mice and $n=7$ tdTomato mice, $p=0.80$, Wilcoxon's rank-sum test) (*right*).

(F) Hemodynamic signal in tdTomato mice evoked by whisker stimulation. The brief whisker stimulation (a single 10 ms pulse) used in the task did not evoke detectable changes in wS1, but a prolonged whisker stimulation (100 pulses each of 10 ms at 100 Hz lasting 1000 ms) evoked a strong reduction of cortical fluorescence ($n = 3$ tdTomato mice).

Figure 2.12. Silicon probe locations, average activity patterns across probes and firing differences in Hit vs Miss trials in different areas, Related to Figure 2.3.

(A-C) Reconstructed location of silicon probes registered to Allen Mouse Brain Atlas in 3D in Novice (A), Expert (B) and overlay of Expert and Novice mice (C).

(D) Time-lapse maps of mean firing rate in Novice and Expert mice in Hit trials. Circles represent different probes and colors show mean z-scored firing rate across the probe at each time window. Neuronal activity patterns are strikingly different between Novice and Expert mice during the delay period (1400 –1900 ms after visual cue onset). Probes from all mice in each group (8 Novice and 22 Expert) are superimposed.

(E) Population firing rate in Novice mice comparing correct vs incorrect Go trials. *Left*, baseline-subtracted (1 s prior to visual cue onset) mean firing rate across cortical areas in Hit and Miss trials of Novice mice are overlaid. *Right*, *p*-value of Hit/Miss comparison in 50 ms consecutive windows (non-parametric permutation test, FDR-corrected) (*right*).

(F) Same as E but for Expert mice. Note prominent differences during the delay period after whisker stimulus across many regions including wS2, DLS, wM2, ALM and tJM1.

Figure 2.13. Unsupervised neuronal clustering, Related to Figures 2.3 and 2.5.

(A) Block diagram indicating the different steps for unsupervised neuronal clustering. Dimensionality reduction and spectral embedding were applied on concatenated trial-type averaged PSTHs of neurons and the results were clustered by fitting a Gaussian mixture model (GMM).

(B) Determination of the number of clusters. Number of optimal clusters ($n=24$) was determined as the minimum of the Bayesian information criterion (BIC) curve. Inset shows magnified version of BIC values around $n=24$.

(C) Spatial distribution of clusters across cortex. Weighted proportion of neurons belonging to different cortical regions (similar to rows of heatmaps in Figure 3D but for all 24 clusters). Sorted (from *left to right*, and then *top to bottom*) based on latency of response onset.

(D) Most prominent firing patterns in different brain regions. For each area the mean firing rate in Hit (black) and Correction rejection (blue) trials are superimposed for the neurons belonging to their two most representative clusters (1st and 2nd rank). Expert (*top*) and Novice (*bottom*) mice. The cluster number is indicated within each frame, as well as the percentage of neurons from the corresponding area belonging to this cluster in parenthesis.

Figure 2.14. Critical early delay processing, Related to Figure 2.5.

(A) Time courses of whisker-evoked calcium signal in selected regions of interest from the data in Figure 5A. Mean of 62 Novice and 82 Expert sessions from 7 mice (\pm SEM). ROI size, 3 x 3 pixels. Activity did not change by learning in the input node wS1, but did diverge in other regions. Note sharp decrease of signal in tJM1 of Expert mice.

(B) Time-lapse maps of mean firing rate immediately after whisker onset. Novice and Expert mice in Hit trials. Same configuration as Figure 2.12D but with higher temporal resolution (10 ms) for 0-200 ms after whisker onset. Note the propagation of excitation in wS1 \rightarrow wS2 \rightarrow wM1 \rightarrow wM2 \rightarrow ALM and transient inhibition of tJM1 in Expert mice.

(C) Sequential propagation of whisker-evoked neuronal response in Hit trials (*left*, Novice; *right*, Expert). Mean z-scored firing rate in the first 100 ms window after whisker stimulus are shown. Brain regions are sorted based on their population-average onset latency in Expert mice.

(D) Wide-field signal immediately after whisker stimulus in Hit and Miss trials. Same as Figure 5A but for Hit vs Miss trials of Expert mice ($n=82$ sessions). From *top to bottom*, average calcium signal in Hit, Miss, Hit-Miss difference, and the statistical significance of the comparison (*p*-value of Wilcoxon signed-rank test, FDR-corrected). The schematic (*top-right*) shows the location of regions of interest plotted in E.

(E) Time courses of whisker-evoked calcium signal for Hit and Miss trials in selected regions of interest from the data in D. ROI size, 3 x 3 pixels.

Figure 2.15. Orofacial movements in Quiet trials and Poisson encoding model, Related to Figure 2.6.

(A) Orofacial movements in selected Quiet trials. The same configuration as Figure 2.1F, *left*. *Left*, grand average movements in all Hit trials without selection (same data as Figure 2.1F). *Right*, grand average movements for selected Quiet trials where mice did not show jaw movements. Note that preparatory movements in the delay period after whisker stimulus disappeared.

(B) Model fit for an example ALM neuron. *Top*, model weights (β) for event variables along the trial timeline are plotted. *Inset*, shows analog variable weights. Weights are shown in units of firing rate (Hz). *Middle*, the overlay of example single-trial firing rate reconstructed from the model (solid lines) and data (dotted lines) are shown for two example Hit (black) and one Correct-rejection (blue) trials. *Bottom*, Average Hit (black) and Correct-rejection (blue) firing rate (PSTHs) reconstructed from the model (plain lines) overlaid with observed data (dotted lines). Orange trace shows PSTH for reduced model after removing delay regressor. Note the high performance of model in reconstructing single trial firing rates and average PSTH.

(C) Model performance. *Top*, fraction of discarded neurons. For each neuron, fit quality was assessed using mutual information (MI) (Cover and Thomas 1991b; Gerstner et al. 2014b) (see Methods), a measure of the difference between the fitted model and constant Poisson model capturing only the mean firing rate. Neurons for which the fitted model did not perform better than the constant model (i.e. $MI \leq 0$) were excluded from the rest of analysis. Note the higher proportion of excluded neurons in Novice mice, suggesting that neurons became more task-related after whisker training. *Bottom*, median MI values across different regions for Expert and Novice mice.

(D) Evaluating significant contribution of individual predictors. For each fitted neuron, contribution of a model predictor was evaluated by refitting the model after excluding that predictor (reduced model; see panel B, orange PSTH) and comparing it to the full model ($p < 0.05$, likelihood ratio test).

(E) Average weight maps of Whisker, Delay and Lick initiation model variables. For each model variable, average model weight map across neurons of superficial (solid border) and deep (dotted border) brain regions of Expert and Novice mice are shown.

(F) Comparison of PSTHs of Quiet trials reconstructed from the GLM model (solid lines) with empirical data (dotted lines). Same configuration as Figure 2.6F but for the other brain regions. Note that the model fitted to all trials (black) reconstructs well Quiet (blue) trials.

Figure 2.16. Spatiotemporal effect of different regions on premature licking and movements, Related to Figure 2.7.

(A) Behavioral impact of optogenetic inactivation across time windows for each brain region (mean \pm SEM) on fraction of Early licks. For each area, Early lick rate in Go (black) and No-Go (red) trials are plotted for Light-off (Off), Baseline (B), Whisker (W), and Delay (D) windows. Asterisks represent significant difference comparing Early licks for light vs light-off trials in Go (black) or No-Go (red) trials ($n=9$ mice; *, $p < 0.05$; Wilcoxon signed-rank test, Bonferroni correction for multiple comparisons).

(B) Changes in preparatory movements in the delay period. Change in orofacial movements (whisker, jaw and tongue speed) and licking pattern (lick spout sensor) during the delay period was quantified in trials with light (over the Delay) vs light-off trials ($n=9$ mice, mean \pm SEM, see methods for movement modulation index definition). For both light and no-light trials only Hit trials are included.

(C) Changes in movement during response window. Similar to (B), but when light was applied and movements were quantified during the response window. Similarly, only Hit trials are included for both light and light-off trials.

Chapter 3 Learning-Related Congruent and Incongruent Changes of Excitation and Inhibition in Distinct Cortical Areas

The text and figures of this chapter are reproduced from the following published journal article:

Vahid Esmaeili, Anastasiia Oryshchuk, Reza Asri, Keita Tamura, Georgios Foustoukos, Yanqi Liu, Romain Guet, Sylvain Crochet and Carl C. H. Petersen. 2022.

“Learning-Related Congruent and Incongruent Changes of Excitation and Inhibition in Distinct Cortical Areas.”

PLOS Biology 20 (5): e3001667.

<https://doi.org/10.1371/journal.pbio.3001667>

My contribution to this paper:

I contributed to the validation of the method to classify cortical neurons to RSU and FSU based on their spike waveforms.

I obtained and fully analyzed optotagging dataset from VGAT-ChR2 mice.

Participated in writing manuscript regarding optotagging experiments and methods.

Actively participated in all discussions and edited all manuscript.

3.1 Abstract

Excitatory and inhibitory neurons in diverse cortical regions are likely to contribute differentially to the transformation of sensory information into goal-directed motor plans. Here, we investigate the relative changes across the mouse sensorimotor cortex in the activity of putative excitatory and inhibitory neurons - categorized as regular or fast spiking according to their action potential waveform - comparing before and after learning of a whisker detection task with delayed licking as a perceptual report. Surprisingly, we found that the whisker-evoked activity of regular versus fast spiking neurons changed in opposite directions after learning in primary and secondary whisker motor cortices, while it changed similarly in primary and secondary orofacial motor cortices. Our results suggest that changes in the balance of excitation and inhibition in local circuits concurrent with changes in the long-range synaptic inputs in distinct cortical regions might contribute to the performance of delayed sensory-to-motor transformation.

3.2 Introduction

Many brain regions are thought to contribute to the performance of goal-directed sensory-to-motor transformations. An increasingly well-defined sensorimotor transformation studied in rodents is the learned association between a whisker sensory input and licking for reward (Knutsen et al. 2006; Brecht 2007; Mehta et al. 2007; Diamond et al. 2008; O'Connor, Peron, et al. 2010; Chen et al. 2013a; Feldmeyer et al. 2013; Miyashita and Feldman 2013; Sachidhanandam et al. 2013; Kwon et al. 2016; Takahashi et al. 2016; Yang et al. 2016; Hong et al. 2018; Isett et al. 2018; Svoboda and Li 2018; Esmaeili and Diamond 2019; Petersen 2019; Esmaeili et al. 2020; Staiger and Petersen 2021). From a cortical perspective considering whisker-dependent tasks requiring licking for the perceptual report, sensory processing is prominent in the somatosensory cortices, whereas neuronal activity linked to motor planning during delay periods is primarily found in premotor cortices, and motor commands are more prominent in the primary motor cortex (Guo et al. 2014b, 2017b; Gilad et al. 2018b; Esmaeili et al. 2021b). We recently showed that in a whisker detection task with delayed licking, the correct execution of the task involves a stereotypical spatiotemporal sequence of whisker deflection-evoked neuronal firing by which the sensory cortex appeared to contribute to exciting frontal cortical regions to initiate neuronal delay period activity (Esmaeili et al. 2021b). Comparing novice and expert mice, we also found that the learning of the task is accompanied by region- and temporal-specific changes in cortical activity (Esmaeili et al. 2021b). (Esmaeili et al. 2021) These experience-dependent changes in evoked-activity likely result from

changes in long-range synaptic inputs and changes within local synaptically-connected neocortical microcircuits.

Neocortex has regional specializations and a columnar organization divided into layers each containing many classes of neurons varying across diverse features (Harris and Mrsic-Flogel 2013; Huang 2014; Tremblay et al. 2016; Luo et al. 2018; Tasic et al. 2018). At the most basic level, neocortical neurons can be classified as excitatory (releasing glutamate) or inhibitory (releasing GABA). Many neocortical excitatory neurons send long-range axons projecting to diverse brain regions, whereas most neocortical inhibitory neurons only have local axonal arborisations, thus contributing primarily to the regulation of local microcircuit activity. The balance between excitation and inhibition is likely to have a major impact on neocortical microcircuit computations and previous work has suggested important changes in this balance across development, brain states, sensorimotor processing and models of brain diseases (Sun et al. 2010; Mateo et al. 2011; Yizhar et al. 2011; Woloszyn and Sheinberg 2012; Haider et al. 2013; Froemke 2015; Antoine et al. 2019; Sohal and Rubenstein 2019). Inhibitory GABAergic neurons can be further divided into many subclasses, with one of the most prominent being the parvalbumin-expressing (PV) neurons. PV cells provide potent inhibition onto excitatory cells by prominently innervating either the soma and proximal dendrites or the axonal initial segment, thus playing a critical role in controlling the discharge of excitatory neurons. At the millisecond timescale, the PV neurons appear specialized for high-speed synaptic computations with fast membrane time-constants and large fast synaptic conductances, receiving substantial excitatory input from many nearby excitatory neurons as well as long-range inputs (Freund and Katona 2007; Isaacson and Scanziani 2011; Avermann et al. 2012; Hu et al. 2014; Cardin 2018; Sermet et al. 2019). Within a neocortical microcircuit, PV neurons are likely to play a critical role in controlling the balance between excitation and inhibition. PV cells typically fire at high rates and have short action potential (AP) durations that can be identified from extracellular recordings. In fact, neurons recorded from extracellular recordings are typically classified based of their AP duration, as regular spiking (RS) units, which have broad AP waveforms and correspond mostly to excitatory neurons; and fast spiking (FS) units, which have narrow AP waveforms and largely correspond to inhibitory PV neurons. Previous whisker-related studies have reported experience-dependent plasticity of both excitatory and inhibitory synaptic transmission, with prominent changes reported in PV GABAergic neurons, for example following whisker deprivation (Chittajallu and Isaac 2010; Gainey et al. 2018). However, it remains unknown how reward-based learning in whisker-dependent tasks might affect the activity of PV neurons, although previous work has revealed prominent changes in PV neuronal activity in mouse motor cortex during learning of a lever-press task (Chen, Kim, et al.

2015) and in visual cortex during learning of a visual discrimination task (Poort et al. 2022).

In the present study, we investigate whether the changes observed during the learning of the whisker detection task with delayed licking are associated with a change in the balance between excitation and inhibition. We used our recently published dataset of high-density silicon probe recordings from six cortical regions previously identified to be important during this behavior (Esmaeili et al. 2021b) and compared the changes in evoked activity of RS and FS units. Interestingly, we found that upon task learning, RS and FS showed opposite changes in some cortical areas, suggesting important changes in local computation, whereas in other regions, RS and FS changed in parallel suggesting rather an overall shift in the synaptic drive to these areas.

3.3 Results

3.3.1 Localisation and classification of cortical neurons

In this study, we further analyzed a data set of extracellular silicon probe recordings of neuronal spiking activity we published recently (Esmaeili et al. 2021b). We focused our analyses on six key neocortical regions: whisker primary somatosensory cortex (wS1), whisker secondary somatosensory cortex (wS2), whisker primary motor cortex (wM1), whisker secondary motor cortex (wM2), anterior lateral motor cortex (ALM) and tongue-jaw primary motor cortex (tjM1) (Fig 3.1A). These regions participate in a whisker detection task with delayed licking to report perceived stimuli (Esmaeili et al. 2021b). Mice first went through pretraining to the task structure, which included a brief light flash to indicate trial onset followed 2 s later by a brief auditory tone to indicate the beginning of the 1-s reporting period, during which the thirsty mice could lick to receive a water reward (Fig 3.1B). We recorded from two separate groups of mice referred to as “Novice” and “Expert” hereafter, while a brief whisker stimulus was introduced 1 s after the visual cue in a randomized half of the trials, and licking in the reporting window was only rewarded in whisker stimulus trials (Fig 3.1B and 3.1C). Expert mice were given additional whisker training through which they learned to lick preferentially in trials with a whisker stimulus (Fig 3.1B and 3.1C). However, Novice mice had not learned the stimulus-reward contingency and licked equally in trials with and without whisker stimulus (Esmaeili et al. 2021). Through the anatomical reconstruction of fluorescently-labeled electrode tracks and registration to a digital mouse brain atlas, here we precisely localize units to specific layers and cortical regions annotated in the Allen Mouse Brain Common Coordinate Framework (Wang et al. 2020) (Fig 3.1D and 3.9). The neuronal location was assigned to the recording

site with the largest amplitude spike waveform along the shank of the silicon probe (Fig 3.1E). Neurons in different cortical regions and layers had diverse firing patterns during task performance (Fig 3.1F and 3.9). We further distinguished neurons according to the duration of the action potential waveform. In both Novice and Expert mice, we found a bimodal distribution of spike duration, which we labeled as FS units (spike duration below 0.26 ms) and RS units (spike duration above 0.34 ms), according to standard nomenclature (Simons 1978; McCormick et al. 1985) (Fig 3.1G and 3.10). Unexpectedly, we found a larger fraction of FS units in sensory areas compared to frontal areas (Fig 3.10), which could in part reflect the differential distribution of PV neurons (Kim et al. 2017) and in part might indicate the known sampling bias of extracellular recordings limited to high-firing neurons, whereas sensory cortex typically has rather sparse activity. During task performance, both FS and RS units had a broad range of baseline firing rates (Fig 3.1H), which appeared to have a near log-normal distribution in both Novice and Expert mice (Fig 3.11). In agreement with previous literature, FS units fired at significantly higher rates than RS units in both Expert and Novice mice (Fig 3.1I and 3.11).

To investigate the classification of FS and RS units, we conducted a new set of recordings in which we measured the impact of stimulating genetically-defined GABAergic neurons in mice expressing channelrhodopsin-2 (ChR2) under the control of the vesicular GABA transporter (VGAT) (Zhao et al. 2011a). Blue light modulated the firing rate of RS and FS neurons in opposite directions, quantified both at the level of the population (Fig 3.1J) and at the level of individual neurons (Fig 3.1K). Overall, light stimulation increased the firing rate of FS units (blue light off: 4.3 ± 4.9 Hz; blue light on: 33.9 ± 32.7 Hz; 51 units recorded in 4 mice; non-parametric permutation test, $p < 10^{-4}$), whereas it decreased the spike rate of RS units (blue light off: 3.2 ± 3.4 Hz; blue light on: 1.3 ± 7.2 Hz; 130 units recorded in 4 mice; non-parametric permutation test, $p = 0.009$) (Fig 3.1L). As a second approach, and to avoid network effects of light stimulation (Sanzeni et al. 2020), we focused only on the first 10-ms window after the onset of light stimulation and identified the opto-tagged neurons based on their fidelity of responses, response onset latency and jitter (Fig 3.1M-O and 3.12). A larger fraction of neurons was opto-tagged among FS neurons compared to RS neurons. These data are therefore consistent with the hypothesis that the majority of FS units are likely to be inhibitory neurons, whereas the majority of RS units are likely to be excitatory neurons.

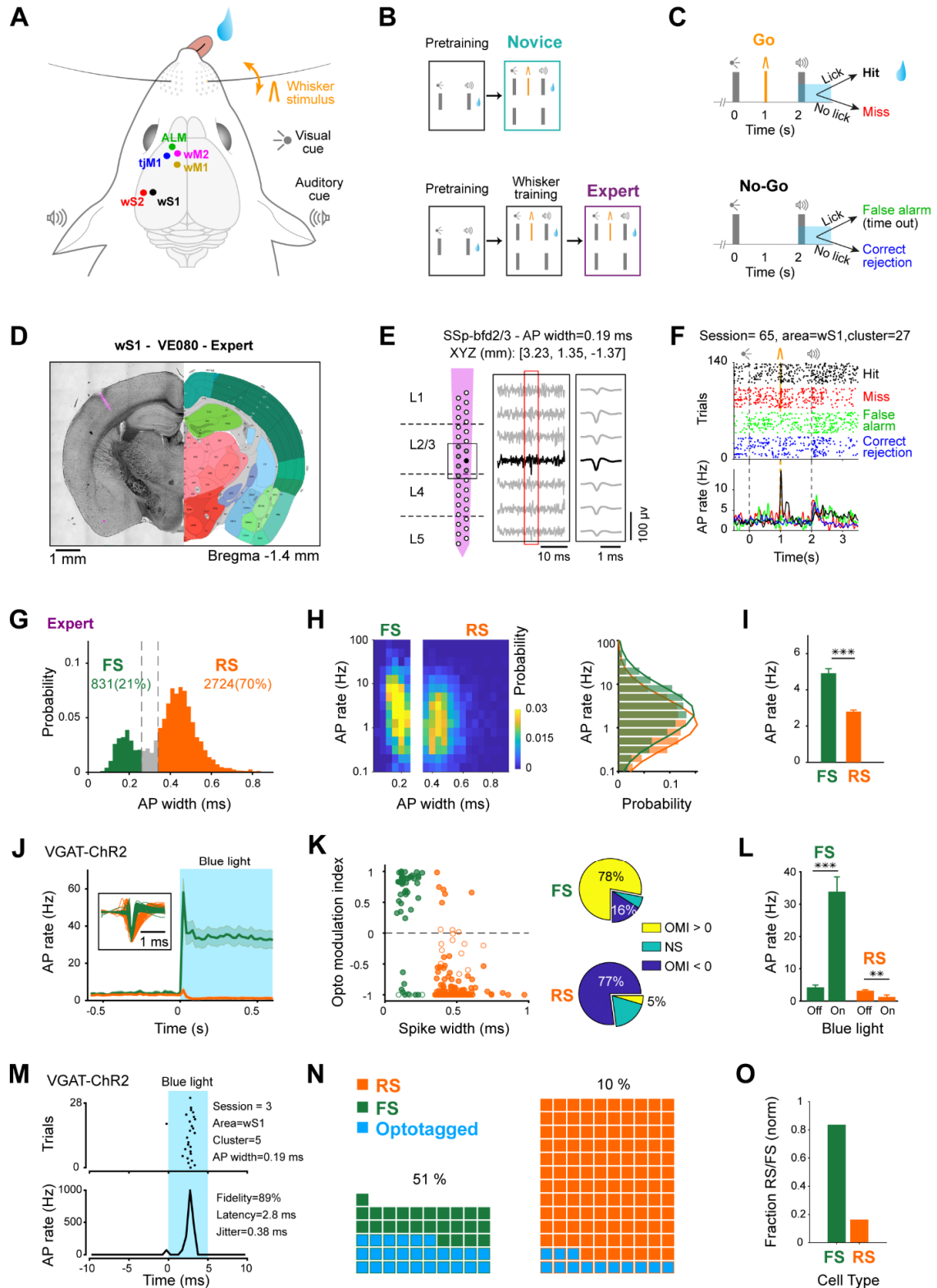


Fig 3.1. Multi-area recordings during delayed whisker detection task and assignment of RS and FS units to cortical sub-divisions.

(A) Schematic of the whisker detection task with the delayed response and the targets of silicon probe recordings.

(B) Training paradigm. Novice and Expert mice were first pretrained in a task, where licking after the auditory cue was rewarded. Expert mice were further trained to only lick in whisker trials.

(C) Final task structure used during recording sessions (for both groups of mice) and behavioral outcomes.

(D) Example coronal section of an Expert mouse brain with the fluorescent track of a probe in wS1, registered to the Allen Mouse Brain Atlas, <https://mouse.brain-map.org> (Wang et al. 2020b).

(E) Reconstructed laminar location of recording sites of the silicon probe shown in (D) according to the Allen Atlas (*left*); filtered recorded raw data of 7 sites around one detected spike; and average extracted spike waveform for this example neuron (*right*). After spike sorting, the position of each cluster (i.e. neuron) was assigned to the location of the recording site with the largest spike amplitude (filled circle), and spike width was calculated on the average spike waveform from this site.

(F) Raster plot and peri-stimulus time histogram for the example neuron shown in (E). Trials are grouped based on the outcome.

(G) Spike width distribution for neurons recorded in Expert mice. Neurons were categorized as fast-spiking (FS, spike width < 0.26 ms) or regular-spiking (RS, spike width > 0.34 ms). Neurons with intermediate spike width (gray bins) were excluded from further analyses.

(H) Baseline AP rate in Expert mice. Spike width distribution vs baseline AP rate (*left*) and overlay of spike rate distribution for RS and FS units. Note the log-normal distribution of baseline firing rates for both RS and FS units. Normal distributions were fitted to the RS and FS histograms (solid lines).

(I) Comparison of mean spike rate in RS vs FS neurons of Expert mice. Error bars: SEM. ***: $p < 0.001$, non-parametric permutation test.

(J-O) Opto-tagging GABAergic neurons in VGAT-ChR2 mice. (J) Grand average firing rate of RS (orange, spike width > 0.34 ms, 130 neurons from 4 mice) and FS (green, spike width < 0.26 ms, 51 neurons from 4 mice) units upon 100-Hz blue light stimulation (shading shows SEM). Note the suppression of activity in RS and the strong increase of activity in FS population. Inset shows the overlay of average spike waveforms for all RS and FS neurons.

(K) Opto modulation index (OMI) vs spike width (*left*) and percentage of modulated neurons (*right*). Each circle represents one neuron, filled circles indicate neurons with significant OMI ($p < 0.05$, non-parametric permutation tests). Pie charts show the percentage of neurons in each group with non-significant modulation (NS), and significant positive (OMI > 0) or negative (OMI < 0) modulation upon blue light stimulation.

(L) Blue light stimulation in VGAT-ChR2 mice increased the activity of narrow-spike neurons labeled as FS; while it suppressed the activity of broad-spike neurons labeled as RS. 100-500 ms after light onset. Error bars: SEM; **: $p < 0.01$; ***: $p < 0.001$.

(M) Raster plot and peri-stimulus time histogram during the first 10-ms of the 100-Hz trains of blue light stimulation for an example opto-tagged neuron.

(N) Waffle plots showing broad-spike (orange) and narrow-spike (green) neurons, and the opto-tagged neurons (blue) in each group. Numbers indicate the percentage of opto-tagged neurons in each group.

(O) Weighted proportion of neurons with narrow (FS) or broad (RS) spike among opto-tagged neurons in (N).

3.3.2 Strong task-modulation of fast-spiking neurons

Many RS units across all six cortical regions change their action potential firing rates in response to the whisker deflection (Esmaeili et al. 2021b). Here, we analyzed the responses of FS units during task performance in Novice and Expert mice (Fig 3.2). Averaged across cortical areas and quantified over the first 100 ms after whisker deflection, FS neurons in Novice mice increased their firing rate by 4.6 ± 7.9 Hz (392 units recorded in 8 mice) which was significantly higher (Wilcoxon rank-sum test, $p = 1 \times 10^{-34}$) than the increase in firing rate of RS neurons of 1.0 ± 2.4 Hz (1089 units recorded in 8 mice) (Fig 3.2A). Task-modulated RS and FS neurons were mainly excited, with only a small fraction showing significant reduction in firing rate (Fig 3.2B). Similarly, for Expert mice, whisker deflection evoked an increase of FS firing rate of 4.7 ± 9.1 Hz (831 units recorded in 18 mice) which was significantly higher (Wilcoxon rank-sum test, $p = 4 \times 10^{-71}$) than the increase in firing rate of RS neurons of 1.1 ± 3.9 Hz (2724 units recorded in 18 mice) (Fig 3.2C). In addition, for Expert mice, FS neurons were more strongly excited during the delay period compared to RS units (change in firing rate of FS neurons: 1.9 ± 4.8 Hz, 831 units recorded in 18 mice; change in firing rate of RS neurons: 0.7 ± 3.2 Hz, 2724 units recorded in 18 mice; Wilcoxon rank-sum test, $p = 1 \times 10^{-30}$). In Novice mice there was little delay period activity in either RS or FS units. The largest fraction of modulated neurons during the delay period were FS units in ALM of Expert mice, which were strongly excited (Fig 3.2D). Analysis of correct rejection trials in Novice and Expert mice, revealed that in the absence of the whisker stimulation neuronal activity remained at baseline levels during the delay period in both RS and FS neurons (Fig 3.13). Thus, the overall task selectivity of FS unit activity changed in a similar manner across learning compared to our previous quantification of RS units (Esmaeili et al. 2021b), with FS units having overall larger responses.

3.3.3 Rapid excitation of FS neurons

Investigating fast sensory processing evoked by the whisker deflection, we found an overall similar sequential recruitment of RS and FS units across cortical areas in both Novice and Expert mice (Fig 3.3, 3.14 and 3.15). The earliest excitation occurred in wS1 and wS2, followed by wM1 and wM2 (Fig 3.3A, 3.3B, 3.14 and 3.15). In wS1 and wS2, FS neurons responded at significantly shorter latency than RS units in both Novice and Expert mice (Fig 3.3C), as described later in more detail. Among the other areas, in Novice mice FS neurons responded with shorter latency than RS units in wM2 (FS: 47.7 ± 38.7 ms, 44/57 units in 8 mice; RS: 61.7 ± 40.7 ms, 126/244 units in 18 mice; Wilcoxon rank-sum test, $p = 0.047$, false discovery rate (FDR) corrected for multiple comparison), whereas in Expert mice FS neurons responded with shorter latency than RS units in wM1 (FS: 33.1 ± 35.1 ms, 101/134 units in 8 mice; RS: $54.2 \pm$

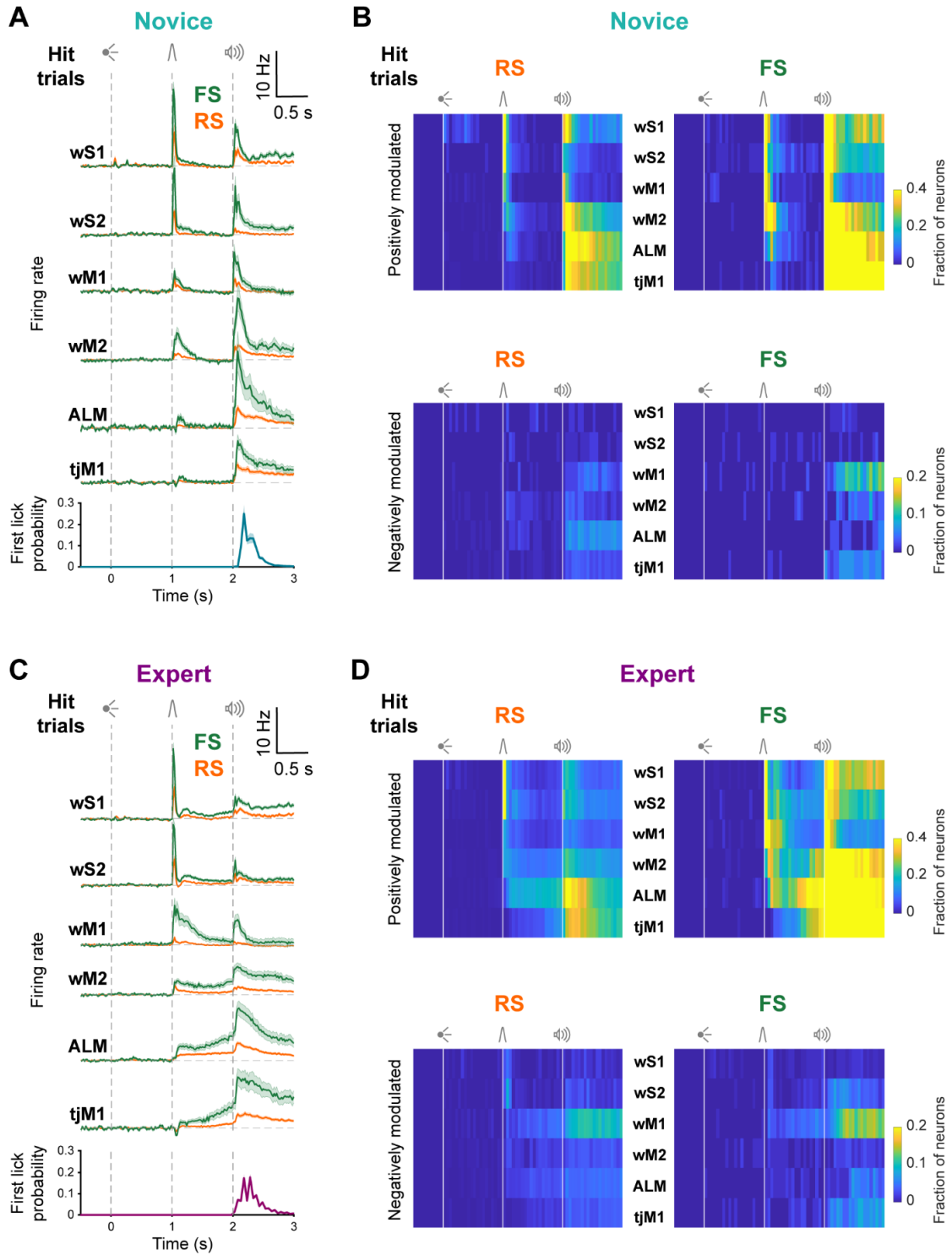


Fig 3.2. FS neurons had similar but larger task-modulation compared to RS neurons in the same region.

(A) Baseline-subtracted (2 s prior to visual onset) population firing rates (mean \pm SEM) of RS and FS neurons from different regions of Novice mice are superimposed for hit trials. wS1: 73 RS units in 7 mice, 103 FS units in 7 mice; wS2: 120 RS units in 8 mice, 68 FS units in 8 mice; wM1: 147 RS units in 7 mice, 66 FS units in 7 mice; wM2: 244 RS units in 7 mice, 57 FS units in 7 mice; ALM: 234 RS

units in 6 mice, 37 FS units in 5 mice; tjM1: 271 RS units in 8 mice, 61 FS units in 8 mice. Average first lick histogram for all Novice mice is shown in the bottom.

(B) Percentage of RS (*left*) and FS (*right*) neurons in different regions of Novice mice which are positively (*top*) or negatively (*bottom*) modulated compared to baseline (non-parametric permutation test, $p < 0.025$). (C) Similar to (A), but for Expert mice. wS1: 258 RS units in 15 mice, 237 FS units in 15 mice; wS2: 342 RS units in 12 mice, 161 FS units in 12 mice; wM1: 452 RS units in 11 mice, 134 FS units in 11 mice; wM2: 401 RS units in 10 mice, 107 FS units in 10 mice; ALM: 766 RS units in 12 mice, 109 FS units in 12 mice; tjM1: 505 RS units in 11 mice, 83 FS units in 11 mice. Average first lick histogram for all Expert mice is shown in the bottom.

(D) Similar to (B), but for Expert mice. Note the difference in color scales for fraction of positively or negatively modulated neurons in b and d.

48.7 ms, 243/452 units in 18 mice; Wilcoxon rank-sum test, $p = 3 \times 10^{-5}$, FDR-corrected for multiple comparison) (Fig 3.3C). Comparing Novice and Expert mice, the latency of RS units increased in wM1, but decreased in wM2, upon whisker learning (Fig 3.3D and 3.14B) (Esmaeili et al. 2021b). In contrast FS units did not significantly change their latency across learning in any of the six cortical regions (Fig 3.3D and 3.14B). These latency differences reveal that task learning is accompanied by fast dynamic changes in the relative timing of the recruitment of FS and RS units across wM1 and wM2.

3.3.4 Fast sensory processing in wS1 and wS2

Having observed the fastest whisker-evoked responses in wS1 and wS2 (Fig 3.3), we further compared RS and FS units in these areas, by focusing on their response in the first 50-ms window (Fig 3.4). The whisker-evoked change in firing rates of RS and FS units in wS1 and wS2 remained unchanged across Novice and Expert mice (Fig 3.4A-3.4C). However, in both regions and both groups of mice, FS units had larger evoked responses compared to RS units (Novice wS1: 6.0 ± 9.6 Hz for 73 RS units vs 13.9 ± 16.1 Hz for 103 FS units in 8 mice, $p < 10^{-4}$; Novice wS2: 4.0 ± 4.6 Hz, for 120 RS units vs 12.2 ± 15.8 Hz for 68 FS units in 8 mice, $p < 10^{-4}$; Expert wS1: 5.3 ± 9.1 Hz for 258 RS units vs 11.9 ± 13.9 Hz for 237 FS units in 18 mice, $p < 10^{-4}$; Expert wS2: 4.3 ± 8.7 Hz for 342 RS units vs 11.5 ± 13.6 Hz for 161 FS units in 18 mice, $p < 10^{-4}$; non-parametric permutation tests, FDR-corrected for multiple comparison) (Fig 3.4C). Neuronal responses in wS1 and wS2 often showed a biphasic response; a fast and sharp evoked response followed by a later secondary wave of spiking activity. While, the fast early response remained unchanged (Fig 3.2A and 3.2C), the late response increased across learning in RS and FS units of both wS1 and wS2 areas (Fig 3.17), consistent with previous work in wS1 in a whisker detection task without a delay period (Sachidhanandam et al. 2013).

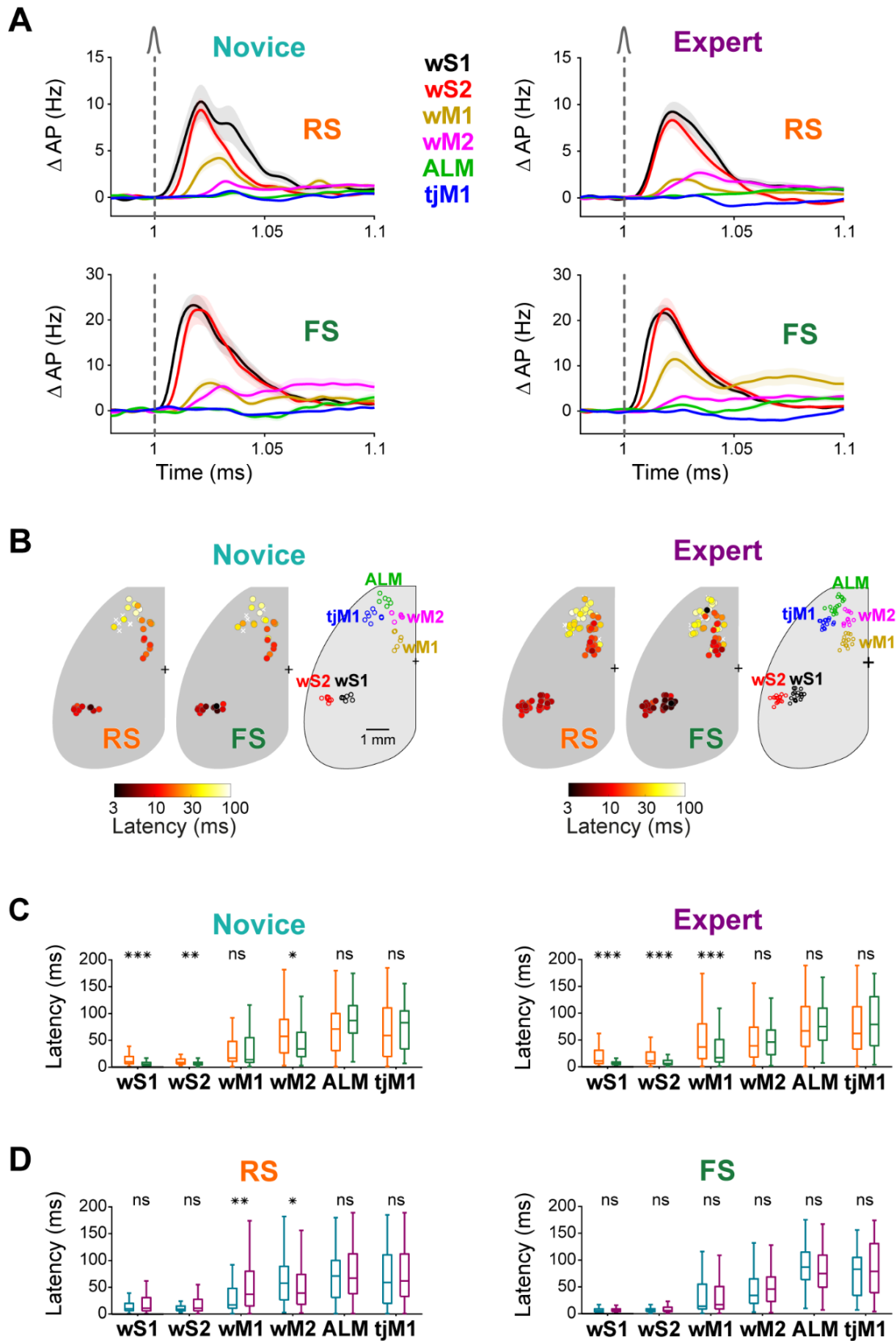


Fig 3.3. Fast propagation of sensory responses across cell classes and cortical regions.

(A) Change in firing rate (mean \pm SEM) of different cortical regions in the first 100-ms window after whisker deflection for RS (*top*) and FS (*bottom*) neurons in Novice (*left*) and Expert (*right*) mice (numbers of units and mice are the same as in Fig 2).

(B) Whisker-evoked response latency maps. For each silicon probe in Novice (*left*) and Expert (*right*) mice, average latency of whisker-evoked response is shown separately for RS and FS units. Circles represent silicon probes and are colored according to the average latency across all responsive neurons recorded on the probe.

(C) Comparison of latency of RS vs FS neurons in Novice (*left*) and Expert (*right*) mice.

(D) Comparison of latency of neurons from Novice vs Expert mice for RS (*left*) and FS (*right*) neurons. In (C) and (D), only neurons with a significant whisker response in the first 200 ms (compared to 200 ms before whisker onset, non-parametric permutation test, $p < 0.05$) were included. Midline represents the median, bottom and top edges show the interquartile range, and whiskers extend to 1.5 times the interquartile range. ***: $p < 0.001$, **: $p < 0.01$, *: $p < 0.05$, ns: $p \geq 0.05$.

The latencies of evoked activity in wS1 and wS2 were shorter for FS units compared to RS units for both Novice and Expert mice (Wilcoxon rank-sum tests FDR-corrected for multiple comparison: Novice wS1 $p = 1 \times 10^{-7}$; Novice wS2 $p = 1 \times 10^{-3}$; Expert wS1 $p = 1 \times 10^{-10}$; Expert wS2 $p = 9 \times 10^{-6}$) (Fig 3.4D). Comparing wS1 and wS2 areas, we found no significant difference in RS units response latencies, whereas FS units in wS1 fired at shorter latencies than FS units in wS2 (Wilcoxon rank-sum test FDR-corrected for multiple comparison, Novice: $p = 1 \times 10^{-4}$, Expert: $p = 3 \times 10^{-4}$). Both wS1 and wS2 therefore responded strongly and similarly to whisker stimulation in both Novice and Expert mice and no significant change was found in the response of RS or FS units across learning (Fig 3.4C and 3.4D).

Optogenetic inactivation by applying blue light in VGAT-ChR2 mice to either wS1 and wS2 during the delivery of the whisker stimulus induced a significant decrease in hit rate (Esmaeili et al. 2021). Here, we reanalyzed this inactivation data in a direct comparison across these two areas, and found a significantly stronger deficit induced by inactivation of wS2 compared to wS1 (wS1: $\Delta \text{hit} = -0.30 \pm 0.13$; wS2: $\Delta \text{hit} = -0.49 \pm 0.12$; Wilcoxon signed-rank test, $p = 0.0039$; 9 mice) (Fig 3.4E). However, potential differences in the spatial extent of the whisker deflection-evoked responses and the efficacy of optogenetic inactivation in wS1 versus wS2 make it difficult to conclude the relative importance of sensory processing in these two areas. Nonetheless, the data suggest that neuronal activity in both wS1 and wS2 is involved in execution of this whisker detection task.

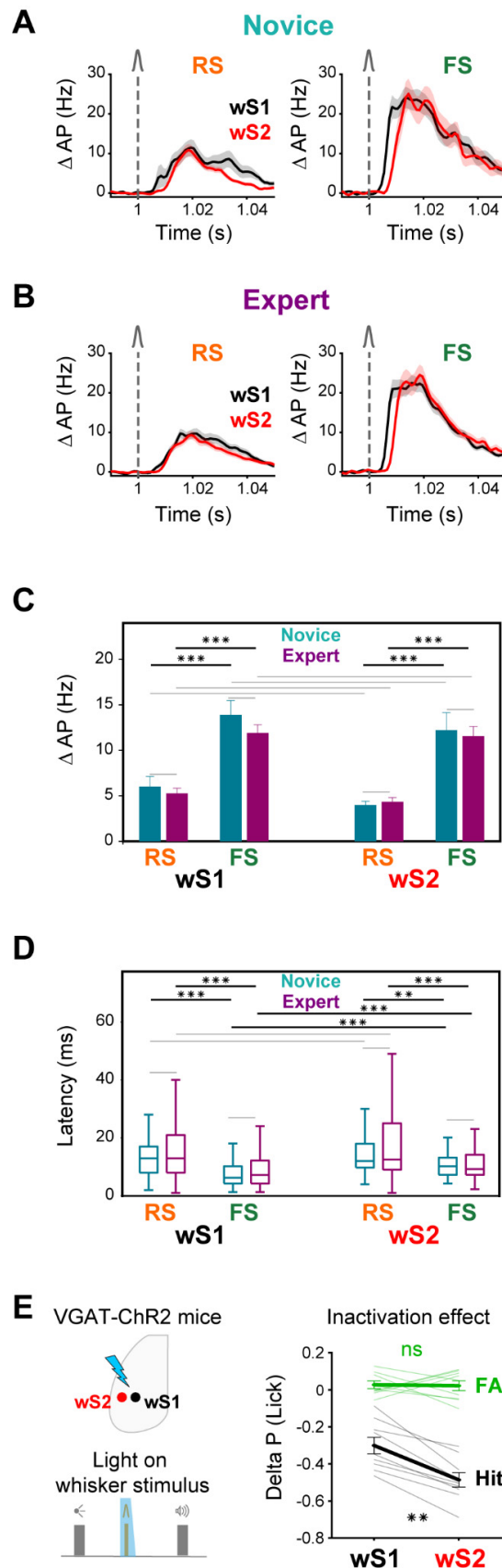
3.3.5 Parallel anatomical pathways from wS1 and wS2 to wM1 and wM2

Neuronal activity in wS1 and wS2 can only contribute to task execution by communicating with other brain regions. Along with various subcortical projections (Sippy et al. 2015; Takahashi et al. 2020), innervation of frontal cortical areas might be of particular importance in connecting sensation and movement (Esmaeili et al. 2020,

2021). Neurons in wS1 have previously been shown to innervate wM1 (Ferezou et al. 2007; Aronoff et al. 2010; Mao et al. 2011; Yamashita et al. 2018), but much less is known about the long-range output of wS2. We, therefore, carried out a set of experiments in which we expressed fluorescent proteins in neurons of wS1 and wS2 to examine their relative innervation targets in frontal cortex (Fig 3.5A). In the example experiment we injected a virus expressing a red fluorescent protein in wS1 and a green fluorescent protein in wS2. The fixed brains were imaged through serial section two photon tomography and registered to the Allen Mouse Brain Common Coordinate Framework (Wang et al. 2020) (Fig 3.5B). As previously shown, wS1 innervates the frontal cortex with a column of axons in a cortical region we label as wM1 (Fig 3.5C). Similarly, wS2 axons project to the frontal cortex in a columnar manner in a region we label as wM2 (Fig 3.5D). The location of wM2 appeared to be more anterior compared to the location of wM1 (Fig 3.5E and 3.5F), which is further confirmed by overlaying the projections (Fig 3.5G). Quantification of the location of the peak on average fluorescence across mice (Fig 3.5G and 3.5H, contours) revealed that wM1 was located at 1.0 mm anterior and 1.0 mm lateral to bregma, while wM2 was located at 1.9 mm anterior and 1.2 mm lateral to bregma. We further quantified wM1 and wM2 locations by averaging among frontal projection centers from individual mice (Fig 3.5H, markers) finding similar results (wM1: 1.0 ± 0.1 mm anterior and 1.0 ± 0.1 mm lateral to bregma across 4 mice; wM2: 1.7 ± 0.1 mm anterior and 1.0 ± 0.3 mm lateral to bregma across 4 mice). The primary and secondary somatosensory cortex, therefore, map onto the frontal cortex in a pattern consistent with mirror-symmetric somatotopy (Mao et al. 2011) and the frontal projections from the visual cortex (Sreenivasan et al. 2017).

3.3.6 Changes in fast sensory processing in wM1 and wM2

We next investigated the changes in whisker deflection-evoked neuronal activity in wM1 and wM2 across task learning. RS and FS neurons in both wM1 and wM2 and in both Novice and Expert mice showed obvious fast sensory-evoked modulation, dominated by units with increased action potential firing (Fig 3.2, 3.3, and 3.6). However, RS and FS neurons changed their activity patterns differentially across learning in these two neighboring cortical areas. In wM1, RS units had a smaller whisker-evoked response in Expert compared to Novice mice (Novice: 1.8 ± 3.0 Hz, 147 units recorded in 7 mice, Expert: 0.9 ± 3.9 Hz, 452 units recorded in 11 mice; non-parametric permutation test, $p = 0.002$) (Fig 3.6A and S10), whereas FS units had a larger response in Expert mice (Novice: 3.1 ± 3.6 Hz, 66 units recorded in 7 mice, Expert: 7.3 ± 16.9 Hz, 134 units recorded in 11 mice; non-parametric permutation test,



$p = 0.0008$) (Fig 3.6B and S3.10). The ratio of RS to FS firing in wM1 is therefore strongly changed in Expert mice in favor of FS units.

Fig 3.4. Fast whisker responses in FS neurons of sensory areas.

(A) Baseline-subtracted (50 ms prior to whisker onset) population firing rate (mean \pm SEM) of RS (*left*) and FS (*right*) neurons in wS1 and wS2 of Novice mice. wS1: 73 RS units in 7 mice, 103 FS units in 7 mice; wS2: 120 RS units in 8 mice, 68 FS units in 8 mice.

(B) Same as (A) but for Expert mice. wS1: 258 RS units in 15 mice, 237 FS units in 15 mice; wS2: 342 RS units in 12 mice, 161 FS units in 12 mice.

(C) Whisker-evoked change in spike rate in the first 50 ms (mean \pm SEM) in wS1 and wS2 for RS and FS units and in Novice and Expert mice. ***: $p < 0.001$. Gray lines show non-significant comparisons.

(D) Latency of the whisker-evoked response in wS1 and wS2. Only neurons with a significant whisker response in the first 100 ms (compared to 100 ms before whisker onset, non-parametric permutation test, $p < 0.05$) were included (Novice wS1: 56/73 RS units, 96/103 FS units, 8 mice; Novice wS2: 97/120 RS units, 57/68 FS units, 8 mice; Expert wS1: 190/258 RS units, 210/237 FS units, 18 mice; Expert wS2: 262/342 RS units, 148/161 FS units, 18 mice). Boxplots represent the distribution of the latency defined as the time to reach to half-maximum response. Midline represents the median, bottom and top edges show the interquartile range, and whiskers extend to 1.5 times the interquartile range. ***: $p < 0.001$, **: $p < 0.01$. Gray lines show non-significant comparisons.

(E) Inactivation of wS1 and wS2. *Left*: Schematic showing the inactivation of wS1 and wS2 areas during whisker stimulus presentation, in VGAT-ChR2 mice (Zhao et al. 2011a; Esmaeili et al. 2021b). Light trials were interleaved with no-light control trials and comprised 1/3 of total trials. *Right*: Change in hit and false-alarm (FA) rate - comparing light and no-light trials - upon optogenetic inactivation of wS1 and wS2. Light colors show individual mice (9 mice), thick lines represent averages, and error bars show SEM. **: $p < 0.01$, ns: $p \geq 0.05$.

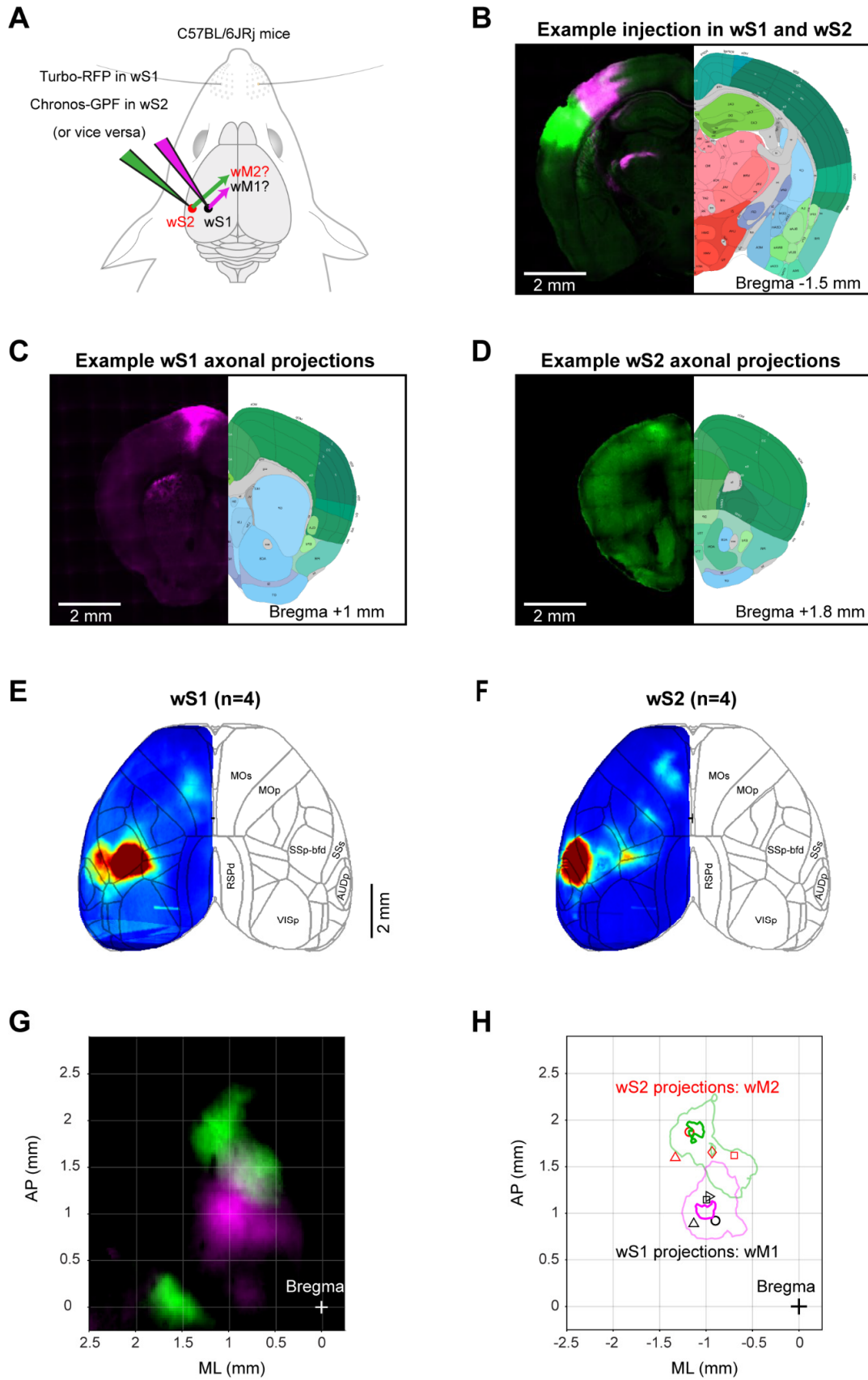


Fig 3.5. Distinct frontal projections of wS1 and wS2.

(A) Schematic of anterograde axonal tracing of wS1 and wS2 projections in the frontal cortex. Fluorescent proteins of different colors were expressed in wS1 and wS2 regions and frontal projection patterns were identified using anatomical reconstructions and registration to Allen Brain Atlas.

(B, C, D) Coronal sections showing example two-color injections in wS1 (magenta) and wS2 (green) and their frontal projection centers. Viral expression in wS1 and wS2 (B) and frontal sections showing the center of frontal projections in wM1 (C) and wM2 (D). All brains were registered to the Allen Mouse Brain Atlas, <https://mouse.brain-map.org>.

(E) Grand average cortical fluorescent map of wS1 projections (4 mice).

(F) Same as (E) but for wS2 projections (4 mice).

(G) Overlay of grand average fluorescent map of wS1 (magenta) and wS2 (green) projections in the frontal cortex.

(H) Center of projections from wS1 and wS2 in the frontal cortex. Contour plots at 95% and 75% maximum of the grand average fluorescent intensity from wS1 (magenta) and wS2 (green) projections, showing the location of wM1 and wM2 respectively. Markers show the center of projections for different mice. Projections in the same mice are indicated with similar markers.

In contrast, we found that neuronal activity in wM2 changed in a very different way across learning compared to wM1. In wM2, whisker deflection evoked an increased action potential firing in RS units of Expert mice compared to Novice mice (Novice: 1.0 ± 2.2 Hz, 244 units recorded in 7 mice, Expert: 1.5 ± 4.5 Hz, 401 units recorded in 10 mice; non-parametric permutation test, $p = 0.016$) (Fig 3.6C and 3.19), but a decreased firing of FS units (Novice: 4.5 ± 6.8 Hz, 57 units recorded in 7 mice, Expert: 2.7 ± 3.9 Hz, 107 units recorded in 10 mice; non-parametric permutation test, $p = 0.021$) (Fig 3.6D and 3.19). The balance of RS to FS unit activity in wM2 is therefore enhanced in favor of RS units across task learning.

To test how the coordination between sensory and motor cortices changed across learning, we quantified inter-areal interactions between wS1->wM1 and wS2->wM2 in the subset of sessions during which we obtained simultaneous paired recordings from these areas (Fig 3.6E and 3.6F). Averaged over individual pairs of neurons, the trial-by-trial correlation between the evoked activity of wS2-RS units with wM2-RS units increased across learning (Novice: 876 neuron pairs recorded in 6 mice, Expert: 583 neuron pairs recorded in 3 mice; Wilcoxon rank-sum test, $p = 0.039$) while it decreased between wS2-RS units and wM2-FS units (Novice: 343 neuron pairs recorded in 6 mice, Expert: 209 neuron pairs recorded in 3 mice; Wilcoxon rank-sum test, $p = 2.9 \times 10^{-4}$). Learning-related changes in firing rates might contribute to these apparent changes in correlations. However, while the activity of wM1-FS units increased across learning, the correlation between wS1-RS units and wM1-FS units did not change significantly, nor did the correlation between wS1-RS units and wM1-RS units. As an additional control, we measured inter-areal pairwise correlations using the spike time tiling coefficient (STTC) method (Cutts and Eglen 2014), which is suggested to be insensitive to firing rate (Fig 3.20B). Quantified using STTC analysis, the only significant increase in correlation across learning was observed between wS2-

RS to wM2-RS units (Novice: 3482 neuron pairs recorded in 6 mice, Expert: 2461 neuron pairs recorded in 3 mice; Wilcoxon rank-sum test, $p = 4.7 \times 10^{-11}$).

Trial-by-trial correlation of the population response showed similar patterns of change across learning in both area pairs as those observed in pair-wise correlation changes (Fig S12A). To further evaluate functional connectivity changes, we identified the number of directional connections (putative direct mono-synaptic connections) based on short-latency sharp peaks in the cross-correlograms between pairs of neurons from whisker sensory and whisker motor cortices (Fig 3.6F and S3.12C). The percentage of connections between wS2-RS units to wM2-RS units increased significantly across learning (Novice: 3 out of 1077 pairs in 6 mice, Expert: 17 out of 1066 pairs in 3 mice; Chi-squared proportion test, $p = 0.0032$).

All together, these data suggest that learning might increase the excitation to inhibition ratio of the sensory-evoked response in wM2, but decreases the ratio in wM1 in favor of inhibition. Increased activity of excitatory neurons in wM2 across learning could arise from the increase in functional connectivity between wS2 to wM2, and could in turn contribute to driving excitation in other frontal areas including ALM, which is known to be important for the motor planning of licking (Guo et al. 2014; Esmaeili et al. 2021).

3.3.7 Neuronal activity in tongue and jaw-related motor cortices

Previous studies have identified motor (tjM1) and premotor (ALM) areas of the neocortex associated with licking (Guo et al. 2014; Mayrhofer et al. 2019). Whisker deflection evoked a rapid decrease in both RS (Fig 3.7A) and FS (Fig 3.7B) neuronal activity in tjM1 of Expert mice (RS Novice: 0.0 ± 1.2 Hz, 271 units recorded in 8 mice, RS Expert: -0.6 ± 1.7 Hz, 505 units recorded in 11 mice; non-parametric permutation test, $p < 0.0001$; FS Novice: -0.2 ± 2.1 Hz, 61 units recorded in 8 mice, FS Expert: -1.5 ± 2.6 Hz, 83 units recorded in 11 mice; non-parametric permutation test, $p = 0.0003$). The observed suppression of neuronal activity in tjM1 evoked by the whisker stimulus in Expert mice was present across superficial and deep layers (Fig 3.13). The suppression of neuronal activity in tjM1 in Expert mice may help suppress early licking (Esmaeili et al. 2021). An active suppression of licking during the response window after the auditory cue is also required in correct rejection trials compared to miss trials, and we previously reported stronger suppression of RS units in correct rejection trials (Esmaeili et al. 2021). Here, we similarly observed a larger reduction of activity of FS neurons during the response window in correct rejection trials compared to miss trials (Fig 3.22). Thus, in periods when licking should be suppressed, there appears to be a decrease in firing of both RS and FS neurons in tjM1 across learning.

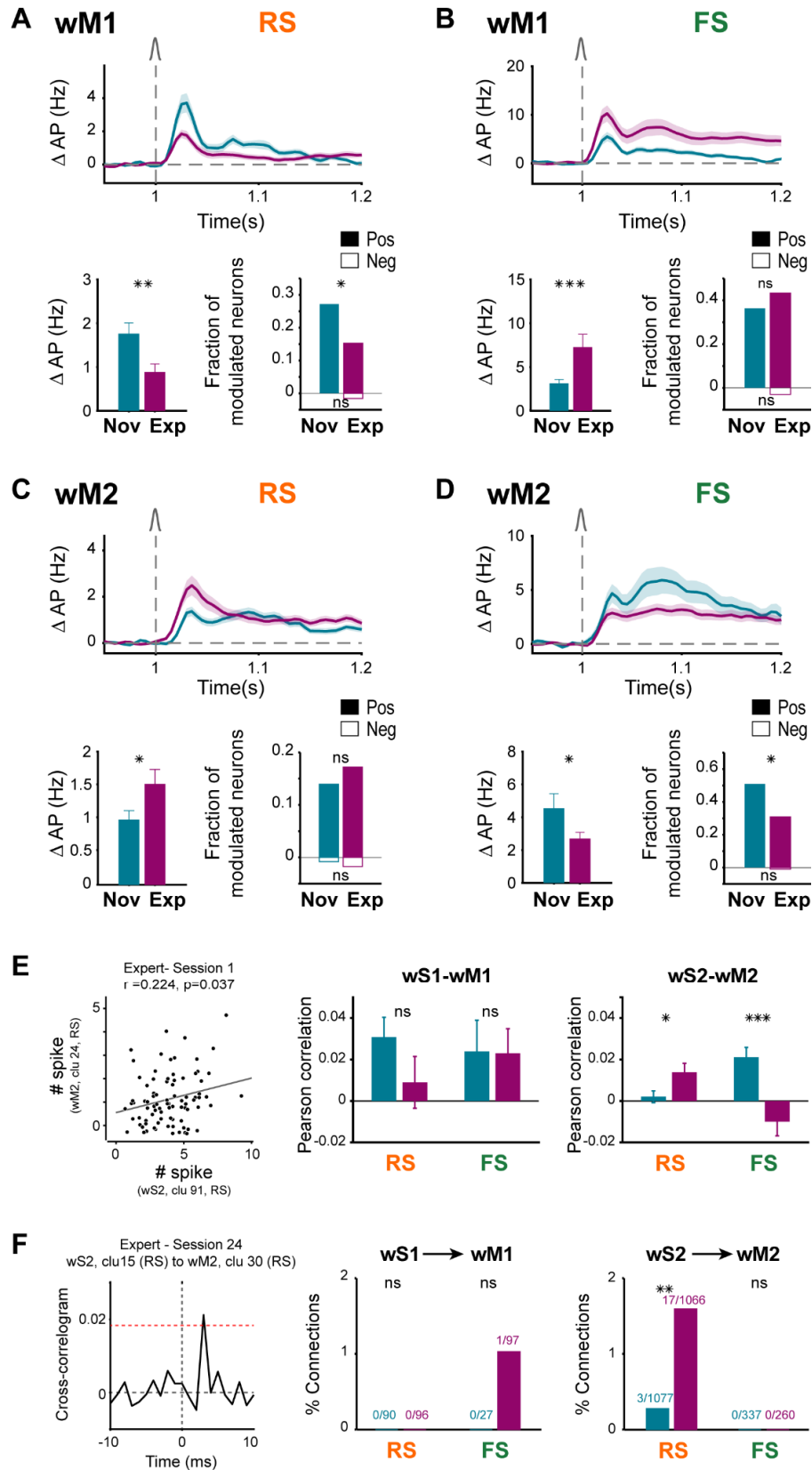


Fig 3.6. Learning differently modulated sensory responses of RS and FS neurons in wM1 and wM2 areas.

(A) Decrease of whisker response in wM1 RS neurons across learning. *Top*: baseline-subtracted (50 ms prior to whisker onset) population firing rate (mean \pm SEM) overlaid for Novice mice (147 neurons in 7 mice) and Expert mice (452 neurons in 11 mice). *Bottom*: Comparison of whisker-evoked response in Novice and Expert mice. Bar plots showing average population rate in 10-90 ms window (mean \pm SEM) after whisker onset and statistical comparison using non-parametric permutation test (*left*) (**: $p < 0.01$; *: $p < 0.05$). The fraction of positively (filled bars) or negatively (empty bars) modulated neurons in the same window (*right*). Modulation of individual neurons compared to a similar window size prior to whisker onset, was identified using non-parametric permutation test ($p < 0.005$). The fractions of modulated neurons in Novice and Expert were compared using a Chi-squared proportion test (*: $p < 0.05$; ns: $p \geq 0.05$).

(B) Increase of whisker response in wM1 FS neurons across learning. Panels are similar to (A) but for wM1 FS neurons in Novice (66 neurons in 7 mice) and Expert mice (134 neurons in 11 mice) (***: $p < 0.001$).

(C) Increase of whisker response in wM2 RS neurons across learning. Panels are similar to (A) but for wM2 RS neurons in Novice (244 neurons in 7 mice) and Expert mice (401 neurons in 10 mice).

(D) Decrease of whisker response in wM2 FS neurons across learning. Panels are similar to (A) but for wM2 FS neurons in Novice (57 neurons in 7 mice) and Expert mice (107 neurons in 10 mice).

(E) Pair-wise correlation between sensory and motor cortices in Novice and Expert mice. *Left*: Scatter plot showing the trial-by-trial correlation between the whisker-evoked response of an example pair of neurons in wS2 and wM2. Each circle represents the response of the neuronal pair in one trial. Circles were jittered slightly for the purpose of visualization. Gray line: least-squares regression. *Middle*: Average pair-wise Pearson correlation of wS1-RS units with wM1-RS (110 neuron pairs in 1 Novice mouse, and 68 neuron pairs in 2 Expert mice) and wS1-RS units with wM1-FS units (44 neuron pairs in 1 Novice mouse, and 89 neuron pairs in 2 Expert mice) separately. *Right*: Average pair-wise Pearson correlation of wS2-RS units with wM2-RS (876 neuron pairs in 6 Novice mouse, and 583 neuron pairs in 3 Expert mice) and wS2-RS units with wM2-FS units (343 neuron pairs in 6 Novice mouse, and 209 neuron pairs in 3 Expert mice). Error bars: SEM. Statistical comparison between Novice and Expert was performed using Wilcoxon rank-sum test (ns: $p \geq 0.05$; *: $p < 0.05$; ***: $p < 0.001$).

(F) Inter-areal functional connectivity identified based on cross-correlograms. *Left*: Example cross-correlogram between a pair of simultaneously recorded neurons from wS2 and wM2. Red dotted line shows the threshold for detecting sharp peaks. A directional connection from wS2 to wM2 was detected as there is a threshold crossing within the time lags between 0-10 ms. *Middle*: Percentage of detected directional connections from wS1-RS units to wM1-RS and wM1-FS units in 1 Novice and 2 Expert mice. *Right*: Percentage of detected directional connections from wS2-RS units to wM2-RS and wM2-FS units in 6 Novice and 3 Expert mice. The numbers on each bar represent the number of identified connections and the total number of recorded pairs. The fractions of connections in Novice and Expert were compared using a Chi-squared proportion test (ns: $p \geq 0.05$; **: $p < 0.01$).

Delay period activity emerges in RS units of ALM after task learning, and is causally involved in motor planning (Esmaeili et al. 2021). Analysis of FS units revealed a similar activity pattern, indicating that in ALM of Expert mice both RS and FS units increased their firing rate after whisker stimulus and remain elevated throughout the delay period (RS Novice: 0.1 ± 0.7 Hz, 234 units recorded in 6 mice, RS Expert: 1.4 ± 4.1 Hz, 766 units recorded in 12 mice; non-parametric permutation test, $p = 0.0001$; FS Novice: 0.2 ± 1.5 Hz, 37 units recorded in 5 mice, FS Expert: 3.7 ± 6.8 Hz, 109 units recorded in 12 mice; non-parametric permutation test, $p = 0.0001$). Furthermore, in Expert compared to Novice mice, a larger fraction of RS and FS units were significantly modulated during the delay, primarily with an increase in firing rate (Fig 3.7C and 3.7D). The delay period activity was more prominent in deeper layers of ALM for both RS and FS neurons (Fig 3.23).

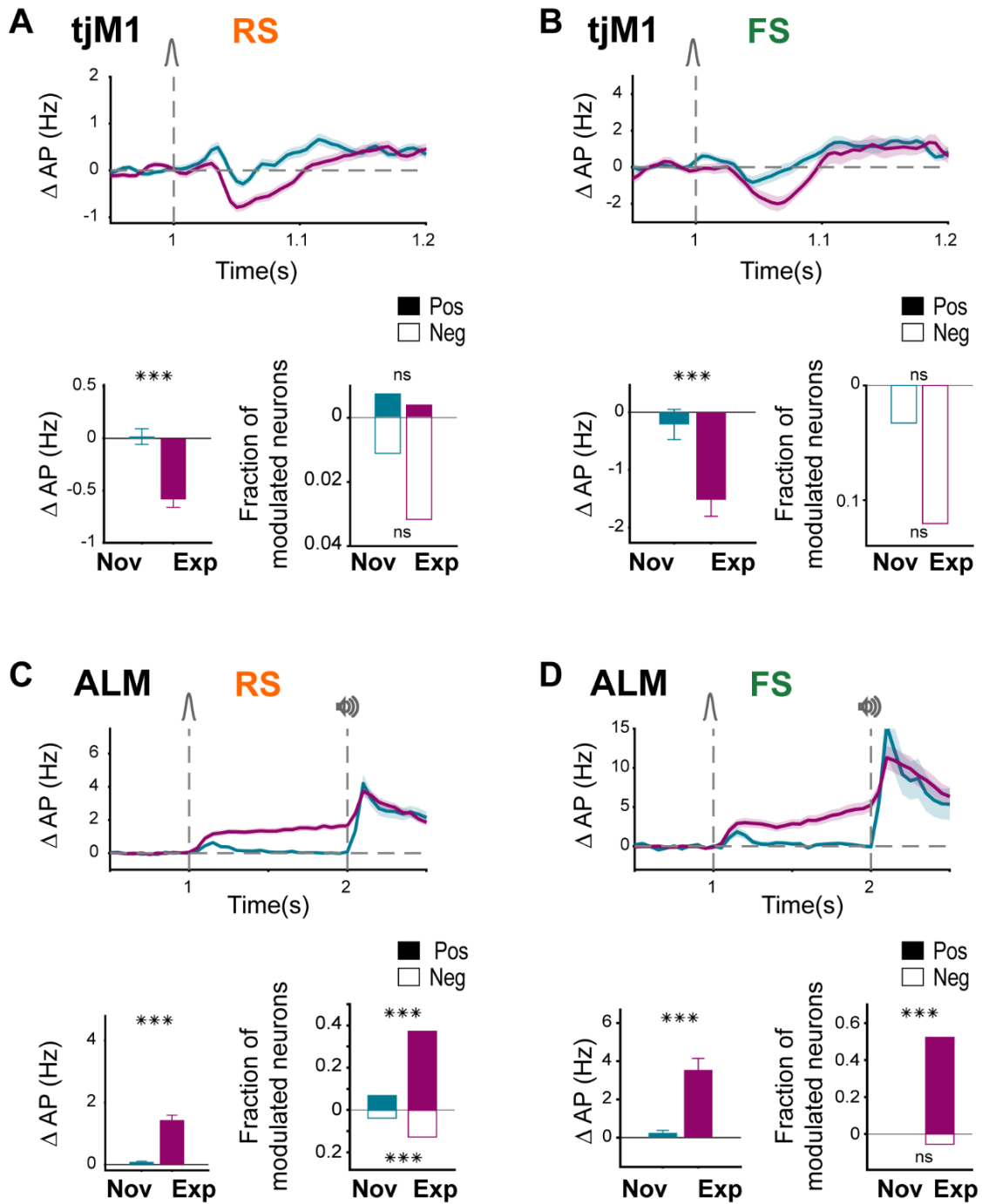


Fig 3.7. FS neuronal responses in tJM1 and ALM changed similarly to RS neurons.

(A) Suppression of tJM1 RS neurons in Expert mice. *Top*: baseline-subtracted (50 ms before whisker onset) firing rate (mean \pm SEM) overlaid for Novice (271 RS units in 8 mice) and Expert mice (505 RS units in 11 mice). *Bottom*: Comparison of whisker-evoked response in Novice and Expert mice. Bar plots showing population rate in 40-90 ms window (mean \pm SEM) after whisker onset and statistical comparison using non-parametric permutation test (*left*, ***: $p < 0.001$); fraction of positively (filled bars) or negatively (empty bars) modulated neurons in the same window (*right*). Modulation of individual neurons compared to a similar window size prior to whisker onset, was identified using non-parametric

permutation test ($p < 0.005$). Fraction of modulated neurons in Novice and Expert were compared using a Chi-squared proportion test (ns: $p > 0.05$).

(B) Suppression of tJM1 FS neurons in Expert mice. Panels are similar to (A) but for tJM1 FS neurons in Novice (61 neurons in 8 mice) and Expert mice (83 neurons in 11 mice).

(C) Delay activity of RS neurons in Expert mice. *Top*: baseline-subtracted (1 s before whisker onset) firing rate (mean \pm SEM) overlaid for Novice (234 RS units in 6 mice) and Expert mice (766 RS units in 12 mice). *Bottom*: Comparison of whisker-evoked response in Novice and Expert mice. Bar plots showing population rate in 200-1000 ms window (mean \pm SEM) after whisker onset and statistical comparison using non-parametric permutation test (*left*, ***: $p < 0.001$); fraction of positively (filled bars) or negatively (empty bars) modulated neurons in the same window (*right*). Modulation of individual neurons compared to a similar window size prior to whisker onset, was identified using non-parametric permutation test ($p < 0.005$). Chi-squared proportion test: ***: $p < 0.001$, ns: $p > 0.05$.

(D) Delay activity of ALM FS neurons in Expert mice. Panels are similar to (C) but for ALM FS neurons in Novice (37 FS units in 5 mice) and Expert mice (109 FS units in 12 mice).

Preparatory movements were prominent during delay periods in Expert mice and accounted for a large part of the neuronal activity during the delay period (Esmaeili et al. 2021b). Nonetheless, investigating the subset of quiet trials without delay period movements, we found that significant neuronal delay period activity still remains in both RS and FS units (Fig 3.24). Therefore, both RS and FS units in ALM develop persistent delay period activity across learning which likely contributes to the storage of a licking motor plan.

3.3.8 Changes in excitation and inhibition across learning

To the extent that we can equate RS units with excitatory neurons and FS units with inhibitory neurons (Fig 3.8A), we can begin to compute changes in the putative balance of excitation and inhibition as the changes in RS and FS firing rates across learning, providing a simple summary for comparisons (Fig 3.8). To do so, for each area (Fig 3.8B) and cell class (RS or FS), we calculated a learning modulation index (LMI) defined as the normalized difference between the mean firing rate in Expert and Novice mice. Positive LMI values indicate an increase in neuronal activity across learning, while negative values represent suppression. The putative excitation and inhibition changed in opposite directions in wM1 (RS LMI = -0.33; FS LMI = 0.38) and wM2 (RS LMI = 0.22; FS LMI = -0.25) (Fig 3.8C and 3.8D). In contrast, putative excitation and inhibition changed in the same direction across learning in ALM (RS LMI = 0.88; FS LMI = 0.87) and tJM1 (RS LMI = -0.92; FS LMI = -0.75) (Fig 3.8C and 3.8D). Subtraction of the LMI of RS from the LMI of FS units as a measure of the change in the putative excitation-inhibition balance across learning, showed a decreased putative excitation-inhibition balance in wM1, but an increased putative excitation-inhibition balance in wM2 (E-I LMI wM1 = -0.72; E-I LMI wM2 = 0.46) (Fig 3.8E and 3.8F). Interestingly, the apparent balance of excitation and inhibition thus appears to change differently across learning in distinct cortical areas.

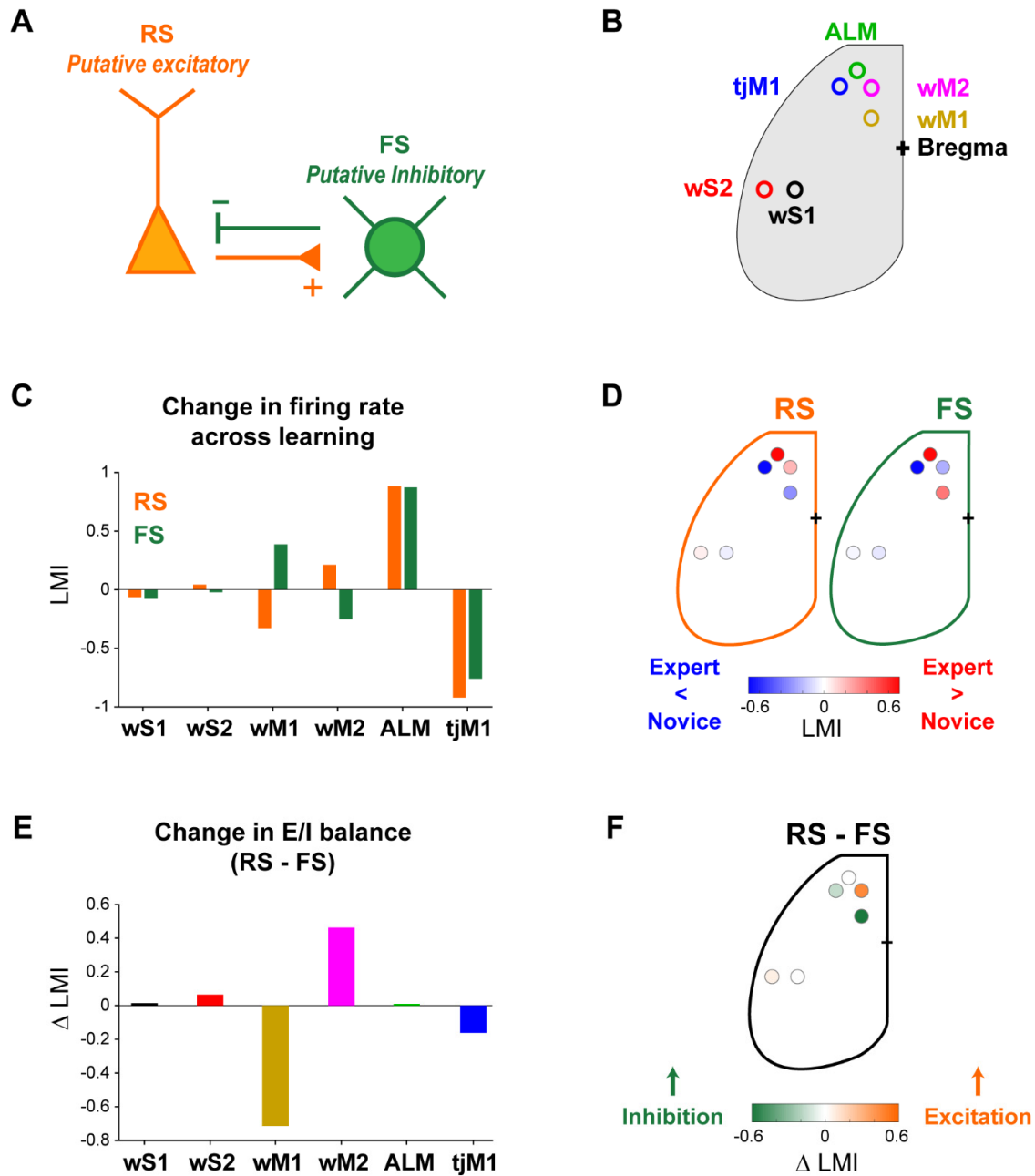


Fig 3.8. Diverse changes of putative excitation-inhibition balance in different cortical regions across learning.

(A) FS (putative PV GABAergic inhibitory) neurons and RS (putative glutamatergic excitatory pyramidal) neurons are typically considered to be strongly and reciprocally connected in local cortical microcircuits providing fast balance of excitation and inhibition.

(B) Schematic showing the location of different cortical regions.

(C) Learning modulation index (LMI) in different cortical regions for RS and FS units, representing learning-induced change in putative excitation and inhibition, respectively. LMI was quantified as the normalized difference between whisker-evoked firing rate in Novice and Expert mice.

(D) Map of the putative excitation-inhibition change across learning, shown as LMI across cortical regions for RS and FS neurons.

(E) Change in the putative excitation-inhibition balance across learning, quantified as difference between LMI of RS and FS neurons in different cortical regions.

(F) Cortical map of the putative excitation-inhibition balance change across learning, calculated as LMI difference between RS and FS neurons.

3.4 Discussion

Comparing neuronal activity across task learning revealed distinct changes in RS and FS units in various neocortical areas. Strikingly, in tJM1 and ALM, RS and FS neurons changed firing rates congruently across learning, but in wM1 and wM2, RS and FS changed firing rate incongruently, pointing toward learning-related changes in the balance of cortical excitation and inhibition, with an overall change across learning towards excitation of wM2 and inhibition of wM1.

In wS1 and wS2, we found that there was little change in overall neuronal activity across learning, consistent with a robust coding of the sensory stimulus in these areas of the somatosensory cortex (Fig 3.4). Our results do not rule out a possible reorganization of neuronal activity across learning with some neurons increasing and others decreasing their response to whisker stimulation. Indeed, in a whisker detection task without a delay period, we previously found in wS1 of expert mice that neurons projecting to wS2 had stronger task-related depolarizations compared to neurons projecting to wM1, whereas we found the converse in naive mice (Yamashita and Petersen 2016). Consistent with an important role for wS2 in whisker detection tasks (Kwon et al. 2016; Le Merre et al. 2018; Esmaeili et al. 2021), here we found that optogenetic inactivation of wS2, as well as wS1 inactivation, induced a strong impairment in task performance (Fig 3.4E).

Neuronal activity in wS1 and wS2 can directly influence the frontal cortex through direct monosynaptic connections with wM1 and wM2, which we characterized anatomically in this study (Fig 3.5). Interestingly, neuronal activity in wM1 and wM2 changed profoundly across learning (Fig 3.6). RS units in wM1 decreased their sensory-evoked response, whereas RS units in wM2 increased their response across learning (Esmaeili et al. 2021). Trial-by-trial correlations (Fig 3.6E) and spike-triggered connectivity analyses (Fig 3.6F) both pointed to the enhanced coupling between wS2-RS units and wM2-RS units, which could, at least in part, result from potentiation of monosynaptic inputs from wS2-RS units to wM2-RS units, although other more complex mechanisms could equally play a role. In contrast, FS units in wM1 increased their response across learning, whereas FS units in wM2 decreased their evoked neuronal activity. Our data thus suggest a differential change in the balance between

excitation and inhibition with learning in wM1 and wM2, with enhanced sensory-evoked inhibition relative to excitation in wM1 but enhanced excitation relative to inhibition in wM2 (Fig 3.8). Changes in inhibitory neuronal activity could contribute importantly to task learning. Increased recruitment of fast inhibition in wM1 across learning could suppress the response of excitatory neurons in wM1. We speculate that suppression of activity in wM1 could enhance whisker detection performance by reducing whisker movements (Sreenivasan, Esmaeili, et al. 2016), which otherwise could cause confounding sensory-reafference signals. On the other hand, the reduced firing of inhibitory neurons in wM2 across learning could allow the excitatory neurons to respond more strongly. Disinhibition of wM2 might be an important step allowing the propagation of whisker sensory information in higher order motor cortex, perhaps contributing to exciting ALM through local intracortical connections (Esmaeili et al. 2021). Interestingly, disinhibition of wS1 has previously been reported to contribute to the execution of a whisker detection task without a delay (Sachidhanandam et al. 2016), suggesting the general importance of considering changes in inhibitory neuronal activity for controlling goal-directed sensorimotor transformations (Hofer et al. 2011; Pinto and Dan 2015; Allen et al. 2017). Several mechanisms could contribute to disinhibition, including the activation of GABAergic neurons preferentially innervating other GABAergic neurons, as found in the auditory cortex during fear learning (Letzkus et al. 2011). Neuromodulation could also play an important role, for example through cholinergic reward signals (Hangya et al. 2015), which could drive the excitation of vasoactive intestinal peptide-expressing GABAergic neurons (Fu et al. 2014; Gasselin et al. 2021), in turn causing disinhibition through their prominent innervation of PV and somatostatin-expressing GABAergic neurons (Lee et al. 2013; Pfeffer et al. 2013; Pi et al. 2013).

In contrast to the divergent changes across learning in RS and FS unit activity in wM1 and wM2, RS and FS units changed their activity patterns in the same way in ALM and tjM1 (Fig 3.7). Suppression of tjM1 activity in Expert mice has a causal role in delayed licking behavior (Esmaeili et al. 2021). The rapid suppression of RS units across learning in tjM1 was mirrored by a rapid suppression of FS unit firing (Fig 3.7A and 3.7B). Overall there was thus no apparent change in the balance of excitation and inhibition in tjM1 across learning (Fig 3.8). The rapid decrease in firing of both RS and FS units evoked by the whisker deflection in Expert mice could result from many different mechanisms, including a possible reduced thalamic or other long-range input to the orofacial sensorimotor cortex.

Neuronal delay period activity in ALM is of critical importance for motor planning of licking (Guo et al. 2014, 2017; Esmaeili et al. 2021). We found that both RS and FS units increase firing rate during the delay period in Expert mice, but not Novice mice (Fig 3.7). Similar to tjM1, there was therefore no apparent change in the balance of excitation and inhibition in ALM across learning (Fig 3.8). Thalamic activity has been

shown to be necessary for maintaining ALM activity during delay periods (Guo et al. 2017b; Gao et al. 2018b; Chabrol et al. 2019b), and increased thalamic input likely excites both RS and FS neurons either directly (Gabernet et al. 2005; Cruikshank et al. 2007; Bagnall et al. 2011; Delevich et al. 2015; Sermet et al. 2019; Rodriguez-Moreno et al. 2020; Anastasiades et al. 2021; Shepherd and Yamawaki 2021) or indirectly through local cortical microcircuitry. ALM neurons in turn, project to thalamic nuclei (Guo et al. 2017b). In agreement with this, we observed larger delay activity in layer 6 of ALM where many corticothalamic neurons are located (Harris and Shepherd 2015) (Fig 3.23).

In future studies, it will be of importance to better define the various classes of neurons beyond our current classification of RS and FS units. For example, diverse classes of GABAergic neurons can be defined through the expression of Cre and Flp recombinase under different promoters (Taniguchi, He, Wu, Kim, Paik, Sugino, Kvitsiani, Kvitsani, et al. 2011; He et al. 2016), enabling functional identification of these neurons through opto-tagging (Kvitsiani et al. 2013). Different classes of excitatory neurons might be best classified through their long-range axonal projections, which could be functionally identified through optogenetic stimulation of axonal branches in target regions (Economo et al. 2018). The current study thus takes a first step towards differentiating neuronal activity in various cortical regions across learning, but further experiments will be needed in order to gain a more complete understanding of neocortical cell type-specific changes, as well as, importantly, investigating subcortical regions which are likely to play profound roles in both learning and execution of goal-directed sensorimotor transformations.

3.5 Materials and Methods

The results in this study are largely based on further analysis of our recently published dataset available Open Access via the CERN database Zenodo (<https://doi.org/10.5281/zenodo.4720013>). The methods used to obtain the published dataset were fully described in the accompanying journal publication (Esmaeili et al. 2021b), and are only briefly introduced here. The new analyses are described in detail below. We also carried out two new series of experiments: i) optogenetic tagging of GABAergic neurons and ii) anatomical analysis of axonal projections from wS1 and wS2 to the frontal cortex. All experimental procedures were approved by the Swiss Federal Veterinary Office (Licences VD1628.7 and VD1889.4) and were conducted in accordance with the Swiss guidelines for the use of research animals. The methods for obtaining the new data are described in detail below. The full data set and analysis code used to generate the figures and results described in this study are available via the Open Access CERN database Zenodo: <https://doi.org/10.5281/zenodo.6511622>.

3.5.1 Behavioral paradigm and electrophysiological recordings

Both Novice and Expert mice were trained in the first stage of the task, where in all trials a visual (trial onset) and auditory cues were presented, and licks during a 1-second response window following the auditory cue were rewarded (Fig 3.1A and 3.1B). To initiate a trial, mice needed to withhold licking (i.e. not touching the water spout) for a quiet period of 2-3 seconds following an inter-trial-interval of 6-8 seconds. Visual cue (200 ms, green LED) and auditory cue (200 ms, 10 kHz tone of 9 dB added on top of the continuous background white noise of 80 dB) were separated with a delay period which gradually was increased to 2 seconds over Pretraining days. Licking before the response period (Early lick) aborted the trial and introduced a 3-5 second timeout. The Expert mice went through a second training phase (Whisker-training), in which only Go trials (i.e. trials with a whisker stimulus) were rewarded. Whisker stimulus (10 ms cosine 100 Hz pulse through a glass tube attached to a piezoelectric driver) was delivered to the right C2 whisker 1 second after the visual cue onset in half of the trials. Electrophysiological data from both groups of mice were acquired during the final task conditions (Fig 1C). Novice mice licked in both Go and No-Go trials; while Expert mice had learned to lick selectively in Go trials (Esmaeili et al. 2021b).

Extracellular recordings were performed using single-shank silicon probes (A1x32-Poly2-10mm-50 s-177, NeuroNexus, MI, USA) with 32 recording sites covering 775 μm of the cortical depth. In each session two probes were inserted in two different brain targets acutely. Probes were coated with Dil (1,1'-Diocetyl-3,3,3',3'-Tetramethylindocarbocyanine Perchlorate, Invitrogen, USA) for post-hoc recovery of

the recording location (see below). The neural data were filtered between 0.3 Hz and 7.5 kHz and amplified using a digital headstage (CerePlex™ M32, Blackrock Microsystems, UT, USA). The headstage digitized the data with a sampling frequency of 30 kHz. The digitized signal was transferred to our data acquisition system (CerePlex™ Direct, Blackrock Microsystems, UT, USA) and stored on an internal HDD of the host PC for offline analysis.

3.5.2 Optogenetic tagging of GABAergic neurons

To evaluate to what extent the categorization of units as RS or FS based on spike width is useful for assessing the activity of excitatory versus inhibitory neurons, we performed simultaneous electrophysiological recordings and blue light stimulations in wS1 in 5 sessions from 4 VGAT-ChR2 mice, which express ChR2 in all neocortical GABAergic neuron types. A craniotomy was made over the C2 barrel column, identified by optical intrinsic imaging. For each mouse, a silicon probe (A1x32-Poly2-10mm-50 s-177-A32, NeuroNexus, MI, USA) was slowly lowered to a depth of ~1000 μm in the C2 barrel column, and an optic fiber (400 μm ; NA = 0.39, Thorlabs) coupled to a 470 nm high power LED (M470F3, Thorlabs, USA) was positioned close to the brain surface and the probe. A 100 Hz train of blue light pulses (50% duty cycle, mean power 1-2 mW) with the duration of 600 ms was applied. Light pulse train was followed by an additional 100 ms ramping down to prevent rebound excitation. In total, 51 FS and 130 RS units were identified in 5 sessions from 4 mice.

3.5.3 Anatomical analysis of axonal projections from wS1 and wS2 to frontal cortex

An AAV1.hSyn.TurboRFP.WRPE.rBG (titer: 6.5×10^{13} vg/ml, AV-1-PV2642, UPenn Vector Core, USA) was injected at the center of C2 barrel column in wS1 (or in the C2 whisker representation in wS2), and an AAV5.Syn.Chronos-GFP.WPRE.bGH (titer: 3.82×10^{13} vg/ml, AV-5-PV3446, UPenn Vector Core, USA) or AAV5.hSyn.hChR2(H134R)-eYFP.WRPE.hGH (titer: 7×10^{12} vg/ml, AV-1-26973P, UPenn Vector Core, USA) was injected in the C2 whisker representation in wS2 (or C2 barrel column in wS1). In total 100 nl of virus was delivered in each area at 300-400 μm and 700-800 μm below the dura, through a glass pipette (PCR Micropipets 1 – 10 ml, Drummond Scientific Company, USA) with a 21 – 27 μm inner tip diameter. After 4 weeks of expression, mice were perfused with phosphate buffered saline (PBS) followed by 4% paraformaldehyde (Electron Microscopy Science, USA) in PBS. The brains were post-fixed overnight at room temperature. Next, we embedded the brains in 3-5 % oxidized agarose (Type-I agarose, Merck KGaA, Germany) and covalently

cross-linked the brain to the agarose by incubating overnight at 4 °C in 0.5 – 1 % sodium borohydride (NaBH₄, Merck KGaA, Germany) in 0.05 M sodium borate buffer. We imaged the brains in a custom-made two-photon serial sectioning microscope, which was controlled using Matlab-based software (ScanImage 2017b, Vidrio Technologies, USA) and BakingTray (<https://github.com/BaselLaserMouse/BakingTray>, version master: 2019/05/20, extension for serial sectioning) (Han et al. 2018b). The setup consists of a two-photon microscope coupled with a vibratome (VT1000S, Leica, Germany) and a high-precision X/Y/Z stage (X/Y: V-580; Z: L-310, Physik Instrumente, Germany). The thickness of a physical slice was set to be 50 µm for the entire brain and we acquired optical sections at 10 µm using a high-precision piezo objective scanner (PIFOC P-725, Physik Instrumente, Germany) in two channels (green channel: 500 – 550 nm, ET525/50, Chroma, USA; red channel: 580 – 630 nm, ET605/70, Chroma, USA). Each section was imaged by 7 % overlapping 1025x1025-µm tiles. A 16x water immersion objective lens (LWD 16x/0.80W; MRP07220, Nikon, Japan), with a resolution of 1 µm in X and Y and measured axial point spread function of ~5 µm full width at half maximum. After image acquisition, the raw images were stitched using a Matlab-based software (StitchIt, <https://github.com/BaselLaserMouse/StitchIt>). The stitched images were then down-sampled by a factor of 25 in X and Y obtaining a voxel size of 25 x 25 x 25 µm, using a Matlab-based software (MaSIV, <https://github.com/alexanderbrown/masiv>) or using the software Fiji (<https://imagej.net/Fiji>). The brains were then registered to Allen Mouse Common Coordinate Framework version 3 (Wang et al. 2020b) using a python-based tool (Brainreg, <https://github.com/brainreg/brainreg>) (Tyson et al. 2022). We then acquired 2-D maps of cortical projection patterns, by only considering layer 2/3 of cortex and calculating 99% intensity levels across cortical depth using custom-developed analysis routine (https://renkulab.io/projects/guier.romain/brainreg/files/blob/notebooks/notebooks_napari_brainreg.ipynb). Grand average 2-D maps of cortical projections (Fig 5E and F) were obtained by first normalizing each mouse's map to its global maximum (i.e. injection site intensity value), and then averaging across mice. The 95% and 75% contours (Fig 5H) for wS1 and wS2 frontal projections sites were calculated on these grand average maps. The center of frontal projection site for individual mice was identified by finding the local maxima in the frontal cortical region (Fig 5H).

3.5.4 Data analysis and statistics

Single neuron whisker-evoked response latency

When measuring the latency of the whisker-evoked response in the firing rate of individual neurons in all cortical areas (Fig 3.3C and 3.3D), the analysis was limited to

the first 200-ms window following the whisker stimulus. First, we examined whether each neuron was modulated (positively or negatively) in the 200-ms window following the whisker stimulus compared to a 200-ms window prior to the whisker onset. For responsive neurons ($p < 0.05$, non-parametric permutation test), latency - calculated on the temporally smoothed peristimulus time histograms (1 ms non-overlapping bins filtered with a Gaussian kernel with $\sigma = 10$ ms) - was defined as the time where the neural activity reached half maximum (half minimum for suppressed neurons) within the 200-ms window. Only responsive neurons are included in boxplots in Fig 3.3C and 3.3D and Fig. 3.14. For wS1 and wS2 regions, where neurons had shorter latencies, we recalculated the latencies with higher temporal resolution (Fig 3.4D). We limited the analysis to 100-ms window following the whisker onset, and calculated latencies on smoothed peristimulus time histograms (1 ms non-overlapping bins filtered with a Gaussian kernel with $\sigma = 5$ ms).

Quantifying opto-tagged neurons

In recordings from VGAT-ChR2 mice (Fig 3.1J-O and 3.12), we quantified the effect of blue light stimulation on firing rates, on both slow and fast time scales. To quantify the effect of light on each individual neuron we first calculated an opto modulation index (OMI, Fig 1K). OMI was defined, in light trials, as the normalized difference between the average firing rate during the light window (100-500 ms after light onset) vs a baseline of similar duration (-400-0 ms prior to light onset):

$$OMI_n = \frac{AP_{light_n} - AP_{baseline_n}}{AP_{light_n} + AP_{baseline_n}}$$

Subsequently, to measure the effect of light stimulation devoid of potential network effects, we focused on the first 10-ms immediately after light onset. We then quantified within this window the following parameters: fidelity, defined as the percentage of trials with at least one spike during this window; latency, as the average delay to first spike in trials with at least one spike during 10-ms window; and jitter as the standard deviation of the latency. We then labeled neurons as opto-tagged with fidelity > 20%, latency < 4.5 ms, and jitter < 2 ms (Fig 3.1M-O and 3.12).

3.5.5 Inter-areal functional connectivity measures

Taking advantage of the subset of sessions with simultaneous paired recordings from whisker sensory and motor cortices, we used two separate methods to examine the changes across learning in the coordination of inter-areal neural activity (Fig 3.6E and 3.6F, and 3.20). First, we measured Pearson correlation between trial-by-trial whisker-evoked responses in pairs of individual neurons recorded from wS1/wS2 (5-55 ms window after whisker onset) and wM1/wM2 (10-90 ms window after whisker

onset) (Fig 6E). For the pair-wise correlation analysis, we only considered neurons with average firing rate > 2.5 Hz within the corresponding analysis windows. Similarly, the Pearson correlation in trial-by-trial average population responses in the same task epochs between pairs of simultaneously recorded areas were quantified (Fig S12A).

As a second measure of pair-wise correlation, which is suggested to be insensitive to firing rate, we applied the spike time tiling coefficient (STTC) approach (Cutts and Eglen 2014). The STTC was calculated during a 1-s window centered on the whisker stimulus (Figure S12B), and was defined for spike trains A and B as:

$$STTC = \frac{1}{2} \left(\frac{P_A - T_B}{1 - P_A T_B} + \frac{P_B - T_A}{1 - P_B T_A} \right)$$

where P_A and P_B are the proportion of spikes from A falling within $\pm\Delta t$ (± 10 ms) of a spike in B and vice versa; and T_A and T_B are the proportion of the total recording time which falls within $\pm\Delta t$ of a spike from B or A respectively.

In addition, we identified directional functional connectivity from wS1 to wM1 and from wS2 to wM2 by calculating cross-correlograms (CCG) during a 1-second window centered on whisker stimulus (Fig 6F and S12C). The CCG was defined as:

$$CCG(\tau) = \frac{\frac{1}{M} \sum_{i=1}^M \sum_{t=1}^N \chi_1^i(t) \chi_2^i(t + \tau)}{\theta(\tau) \sqrt{\lambda_1 \lambda_2}}$$

where M is the number of trials, N is the number of bins in the trial, χ_1^i and χ_2^i are the spike trains of the two units on trial i , τ is the time lag relative to reference spikes, and λ_1 and λ_2 are the mean firing rates of the reference and target units respectively. $\theta(\tau)$ is the triangular function that corrects for the overlap time bins caused by the sliding window (Perkel et al. 1967). Neurons with firing rate > 1 Hz within the analysis window were included in this analysis.

To better capture fast timescale changes related to feedforward connections, cross-correlograms were corrected by subtracting a jittered version (Smith and Kohn 2008; Siegle et al. 2021) (Fig S12C):

$$CCG_{corrected} = CCG - CCG_{jittered}$$

The jittered CCG was produced as the average of 100-times resampling the original dataset where spike times within each 25-ms window were randomly permuted across different trials. This method, removes the stimulus-locked and slow timescale correlations larger than the jitter window, while preserving the trial-averaged PSTH and a number of spikes for each unit (Harrison and Geman 2009). For each pair of recorded units, the significant directional connection from reference to target neuron was identified if the maximum CCG within time lags between 0 to 10 ms was larger than 6-fold standard deviation of the jitter-corrected CCG flanks (between ± 50 -100 ms).

For both analytical methods, in wS1/wS2 we focused only on the RS units, as they are known to have long-range projections. In wM1/wM2, we quantified correlations and directional connections separately for RS and FS units.

3.5.6 Quantifying learning modulation index

The learning modulation index (LMI) for each cell class ('cc', i.e. RS or FS) and cortical area ('a', i.e. wS1, wS2, wM1, wM2, ALM, or tJM1) was defined as the normalized difference of whisker-evoked response in Novice and Expert mice (Fig 3.8C and 3.8D):

$$LMI_{ct,a} = \frac{\Delta AP_{Expert_{cc,a}} - \Delta AP_{Novice_{cc,a}}}{|\Delta AP_{Expert_{cc,a}}| + |\Delta AP_{Novice_{cc,a}}|}$$

where ΔAP is the grand average change in firing rate (compared to pre-whisker baseline) across all neurons from that mouse group, cortical region and cell class.

3.5.7 Statistics

Data are represented as mean \pm SEM unless otherwise noted. The Wilcoxon signed-rank test was used to assess significance in paired comparisons; and the Wilcoxon rank-sum test was used for unpaired comparisons (Matlab implementations). Analysis of spiking activity was performed using non-parametric permutation test. Comparisons of the number of modulated neurons were performed using a Chi-squared proportion test. The statistical tests used and n numbers are reported explicitly in the main text or figure legends. P-values are corrected for multiple comparisons when necessary and methods are indicated in the main text or figure legends.

Acknowledgments

This work was supported by the Swiss National Science Foundation (310030B_166595, 31003A_182010 and CRSII5_177237) (CCHP), the European Research Council (ERC-2011-ADG 293660) (CCHP), European Union's Marie Skłodowska-Curie Actions (665667, 798617) (KT), the Research Foundation for Opto-science and Technology (KT), the Brain Science Foundation (KT), the Japan Society for the Promotion of Sciences (KT), and the Ichiro Kanehara Foundation (KT). The funders had no role in study design, data collection, and analysis, decision to publish, or preparation of the manuscript.

Author Contributions

VE, KT, SC, and CCHP conceptualized the study; VE and RA analyzed the published dataset; VE and AO obtained and analyzed optogenetic tagging data; VE, RG, GF, and YL obtained and analyzed anatomical data; VE, KT, SC, and CCHP wrote the manuscript; all authors discussed and edited the manuscript; and CCHP provided overall supervision.

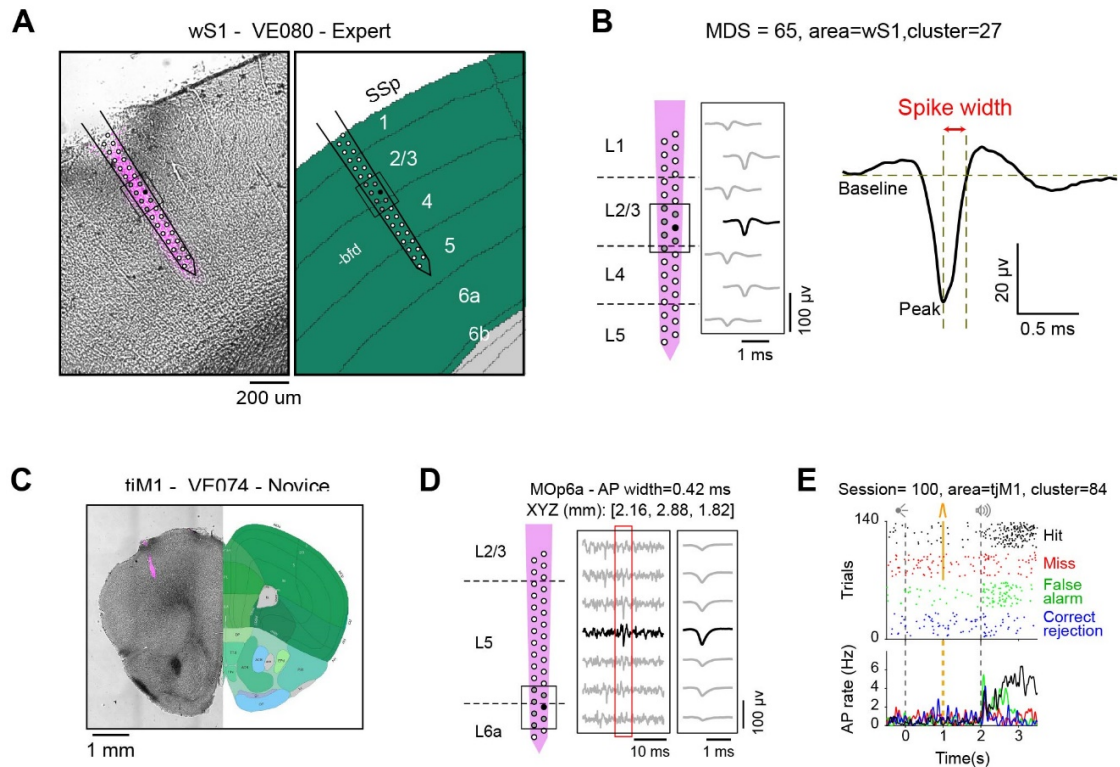


Fig 3.9. Anatomical localization of neurons.

(A) Magnified example fluorescent track of the silicon probe in wS1 shown in Fig 3.1D, and location of different probe sites after registration to the Allen Mouse Brain Atlas, <https://mouse.brain-map.org>. The small rectangular box and black recording site highlight the location of the example neuron shown in (B).

(B) Silicon probe, example shown in (A), with site locations across cortical layers and example neuron recorded on the probe. Spikes from each neuron were observed across several sites (shown with circles) of the silicon probe. For calculating the spike width for each neuron, the average spike waveform extracted from the recording site with the largest spike peak amplitude (filled circle) was used. Spike width was defined as the time between the spike peak (minimum) to the time voltage came back to baseline level. Gray horizontal line shows spike baseline, and vertical lines mark where spike width was measured.

(C) Example coronal section of a Novice mouse brain with fluorescent track of a single shank silicon probe in tjM1, registered to the Allen Mouse Brain Atlas, <https://mouse.brain-map.org>. (D) Reconstructed location of different recording sites of the example silicon probe shown in (C) according to Allen Atlas (*left*), filtered recorded raw data of 7 probe sites around one detected spike, and average extracted spike waveform for this example neuron (*right*). After spike sorting, the position of each neuron was assigned to the location of recording site across the probe with the largest spike amplitude (filled circle).

(E) Raster plot and peri-stimulus time histogram (PSTH) for the example neuron shown in (D). Trials are grouped and colored based on trial outcome.

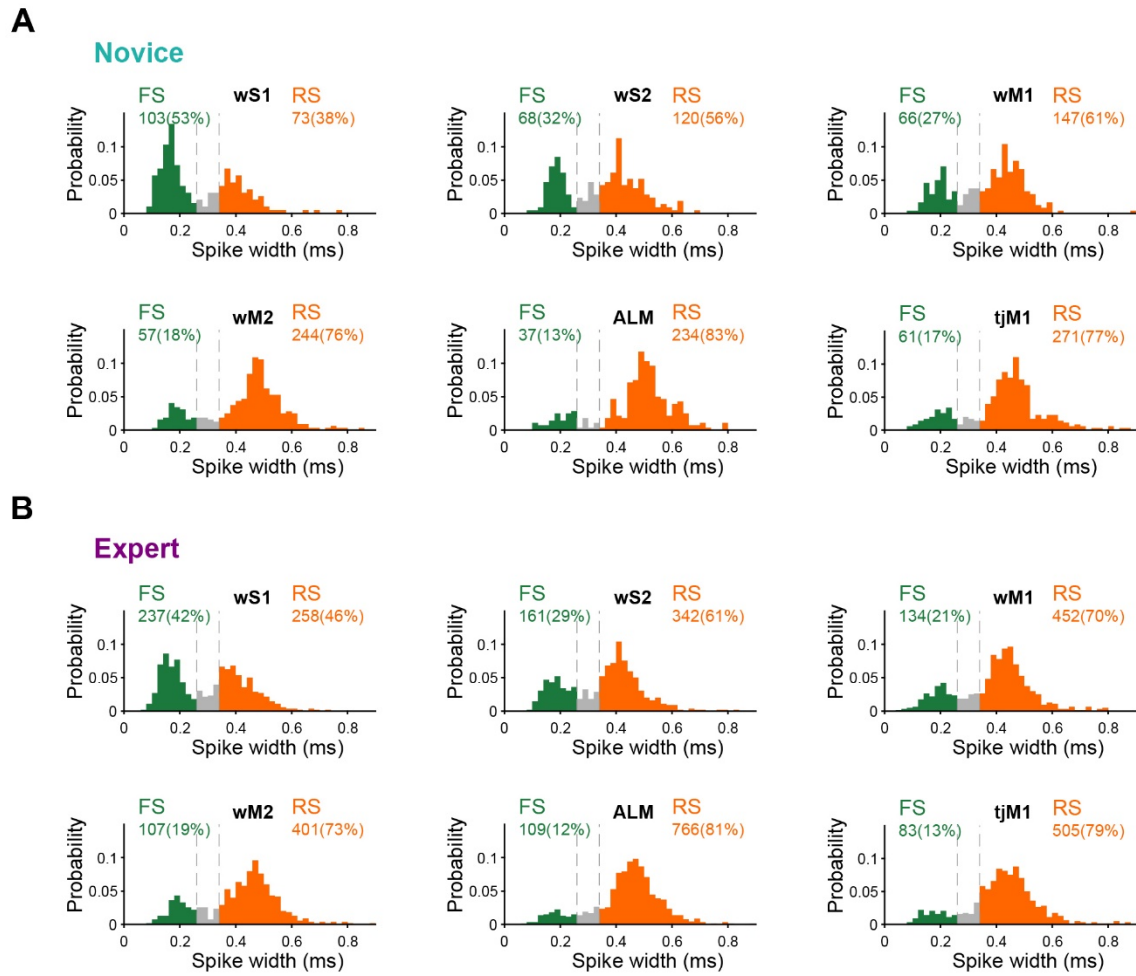


Fig.3.10. Distribution of spike width in different cortical areas.

(A) Spike width distribution for neurons recorded from Novice mice shown separately for different cortical regions. Neurons were categorized as fast-spiking (FS, spike width < 0.26 ms) or regular-spiking (RS, spike width > 0.34 ms) in all areas. Neurons with intermediate spike width (gray bars) were excluded from the rest of analysis. Percentage of neurons in each area tagged as RS or FS are shown.

(B) Same as (A) but for Expert mice. A smaller percentage of FS neurons appears to be found in frontal regions in both Novice (A) and Expert mice (B).

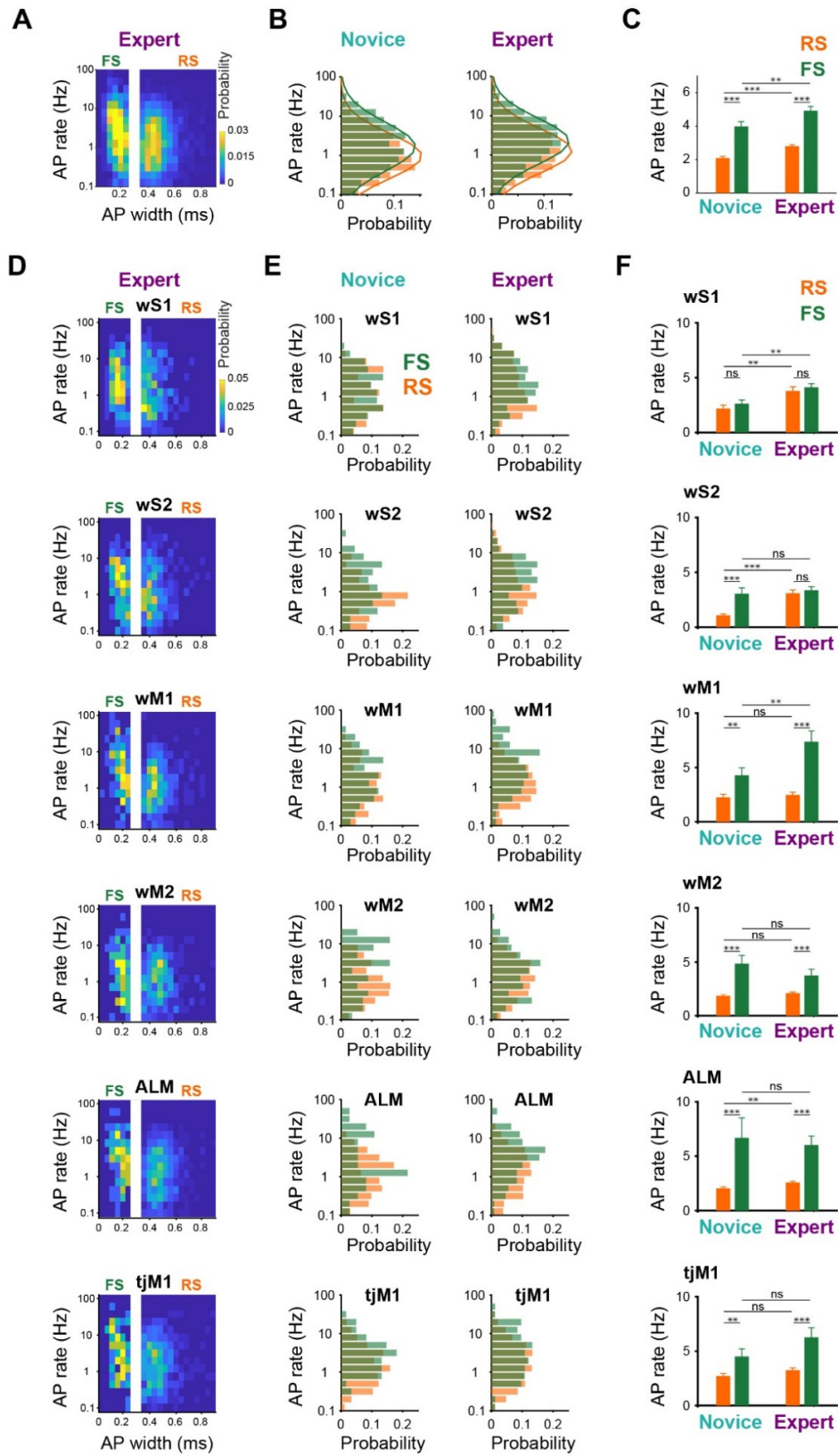


Fig. 3.11. Baseline firing rates of RS and FS neurons.

(A) Spike width distribution vs spike rate for all neurons recorded from Novice mice.

(B) Spike rate distribution for RS and FS units in Novice (*left*) and Expert (*right*) mice. Note the log-normal distribution of baseline firing rates for both RS and FS units in Novice and Expert mice. Normal distributions were fit to the RS and FS histograms (solid lines).

(C) Comparison of mean spike rate in RS vs FS neurons of Novice and Expert mice. Error bars: SEM. ***: $p < 0.001$, **: $p < 0.01$, *: $p < 0.05$, ns: $p \geq 0.05$, non-parametric permutation test, FDR-corrected for multiple comparison.

(D-F) Same as (A-C), but showing data separately for different cortical areas.

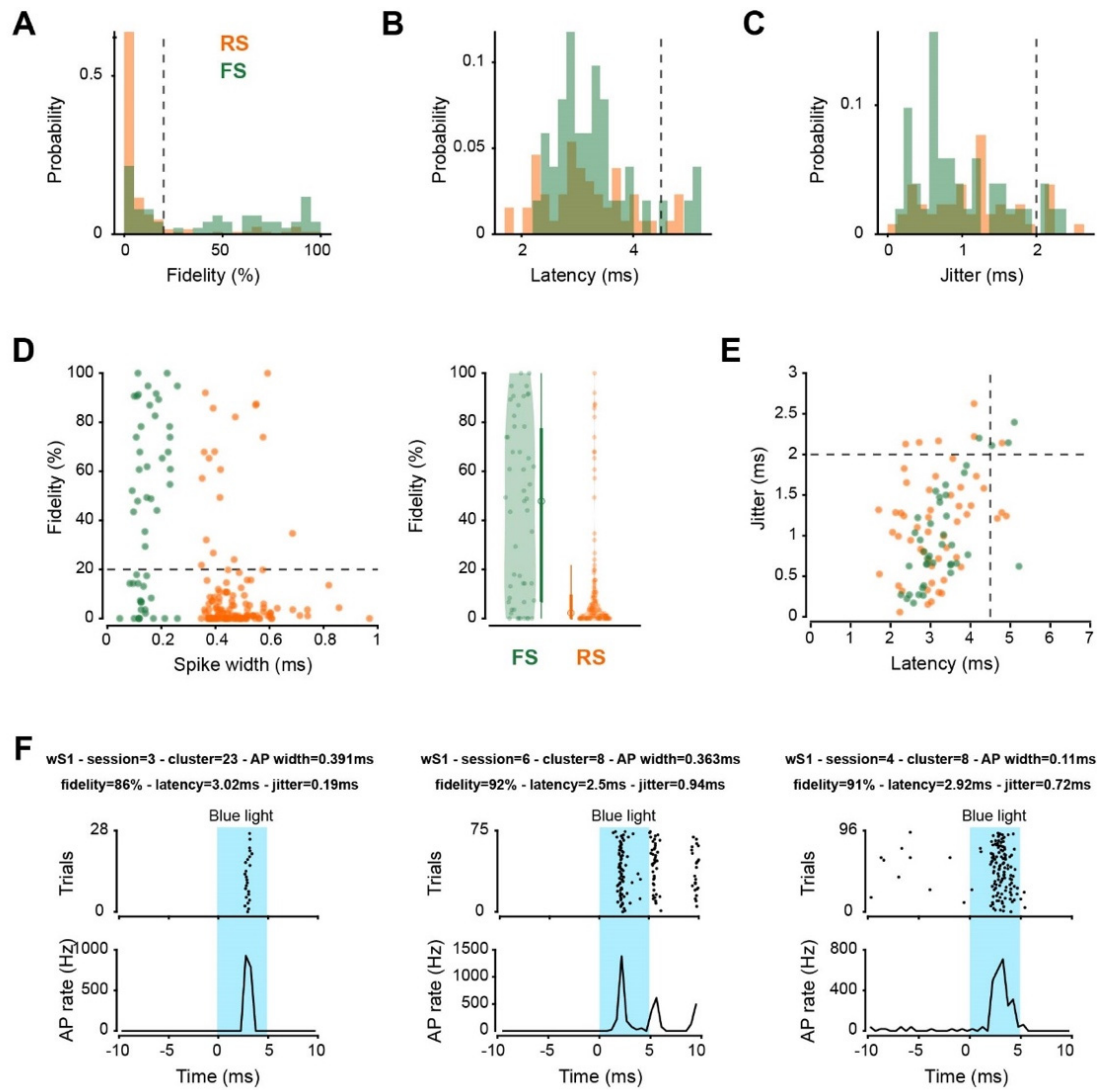


Fig. 3.12. Opto-tagging GABAergic neurons in VGAT-ChR2 mice.

(A-C) Criteria for labeling neurons as opto-tagged upon blue light stimulation in VGAT-ChR2 mice. Probability distribution of fidelity scores (A), first spike latency (B), and jitter (C) for RS units (orange, spike width > 0.34 ms, 130 neurons from 4 mice) and FS units (green, spike width < 0.26 ms, 51 neurons from 4 mice) measured in the first 10-ms window of blue light stimulation. The thresholds for detection of opto-tagged cells (dotted vertical lines) were defined based on previous literature and dips in the observed probability distributions (i.e. fidelity > 20%, latency < 4.5 ms, jitter < 2 ms).

(D) Scatter plot of spike width versus fidelity (left) and distribution of fidelity scores shown with violin plots and bar plots (right).

(E) Scatter plot of latency versus jitter of light-evoked response for RS and FS units.

(F) Raster plot and peri-stimulus time histogram during the first 10-ms of 100-Hz blue light stimulation for three example opto-tagged neurons.

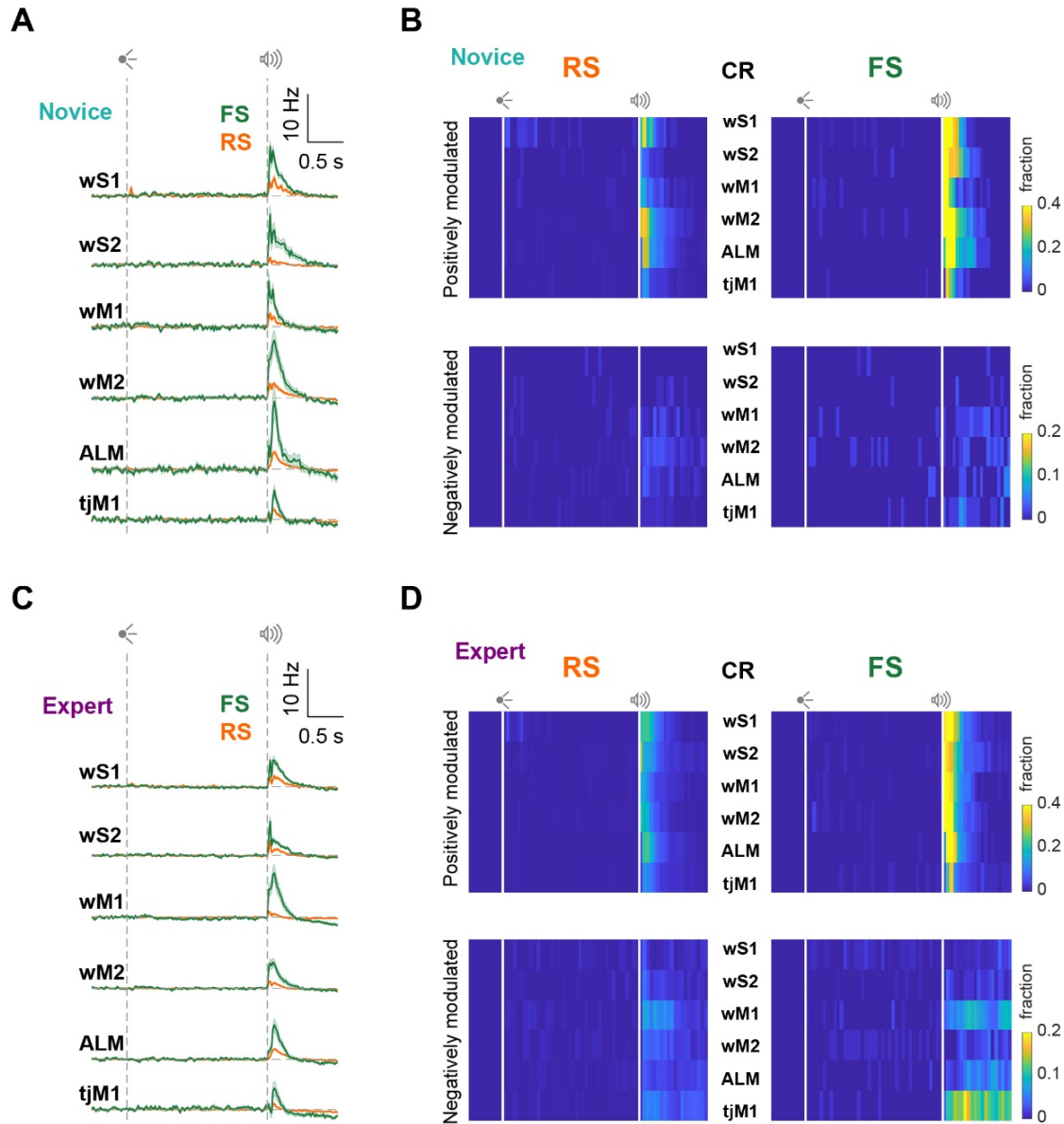


Fig. 3.13. FS neurons remain at baseline level during correct rejection trials.

(A) Baseline-subtracted (2 s prior to visual onset) population firing rates (mean \pm SEM) of RS and FS neurons from different regions of Novice mice are superimposed in correct rejection trials. wS1: 73 RS units in 7 mice, 103 FS units in 7 mice; wS2: 120 RS units in 8 mice, 68 FS units in 8 mice; wM1: 147 RS units in 7 mice, 66 FS units in 7 mice; wM2: 244 RS units in 7 mice, 57 FS units in 7 mice; ALM: 234 RS units in 6 mice, 37 FS units in 5 mice; tJM1: 271 RS units in 8 mice, 61 FS units in 8 mice.

(B) Percentage of RS (*left*) and FS (*right*) neurons in different regions of Novice mice which are positively (*top*) or negatively (*bottom*) modulated compared to baseline (non-parametric permutation test, $p < 0.05$) in correct rejection trials.

(C) Similar to (A), but for Expert mice. wS1: 258 RS units in 15 mice, 237 FS units in 15 mice; wS2: 342 RS units in 12 mice, 161 FS units in 12 mice; wM1: 452 RS units in 11 mice, 134 FS units in 11 mice; wM2: 401 RS units in 10 mice, 107 FS units in 10 mice; ALM: 766 RS units in 12 mice, 109 FS units in 12 mice; tJM1: 505 RS units in 11 mice, 83 FS units in 11 mice.

(D) Similar to (B), but for Expert mice. There appears to be stronger suppression of both RS and FS neurons of tjM1 during the response window in Expert compared to Novice mice.

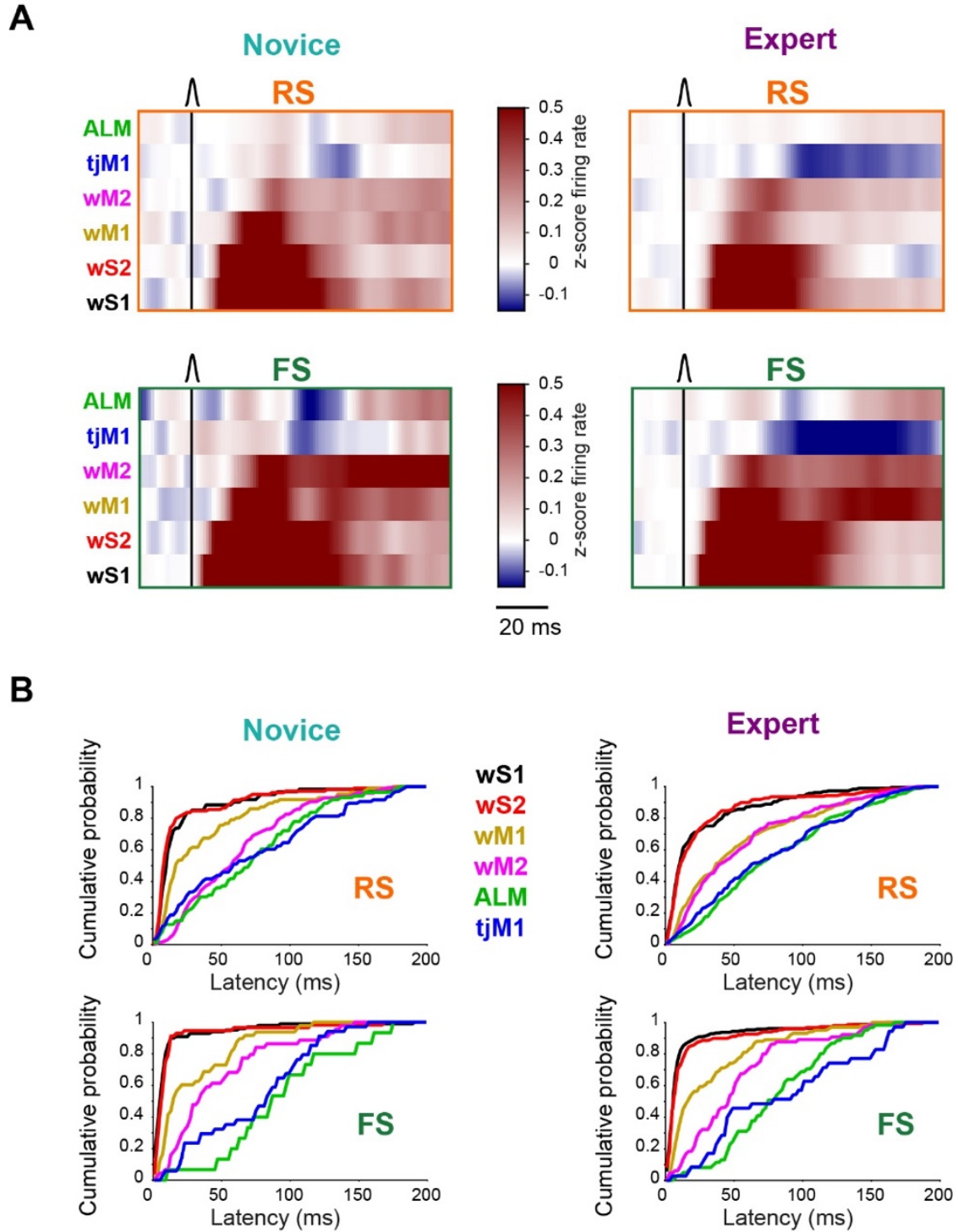


Fig. 3.14. Sequential activation of cortical regions upon whisker stimulation.

(A) Sequential propagation of whisker-evoked spiking responses in hit trials for RS (*top*) and FS (*bottom*) neurons from Novice (*left*) and Expert (*right*) mice. Mean z-scored firing rate in the first 100 ms window after whisker stimulus is shown. Brain regions are sorted based on their population-average onset latency in RS neurons of Expert mice.

(B) Cumulative distribution of latency of individual neurons for different cortical areas in RS (*top*) and FS (*bottom*) neurons from Novice (*left*) and Expert (*right*) mice. Only neurons with significant modulation in the 200 ms window following whisker stimulus compared to a 200 ms window prior to the whisker stimulus are included ($p < 0.05$, non-parametric permutation test). Latency was defined at the half maximum (minimum for suppressed neurons) response within the 200 ms window.

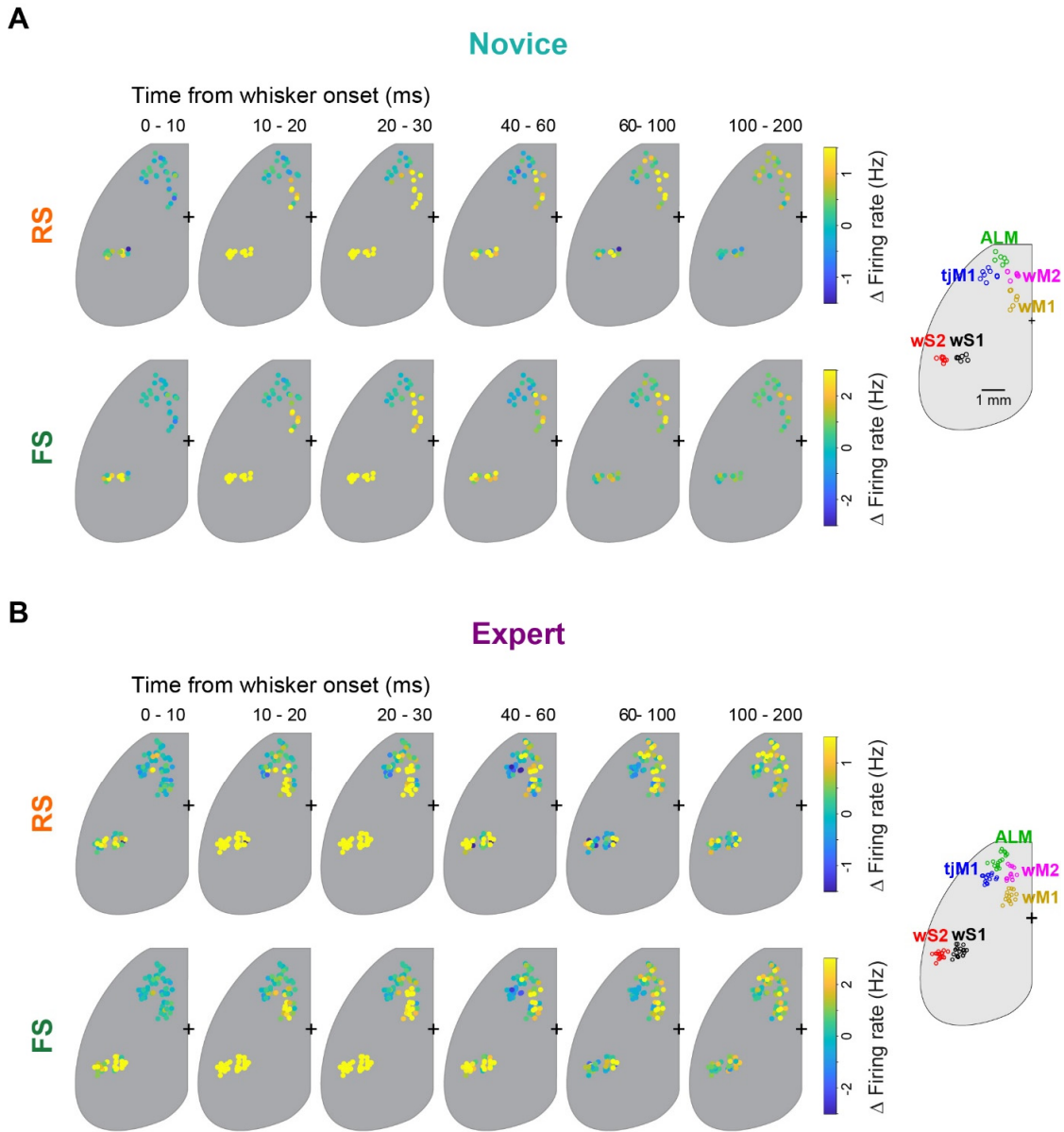


Fig. 3.15. Early sensory response map across different probes.

(A) Time-lapse maps of whisker-evoked firing rate in RS (*top*) and FS (*bottom*) neurons of Novice mice in hit trials. Circles represent different probes and colors show mean baseline-subtracted (50 ms before whisker onset) firing rate across each probe at different time windows. Probes from all Novice mice (43 probes in 8 mice) are superimposed.

(B) Same as (A) but for Expert mice (90 probes in 18 mice).

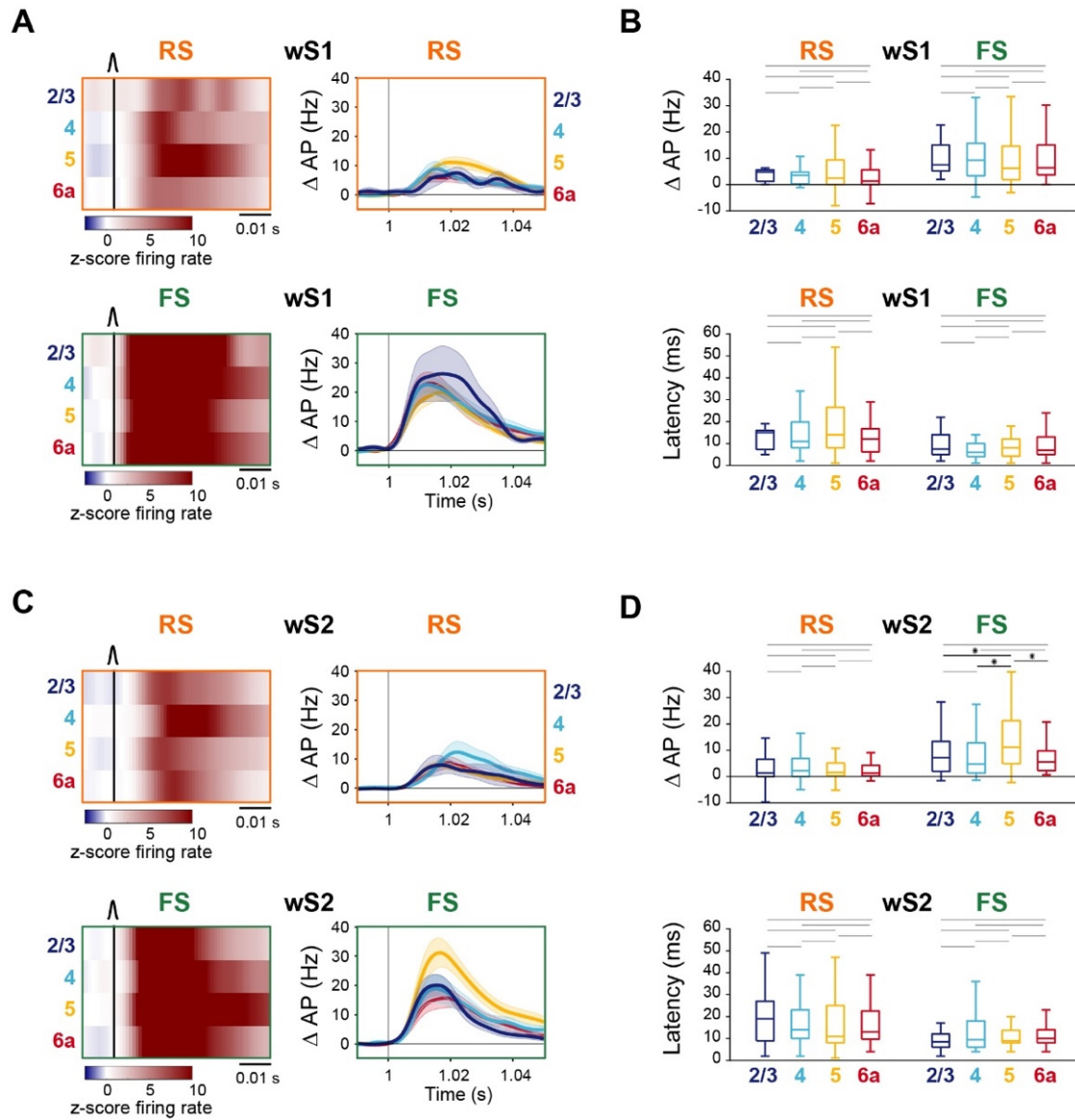


Fig. 3.16. Faster and larger sensory response in FS neurons across all layers of wS1 and wS2.

(A) Mean z-scored firing rate (*left*) and baseline-subtracted firing rate (*right*) of RS (*top*) and FS (*bottom*) neurons across different cortical layers of wS1.

(B) Boxplots representing the distribution of firing rate change (*top*) and response latency (*bottom*) of RS and FS units in different layers of wS1. Only neurons with a significant whisker response in the first 100 ms (compared to 100 ms before whisker onset, non-parametric permutation test, $p < 0.05$) were included. Midline represents the median, bottom and top edges show the interquartile range, and whiskers extend to 1.5 times the interquartile range. *: $p < 0.05$. Gray lines show non-significant comparisons. Firing rate change was compared using non-parametric permutation test and latencies were compared using Wilcoxon rank-sum test.

(C-D) Same as (A-B), but for wS2 neurons.

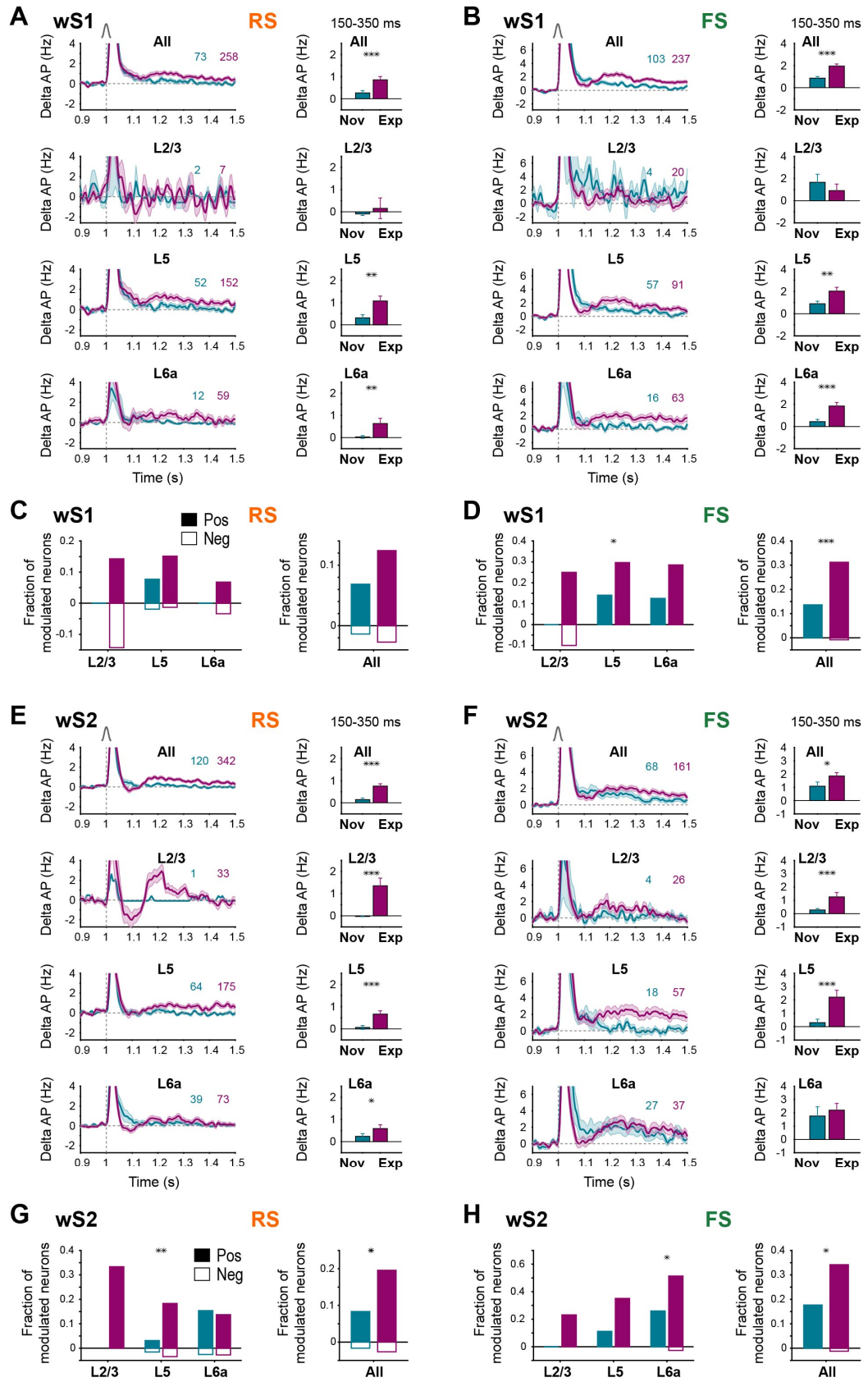


Fig. 3.17. Layer-specific quantification of RS and FS neuronal responses during the secondary late response in wS1 and wS2 across learning.

(A) Increase of late whisker response in wS1 RS neurons across learning. *Left*: baseline-subtracted (200 ms prior to whisker onset) population firing rate (mean \pm SEM) for all neurons and different cortical layers (L2/3, L5 and L6a) separately overlaid for Novice and Expert mice. The number of neurons is indicated on the figure. *Right*: change in average spike rate quantified in 150-350 ms window after whisker onset relative to similar window size before whisker onset. ***: $p < 0.001$, **: $p < 0.01$, *: $p < 0.05$, ns: $p \geq 0.05$, non-parametric permutation test, FDR-corrected for multiple comparison.

(B) Increase of late whisker response in wS1 FS neurons across learning. Panels are similar to (A) but for wS1 FS neurons in Novice and Expert mice. (C) Fraction of wS1 RS neurons across different layers with significant positive (filled bars) or negative (empty bars) modulation late after whisker stimulus (150-350 ms window after whisker onset relative to similar window size before whisker onset). Positive or negative modulation of neurons was quantified using non-parametric permutation test ($p < 0.005$). ***: $p < 0.001$, **: $p < 0.01$, *: $p < 0.05$, ns: $p \geq 0.05$, Chi-squared proportion test. Fractions are reported for groups with more than five neurons.

(D) Similar to (C) but for wS1 FS neurons.

(E-H) Similar to (A-D) but for wS2.

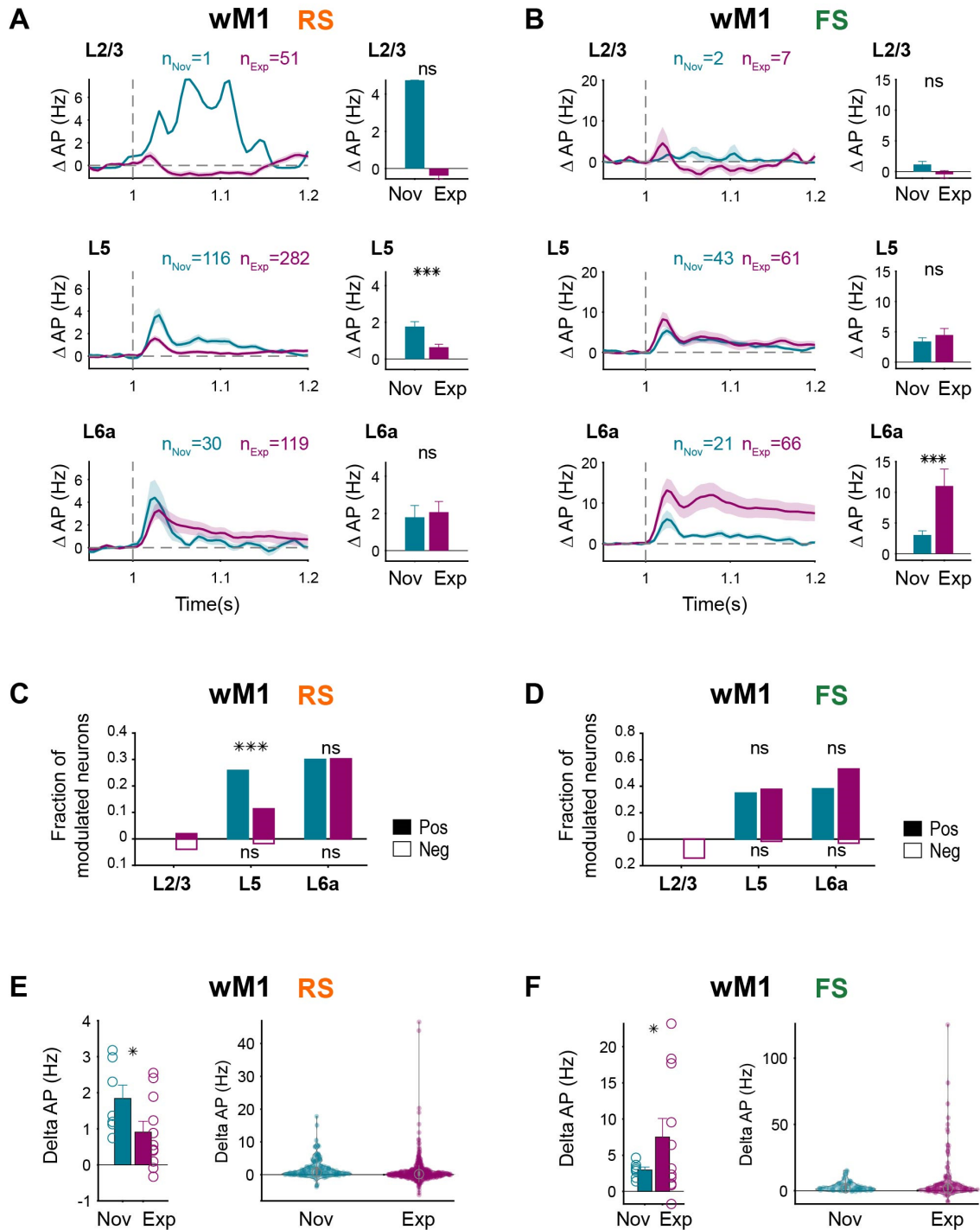


Fig. 3.18. Layer-specific quantification of RS and FS neurons in wM1 across learning.

(A) Decrease of early whisker response in wM1 RS neurons across learning. *Left*: baseline-subtracted (50 ms prior to whisker onset) population firing rate (mean \pm SEM) for different cortical layers (L2/3, L5 and L6a) overlaid for Novice (147 neurons in 7 mice) and Expert (452 neurons in 11 mice) mice. The number of neurons for each layer is indicated on the figure. *Right*: change in average spike rate quantified in 10-90 ms window after whisker onset relative to similar window size before whisker

onset. ***: $p < 0.001$, ns: $p \geq 0.05$, non-parametric permutation test, FDR-corrected for multiple comparison.

(B) Increase of whisker response in wM1 FS neurons across learning. Panels are similar to (A) but for wM1 FS neurons in Novice (66 neurons in 7 mice) and Expert (134 neurons in 11 mice) mice.

(C) Fraction of wM1 RS neurons across different layers with significant positive (filled bars) or negative (empty bars) modulation early after whisker stimulus (10-90 ms window after whisker onset relative to similar window size before whisker onset). Positive or negative modulation of neurons was quantified using non-parametric permutation test ($p < 0.005$). ***: $p < 0.001$, ns: $p \geq 0.05$, Chi-squared proportion test. Fractions are reported for groups with more than five neurons.

(D) Similar to (C) but wM1 FS neurons.

(E) Mouse-by-mouse variability and distribution of whisker-evoked response in RS units in wM1 of Novice and Expert mice. (*Left*) Bar plots showing average firing rate across mice in 10-90 ms window (mean \pm SEM, 7 Novice and 11 Expert mice) after whisker onset and statistical comparison using non-parametric permutation test (*: $p < 0.05$). Circles show individual mice. (*Right*) Violin plots showing the distribution of whisker-evoked response in 10-90 ms window for all neurons recorded in Novice (147 neurons in 7 mice) and Expert mice (452 neurons in 11 mice).

(F) Same as (E) but for wM1 FS units in Novice (66 neurons in 7 mice) and Expert mice (134 neurons in 11 mice).

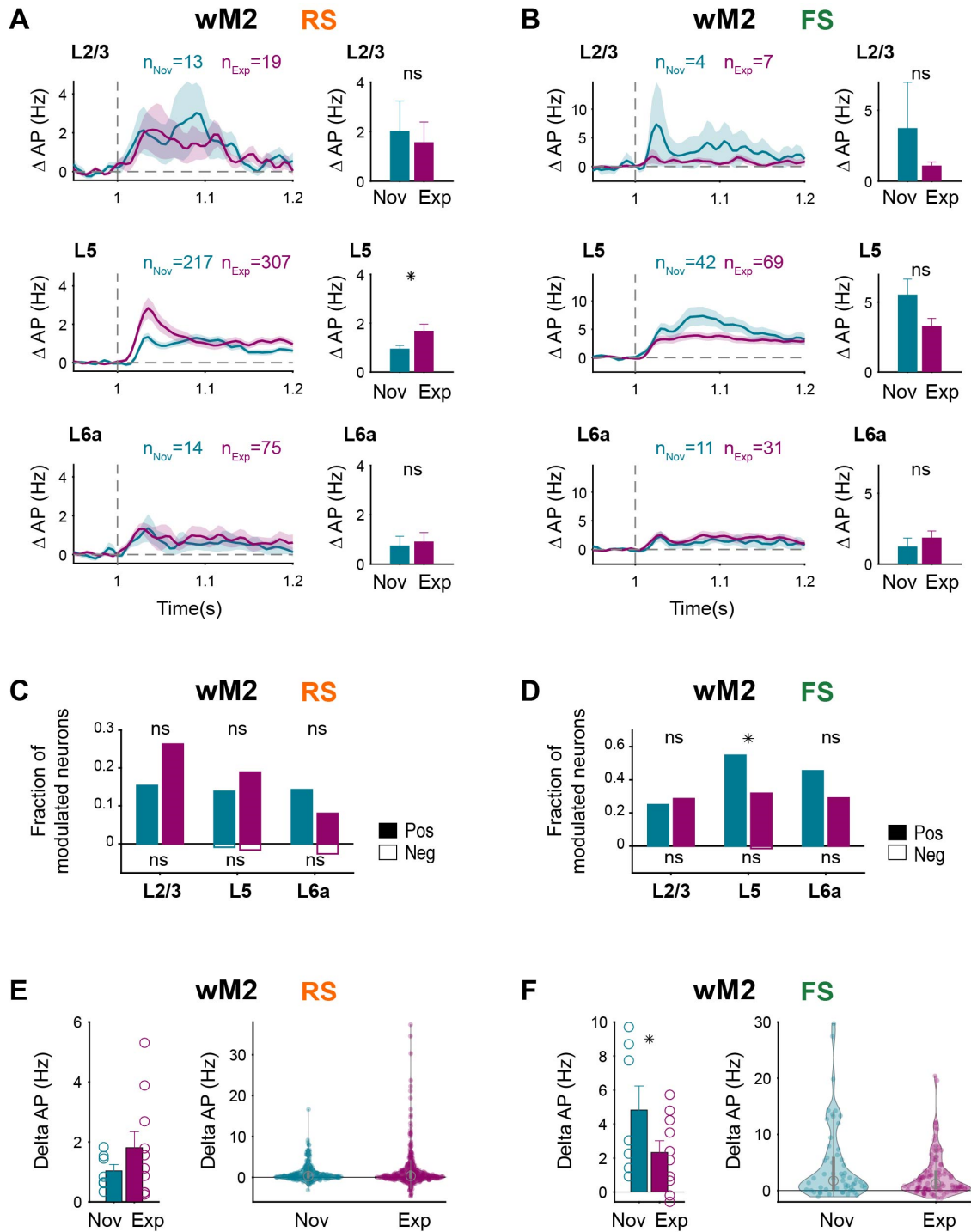


Fig. 3.19. Layer-specific quantification of RS and FS neuronal activity in wM2 across learning.

(A) Increase of early whisker response in wM2 RS neurons across learning. *Left*: baseline-subtracted (50 ms prior to whisker onset) population firing rate (mean \pm SEM) for different cortical layers (L2/3, L5 and L6a) overlaid for Novice mice (244 neurons in 7 mice) and Expert mice (401 neurons in 11 mice). The number of neurons for each layer is indicated on the figure. *Right*: change in average spike rate quantified in 10-90 ms window after whisker onset relative to similar window size before

whisker onset. *: $p < 0.05$, ns: $p \geq 0.05$, non-parametric permutation test, FDR-corrected for multiple comparison.

(B) Decrease of whisker response in wM2 FS neurons across learning. Panels are similar to (A) but for wM2 FS neurons in Novice mice (57 neurons in 7 mice) and Expert mice (107 neurons in 10 mice).

(C) Fraction of wM2 RS neurons across different layers with significant positive (filled bars) or negative (empty bars) modulation early after whisker stimulus (10-90 ms window after whisker onset relative to similar window size before whisker onset). Positive or negative modulation of neurons was quantified using non-parametric permutation test ($p < 0.005$). *: $p < 0.05$, ns: $p \geq 0.05$, Chi-squared proportion test. Fractions are reported for groups with more than five neurons.

(D) Similar to (C) but wM2 FS neurons.

(E) Mouse-by-mouse variability and distribution of whisker-evoked response in RS units in wM2 of Novice and Expert mice. (*Left*) Bar plot showing average firing rate across mice in 10-90 ms window (mean \pm SEM, 7 Novice and 10 Expert mice) after whisker onset and statistical comparison using non-parametric permutation test (*: $p < 0.05$). Circles show individual mice. (*Right*) Violin plots showing the distribution of whisker-evoked response in 10-90 ms window for all neurons recorded in Novice (244 neurons in 7 mice) and Expert mice (401 neurons in 10 mice).

(F) Same as (E) but for wM2 FS units in Novice (57 neurons in 7 mice) and Expert mice (107 neurons in 10 mice).

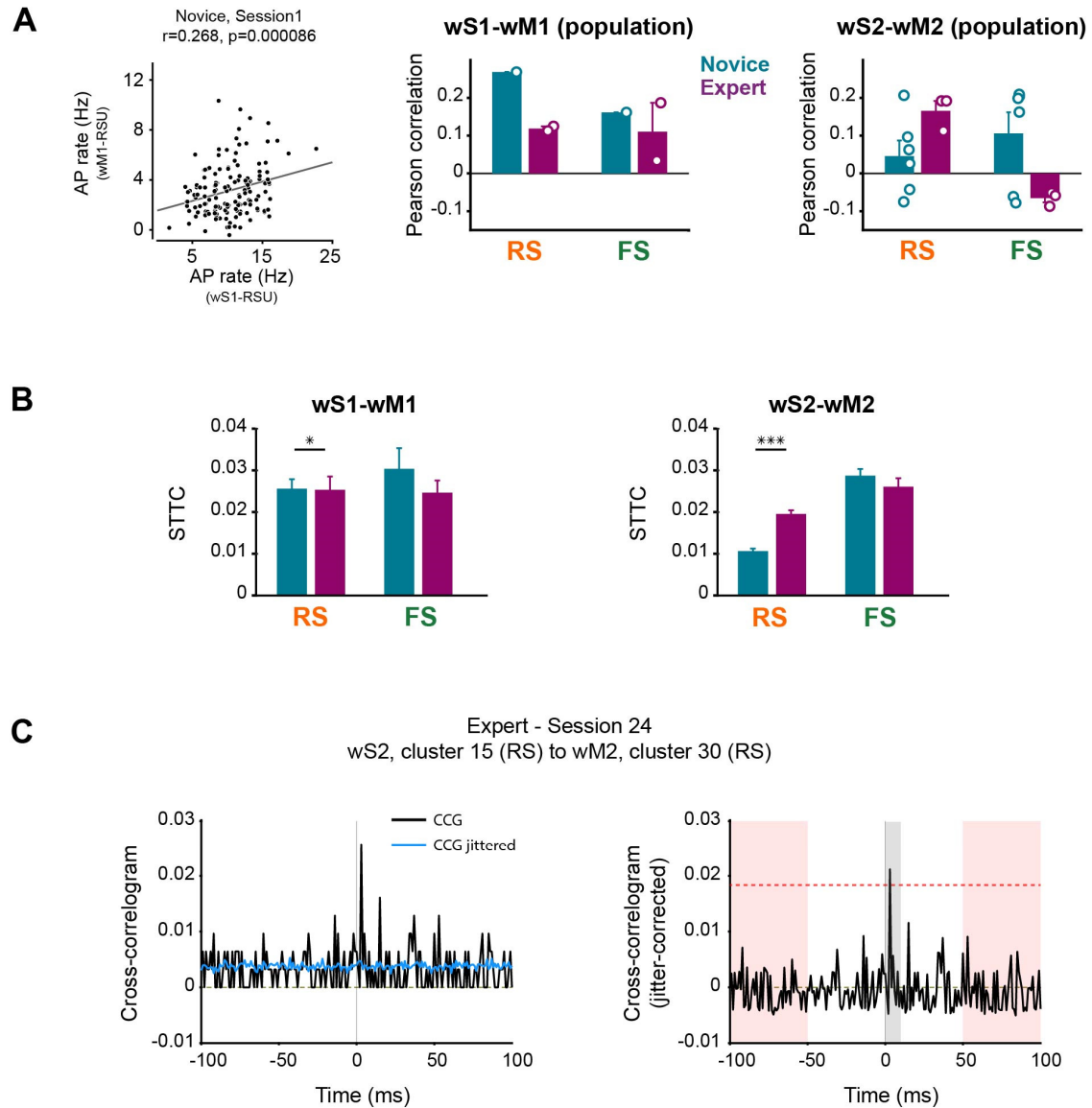


Fig. 3.20. Inter-areal functional connectivity.

(A) Inter-areal correlation of population response in Novice and Expert mice. (*Left*) Scatter plot of trial-by-trial average population response between wS1-RS units and wM1-RS units for an example Novice session. Circles were jittered slightly for the purpose of visualization. Gray line: least-squares regression. (*Middle*) Pearson correlation of trial-by-trial average population response of wS1-RS units vs wM1-RS, and wS1-RS units vs wM1-FS units (1 Novice and 2 Expert mice). (*Right*) Pearson correlation of trial-by-trial population average response of wS2-RS units vs wM2-RS, and wS2-RS units vs wM2-FS units (6 Novice and 3 Expert mice). Circles show individual sessions. Error bars: SEM.

(B) Pair-wise correlation between sensory and motor cortices in Novice and Expert mice using the spike time tiling coefficient (STTC) method. *Left*: Average pair-wise STTC correlation of wS1-RS units with wM1-RS (308 neuron pairs in 1 Novice mouse, and 398 neuron pairs in 2 Expert mice) and wS1-RS units with wM1-FS units (112 neuron pairs in 1 Novice mouse, and 139 neuron pairs in 2 Expert mice) separately. *Right*: Average pair-wise Pearson correlation of wS2-RS units with wM2-RS (3482 neuron pairs in 6 Novice mouse, and 2461 neuron pairs in 3 Expert mice) and wS2-RS units with wM2-FS units (821 neuron pairs in 6 Novice mouse, and 532 neuron pairs in 3 Expert mice). Error bars: SEM. Statistical comparison between Novice and Expert was performed using Wilcoxon rank-sum test (ns: $p \geq 0.05$; *: $p < 0.05$; ***: $p < 0.001$).

(C) Example cross-correlogram (CCG) from pair of neurons recorded simultaneously in wS2 and wM2 of an Expert mouse with a significant connection; same example pair as shown in Figure 6F, but with CCG from -100 to 100 ms time lags. Jitter correction method (*left*), and detection of significant functional connections (*right*). Significant connections were detected if any threshold crossing happened within 0 to 10 ms time lags (gray bar) of the jitter-corrected CCG. Threshold (red dotted line) was defined as 6-fold standard deviation of the jitter-corrected CCG flanks (red bars).

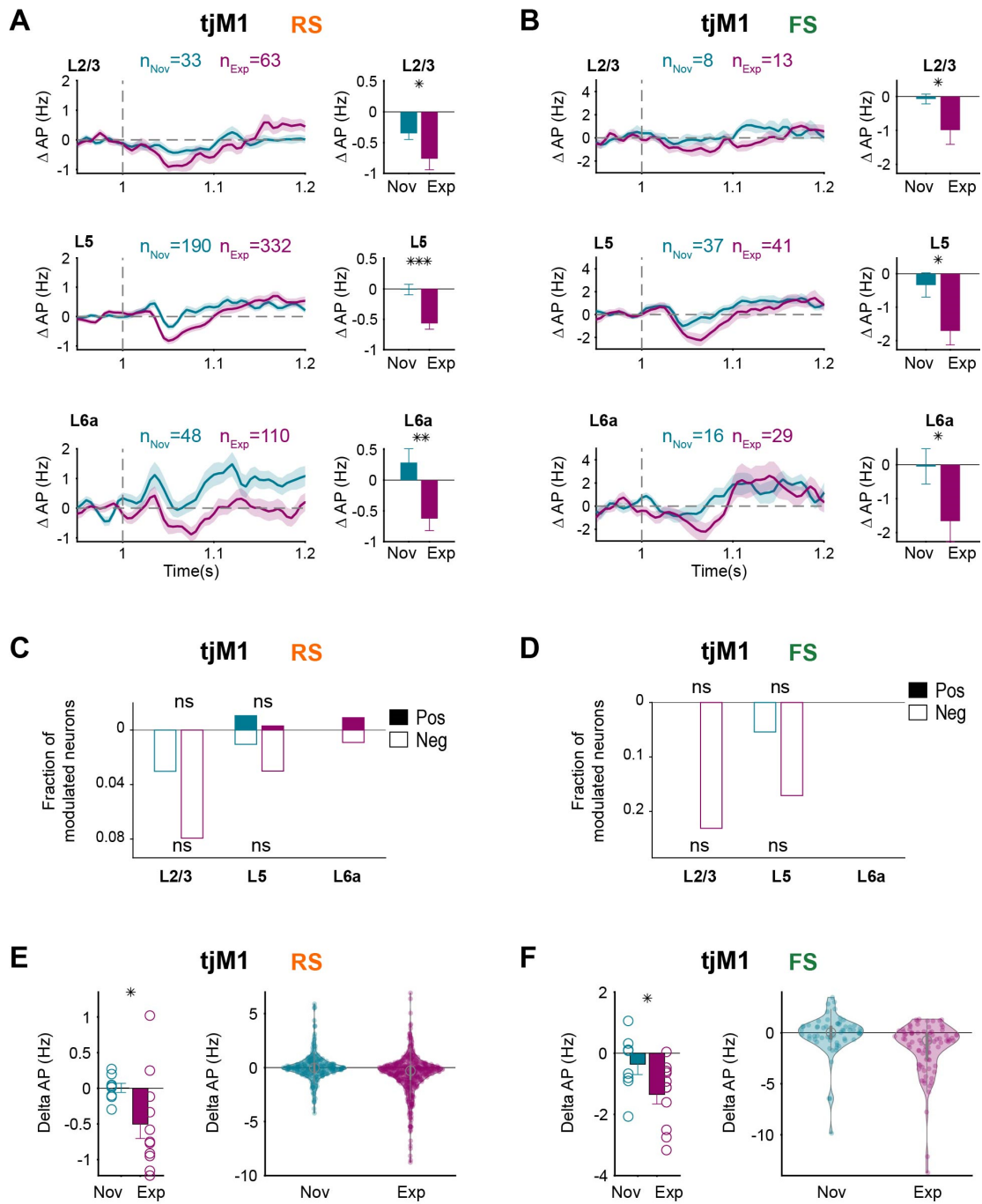


Fig. 3.21. Layer-specific quantification of RS and FS neurons in tjM1 across learning.

(A) Suppression of activity in tJM1 RS neurons across learning. *Left*: baseline-subtracted (50 ms prior to whisker onset) population firing rate (mean \pm SEM) for different cortical layers (L2/3, L5 and L6a) overlaid for Novice mice (271 neurons in 8 mice) and Expert mice (505 neurons in 11 mice). The number of neurons for each layer is indicated on the figure. *Right*: change in average spike rate quantified in 40-90 ms window after whisker onset relative to similar window size before whisker onset. ***: $p < 0.001$, **: $p < 0.01$, *: $p < 0.05$, non-parametric permutation test, FDR-corrected for multiple comparison.

(B) Suppression of activity in tJM1 FS neurons across learning. Panels are similar to (A) but for tJM1 FS neurons in Novice mice (61 neurons in 8 mice) and Expert mice (83 neurons in 11 mice).

(C) Fraction of tJM1 RS neurons across different layers with significant positive (filled bars) or negative (empty bars) modulation early after whisker stimulus (40-90 ms window after whisker onset relative to similar window size before whisker onset). Positive or negative modulation of neurons was quantified using non-parametric permutation test ($p < 0.005$). ns: $p \geq 0.05$, Chi-squared proportion test. Fractions are reported for groups with more than five neurons.

(D) Similar to (C) but tJM1 FS neurons.

(E) Mouse-by-mouse variability and distribution of whisker-evoked response in RS units in tJM1 of Novice and Expert mice. (*Left*) Bar plots showing average firing rate across mice in 40-90 ms window (mean \pm SEM, 8 Novice and 11 Expert mice) after whisker onset and statistical comparison using non-parametric permutation test (*: $p < 0.05$). Circles show individual mice. (*Right*) Violin plots showing the distribution of whisker-evoked response in 40-90 ms window for all neurons recorded in Novice (271 neurons in 8 mice) and Expert mice (505 neurons in 11 mice).

(F) Same as (E) but for tJM1 FS units in Novice (61 neurons in 7 mice) and Expert mice (83 neurons in 11 mice).

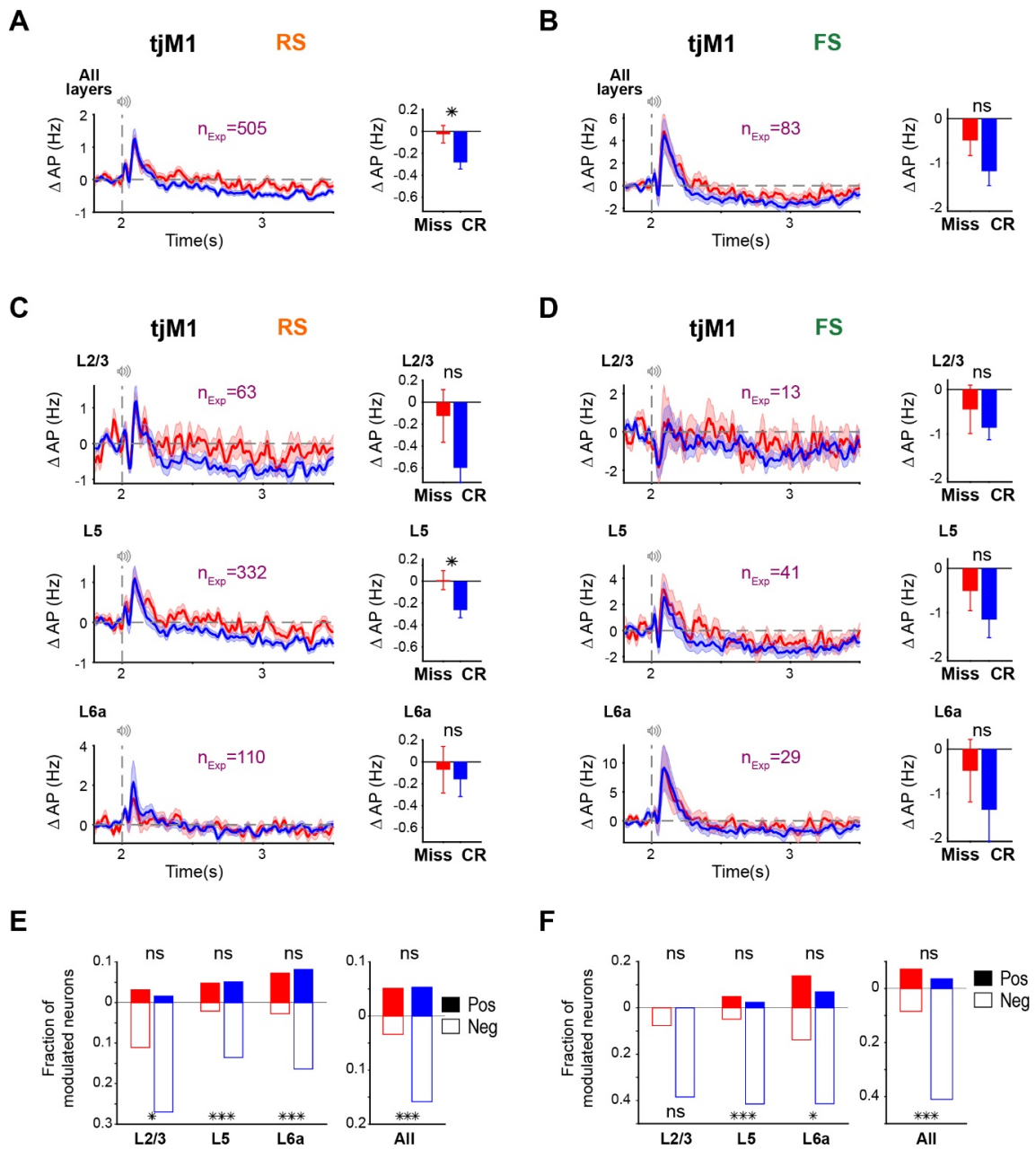


Fig. 3.22. Suppression of activity in tJM1 during response window in no-lick trials of Expert mice.

(A) Stronger suppression of tJM1 RS neurons in correct rejection vs miss trials. *Left*: baseline-subtracted (200 ms prior to auditory onset) population firing rate (mean \pm SEM) overlaid for correct rejection (blue) and miss trials (red) in Expert mice (505 neurons in 11 mice). *Right*: change in average spike rate quantified in 200-1000 ms window after auditory onset relative to a 200-ms window prior to auditory onset. *: $p < 0.05$, ns: $p \geq 0.05$, non-parametric permutation test.

(B) Similar to (A) but for FS neurons (83 neurons in 11 mice).

(C) Similar to (A) but separately for RS neurons of different cortical layers. The number of neurons for each layer is indicated on the figure. *: $p < 0.05$, ns: $p \geq 0.05$, non-parametric permutation test, FDR-corrected for multiple comparison.

(D) Similar to (C) but for FS neurons.

(E) Fraction of tJM1 RS neurons across different layers with significant positive (filled bars) or negative (empty bars) modulation in correct rejection and miss trials, quantified during response window (200-1000 ms window after auditory onset relative to 200-ms window before auditory onset). Positive or negative modulation of neurons was quantified using non-parametric permutation test ($p < 0.005$). ***, $p < 0.001$, *: $p < 0.05$, ns: $p \geq 0.05$, Chi-squared proportion test.

(F) Similar to (E) but tJM1 FS neurons.

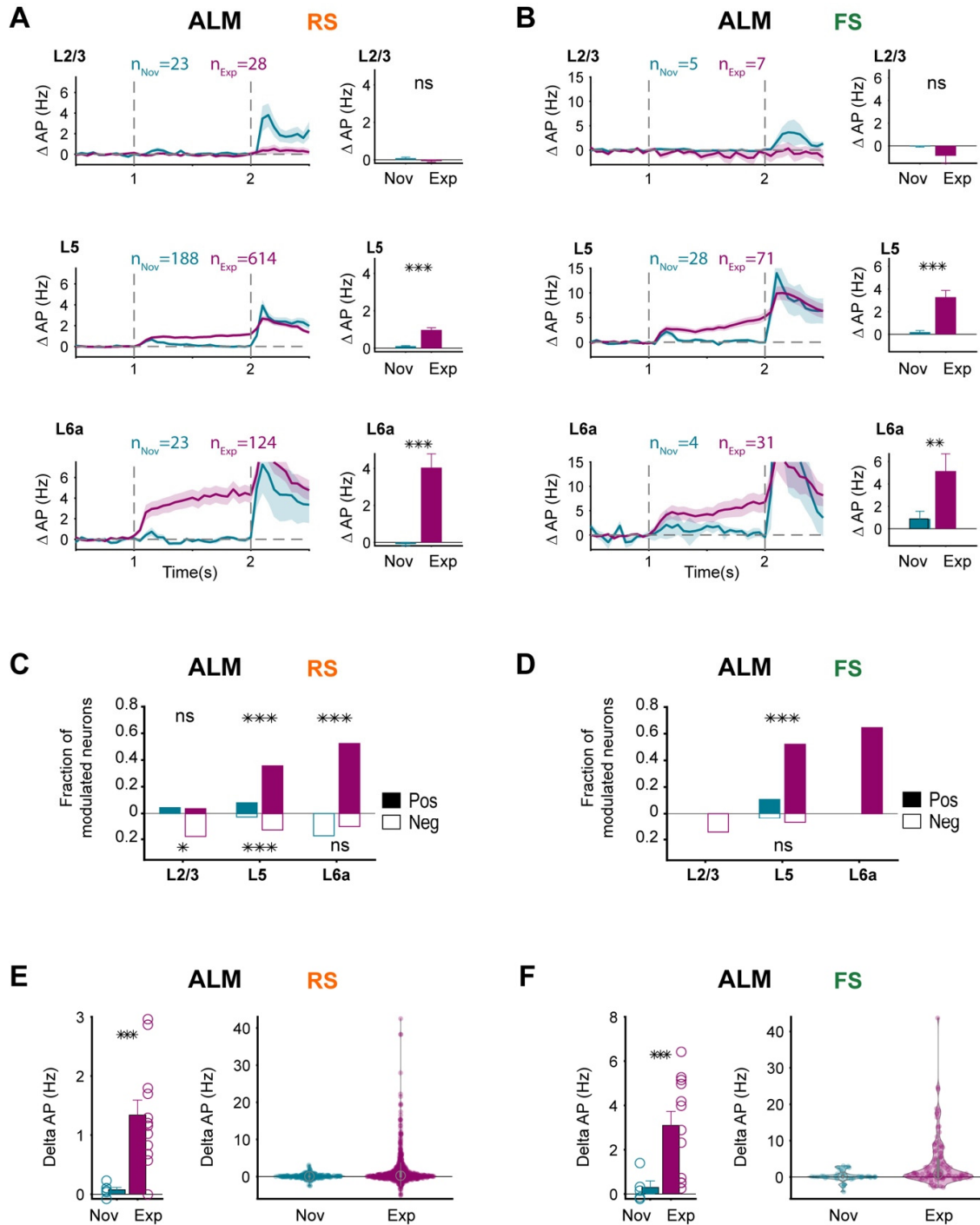


Fig. 3.23. Layer-specific quantification of RS and FS neuronal activity in ALM.

(A) Delay activity in ALM RS neurons upon learning. *Left*: baseline-subtracted (1 s prior to whisker onset) population firing rate (mean \pm SEM) for different cortical layers (L2/3, L5 and L6a) overlaid for Novice mice (234 neurons in 6 mice) and Expert mice (766 neurons in 12 mice). The number of neurons for each layer is indicated on the figure. *Right*: change in average spike rate quantified in 200-1000 ms window after whisker onset relative to similar window size before whisker onset. ***: $p < 0.001$, **: $p < 0.01$, ns: $p \geq 0.05$, non-parametric permutation test, FDR-corrected for multiple comparison.

(B) Delay activity in ALM FS neurons upon learning. Panels are similar to (A) but for ALM FS neurons in Novice mice (37 neurons in 5 mice) and Expert mice (109 neurons in 12 mice).

(C) Fraction of ALM RS neurons across different layers with significant positive (filled bars) or negative (empty bars) modulation during delay period (200-1000 ms window after whisker onset relative to similar window size before whisker onset). Positive or negative modulation of neurons was quantified using non-parametric permutation test ($p < 0.005$). ***: $p < 0.001$, *: $p < 0.05$, ns: $p \geq 0.05$, Chi-squared proportion test. Fractions are reported for groups with more than five neurons.

(D) Similar to (C) but for ALM FS neurons.

(E) Mouse-by-mouse variability and distribution of delay activity of RS units in ALM of Novice and Expert mice. (*Left*) Bar plots showing average firing rate across mice in 200-1000 ms window (mean \pm SEM, 6 Novice and 12 Expert mice) after whisker onset and statistical comparison using non-parametric permutation test (*: $p < 0.05$). Circles show individual mice. (*Right*) Violin plots showing the distribution of delay activity in 200-1000 ms window for all neurons recorded in Novice (234 neurons in 6 mice) and Expert mice (766 neurons in 12 mice).

(F) Same as (E) but for ALM FS units in Novice (37 neurons in 5 mice) and Expert mice (109 neurons in 12 mice).

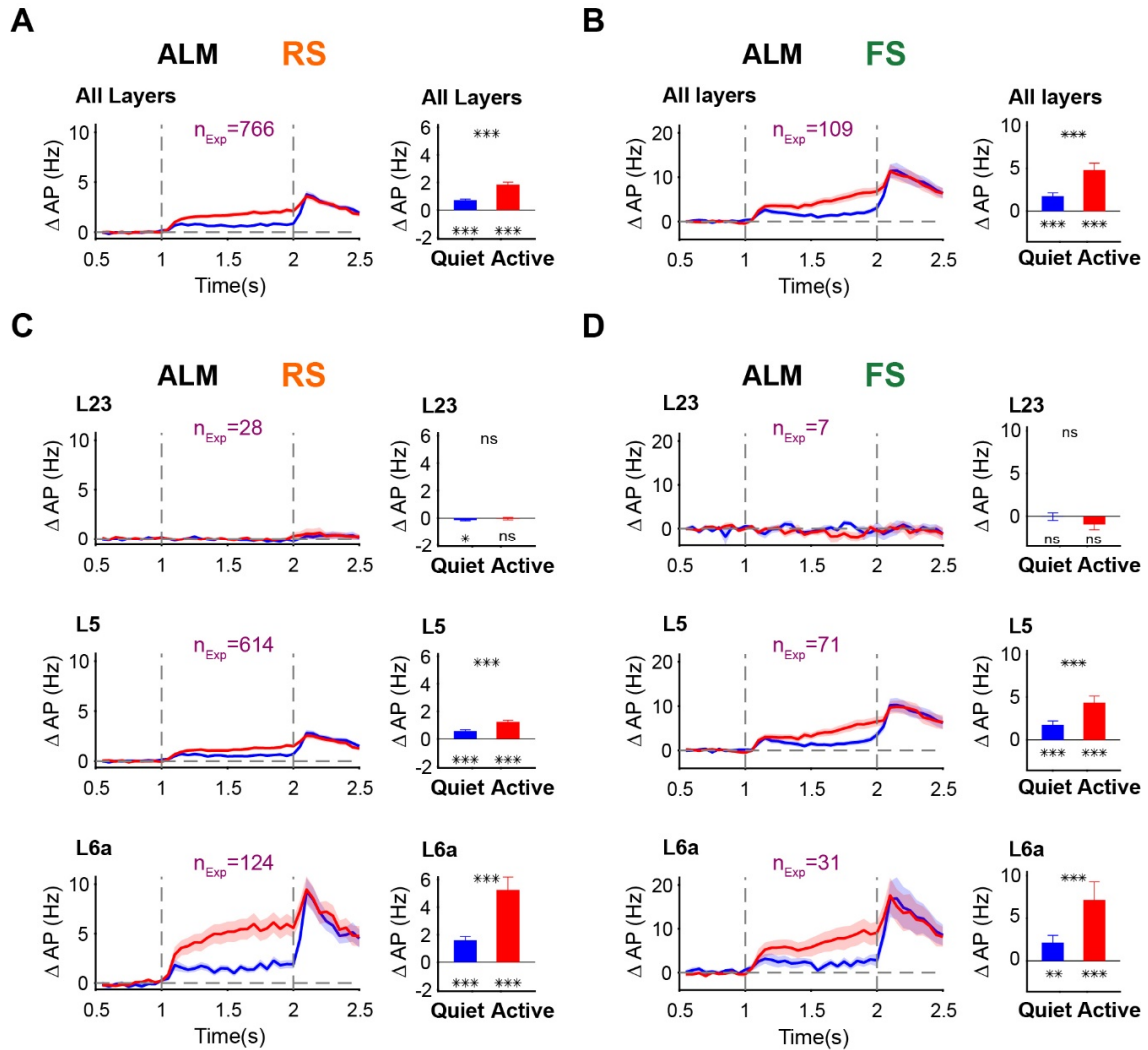


Fig. 3.24. Preparatory neuronal activity in ALM is decreased, but remains significant in quiet trials devoid of movements.

(A) Larger delay period activity of ALM RS neurons in Active vs Quiet hit trials. *Left*: baseline-subtracted (1 s prior to whisker onset) population firing rate (mean \pm SEM) overlaid for Quiet (blue) and Active (red) hit trials in Expert mice (766 RS units in 12 mice). *Right*: change in average spike rate quantified in 200-1000 ms window after whisker onset relative to a 1-s window prior to whisker onset. ***: $p < 0.001$, non-parametric permutation test. Asterisks below the bars represent the p value for comparing delay activity in each trial type compared to baseline, while asterisks above the bars represent the p value of the comparison between delay activity in Quiet and Active hit trials.

(B) Similar to (A) but for FS neurons (109 FS units in 12 mice).

(C) Similar to (A) but separately for RS neurons of different cortical layers. The number of neurons for each layer is indicated on the figure. ***: $p < 0.001$, ns: $p \geq 0.05$, non-parametric permutation test, FDR-corrected for multiple comparison.

(D) Similar to (C) but for FS neurons.

Chapter 4 Representation of sensory, motor and decision information in sensory, motor and medial prefrontal cortices of mice

Paper in preparation

“Representation of sensory, motor and decision information in sensory, motor and medial prefrontal cortices of mice.”

Anastasiia Oryshchuk, Christos Sourmpis, Reza Asri, Vahid Esmaeili, Alireza Modirshanechi, Wulfram Gerstner, Carl C.H. Petersen¹ and Sylvain Crochet¹

1: These authors contributed equally

My contribution to this paper:

For this Chapter together with C.H. Petersen¹ and Sylvain Crochet¹ I conceptualized and design the study.

I developed neural and behavioral experiment setups I acquired all the behavioral, electrophysiological and optoinhibition experimental data. I obtained a big part of histological data, and imaged all the samples.

I analyzed all movements, electrophysiological and behavioral data.

I wrote the manuscript and made a vast majority of the figures.

4.1 Summary

Goal-directed behavior requires the processing of incoming sensory information, making appropriate decisions, and generating relevant motor outputs. Yet, how sensorimotor transformation arises within the brain remains to be precisely determined. Here we investigated the contribution of the whisker primary somatosensory cortex (wS1), the medial prefrontal cortex (mPFC), and the tongue-jaw primary motor cortex (tjM1) in the transformation of a whisker sensory stimulus into licking motor output. We trained mice to perform a psychophysical whisker detection task, in which they learned to lick for reward in response to a brief single-whisker stimulus of variable amplitude. Combining high-density extracellular recordings with careful movement monitoring using high-speed video filming allowed to dissociate sensory, motor, and decision-related activity. We observed strong sensory responses in wS1 encoding the presence and the amplitude of the stimuli, whether the mouse responded or not by licking, whereas graded responses were only observed in mPFC and tjM1 when the mouse licked. Strong lick-related activity was observed in all three cortical areas, but tjM1 best encoded jaw kinematics. Decision neurons – defined as neurons with significant selectivity between Hit and Miss trials just after the whisker stimulus, and between Hit and Spontaneous licks just before the lick onset time – were found in all three areas but with the highest proportion in wS1. Finally, examining sessions with simultaneous recordings from wS1 and mPFC, we found that failure in the sensorimotor transformation (Miss) could occur at different levels, but regardless of the evoked activity in wS1, the response of mPFC was always higher in Hit trials compared to Miss trials. Altogether, our study suggests a representation of sensory, motor, and decision information more distributed across cortical areas than anticipated.

4.2 Introduction

Learning to generate the appropriate action in response to a given external stimulus is a key function for the survival of any animal, also referred to as sensorimotor transformation. It requires the succession of several processes starting with sensory perception, then decision-making, and finally motor execution. In mammals, even simple sensorimotor transformations involve a large and distributed network of cortical and subcortical areas, including sensory, motor, associative, and high-order cortical areas, as well as striatum, superior-colliculus, cerebellum or midbrain (Romo and de Lafuente 2013; Svoboda and Li 2018; Crochet et al. 2019; Gallero-Salas et al. 2021; Sych et al. 2022; Cruz et al. 2023). Early work in non-human primates has suggested a progressive transformation of sensory signal into a decision and then motor command, as the information flows from sensory to frontal and motor cortical areas,

with sensory areas mostly encoding the physical qualities of the sensory stimulus and frontal regions encoding the decision (to initiate the motor response) (de Lafuente and Romo 2005; Romo and de Lafuente 2013; Alvarez et al. 2015). However, recent studies have reported the presence of decision information and motor-related activity at the early stage of the sensorimotor transformation, in sensory areas (Steinmetz et al. 2019b; Lee et al. 2020; Buetfering et al. 2022; Francis et al. 2022), thus challenging the idea of a segregated representation of different task dimensions across brain areas. In addition, motor activity has been shown to have a broad impact on neuronal activity brain wide, and could constitute a confounding factor with decision-related activity (Musall et al. 2019; Steinmetz et al. 2019; Stringer et al. 2019; Esmaeili et al. 2021; Avitan and Stringer 2022). Therefore, it remains unclear which neuronal computations happen at each stage of the sensorimotor transformation and how sensory, motor, and decision-related information are represented by the neuronal activity of different brain areas.

Sensorimotor transformations can be studied in head-fixed mice allowing for precise measurements of neuronal activity with cellular resolution and monitoring of fine movements with high-temporal resolution (Mathis et al. 2018; Steinmetz et al. 2019; Esmaeili et al. 2021). A simple sensorimotor transformation commonly studied in mice is the learned association between a sensory stimulus delivered to a whisker and the action of licking a water spout to obtain a reward (whisker-detection task) (O'Connor et al. 2010; Chen et al. 2013; Sachidhanandam et al. 2013; Takahashi et al. 2016; Yang et al. 2016; Hong et al. 2018, 2018; Esmaeili et al. 2020). Over the last decade, correlational and causal studies have started to define the neuronal circuits involved in the transformation of the whisker stimulus into the action of licking for reward (Esmaeili et al. 2020). The primary whisker somatosensory cortex (wS1) has been identified as a starting point in the network of cortical areas involved in sensorimotor transformation. The neurons in wS1 receive whisker-related sensory information from the ventral posterior medial thalamus (VPM) with a one-to-one correspondence between the whiskers at the periphery and the barrel columns in the cortex (Feldmeyer et al. 2013; Adibi 2019; Petersen 2019; Staiger and Petersen 2021). Neurons in wS1 have been shown to encode different properties of the sensory stimuli applied to the whiskers, such as velocity, timing, texture, and egocentric angular position (Crochet et al. 2011; Chen et al. 2013b; Yu et al. 2019; Staiger and Petersen 2021). The activity of wS1 is necessary for the execution of whisker-detection or discrimination tasks (Sachidhanandam et al. 2013; Guo et al. 2014; Kwon et al. 2016a; Le Merre et al. 2018; Takahashi et al. 2020). The response of wS1 neurons to a whisker stimulus changes with the learning of a whisker-detection or discrimination task in a projection-specific manner (Chen, Margolis, et al. 2015; Yamashita and Petersen 2016; Vavladeli et al. 2020). In a simple whisker-detection task, when the mouse licks in response to the whisker stimulus, wS1 neurons respond typically with a short-

latency, fast and high-amplitude depolarization followed by a secondary and broader depolarization. The first rapid depolarization likely corresponds to a rapid sensory-evoked response driven by thalamic inputs, independently of the mouse behavioral report. The secondary depolarization, more pronounced when the mouse licks in response to the whisker stimulus than when it fails to respond, possibly represents perception-related cortico-cortical processing (Sachidhanandam et al. 2013; Yamashita and Petersen 2016). The perception of the whisker stimulus leading to behavioral response appears to rely both on cortico-cortical interactions between wS1 and wS2 (Kwon et al. 2016; Yamashita and Petersen 2016; Yang et al. 2016) and local amplification of the sensory signal through active dendritic processing (Takahashi et al. 2016, 2020).

At the other end of the sensorimotor transformation, a region of the motor cortex controlling tongue and jaw movements has been recently identified, which we refer to as the tongue/jaw primary motor cortex (tjM1). Similarly to wM1, tjM1 receives direct synaptic inputs from its corresponding somatosensory area, the tongue/jaw primary somatosensory cortex. Neurons in tjM1 have high selectivity for the direction and amplitude of tongue protrusion during licking, and optogenetic stimulation of tjM1 neurons reliably evokes jaw opening (Mayrhofer et al. 2019; Xu et al. 2022). Conversely, inhibition of tjM1 strongly suppresses licking in different tasks requiring licking in response to a sensory stimulus, with or without a delay (Mayrhofer et al. 2019; Esmaili et al. 2021), or sequential directional licking (Xu et al. 2022). Thus tjM1 is a likely endpoint for the sensorimotor transformation in which a brief whisker deflection is converted into goal-directed licking in order to obtain the reward. The neurons in wS1 and wS2 do not project directly to tjM1 and the exact circuits linking the whisker sensory areas to the tongue/jaw motor areas remain to be determined.

Regarding the decisional component of the sensorimotor transformation, several studies have pointed to an important role played by the medial prefrontal cortex (mPFC) in goal-directed behaviors and decision-making (Le Merre et al. 2021; Klein-Flügge et al. 2022). Although the medial prefrontal cortex (mPFC) is believed to guide behavior by integrating different rules in complex tasks, it also appears to be necessary for the execution of simple sensory detection (Le Merre et al. 2018; Esmaili et al. 2021) or discrimination tasks in mice (Pinto and Dan 2015; Otis et al. 2017; Lak et al. 2020). Similar to what has been found in non-human primates, mPFC neurons in rodents display a large variety of task-related activity: they respond to behaviorally relevant sensory cues (Pinto and Dan 2015; Otis et al. 2017; Le Merre et al. 2018), the subject's motor output (Pinto and Dan 2015; Lak et al. 2020; Kim et al. 2021; Lui et al. 2021), and may guide the subject's choices by encoding reward expectations, action-outcome and context (Moorman and Aston-Jones 2015; Lak et al. 2020; Lui et al. 2021; Spellman et al. 2021).

In this study, we aimed at investigating how sensory, decision, and motor information are encoded at different stages of the sensorimotor transformation. We, therefore, recorded the neuronal activity in mice performing a whisker sensory detection task from the first cortical area receiving the sensory input (wS1), from the motor area controlling the motor output (tjM1), and from the mPFC, an area expected to be involved in the decision process. In order to disentangle sensory, motor, and decision information, and following the idea of the pioneering work in non-human primates (Romo and de Lafuente 2013b) and previous studies in rodents (Stuttgen and Schwarz 2008; Takahashi et al. 2016; Lee et al. 2020), we developed a psychophysical version of the whisker detection task in which head-restrained mice are trained to respond to a whisker stimulus of variable amplitude by licking for reward. High-speed video filming of orofacial movements during the recording allowed to carefully take into account the impact of task-related movements on neuronal activity.

We found that purely sensory information was mostly found in the activity of wS1 neurons whereas licking-related activity was broadly distributed across the three areas. When mice licked in response to the whisker stimulus, the neuronal response increased with the stimulus amplitude in all three cortical areas, but aligning the neuronal activity to the jaw opening onset time, revealed graded responses preceding the jaw onset in wS1 and to a lesser extent mPFC, but not in tjM1. We defined decision neurons as neurons with significant selectivity between Hit and Miss trials just after the whisker stimulus, and between Hit and Spontaneous lick just before movement onset. Surprisingly, decision neurons were found in all three areas but were more abundant in wS1. Finally, using simultaneous recordings in wS1 and mPFC, we could compare the population activity for the same Hit and Miss trials in the two areas. When selecting Hit and Miss trials with similar sensory-evoked population activity, or Miss trials with higher sensory-evoked activity than Hit trials in wS1, the population activity in mPFC was always significantly higher for Hit trials. We conclude that while sensory information is primarily encoded in the sensory area, motor and decision information are broadly distributed and a decision may result from the concerted activity of neurons distributed across many brain regions rather than from the activity of a pool of decision neurons in a dedicated area.

4.3 Results

4.3.1 wS1, mPFC and tjM1 are necessary for the execution of a psychophysical whisker detection task in mice

We recorded the extracellular neuronal activity from three cortical regions: the primary whisker somatosensory cortex (wS1), medial prefrontal cortex (mPFC), and tongue and jaw motor cortex (tjM1) while mice performed a whisker-based psychophysical detection task (Figure 4.1A). In this task, thirsty mice learned to respond to a brief whisker stimulation of various amplitudes by licking the water spout in order to receive the reward. A light metal particle was attached to the right C2 whisker and a magnetic coil was placed underneath the head of the mouse allowing the delivery of brief (1 ms) and well-controlled whisker deflections (Figure 4.9). Licking was monitored online using a piezo-film attached to the water spout. During the recording sessions, we monitored mouse orofacial movements through high-speed video filming at 200 fps. A camera positioned above the mouse captured the horizontal movements of the right C2 whisker. A mirror was positioned on the side to capture tongue and jaw movements with the same camera. We used DeepLabCut (Mathis et al. 2018) to extract the whisker angle, and displacement of the jaw and the tongue from the high-speed videos, aligned to the neuronal activity (Figure 4.1B). Based on the jaw trace, we identified the onset time of the jaw opening following the whisker stimulus, as the reaction time of the animal for each trial. In Hit trials, the whisker stimulus was typically followed by a small-amplitude and brief retraction of the right C2 whisker, immediately followed by a high-amplitude protraction and then the opening of the jaw and tongue (Figure 4.1B and D).

The temporal structure of the psychophysical detection task was very similar to that of the simple whisker detection task used in our previous studies (Sachidhanandam et al. 2013; Sippy et al. 2015; Yamashita and Petersen 2016; Kyriakatos et al. 2017; Le Merre et al. 2018). Trials were not cued to the mouse and started after a random 6-12 s of intertrial-interval that included a 2.5-3.5 s no-lick window during which mice were required not to lick in order to initiate a trial (Figure 4.1C). Stimulus “Go” trials and no-stimulus “No-Go” trials were presented with equal probabilities. In stimulus trials, four different stimulus amplitudes – 1°, 1.8°, 2.5°, and 3.3°, measured as the amplitude of the first downward whisker deflection (Figure 4.10) – were presented with equal probabilities. All trial types were interleaved in a pseudo-randomized manner in blocks of 20 trials. Like any other Go/No-Go task, four trial outcomes could occur: Hit trial when the mouse licked within the 1 s response window after the whisker stimulation; Miss trial when the mouse did not lick after the whisker stimulus; False alarm when the mouse licked in a no-stimulus trial; Correct rejection

when the mouse did not respond in a no-stimulus trial. Only Hit trials were rewarded; Miss, False alarm, and Correct rejection trials were neither punished nor rewarded.

In this study, the stimulus strengths used were calibrated across the physiological range of whisker deflection and the mouse's ability to detect them. We determined psychometric curves for each mouse performing the whisker-based detection task by fitting the performance for the different amplitudes with a sigmoid function using a maximum likelihood method (See 4.6 Methods). Figure 1D shows the individual psychometric curves fitted to each of the 29 electrophysiological recording sessions (19 mice) used in this study. Overall the psychometric curves were comparable across mice and sessions, although the near-threshold stimulus amplitude could vary and was therefore computed for each session.

To test the necessity of wS1, mPFC, and tJM1 for the execution of the psychophysical detection task, we performed focal and temporally-precise optogenetic inactivations in VGAT-ChR2 mice (Zhao et al. 2011; Guo et al. 2014) (Figure 4.1E). Blue (470 nm) light pulses (100 Hz train; 50% duty-cycle; 5 mW mean power; 100 ms before to 1 s after whisker stimulus) were delivered through a 200 μ m optic fiber in 30% of all trials and were randomly interleaved across each session. We performed unilateral photoinhibition of all areas on the left hemisphere. Notably, in our task, the reward spout was positioned to the right side of the mouse, and the mouse had to execute a rightward lick in order to reach it.

On average we observed a significant decrease in lick probability for all stimulus amplitudes when inactivating wS1, tJM1 and mPFC, but not when inactivation was applied to the forepaw primary somatosensory cortex (fpS1) located about 1 mm anterior to wS1 (Table 4.1). We computed the detection threshold for light-on and light-off conditions and observed a reliable and significant shift of the detection threshold towards higher stimulus intensities during wS1 inactivation (wS1: detection threshold light = 2.97 ± 0.36 deg vs no-light = 2.00 ± 0.28 deg, mean \pm SD. $P = 4.88 \times 10^{-4}$ Wilcoxon signed-rank test), but not for the other areas (mPFC: detection threshold light = 2.45 ± 0.61 deg vs no-light = 2.16 ± 0.49 deg, mean \pm SD. $P = 0.17$ Wilcoxon signed-rank test. wM1: detection threshold light = 2.32 ± 0.69 deg vs no-light = 2.11 ± 0.50 deg, mean \pm SD. $P = 0.21$ Wilcoxon signed-rank test. fpS1: detection threshold light = 1.90 ± 0.37 deg vs no-light = 1.94 ± 0.28 deg, mean \pm SD. $P = 0.47$ Wilcoxon signed-rank test). We concluded that all three cortical areas are involved in the execution of the psychophysical detection task. Inactivation of wS1 seems to shift the detection probability to a higher amplitude whereas inactivation of mPFC and tJM1 resulted in a general decrease of the response probability but did not affect the detection threshold (Figure 4.1E).

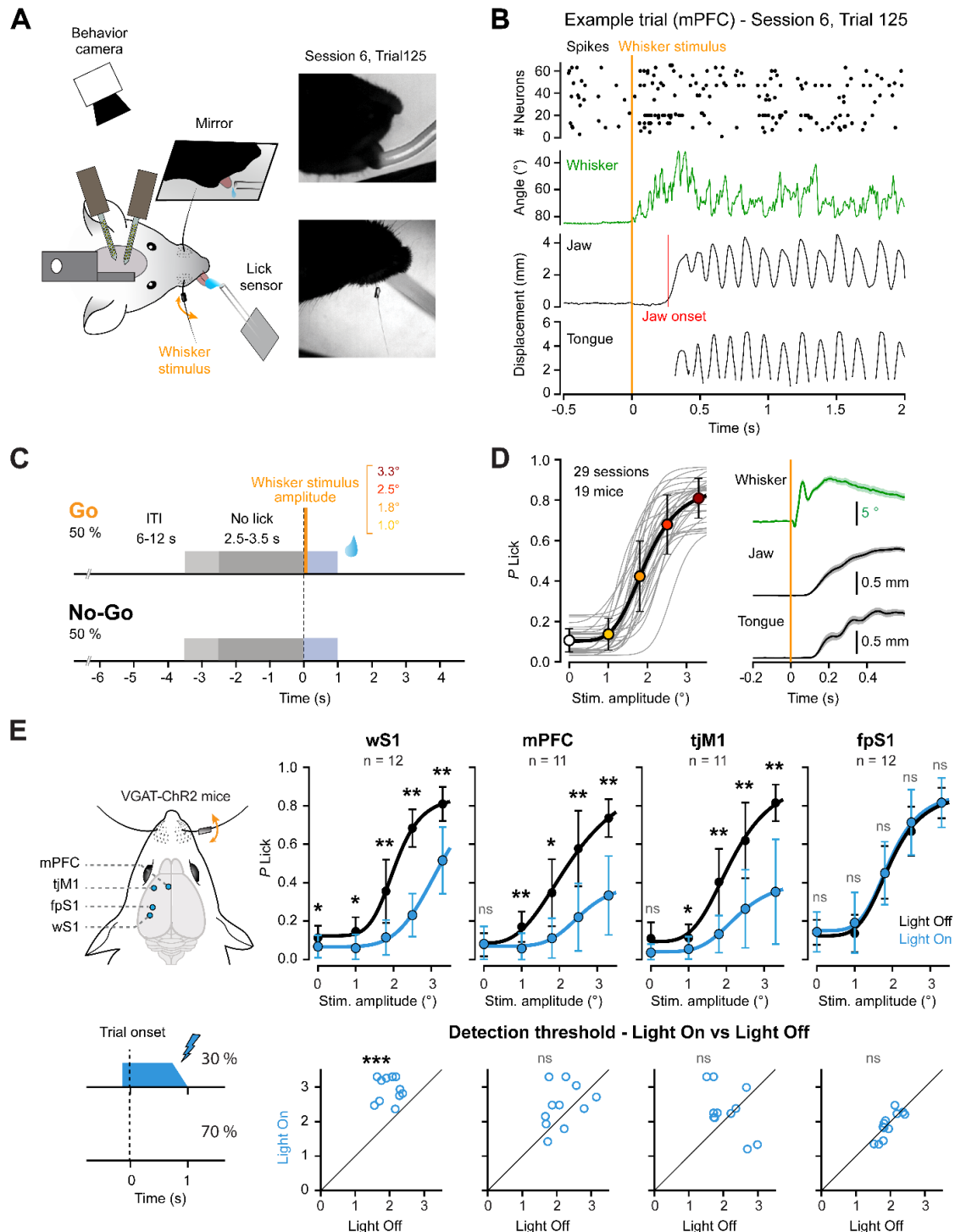


Figure 4.1. A psychometric whisker-based tactile detection task involving wS1, mPFC, and tJM1.

(A) Schematic representation of the experimental set-up. Head-restrained, water-restricted mice were trained to respond to a brief stimulus delivered to the right C2 whisker by licking a water spout positioned to their right to obtain a water reward. Once trained, the neuronal activity of wS1, tJM1, or mPFC was recorded using a high-density extracellular recording silicon probe. Facial movements were

filmed using a high-speed video camera and whisker angular position, jaw opening, and tongue protrusion were tracked offline with DeepLabCut.

(B) Example recording of a single whisker-stimulus trial showing (from top to bottom) the raster plot of the neuronal activity recorded in mPFC (neurons were sorted according to recording depth), the whisker angular position (green), the jaw and tongue displacement (black). Upward deflections indicate respectively whisker protraction, jaw opening, and tongue protrusion. The red line on the jaw movement trace indicates the jaw opening onset time.

(C) Task structure: following a 6-12 s intertrial interval, each trial was preceded by a 2.5-3.5 s No-lick window during which mice were required not to lick. Licking during the No-lick window resulted in postponing the trial onset. In 50% of the trials, a whisker stimulus of variable amplitude was presented (Go trials), and licking within the 1 s response window immediately after was rewarded by a drop of sweet water (Hit). In the other 50% of the trials, no whisker stimulus was presented (NoGo trials), and licking during the response window (False alarm) was neither punished nor rewarded.

(D) *Left*, Lick probability as a function of the whisker stimulus amplitude for the 29 recording sessions (19 mice). Thin grey lines show the psychometric function fitted for each individual session; the thick black line shows the psychometric function fitted to the averaged performance (circles and error bars indicate mean \pm SD). *Right*, Average movements evoked by the whisker stimulus (all stimulus trials) for the 29 sessions.

(E) *Left*, Focal optogenetic inactivation during the entire response window was performed in VGAT-ChR2 mice for wS1, tJM1, mPFC, and fpS1 in 30% of the trials. *Right top*, Averaged performance (lick probability) as a function of the whisker stimulus amplitude for control (no-light, black) and test (light, blue) trials for the 4 cortical areas (Table 4.1). Statistical significance between no-light and light trials was assessed using Wilcoxon signed-rank test with Bonferroni correction for each area (5 tests): ns, $p > 0.05$; *, $p < 0.05$; **, $p < 0.01$; *** (Table 1). *Right bottom*, the Detection threshold, as a middle point of the fitted sigmoid was computed for each inactivation session for control and test trials for the 4 cortical areas. X and y-axis correspond to a whisker stimulus amplitude range. Statistical significance for the change in the detection threshold during no-light and light trials was assessed using Wilcoxon signed-rank test (ns, $p < 0.01$; ***); wS1 $p = 4.88 \times 10^{-4}$; mPFC $p = 0.17$; tJM1 $p = 0.21$; fpS1 $p = 0.47$).

Table 4.1. Optoinhibition : average lick probability (P_{lick}) and statistical differences (Wilcoxon signed-rank test with Bonferroni correction) (Related to Figure 4.1E).

Area	N mice	N sessions	Stimulus amplitude										
			0°		1°		1.8°		2.5°		3.3°		
			Light Off / On										
			Off	On	Off	On	Off	On	Off	On	Off	On	
wS1	12	12	mean	0.11	0.07	0.15	0.06	0.36	0.12	0.68	0.23	0.81	0.52
			± SD	± 0.06	± 0.06	± 0.07	± 0.07	± 0.16	± 0.09	± 0.10	± 0.11	± 0.09	± 0.17
			P	0.03		0.01		2.44 x 10 ⁻³		2.44 x 10 ⁻³		2.44 x 10 ⁻³	
mPFC	11	11	mean	0.08	0.08	0.17	0.06	0.35	0.11	0.58	0.22	0.74	0.33
			± SD	± 0.06	± 0.09	± 0.08	± 0.08	± 0.17	± 0.10	± 0.20	± 0.18	± 0.10	± 0.21
			P	1		4.88 x 10 ⁻³		0.02		4.88 x 10 ⁻³		4.88 x 10 ⁻³	
tjM1	11	11	mean	0.11	0.04	0.11	0.05	0.40	0.13	0.62	0.26	0.82	0.35
			± SD	± 0.08	± 0.05	± 0.07	± 0.08	± 0.17	± 0.10	± 0.20	± 0.20	± 0.10	± 0.27
			P	0.16		0.03		0.01		0.01		4.88 x 10 ⁻³	
fpS1	12	12	mean	0.14	0.14	0.14	0.19	0.45	0.45	0.67	0.71	0.81	0.82
			± SD	± 0.06	± 0.10	± 0.10	± 0.16	± 0.14	± 0.16	± 0.13	± 0.17	± 0.08	± 0.13
			P	1		1		1		0.65		1	

4.3.2 Patterns of cortical activity across cortical areas

To investigate cortical dynamics with a high temporal resolution, we carried out high-density extracellular recordings with silicon probes from the three cortical areas wS1, mPFC, and tjM1. We recorded simultaneously from 2 cortical areas across 29 sessions in 19 mice. The probes were coated with DiI (1,1'-Diocetadecyl-3,3,3',3'-Tetramethylindocarbocyanine Perchlorate, Invitrogen, USA) for precise anatomical localization and registration to the Allen brain atlas (Shamash et al. 2018) (Figure 4.11). In total, we recorded 2,001 single units (651 in wS1, 795 in mPFC, and 555 in tjM1) that satisfied quality criteria (Hill et al. 2011) (see 4.6 Methods).

Based on spike waveform each neuron was classified as a regular spiking unit (RSU, presumably excitatory neurons) or a fast spiking unit (FSU, presumably inhibitory interneurons) (Esmaili et al. 2022). Single neurons across cortical areas exhibited different patterns of activity when aligned to the stimulus onset or the jaw opening onset (Figure 4.2A). On average, we observed an increase in activity in all three areas. wS1 exhibited a first short-latency and pronounced increase in firing rate immediately after the whisker stimulus, followed by a second and smaller phase, similar to what has been observed in the membrane potential of wS1 excitatory neurons (Sachidhanandam et al. 2013; Yamashita and Petersen 2016). mPFC exhibited a transient increase in firing rate, whereas tjM1 showed a more prolonged and sustained activity. When aligned to the jaw onset, all three areas showed an increase in firing rate that started before the onset of the jaw opening (Figure 4.2B).

To test for the task-specific aspect of the neuronal activity evoked by the whisker stimulus, we also recorded from the same areas in other mice passively exposed to the same whisker stimuli that were not predictive of the reward (R- mice). R- mice did not learn to lick in response to the whisker stimulus (Figure 4.13A-B) and the overall pattern of neuronal activity was in sharp contrast with the activity recorded in mice trained in the detection task (R+). In R- mice, the whisker stimulus evoked a sharp and fast increase in firing rate in wS1, but without the secondary increase in firing rate. Little or no response was observed in mPFC and tjM1 following the whisker stimulus (Figure 4.13C-D). When aligned to the jaw onset, all three areas showed an increase in firing rate that started before the onset of the jaw opening, similar to what was observed in R+ mice (Figure 4.13C-D).

Neurons exhibiting similar firing patterns across trial types are expected to encode similar information about the task, hence it is important to understand if a single pattern is uniquely represented in one brain region or distributed across brain regions (Esmaili et al. 2021). To answer this question we performed unsupervised clustering based on the temporal firing patterns in different trial types of all neurons recorded in R+ mice pooled together (see 4.6 Methods). We considered five trial types: Miss and Hit trials aligned to the whisker stimulation onset, Hit and Spontaneous Licks (including

False alarms) trials aligned to the jaw onset, and periods of free whisking (without jaw movements) aligned to the onset of whisking. The Gaussian mixture model revealed 16 distinct clusters based on minimum Bayesian information criteria (BIC) (Figure 4.12). Figure 2C shows a heat-map of the normalized neuronal activity of each recorded neuron grouped by clusters that are sorted according to their mean response latency in Hit trials, aligned to the whisker stimulus. We also computed the relative proportion of each cluster in each cortical area. Clusters with strong and short latency responses to the whisker stimulus in both Hit and Miss trials (like clusters 1 and 2) were predominantly found in wS1. However, some clusters with sensory evoked response in the absence of movement (Miss trials) (like clusters 10 and 16) were also found in mPFC and tJM1 (Figure 4.14). Clusters with prominent responses during Hit and Spontaneous licks were more broadly distributed, although the two clusters with the strongest response during spontaneous lick and no response in Miss trials (pure motor clusters, 5 and 6) were more abundant in tJM1 (Figure 4.14). Some clusters appeared to have very selective activity for one trial type: clusters 8 and 9 were only active in Hit trials, but not in Miss or Spontaneous lick trials; clusters 11 and 13 were selectively active in Spontaneous lick trials, but not in Hit trials. These clusters were mostly found in mPFC and tJM1 (Figure 4.14).

4.3.3 Graded responses to the whisker stimulus during Hit trials in all three areas

The main goal of this study was to test how sensory, decision, and motor information are represented in sensory, higher-order, and motor areas. We hypothesized that purely sensory neurons would show sensory-evoked activity that would correlate with the strength of the whisker stimulus, regardless of the behavioral response (Hit or Miss), and no motor-related activity (Spontaneous lick); purely motor neurons should show similar activity whenever the mouse licked, whether it was preceded by the whisker stimulus or not (Hit or Spontaneous lick), and no response to the sensory stimulus alone (Miss). In this study, we will define sensory-guided decision as the decision to lick in response to the whisker stimulus. Thus, sensory-guided decision neurons should show similar activity in Hit trials, regardless of the stimulus strength, and no response to the sensory stimulus alone (Miss) or to the motor activity alone (Spontaneous lick) (Figure 4.3A). Then, only the 'sensory' neurons should exhibit a graded response to the whisker stimulus as a function of the stimulus amplitude.

We computed the mean PSTHs for Hit trials, aligned to the whisker stimulus for each area. Because our clustering analysis revealed both positive and negative responses to the whisker stimulus, we first computed the Selectivity Index (SI) of each neuron using receiver operating characteristic (ROC) analysis and comparing Hit vs Correct rejection trials. We then computed the mean PSTHs and SI separately for the

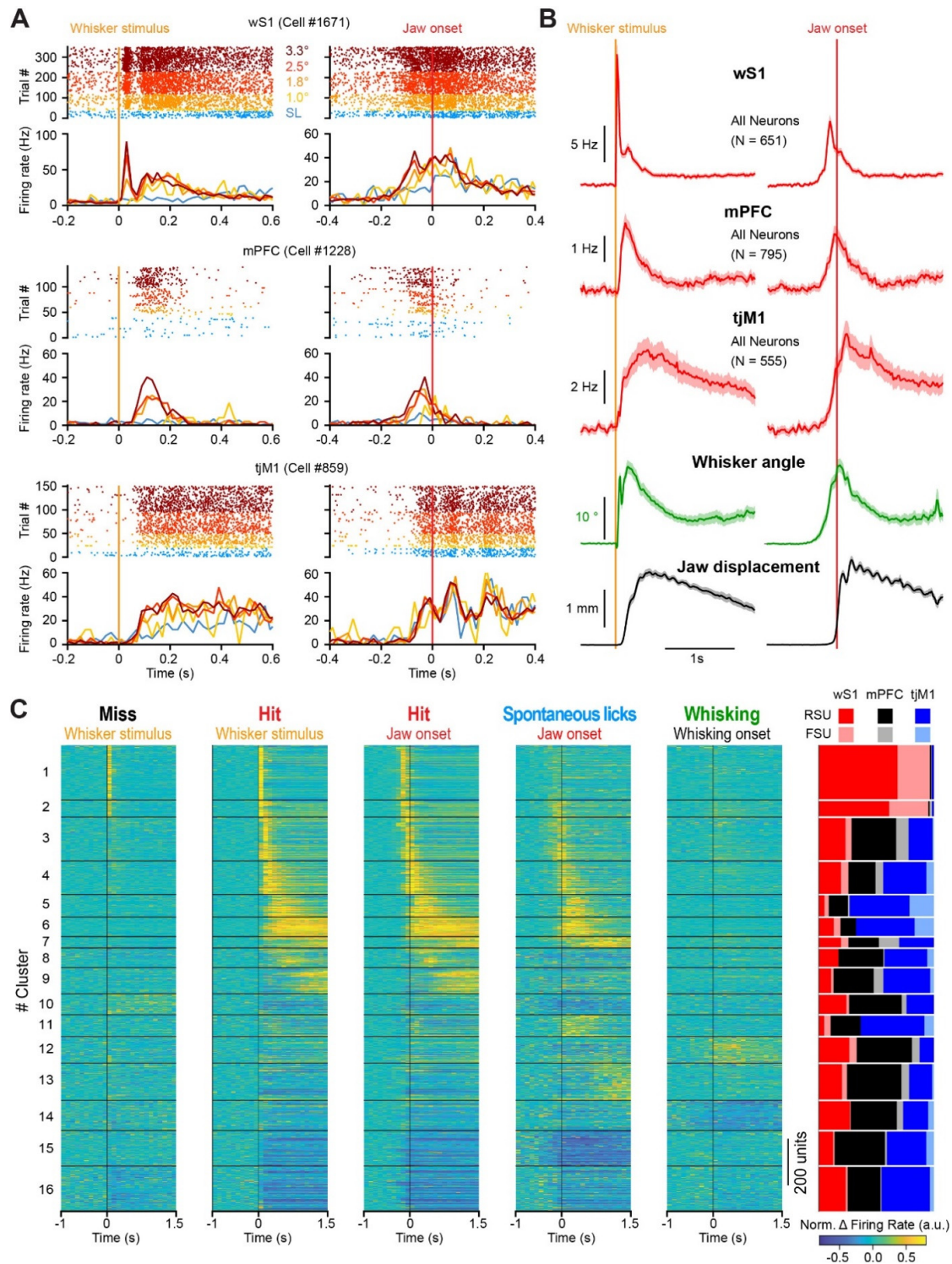


Figure 4.2. Cortical activity patterns during task execution.

(A) Examples of recorded neurons from the three areas in R+ mice. The activity of all lick trials (Hit and Spontaneous lick) for each neuron was aligned to the whisker stimulus onsets (orange, left column), or to the jaw onsets (red, right column). Top row wS1 (RSU) neuron #1671, middle row mPFC (RSU) neuron #1228, bottom row tJM1 (RSU) neuron #859. For each panel, the top part displays a raster plot of the neuronal activity with all trials sorted by stimulus amplitude (Spontaneous Licks (SL) blue;

Stimulus amplitude 1.0° yellow; 1.8° orange; 2.5° red; 3.3° dark red). *The bottom part* displays the peristimulus time histograms (PSTHs, 0.02 s bin) averaged across trials with the same stimulus amplitudes (same color code as raster plot).

(B) *Top*, Average PSTHs (0.02 s bin) for Hit trials of the strongest whisker stimulus (amp. 3.3°), for wS1, mPFC, tJM1 (shown in red as mean \pm SEM) aligned to the whisker stimulus onset (orange, left column), or to the jaw onset (red, right column). RSUs and FSUs are pooled together. *Bottom*, average whisker angle (green) and jaw displacement (black) (29 sessions) aligned to whisker stimulus (left) or jaw onset time (right).

(C) *Left panel*, Heatmap showing the averaged and normalized activity (0.1 s bin size) of each of the 2001 neurons recorded in R+ mice for different trial types and alignment, after clustering using a Gaussian Mixture Model (GMM) (Esmaeili et al. 2021). From left to right: Miss trials aligned to the stimulus onset, Hit trials aligned to the stimulus onset, Hit trials aligned to the jaw onsets, Spontaneous Licks aligned to the jaw onset, and Free Whisking aligned to the whisking onset. The clusters are sorted according to their response latency in Hit trials, stimulus aligned. *Right panel*, Repartition of the neurons of each cluster across the three cortical areas (wS1 red, mPFC black, tJM1 blue) and neuron types (FSUs shown in lighter colors compared to RSUs). The proportions are computed and normalized according to the total number of neurons in each area.

neurons with positive and negative SI. The mean SI and proportion of cells with significant SI increased strongly from the first 50 ms bin in wS1 and increased also markedly in mPFC and tJM1 in the next 50 ms bin (Figure 4.3B-C). To test whether the presence of the whisker stimulus in Hit trials was encoded at the level of the neuronal population dynamic in each area, we used a logistic regression approach to classify Hit vs Spontaneous lick on a single-trial base. In agreement with the SI, we found that it was possible to decode with high accuracy Hit trials from False alarm trials in the first 200 ms following the whisker stimulus from all three areas (decoding accuracy wS1: 0.83 ± 0.07 ; mPFC: 0.76 ± 0.07 ; tJM1: 0.75 ± 0.09 ; mean \pm SD. Data vs Shuffled: wS1 $P = 3.10 \times 10^{-4}$; mPFC $P = 5.49 \times 10^{-4}$; tJM1 $P = 1.83 \times 10^{-4}$; Wilcoxon signed rank test) (Figure 4.3D).

Unexpectedly, we observed a graded response to the whisker stimulus in Hit trials in all three areas, especially for the neurons with positive SI (Figure 4.3B and E, Tables 4.2 and 4.3). However, when looking at individual neurons, we found that the mean Pearson correlation (r) between the evoked activity and the stimulus amplitude was higher in wS1 than in mPFC or tJM1 (Mean Pearson coefficient r : wS1 = 0.21 ± 0.01 ; mPFC = 0.05 ± 0.01 ; tJM1 = 0.01 ± 0.01 . wS1 vs mPFC, $P = 3.70 \times 10^{-34}$; wS1 vs tJM1, $P = 1.68 \times 10^{-42}$; mPFC vs tJM1, $P = 5.23 \times 10^{-6}$. Wilcoxon-Mann-Whitney rank sum test with Bonferroni correction) (Figure 4.3F). Interestingly, the whisker protraction that followed the whisker stimulus in Hit trials also increased in amplitude with the stimulation strength (Figure 4.15). Thus, when mice responded to the whisker stimulus, the evoked activity correlated with the stimulus amplitude in all three areas.

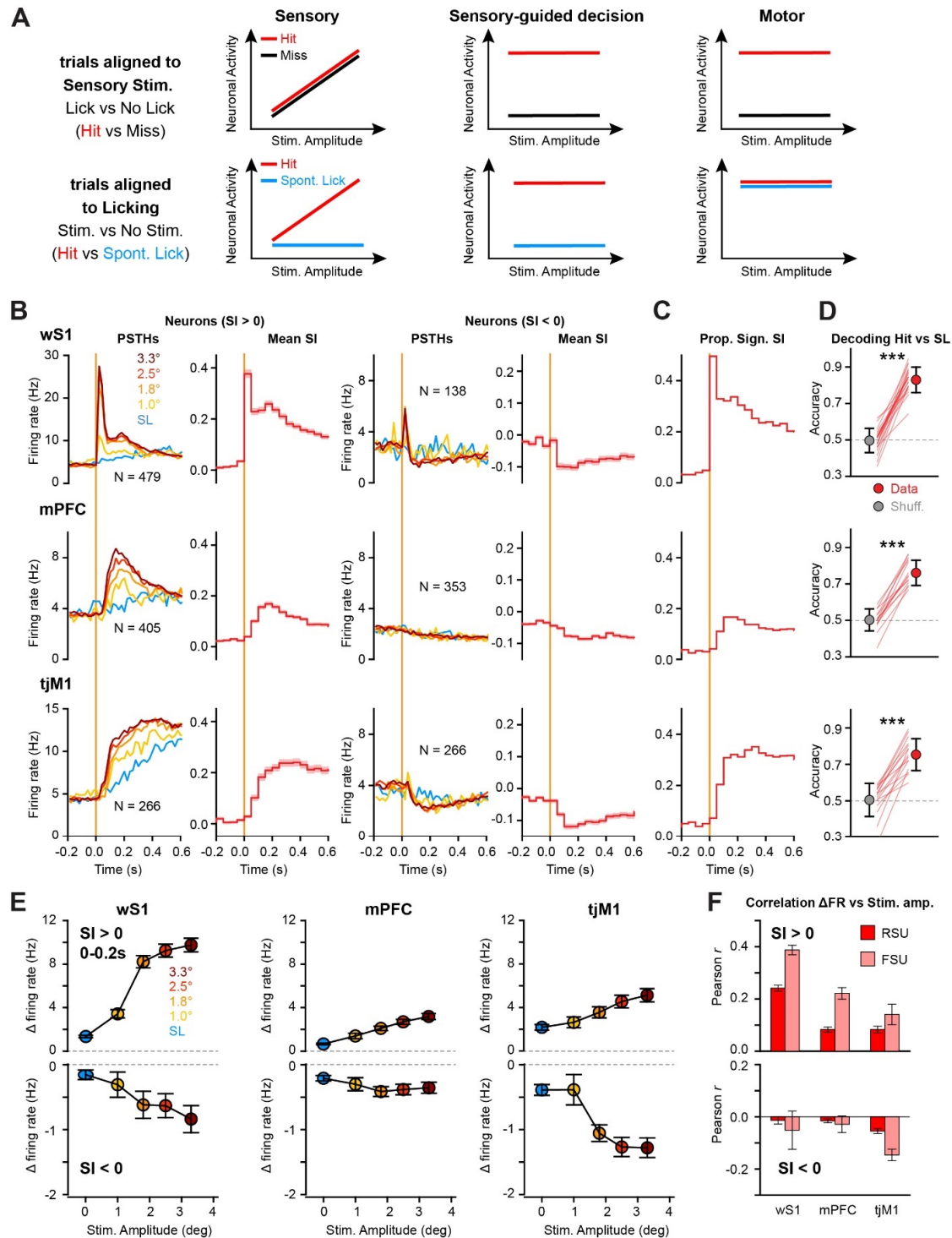


Figure 4.3. Graded evoked responses in Hit trials in all three regions.

(A) Hypothetical outcomes of neuronal responses in psychophysical sensory detection task. Purely Sensory neurons should show increased evoked activity with stimulus amplitude when aligned to the stimulus onset, irrespective of the behavioral outcome (Hit or Miss), and no response during Spontaneous lick. Sensory-guided decision neurons, should show selective activity for Hit trials, irrespective of the stimulus amplitude, and no activity for Miss or Spontaneous lick trials. Purely motor

neurons should show a similar response for Hit and spontaneous lick trials, irrespective of the stimulus amplitude, and no response for Miss trials.

(B) Whisker stimulus evoked neuronal activity and selectivity index (SI) in Hit trials for the three cortical areas (*Top row*, wS1; *Middle row*, mPFC and *Bottom row*, tJM1). Each neuron was classified as positively ($SI > 0$) or negatively ($SI < 0$) modulated neurons based on ROC analysis comparing Hit vs Correct Rejection (CR) trials. For positively and negatively modulated neurons, we computed the grand-average PSTHs (0.02 s bin) for lick trials (Hit and Spontaneous lick) for each stimulus amplitude, aligned to the stimulus (or trial) onset time (*Left column*). We also computed the mean SI (0.05 s bin) (*Right column*). Both FSUs and RSUs were included. The number of neurons is indicated for each category and area.

(C) Proportion of cells with significant SI (Hit vs CR) based on the non-parametric permutation test for each 50 ms time bin after False discovery rate correction (FDR).

(D) A logistic regression approach was used to classify Hit vs Spontaneous lick on a single-trial base from the population activity in each area. The decoding was performed on 0.1 s bins aligned to the trial onset time. The highest accuracy obtained from the real data (Data, red filled circle) and after label shuffling (Shuff., grey filled circle) are plotted for each area. Individual sessions are plotted as thin red lines. The grey dotted line indicates the theoretical chance level. Statistical significance between data and label-shuffled decoding accuracy was assessed using Wilcoxon signed-rank test with FDR correction across 9 time bins (***, $P < 0.001$): wS1, $P = 3.1 \times 10^{-4}$; mPFC, $P = 5.5 \times 10^{-4}$; tJM1, $P = 1.8 \times 10^{-4}$.

(E) Quantification of the evoked responses (0-0.2s for each area and for positively ($SI > 0$, *Top*) and negatively modulated neurons ($SI < 0$, *Bottom*). The delta firing rate was computed by subtracting the mean baseline response (0.5 s window before the stimulus) from the mean evoked response (0-0.2 s after the stimulus) individually for each neuron and amplitude. Data represented as a mean \pm SEM and values can be found in Table 4.2. The difference in evoked responses across stimulus amplitudes was assessed using a Kruskal-Wallis test to test for independent samples (neurons with $SI > 0$: wS1, $P = 6.2 \times 10^{-78}$; mPFC, $P = 1.7 \times 10^{-19}$; tJM1, $P = 1.9 \times 10^{-4}$; neurons with $SI < 0$: wS1, $P = 0.67$; mPFC, $P = 9.6 \times 10^{-3}$; tJM1, $P = 5.8 \times 10^{-15}$). Then followed by multiple comparison tests (P -values for all comparisons are displayed in Table 4.3).

(F) Mean Pearson coefficient of correlation between delta firing rate and stimulus amplitude computed for positively ($SI > 0$) and negatively ($SI < 0$) modulated RSU and FSU neurons in each area. The difference between mean Pearson coefficient was assessed using a Kruskal-Wallis test, followed by multiple comparison tests (P -values for all comparisons are displayed in Table 4.4).

Table 4.2. Mean and SEM of the delta firing rate of early (0-0.2 s) sensory-evoked responses during Hit and Spontaneous lick trials for the different stimulus amplitudes (related to Fig. 4.3E).

neurons with $SI > 0$						
Area	measures	Stimulus amplitudes (degrees)				
		0	1	1.8	2.5	3.3
wS1	mean	1.27	3.40	8.10	9.12	9.59
	\pm SEM	± 0.12	± 0.37	± 0.55	± 0.59	± 0.61
mPFC	mean	0.58	1.55	2.27	2.95	3.42
	\pm SEM	± 0.08	± 0.27	± 0.20	± 0.24	± 0.28
tJM1	mean	2.44	3.10	4.13	5.15	5.70
	\pm SEM	± 0.31	± 0.54	± 0.56	± 0.64	± 0.67
neurons with $SI < 0$						
Area	measures	Stimulus amplitudes (degrees)				
		0	1	1.8	2.5	3.3
wS1	mean	-0.18	-0.46	-0.72	-0.79	-0.98
	\pm SEM	± 0.08	± 0.23	± 0.22	± 0.19	± 0.21
mPFC	mean	-0.22	-0.29	-0.45	-0.48	-0.39
	\pm SEM	± 0.04	± 0.10	± 0.07	± 0.07	± 0.07
tJM1	mean	-0.11	-0.42	-1.09	-1.19	-1.05
	\pm SEM	± 0.09	± 0.22	± 0.12	± 0.13	± 0.14

Table 4.3. *P*-values obtained from multiple comparison tests of the delta firing rate for different stimulus amplitudes (Fig. 4.3 E).

neurons with SI>0											
Area	label 1	label 2	p-value	Area	label 1	label 2	p-value	Area	label 1	label 2	p-value
	Amp°	Amp°			Amp°	Amp°			Amp°	Amp°	
wS1	0	1	0.01	mPFC	0	1	0.65	tjM1	0	1	0.90
wS1	0	1.8	0.00	mPFC	0	1.8	2.03×10^{-7}	tjM1	0	1.8	0.74
wS1	0	2.5	0.00	mPFC	0	2.5	1.14×10^{-11}	tjM1	0	2.5	0.03
wS1	0	3.3	0.00	mPFC	0	3.3	3.37×10^{-13}	tjM1	0	3.3	0.02
wS1	1	1.8	2.55×10^{-21}	mPFC	1	1.8	2.21×10^{-4}	tjM1	1	1.8	0.22
wS1	1	2.5	0.00	mPFC	1	2.5	1.06×10^{-7}	tjM1	1	2.5	1.43×10^{-3}
wS1	1	3.3	0.00	mPFC	1	3.3	6.63×10^{-9}	tjM1	1	3.3	9.48×10^{-4}
wS1	1.8	2.5	0.54	mPFC	1.8	2.5	0.57	tjM1	1.8	2.5	0.45
wS1	1.8	3.3	0.50	mPFC	1.8	3.3	0.30	tjM1	1.8	3.3	0.38
wS1	2.5	3.3	1.00	mPFC	2.5	3.3	0.99	tjM1	2.5	3.3	1.00

neurons with SI<0											
Area	label 1	label 2	p-value	Area	label 1	label 2	p-value	Area	label 1	label 2	p-value
	Amp°	Amp°			Amp°	Amp°			Amp°	Amp°	
wS1	0	1	0.97	mPFC	0	1	0.79	tjM1	0	1	0.75
wS1	0	1.8	0.86	mPFC	0	1.8	0.02	tjM1	0	1.8	1.89×10^{-9}
wS1	0	2.5	0.83	mPFC	0	2.5	0.03	tjM1	0	2.5	1.65×10^{-9}
wS1	0	3.3	0.60	mPFC	0	3.3	0.21	tjM1	0	3.3	1.84×10^{-6}
wS1	1	1.8	1.00	mPFC	1	1.8	0.31	tjM1	1	1.8	2.50×10^{-6}
wS1	1	2.5	0.99	mPFC	1	2.5	0.36	tjM1	1	2.5	2.24×10^{-6}
wS1	1	3.3	0.92	mPFC	1	3.3	0.86	tjM1	1	3.3	5.91×10^{-4}
4wS1	1.8	2.5	1.00	mPFC	1.8	2.5	1.00	tjM1	1.8	2.5	1.00
wS1	1.8	3.3	0.99	mPFC	1.8	3.3	0.89	tjM1	1.8	3.3	0.78
wS1	2.5	3.3	1.00	mPFC	2.5	3.3	0.92	tjM1	2.5	3.3	0.77

Table 4.4. *P*-values obtained from multiple comparison tests of the mean Pearson correlation coefficient different stimulus amplitudes (Fig. 4.3 F).

			FSU						RSU					
			SI<0			SI>0			SI<0			SI>0		
			tjM1	mPFC	wS1	tjM1	mPFC	wS1	tjM1	mPFC	wS1	tjM1	mPFC	
RSU	SI>0	wS1	0	1.74 $\times 10^{-7}$	0.03	0.43	1.00	3.62 $\times 10^{-5}$	0	0	0	1.10 $\times 10^{-14}$	5.20 $\times 10^{-17}$	
		mPFC	3.29 $\times 10^{-9}$	0.24	0.96	0.95	5.92 $\times 10^{-5}$	0	1.31 $\times 10^{-14}$	2.48 $\times 10^{-8}$	1.11 $\times 10^{-3}$	1.00		
		tjM1	2.84 $\times 10^{-8}$	0.34	0.98	0.91	5.25 $\times 10^{-5}$	0	5.93 $\times 10^{-11}$	8.05 $\times 10^{-6}$	9.23 $\times 10^{-3}$			
	SI<0	wS1	0.01	1.00	1.00	9.70 $\times 10^{-3}$	9.24 $\times 10^{-12}$	0	0.50	1.00				
		mPFC	0.01	1.00	1.00	1.18 $\times 10^{-3}$	1.03 $\times 10^{-16}$	0	0.39					
		tjM1	0.39	1.00	1.00	5.40 $\times 10^{-6}$	0	0						
	FSU	SI>0	wS1	0	2.52 $\times 10^{-14}$	9.89 $\times 10^{-5}$	4.90 $\times 10^{-5}$	0.02						
			mPFC	1.65 $\times 10^{-17}$	1.40 $\times 10^{-5}$	0.07	0.75							
			tjM1	1.62 $\times 10^{-7}$	0.08	0.71								
SI<0		wS1	0.86	1.00										
		mPFC	0.51											

4.3.4 Purely sensory responses in the absence of licking are mostly restricted to neurons in wS1

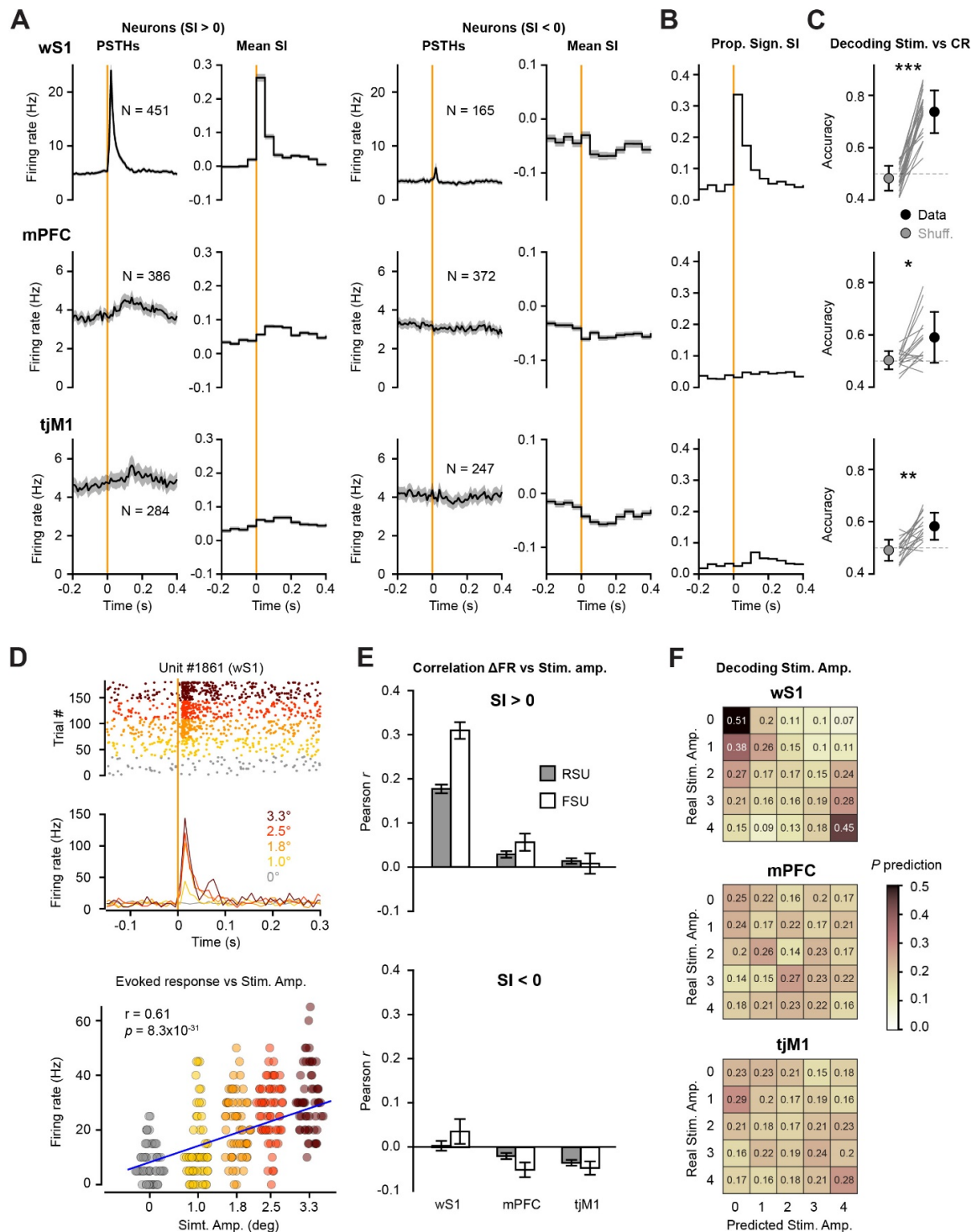
We next considered purely sensory-evoked responses in the absence of licking by analyzing Miss trials. We first computed the SI of each neuron comparing Miss and Correct rejection trials. On average, wS1 neurons had much higher SI than mPFC and tjM1 (max positive SI wS1 = 0.26 ± 0.011 ; mPFC = 0.08 ± 0.005 ; tjM1 = 0.068 ± 0.0053 . wS1 vs mPFC, $P = 6.43 \times 10^{-33}$; wS1 vs tjM1, $P = 5.98 \times 10^{-34}$; mPFC vs tjM1, $P = 0.20$ Wilcoxon-Mann-Whitney rank sum test with Bonferroni correction) and the proportion of cells with significant SI was also much higher in wS1 (proportion of cells with significant SI, wS1 = 0.34; mPFC = 0.047; tjM1 = 0.07. wS1 vs mPFC, $P = 2.74 \times 10^{-44}$; wS1 vs tjM1, $P = 3.36 \times 10^{-28}$; mPFC vs tjM1, $P = 0.09$. Chi-square test with Bonferroni correction) (Figure 4.4A-B). The evoked activity in Miss trials in the three cortical areas was very similar to that evoked in R- mice (Figure 4.16A-B and 4.17A-B). Accordingly, we were able to decode the presence of the stimulus with the highest accuracy from the population activity in wS1 (decoding accuracy Hit vs Correct rejection wS1: 0.74 ± 0.08 ; mean \pm SD) (Figure 4.4C). Nonetheless, in mice trained in the whisker detection task (R+), neurons in mPFC and tjM1 still contained some

information about the sensory stimulus and it was possible to decode the presence of the stimulus above chance level from mPFC and tjM1 population activity (decoding accuracy mPFC: 0.59 ± 0.10 ; tjM1: 0.58 ± 0.05 ; mean \pm SD; wS1, $P = 2.68 \times 10^{-4}$; mPFC, $P = 0.023$; tjM1, $P = 0.0021$. Wilcoxon signed-rank test, with FDR correction across bins). That was not the case in R- mice (decoding accuracy wS1 = 0.74 ± 0.09 ; mPFC = 0.52 ± 0.02 ; tjM1 = 0.54 ± 0.01 ; mean \pm SD; wS1, $P = 0.035$; mPFC, $P = 0.12$; tjM1, $P = 0.087$. Wilcoxon signed-rank test, with FDR correction across bins) (Figure 4.16C and 4.17A).

We also computed the Pearson coefficient of correlation between the evoked change in firing rate and the stimulus amplitude for each neuron (Figure 4.4D). We found a much stronger mean correlation for the neurons in wS1 compared to mPFC and tjM1 (Mean Pearson coefficient r : wS1 = 0.15 ± 0.008 ; mPFC = 0.0022 ± 0.0048 ; tjM1 = 0.0063 ± 0.0046 . wS1 vs mPFC, $P = 8.54 \times 10^{-51}$; wS1 vs tjM1, $P = 5.41 \times 10^{-50}$; mPFC vs tjM1, $P = 1$. Wilcoxon-Mann-Whitney rank sum test with Bonferroni correction) (Figure 4.4E). In fact, it was possible to decode the stimulus amplitude from the population activity in wS1 above the chance level, but not from mPFC or tjM1 (Figure 4.4F). This was similarly observed in R- mice (Figure 4.16D-F). Thus, despite the fact that some sensory information seems to reach mPFC and tjM1 in mice trained in the whisker detection task, wS1 is the only area to encode both the presence of the stimulus and the strength of the stimulus when the mouse did not lick.

4.3.5 Purely motor response in the absence of sensory stimulus is broadly distributed

Similarly to *purely sensory* responses, we investigated *purely motor* responses by focusing on Spontaneous lick trials that were not triggered by a whisker stimulus. We computed the SI for each neuron by comparing their activity 100 ms before and 100 ms after jaw onset time to the no-lick window preceding the trial. We found high SI immediately before and after jaw onset time in all three areas (Figure 4.5A), in both groups of mice (R+ and R-) (Figure 4.18A-B). Just around jaw onset time, tjM1 had the highest SI and highest proportion of neurons with significant SI, followed by wS1 and then mPFC (max positive SI just around jaw onset wS1 = 0.21 ± 0.012 ; mPFC = 0.14 ± 0.01 ; tjM1 = 0.27 ± 0.019 . wS1 vs mPFC, $P = 5.20 \times 10^{-4}$; wS1 vs tjM1, $P = 0.22$; mPFC vs tjM1, $P = 2.13 \times 10^{-6}$ Wilcoxon-Mann-Whitney rank sum test with Bonferroni correction; proportion of cells with significant SI, wS1 = 0.14; mPFC = 0.05; tjM1 = 0.17. wS1 vs mPFC, $P = 1.19 \times 10^{-3}$; wS1 vs tjM1, $P = 0.42$; mPFC vs tjM1, $P = 6.91 \times 10^{-5}$. Chi-square test) (Figure 4.5B). It was possible to decode with high accuracy jaw opening from the population activity before and after jaw onset time from all three areas, with similar accuracy from wS1 and tjM1 and lower accuracy from mPFC (decoding accuracy wS1: before 0.77 ± 0.09 and after 0.85 ± 0.05 ; mPFC before



stimulus onset time (*Left column*). We also computed the mean SI (0.05 s bin) (*Right column*). Both FSUs and RSUs were included. The number of neurons is indicated for each category and area.

(B) Proportion of cells with significant SI (Miss vs CR) based on the non-parametric permutation test for each 50 ms time bin after False discovery rate correction (FDR).

(C) A logistic regression approach was used to classify Miss vs CR on a single-trial base from the population activity in each area. The decoding was performed on 0.1 s bins aligned to the trial onset time. The highest accuracy obtained from the real data (Data, black filled circle) and after label shuffling (Shuff., grey filled circle), are plotted for each area. Individual sessions are plotted as thin grey lines. The grey dotted line indicates the theoretical chance level. Statistical significance between data and label-shuffled decoding accuracy was assessed using Wilcoxon signed-rank test with FDR correction across 9 time bins (*, $0.05 > P > 0.01$; **, $0.01 > P > 0.001$; ***, $P < 0.001$): wS1, $P = 2.7 \times 10^{-4}$; mPFC, $P = 0.02$; tjM1, $P = 2.1 \times 10^{-3}$.

(D) Example wS1 neuron (neuron #1861). *Top*, raster plot for all Miss trials aligned to the whisker stimulus and sorted according to the stimulus amplitudes and corresponding PSTHs. (0.01 s bin). *Bottom*, distribution of evoked response (firing rate computed 0-200 ms after the whisker stimulus) for single trials as a function of stimulus amplitude. Linear correlation was assessed using Pearson correlation (correlation coefficient $r = 0.61$, $p = 8.3 \times 10^{-31}$, non-parametric permutation test). The blue line is a linear fit to the data.

(E) Mean Pearson coefficient of correlation averaged across neurons for positively (SI > 0, Top) and negatively (SI < 0, Bottom) modulated RSU (filled grey bars) and FSU (open bars) neurons from each area. The difference between mean Pearson coefficient was assessed using a Kruskal-Wallis test, followed by multiple comparison tests (P -values for all comparisons are displayed in Table 4.5).

(F) Multinomial logistic regression approach was used to decode the stimulus amplitude from the population activity 100 ms after stimulus onset in Miss trials on a single trial basis. The Confusion matrices display the probability of correctly predicting the stimulus amplitude (Predicted) depending on the actual stimulus amplitude (Real) for each area. Chance level = 0.2.

Table 4.5. P -values obtained from multiple comparison tests of the mean Pearson correlation coefficient different stimulus amplitudes (Fig.4.4 E).

			FSU						RSU				
			SI<0			SI>0			SI<0			SI>0	
			tjM1	mPFC	wS1	tjM1	mPFC	wS1	tjM1	mPFC	wS1	tjM1	mPFC
RSU	SI>0	wS1	2.50 $\times 10^{-14}$	5.15 $\times 10^{-15}$	0.02	1.75 $\times 10^{-6}$	1.39 $\times 10^{-3}$	2.66 $\times 10^{-3}$	0	0	0	0	0
		mPFC	0.04	0.02	1.00	0.99	0.99	0	1.75 $\times 10^{-6}$	2.90 $\times 10^{-4}$	0.68	1.00	
		tjM1	0.16	0.09	1.00	1.00	0.86	0	7.01 $\times 10^{-4}$	0.05	0.99		
	SI<0	wS1	0.67	0.51	1.00	1.00	0.42	0	0.23	0.92			
		mPFC	0.99	0.94	0.96	1.00	0.01	0	0.93				
		tjM1	1.00	1.00	0.69	0.93	5.55 $\times 10^{-4}$	0					
FSU	SI>0	wS1	0	0	1.96 $\times 10^{-5}$	5.02 $\times 10^{-12}$	5.38 $\times 10^{-9}$						
		mPFC	0.02	9.65 $\times 10^{-3}$	1.00	0.83							
		tjM1	0.93	0.86	1.00								
	SI<0	wS1	0.71	0.61									
		mPFC	1.00										

0.63 \pm 0.10 and after 0.77 \pm 0.07; tjM1: before 0.77 \pm 0.01 and after 0.91 \pm 0.06; Mean \pm SD. Data vs Shuffled: wS1 PBefore = 8.94×10^{-5} , PAfter = 8.94×10^{-5} ; mPFC PBefore = 1.53×10^{-3} , PAfter = 3.66×10^{-4} ; tjM1 PBefore = 3.30×10^{-4} , PAfter = 1.37

$\times 10^{-4}$; Wilcoxon signed rank test, FDR corrected across bins) (Figure 4.5C). It was also possible to decode licking from the population activity in all three areas in R-, before and after lick onset time (Figure 4.18C). Thus the initiation of licking seems to be broadly represented across cortical areas, irrespective of the task performed, in good agreement with recent studies (Steinmetz et al. 2019; Stringer et al. 2019).

We postulated that cortical areas involved in motor control should not only encode the movement initiation but also the fine kinematics of the movement. Therefore, we measured the correlation between neuronal activity and the phase of the jaw movement during long lick bouts when the mice collected the reward in Hit trials (Berens 2009). To avoid contamination for the whisker stimulus we excluded the first 500 ms following the stimulus in Hit trials (Figure 4.5D-E). We found the highest proportion of neurons with significant jaw-phase correlation in tJM1, but also a high proportion in wS1 which may be due to the close correlation of orofacial movements, including whisker movement, during licking (Total proportion of neurons in wS1 = 0.46, mPFC = 0.16 and tJM1 = 0.66; tJM1 vs wS1 $P = 3.8 \times 10^{-13}$, tJM1 vs mPFC $P = 6.3 \times 10^{-81}$ and wS1 vs mPFC $P = 1.54 \times 10^{-35}$, Chi-square test) (Figure 4.5E and 4.19). In good agreement, we could decode jaw displacement with the highest accuracy from tJM1, followed by wS1 and then mPFC (correlation between predicted and real jaw movement: wS1 0.28 ± 0.06 ; mPFC 0.21 ± 0.02 ; and tJM1 0.47 ± 0.16 ; mean \pm SD. tJM1 vs wS1 $P = 0.0032$, tJM1 vs mPFC $P = 3.02 \times 10^{-4}$ and wS1 vs mPFC $P = 0.0021$, Wilcoxon-Mann-Whitney rank sum test with Bonferroni correction) (Figure 4.5F). By analyzing reward collection in R- mice, we found similar proportions of cells with phase correlation with jaw movement and similar accuracy when decoding jaw position compared to mice performing the whisker detection task (Figure 4.18D-E and 4.19).

4.3.6 Motor and sensory information in Hit trials

Our previous analyses showed a broad impact of motor activity on neuronal activity across cortical areas. We thus tested to what extent motor-related activity could explain the graded response observed in mPFC and tJM1. We hypothesized that the stimulus strength could impact the distribution, and therefore the mean, of the response latency. We computed the mean response latency across all sessions and found that indeed stronger stimulus resulted in significantly shorter response latency on average (Figure 4.6A and Table 4.5). However, looking at the response latency distribution, it appeared that the increase in stimulus amplitude mostly resulted in a narrower distribution around the mode rather than a shift of the mode (Figure 4.6B).

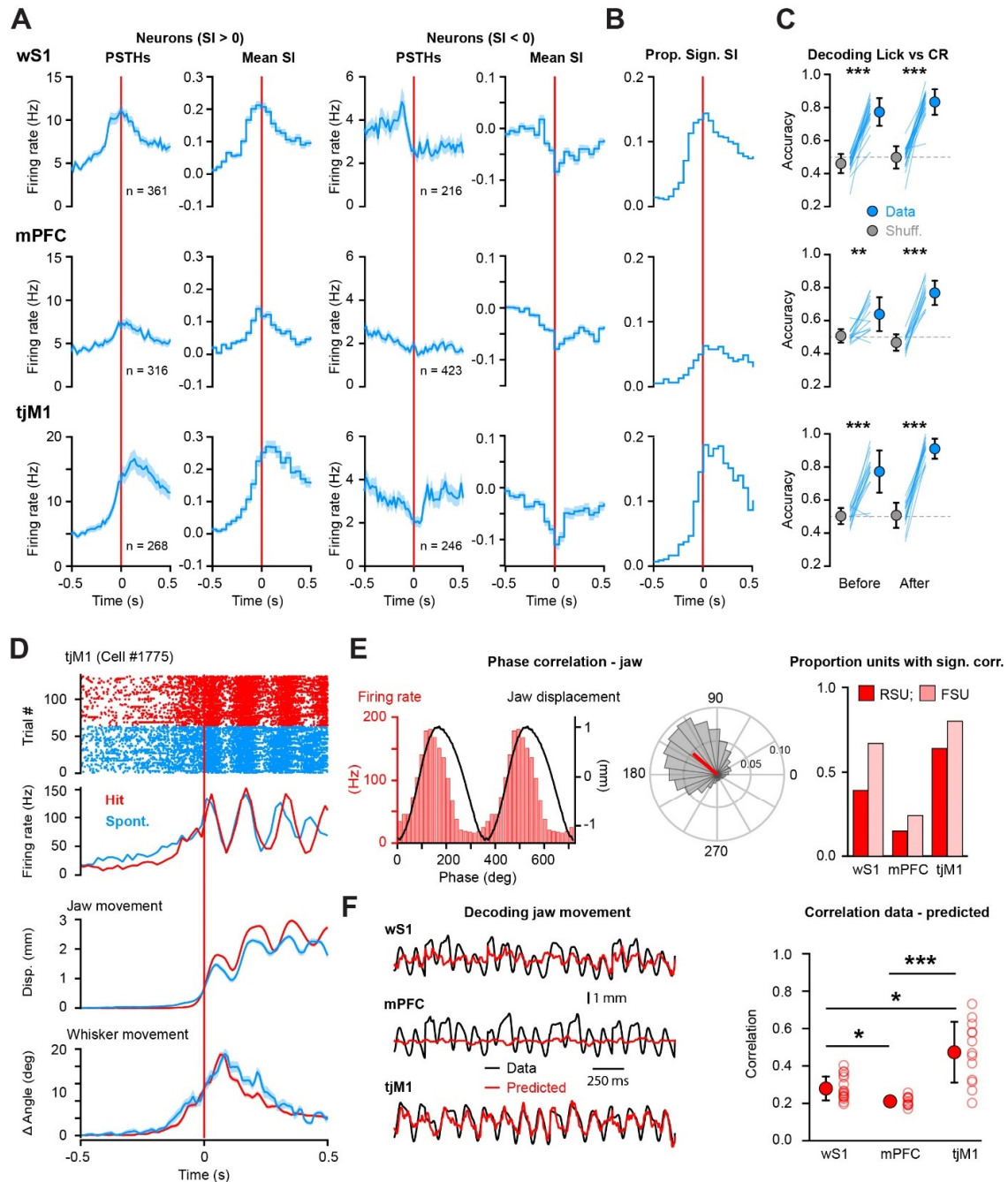


Figure 4.5. Purely motor-related activity in the absence of sensory stimulus.

(A) lick evoked neuronal activity and selectivity index (SI) in Spontaneous lick trials for the three cortical areas (Top row, wS1; Middle row, mPFC and Bottom row, tJM1). Each neuron was classified as a positively (SI > 0) or negatively (SI < 0) modulated neuron according to their maximum Selectivity Index (SI) within a 0.2 s window around the jaw onset (from - 0.1 s to 0.1 s) based on ROC analysis comparing Spontaneous lick vs No lick time window (baseline). For positively and negatively modulated neurons, we computed the grand-average PSTHs (0.02 s bin), aligned to the jaw movement onset time

(Left column). We also computed the mean SI (0.05 s bin) (Right column). Both FSUs and RSUs were included. The number of neurons is indicated for each category and area.

(B) Proportion of cells with significant SI (Spontaneous lick vs baseline) based on the non-parametric permutation test for each 50 ms time bin after False discovery rate correction (FDR).

(C) A logistic regression approach was used to classify Spontaneous Licks vs Correct Rejection (CR) on a single-trial basis from the population activity in each area. The decoding was performed on 0.1 s bins aligned to the jaw movement onset time. The accuracy obtained from the real data (Data, black filled circle) and after label shuffling (Shuff., grey filled circle) are plotted for each area for the 0.1 s bins immediately before and after jaw onset. Individual sessions are plotted as thin blue lines (wS1, 21 sessions; mPFC, 15 sessions; tjM1, 17 sessions). The grey dotted line indicates the theoretical chance level. Statistical significance between data and label-shuffled decoding accuracy was assessed using Wilcoxon signed-rank test with FDR correction across 9 time bins (**, $0.01 > P > 0.001$; ***, $P < 0.001$): wS1_{Before}, $P = 8.9 \times 10^{-5}$; wS1_{After}, $P = 8.9 \times 10^{-5}$; mPFC_{Before}, $P = 1.5 \times 10^{-3}$; mPFC_{After}, $P = 3.7 \times 10^{-4}$; tjM1_{Before}, $P = 3.3 \times 10^{-4}$; tjM1_{After}, $P = 1.4 \times 10^{-4}$.

(D) Example tjM1 neuron (neuron #1775). *Top*, raster plot for all Hit (red) and Spontaneous lick (blue) trials aligned to the jaw movement onset and corresponding PSTHs. (0.02 s bin). *Bottom*, Average jaw, and whisker movements for the same trials.

(E) Modulation of neuronal activity by the phase of jaw movement. *Left*, Jaw phase-modulation for the same example cell as in *panel (D)* was quantified based on licking bouts during reward collection. The mean jaw phase (black line, two full cycles are displayed) is overlaid with the distribution of mean firing rates across jaw phases. *Middle*, Polar plot displaying spike probability across different phases of the jaw movement (grey bars) for the example neuron. The red line indicates the mean resultant vector \bar{r} and its length R ($\bar{r} = 139^\circ$, $R = 0.036$, $P = 4.2 \times 10^{-1103}$, Rayleigh test). *Right*, Proportion of cells with significant jaw-phase correlation was assessed by testing the uniformity of the spike probability distribution around the circle with Rayleigh test.

(F) Continuous decoding of jaw movement from neuronal population activity was performed using linear regression for the continuous signal regression approach. *Left*, example real (Data, black) and predicted (red) jaw traces from three recording sessions from wS1, mPFC, and tjM1. *Right*, the correlation coefficient between real and predicted jaw traces for each area. Empty circles indicate individual sessions, filled red circles with error bars indicate mean \pm SD for each area. Comparison between areas: Kruskal-Wallis test, $P = 6.6 \times 10^{-6}$; multiple comparison tests (*, $0.05 > P > 0.01$; **, $0.01 > P > 0.001$; ***, $P < 0.001$): wS1 vs mPFC, $P = 0.02$; wS1 vs tjM1 $P = 0.02$; mPFC vs tjM1 $P = 3.1 \times 10^{-6}$.

Considering the evoked neuronal activity, we would expect sensory-driven activity to be stable in time relative to the whisker stimulus and licking-related activity to follow the response latency (Figure 4.6C). To assess whether response latency could affect the neuronal response, we computed PSTHs for the stimulus amplitude 2.5° for 3 ranges of response latency: below 150 ms (0.12 ± 0.018 ms, mean \pm SD); between 150 and 300 ms (0.20 ± 0.024 ms, mean \pm SD); and above 300 ms (0.42 ± 0.077 ms, mean \pm SD). We found that the peak of the evoked response in wS1 and mPFC was largely unchanged by the response latency, whereas in tjM1, we observed a clear drift of the peak of the response as the latency increased. This suggested that the difference in the mean response latency might account for the graded response in Hit trials in tjM1, when aligned to the stimulus onset (Figure 4.6D).

A way to correct for the difference in response latency is to realign the neuronal activity to the movement onset time. In the hypothetical case of pure motor encoding, the evoked response should be similar for all stimulus amplitudes when aligned to the

motor onset. Indeed, when aligned to the jaw onset time, we did not observe any graded response with stimulus amplitude in tjM1. In wS1 a clear graded response was observed before jaw onset, in agreement with the presence of a sensory-evoked response. Interestingly, we also observed a graded response before jaw onset in mPFC, suggesting that the neuronal activity in this area still contained information about the sensory stimulus (Figure 4.6E). We quantified how much the activity was different compared to spontaneous lick 200 ms before the onset of the jaw opening for the three areas. We found that the difference in firing rate increased significantly with stimulus amplitude for neurons with positive SI in both wS1 and mPFC. That was much less true in tjM1 (Figure 4.6F and Tables 4.6 and 4.7). We also computed the Pearson coefficient of correlation between the difference in firing rate and the stimulus amplitude for each neuron and found the highest mean correlation in wS1, then in mPFC, and the lowest correlation in tjM1 (Mean Pearson coefficient r : wS1 = 0.13 ± 0.0077 ; mPFC = 0.05 ± 0.0053 ; tjM1 = 0.016 ± 0.007 . wS1 vs mPFC, $P = 5.24 \times 10^{-14}$; wS1 vs tjM1, $P = 1.34 \times 10^{-21}$; mPFC vs tjM1, $P = 0.0016$. Wilcoxon-Mann-Whitney rank sum test with Bonferroni correction) (Figure 4.6G). Altogether, these analyses confirm that tjM1 predominantly encodes Licking-related information during the task, whereas wS1 and mPFC encode a mixture of sensory and motor information.

4.3.7 Decision encoding

In this study, we were interested in understanding the neuronal circuits that make the link between the whisker sensory stimulus and the action of licking (sensory-guided decision). Therefore, we defined decision-related activity as a neuronal activity that would show selectivity for Hit vs Miss trials just after the whisker stimulus and for Hit vs Spontaneous lick just before lick onset. We computed the SI for each neuron for Hit vs Miss trials aligned to the stimulus onset for the near-threshold stimulus amplitude, and for Hit vs spontaneous lick trials aligned to jaw opening onset for stimulus amplitudes 1.8° , 2.5° , and 3.3° .

All three areas showed high Hit vs Miss SI, with wS1 showing the earliest increase with high SI (positive SI in the first 50 ms wS1 = 0.21 ± 0.01 ; mPFC = 0.1 ± 0.01 ; tjM1 = 0.072 ± 0.01 . wS1 vs mPFC, $P = 1.35 \times 10^{-15}$; wS1 vs tjM1, $P = 4.05 \times 10^{-20}$; mPFC vs tjM1, $P = 0.025$. Wilcoxon-Mann-Whitney rank sum test with Bonferroni correction) and the highest proportion of neurons with significant SI in the first 50 ms following stimulus onset (proportion of cells with significant SI in the first 50 ms, wS1 = 0.17; mPFC = 0.028; tjM1 = 0.038. wS1 vs mPFC, $P = 0.33$; wS1 vs tjM1, $P = 0.76$; mPFC vs tjM1, $P = 0.54$. Chi-square test with Bonferroni correction) (Figure 4.7A-B).

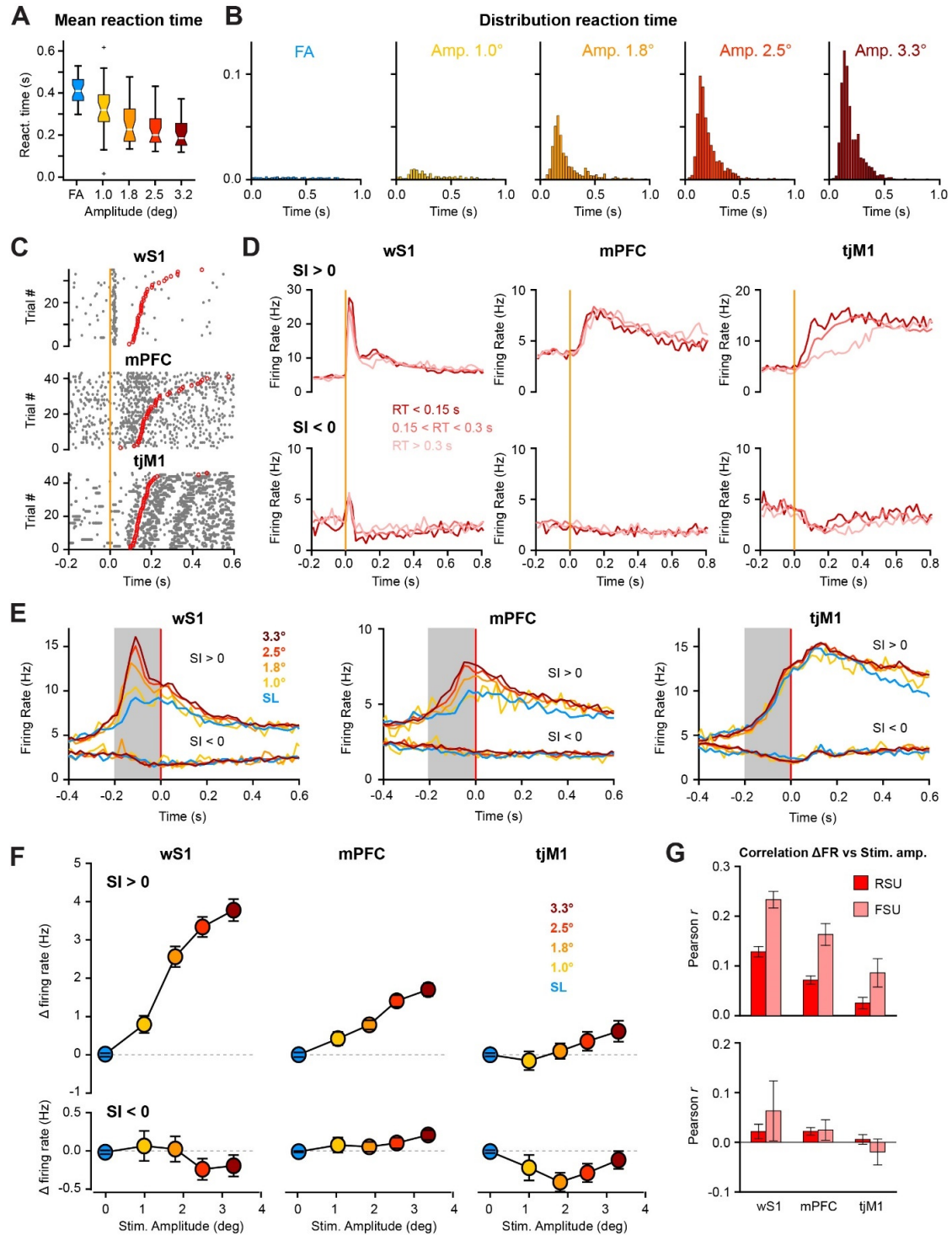


Figure 4.6. Motor and sensory-evoked activity in Hit trials.

(A) Mean reaction time (calculated as the jaw opening time) for different amplitudes across sessions ($n=29$ sessions, 19 mice). On each box of the plot, the central mark indicates the median reaction time and the bottom and top edges of the box indicate the 25th and 75th percentiles, respectively. Kruskal-Wallis test $P = 1.15 \times 10^{-12}$. See Table 4.6 for multiple comparison test between amplitudes.

(B) Distribution of reaction times averaged across sessions for the spontaneous lick (False alarm) and Hit trials for different stimulus amplitudes. The histograms were normalized by the total number of lick trials in each condition.

(C) Examples of raster plots of for Hit trials (amplitude 2.5°), aligned to the whisker stimulus (*orange vertical line*) and sorted by their reaction time (*red circles* indicate jaw opening time for each trial): *top panel* wS1 (neuron #1012), *middle panel* mPFC (neuron #698), *bottom panel* tJM1 (neuron #853).

(D) Mean PSTHs (0.02 s bin), for stimulus amplitude 2.5°, averaged across trials with different reaction times and aligned to the stimulus onset: early reaction times (RT < 0.15 s, dark red); intermediate reaction times (0.15 < RT < 0.3 s, light red); late reaction times (RT > 0.3 s, pink). All units are divided into neurons with SI > 0 (*upper row*), and neurons with SI < 0 (*lower row*) according to their max Hit vs correct rejection SI within the first 0.2 s (same as for figure 4.3B). *Left column* wS1, *middle* mPFC, *right* tJM1.

(E) Neuronal responses for Hit trials for three cortical areas aligned to the jaw onset: *left* wS1, *middle* mPFC, *right* tJM1. Mean PSTHs (0.02 s bin) for Hit trials sorted for different stimulus amplitudes and Spontaneous Licks, averaged across neurons with SI > 0 (*Top*) and neurons with SI < 0 (*Bottom*), according to the classification in figure 4.3B.

(F) Quantification of the firing rate during 0.2 s before the jaw onset (highlighted by *the grey area in E*). Mean delta firing rate (Hit – Spontaneous lick) across neurons (mean ± SEM values can be found in Table 4.7). Kruskal-Wallis test : wS1 SI>0, $P = 9.91 \times 10^{-75}$; wS1 SI<0, $P = 0.31$; mPFC SI>0, $P = 1.20 \times 10^{-31}$; mPFC SI<0, $P = 3.75 \times 10^{-6}$; tJM1 SI>0, $P = 1.86 \times 10^{-4}$; tJM1 SI<0, $P = 0.13$. See Table 4.8 for multiple comparison tests between amplitudes.

(G) Mean Pearson coefficient of correlation between delta firing rate and stimulus amplitude computed for positively (SI>0) and negatively (SI<0) modulated RSU and FSU neurons in each area. The difference between the mean Pearson coefficient was assessed using a Kruskal-Wallis test, followed by multiple comparison tests (P -values for all comparisons are displayed in Table 4.9).

Table 4.6. P values for Multiple Comparison Test between reaction times for different amplitudes (related to Figure 4.6A).

label 1	label 2	p-value
Amp °	Amp °	
0	1	0.09
0	1.8	2.16×10^{-6}
0	2.5	1.37×10^{-8}
0	3.3	2.80×10^{-10}
1	1.8	0.05
1	2.5	3.06×10^{-3}
1	3.3	2.82×10^{-4}
1.8	2.5	0.91
1.8	3.3	0.59
2.5	3.3	0.98

Table 4.7. Quantification of delta firing rate (related to Figure 4.6F).

neurons with SI>0						
(Hz)	Area	Stimulus amplitudes (degrees)				
		0 (SL)	1	1.8	2.5	3.3
wS1	mean	0.01	0.78	2.55	3.33	3.77
	± SEM	± 0.03	± 0.23	± 0.27	± 0.26	± 0.29
mPFC	mean	-0.01	0.41	0.77	1.40	1.69
	± SEM	± 0.02	± 0.18	± 0.12	± 0.15	± 0.17
tjM1	mean	-0.01	-0.17	0.09	0.34	0.60
	± SEM	± 0.04	± 0.24	± 0.20	± 0.25	± 0.27
neurons with SI<0						
(Hz)	Area	Stimulus amplitudes (degrees)				
		0 (SL)	1	1.8	2.5	3.3
wS1	mean	-0.02	0.07	0.03	-0.24	-0.19
	± SEM	± 0.02	± 0.20	± 0.17	± 0.14	± 0.14
mPFC	mean	-0.01	0.08	0.06	0.10	0.21
	± SEM	± 0.01	± 0.10	± 0.06	± 0.07	± 0.06
tjM1	mean	-0.01	-0.22	-0.41	-0.29	-0.12
	± SEM	± 0.02	± 0.17	± 0.12	± 0.12	± 0.12

Table 4.8. Multiple comparison Kruskal-Wallis test to identify significant differences between mean delta firing rates for different stimulus amplitudes (related to Figure 4.6F).

cells with SI>0											
Area	label 1 Amp°	label 2 Amp°	p-value	Area	label 1 Amp°	label 2 Amp°	p-value	Area	label 1 Amp°	label 2 Amp°	p-value
wS1	0	1	4.52×10^{-5}	mPFC	0	1	0.03	tjM1	0	1	0.20
wS1	0	1.8	0	mPFC	0	1.8	2.58×10^{-8}	tjM1	0	1.8	1.00
wS1	0	2.5	0	mPFC	0	2.5	9.01×10^{-19}	tjM1	0	2.5	0.89
wS1	0	3.3	0	mPFC	0	3.3	0	tjM1	0	3.3	0.11
wS1	1	1.8	9.36×10^{-10}	mPFC	1	1.8	0.02	tjM1	1	1.8	0.13
wS1	1	2.5	2.59×10^{-23}	mPFC	1	2.5	1.86×10^{-8}	tjM1	1	2.5	0.02
wS1	1	3.3	0	mPFC	1	3.3	5.92×10^{-14}	tjM1	1	3.3	0.00
wS1	1.8	2.5	6.06×10^{-3}	mPFC	1.8	2.5	0.02	tjM1	1.8	2.5	0.95
wS1	1.8	3.3	1.24×10^{-4}	mPFC	1.8	3.3	2.23×10^{-5}	tjM1	1.8	3.3	0.16
wS1	2.5	3.3	0.87	mPFC	2.5	3.3	0.41	tjM1	2.5	3.3	0.55
cells with SI<0											
Area	label 1 Amp°	label 2 Amp°	p-value	Area	label 1 Amp°	label 2 Amp°	p-value	Area	label 1 Amp°	label 2 Amp°	p-value
wS1	0	1	0.82	mPFC	0	1	0.98	tjM1	0	1	0.36
wS1	0	1.8	1.00	mPFC	0	1.8	0.16	tjM1	0	1.8	0.79
wS1	0	2.5	0.88	mPFC	0	2.5	0.04	tjM1	0	2.5	0.90
wS1	0	3.3	0.98	mPFC	0	3.3	0.00	tjM1	0	3.3	0.98
wS1	1	1.8	0.59	mPFC	1	1.8	0.04	tjM1	1	1.8	0.96
wS1	1	2.5	0.26	mPFC	1	2.5	0.01	tjM1	1	2.5	0.88
wS1	1	3.3	0.46	mPFC	1	3.3	0.00	tjM1	1	3.3	0.12
wS1	1.8	2.5	0.98	mPFC	1.8	2.5	0.98	tjM1	1.8	2.5	1.00
wS1	1.8	3.3	1.00	mPFC	1.8	3.3	0.35	tjM1	1.8	3.3	0.44
wS1	2.5	3.3	1.00	mPFC	2.5	3.3	0.72	tjM1	2.5	3.3	0.59

Table 4.9. *P*-values obtained from multiple comparison tests of the mean Pearson correlation coefficient different stimulus amplitudes (Fig.4.6 G).

			FSU						RSU				
			SI<0			SI>0			SI<0			SI>0	
			tjM1	mPF C	wS1	tjM1	mPF C	wS1	tjM1	mPFC	wS1	tjM1	mPF C
RS U	SI>0	wS1	6,34 $\times 10^{-5}$	0,11	0,99	0,99	0,97	5,91 $\times 10^{-5}$	3,34 $\times 10^{-12}$	3,90 $\times 10^{-12}$	6,71 $\times 10^{-6}$	1,70 $\times 10^{-8}$	0,02
		mPF C	0,05	0,89	1,00	1,00	0,03 $\times 10^{-12}$	2,51 $\times 10^{-12}$	9,16 $\times 10^{-4}$	5,15 $\times 10^{-3}$	0,22	0,08	
		tjM1	0,88	1,00	1,00	0,71	8,48 $\times 10^{-6}$	2,94 $\times 10^{-21}$	0,99	1,00	1,00		
	SI<0	wS1	0,94	1,00	1,00	0,72	5,11 $\times 10^{-5}$	3,50 $\times 10^{-16}$	1,00	1,00			
		mPF C	0,95	1,00	1,00	0,52	5,24 $\times 10^{-7}$	0	1,00				
		tjM1	1,00	1,00	1,00	0,28	8,82 $\times 10^{-8}$	0					
	FSU	SI>0	wS1	1,51 $\times 10^{-11}$	1,46 $\times 10^{-5}$	0,28	0,01	0,57					
			mPF C	2,91 $\times 10^{-5}$	0,03	0,90	0,80						
			tjM1	0,18	0,90	1,00							
SI<0		wS1	0,99	1,00									
		mPF C	1,00										

wS1 also showed the highest Hit vs Spontaneous Lick SI (positive SI before lick onset wS1 = 0.14 ± 0.01 ; mPFC = 0.075 ± 0.01 ; tjM1 = 0.065 ± 0.01 . wS1 vs mPFC, $P = 6.1.73 \times 10^{-6}$; wS1 vs tjM1, $P = 5.26 \times 10^{-7}$; mPFC vs tjM1, $P = 0.71$ Wilcoxon-Mann-Whitney rank sum test with Bonferroni correction) and the highest proportion of neurons with significant SI before jaw onset, whereas the mean SI and proportion of neurons with significant SI was rather low in both mPFC and tjM1 (proportion of cells with significant SI before lick onset, wS1 = 0.18; mPFC = 0.053; tjM1 = 0.058. wS1 vs mPFC, $P = 5.09 \times 10^{-14}$; wS1 vs tjM1, $P = 3.06 \times 10^{-10}$; mPFC vs tjM1, $P = 0.70$. Chi-square test) (Figure 4.7C-D). Plotting the SI for Hit vs Spontaneous lick trials ($SI_{Hit/SL}$) against the SI for Hit vs Miss trials ($SI_{Hit/Miss}$), we found that the majority of the neurons tended to have a positive SI for both, i.e. a higher response in Hit trials. We then selected the neurons with significant SI for both that we considered as sensory-guided decision neurons (Figure 4.7E). Decision neurons were more abundant in wS1 and in similar proportions in mPFC and tjM1 (Total proportion of decision neurons in wS1 = 0.18, mPFC = 0.058 and tjM1 = 0.073; tjM1 vs wS1 $P = 1.02 \times 10^{-7}$, tjM1 vs mPFC $P = 0.26$ and wS1 vs mPFC $P = 1.10 \times 10^{-12}$, Chi-square test). Interestingly, FSUs (presumably inhibitory interneurons) had a higher proportion of decision neurons in all

three areas (wS1 RSU vs FSU, $P = 6.46 \times 10^{-11}$; mPFC RSU vs FSU, $P = 5.12 \times 10^{-4}$; tjM1 RSU vs FSU, $P = 4.83 \times 10^{-5}$, Chi-square test) (Figure 4.7F). Finally, we computed the PSTHs aligned to the whisker stimulus and to the jaw onset for the sensory-guided decision neurons with positive SI in the three areas. Interestingly, decision neurons in wS1 had still a marked sensory-evoked response in Miss trials. Decision neurons in tjM1 had a pronounced motor response during spontaneous lick trials. But decision neurons in mPFC had only little sensory-evoked response in Miss trials and motor-related activity in Spontaneous lick trials, and thus appeared to have the highest contrast in their activity between Hit vs Miss trials and between Hit vs spontaneous lick trials (Figure 4.7G). We then verified which proportion of cells among sensory-guided decision neurons were still significantly encoding sensory information (neurons with significant SI for Miss vs Correct rejection trials during 200 ms after the stimulus onset), motor information (neurons with significant SI for Spontaneous licks vs Correct rejection trials during 200 ms before the jaw onset), sensory plus motor, or were selectively responding only in Hit trials (but not in Miss trials and not during Spontaneous licks), which we called “gated” neurons (Figure 4.8). As anticipated from the average responses of decision neurons, we observed that the majority of wS1 decision neurons still encoded sensory- and motor-related signals, the majority of tjM1 decision neurons still encoded motor-related signals, however, the majority of mPFC decision neurons were gated neurons. By comparing proportions of gated neurons between areas we observed a significantly higher proportion in mPFC (proportion of “gated” neurons among decision neurons, by considering RSU and FSU together: wS1 0.12; mPFC 0.37; tjM1 0.18; $p = 9.22 \times 10^{-4}$; Chi-squared test) (Figure 4.8A) After looking separately at RSU and FSU units we still observed a significantly higher proportion of gated neurons in mPFC among FSU but not RSU (RSU $p = 0.11$; FSU $p = 0.0011$; Chi-squared test) (Figure 4.8B-C). Overall, decision neurons were recorded from deeper layers 5 and 6 in all three regions (Figure 4.8D). In conclusion, decision-related information was found in all three areas but predominantly in wS1. But the activity of mPFC decision neurons appeared to be more selectively gated in Hit trials.

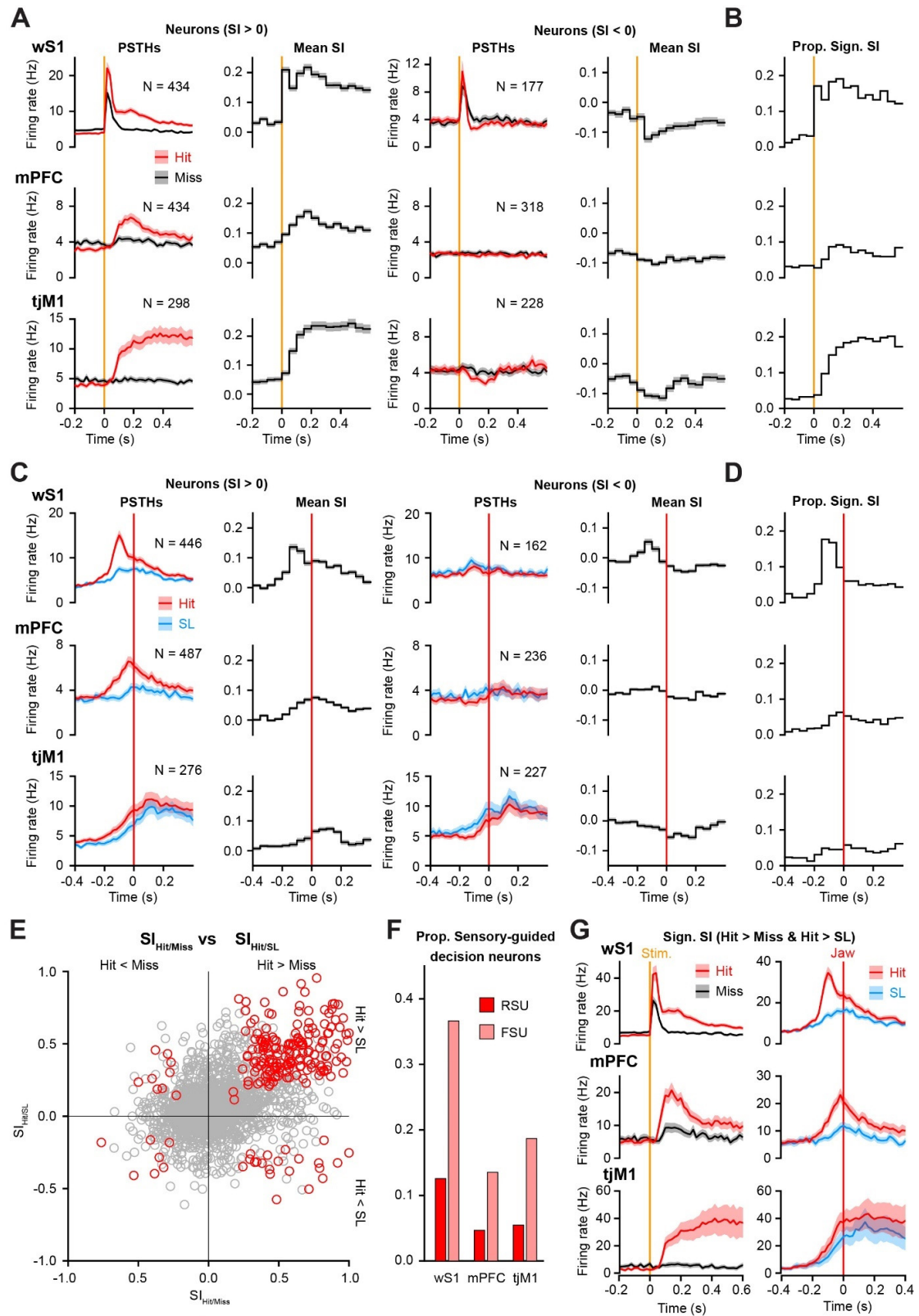


Figure 4.7. Decision-related information is encoded in all three regions.

(A) Comparison of Hit (*red*) and Miss (*black*) neuronal responses for the near-threshold stimulus amplitude aligned to the whisker stimulus (*orange vertical line*). All neurons were subdivided into neurons with $SI > 0$ (stronger response for Hit) and neurons with $SI < 0$ (stronger response for Miss) according to their maximum Selectivity Index (SI) right after the whisker stimulus (0-0.2 s) onset. SI was defined based on ROC analysis of Hit vs Miss trials for near-threshold amplitude. Sessions were truncated after the mouse missed 4 stimuli in a row for the strongest stimulus amplitude. *Left column*, grand-average PSTHs (0.02 s bin) for Hit (*red*) and Miss (*black*) trials. *Right column*, Mean SI Hit vs Miss (50 ms time bin).

(B) Proportion of neurons with significant selectivity for Hit versus Miss (for the near-threshold amplitude) based on the non-parametric permutation test from ROC computed for 50 ms time bins. *P*-values were FDR corrected for a total of 30 bins for each area.

(C) Same as (A) but for the comparison between of Hit trials for the strongest amplitude (3.3°) vs Spontaneous Licks, aligned to the jaw onset. SI was defined based on 0.2 s time window before the jaw onset. Neurons with $SI > 0$ respond stronger in Hit before the jaw onset, compared to Spontaneous lick. Neurons with $SI < 0$ respond stronger in Spontaneous licks compared to Hit.

(D) Same as (B) but for Hit (strong amplitude 3.3°) versus Spontaneous Lick.

(E) Distribution of Hit vs Miss SI against Hit vs SL SI for each recorded neuron. Neurons with both significant SIs are highlighted in red.

(F) Proportion of neurons with both significant SIs (sensory-guided decision neurons) recorded in each area normalized by the number of recorded neurons from each area and each cell type.

(G) Responses of neurons with both significant and positive SIs. *Left*, Grand-average PSTHs (0.02 s bin) for Hit and Miss trials (for the threshold stimulus amplitude) aligned to the stimulus. *Right*, Grand-average average PSTHs (0.02 s bin) for Hit (strong stimulus amplitude 3.3°) and spontaneous lick trials aligned to the jaw onset.

Table 4.10. Distribution of decision neurons across areas and layers (Fig.4.8 D).

wS1	neurons		mPFC	neurons		tjM1	neurons	
layers	number	proportion	layers	number	proportion	layers	number	proportion
SSp-bfd2/3	4	0.093	ACAv5	3	0.065	MOp2/3	4	0.089
SSp-bfd4	28	0.15	ILA1	1	0.071	MOp5	10	0.055
SSp-bfd5	55	0.2	ILA2/3	1	0.017	MOp6a	4	0.29
SSp-bfd6a	30	0.25	ILA5	6	0.051	MOs5	5	0.028
			ILA6a	1	0.031	MOs6a	17	0.22
			ORBm5	1	0.016			
			PL2/3	2	0.022			
			PL5	27	0.078			
			PL6a	3	0.16			

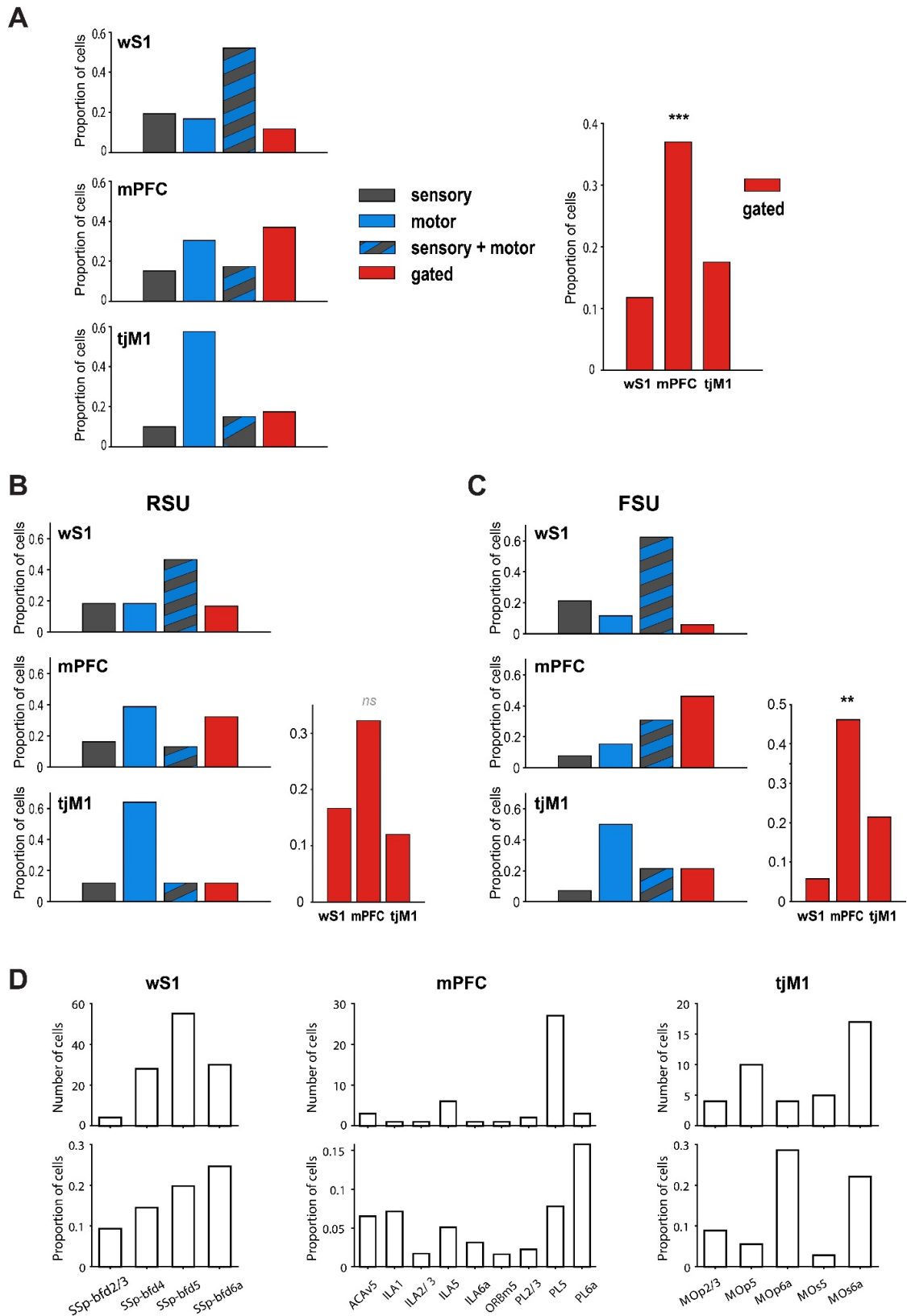


Figure 4.8. Decision “gated” neurons are mostly found in mPFC.

(A) Different types of decision neurons across areas (both RSU and FSU are included). Decision neurons (significant SI for both Hit vs Miss trials and Hit vs Spontaneous Licks) were further categorized as *sensory* (significant SI for Miss trials vs Correct rejection trials from 0 to 200 ms after the stimulus onset), *motor* (significant SI for Spontaneous lick vs Correct rejection trials from -200 to 0 ms aligned to the jaw onset, blue bars), *sensory + motor* (both *sensory* and *motor*) or *gated* (neurons selectively responsive in Hit trials, i.e. neither *sensory* nor *motor*; red bars). *Left panel*, proportion of decision neurons for each category across cortical areas: grey bars, *sensory* neurons (wS1 0.19; mPFC 0.15; tjM1 0.1); blue bars, *motor* neurons (wS1 0.17; mPFC 0.3; tjM1 0.57); bars with blue and grey strips, *sensory + motor* (wS1 0.52; mPFC 0.17; tjM1 0.15); red bars, *gated* (wS1 0.12; mPFC 0.37; tjM1 0.18). *Right panel*, comparison of proportions of gated neurons for three cortical regions (wS1 0.12; mPFC 0.37; tjM1 0.18; $p = 9.22 \times 10^{-4}$; Chi-squared test).

(B) Same as in A but only including RSU. Proportion of *sensory* neurons: wS1 0.18; mPFC 0.16; tjM1 0.12. Proportion of *motor* neurons: wS1 0.18; mPFC 0.39; tjM1 0.64. Proportion of *sensory + motor*: wS1 0.47; mPFC 0.13; tjM1 0.12. Proportion of *gated* neurons: wS1 0.17; mPFC 0.32; tjM1 0.12. Comparison of proportions of gated neurons across areas $p = 0.11$, Chi-squared test.

(C) Same as in A but only including FSU. Proportion of *sensory* neurons: wS1 0.21; mPFC 0.08; tjM1 0.07. Proportion of *motor* neurons: wS1 0.11; mPFC 0.15; tjM1 0.5. Proportion of *sensory + motor*: wS1 0.62; mPFC 0.31; tjM1 0.21. Proportion of *gated* neurons: wS1 0.058; mPFC 0.46; tjM1 0.21. Comparison of proportions of gated neurons across areas $p = 0.0011$, Chi-squared test.

(D) Distribution of decision neurons across recorded areas and layers. Upper row, number of decision neurons; lower row, proportion of decision neurons (number of decision neurons divided by the number of recorded neurons in each layer). Numbers and proportions are displayed in Table 4.10.

4.3.8 Multiple decision points in the sensorimotor transformation

Failure in the sensorimotor transformation (Miss) could probably come from different origins. The mouse may fail to perceive the sensory stimulus and therefore not respond, but the mice may also feel the stimulus but decide not to lick. Thus, the failure could occur at different stages of the process. Taking advantage of the session with simultaneous recordings of wS1 and mPFC, we selected trials based on the evoked population activity in wS1 in the first 50 ms, assuming that it would represent the sensory information reaching wS1 and broadcasted to downstream areas.

Due to the nature of our task, the sensory-evoked activity in wS1 was much higher for Hit than for Miss trials when considering all stimulus amplitudes, but the distributions of the evoked activity for Hit and Miss trials were broad and largely overlapping (Figure 4.9A). Thus, we could select Hit and Miss trials with similar evoked activity in wS1 (Figure 9A) and then compare the evoked activity for the same trials in mPFC (Figure 9B). Even when selecting trials with similar evoked population activity in wS1, mPFC population activity was still much higher for Hit trials, compared to Miss trials (Figure 9B-C). We then selected Miss trials with high evoked activity in wS1 and compared them with Hit trials with low evoked activity. Interestingly, even in this situation, mPFC activity was still higher for Hit trials compared to Miss trials. Suggesting that regardless of the sensory processing in wS1, mPFC keeps track of the final decision to lick or not to lick.

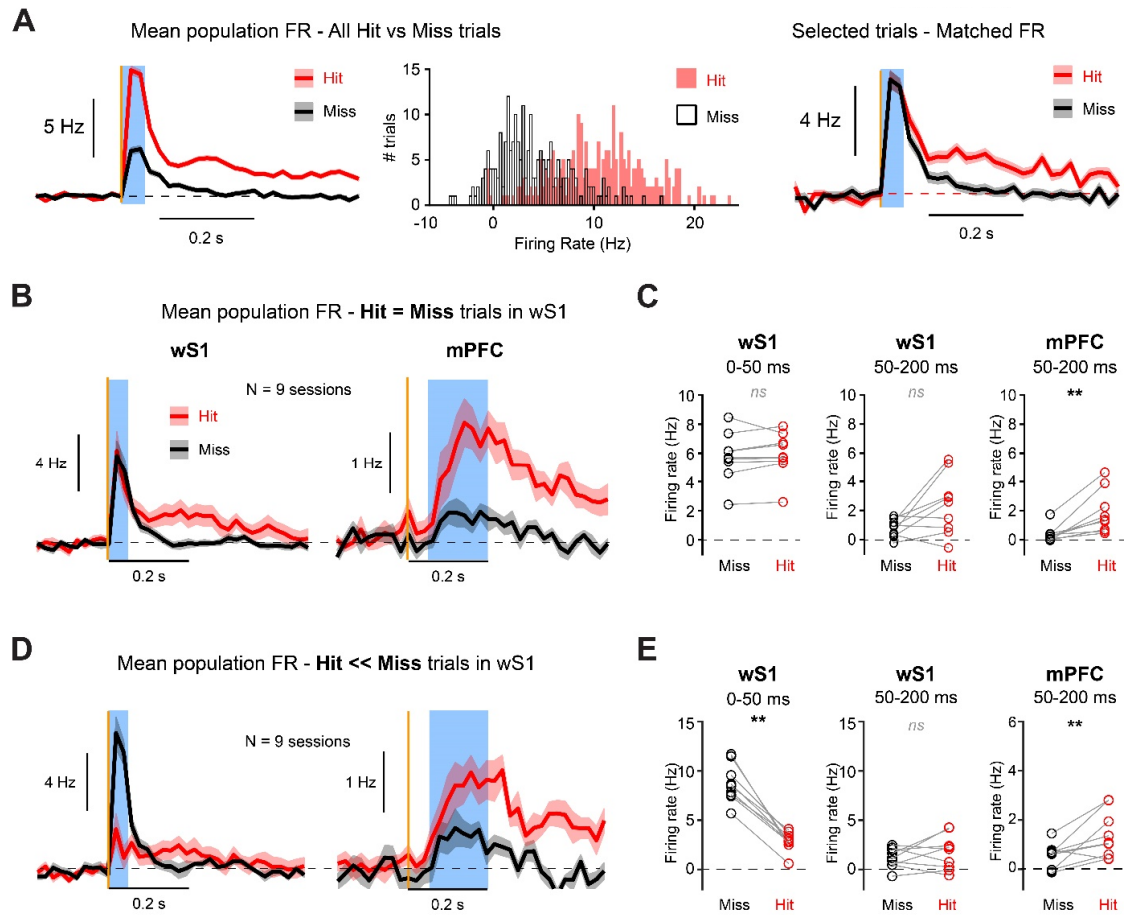


Figure 4.9. Multiple decision points in the sensorimotor transformation.

(A) Example wS1 recording from one session (Mouse AO051). *Left*, Population PSTHs (0.2 s time bin) for Hit and Miss trials (all stimulus amplitudes) aligned to the whisker stimulus. *Middle*, Distribution of neuronal population firing rates during early sensory evoked responses (0-50 ms, blue shaded area) across Hit (red filled bars) and Miss (black open bars) trials (Distribution binned with 0.25 Hz), note the overlap between the two distributions. *Right*, Mean PSTHs for selected trials with matched firing rates during the early 0-50 ms sensory-evoked response in wS1 (Matched-FR trials). Matched trials were selected based the wS1 population firing rate with overlap between Hit and Miss distributions.

(B) Grand-average PSTHs for selected Hit and Miss Matched-FR trials (averaged across 9 sessions with simultaneous recordings from wS1 and mPFC). *Left*, wS1 activity. *Right*, mPFC activity.

(C) Quantification of the mean delta firing rate across Matched-FR trials during the early time window (0-50 ms) for wS1 (*left panel*) (Hit vs Miss: wS1, $P = 0.82$; Wilcoxon signed-rank test) and the later time window (50-200 ms) for wS1 (*middle panel*) and for mPFC (*right panel*) (Hit vs Miss: wS1, $P = 0.074$; mPFC, $P = 3.90 \times 10^{-3}$; Wilcoxon signed-rank test). Circles and lines represent mean values for each session.

(D) Grand-average PSTHs for selected Miss trials with high firing rate, and Hit trials with low firing rate (averaged across 9 sessions with simultaneous recordings from wS1 and mPFC). *Left*, wS1 activity. *Right*, mPFC activity.

(E) Quantification of the mean delta firing rate during the early time window (0-50 ms) for wS1 (*left panel*) (Hit vs Miss: wS1, $P = 0.0039$; Wilcoxon signed-rank test) and the later time window (50-200 ms) for wS1 (*middle panel*) and mPFC (*right panel*) (Hit vs Miss: wS1, $P = 0.43$; mPFC, $P = 0.0078$; Wilcoxon signed-rank test) after selecting Miss trials with high firing rate and Hit trials with low firing rate. Circles and lines represent mean values for each session.

4.4 Discussion

Detecting sensory stimuli in the presence of temporal uncertainty is a challenging task for the brain. The brain must constantly process incoming sensory information and, based on that information, make decisions to execute an action, even when the sensory stimuli are ambiguous. Our study provides new insights into the intricate process of sensorimotor transformation during a sensory detection task in which mice are required to report by licking when a whisker sensory stimulus is delivered. We have employed a classical psychophysical approach – delivering sensory stimuli of variable amplitudes – and carefully monitored the mice's orofacial movements, to disentangle sensory, motor, and decision information. By systematically comparing the neuronal activity and computation of the cortical sensory input area (wS1), a presumably decision area (mPFC), and the motor output area (tjM1), we revealed four key findings that we will further discuss below: (1) we observed the most prominent sensory representation in wS1, which encoded the amplitude of the sensory stimuli even in the absence of licking in trained mice, and in the absence of goal-directed behavior in R-mice. However, we also observed marked Hit-Miss response difference in wS1, even at short latency (first 50 ms), that correlated on a trial-to-trial basis with the perceptual reports of the mouse; (2) licking evoked strong neuronal responses in all three cortical regions, however tjM1 neurons best encoded fine kinematics of the jaw phase; (3) we found decision-related activity in all three cortical areas, but with the highest proportion of neurons, and the shortest latency (within the first 50 ms), in wS1; (4) even though wS1 revealed strong choice encoding, it was not a final decision area: trials with the same sensory-evoked activity in wS1 could lead to opposite perceptual decisions (Hit or Miss), nonetheless, the activity in mPFC for those trials was still differential with the highest activity for Hit trials.

4.4.1 Early Hit Miss difference in wS1 contributes to the perception

In the detection tasks, the comparison between Hit and Miss trials is a valuable tool for studying sensory perception. It provides a way to quantify the subject's performance and analyze the underlying neural mechanisms. However, in simple Go-NoGo tasks, miss trials are often ambiguous as they can result from a failure in the sensorimotor transformation or from a disengagement due to loss of motivation. It is particularly the case when the sensory stimulus is strong, far above the perceptual threshold, in which case Miss trials tend to be mostly observed towards the end of the session, as the animal reaches satiation (Allen et al. 2019; Lee et al. 2020; Matteucci et al. 2022).

Previous studies using above-threshold whisker stimuli have reported Hit-Miss differences in the late (50-200 ms) sensory-evoked response in wS1, but little or no change in the early (0-50 ms) sensory-evoked response (Sachidhanandam et al. 2013; Yamashita and Petersen 2016; Kyriakatos et al. 2017; Le Merre et al. 2018; Vaviladeli et al. 2020; Esmaeili et al. 2021). This result was interpreted as a high reliability of the fast bottom-up sensory input transmitted to the cortex via the thalamus. In good agreement, only little and transitory decision information was found in thalamocortical neurons (Yang et al. 2016). Presumably, a strong whisker stimulus would reliably evoke a high number of spikes in wS1 neurons, therefore a failure to lick probably reflects a deficiency in the downstream sensorimotor process, likely resulting from attentional or motivational influences.

In our psychophysical task, the use of different stimulus intensities allowed us to investigate the correlates of sensory perception for near-threshold stimuli that led to Miss or Hit trials in similar proportion and throughout the sessions. Importantly, we also analyzed Hit-Miss differences for trials occurring before mice disengaged by excluding trials occurring after four consecutive misses for the strongest amplitude. By doing this, we found that even the early (< 50 ms) sensory-evoked response in wS1 correlated with the mice's behavioral response. About seventeen percent (17.05%) of neurons in wS1 had significant Hit-Miss selectivity in the first 50 ms bin (Figure 4.7B). This suggests that for weak sensory stimuli, an absence of behavioral response can already occur due to a failure in the early sensory processing in primary sensory areas. Interactions between the bottom-up sensory input and ongoing spontaneous cortical activity may result in variable sensory-evoked responses, and therefore behavioral responses, for near-threshold stimuli.

4.4.2 Widespread movement-related activity

Over the last decade, many studies have established that motor activity has a global impact on nearly all brain areas and that task-driven computations are embedded within a broader context of movement-related information (Poulet and Crochet 2018; Ayaz et al. 2019; Musall et al. 2019; Steinmetz et al. 2019; Stringer et al. 2019). Recent studies have demonstrated that both instructed and uninstructed movements were the best predictors of neural activity in many brain areas (Musall et al. 2019; Steinmetz et al. 2019; Esmaeili et al. 2021). In good agreement, we found that neuronal activity in wS1, mPFC, and tJM1 was strongly modulated by spontaneous licking, independently of the task (R+ and R- mice). Interestingly, the activity changed in all three areas before movement onset and it was possible to decode movement significantly from all three areas both before and after movement onset (Figure 4.5 and 4.18).

Clustering also revealed different patterns of neuronal modulation by movements, with some neuronal populations being strongly excited and others strongly inhibited during licking (Figure 4.2, and 4.14). The temporal dynamics were also different with some clusters modulated briefly around the onset of the movement (clusters 2, 3, or 4), others throughout (clusters 6, 7, or 15), and yet others late after the lick onset (clusters 13). We also identified clusters – 12 and 14 – that increased and decreased firing rates respectively, during whisking in the absence of licking. These clusters were also composed of neurons from all three cortical areas. Interestingly those two clusters did not respond much during licking. Similarly, many lick-related clusters did not respond much during whisking in the absence of licking, indicating that different movements are encoded by some specific pools of neurons, but not specific areas.

When investigating the encoding of fine movement kinematics, such as the jaw phase during licking or the whisker phase during whisking, we found more specific representations in dedicated areas (Figure 4.5D-F, and 4.19). Many neurons with jaw-phase modulation were found in both tjM1 and wS1, probably due to the fact that whisker movement and jaw movement are phase-correlated during licking. However, the proportion of neurons with significant jaw-phase modulation but no whisker-phase modulation was the highest in tjM1 (Figure 4.19) and the population activity of tjM1 was best at decoding jaw movements (Figure 4.5E and 4.18E). This finding is in agreement with other recent studies showing that tjM1 neurons encode both the direction and amplitude of tongue movements during licking (Mayrhofer et al. 2019; Xu et al. 2022).

Finally, when mice licked in response to the whisker stimulus, the activity of tjM1 was mostly modulated by the reaction time of the mouse. When aligning the neuronal activity to the jaw opening onset time, little difference was observed in the neuronal activity when comparing the different stimulus amplitudes or even spontaneous licking. Thus our results confirm that tjM1 seems to be involved mostly in the execution of licking.

4.4.3 Multiple decision points along the sensorimotor transformation

Hit-Miss differences are commonly used to characterize a subject's perceptual decision in detection tasks. However, in standard Go-NoGo tasks in which the subject is required to act in response to the Go stimulus and not to act in response to the No-Go stimulus, decision and motor responses are highly correlated, and thus difficult to disentangle. Therefore, to accurately assess decision coding, one must consider both the perceptual report of the mouse and carefully control for motor-related activity. Imposing a delay between the presentation of the stimulus and the behavioral response can help to distinguish decision- and motor-related information to some

extent but anticipatory movements during the delay period need to be taken into consideration (Esmaeili et al. 2021). To address this issue in our study, we proposed a more stringent definition of decision information coding, where a neuron region is considered as encoding decision if it can distinguish between Hit and Miss trials just after the stimulus presentation, as well as between Hit trials and spontaneous licking just before the movement initiation (sensory-guided decision). By doing so, we have identified a small proportion of decision neurons in all three areas, but with the highest proportion in wS1. Neurons encoding behavioral decision have been found in previous studies in wS1 (Sachidhanandam et al. 2013; Takahashi et al. 2016; Yang et al. 2016), as well as in the primary auditory cortex as mice performed an auditory discrimination task (Francis et al. 2022). In line with these findings, a recent study has identified decision neurons in wS1 as mice performed a two-alternative forced-choice texture discrimination task, and provided causal evidence of the role of these neurons in driving behavior and enhancing performance (Buetfering et al. 2022). Thus primary sensory areas in rodents seem to contain more decision-related information than previously reported in non-human primates (Romo and de Lafuente 2013).

However, one may also argue that perception and decision are intimately intricated in our task and that the decision information contained in wS1 neuronal activity may reflect the perception of the sensory stimulus rather than the decision to lick in response to this sensory stimulus. Importantly, in our analysis on the decision process, we have excluded the end of the sessions, when mice disengage due to satiation. In this situation, mice most likely licked every time they perceived the stimulus. Hence the sensory-guided decision information found in wS1 may reflect more the success or failure of the sensory perception (detection) rather than a decision to lick or not. In good agreement, the optogenetic inactivation of wS1 did increase significantly the threshold for detection, which was not the case for mPFC or tJM1 (Figure 4.1E).

When comparing the evoked activity for the same trials in wS1 and mPFC, we found that regardless of the sensory-evoked activity in wS1, the activity in mPFC was always higher for Hit trials compared to Miss trials. In particular, even when selecting Miss trials with higher sensory-evoked activity in wS1 compared to Hit trials, the activity in mPFC was still higher for Hit trials (Figure 4.9). This suggests that beyond the first decision based on the sensory detection in wS1, a latter decision point may still exist in mPFC, partly based on the sensory detection in wS1, but not only. In agreement, another study also reported two types of Miss trials in a texture discrimination task, based on whether or not the evoked activity in wS1 could categorize the two stimuli, suggesting that some Miss trials resulted from a lack of sensory discrimination whereas in other trials the activity in wS1 could identify correctly the stimulus, but nonetheless, the mice decided no to lick (Buetfering et al. 2022).

Finally, we also observed neurons reflecting choice information in the tjM1. However, the difference between stimulus-driven licks (Hits) and spontaneous licks before the movement initiation (jaw onset) was very small (Figure 4.7G) which arguably might reflect small differences in lick kinematic reflecting mice's confidence in licking after a whisker stimulus versus licking spontaneously.

Altogether, our study suggests that decision does not come from the activity of a single pool of neurons in a given area but rather results from the concerted activity of several pools of neurons distributed across brain areas. Interestingly, in our study we found that FSUs – presumably GABAergic inhibitory interneurons – had a much higher proportion of decision neurons, suggesting an important role played by local GABAergic interneurons in the local computation of decision. This is in line with several studies also pointing to an important role of GABAergic interneurons in the processes of a decision in sensorimotor transformation (Pinto and Dan 2015; Sachidhanandam et al. 2016; Esmaeili et al. 2022).

4.4.4 Role of mPFC in sensorimotor transformation

Previous investigations have reported evoked responses for behaviorally relevant sensory stimuli that developed during learning in mPFC (Pinto and Dan 2015; Otis et al. 2017; Le Merre et al. 2018; Peters et al. 2022). In good agreement, we found that neurons in mPFC had prominent evoked responses when mice responded to the whisker stimulus, but not in mice that were passively exposed to unrewarded whisker stimuli (R- mice) (Figure 4.16). We also found that mPFC is strongly driven by motor-related activity both before and after jaw movement onset time, in both whisker-rewarded and non-rewarded mice (Figure 4.5 and 4.18). Thus, the question remains whether the mPFC actually contains any sensory-related activity or mostly motor-related activity.

By analyzing no-lick trials (Miss) in R+ mice, we found that the response of mPFC neurons to the whisker stimulus was strongly reduced compared to Hit trials. Nonetheless, a sensory-evoked response persisted, which was not correlated with the amplitude of the sensory stimulus, but allowed to significantly decode the presence of the stimulus (Figure 4.4C). In addition, by aligning the neuronal activity to the jaw movement onset, a graded response that correlated with stimulus amplitude persisted before the movement onset in mPFC (Figure 4.6E-G). This graded response could represent an encoding of the stimulus amplitude or an increase in reward expectation for stronger stimuli (Lak et al. 2020).

In contrast to the expected role of mPFC in decision-making, the proportion of decision neurons was not higher in mPFC than in wS1 or tjM1 (Figure 4.7). However, mPFC decision neurons appeared to have the highest contrast between Hit and Miss

responses, and Hit and Spontaneous lick activity (Figure 4.7G). Furthermore, when comparing the evoked activity in wS1 and mPFC for the same Hit and Miss trials, we found that mPFC activity always tracked correctly the behavioral response, with higher activity for Hit trials, regardless of the activity in wS1 (Figure 4.9).

Thus, altogether our results show that mPFC activity encodes a mixture of task-related sensory, motor, and decision information, in good agreement with previous studies (Pinto and Dan 2015; Otis et al. 2017; Le Merre et al. 2018; Lak et al. 2020; Kim et al. 2021; Peters et al. 2022). However, the exact role of mPFC in sensorimotor transformation remains unclear. Inactivation of mPFC strongly impairs mice performance in sensory detection or discrimination tasks (Figure 4.1E) (Pinto and Dan 2015; Le Merre et al. 2018; Esmaili et al. 2021), but whether mPFC activity is really involved in decision-making on a trial-by-trial basis is not certain considering mPFC response latency. Alternatively, the role of mPFC could be to keep track of trial history, outcome, and context (Moorman and Aston-Jones 2015; Lak et al. 2020; Lui et al. 2021; Spellman et al. 2021) to instruct other brain areas about the appropriate behavioral response (Brockett et al. 2022). In our study, we focused our analysis on the neuronal activity immediately after the sensory stimulus or before movement, but we also observed some clusters with a high proportion in mPFC, that exhibit late and selective activity on Hit trials or Spontaneous lick trials. Such neurons could play an important role in encoding trial feedback that may be used for learning or updating behavior on a trial-by-trial basis.

4.5 Conclusion

By systematically comparing the neuronal activity and computation of the cortical sensory input area (wS1), a potential decision area (mPFC), and the motor output area (tjM1), we have uncovered that the representation of sensory information, decision-making, and motor action is not a discrete function of each individual brain region, but rather distributed and encoded across all three regions. We propose that the decision to lick after the whisker stimulus is a gradual process involving the flow of information from the primary somatosensory (wS1) to the primary motor (tjM1) cortex, and that failure in signal processing can occur at any level.

Author contributions

AO, CCHP and SC conceptualized the study; AO developed neural and behavioral experiment setups; AO obtained neural and behavioral data; AO obtained histological data; AO, CS and RA analyzed the data; VE, AM and WG advised clustering and decoding of neuronal data; AO, CCHP and SC wrote the manuscript; all authors discussed and edited the manuscript; and CCHP and SC provided overall supervision.

Declaration of interests

The authors declare no conflict of interest

4.6 Methods

4.6.1 Experimental model and subject details

All procedures were approved by Swiss Federal Veterinary Office (License number VD-1628) and were conducted in accordance with the Swiss guidelines for the use of research animals. For optogenetic inactivation, we used VGAT-ChR2 mice [B6.Cg-Tg(Slc32a1-COP4*H134R/EYFP)8Gfng/J, JAX: 014548] (Zhao et al. 2011b; Guo et al. 2014a). For electrophysiological recording, we used C57BL/6 wild-type mice, and VGAT-ChR2 mice. Adult male and female mice were at least 6 weeks old at the time of head-post implantation (see below). Mice were kept in a reverse light/dark cycle (light 7 p.m. to 7 a.m.), in ventilated cages at a temperature of $22 \pm 2^\circ\text{C}$ with food available ad libitum. Water was restricted to 1 ml a day during behavioral training with at least 2 days of free access to water in the cage every 2 weeks. All mice were weighed and inspected daily during behavioral training.

Experimental design

This study did not involve randomization or blinding. We did not estimate sample-size before carrying out the study.

4.6.2 Implantation of metal headpost

Mice were first implanted with a metal head-post under anesthesia using a mixture of ketamine and xylazine (ketamine: 125 mg/kg, xylazine: 10 mg/kg, i.p.). Carprofen was injected (100 μl at 0.5 mg/ml, i.p.) for analgesia before the start of surgery. Body temperature was kept at 37°C throughout the surgery with a heating pad. An ocular ointment (VITA-POS, Pharma Medica AG, Switzerland) was applied over the eyes to prevent them from drying. A mix of lidocaine and bupivacaine was injected below the scalp as a local analgesic before skin incision. A povidone-iodine solution (Betadine, Mundipharma Medical Company, Bermuda) was used for skin disinfection. To expose the skull, a part of the scalp was removed with surgical scissors. The periosteal tissue was removed with cotton buds and a scalpel blade. After disinfection with Betadine and rinsing with Ringer solution, the skull was dried well with cotton buds. A thin layer of super glue (Loctite super glue 401, Henkel, Germany) was then applied across the dorsal part of the skull and a custom-made head fixation implant was glued to the right hemisphere without a tilt and parallel to the midline. A second thin layer of the glue was applied homogeneously on the left hemisphere. After the glue had dried, the head implant was further secured with self-curing denture acrylic (Paladur, Kulzer, Germany; Ortho-Jet, LANG, USA). A chamber

was made by building a wall with denture acrylic along the edge of the bone covering the left hemisphere. Particular care was taken to ensure that the left hemisphere of the dorsal cortex was free of denture acrylic and only covered by super glue for optical access. This intact, transparent skull preparation was used to perform intrinsic optical signal imaging (IOS) experiments. Mice were returned to their home cages and ibuprofen (Algifor Dolo Junior, VERFORA SA, Switzerland) was added to the drinking water for three days after surgery.

4.6.3 Skull preparation and craniotomies

For electrophysiological recordings, up to 3 small craniotomies were made over the regions of interest using a dental drill under isoflurane anesthesia (2-3% in O₂). The craniotomies were protected using a silicon elastomer (Kwik-Cast, World Precision Instruments, Sarasota, FL, USA). Regions of interest were the whisker primary somatosensory cortex (wS1), the medial prefrontal cortex (mPFC), and the tongue-jaw primary motor cortex (tjM1), selected based on previous studies (Le Merre et al. 2018a; Mayrhofer et al. 2019b; Esmaeili et al. 2021a) and IOS imaging. IOS was performed under isoflurane anesthesia (1-1.5% with O₂) to map the C2-whisker representation in wS1. A piezoelectric actuator was used to vibrate the right C2 whisker. An increase in absorption of red light (625 nm) upon sensory stimulation indicated the functional location of the corresponding sensory cortex. For the other regions, stereotaxic coordinates relative to bregma were used: tjM1: AP 2.0 mm; Lat 2.0 mm; mPFC: AP 2 mm; Lat 0.5 mm. For optogenetic inactivation experiments, the bone over the regions of interest was thinned and a thin layer of superglue was applied to protect the skull for stable optical access over days. For the inactivation of mPFC, a small craniotomy was made for the insertion of an optical fiber.

4.6.4 Behavioral paradigm

Head-restrained, water-restricted mice were trained in either of two different behavioral tasks. Whisker-rewarded (R+) mice were trained in a psychometric version of a whisker-detection task to lick for water reward in response to a brief single-whisker deflection of variable amplitude. Whisker-non-rewarded mice (R-) were trained to lick for the reward at random times while being exposed to the same range of whisker stimuli that were not predictive of the reward delivery.

The task structure closely resembles the previously used simple whisker detection task (Sachidhanandam et al. 2013; Yamashita and Petersen 2016; Le Merre et al. 2018) but with varying strengths of the whisker stimulation. The new trial started

without any preceding cues following a variable 6-12 s inter-trial interval that included a variable 2.5-3.5 s no-lick period, during which mice were required not to lick to initiate a trial. Stimulus trials and No Stimulus trials (catch trials) were presented with equal probabilities. Stimulus trials included four whisker stimulus amplitudes 1, 1.8, 2.5, and 3.3 degrees of the C2 whisker deflection also with equal probabilities. All trial types were presented in a pseudo-randomized manner. Mice were required to lick the water spout within a 1-s response window following the whisker stimulus in order to receive a drop of sweet water (sucrose concentration 0.02 gr/ml) as a reward. Contacts of the tongue with the water spout were detected online by a piezo-electric sensor. Trials when the mouse licked the water spout within the 1 s response window after a whisker stimulus, were considered as Hit trials, and were rewarded with a drop (4 μ l) of sweet water; if the mouse did not lick within the response window after a whisker stimulus, no reward was delivered, and the trial was classified as Miss trial; if mice licked within the response window when no whisker stimulation was delivered (catch trials), the trial was classified as False alarm; if no licking occurred during catch trials, they were considered as Correct rejection.

Mice were trained daily with one training session a day and a break of 2 days with free access to water every 2 weeks. Training of naive animals started with two days of free-licking and handling, within which mice were gradually accustomed to the experimenter, head-fixation, and the association of licking the reward spout with occasional water delivery. Following the training, on the second day, all whiskers apart from C2 were trimmed. On the third day, mice began training in the whisker detection task: at the beginning of the session, animals were presented with a few associative trials during which mice received automatic water rewards paired with the whisker stimulation of a strong whisker stimulation amplitude (3.3 deg) to build an association between the whisker deflection and the reward; after a few associative trials, mice rapidly learned the task and licked in response to the whisker stimulus. The next training sessions aimed to improve the performance of the mice by increasing the ratio between hit and false-alarm rate. The proportion of Stimulus trials and Catch trials was progressively increased with training days from 70% Stimulus / 30% Catch trials at the beginning of training to 50% / 50% at the end. The inter-trial interval was progressively increased with training days from 5-6 seconds to 6-12 seconds for final experiments, making the mouse calmer (decrease of spontaneous licking). During the first few training days (3-5), the strength of the magnetic pulse was kept close to the maximum (3.3 deg of whisker deflection) that could be easily detected by the mouse. When the mouse displayed a good level of performance (hit rate > 70%; false-alarm rate < 30%) the strength of the stimulation was gradually decreased to 2.5 deg, making the whisker stimulus more difficult to detect. During these sessions, to facilitate the mice's performance, a short block of 10-40 trials with the highest whisker stimulus amplitude was always presented at the beginning. When the performance became stable with a

false alarm rate below 30 % and hit rate above 70 % with the 2.5 deg stimulus amplitude, the mouse was considered as well trained, and psychophysical experiments were introduced.

In this study, the stimulus strengths used were carefully calibrated to span a large range of detection probability. After learning of the detection task, mice were tested with the psychophysical paradigm deflecting their C2 whiskers at 4 different amplitudes (1, 1.8, 2.5, 3.3 deg) and no stimulus during catch trials. For recording sessions, four whisker stimulation trials with different amplitudes were presented with equal probability. Each recording session started with a few (5-10) strong whisker stimulations (3.3 deg) followed by all trial types. These few starting trials were not included in the analysis and were used to reduce the effect of over-motivation at the beginning of the session when animals are water deprived.

All stimuli for the psychophysical detection task were specifically designed to be very precise in duration, shape, and magnitude. In our detection task, the stimulus is a brief magnetic pulse that is generated by a custom-made magnetic coil that is controlled by the behavioral algorithm through a high-power amplifier. Magnetic pulses of around 1 ms duration and varying in amplitude were achieved by applying biphasic voltage pulses (0.5 ms positive and 0.5 ms negative step) with different amplitudes to the coil. To measure whisker deflection elicited by the stimulations of different amplitudes a naive mouse was deeply anesthetized with pentobarbital and implanted with the head post. All whiskers apart from the C2 whisker were trimmed. The mouse was placed on the behavioral setup. The metal particle was positioned 1 mm from the base of the mouse whisker and a small (2 mm in diameter) round piece of paper was placed on top. Then high-precision infrared displacement sensor was positioned just 1 mm above the white piece of paper that was used as a reflector. All whisker stimulation amplitudes were applied in an interleaved manner and the whisker displacements were recorded.

Whisker-non-rewarded mice (R-) were trained to lick for a reward at random times while being exposed to the same range of whisker stimuli that were not predictive of the reward delivery. Whisker-non-rewarded group of mice was exposed to the whisker stimulation for a similar number of days as the whisker-rewarded group of mice. Similarly, during the first week of training, R- mice were only presented with the strong whisker stimulation and after for a few days with an amplitude of 2.5 deg, and after were introduced to the four different amplitudes of the whisker stimulation. The trial structure was kept with the maximum similarity to R+ mice. The new trial started after 8-12 seconds of intertrial interval plus 2.5-3.5 seconds of the no-lick window, followed by 2 s of response window. If by chance the mouse licked within the response window it received a reward with a 70% probability. Whisker stimulation was completely independent of the trial structure and could occur at any time and the probability was calculated to match the probability of stimuli appearing in R+ mice. For later analysis

of Miss trials only whisker stimulation with 2.5 s no-lick quiet window baseline and no lick 1 s after the stimulation were considered. As spontaneous licks only non-rewarded licks with 2.5 s no lick and no stimulus baseline, and no stimulus 1 s after the lick were considered.

4.6.5 Electrophysiological recordings

Acute recordings were performed on both groups of mice once they passed the training criteria (more than 70% Hit rate for the strong whisker stimulus amplitude and less than 30 % False alarm; for three consecutive days of the psychophysical version of the detection task). One or two recording sessions were done for each mouse over two consecutive days. Extracellular spikes were recorded using single-shank silicon probes (A1x32-Poly2-10mm-50 s-177, NeuroNexus, MI, USA) with 32 recording sites covering 775 μm of the cortical depth. In each session, two probes were inserted in two different brain targets acutely. Before insertion probes were coated with DiI (1,1'-Diocetyl-3,3,3',3'-Tetramethylindocarbocyanine Perchlorate, Invitrogen, USA) for post-hoc recovery of the recording location (see below). The neural data were filtered between 0.3 Hz and 7.5 kHz and amplified using a digital headstage (CerePlex™ M32, Blackrock Microsystems, UT, USA). The headstage digitized the data with a sampling frequency of 30 kHz. The digitized signal was transferred to our data acquisition system (CerePlex™ Direct, Blackrock Microsystems, UT, USA) and stored on an internal HDD of the host PC for offline analysis. One or two silicon probes were connected to an external reference silver wire that was placed to the recording chamber filled with the Ringer. During recording, the CerePlexDirect (from BlackRockMicrosystems) software was used to monitor probe insertion and the quality of the recordings. After probes were inserted, mice were left for 30 min for the probes and brain to stabilize after which the behavioral session and recording were started.

4.6.6 Optogenetic manipulations

To achieve an inhibition of a given brain region we activated GABA-ergic interneurons expressing ChR2 that in turn inhibited pyramidal cells (Guo et al. 2014). Optogenetic stimulation of three superficial cortical areas wS1, tjM1, and fpS1 was achieved through transparent skull preparation, plus skull thinning above the area of interest to facilitate the penetration of the light into the cortex. Blue light pulses were delivered through a 200 μm optic fiber (0.22NA, M84L01, Thorlabs, USA) positioned right above the area of interest. During the experiments, the rest of the exposed skull was covered with Kwik-cast to avoid inhibition of other cortical areas. For mPFC inhibition, a cannula (CFMXA05, Thorlabs USA) of 200 μm was implanted with the tip

inserted to around 1500 μm depth below the pia ($n=9$ mice), or acutely lowered to a similar depth above mPFC ($n=3$ mice). The optic fiber was coupled to a 470 nm high-power LED (M470F3, Thorlabs, USA). C2 barrel column of wS1 and fpS1 were localized using the IOS stimulating C2 whisker or the paw of the mouse respectively. tjM1 and mPFC were targeted using stereotactic coordinates: tjM1, AP X mm, Lateral X mm; mPFC, AP X mm, Lateral X mm, depth X μm from pia with Xdeg lateral angle from the vertical.

Optogenetic inactivations were performed in 13 Expert VGAT-ChR2 mice inhibiting one area of interest per session. The order for the areas was randomized across mice. Testing sessions started when mice reached Expert levels of performance ($d\text{-prime} > 1$ for the strongest whisker stimulus amplitude). An ambient blue masking light was used in the training sessions as well as on testing days. Light trials were randomly interleaved with light-off control trials and made up 30 % of the Go and No-Go trials. On light trials, a 100 Hz train of blue light pulses (50% duty cycle, mean power 5 mW) was applied 100 ms before and 900 ms after trial onset, terminated by an additional 100 ms ramping down to prevent rebound excitation.

4.6.7 Histology and localization of electrode/optical fiber tracks

At the end of the experiments, mice were perfused with phosphate-buffered saline (PBS) followed by 4% paraformaldehyde (PFA, Electron Microscopy Science, USA) in PBS. Brains were post-fixed overnight at room temperature. Fluorescent Dil tracks were imaged with a fluorescence microscope (Leica DM5500) in serial 100- μm coronal sections cut with a vibratome (VT 1000S; Leica, Wetzlar, Germany). Matlab-based software (Allen CCF tools, <https://github.com/cortex-lab/allenCCF>) was used to register brain slices and probe locations to Allen mouse brain atlas (Shamash et al. 2018).

4.6.8 Behavioral data analysis

All analysis was performed using custom-written codes in Matlab. To quantify the performance of the animals during the psychophysical detection task we computed the Hit rate (number of Hit trials/number of Stimulus trials) for each stimulus amplitude and the False-Alarm (FA) rate (number of FA/number of Catch trials). To construct psychometric curves we fitted detection performance across stimulus intensities with a sigmoidal function by using the “fit” function in Matlab.

Fitting model: $f(x) = ((\alpha - \beta) / (1 + (x/\gamma)^\lambda)) + \beta$

Where x is stimulus intensity, $f(x)$ is the detection probability, α and β define the lapse rate of the curve, γ defines the middle point and λ the slope of the curve. α , β , γ , λ are free parameters that were fitted using a maximum likelihood method. The detection threshold was defined as the middle point of the psychometric curve and the sensitivity was defined as the slope (λ) of the curve. For the construction of individual session psychometric functions, the analysis of optogenetic inactivation, the analysis of Hit trials, and the comparison of Hit vs Miss trials we only selected the trials before mice disengaged from the task by cutting the end of each behavioral session if the mouse missed 4 strongest whisker stimuli in a row. For analysis of the purely sensory-evoked activity in no-lick trials (Miss), all trials were considered to increase the number of trials for all stimulus amplitude. We also defined Spontaneous licks as all non-rewarded licks with at least 2.5 s of no-lick baseline. Spontaneous licks that occurred within the response window of catch trials were considered as False alarms. For the analysis of motor activity, all spontaneous licks (including False alarms) were included.

4.6.9 Quantification of orofacial movements

We monitored the orofacial movements of mice during each behavioral session using a high-speed camera (CL 600 X 2/M, Optronics, Germany; 200 or 500 Hz frame rate, 0.5- or 1 ms exposure, and 512x512-pixel resolution). Continuous movements of the left C2 whisker, tongue, and jaw were filmed under blue and infrared light illumination. A high-speed camera was positioned above the mouse and focused on the C2 whisker. We also used the side mirror to capture the motion of the tongue and the jaw. To extract the position of each body part in time we used the Python-based toolbox DeepLabCut 2.2b7 (DLC), a software that uses deep learning networks for markerless pose estimation (Mathis et al. 2018). To train the network and to improve its ability to generalize, we first created a joint video that consisted of a sample of random frames of Hit trials from all recorded sessions. We trained the network on around 200 labeled frames using the k-means automatic extraction algorithm for the maximum number of iterations (1030000 iterations). Afterward, we used the trained network to extract the position of several body parts (the C2 whisker base and middle points, the tongue, the jaw, and the nose tips) for all the video filming data, for all the sessions and mice. For most sessions, we observed high-quality performance of the network, but for a small subset of sessions, we further improved it by refining the labels of 20 outlier frames and retraining the network. We filtered out all body part position estimations below the 60% likelihood. Using the X and Y extracted coordinates for each body part we then performed the following calculations:

We calculated the whisker angle as:

$$\theta(t) = \arctan\left(\frac{m(t)_{\text{whisker}} - m_{\text{midline}}}{1 + m(t)_{\text{whisker}} \cdot m_{\text{midline}}}\right)$$

$$\text{where } m_{\text{whisker}}(t) = \frac{y(t)_{wh_2} - y(t)_{wh_1}}{x(t)_{wh_2} - x(t)_{wh_1}} \quad \text{and} \quad m_{\text{midline}} = \frac{y_{ml_2} - y_{ml_1}}{x_{ml_2} - x_{ml_1}}$$

With (x_{wh_1}, y_{wh_1}) as the coordinates of the whisker base and (x_{wh_2}, y_{wh_2}) as the coordinates of the whisker midpoint that were estimated by DLC for each point in time; (x_{ml_1}, y_{ml_1}) and (x_{ml_2}, y_{ml_2}) are coordinates of the mouse face midline.

We calculated jaw and tongue displacement as:

$$d(t) = \sqrt{(x(t)_2 - x_1)^2 + (y(t)_2 - y_1)^2}$$

For the jaw with (x_2, y_2) as coordinates of the jaw tip for each point in time and (x_1, y_1) coordinates of the resting (closed) position of the jaw.

For the tongue with (x_2, y_2) as coordinates of the tongue tip for each point in time and (x_1, y_1) coordinates of the resting (closed) position of the jaw. The jaw and tongue traces were then mean-filtered (10 ms) and multiplied by pixel size to get a real displacement in mm.

From whisker traces, we identified epochs of *Free whisking* defined as periods with whisker angular velocity $= \dot{\theta} = \frac{d\theta}{dt}$ higher than 200 deg.s for at least 300 ms. For our analyses, we then selected Free whisking epochs that were preceded by at least 500 ms of no-whisking baseline and no jaw movements.

From the jaw displacement traces we defined the onset of licking for each licking episode by (1) finding the peaks higher than the threshold (mean + SD of the concatenated over trials jaw vector for each session) and prominence higher than 1/3 of the threshold; (2) identifying a first peak of the licking episode; (3) moving backward till reaching 1/7 of the threshold.

4.6.10 Electrophysiology data

Acquired electrophysiological data were first preprocessed, after clustered with Kilosort2, an open-source spike sorting software suited for dense multielectrode recordings (Stringer et al. 2019; Pachitariu et al. 2023) (<https://github.com/MouseLand/Kilosort/releases/tag/v2.0>), following the automatic clustering we manually refined all clusters. We first removed the artifact caused by the magnetic coil (used for the whisker stimulation) by substituting 3 ms of the signal after the coil onsets with the line from each channel separately. Common average

referencing, temporal filtering, channel whitening, and drift correction steps were automatically performed by Kilosort2, afterwards spiking activity on each probe was detected and sorted into different clusters. (Pachitariu et al. 2023). After an automated clustering step, clusters were manually inspected and refined using Phy Template GUI (<https://phy.readthedocs.io/>) following the guidelines (https://phy.readthedocs.io/en/latest/sorting_user_guide/) (by S. Lenzi and N. Steinmetz). Only clusters classified as “good units” were selected. For the final analyses, to assess the quality of spike sorting results and to reduce the bias of an experimenter, we selected only “well-isolated” units based on the sorting quality matrix (Schmitzer-Torbert et al. 2005; Hill, Mehta, and Kleinfeld 2011, <https://github.com/cortex-lab/sortingQuality>). For each unit we quantified “ISI Violation rate”, as an estimated false positive rate of the spikes that could come from another neuron, based on the rate of refractory period violations (Hill et al. 2011); “Isolation Distance” estimates how distant are the spikes of the cluster x from the other spikes recorded on the same electrode (Harris et al. 2001; Schmitzer-Torbert et al. 2005).

We then categorized all single units as regular spiking (RSU) or fast-spiking neurons based on the duration of the spike waveform as described in Chapter 3.5 (Esmaeili et al. 2022).

4.6.11 Receiver Operating Characteristic (ROC) analysis

First to account for the shift in the distributions of the whisker stimulus amplitudes we subselected equal numbers of Hit and Miss trials for each stimulus amplitude individually by downsampling to the minimal number of conditions. For example, if for the strong whisker stimulus we have 80 Hit trials and 20 Miss trials, we would consider all Misses and randomly subselect 20 Hits. We excluded the smallest whisker stimulus from this analysis as we observed minimum or no sensory-evoked response.

To quantify the selectivity of neuronal firing rate for stimulus we built ROC curves comparing the distribution of firing rate in bins of 50 ms for Miss and Correct-rejection trials. We subtracted the baseline from every single trial, computed as the mean firing rate during 500 ms before the trial onset when the mouse was quiet. The selectivity index (SI) was defined by scaling and shifting the area under the ROC curve (AUC) between -1 and 1:

$$\text{Selectivity index} = 2 \times (\text{AUC} - 0.5),$$

Where positive selectivity reflects higher activity in Miss than Correct-rejection trials and vice versa. We then split all recorded neurons into positively or negatively modulated according to their maximum absolute SI in the first 4 bins (from 0 to 200 ms after the Stimulus/NoStimulus onset). To examine the significance of selectivity, the

area under the ROC curve (AUC) was then compared to a shuffled distribution (AUC shuffled), obtained by shuffling the tags of the trial types 100 times and performing non-parametric permutation tests. P-values were corrected by False discovery rate (FDR) correction to account for all bins tested. We then calculated the proportion of neurons with significant SI for each bin.

By performing similar calculations, we also quantified Hit versus Correct-rejection selectivity aligned to the trial onset (Fig 4.3).

For Hit versus Spontaneous Licks aligned to the jaw onset we selected only Hits for the strong whisker stimulus; and to assess selectivity between Hit versus Miss trials we selected only the near-threshold amplitude to eliminate possible confounds of stimulus amplitude. The near-threshold amplitude was then defined for each session based on mouse performance as the magnitude of the whisker stimulation that was the closest to the detection threshold of the psychometric function obtained by fitting lick probability as described before.

Similarly, to quantify the selectivity of single units during spontaneous licks we built ROC curves comparing the distribution of spiking activity in bins of 50 ms around lick onsets to a baseline distribution (10 bins of 50 ms before trial onset). The area under the ROC curve was then compared to examine the lick selectivity beyond baseline fluctuations.

4.6.12 Clustering neuronal responses

For clustering the neuronal response patterns recorded in the mice performing the whisker detection task (R+ mice), all 2001 neurons were included in the analysis. We considered five trial types: Miss trials aligned to the stimulus onset, Hit trials aligned to the stimulus onset, Hit trials aligned to jaw movement onset, Spontaneous Licks aligned to jaw movement onset, free whisking aligned to the onset of whisker movement (without jaw movement). To account for the shift in the Hit and Miss distributions of the whisker stimulus amplitudes we subselected equal numbers of Hit and Miss trials for each stimulus amplitude individually by downsampling to the minimal number of conditions. We excluded the smallest whisker stimulus from this analysis as we observed minimum or no sensory-evoked response.

We then for each neuron computed mean time-varying PSTHs with the 100 ms bin size for each of the trial types. We considered 2.5 s duration of each trial type with 1 s baseline and 1.5 s response for both stimulus and lick alignment. For each of the trial types we subtracted its baseline (mean response from -0.5 s to 0 s for stimulus-aligned trials, and from -1 s to -0.5 s for jaw and whisker onset alignments). We then concatenated PSTHs for all five trial types for each neuron resulting in a vector of 125

firing rate values and normalized to the range of values across these 125 bins. We then concatenated the PSTH vectors for all neurons resulting in an activity matrix $X \in \mathbb{R}^{2001 \times 125}$ where each row i corresponds to the concatenated normalized firing rate of the neuron i across different trial types. Principal Component Analysis (PCA) and spectral embedding were used to reduce redundancy and detect non-convex clusters, respectively as described in Chapter 2.5 (Esmaeili et al. 2021). Neurons were then clustered using a Gaussian Mixture Model (GMM). The number of clusters was selected based on the minimum Bayesian information criterion (BIC) (Engelhard et al. 2019) (Figure S3). Clusters were then manually sorted for visualization purposes.

4.6.13 Decoding of behavioral variables

For decoding behavioral signals and the subject's performance from the neuronal spiking activity we pulled together RSUs and FSUs. Decoding was always performed on the single session-level. Depending on the nature of the signal that we decoded we used: (1) logistic regression for binary signal classification, e.g. Miss vs Correct rejection (CR), CR vs False Alarm (FA) trials, Hit vs FA, Hit vs CR to predict whisker stimulus onset, and jaw onset; (2). linear Regression for continuous signal regression, e.g. jaw displacement trace; (3). multinomial logistic regression for the stimulus amplitude classification, e.g. during Miss trials. Our decoders can be differentiated into trial-based, and continuous-based decoders. In trial-based decoders, we split the spiking activity in non-overlapping windows of 0.1 s and we use as input the firing rate of each neuron for this time period for signal prediction. Input data was always normalized to have an equal number of testing conditions (stimulus equalized or lick equalized). For example, for the prediction of the whisker stimulus, we selected the same number of Miss vs CR trials. For the prediction of whisker stimulus onset and jaw onset from Hit and Miss trials stimulus amplitudes 1.8, 2.5, and 3.3 were pulled together. For trial-based prediction of the stimulus amplitudes, an equal number of trials for each amplitude was selected. Trials equalization was always achieved by downsampling. For continuous-based decoding, we use either causal 5ms kernels that extend for 50 ms for every neuron. Based on the activity of these 50ms we predict the behavioral signal at each timestep. For the continuous prediction of the jaw trace, we used as an input licking episodes when the mouse was collecting the reward.

We estimated the accuracy or the explained variance using 5-fold stratified cross-validation in order to ensure that our labels/conditions have the same data distribution in the training and test set. In order to avoid overfitting we used L2-regularization where the strength of the regularization was determined with a small grid search with nested cross-validation. To estimate the significance of the decoding results, we compared our results with the average measure of 20 label-shuffled splits with the Wilcoxon

signed-rank test. Finally, to correct for the multiple tests we used False Discover Rate (FDR) correction. Every session-area pair that had less than 8 neurons or had less than 10 trials per label/condition was not used in our algorithm.

4.6.14 Pearson correlations

To assess the linear correlation between neuronal responses and amplitudes of the whisker stimulations, we computed the trial-by-trial Pearson coefficient of correlation for each neuron. For Miss trials, we considered mean responses over the first 0.1s after the whisker stimulus. For Hit trials, we considered a 0.2 s time window after the whisker stimulus and a 0.2 s time window before the jaw onset. The number of trials for each amplitude (0, 1, 1.8, 2.5, 3.3) was adjusted as a mean number of trials among amplitudes 1, 1.8, 2.5, 3.3. To identify significantly modulated units we performed a t-test ($p < 0.05$). To obtain mean correlation plots we separately averaged the coefficients of correlation for positive ($SI > 0$) and negative ($SI < 0$) RSUs and FSUs.

4.6.15 Phase-modulation analysis

For phase-modulation analyses of the jaw trace, we selected licking episodes when mice were collecting the reward. We excluded the first 200 ms from each lick sequence and ensured that there were no stimuli before for 500 ms to avoid extra sensory or decision information. The lick sequences were then smoothed using a Gaussian filter with a 20 ms size and downsampled to 200 Hz for R+ mice to match R-video filming frequency. All sequences from one session were concatenated into one vector and the mean was subtracted from each data point. This jaw vector was transformed to a complex-value analytic signal using the Hilbert transform. The neuronal firing rate and spike count of corresponding time were calculated for 5 ms bins to match the jaw phase vector. We binned the full phase (0-360°) to 100 bins which accounted for the 3.6° range. A phase of 0° corresponds to the trough of the oscillation and a phase of 180° to the peak of the oscillation. For each neuron, we quantified the mean resultant vector of the phase preference \bar{r} as

$$\bar{r} = \frac{1}{N} \sum_i \begin{pmatrix} \cos a_i \\ \sin a_i \end{pmatrix} \quad \text{where } N \text{ is the sample size and } a \text{ is a phase}$$

And then its resultant vector length as $R = \|\bar{r}\|$

We tested whether a data sample (neuronal spike count) was distributed uniformly around the circle (jaw phase) or had a common mean direction using

Rayleigh test, which tested for non-uniformity of circular data against the von Mises distribution. P value was calculated as the following

$$p = \exp \left[\sqrt{1 + 4N + 4(N^2 - (R \cdot N)^2)} - (1 + 2N) \right]$$

where N is the sample size and R is the resultant vector length.

Circular statistics were performed using the CircStat toolbox for Matlab (Berens 2009). Values in the text and figures are reported as circular mean \pm circular SD.

Whisker phase-modulation analysis was performed in the same way as for the jaw. We selected all episodes of the free whisking and put a very strict threshold on the jaw movements. The idea was to select only whisking moments when the mouse is not licking. was but by taking into account concatenated

In the end, we quantified the proportion of units with significant phase correlation for the jaw and the whisker movements for each area.

4.6.16 Analysis of paired recordings

We analyzed 9 sessions (9 mice) with simultaneous recording in wS1 and mPFC. We first for each trial substracted its baseline, computed by averaging firing rates during 0.5 s before the stimulus onset of this trial. For this analysis, all stimulus amplitudes were pulled together. To select wS1-FR matching trials we (1) computed mean response during the first 50 ms period after the stimulus onset in wS1 for Hit and Miss trials, (2) plotted the distribution of Hit and Miss trials with a size of the bin 0.2 Hz, and (3) subselected randomly an equal number of Hits and Misses (by downsampling) that had firing rate within the distributions overlap. A subselection of trials resulted in having a very similar sensory-evoked response for Hit and Miss trials in wS1 for each session. We after plotted PSTHs from mPFC for each session for corresponding wS1-FR matching trials. We after restricted our analysis: (1) we divided an overlapping distribution of Hit and Miss trials from wS1 equally into two nonoverlapping parts; (2) subselected the left side of the distribution (with the smallest firing rates) and kept only Hit trials, and subselected the right part of the overlapping distribution and kept Miss trials. The second subselection is an extreme version of the previous selection resulting in a much stronger sensory-evoked response in Miss trials. The significance was assessed by comparing mean responses across sessions for Hit and Miss with the Wilcoxon signed-rank test.

4.6.17 Statistics

Data are represented as mean \pm SEM (when the mean is computed across neurons) or mean \pm SD (when the mean is computed across sessions) unless otherwise noted. The Wilcoxon signed-rank test was used to assess significance in paired comparisons; and the Wilcoxon rank-sum test was used for unpaired comparisons (Matlab implementations). Analysis of spiking activity, selectivity of calcium signals, and involvement index were performed using a non-parametric permutation test. The statistical tests used and n numbers are reported explicitly in the main text or figure legends. P-values are corrected for multiple comparisons and methods are indicated in figure legends.

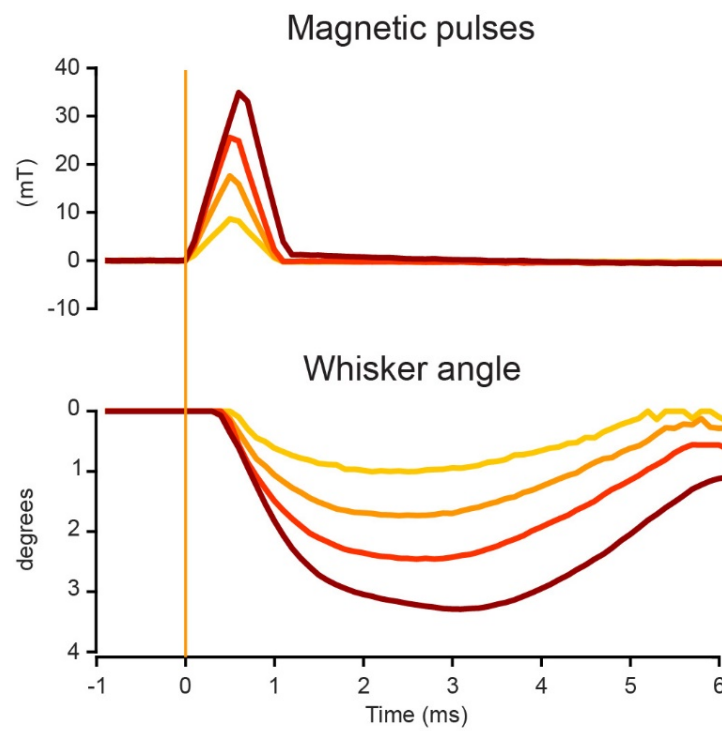


Figure 4.10 Calibration of the magnetic whisker stimulus

Brief (1 ms) magnetic pulses of various amplitudes (*Top*) were used to evoke fast downward deflections of the right C2 whisker (*Bottom*) with peak amplitude ranging from 1.0° to 3.3°.

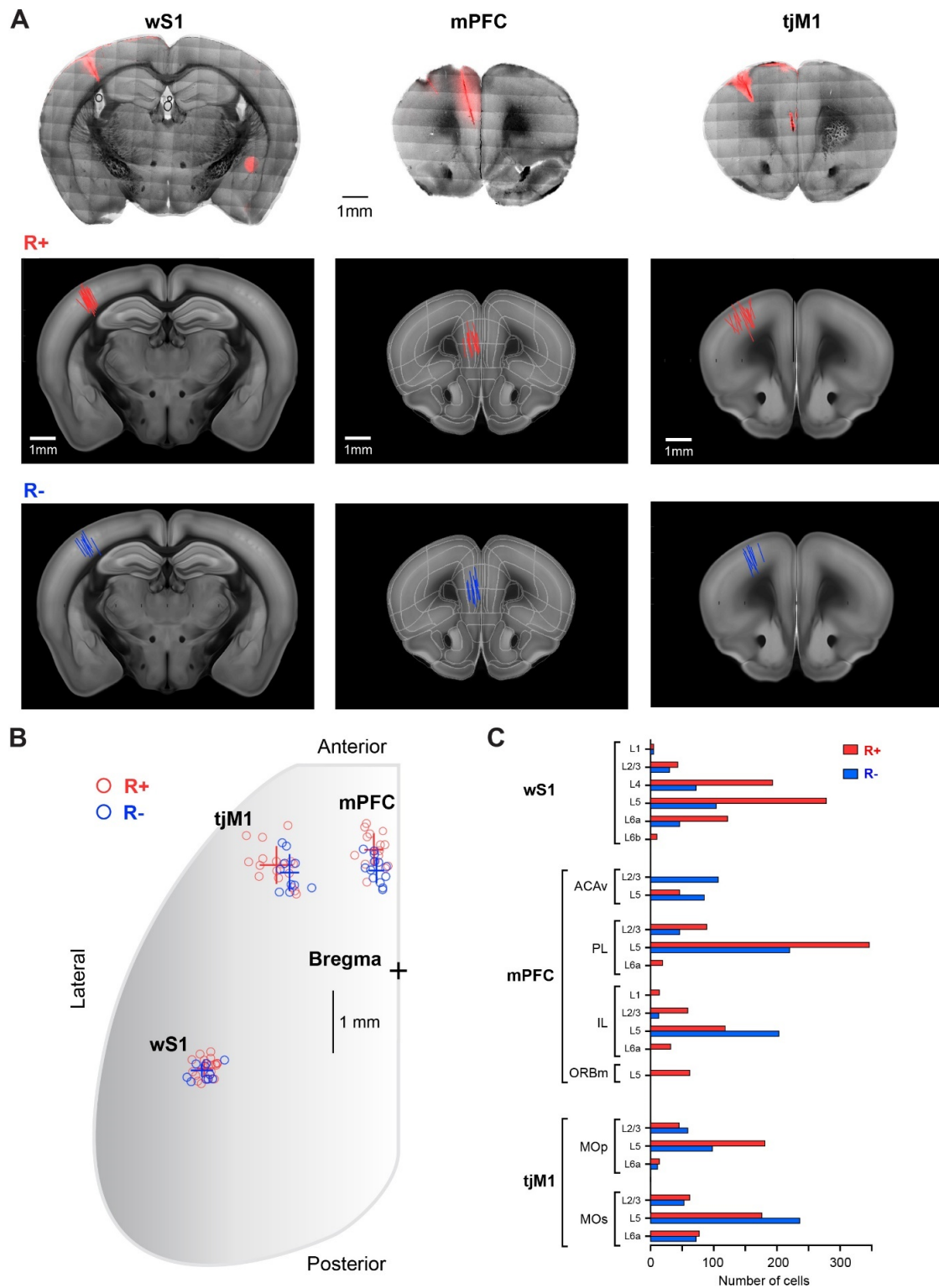


Figure 4.11. Anatomical localization and registration of the recording probes.

(A) *Top*, Three examples photomicrograph of the track of the recording probes labeled with the fluorescent Dil (red). *Bottom*, Superposition of the tracks of the probes on top of the coronal section

from the Allan Reference Atlas, for mice trained in the whisker detection task (R+) and mice exposed to the non-rewarded whisker stimuli (R-).

(B) Top-view of the position of the recording probes in R+ (red) and R- (blue) mice.

(C) Distribution of the recorded neurons in the different brain areas for R+ (red) and R- (blue) mice.

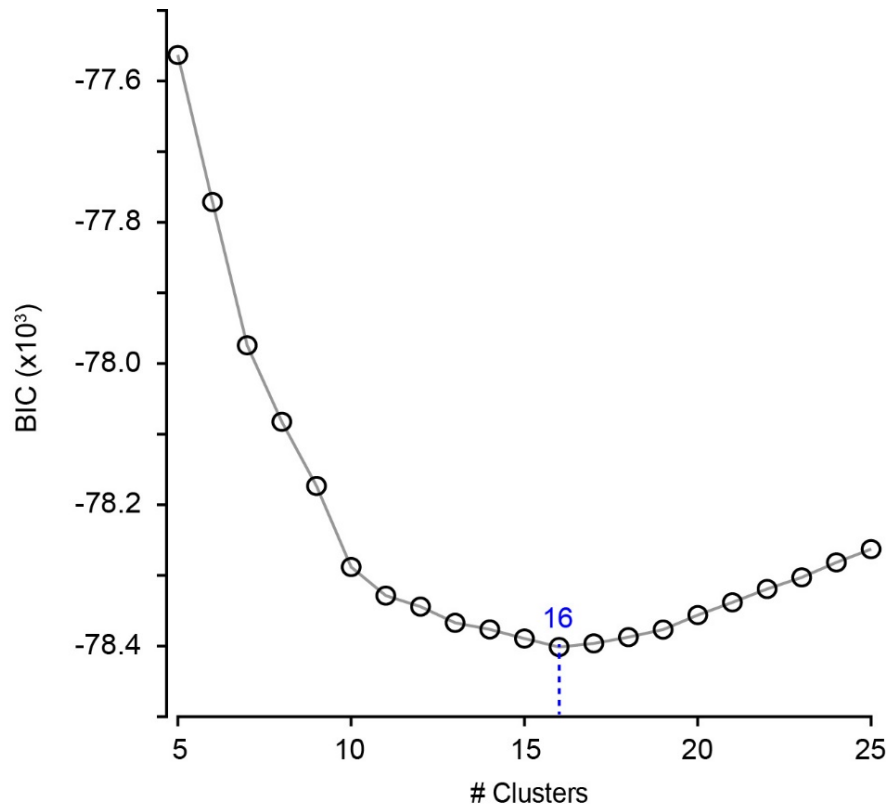


Figure 4.12. Bayesian information criteria curve for the number of clusters

Bayesian information criteria (BIC) were computed for models with a different number of clusters. The optimal number of clusters (16) was defined by the minimum in the BIC curve.

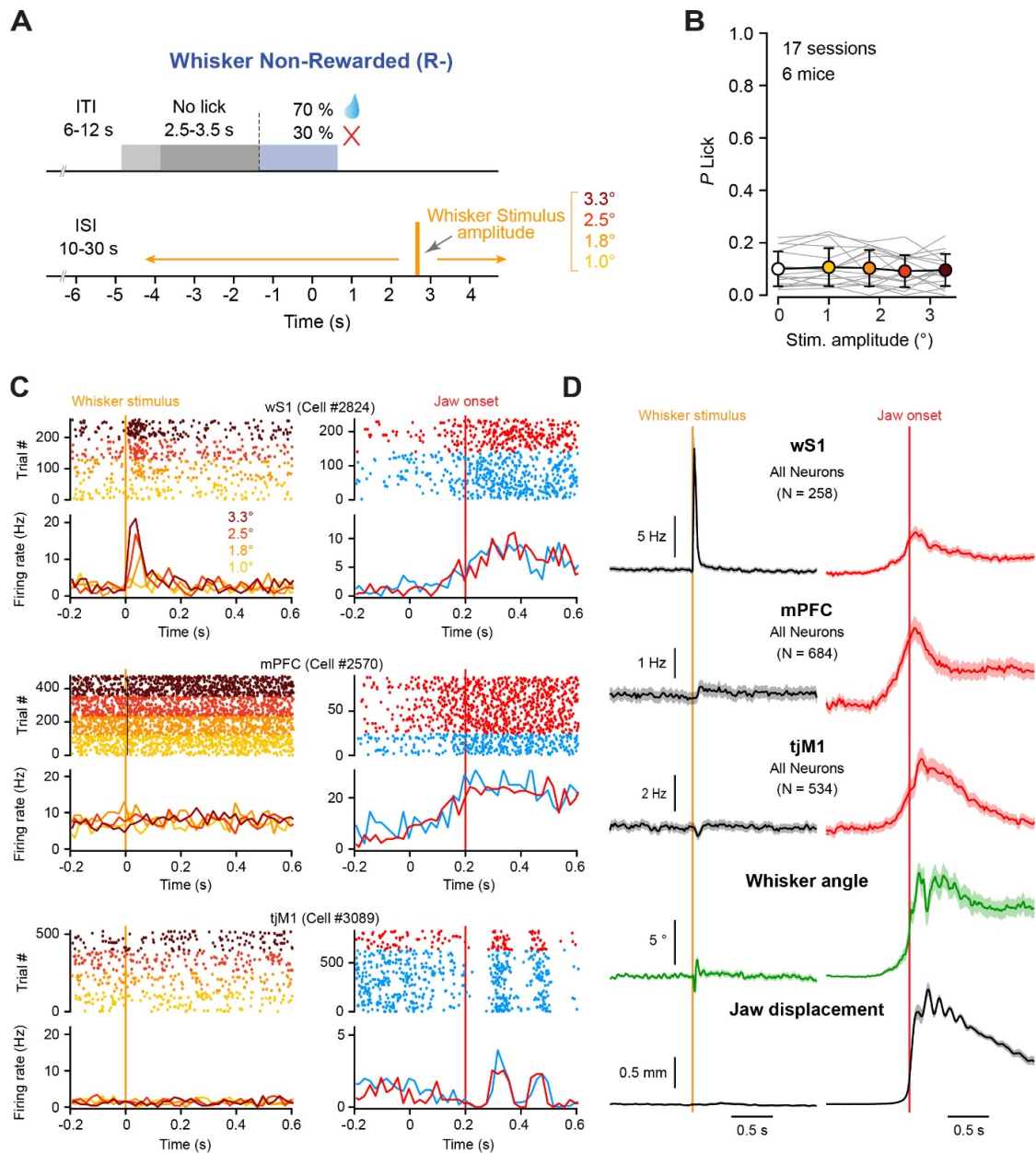


Figure 4.13. High-density extracellular recordings in mice exposed to the non-rewarded whisker stimuli.

(A) Task structure of the whisker non-rewarded mice (R-). Head-restrained water-restricted mice were trained in a free-licking task with a similar structure as the whisker-detection task (R+ mice). Mice were rewarded with a 70% of probability if they licked within 2 s response windows that were separated by a 6-12 s intertrial interval and a 2.5-3.5 s No-lick window during which mice were required not to lick. Unlike R+ mice, no cue indicated to the R- mice the onset of the response window. In addition, whisker stimuli of variable amplitude were presented at random times (10-30 s inter-stimulus interval) and were uncorrelated to the task structure, therefore mice did not associate the whisker stimulus to the reward availability.

(B) Lick probability as a function of the whisker stimulus amplitude for the 17 recording sessions (6 mice). Thin grey lines show the lick probability for each individual session; the thick black line shows the averaged performance (circles and error bars indicate mean \pm SD).

(C) Examples of recorded neurons from the three areas in R- mice. *Left column*, The activity of all stimulus trials for each neuron was aligned to the whisker stimulus onsets (orange). *Right column*, The activity of all Lick trials (rewarded, red and non-rewarded, blue) for each neuron was aligned to the jaw onsets (red). *Top row* wS1 (RSU) neuron #2824, *middle row* mPFC (RSU) neuron #2570, *bottom row* tJM1 (RSU) neuron #3089. For the stimulus aligned plots, *the top part* displays a raster plot of the neuronal activity with all trials sorted by stimulus amplitude (Stimulus amplitude 1.0° yellow; 1.8° orange; 2.5° red; 3.3° dark red). *The bottom part* displays the peristimulus time histograms (PSTHs, 0.02 s bin) averaged across trials with the same stimulus amplitudes (same color code as raster plot). For the jaw onset aligned plots, *the top part* displays a raster plot of the neuronal activity with all rewarded (red) and non-rewarded (blue) lick trials. *The bottom part* displays the peristimulus time histograms (PSTHs, 0.02 s bin) averaged across similar trials (same color code as raster plot).

(D) *Top left*, Average PSTHs (0.02 s bin) for Stimulus trials of the strongest whisker stimulus (amp. 3.3°), for wS1, mPFC, tJM1 (shown in black as mean \pm SEM) aligned to the whisker stimulus onset (orange). *Top right*, Average PSTHs (0.02 s bin) for Lick trials for wS1, mPFC, tJM1 (shown in red as mean \pm SEM) aligned to the jaw onset (red). *Bottom*, average whisker angle (green) and jaw displacement (black) (17 sessions) aligned to whisker stimulus (*left*) or jaw onset time (*right*).

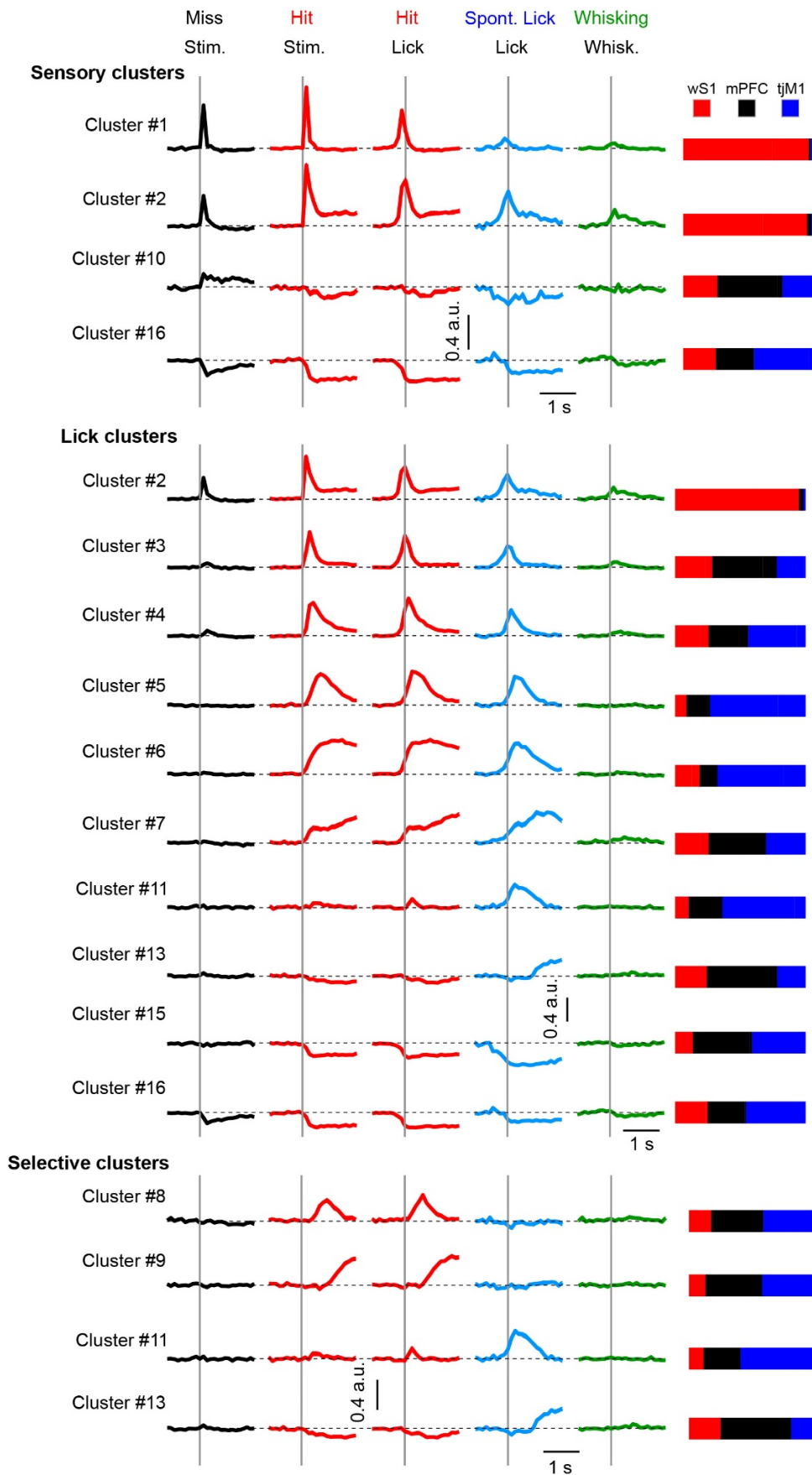


Figure 4.14. Neuronal clusters of interest.

Mean normalized PSTHs (0.1 s bin size) for different clusters (*rows*). Average PSTH for each cluster computed for Miss trials stimulus aligned (*black*), Hit trials stimulus and lick aligned (*red*), Spontaneous licks aligned to lick onset (*blue*), and spontaneous whisking aligned to the whisking onset (*green*). Bar on the right display the proportion of cells from a given cluster in each area. The clusters were selected by visual inspection as Sensory (*Top*) if they displayed an evoked activity in Miss trials, Lick if they exhibit activity in Spontaneous lick trials (Middle), and Selective if they were only active in one of the lick trial types (either Hit or Spontaneous lick, but not both).

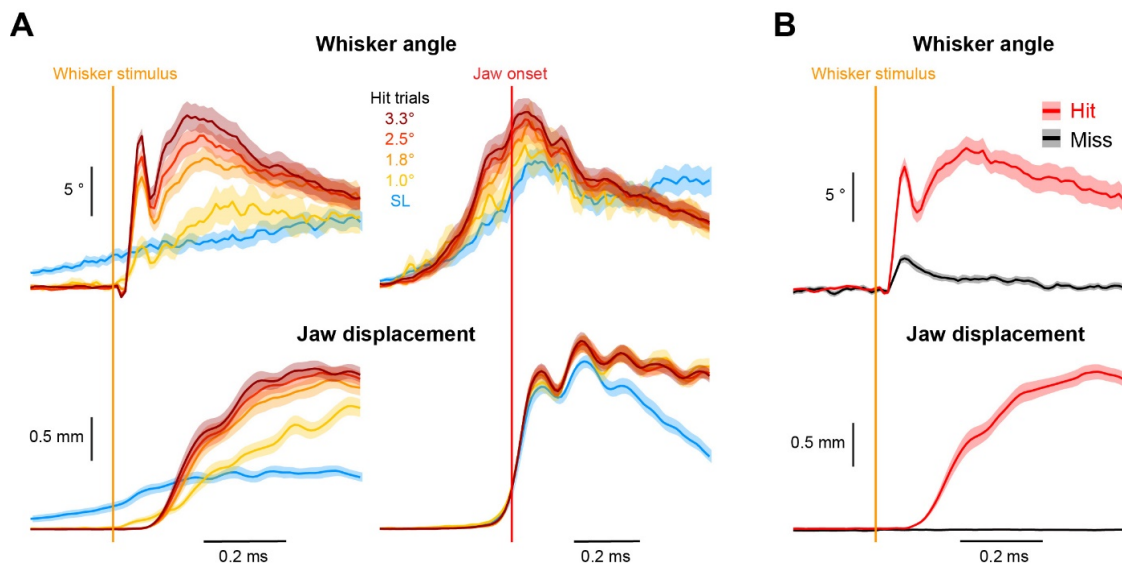


Figure 4.15. Evoked whisker and jaw movements.

(A) *Left panels*, stimulus-aligned whisker angle (*top*), and jaw displacement (*bottom*) for Hit trials of different whisker stimulus amplitudes and Spontaneous lick (SL) trials. *Right panels* same as the *left* but movements are aligned to the jaw onset.

(B) Stimulus-aligned whisker angle (*top*), and jaw displacement (*bottom*) for Hit (red) and Miss (black) trials for the near-threshold stimulus amplitude.

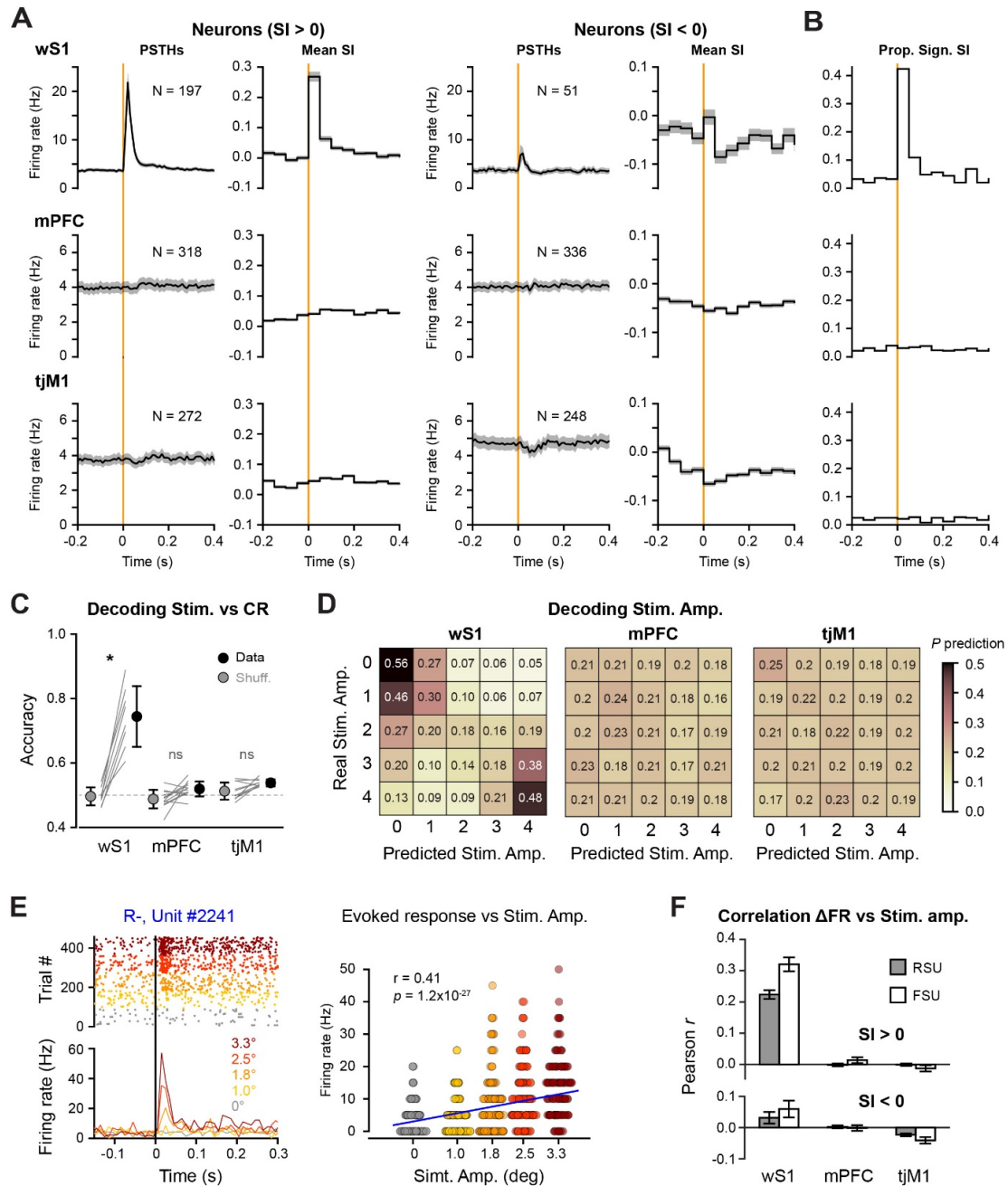


Figure 4.16. Purely sensory-evoked responses in R- mice.

(A) Whisker stimulus-evoked neuronal activity and selectivity index (SI) in stimulus trials (whisker stimulus amplitude 1.8°, 2.5° and 3.3°) for the three cortical areas (*Top row*, wS1; *Middle row*, mPFC, and *Bottom row*, tjM1). Each neuron was classified as positively (SI > 0) or negatively (SI < 0) modulated neurons based on ROC analysis comparing Stimulus vs No Stimulus trials. For positively and negatively modulated neurons, we computed the grand-average PSTHs (0.02 s bin), aligned to the stimulus onset time (*Left column*). We also computed the mean SI (0.05 s bin) (*Right column*). Both FSUs and RSUs were included. The number of neurons is indicated for each category and area.

(B) Proportion of cells with significant SI (Stim vs No Stim) based on the non-parametric permutation test for each 50 ms time bin after False discovery rate correction (FDR).

(C) A logistic regression approach was used to classify Stim vs No Stim on a single-trial basis from the population activity in each area. The decoding was performed on 0.1 s bins aligned to the trial onset time. The highest accuracy obtained from the real data (Data, black filled circle) and after label shuffling (Shuff., grey filled circle) are plotted for each area. Individual sessions are plotted as thin grey lines. The grey dotted line indicates the theoretical chance level. Statistical significance between data and label-shuffled decoding accuracy was assessed using Wilcoxon signed-rank test with FDR correction across 9 time bins (*, $0.05 > P > 0.01$): wS1, $P = 0.035$; mPFC, $P = 0.12$; tjM1, $P = 0.087$.

(D) Multinomial logistic regression approach was used to decode the stimulus amplitude from the population activity 100 ms after stimulus onset in Stim trials on a single-trial basis. The Confusion matrices display the probability of correctly predicting the stimulus amplitude (Predicted) depending on the actual stimulus amplitude (Real) for each area. Chance level = 0.2.

(E) Example wS1 neuron (neuron #2241). *Top*, raster plot for all Stim trials aligned to the whisker stimulus and sorted according to the stimulus amplitudes and corresponding PSTHs. (0.01 s bin). *Bottom*, distribution of evoked response (firing rate computed 0-200 ms after the whisker stimulus) for single trials as a function of stimulus amplitude. Linear correlation was assessed using Pearson correlation (correlation coefficient $r = 0.41$, $p = 1.2 \times 10^{-27}$, non-parametric permutation test). The blue line is a linear fit to the data.

(F) Mean Pearson coefficient of correlation averaged across neurons for positively ($SI > 0$, Top) and negatively ($SI < 0$, Bottom) modulated RSU (filled grey bars) and FSU (open bars) neurons from each area. The difference between the mean Pearson coefficient was assessed using a Kruskal-Wallis test, followed by multiple comparison tests (P -values for all comparisons are displayed in Table 4.11).

Table 4.11. P -values obtained from multiple comparison tests of the mean Pearson correlation coefficient different stimulus amplitudes (Fig. 4.16F).

			FSU						RSU				
			SI<0			SI>0			SI<0			SI>0	
			tjM1	mPFC	wS1	tjM1	mPFC	wS1	tjM1	mPFC	wS1	tjM1	mPFC
RSU	SI>0	wS1	0	1.89 $\times 10^{-17}$	0.21	1.54 $\times 10^{-12}$	5.91 $\times 10^{-11}$	0.97	0	0	5.69 $\times 10^{-7}$	0	0
		mPFC	0.16	1.00	0.49	1.00	0.99	0	0.10	1.00	0.93	1.00	
		tjM1	0.15	1.00	0.52	1.00	0.99	0	0.10	1.00	0.95		
	SI<0	wS1	0.05	0.97	1.00	0.85	1.00	3.73 $\times 10^{-8}$	0.09	0.98			
		mPFC	0.08	1.00	0.60	1.00	1.00	0	0.03				
		tjM1	1.00	0.79	0.04	1.00	0.12	0					
FSU	SI>0	wS1	0	1.88 $\times 10^{-17}$	0.04	1.26 $\times 10^{-13}$	8.18 $\times 10^{-12}$						
		mPFC	0.07	1.00	0.96	0.95							
		tjM1	0.98	1.00	0.39								
	SI<0	wS1	0.02	0.60									
		mPFC	0.50										

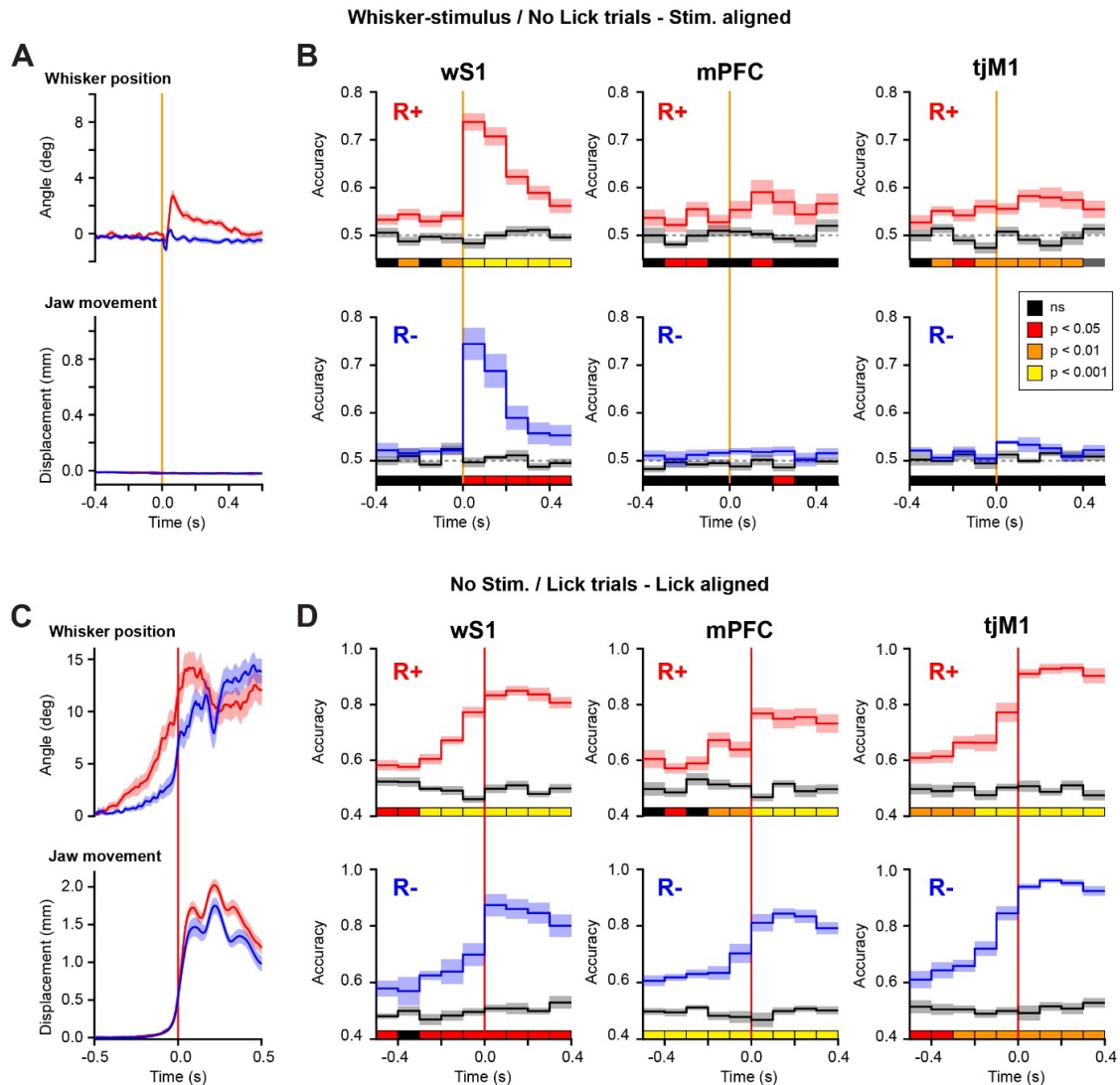


Figure 4.17. Decoding of sensory stimulus and licking in R+ and R- mice.

(A) Whisker angle and jaw displacement aligned to the stimulus onset for whisker rewarded (R+, red) and whisker non-rewarded (R-, blue) group of mice.

(B) Decoding accuracy of Stimulus-NoLick trials vs NoStimulus-NoLick trials for R+ mice (red) and R- mice (blue) based on neuronal population activity using logistic regression. Decoding was performed on 0.1 s bins for wS1 (left), mPFC (middle), and tJM1(right). Black lines correspond to prediction accuracy from the shuffled data. Color-coded on the bottom of each graph: P-value Data vs Shuffled (Wilcoxon signed-rank test, FDR corrected across 9 bins).

(C) same as (A) but aligned to the jaw onset.

(D) same as (B) but for Spontaneous Licks vs NoStimulus-NoLick trials aligned to the jaw onset.

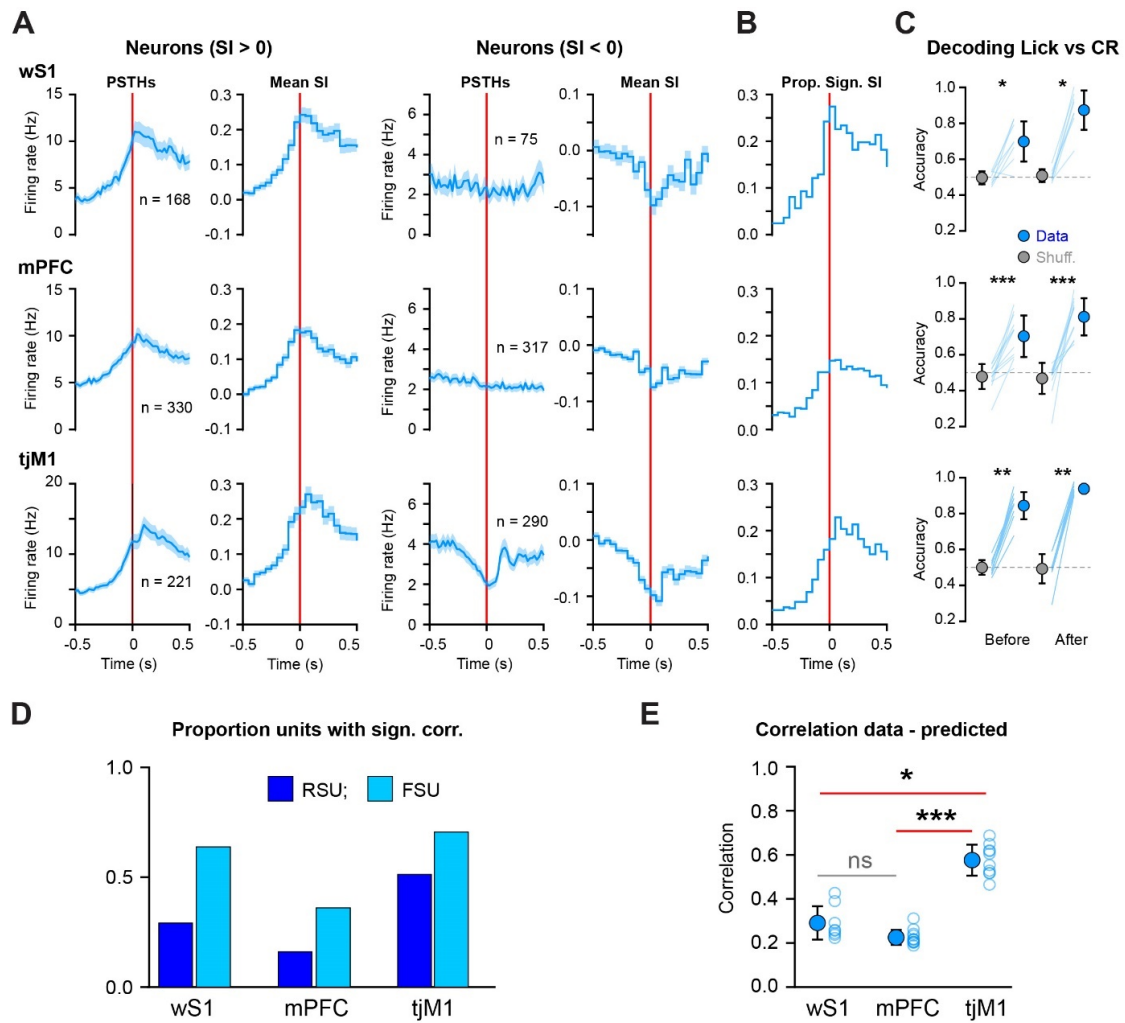


Figure 4.18. Purely motor activity in R- mice.

(A) lick evoked neuronal activity and selectivity index (SI) in Spontaneous lick trials for the three cortical areas (*Top row*, wS1; *Middle row*, mPFC and *Bottom row*, tJM1). Each neuron was classified as positively (SI > 0) or negatively (SI < 0) modulated neuron according to their maximum Selectivity Index (SI) within a 0.2 s window around the jaw onset (from - 0.1 s to 0.1 s) based on ROC analysis comparing Spontaneous lick vs No lick time window (baseline). For positively and negatively modulated neurons, we computed the grand-average PSTHs (0.02 s bin), aligned to the jaw movement onset time (*Left column*). We also computed the mean SI (0.05 s bin) (*Right column*). Both FSUs and RSUs were included. The number of neurons is indicated for each category and area.

(B) Proportion of cells with significant SI (Spontaneous lick vs baseline) based on the non-parametric permutation test for each 50 ms time bin after False discovery rate correction (FDR).

(C) A logistic regression approach was used to classify Spontaneous Licks vs Correct Rejection (CR) on a single-trial basis from the population activity in each area. The decoding was performed on 0.1 s bins aligned to the jaw movement onset time. The accuracy obtained from the real data (Data, black filled circle) and after label shuffling (Shuff., grey filled circle) are plotted for each area for the 0.1 s bins immediately before and after jaw onset. Individual sessions are plotted as thin blue lines (wS1, 8 sessions; mPFC, 12 sessions; tJM1, 10 sessions). The grey dotted line indicates the theoretical chance level. Statistical significance between data and label-shuffled decoding accuracy was assessed using Wilcoxon signed-rank test with FDR correction across 9 time bins (**, 0.01 > P > 0.001; ***, P < 0.001):

wS1_{Before}, $P = 0.02$; wS1_{After}, $P = 0.01$; mPFC_{Before}, $P = 6.28 \times 10^{-4}$; mPFC_{After}, $P = .28 \times 10^{-4}$; tjM1_{Before}, $P = 2.93 \times 10^{-3}$; tjM1_{After}, $P = 2.93 \times 10^{-3}$. Mean \pm SD can be found in Table 4.12

(D) Proportion of cells with significant jaw-phase correlation assessed by testing the uniformity of the spike probability distribution around the circle with Rayleigh test.

(F) Continuous decoding of jaw movement from neuronal population activity was performed using linear regression for the continuous signal regression approach. The correlation coefficient between real and predicted jaw traces for each area. Empty circles indicate individual sessions, filled red circles with error bars indicate mean \pm SD for each area. Comparison between areas: Kruskal-Wallis test, $P = 1.3 \times 10^{-5}$; multiple comparison tests (*, $0.05 > P > 0.01$; **, $0.01 > P > 0.001$; ***, $P < 0.001$): wS1 vs mPFC, 0.18; wS1 vs tjM1 $P = 0.027$; mPFC vs tjM1 $P = 6.7 \times 10^{-6}$.

Table 4.12. Mean and SD accuracy for real and shuffle data when decoding Spontaneous licks versus Correct rejection trials (related to Figure 4.18C).

Area	mean	SD	mean_Shuf	SD_Shuf	bin
wS1	0.70	± 0.11	0.50	± 0.04	50 ms time window before the jaw onset
mPFC	0.70	± 0.12	0.48	± 0.07	
tjM1	0.84	± 0.08	0.50	± 0.04	
wS1	0.87	± 0.11	0.51	± 0.04	50 ms time window after the jaw onset
mPFC	0.81	± 0.10	0.47	± 0.09	
tjM1	0.94	± 0.03	0.49	± 0.08	

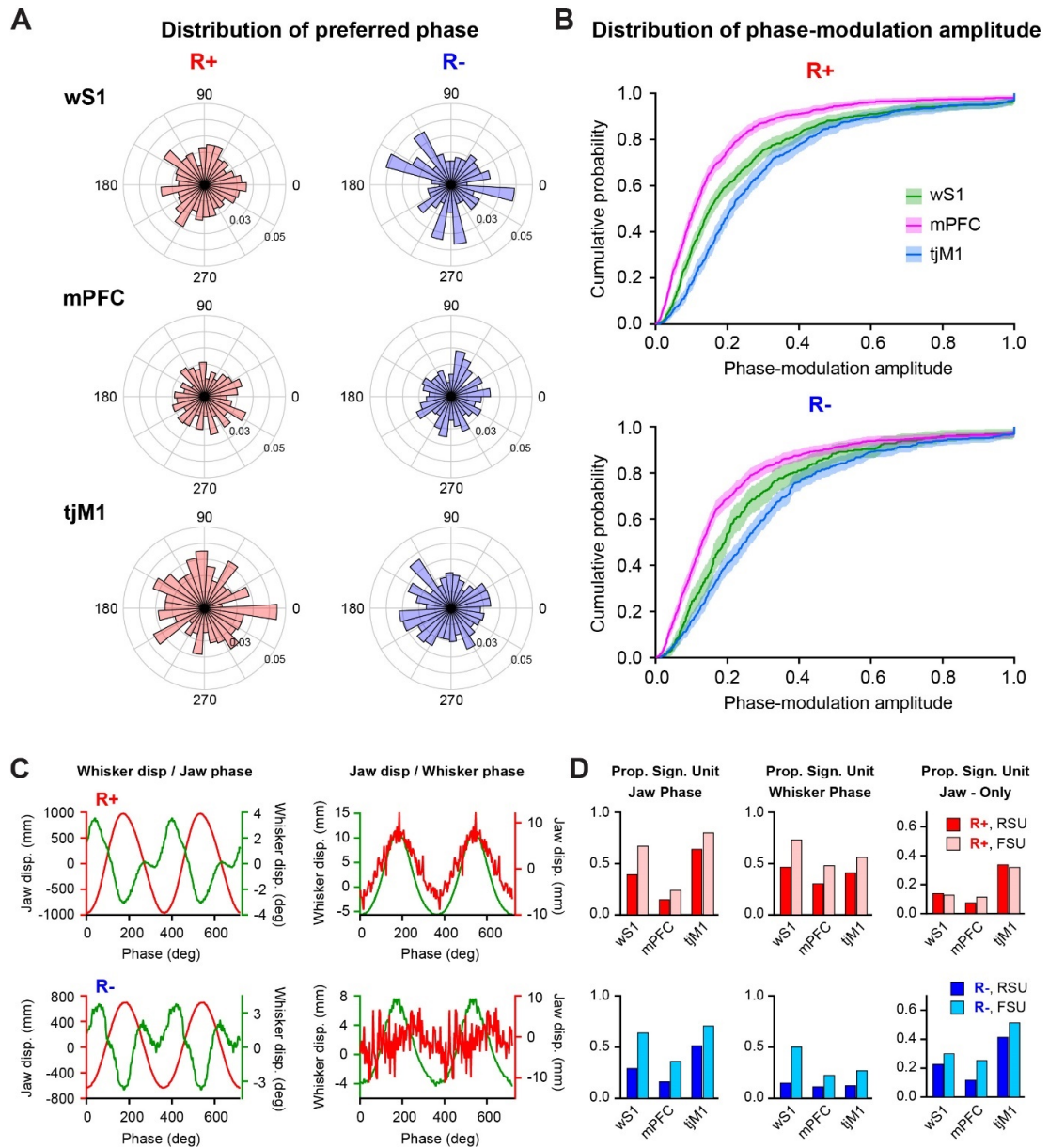


Figure 4.19. Jaw-phase correlation and encoding in R+ and R- mice.

(A) Distribution of preferred jaw-phase (mean resultant vector \bar{r}) for all neurons obtained from the phase correlation analysis. *Left column* for whisker-rewarded mice (R+), *right column* for whisker non-rewarded mice (R-).

(B) Normalised cumulative distribution of the length (R) of the mean resultant vector \bar{r} for all neurons. *Top*, whisker-rewarded mice ($R+$); *bottom*, whisker non-rewarded mice ($R-$).

(C) *Left*, whisker angle (green) as a function of the jaw-phase (red) during licking for whisker-rewarded mice (R+, Top), and whisker non-rewarded mice (R-, Bottom). *Right*, jaw movement (red) as a function of the whisker phase during whisking without licking.

(D) *Left*, Proportion of cells with significant jaw-phase coding, as assessed by testing the uniformity of the spike probability distribution around the circle (jaw phase) with Rayleigh test. *Middle*, Same as a left panel but for the proportion of cells with significant whisker-phase coding. *Right*,

Proportion of significant cells with jaw-phase coding, excluding the cells that have significant whisker-phase coding. *Upper panels* for whisker-rewarded mice (R+), *bottom panels* for whisker non-rewarded mice (R-). Proportions of cells can be found in Table 4.12.

Table 4.13. Proportion of cells with significant jaw-phase correlation, whisker-phase correlation, and jaw-phase correlation but no whisker-phase correlation (related to Figure 4.19D).

		Jaw phase		Whisker phase		Jaw (excluding whisker)	
		R+	R-	R+	R-	R+	R-
wS1	RSU	0.39	0.29	0.46	0.15	0.13	0.23
	FSU	0.65	0.63	0.72	0.50	0.13	0.30
mPFC	RSU	0.14	0.16	0.30	0.11	0.07	0.12
	FSU	0.23	0.36	0.48	0.22	0.10	0.25
tjM1	RSU	0.63	0.51	0.41	0.12	0.33	0.41
	FSU	0.80	0.70	0.53	0.26	0.35	0.51

Chapter 5 Conclusions and Future Perspectives

At the end of my thesis, I would like to discuss all our findings and compare them to existing knowledge about sensorimotor transformation in different goal-directed tasks and different sensory modalities. I will discuss possible roles and functions of primary sensory and primary motor cortical regions, beyond their traditional roles in sensory processing or motor execution. I will share my vision of how the frontal cortex can orchestrate the behavior and cover the possible roles of the mPFC during the whisker detection task. Finally and importantly, I will describe how wS1 and tjM1 can be linked during the execution of goal-directed behavior. Finally, I will provide a detailed account of the neural circuits in the mouse brain that mediate the transformation of whisker sensory input into licking motor output via reward-based learning.

In Chapter 2 (Esmaeili et al. 2021), using multiple technical approaches, we demonstrated the temporally distinct recruitment of various cortical regions involved in the sensorimotor transformation in a delayed-licking task. Three key findings were identified through the analysis of learning-induced changes in neural activity. Firstly, widespread neuronal activity in the delay period could largely be explained by preparatory movements, but acritical and non-movement related activity was predominantly localized to a small region of the secondary motor cortex including the ALM. Inactivation of ALM during the delay period significantly reduced the probability of correct stimulus detection, indicating its importance in delayed sensorimotor transformation. Additionally, we observed a fraction of delay-encoding neurons which was also significantly enhanced by learning in other cortical areas, including wS2, wM1, wM2, and tjM1. Secondly, our study proposed a putative corticocortical signaling pathway that links the sensory to the motor cortex through learning. Rapid sequential activation of cortical areas evoked by whisker-deflection was observed, with the earliest cortical response occurring in wS1 and wS2. The sensory response in wM2 showed the earliest significant increase in whisker-evoked firing and a decrease in response latency across learning, suggesting it may serve as a key node in the corticocortical network which converts a whisker sensory stimulus into longer-lasting preparatory neuronal activity. Thirdly, we found a transient suppression of neuronal activity in the tongue and jaw primary motor cortex (tjM1) immediately after the whisker stimulus, likely contributing to the withholding of licking during the delay period. Accordingly, optoinhibition of tjM1 during the delay period decreased early licks, whereas optoactivation of tjM1 during the delay period increased early licks.

Importantly optogenetic inactivation of *tjM1* during the response window demonstrated its causal role in the execution of directional lick.

In Chapter 3 (Esmaeili et al. 2022) we focused in more detail on the putative corticocortical signaling pathway linking the sensory to the motor cortex through learning, by performing further analyses of the data presented in Chapter 2. In particular, while we only presented the activity of presumably excitatory neurons (RSUs) in Chapter 2, we present a detailed comparison of presumably excitatory and inhibitory (FSUs) neurons in Chapter 3. We first validated our classification of RSUs and FSUs based on spike waveforms using optotagging. Then we showed that the patterns of changes during the learning of the whisker detection task with delay in RSU and FSU activity differed across different cortical areas. Specifically, in *tjM1* and *ALM*, RSU and FSU neurons changed firing rates congruently across learning, suggesting changes in the external inputs driving these regions. In contrast, in *wM1* and *wM2*, RSU and FSU neurons changed firing rate incongruently, suggesting a differential change in the balance between excitation and inhibition with learning, with enhanced sensory-evoked inhibition relative to excitation in *wM1*, and enhanced excitation relative to inhibition in *wM2*. Lastly, we presented direct anatomical evidence for a direct monosynaptic connection between *wS2* and *wM2*, and showed a selective increase in functional connectivity between *wS2* and *wM2* after learning of the task. Overall, in Chapters 2 and 3, we provided insight into the neural mechanisms underlying learning and execution of a delayed sensorimotor transformation, with a special emphasis on the *wS2* → *wM2* neuronal pathway.

In Chapter 4, we investigated the neuronal activity and computation of the cortical sensory input area (*wS1*), a presumably decision area (*mPFC*), and the motor output area (*tjM1*). We revealed that the representation of sensory information, decision-making, and motor action are not discrete functions of each individual brain region, but are rather distributed and encoded across all three regions. However, we found that purely sensory information (encoding of the amplitude of the whisker stimuli during Miss trials) was mostly encoded in the activity of *wS1* neurons. We observed broadly distributed unspecific licking-related activity across the three areas, however, *tjM1* activity encoded the kinematic of the licking movements. We defined sensory-guided decision neurons as neurons with significant selectivity between Hit and Miss trials just after the whisker stimulus, and between Hit and Spontaneous lick just before movement onset. Surprisingly, decision neurons were found in all three areas but were more abundant in *wS1*. By examining sessions with simultaneous recordings from *wS1* and *mPFC*, we found that failure in the sensorimotor transformation (Miss) could occur at different levels, but regardless of the evoked activity in *wS1*, the response of *mPFC* was always higher in Hit trials compared to Miss trials. We finally proposed that the decision to lick after the whisker stimulus is a gradual process involving the flow of

information from the primary somatosensory (wS1) to the primary motor (tjM1) cortex, and that failure in signal processing can occur at any level.

5.1 Role of primary sensory cortex in goal-directed sensorimotor transformation

The role of primary sensory cortical areas in sensorimotor transformation during perceptual decision tasks is still largely debated: first, although there seems to be a general agreement that primary sensory areas play a critical role in complex sensory discrimination tasks, their involvement in simple sensory detection tasks remains controversial (Stüttgen and Schwarz 2018), second, even though primary sensory areas might be critical for perceptual task execution, it remains unclear whether their role is limited to encoding the nature and properties of the stimuli or also contribute to decision making or other functions.

In order to determine the specific function of the brain region one needs to combine correlative and manipulative strategies. Correlative evidence is often provided by recording neuronal activity with different methods and correlating it to the subject's behavior or external world variables. Manipulative evidence can be provided by lesioning, inactivating, or stimulating a brain area or a specific neuronal population. However, each of these strategies has its own limitations, and therefore, a combination of methods is necessary to obtain conclusive results (Panzeri et al. 2017).

The necessity of primary sensory areas in goal-directed sensorimotor tasks

I will start with correlation studies in the whisker primary somatosensory cortex. Sensory-evoked responses in wS1 caused by single-whisker stimulation were investigated over a decade using a lot of different technics and approaches. Electrophysiological data due to its high temporal resolution, either obtained by a whole-cell recording of single neurons (Sachidhanandam et al. 2013; Yamashita and Petersen 2016), or local field potential recording (Le Merre et al. 2018), or extracellular recordings of a larger population of single neurons (Stüttgen and Schwarz 2008; Stüttgen et al. 2011) (as used in this thesis work), always revealed biphasic sensory evoked responses driven by the whisker stimulus in the goal-directed detection tasks. The early sensory-evoked response (0-50 ms), is believed to represent information about the sensory stimulus (Sachidhanandam et al. 2013). Recordings from our psychophysical task (Chapter 4) further demonstrated that this early sensory-evoked response linearly increases in amplitude as a function of the strength of the whisker stimulus, which is in line with other studies in the field (Romo and de Lafuente 2013). This graded sensory evoked response was observed in both Hit and Miss trials, and

even after realignment of the trials to the licking onset in Hit trials. Moreover, we also observed early graded responses in mice that passively received the whisker stimulus which was not predictive of the reward, pointing out that the primary function of wS1 is to encode information about the physical features of the sensory stimulus. Barrel cortex neurons were shown to be activated by the single whisker stimulus close to a perceptual threshold also in previous study in rat performing a whisker-detection task (Stuttgen and Schwarz 2008). In this study, the activation of wS1 neurons was highly correlated with behavioral reports, as psychometric data could be brought into close alignment with neurometric data. Similar results were observed using the 2-photon functional Ca²⁺ imaging of the apical dendrite of L5 neurons in the barrel cortex. The dendritic evoked activity increased as a function of the single whisker deflection strength (Takahashi et al. 2016, 2020).

Primary somatosensory neurons also encode the amplitude of the vibration stimulation applied to the all whisker pad in rodents (Fassihi et al. 2017; Lee et al. 2020; Zareian et al. 2021), and similarly, in monkeys, the amplitude of the vibrotactile stimulation applied to the fingertip is encoded by primary somatosensory region (de Lafuente and Romo 2005, 2006). Barrel neurons can also well discriminate between vibrotactile signals consisting of pulse sequences (Lak et al. 2008; Gerdjikov et al. 2010; Musall et al. 2014), or consisting of white noise sequences applied with different kinematic properties and frequency composition (Maravall et al. 2007). A list of studies also shows that barrel neurons correlate with the coarseness of textures (Chen et al. 2013; Garion et al. 2014; Chen, Margolis, et al. 2015), and the whisker deflection direction (Andermann et al. 2004; Kerr et al. 2007). There is thus general agreement that the neuronal activity in wS1 encodes the physical features of the sensory stimulus. But to what extent does the neuronal activity in wS1 correlate with perception and behavioral reports?

Recent studies have demonstrated that the magnitude of stimulus-evoked activity in barrel neurons is positively correlated with the likelihood of a behavioral response, as assessed using repeated presentations of the same stimulus (Sachidhanandam et al. 2013; Yang et al. 2016). Previously observed in our laboratory, the early sharp response (0-50 ms) evoked by the single whisker stimulation had similar amplitudes for Hit and Miss trials (successful and unsuccessful stimulus detection), whereas the secondary sensory-evoked response (50-400 ms after the stimulus) was prominent only in Hit trials (Sachidhanandam et al. 2013; Yamashita and Petersen 2016; Kyriakatos et al. 2017; Le Merre et al. 2018). Further supported by optogenetic inactivation experiments (Sachidhanandam et al. 2013), the current belief was that early sensory evoked response encodes sensory information about the stimulus, whereas late response contributes to sensory perception and trial-by-trial correlates with the mouse perceptual reports (Sachidhanandam et al. 2013; Yamashita and Petersen 2016; Kyriakatos et al. 2017; Le Merre et al. 2018). The absence of difference

between Hit and Miss trials for the early sensory evoked response in wS1 was also observed in our study in the delay task (Chapter 2), however, in the psychophysical version of the detection task (Chapter 4), we observed a Hit/Miss difference already within the first 50 ms after the stimulus onset, which also correlated on a trial-by-trial basis with mice perceptual reports for the near-threshold whisker stimulation. Furthermore, we revealed that around 20% of wS1 neurons were highly selective for Hit/Miss within the first 50 ms after the stimulus presentation. The observed difference most probably resulted from the saliency of the whisker stimulation that was used in different experiments. Presumably, near-threshold detection stimuli used in the psychophysical task could lead to the Miss trial due to the failure in detecting or perceiving the stimulus *per se*, rather than due to the failure in a decision to lick.

In addition to studying the correlation between different stimuli and neuronal activity in wS1 comes manipulative studies. Rodents can be trained to detect weak electrical stimulation (Romo et al. 1998; Butovas and Schwarz 2007) or optogenetic activation (Huber et al. 2008; Sachidhanandam et al. 2013c; Musall et al. 2014) of the barrel cortex, both of which were capable of eliciting behavioral responses. This suggests that direct stimulation of the primary somatosensory cortex (wS1) can serve as a substitute for whisker stimulation, indicating that neural activity in the wS1 plays a causal role in sensory perception and drives downstream circuits involved in the transformation of sensory input into motor output.

Another manipulative strategy is transient or permanent inactivation using pharmacology, optogenetics, or lesion. Transient pharmacological inactivation of wS1 impaired the detection of multi-whisker (Miyashita and Feldman 2013a) or single-whisker (Sachidhanandam et al. 2013c; Le Merre et al. 2018c) stimulation, and the same is true for transient optogenetic inhibition during single whisker detection task (Sachidhanandam et al. 2013; Kwon et al. 2016; Takahashi et al. 2016, 2020; Yang et al. 2016; Hong et al. 2018; Le Merre et al. 2018; Mayrhofer et al. 2019). Results from experiments described in my thesis also show that optogenetic blocking of the sensory-evoked responses in wS1 led to a strong reduction of the detection probability in both delay and psychophysical detection tasks. In the delay task (Chapter 2 (Esmaeili et al. 2021)). Similar temporal involvement of wS1 along the trial was demonstrated in the whisker discrimination task where the mouse had to detect the position of the poll, where wS1 inactivation decreased the performance during sample and delay epochs (Guo et al. 2014). In our psychophysical task (Chapter 4), wS1 inactivation altered mouse perception by increasing the mouse detection threshold consistent with another study in a very similar whisker detection task where wS1 inactivation shifted the detection threshold towards higher whisker stimulation but did not alter the slope of the psychometric curve (Takahashi et al. 2016). Hence, we believe that neuronal responses in wS1 are crucial for processing whisker sensory information and routing it to higher cortical regions.

Similar transient inactivation effects were observed in other primary sensory cortices. Optogenetic inactivation of the primary somatosensory cortex also revealed its role in forelimb motor adaptation. S1 photoinhibition impaired mice's ability to update motor commands to the change in the environment but not the execution of already-adapted motor commands. This finding indicates that cortical processing of somatosensory feedback via S1 plays an important role and direct projections from the spinal cord to the cerebellum are not sufficient to support motor adaptations in the forelimb motor adaptation task (Mathis et al. 2017).

In the visual discrimination task, where depending on the position of the visual stimulus (right or left) the mouse has to turn the wheel left or right respectively, optogenetic inactivation of the primary visual cortex (V1) biases mice choices by reducing the choice of contralateral side (contralateral to the hemisphere of inactivation). The authors observed a lot of sensory information coding in V1 and other visual and frontal regions. Interestingly inactivation of all regions that encoded sensory stimulus biased the mice's performance in the same way. However they didn't observe choice-related coding in V1, but a lot of movement-related activity. (Zatka-Haas et al. 2021).

The available evidence from both correlative and manipulative studies suggests that wS1 is involved in whisker-mediated detection. However, there are two important caveats to consider. First, experiments that demonstrate impairments in a specific behavioral function after transient inactivation of a brain region do not necessarily imply a causal role for that region, as downstream targets may be affected, altering their excitation-inhibition balance (Otchy et al. 2015). Therefore, it is crucial to investigate whether permanent lesions of wS1 impair stimulus detection. A classic study by Hutson and Masterton postulates that stimulus detection won't be impaired after a permanent lesion of the barrel cortex (Hutson and Masterton 1986). One could argue that over the recovery time after the lesion, circuit reorganization could occur and compensate for the loss of the lesioned area, however, a recent study from Hong et al. demonstrated that mice were still able to perform a whisker detection task above chance level one day after a complete lesion of wS1 and fully recovered performance the day after, arguing that plasticity would not have time to occur in a such short time (Hong et al. 2018). Importantly they also demonstrated that brief optogenetic inhibition decreased the mice's performance. This constellation of findings – impairment through transient but not permanent inactivation can possibly be explained by the involvement of wS1 in the execution of the whisker detection task during the normally functional intact brain, which might not be a case after the permanent injury. Blocking or altering the function of neuronal structures has been promoted as a means of uncovering the "causal roles" of these structures in specific functions. However, as with correlative neuroscience, the manipulative approach is plagued by uncertainties.

It is commonly accepted for other primary cortical regions that the temporary inactivation of a particular brain region can impair task performance on sensory simple detection or discrimination tasks, while the effects of permanently lesioning the same area may be minor. The involvement of the auditory cortex (AC) is controversial even for the discrimination of two distinct sounds. Indeed, lesions or reversible silencing of the auditory cortex led to small deficits or had little effect, depending on task conditions, silencing methods, and animal models (Talwar et al. 2001; Rybalko et al. 2006; Jaramillo and Zador 2010; Pai et al. 2011; Gimenez et al. 2015; Ceballo et al. 2019). Thus, the auditory cortex does not seem to be always necessary for simple sound discrimination. It seems that the complexity of the task often determines the necessity of the primary sensory region, however, the level of this complexity is not the same in all sensory systems. For example, the auditory cortex is not required for the discrimination of the pure tones task but it is necessary when the mouse has to discriminate between two frequency-modulated sounds (Ceballo et al. 2019). In the visual detection task when the mouse had to detect orientation changes of the visual stimuli, silencing of V1 activity abolished detection in conditions of high task complexity (low-saliency stimuli) but not low task complexity (Lohuis et al. 2021). Another evident example comes from human studies when subjects with primary visual cortex lesions display residual visual abilities, a phenomenon termed “blindsight” (Sanders et al. 1974; Schmid et al. 2010). A similar effect was observed in the motor cortex in rats performing the lever-pressing task (Kawai et al. 2015). Well-trained rats could execute motor sequences without a motor cortex. Altogether, these studies suggest that the cortex might be dispensable for the execution of simple sensorimotor tasks.

Even though the necessity of primary sensory regions for detection is still questionable, their role in more complex discrimination tasks is more strongly supported. In object discrimination task using freely moving whiskers, pharmacological and optogenetic inactivation of the primary somatosensory cortex abolishes mice performance (O’Connor, Clack, et al. 2010; Guo et al. 2014). Lesion of wS1 does permanently impairs performance in a shape discrimination task (Rodgers et al. 2021). Lesion of the primary auditory cortex also impairs the discrimination of frequency-modulated sounds (Ceballo et al. 2019).

In conclusion, the necessity of primary sensory cortical areas in the execution of simple sensorimotor transformations remains highly controversial, largely due to the different possible interpretations of lesion vs temporary inactivation approaches. We would like to argue that a possible explanation could be the likely existence of several parallel and partially redundant pathways that could be recruited by the sensorimotor transformation. If the temporal inactivation of a given area impairs performance, it probably indicates the necessity of this area for the execution of the task, but more a permanent inactivation could rapidly recruit alternative pathways to compensate for the

loss of the lesioned area. Further experiments combining large-scale longitudinal neuronal recording and manipulation would be necessary to address this question.

Role of primary sensory areas in perceptual-decision making

The involvement of primary sensory cortical regions in perceptual decision-making is intricate. Although these regions are conventionally considered as crucial intermediaries between peripheral sensory inputs and the decision-making centers, several observations contradict this simplified notion, indicating a more complex role of primary sensory areas in perceptual decisions. Oppose to multiple results demonstrating that primary sensory regions provide information on sensory inputs but not decisions (de Lafuente and Romo 2006; Romo and de Lafuente 2013; Guo et al. 2014; Rossi-Pool et al. 2016; Fassihi et al. 2017; Zatka-Haas et al. 2021), one of our interesting findings was that wS1 also strongly encodes sensory-guided decision, i.e. the decision to lick in response to the whisker stimulus (Chapter 4). This is not a completely novel finding, in fact, it was already reported in several papers (Kwon et al. 2016; Takahashi et al. 2016; Yang et al. 2016; Buetfering et al. 2022). However, in many previous studies, the decision (or choice) was generally considered simply as Hit/Miss difference, or task-related movements were not carefully taken into account. However, we observed that simply licking, which is also present in Hit trials, caused strong responses in the wS1. This is in line with other studies showing widespread motor-related cortical activity (Musall et al. 2014; Steinmetz et al. 2019; Stringer et al. 2019). Hence in our project, we proposed a stronger definition of sensory-guided decision, where the neuron – or a brain region – has to distinguish between Hit and Miss trials early after the stimulus, while also differentiating between Hit and Spontaneous licking events before the movement onset. Thus, we refer here to sensory-guided decision as a decision signal that links the sensory cue to the appropriate motor action, i.e., not just a motor command that triggers the action, but rather a signal that is used to make the choice to lick in response to the whisker stimulus. Surprisingly among the three areas we studied, we observed the highest proportion of these neurons in wS1. This finding probably makes sense if we think of wS1 as the first stage of the sensorimotor transformation, which is likely more efficient to extract categorical and task-relevant interpretations of the sensory signals instead of just extracting physical features of the sensory stimulus. The categorical interpretation of the sensory stimuli already at the level of wS1 might be an even more efficient strategy if we consider that the actual task of the mouse is stimulus detection and not a discrimination of the stimulus amplitude for example. Hence, these very early choice signals in wS1 might reflect the success or failure in sensory perception or detection of the stimuli. In line with our results is a very recent work that identified decision neurons in wS1 that carry categorical information about the trial type and

demonstrated that selective photostimulation of these decision neurons was driving behavior and enhancing mice performance (Buetfering et al. 2022).

In rodents, primary sensory areas have been shown to represent more complex functions than initially believed. Studies have reported important reward-related signals in primary sensory areas. In wS1 of mice performing a whisker based object-detection task, the activity of L2/3 and L5 apical dendrites, as well as of the somata of L2/3 excitatory neurons tracks reward delivery, independently of sensory or motor signals (Lacefield et al. 2019). Another study in mice described the role of S1 in reward processing. The orbitofrontal cortex (OFC) propagated reward information to S1 during tactile reversal learning (Banerjee et al. 2020). Researchers found that the lateral OFC responded to the mismatch between expected outcomes and actual outcomes caused by rule reversals during tactile reversal learning. This mismatch triggered a reward-dependent value-prediction error signal that was encoded and propagated by a subset of OFC neurons. The signal was then sent via feedback projections to S1, which was responsible for updating sensory representations and adjusting the animals' behavior. The study suggested that reward feedback to S1 played a crucial role in shaping representations and updating predictions in mice (Banerjee et al. 2020). Similar findings have also been observed in the rat primary visual cortex (V1). Specifically, when visual stimuli were associated with subsequent reward, a significant number of neurons in V1 could accurately predict reward timing and value (Shuler and Bear 2006; Ramesh et al. 2018; Banerjee et al. 2023). Another study investigated the effects of reward on the representation of sensory stimuli in V1 of monkeys and found that the relative value of a stimulus influences V1 activity (Stanisor et al. 2013).

Several other studies implicated top-down control of sensory processing. The work of Gilbert & Li indicated task-dependent modulation of V1 responses in monkeys during vernier/bisection tasks (Gilbert and Li 2013). Roelfsema et al revealed context-dependent processing in V1 of monkeys performing line tracing task showing that task demands modulate the V1 activity (Roelfsema et al. 1998). Context-dependent processing in primary sensory cortices could thus be important. In addition, locomotion was shown to alter responses in the primary sensory cortex. Researchers investigated how the primary visual cortex (V1) in mice integrates signals related to visual speed and run speed during navigation in a virtual environment by recording V1 activity. The study found that almost half of the V1 neurons were driven by combinations of visual speed and run speed, performing a weighted sum of the two speeds. As a population, the V1 neurons predicted a linear combination of visual and run speeds better than either speed alone, indicating that V1 play an important role in integrating visual motion and locomotion during navigation in mice (Saleem et al. 2013).

Hence, neurons of primary sensory cortices in addition to encoding sensory input, also integrate them with contextual information such as reward (Shuler and Bear 2006; Stanisor et al. 2013; Ramesh et al. 2018; Banerjee et al. 2023), expectation(Jaramillo

and Zador 2010; Keller et al. 2012), attention (Reynolds and Heeger 2009; Gilbert and Li 2013) and motor action (Poulet and Petersen 2008; Saleem et al. 2013; Ayaz et al. 2019). The early integration of sensory-, contextual-, reward- related signals at early stage of the sensorimotor transformation is certainly an optimal solution to rapidly shape animal's behavior in an ever changing environment.

5.3 Cortical control of planning and executing licking as a motor output

As previously stated, animals often communicate their choices in various behavioral tasks by licking as a means to receive a reward. This is commonly referred to as the “motor output” of the sensorimotor transformation process. The brain must effectively plan, coordinate and regulate the movements of the tongue and jaw to enable successful licking.

In contrast to sensory areas, neuronal activity in motor areas correlates best with motor action. The neuronal activity in the whisker motor cortex (wM1) is correlated to whisker movements (Hill et al. 2011; Sreenivasan, Kyriakatos, et al. 2016). Optogenetic activation of the whisker motor cortex elicits whisker protraction whereas opto-inhibition strongly reduces whisker movements (Sreenivasan, Kyriakatos, et al. 2016; Auffret et al. 2018) suggesting an important role for wM1 in the control of whisking initiation (Sreenivasan, Esmaili, et al. 2016; Ebbesen et al. 2017). Although wM1 receives direct inputs from wS1 (Yamashita et al. 2018; Liu et al. 2022), wM1 does not control licking and, in fact, is not necessary for the execution of the whisker-based detection task (Le Merre et al. 2018). Recently, another region of the motor cortex, referred to as the tongue/jaw primary motor cortex (tjM1), was identified as controlling jaw movements. The activity of the neurons in tjM1 encodes licking movements with high selectivity for the direction of the licking, and unilateral activation of tjM1 drives licking in the contralateral direction while unilateral inhibition impairs contralateral licking (Mayrhofer et al. 2019). In our delay licking whisker detection task (Chapter 2 (Esmaili et al. 2021)), where the mouse had to actively suppress lick initiation until the go cue, active lick suppression was reflected in tjM1 activity. We observed a transient inhibition after the whisker stimulus in the trials where the mouse successfully withheld the licking during the delay, and inversely excitation during the trials with premature licking. Importantly optogenetic manipulation experiments confirmed the hypothesis that inhibition of tjM1 on the population level might correspond to active lick suppression. Our experiments revealed that the inactivation of tjM1 during the delay period significantly decreased the number of these premature licks and inversely activation of tjM1 increased the probability of early licks during the

delay period. And as expected inhibition of tjM1 during the response window significantly decreased the licking probability of mice. Therefore, tjM1 exhibited a crucial role in suppressing premature licking during the delay period. Research conducted on human subjects has indicated that inhibitory mechanisms play a crucial role in preventing inappropriate actions from being executed (Chikazoe et al. 2009; Duque et al. 2017). Furthermore, Cohen et al. (Cohen et al. 2010) suggested that parallel suppression and activation during a delay period may be a universal principle of response preparation that is preserved across different species.

These are important pieces of evidence to support the motor function of the tjM1, however, to investigate whether tjM1 controls the execution of the lick, we hypothesized that it should encode information about the fine kinematics of the jaw and the tongue. Our analysis (Chapter 4) revealed that tjM1 indeed encodes the phase of a jaw motion, which is congruent with previous research in the field showing that tjM1 encodes the length and angle of the tongue and the jaw (Xu et al., 2022). Recordings from our psychophysical task revealed a high proportion of neurons exhibiting significant phase coding of the jaw. We were also able to predict the actual jaw displacement in time with high accuracy based on the activity of tjM1 neurons. Our results indicate that encoding licking and jaw displacement is an intrinsic function of tjM1 and independent of the goal-directed task training, as was supported by our recordings from the whisker non-rewarded group of mice. Thus, tjM1 is a likely endpoint for the sensorimotor transformation in which a brief whisker deflection is converted into goal-directed licking in order to obtain a reward. Other primary motor regions demonstrated precise motor control in mice. For example, forelimb M1 activity encodes oromaneal kinematics during food handling and feeding behavior (Barrett et al. 2022).

During perceptual decision tasks, motor output is often planned before the execution and only released after specific sensory events, like a go cue (Inagaki et al. 2022). Therefore, planning and execution of the movement may be associated with different patterns of neuronal activity and involve different brain regions and different neuronal populations. It has been suggested that persistent or ramping up neuronal activity during the delay period may contribute to motor planning (Guo et al. 2014), the process that connects past experiences with future movements. In our delayed-response licking task (Chapter 2 (Esmaeili et al. 2021)) the activity of broad regions of the cortex was modulated during the delay period in Hit (correct) trials, however, only a small region of the secondary motor cortex including ALM remained activated after selecting trials without any uninstructed movements. ALM inactivation during the delay period strongly affected mice performance by reducing the hit rate. Hence, essential neuronal delay epochs activity appeared to be predominantly localized to ALM, which is in good agreement with other studies in closely-related tasks (Guo et al. 2014; Li et al. 2015). Several studies described a large proportion of neurons in the ALM exhibiting

preparatory activity that can predict the direction of the licking (Guo et al. 2014a; Chen et al. 2017). Moreover, optogenetic manipulations have provided evidence that preparatory activity in the ALM underlies motor planning (Guo et al. 2014; Li et al. 2015, 2016; Svoboda and Li 2018).

Overall, various brain regions, including the frontal and parietal cortex, have been implicated in motor planning (Fuster and Alexander 1971; Erlich et al. 2011; Ames et al. 2014; Guo et al. 2014; Liu et al. 2014). Neural activity during motor planning is also referred to as "preparatory activity". In nonhuman primates, preparatory activity has been detected in the primary motor cortex and premotor cortex (Tanji and Evarts 1976; Riehle and Requin 1989; Churchland et al. 2010), the parietal cortex (Maimon and Assad 2006), and subcortical regions such as the striatum, the superior colliculus, and the motor-related thalamus (Alexander and Crutcher 1990; Tanaka 2007; Ding and Gold 2010).

But ALM has been also identified as an important region for movement release and initiation. Researchers investigated the transition from motor planning to execution of directional licking evoked by the "Go cue" (Inagaki et al. 2022) in the delayed-response task (Guo et al. 2014). They proposed a multi-regional neuronal circuit that is critical for reorganizing ALM activity in response to the "Go-cue" and initiating planned directional licking. It has been shown that "Go-cue" activity first was encoded in ALM-projecting thalamic neurons, and shortly after in ALM (Dacre et al. 2021; Inagaki et al. 2022). Similarly, short-latency "Go-cue" evoked responses were observed in pedunculopontine nucleus (PPN) and midbrain reticular nucleus (MRN), among other areas. Which presumably signals the Go cue information to ALM via the thalamus. Consistent with a role in motor release, optogenetic stimulation of thalamus-projecting PPN/MRN neurons triggered directional licking and modulated ALM activity similar to the Go cue (Inagaki et al. 2022).

Several studies have described the role of ALM for motor planning but also the execution of directional licking in mice (Komiya et al. 2010; Guo et al. 2014; Li et al. 2015; Economo et al. 2018). Stimulation of ALM triggers rhythmic licking (Komiya et al. 2010; Li et al. 2015). ALM also forms reciprocal connections with parts of the thalamus which in turn receives input from the basal ganglia, cerebellum, and midbrain. Therefore, ALM projecting thalamus forms a processing hub essential for orofacial movement initiation by linking subcortical structures and ALM (Guo et al. 2017, 2018). Another piece of evidence supporting the role of ALM in licking execution is the fact that ALM pyramidal tract (PT) neurons project to a brainstem center controlling directional licking (Economo et al. 2018) and related areas in the superior colliculus (Rossi et al. 2016). Projection-specific recordings showed that activity consistent with a motor command rose around the movement initiation in PT neurons, but not intratelencephalic (IT) neurons.

To conclude, both *tjM1* and *ALM* seem to be involved in the execution of directional licking, however, the distinction between the licking-related coding represented in *ALM* and/or *tjM1* is yet to be discovered. According to a recent study (Xu et al. 2022), there may be a difference in how the brain encodes information related to different tongue movements. Specifically, it has been suggested that *ALM* (a presumably premotor region involved in tongue movements), is primarily responsible for processing abstract task-related variables, such as the intended direction of a lick and the distance to a reward. In contrast, the areas known as *tjM1* and *tjS1* appear to be more involved in coordinating the specific movements of the tongue during each individual lick, such as the angle, velocity, and length of the tongue's movement (Xu et al. 2022). Further research may shed additional light on the specific anatomical and functional properties of these brain regions, leading to a better understanding of how the brain processes sensorimotor information during goal-directed licking. In order to understand the coding differences between these two brain regions one can design a more demanding behavioral task. It's possible to envision a scenario where an animal must adjust its motor output to a constantly changing environment. Sensorimotor tasks of this nature could provide a valuable means of studying the patterns of neural activity in brain regions responsible for controlling orofacial movements.

5.3 Role of the frontal cortex (PFC) in goal-directed behavior

Where is the whisker sensory information transformed into motor output then? We believe that *wS1* is the first cortical area that processes whisker sensory information by extracting physical features of the stimulus (de Lafuente and Romo 2006; Feldmeyer et al. 2013; Romo and de Lafuente 2013; Takahashi et al. 2016; Stüttgen and Schwarz 2018), and in addition, it extracts categorical decision information that would lead to a decision to lick or not (Kwon et al. 2016a; Yang et al. 2016a; Buetfering et al. 2022). However, the extraction of features from the stimulus along the sensory pathway is likely influenced by top-down modulation from higher cortical areas very early in the pathway (Churchland 1995; Roelfsema et al. 1998; Shuler and Bear 2006; Jaramillo and Zador 2010; Saleem et al. 2013; Stanisor et al. 2013; Banerjee et al. 2020). These intervening decision variables could then influence downstream feature extraction as well as modulate the behavior of the mouse to optimize the performance of the task. At the same time, the performance of sensory decision-making tasks depends on the ability to learn and comprehend the actual rules of the task. These high-level aspects of goal-directed behavior, are thought to involve brain regions such as the prefrontal cortex (PFC) (Pennartz et al. 2011; Euston et al. 2012).

As described before in the introduction (Chapter 1.4) PFC is subdivided into three prefrontal subregions. (1) The dorsomedial PFC (dmPFC), includes the secondary motor cortex, part of which is wM2 and ALM. The functions of ALM in motor planning and execution were covered in a paragraph before, and the functions of wM2 will be covered in the next paragraph. (2) The ventromedial PFC (vmPFC), includes prelimbic (PL) and infralimbic (IL) areas, which I will jointly refer to as the mPFC region. (3) The ventrolateral PFC (vlPFC), includes the medial, ventro-lateral, and lateral divisions of orbitofrontal cortex (OFC).

The mPFC is believed to guide behavior by integrating task-relevant information. Inactivation experiments have shown its necessity for the execution of sensory discrimination tasks in mice (Pinto and Dan 2015; Otis et al. 2017; Lak et al. 2020). A recent study from our laboratory has indicated that the mPFC may play an important role in the learning and maintenance of even simple sensorimotor transformations like whisker detection task (Le Merre et al. 2018). In agreement, here (Chapter 4), I found that optogenetic inactivation of mPFC in the psychophysical detection task also decreased stimulus detection probability, indicating its involvement in the task. However, the precise computations that occur in this region during sensory detection or discrimination tasks remained largely unknown.

To begin with, we have not observed any sensory responses to the whisker stimulus in mPFC in mice that passively received the stimulations that were not predictive of reward (Chapter 4), similar to what was observed in previous studies (Pinto and Dan 2015; Le Merre et al. 2018). However, we observed small responses in Miss trials in trained mice where a whisker stimulus was predicting reward availability. These results again support the hypothesis that mPFC encodes only behaviorally relevant stimuli (Le Merre et al. 2018) and reward predictive cues (Pinto and Dan 2015).

Although mice trained for the psychophysical detection task showed little response to sensory stimuli in the mPFC during Miss trials, this information was enough to predict the presence of the stimulation in comparison with no stimulus trials. In contrast, mPFC neurons revealed strong sensory-driven responses in Hit trials which increased linearly as a stimulus strength increased. Importantly this graded sensory-driven response in mPFC was preserved and appeared before the jaw onset when realigning trials to the lick onset. To sum up we observed little responses in Miss trials and strong and graded responses in Hit trials, which could be entirely explained by movements. There could be several possible explanations for this graded response in Hit trials, mPFC could reflect sensory information about the relevant reward predictive cues (Pinto and Dan 2015; Otis et al. 2017); it can reflect the sensory confidence of the mouse in getting rewards (Lak et al. 2020), or anticipatory coding of upcoming rewards (Lak et al. 2020; Kim et al. 2021; Lui et al. 2021). However, the design of the task did not allow for a deeper understanding of the nature of the graded

response in the mPFC. In order to reveal the correlation between reward and observed graded response in Hit trials in mPFC, one could manipulate the size of the reward (Lak et al. 2020) or omit the reward in some trials.

Our study (Chapter 4) also supports prior research demonstrating that the mPFC plays an important role in choice-related activity during goal-directed behavior (Euston et al. 2012; Pinto and Dan 2015; Esmaeili and Diamond 2019; Kim et al. 2021; Lui et al. 2021). Through careful Hit vs Miss comparison for the near-threshold stimuli in combination with Hit vs Spontaneous Lick analysis, we identified sensory-guided decision neurons. Even though we observed the highest proportion of decision neurons in wS1, mPFC decision neurons revealed marked differential responses with almost no response for Miss trials and Spontaneous licks, and high responses for Hit trials. Our simultaneous recordings of wS1 and mPFC revealed that in some trials the same sensory-evoked responses in wS1 at the population level could still lead to differential behavioral outcomes (evoking Hit or Miss). These trials with similar evoked activity in wS1 still led to stronger evoked activity in Hit trials and smaller evoked activity in Miss trials at the level of mPFC. Suggesting that mPFC likely keeps track of trial outcomes (Huo et al. 2020). In good agreement, the study from Lui et al., revealed that some mPFC neurons encoded the sensory cue (a specific odor), but even more of them encoded sensory stimulus-driven choice of the mouse during a two-alternative choice task. (Lui et al. 2021a). Anticipatory coding of upcoming rewards by individual mPFC neurons was also reported in the membrane potential dynamics in mice performing behaviors in which the sensory stimulus predicted rewards with different delays and with different probabilities. However, it should be noted that the anticipatory activity of mPFC neurons was correlated with anticipatory licking, thus motor-related activity could have contributed to the activity of mPFC (Kim et al. 2021).

Another region of the prefrontal cortex is supposed to play an important role for reward expectation. Indeed, the representation of expected value coding in the orbitofrontal cortex (OFC) is long-standing in the literature and was observed in different species (Sugrue et al. 2005; Lee et al. 2012; Daw 2013). Neurons in OFC are not sensitive to spatial locations of targets linked to specific rewards but rather encode action values related to specific goals or objects (Tremblay and Schultz 1999; Wallis and Miller 2003). One good example is a monkey choosing between two different flavors of juice, in this case, neurons in the OFC signaled the action value functions associated with specific juice flavors and not the directions of eye movements (Padoa-Schioppa and Assad 2006).

However, there is an ongoing debate regarding the OFC's specific function, with some studies emphasizing its role in making current choices (Padoa-Schioppa and Conen 2017), while others highlight its role in learning (Schoenbaum et al. 2009; Song et al. 2017; Miller et al. 2022), or even both (Liu et al. 2020). Researchers have demonstrated that in mice performing a Go/No-Go visual task, the OFC projection to

the visual primary cortex (V1) mediated the outcome-expectancy modulation of V1 responses to the non-rewarded (No-Go) stimulus (Liu et al. 2020). Furthermore, in this study, chronic optogenetic inactivation of OFC projection to V1 impaired, whereas chronic activation of SST interneurons in V1 improved, the learning of the Go/No-Go task, without affecting the immediate choice of the mouse. Thus, OFC top-down projection to V1 seemed to be crucial for driving associative learning. It has been shown also that the OFC propagates reward information to the primary somatosensory cortex (S1) during tactile reversal learning in mice (Banerjee et al. 2020). Hence it will be interesting to record the neuronal activity of OFC in our psychophysical detection task, possibly during learning, and compare its activity with that of mPFC.

Another important function attributed to mPFC in the literature is its involvement in working memory. Persistent activity in mPFC is often reported when the animal needs to hold information for a short amount of time (Liu et al. 2014; Rikhye et al. 2018; Esmaeili and Diamond 2019; Nakajima et al. 2019). In our delayed-licking task (Chapter 2 (Esmaeili et al. 2021)), we did not observe any persistent activity during the delay period in mPFC that could support the maintenance of the motor plan, nonetheless, mPFC optogenetic inactivation had the largest impact on the hit rate across all the tested brain regions. Importantly, mPFC inactivation during all task epochs (including the baseline) impaired mice performance. Lesions of mPFC also produced pronounced deficits in different delayed response tasks in rodents (Brito and Brito 1990; Delatour and Gisquet-Verrier 1996, 1999, 2000; Floresco et al. 1997). This observation suggests that mPFC might not be solely important for some specific step of sensorimotor transformation but rather be related to the representation of the task rules (Durstewitz et al. 2010), behavioral strategy (Powell and Redish 2016) or motivation (Popescu et al. 2016).

Another important conclusion from both the psychophysical (Chapter 4) and the delayed licking (Chapter 2 (Esmaeili et al. 2021)) tasks, was that mPFC activity is strongly modulated by movements. In all groups of mice, trained for the delayed-response task, the psychophysical detection task, and the task with non-rewarded whisker stimuli, licking *per se* evoked large excitation and inhibition. Hence, in the future, it would be important to carefully take into consideration this strong motor component and account for it when interpreting other functions of mPFC.

During my thesis work, I revealed coding properties of mPFC that contribute to our understanding of its functions however it is still unclear whether mPFC provides top-down modulation to the sensory processing pathway that transforms whisker stimulus into motor output, sort of orchestrating the whole behavior; or mPFC is one of the stops on the way of the linear, hierarchical transformation path from wS1 to tJM1. Or maybe both at the same time. Another important question to investigate is how whisker stimulus-driven signals reach the mPFC, as it does not receive important direct axonal projections from wS1; although, some detailed tracing methods have revealed

long-range projections from S1 to L5 neurons in the medial prefrontal cortex (mPFC) (DeNardo et al. 2015). Further tracing and functional connectivity studies will be necessary to fully understand how sensory signals flows and are integrated in mPFC.

5.4 Neuronal circuits for the transformation of whisker stimulus into a goal-directed licking

In the previous sections, I presented our new insights on the processing of whisker sensory information in wS1 and cortical control of licking by tjM1, and how this transformation might be influenced by higher-order frontal regions such as mPFC. However, a critical question remains: how are these two processes linked in goal-directed sensorimotor transformation? In other words, how does sensory information from the whiskers drive the motor response of licking? Although tjM1 receives direct sensory inputs from the tongue/jaw primary sensory cortex, it does not receive input from wS1. Therefore, the transformation of the whisker sensory information into a motor command must transit through other cortical or subcortical areas. How and where in the brain this sensorimotor transformation occurs is a difficult question that doesn't have a clear answer yet, but I will describe the current hypothesis based on previous experiments from the laboratory and our new findings.

A study from our laboratory demonstrated that even during the execution of a simple whisker-based detection task in mice, sensory-related neuronal activity rapidly spreads across multiple cortical areas, reaching the medial prefrontal cortex and dorsal hippocampus with short latencies (< 50 ms) (Le Merre et al. 2018). In our delayed-licking task, we observed as well a sequential activation of many areas: starting with wS1, then wS2, wM1, wM2, DLS, PPC, tjM1, dCA1, ALM, and mPFC based on their mean population latency. Hence, sensorimotor transformation recruits a large network of cortical and subcortical areas that is necessary for converting sensory information into motor commands. Several other studies have demonstrated a broadly distributed representation of task variables across brain regions during goal-directed behavior using high-density electrophysiology, imaging, or both techniques (Allen et al. 2017, 2019; Steinmetz et al. 2019; Stringer et al. 2019)

Transformation of whisker sensory stimulus into goal-directed licking in the cortex starts in wS1/wS2 areas. As I already mentioned wS1 has direct projections to wM1 and to wS2, which forms parallel pathways sending whisker sensory information to these two regions (Kwon et al. 2016; Yamashita and Petersen 2016; Yamashita et al. 2018; Liu et al. 2022). We also know that wS1 and wS2 form feedback loops that might be important for stimulus perception (Kwon et al. 2016; Esmaeili et al. 2020). But much less is known about the long-range output of wS2. We, therefore, identified its relative innervation targets in the frontal cortex (Chapter 3 (Esmaeili et al. 2022)). The results

showed that wS1 innervates largely the frontal cortex in a region labeled wM1, while wS2 axons project to a more anterior region labeled wM2. Thus, we hypothesized that the stimulus-evoked signals from wS1 and wS2 were transmitted to wM1 and wM2 respectively, by parallel anatomical pathways. Then wM2 might project in turn to tjM2/ALM and tjM1 in order to drive licking (Esmaeili et al. 2020). In support of this hypothesis, we demonstrated that wM2 is a key node in converting whisker sensory input to a licking motor output during a delayed-response whisker detection task (Chapter 2 (Esmaeili et al. 2021)): (1) wM2 showed the earliest augmentation of sensory evoked response across the learning of delay detection task compare to other recorded regions, (2) and in addition, decreased across learning response latency. Moreover, (3) after comparing Hit and Miss trials wM2 was the first to exhibit choice-related activity, followed by ALM activation that ramped up during the delay period. ALM activity also became prominent after learning. Even though delay activity was observed in several brain regions it persisted only in the secondary motor cortex including ALM after selecting quiet trials without any movements, presumably encoding motor planning. Hence our results from delay detection task revealed that wM2 and ALM are likely the most important regions for motor planning.

Top-down projections from M2 to sensory areas have been shown to play a crucial role in sensory discrimination across multiple modalities such as vision and forelimb somatosensation (Manita et al. 2015; Zhang et al. 2016). Additionally, M2 has been implicated in an adaptive sensorimotor task that requires mice to shift between multiple auditory-motor mappings in a flexible manner (Siniscalchi et al. 2016). Therefore, M2 may provide top-down feedback to S1/S2 to emphasize or attenuate incoming sensory input.

As mentioned in our recent review (Esmaeili et al. 2020), in order to achieve this routing of the signal from wS1/wS2 to wM2, ALM, and tjM1 the synaptic connections between the neuronal circuits need to be altered through reward-based learning, with numerous cortical and subcortical regions likely involved, utilizing various neurotransmitters. One such neurotransmitter is acetylcholine, which has been demonstrated to increase in the cortex in response to reward-related signals (Hangya et al. 2015).

Another crucial neurotransmitter to consider is dopamine, as its activity in midbrain dopaminergic neurons has been linked to reward signals in the brain. In response to unexpected rewards, there is a transient increase in the activity of midbrain dopaminergic neurons, which have prominent projections to the striatum. Dopaminergic signaling can affect synaptic plasticity in the striatum by acting on dopamine type 1 receptors (D1Rs), promoting long-term potentiation of glutamatergic synaptic input onto direct pathway striatonigral projection neurons (dSPNs), which helps reinforce rewarded behaviors. In the context of the whisker detection task, enhanced sensory signals were found in D1R-expressing dSPNs compared to the

D2R-expressing indirect pathway striatopallidal neurons (Sippy et al. 2015, 2021). Finally, but never the less very important, the aforementioned flow of activity is likely being under the direct control of higher-order brain areas such as the mPFC and the hippocampus (Le Merre et al. 2018).

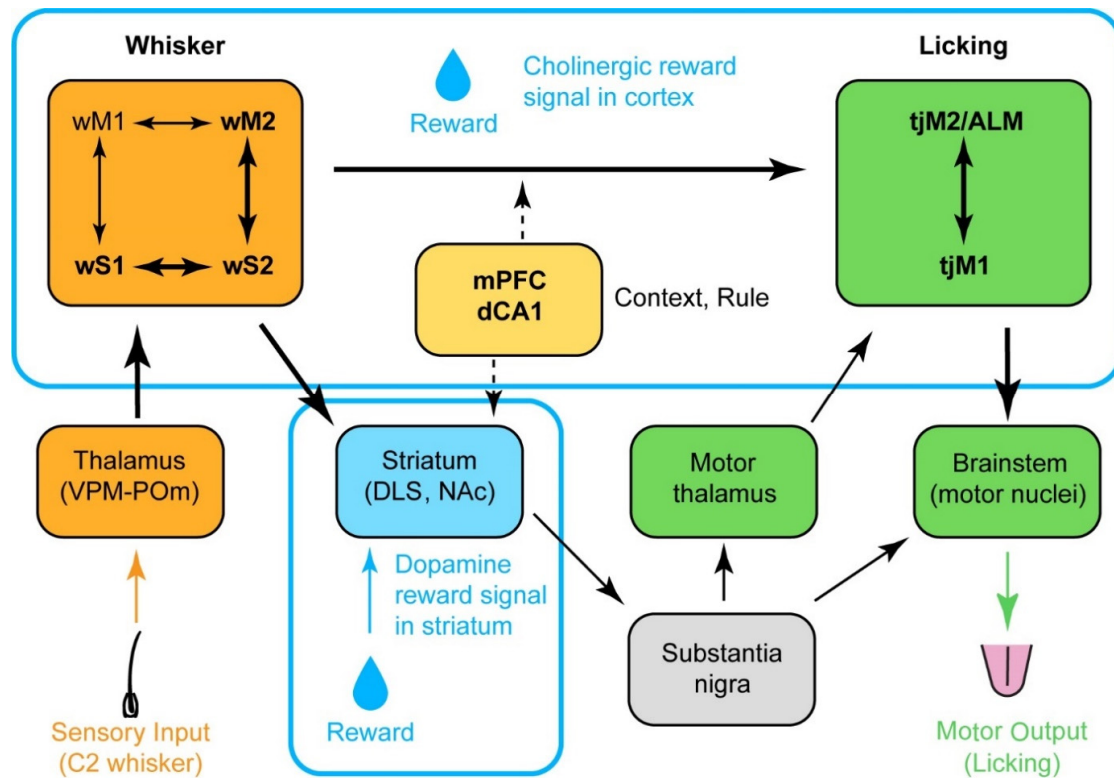


Figure 5.1. Pathways underlying transformation of whisker stimulus into a goal-directed licking

Several cortical and subcortical circuits are involved in the sensorimotor transformation of a whisker sensory input to licking motor output. Whisker module that includes reciprocally connected parallel pathways wS1, wS2, and wM1, wM2 which process sensory whisker information that is streamed from the Thalamus. The licking module includes tjM2/ALM and tjM1 areas that plan and execute the licking motor output, which is routed to the brainstem motor nuclei, which in turn control motor neurons. The flow of the signal is under the direct control of higher-order brain areas like the mPFC and the hippocampus which might set the context and rules of the detection task. These complex interactions are modulated by acetylcholine reward signals in the cortex, and by dopamine reward signals in the striatum, which could be important for learning and plasticity.

Above I provided insights into the current understanding of cortical neural circuits and their mechanisms that underlie simple sensorimotor transformations in goal-directed behaviors. Although the neocortex and striatum play a critical role in this process, it is probable that several other subcortical regions, such as the midbrain, brainstem, colliculus, and cerebellum, also contribute significantly to sensorimotor transformations. However, further research is needed to gain a comprehensive

understanding of these regions' involvement. Moreover, the investigation of complex tasks that incorporate delays and directional licking can be beneficial in disentangling sensory processing, decision-making, and motor commands, thereby aiding in a better understanding of the underlying neural processes.

To sum up, simple sensorimotor transformations of a whisker stimulus to licking during reward-based learning are recruiting different excitatory, inhibitory, and neuromodulatory cortical and subcortical neuronal circuits which are still to be discovered and fully characterized

5.5 Closing remarks

The transformation of sensory input into goal-directed motor output is a fundamental process in the brain, yet its underlying neocortical circuits remain highly unknown. Understanding these highly interconnected neural networks is a major objective of modern neuroscience. As demonstrated in this thesis, solving this multifaceted problem requires careful examination of the activity of many brain areas, careful analysis of movements of the subject, and designing more and more elaborated behaviors that would include delayed licking or psychophysics. However, the continuous development of technology provides additional tools for future research, and the years to come may revolutionize our current knowledge of the mammalian brain. Advancements in electrophysiological and imaging techniques, optogenetics, and other cutting-edge tools will undoubtedly aid in these efforts.

This work sheds light on the fundamental and sophisticated neural computations performed by the mouse neocortex and the findings presented in this thesis provide a crucial piece of the puzzle and move us closer to a more comprehensive understanding of neocortical functions.

Future studies should focus on describing with high spatial and temporal resolution how sensory information flows between brain areas and is gradually transformed into motor command. Understanding functional connectivity between areas during a specific behavioral task is still a challenge in modern neuroscience. It has been addressed using wide-field imaging of the dorsal neocortex, allowing observation of progressive propagation of signals in time (Allen et al. 2017; Musall et al. 2019; Engel et al. 2021; Gallero-Salas et al. 2021), however, the deeper cortical structure like mPFC cannot be observed in such a way. One possibility to answer this question would be to map functional connectivity with high-density extracellular recording probes simultaneously from a big number of brain regions (Steinmetz et al. 2019; Huo et al. 2020). The advantage of silicon probes with multi-recording channels is the possibility to collect neural activity from a big population of neurons (Jun et al. 2017). A combination of recordings of hundreds of neurons simultaneously with

optogenetic perturbations would allow us to better dissect the functional circuit involved in the sensorimotor transformation. An important approach would be to use an optotagging technique to understand the projection targets of neurons, and to understand which exact information is transmitted from one region to another. The final ultimate goal would be to address more precisely the response of mPFC neurons depending upon their cell type, location, and projection targets in order to solve the puzzle of mPFC heterogeneous coding of task relevant variables.

Another must-have for all future experiments is the careful monitoring of orofacial movements. More and more studies show that uninstructed movements can explain neuronal activity better than task-related variables, and that task-relevant information is embedded on top of movement information coding (Musall et al. 2014; Steinmetz et al. 2019). This makes a lot of sense because it is crucial for the brain to have information about the position of the body in space. Careful movement monitoring becoming an important routine and advances in machine learning algorithms for tracking the position of different body parts on the video (Mathis et al. 2018) provide a precise reconstruction of the body in time and space.

References

- Abbe E. 2018. Community Detection and Stochastic Block Models. now Publishers Inc.
- Adibi M. 2019. Whisker-mediated touch system in rodents: from neuron to behavior. *Front Syst Neurosci.* 13:40.
- Ahl AS. 1986. The role of vibrissae in behavior: A status review. *Vet Res Commun.* 10:245–268.
- Ährlund-Richter S, Xuan Y, van Lunteren JA, Kim H, Ortiz C, Pollak Dorocic I, Meletis K, Carlén M. 2019. A whole-brain atlas of monosynaptic input targeting four different cell types in the medial prefrontal cortex of the mouse. *Nat Neurosci.* 22:657–668.
- Alexander GE, Crutcher MD. 1990. Functional architecture of basal ganglia circuits: neural substrates of parallel processing. *Trends Neurosci.* 13:266–271.
- Allen WE, Chen MZ, Pichamoorthy N, Tien RH, Pachitariu M, Luo L, Deisseroth K. 2019. Thirst regulates motivated behavior through modulation of brainwide neural population dynamics. *Science.* 364:eaav3932.
- Allen WE, Kauvar IV, Chen MZ, Richman EB, Yang SJ, Chan K, Gradinaru V, Deverman BE, Luo L, Deisseroth K. 2017a. Global Representations of Goal-Directed Behavior in Distinct Cell Types of Mouse Neocortex. *Neuron.* 94:891-907.e6.
- Alvarez M, Zainos A, Romo R. 2015. Decoding stimulus features in primate somatosensory cortex during perceptual categorization. *Proc Natl Acad Sci U A.* 112:4773–4778.
- Ames KC, Ryu SI, Shenoy KV. 2014. Neural Dynamics of Reaching Following Incorrect or Absent Motor Preparation. *Neuron.* 81:438–451.
- Amodio DM, Frith CD. 2006. Meeting of minds: the medial frontal cortex and social cognition. *Nat Rev Neurosci.* 7:268–277.
- Anastasiades PG, Collins DP, Carter AG. 2021. Mediodorsal and Ventromedial Thalamus Engage Distinct L1 Circuits in the Prefrontal Cortex. *Neuron.* 109:314-330.e4.
- Andermann ML, Kerlin AM, Roumis DK, Glickfeld LL, Reid RC. 2011. Functional specialization of mouse higher visual cortical areas. *Neuron.* 72:1025–1039.
- Andermann ML, Ritt J, Neimark MA, Moore CI. 2004. Neural Correlates of Vibrissa Resonance: Band-Pass and Somatotopic Representation of High-Frequency Stimuli. *Neuron.* 42:451–463.
- Antoine MW, Langberg T, Schnepel P, Feldman DE. 2019. Increased Excitation-Inhibition Ratio Stabilizes Synapse and Circuit Excitability in Four Autism Mouse Models. *Neuron.* 101:648-661.e4.
- Arabzadeh E, Zorzin E, Diamond ME. 2005. Neuronal Encoding of Texture in the Whisker Sensory Pathway. *PLOS Biol.* 3:e17.
- Aronoff R, Matyas F, Mateo C, Ciron C, Schneider B, Petersen CCH. 2010a. Long-range connectivity of mouse primary somatosensory barrel cortex. *Eur J Neurosci.* 31:2221–2233.
- Aruljothi K, Marrero K, Zhang Z, Zareian B, Zagha E. 2020. Functional Localization of an Attenuating Filter within Cortex for a Selective Detection Task in Mice. *J Neurosci.* 40:5443–5454.
- Auffret M, Ravano VL, Rossi GMC, Hankov N, Petersen MFA, Petersen CCH. 2018. Optogenetic Stimulation of Cortex to Map Evoked Whisker Movements in Awake Head-Restrained Mice. *Neuroscience.* 368:199.
- Avermann M, Tomm C, Mateo C, Gerstner W, Petersen CCH. 2012. Microcircuits of excitatory and inhibitory neurons in layer 2/3 of mouse barrel cortex. *J Neurophysiol.* 107:3116–3134.
- Avitan L, Stringer C. 2022. Not so spontaneous: Multi-dimensional representations of behaviors and context in sensory areas. *Neuron.* 110:3064–3075.
- Ayaz A, Stauble A, Hamada M, Wulf MA, Saleem AB, Helmchen F. 2019. Layer-specific integration of locomotion and sensory information in mouse barrel cortex. *Nat Commun.* 10:2585.
- Bagnall MW, Hull C, Bushong EA, Ellisman MH, Scanziani M. 2011. Multiple clusters of release sites formed by individual thalamic afferents onto cortical interneurons ensure reliable transmission. *Neuron.* 71:180–194.

- Baker A, Kalmbach B, Morishima M, Kim J, Juavinett A, Li N, Dembrow N. 2018. Specialized Subpopulations of Deep-Layer Pyramidal Neurons in the Neocortex: Bridging Cellular Properties to Functional Consequences. *J Neurosci.* 38:5441–5455.
- Banerjee A, Parente G, Teutsch J, Lewis C, Voigt FF, Helmchen F. 2020. Value-guided remapping of sensory cortex by lateral orbitofrontal cortex. *Nature.* 585:245–250.
- Banerjee A, Wang BA, Teutsch J, Helmchen F, Pleger B. 2023. Analogous cognitive strategies for tactile learning in the rodent and human brain. *Prog Neurobiol.* 222:102401.
- Bar NS, Skogestad S, Marçal JM, Ulanovsky N, Yovel Y. 2015. A Sensory-Motor Control Model of Animal Flight Explains Why Bats Fly Differently in Light Versus Dark. *PLoS Biol.* 13:e1002046.
- Barrett JM, Martin ME, Shepherd GMG. 2022. Manipulation-specific cortical activity as mice handle food. *Curr Biol.* 32:4842–4853.e6.
- Barthas F, Kwan AC. 2017. Secondary Motor Cortex: Where ‘Sensory’ Meets ‘Motor’ in the Rodent Frontal Cortex. *Trends Neurosci.* 40:181–193.
- Beier KT, Steinberg EE, DeLoach KE, Xie S, Miyamichi K, Schwarz L, Gao XJ, Kremer EJ, Malenka RC, Luo L. 2015. Circuit Architecture of VTA Dopamine Neurons Revealed by Systematic Input-Output Mapping. *Cell.* 162:622–634.
- Benjamini Y, Hochberg Y. 1995. Controlling the False Discovery Rate: A Practical and Powerful Approach to Multiple Testing. *J R Stat Soc Ser B Methodol.* 57:289–300.
- Berens P. 2009. CircStat: A MATLAB Toolbox for Circular Statistics. *J Stat Softw.* 31:1–21.
- Berg RW, Kleinfeld D. 2003. Rhythmic Whisking by Rat: Retraction as Well as Protraction of the Vibrissae Is Under Active Muscular Control. *J Neurophysiol.* 89:104–117.
- Bethge P, Carta S, Lorenzo DA, Egolf L, Goniotaki D, Madisen L, Voigt FF, Chen JL, Schneider B, Ohkura M, Nakai J, Zeng H, Aguzzi A, Helmchen F. 2017. An R-CaMP1.07 reporter mouse for cell-type-specific expression of a sensitive red fluorescent calcium indicator. *PLoS One.* 12:e0179460–e0179460.
- Bisley JW, Goldberg ME. 2006. Neural Correlates of Attention and Distractibility in the Lateral Intraparietal Area. *J Neurophysiol.* 95:1696–1717.
- Boothe R. 2021. Signal Detection Theory, Part 1. CodeX.
- Brecht M. 2007. Barrel cortex and whisker-mediated behaviors. *Curr Opin Neurobiol.* 17:408–416.
- Brecht M, Preilowski B, Merzenich MM. 1997. Functional architecture of the mystacial vibrissae. *Behav Brain Res.* 84:81–97.
- Brecht M, Roth A, Sakmann B. 2003. Dynamic receptive fields of reconstructed pyramidal cells in layers 3 and 2 of rat somatosensory barrel cortex. *J Physiol.* 553:243–265.
- Brecht M, Sakmann B. 2002. Dynamic representation of whisker deflection by synaptic potentials in spiny stellate and pyramidal cells in the barrels and septa of layer 4 rat somatosensory cortex. *J Physiol.* 543:49–70.
- Brecht M, Schneider M, Sakmann B, Margrie TW. 2004. Whisker movements evoked by stimulation of single pyramidal cells in rat motor cortex. *Nature.* 427:704–710.
- Brito GNO, Brito LSO. 1990. Septohippocampal system and the prelimbic sector of frontal cortex: A neuropsychological battery analysis in the rat. *Behav Brain Res.* 36:127–146.
- Britten KH, Shadlen MN, Newsome WT, Movshon JA. 1992. The analysis of visual motion: a comparison of neuronal and psychophysical performance. *J Neurosci Off J Soc Neurosci.* 12:4745–4765.
- Brockett AT, Tennyson SS, deBettencourt CA, Kallmyer M, Roesch MR. 2022. Medial prefrontal cortex lesions disrupt prepotent action selection signals in dorsomedial striatum. *Curr Biol.* 32:3276–3287.e3.
- Bruce V, Green PR, Georgeson MA. 2003. Visual Perception: Physiology, Psychology, & Ecology. Psychology Press.
- Buetfering C, Zhang Z, Pitsiani M, Smallridge J, Boven E, McElligott S, Häusser M. 2022. Behaviorally relevant decision coding in primary somatosensory cortex neurons. *Nat Neurosci.* 25:1225–1236.

- Burt C. 1960. GUSTAV THEODOR FECHNER ELEMENTE DER PSYCHOPHYSIK 1860. *Br J Stat Psychol.* 13:1–10.
- Buse A. 1982. The Likelihood Ratio, Wald, and Lagrange Multiplier Tests: An Expository Note. *Am Stat.* 36:153–157.
- Butovas S, Schwarz C. 2007. Detection psychophysics of intracortical microstimulation in rat primary somatosensory cortex. *Eur J Neurosci.* 25:2161–2169.
- Buzsáki G. 2004. Large-scale recording of neuronal ensembles. *Nat Neurosci.* 7:446–451.
- Carandini M, Churchland AK. 2013. Probing perceptual decisions in rodents. *Nat Neurosci.* 16:824–831.
- Cardin JA. 2018. Inhibitory Interneurons Regulate Temporal Precision and Correlations in Cortical Circuits. *Trends Neurosci.* 41:689–700.
- Ceballo S, Piwowska Z, Bourg J, Daret A, Bathellier B. 2019. Targeted Cortical Manipulation of Auditory Perception. *Neuron.* 104:1168–1179.e5.
- Chabrol FP, Blot A, Mrcic-Flogel TD. 2019a. Cerebellar Contribution to Preparatory Activity in Motor Neocortex. *Neuron.* 103:506–519.e4.
- Chen JL, Carta S, Soldado-Magraner J, Schneider BL, Helmchen F. 2013a. Behaviour-dependent recruitment of long-range projection neurons in somatosensory cortex. *Nature.* 499:336–340.
- Chen JL, Margolis DJ, Stankov A, Sumanovski LT, Schneider BL, Helmchen F. 2015. Pathway-specific reorganization of projection neurons in somatosensory cortex during learning. *Nat Neurosci.* 18:1101–1108.
- Chen JL, Voigt FF, Javadzadeh M, Krueppel R, Helmchen F. 2016. Long-range population dynamics of anatomically defined neocortical networks. *eLife.* 5:e14679.
- Chen SX, Kim AN, Peters AJ, Komiyama T. 2015. Subtype-specific plasticity of inhibitory circuits in motor cortex during motor learning. *Nat Neurosci.* 18:1109–1115.
- Chen T-W, Li N, Daie K, Svoboda K. 2017. A Map of Anticipatory Activity in Mouse Motor Cortex. *Neuron.* 94:866–879.e4.
- Chikazoe J, Jimura K, Hirose S, Yamashita K, Miyashita Y, Konishi S. 2009. Preparation to inhibit a response complements response inhibition during performance of a stop-signal task. *J Neurosci Off J Soc Neurosci.* 29:15870–15877.
- Chittajallu R, Isaac JTR. 2010. Emergence of cortical inhibition by coordinated sensory-driven plasticity at distinct synaptic loci. *Nat Neurosci.* 13:1240–1248.
- Churchland MM, Yu BM, Cunningham JP, Sugrue LP, Cohen MR, Corrado GS, Newsome WT, Clark AM, Hosseini P, Scott BB, Bradley DC, Smith MA, Kohn A, Movshon JA, Armstrong KM, Moore T, Chang SW, Snyder LH, Lisberger SG, Priebe NJ, Finn IM, Ferster D, Ryu SI, Santhanam G, Sahani M, Shenoy KV. 2010. Stimulus onset quenches neural variability: a widespread cortical phenomenon. *Nat Neurosci.* 13:369–378.
- Churchland P. 1995. Large-scale neuronal theories of the brain. *Comput Amp Math Appl.*
- Cohen O, Sherman E, Zinger N, Perlmutter S, Prut Y. 2010. Getting ready to move: transmitted information in the corticospinal pathway during preparation for movement. *Curr Opin Neurobiol.* 20:696–703.
- Cover TM, Thomas JA. 1991a. Elements of information theory, Wiley series in telecommunications. New York: Wiley.
- Creem-Regehr SH. 2009. Sensory-motor and cognitive functions of the human posterior parietal cortex involved in manual actions. *Neurobiol Learn Mem, Special Issue: Parietal Cortex.* 91:166–171.
- Crochet S, Lee S-H, Petersen CCH. 2019. Neural Circuits for Goal-Directed Sensorimotor Transformations. *Trends Neurosci.* 42:66–77.
- Crochet S, Petersen CCH. 2006. Correlating whisker behavior with membrane potential in barrel cortex of awake mice. *Nat Neurosci.* 9:608–610.
- Crochet S, Poulet JF, Kremer Y, Petersen CC. 2011. Synaptic mechanisms underlying sparse coding of active touch. *Neuron.* 69:1160–1175.

- Cruikshank SJ, Lewis TJ, Connors BW. 2007. Synaptic basis for intense thalamocortical activation of feedforward inhibitory cells in neocortex. *Nat Neurosci.* 10:462–468.
- Cruz KG, Leow YN, Le NM, Adam E, Huda R, Sur M. 2023. Cortical-subcortical interactions in goal-directed behavior. *Physiol Rev.* 103:347–389.
- Cul AD, Baillet S, Dehaene S. 2007. Brain Dynamics Underlying the Nonlinear Threshold for Access to Consciousness. *PLOS Biol.* 5:e260.
- Cunningham JP, Yu BM, Shenoy KV, Sahani M. 2007. Inferring Neural Firing Rates from Spike Trains Using Gaussian Processes. In: Platt J,, Koller D,, Singer Y,, Roweis S, editors. *Advances in Neural Information Processing Systems*. Curran Associates, Inc.
- Cutts CS, Eglén SJ. 2014. Detecting pairwise correlations in spike trains: an objective comparison of methods and application to the study of retinal waves. *J Neurosci Off J Soc Neurosci.* 34:14288–14303.
- Dacre J, Colligan M, Clarke T, Ammer JJ, Schiemann J, Chamosa-Pino V, Claudi F, Harston JA, Eleftheriou C, Pakan JMP, Huang C-C, Hantman AW, Rochefort NL, Duguid I. 2021. A cerebellar-thalamocortical pathway drives behavioral context-dependent movement initiation. *Neuron.* 109:2326–2338.e8.
- Dahmen J, Kayaalp ME, Ollivier M, Pareek A, Hirschmann MT, Karlsson J, Winkler PW. 2023. Artificial intelligence bot ChatGPT in medical research: the potential game changer as a double-edged sword. *Knee Surg Sports Traumatol Arthrosc.*
- Daw ND. 2013. Neuroeconomics: Chapter 16. *Advanced Reinforcement Learning*. Elsevier Inc. Chapters.
- De Lafuente V, Romo R. 2005a. Neuronal correlates of subjective sensory experience. *Nat Neurosci.* 8:1698–1703.
- De Lafuente V, Romo R. 2006. Neural correlate of subjective sensory experience gradually builds up across cortical areas. *Proc Natl Acad Sci U S A.* 103:14266–14271.
- DeCarlo LT. 1998. Signal detection theory and generalized linear models. *Psychol Methods.* 3:186.
- Dehaene S, Changeux J-P. 2011. Experimental and Theoretical Approaches to Conscious Processing. *Neuron.* 70:200–227.
- Delatour B, Gisquet-Verrier P. 1996. Prelimbic cortex specific lesions disrupt delayed-variable response tasks in the rat. *Behav Neurosci.* 110:1282–1298.
- Delatour B, Gisquet-Verrier P. 1999. Lesions of the prelimbic-infralimbic cortices in rats do not disrupt response selection processes but induce delay-dependent deficits: Evidence for a role in working memory? *Behav Neurosci.* 113:941–955.
- Delatour B, Gisquet-Verrier P. 2000. Functional role of rat prelimbic-infralimbic cortices in spatial memory: evidence for their involvement in attention and behavioural flexibility. *Behav Brain Res.* 109:113–128.
- Delevich K, Tucciarone J, Huang ZJ, Li B. 2015. The mediodorsal thalamus drives feedforward inhibition in the anterior cingulate cortex via parvalbumin interneurons. *J Neurosci Off J Soc Neurosci.* 35:5743–5753.
- DeNardo LA, Berns DS, DeLoach K, Luo L. 2015. Connectivity of mouse somatosensory and prefrontal cortex examined with trans-synaptic tracing. *Nat Neurosci.* 18:1687–1697.
- Deschênes M, Timofeeva E, Lavallée P. 2003. The Relay of High-Frequency Sensory Signals in the Whisker-to-Barreloid Pathway. *J Neurosci.* 23:6778–6787.
- Diamond ME, Arabzadeh E. 2013. Whisker sensory system – From receptor to decision. *Prog Neurobiol.* 103:28–40.
- Diamond ME, von Heimendahl M, Knutsen PM, Kleinfeld D, Ahissar E. 2008a. “Where” and “what” in the whisker sensorimotor system. *Nat Rev Neurosci.* 9:601–612.
- Ding L, Gold JJ. 2010. Caudate Encodes Multiple Computations for Perceptual Decisions. *J Neurosci.* 30:15747–15759.
- Duque J, Greenhouse I, Labruna L, Ivry RB. 2017. Physiological Markers of Motor Inhibition during Human Behavior. *Trends Neurosci.* 40:219–236.

- Durstewitz D, Vitoz NM, Floresco SB, Seamans JK. 2010. Abrupt Transitions between Prefrontal Neural Ensemble States Accompany Behavioral Transitions during Rule Learning. *Neuron*. 66:438–448.
- Ebbesen CL, Doron G, Lenschow C, Brecht M. 2017. Vibrissa motor cortex activity suppresses contralateral whisking behavior. *Nat Neurosci*. 20:82–89.
- Economo MN, Viswanathan S, Tasic B, Bas E, Winnubst J, Menon V, Graybiel LT, Nguyen TN, Smith KA, Yao Z, Wang L, Gerfen CR, Chandrashekar J, Zeng H, Looger LL, Svoboda K. 2018a. Distinct descending motor cortex pathways and their roles in movement. *Nature*. 563:79–84.
- Egger R, Narayanan RT, Guest JM, Bast A, Udvardy D, Messori LF, Das S, de Kock CPJ, Oberlaender M. 2020. Cortical Output Is Gated by Horizontally Projecting Neurons in the Deep Layers. *Neuron*. 105:122–137.e8.
- Eimer M. 1993. Effects of attention and stimulus probability on ERPs in a Go/Nogo task. *Biol Psychol*. 35:123–138.
- El-Boustani S, Sermet BS, Foustoukos G, Oram TB, Yizhar O, Petersen CCH. 2020. Anatomically and functionally distinct thalamocortical inputs to primary and secondary mouse whisker somatosensory cortices. *Nat Commun*. 11:3342.
- Else H. 2023. Abstracts written by ChatGPT fool scientists. *Nature*. 613:423–423.
- Emken JL, Benitez R, Reinkensmeyer DJ. 2007. Human-robot cooperative movement training: Learning a novel sensory motor transformation during walking with robotic assistance-as-needed. *J NeuroEngineering Rehabil*. 4:8.
- Engel TA, Schölvink ML, Lewis CM. 2021. The diversity and specificity of functional connectivity across spatial and temporal scales. *NeuroImage*. 245:118692.
- Engelhard B, Finkelstein J, Cox J, Fleming W, Jang HJ, Ornelas S, Koay SA, Thiberge SY, Daw ND, Tank DW, Witten IB. 2019. Specialized coding of sensory, motor and cognitive variables in VTA dopamine neurons. *Nature*. 570:509–513.
- Erllich JC, Bialek M, Brody CD. 2011. A cortical substrate for memory-guided orienting in the rat. *Neuron*. 72:330–343.
- Esmaili V, Diamond ME. 2019a. Neuronal Correlates of Tactile Working Memory in Prefrontal and Vibrissa Somatosensory Cortex. *Cell Rep*. 27:3167–3181.e5.
- Esmaili V, Oryshchuk A, Asri R, Tamura K, Foustoukos G, Liu Y, Guet R, Crochet S, Petersen CCH. 2022. Learning-related congruent and incongruent changes of excitation and inhibition in distinct cortical areas. *PLOS Biol*. 20:e3001667.
- Esmaili V, Tamura K, Foustoukos G, Oryshchuk A, Crochet S, Petersen CC. 2020a. Cortical circuits for transforming whisker sensation into goal-directed licking. *Curr Opin Neurobiol*, Whole-brain interactions between neural circuits. 65:38–48.
- Esmaili V, Tamura K, Muscinelli SP, Modirshanechi A, Boscaglia M, Lee AB, Oryshchuk A, Foustoukos G, Liu Y, Crochet S, Gerstner W, Petersen CCH. 2021a. Rapid suppression and sustained activation of distinct cortical regions for a delayed sensory-triggered motor response. *Neuron*. 109:2183–2201.e9.
- Euston DR, Gruber AJ, McNaughton BL. 2012a. The Role of Medial Prefrontal Cortex in Memory and Decision Making. *Neuron*. 76:1057–1070.
- Fassihi A, Akrami A, Pulecchi F, Schönfelder V, Diamond ME. 2017. Transformation of Perception from Sensory to Motor Cortex. *Curr Biol*. 27:1585–1596.e6.
- Fechner GT. 1948. Elements of psychophysics, 1860. In: Readings in the history of psychology. Century psychology series. East Norwalk, CT, US: Appleton-Century-Crofts. p. 206–213.
- Feldmeyer D, Brecht M, Helmchen F, Petersen CC, Poulet JF, Staiger JF, Luhmann HJ, Schwarz C. 2013a. Barrel cortex function. *Prog Neurobiol*. 103:3–27.
- Ferezou I, Haiss F, Gentet LJ, Aronoff R, Weber B, Petersen CCH. 2007a. Spatiotemporal Dynamics of Cortical Sensorimotor Integration in Behaving Mice. *Neuron*. 56:907–923.
- Ferrero DM, Lemon JK, Flügge D, Pashkovski SL, Korzan WJ, Datta SR, Spehr M, Fendt M, Liberles SD. 2011. Detection and avoidance of a carnivore odor by prey. *Proc Natl Acad Sci*. 108:11235–11240.

- Floresco SB, Seamans JK, Phillips AG. 1997. Selective roles for hippocampal, prefrontal cortical, and ventral striatal circuits in radial-arm maze tasks with or without a delay. *J Neurosci*. 17:1880–1890.
- Francis NA, Mukherjee S, Koçillari L, Panzeri S, Babadi B, Kanold PO. 2022. Sequential transmission of task-relevant information in cortical neuronal networks. *Cell Rep*. 39:110878.
- Freund TF, Katona I. 2007. Perisomatic inhibition. *Neuron*. 56:33–42.
- Fritsch G, Hitzig E. 1870. Über die elektrische Erregbarkeit des Grosshirns *Archiv für Anatomie. Physiol Wiss Med*. 300–332.
- Froemke RC. 2015. Plasticity of cortical excitatory-inhibitory balance. *Annu Rev Neurosci*. 38:195–219.
- Fu Y, Tucciarone JM, Espinosa JS, Sheng N, Darcy DP, Nicoll RA, Huang ZJ, Stryker MP. 2014. A cortical circuit for gain control by behavioral state. *Cell*. 156:1139–1152.
- Funahashi S, Bruce CJ, Goldman-Rakic PS. 1989. Mnemonic coding of visual space in the monkey's dorsolateral prefrontal cortex. *J Neurophysiol*. 61:331–349.
- Fuster JM, Alexander GE. 1971. Neuron Activity Related to Short-Term Memory. *Science*. 173:652–654.
- Fuster JM, Bodner M, Kroger JK. 2000. Cross-modal and cross-temporal association in neurons of frontal cortex. *Nature*. 405:347–351.
- Gabernet L, Jadhav SP, Feldman DE, Carandini M, Scanziani M. 2005. Somatosensory integration controlled by dynamic thalamocortical feed-forward inhibition. *Neuron*. 48:315–327.
- Gainey MA, Aman JW, Feldman DE. 2018. Rapid Disinhibition by Adjustment of PV Intrinsic Excitability during Whisker Map Plasticity in Mouse S1. *J Neurosci Off J Soc Neurosci*. 38:4749–4761.
- Gallero-Salas Y, Han S, Sych Y, Voigt FF, Laurenczy B, Gilad A, Helmchen F. 2021a. Sensory and Behavioral Components of Neocortical Signal Flow in Discrimination Tasks with Short-Term Memory. *Neuron*. 109:135–148.e6.
- Gao Z, Davis C, Thomas AM, Economo MN, Abrego AM, Svoboda K, De Zeeuw CI, Li N. 2018a. A cortico-cerebellar loop for motor planning. *Nature*. 563:113–116.
- Garion L, Dubin U, Rubin Y, Khateb M, Schiller Y, Azouz R, Schiller J. 2014. Texture coarseness responsive neurons and their mapping in layer 2–3 of the rat barrel cortex in vivo. *eLife*. 3:e03405.
- Gasselin C, Hohl B, Vernet A, Crochet S, Petersen CCH. 2021. Cell-type-specific nicotinic input disinhibits mouse barrel cortex during active sensing. *Neuron*. 109:778–787.e3.
- Georgopoulos AP, Ashe J, Smyrnis N, Taira M. 1992. The Motor Cortex and the Coding of Force. *Science*. 256:1692–1695.
- Gerdjikov TV, Bergner CG, Stüttgen MC, Waiblinger C, Schwarz C. 2010. Discrimination of vibrotactile stimuli in the rat whisker system: behavior and neurometrics. *Neuron*. 65:530–540.
- Gerstner W, Kistler WM, Naud R, Paninski L. 2014. *Neuronal dynamics: From single neurons to networks and models of cognition*. Cambridge University Press.
- Gilad A, Gallero-Salas Y, Groos D, Helmchen F. 2018a. Behavioral Strategy Determines Frontal or Posterior Location of Short-Term Memory in Neocortex. *Neuron*. 99:814–828.e7.
- Gilbert CD, Li W. 2013. Top-down influences on visual processing. *Nat Rev Neurosci*. 14:350–363.
- Gimenez TL, Lorenc M, Jaramillo S. 2015. Adaptive categorization of sound frequency does not require the auditory cortex in rats. *J Neurophysiol*. 114:1137–1145.
- Goard MJ, Pho GN, Woodson J, Sur M. 2016. Distinct roles of visual, parietal, and frontal motor cortices in memory-guided sensorimotor decisions. *eLife*. 5:e13764.
- Gold JI, Shadlen MN. 2002. Banburismus and the Brain: Decoding the Relationship between Sensory Stimuli, Decisions, and Reward. *Neuron*. 36:299–308.
- Goldstein EB, Brockmole JR. 2017. *Sensation and Perception*. Cengage Learning Asia Pte Limited.
- Gomez P, Ratcliff R, Perea M. 2007. A Model of the Go/No-Go Task. *J Exp Psychol Gen*. 136:389–413.

- Gong S, Doughty M, Harbaugh CR, Cummins A, Hatten ME, Heintz N, Gerfen CR. 2007. Targeting Cre recombinase to specific neuron populations with bacterial artificial chromosome constructs. *J Neurosci Off J Soc Neurosci*. 27:9817–9823.
- Gorski JA, Talley T, Qiu M, Puelles L, Rubenstein JLR, Jones KR. 2002. Cortical excitatory neurons and glia, but not GABAergic neurons, are produced in the Emx1-expressing lineage. *J Neurosci Off J Soc Neurosci*. 22:6309–6314.
- Guo K, Yamawaki N, Svoboda K, Shepherd GMG. 2018. Anterolateral Motor Cortex Connects with a Medial Subdivision of Ventromedial Thalamus through Cell Type-Specific Circuits, Forming an Excitatory Thalamo-Cortico-Thalamic Loop via Layer 1 Apical Tuft Dendrites of Layer 5B Pyramidal Tract Type Neurons. *J Neurosci Off J Soc Neurosci*. 38:8787–8797.
- Guo ZV, Inagaki HK, Daie K, Druckmann S, Gerfen CR, Svoboda K. 2017a. Maintenance of persistent activity in a frontal thalamocortical loop. *Nature*. 545:181–186.
- Guo ZV, Li N, Huber D, Ophir E, Gutnisky D, Ting JT, Feng G, Svoboda K. 2014a. Flow of cortical activity underlying a tactile decision in mice. *Neuron*. 81:179–194.
- Haber SN, Liu H, Seidlitz J, Bullmore E. 2022. Prefrontal connectomics: from anatomy to human imaging. *Neuropsychopharmacology*. 47:20–40.
- Haider B, Häusser M, Carandini M. 2013. Inhibition dominates sensory responses in the awake cortex. *Nature*. 493:97–100.
- Han Y, Kebschull JM, Campbell RAA, Cowan D, Imhof F, Zador AM, Mrsic-Flogel TD. 2018a. The logic of single-cell projections from visual cortex. *Nature*. 556:51–56.
- Hangya B, Ranade SP, Lorenc M, Kepecs A. 2015a. Central Cholinergic Neurons Are Rapidly Recruited by Reinforcement Feedback. *Cell*. 162:1155–1168.
- Hanks TD, Kopec CD, Brunton BW, Duan CA, Erlich JC, Brody CD. 2015. Distinct relationships of parietal and prefrontal cortices to evidence accumulation. *Nature*. 520:220–223.
- Harris JA, Mihalas S, Hirokawa KE, Whitesell JD, Choi H, Bernard A, Bohn P, Caldejon S, Casal L, Cho A, Feiner A, Feng D, Gaudreault N, Gerfen CR, Graddis N, Groblewski PA, Henry AM, Ho A, Howard R, Knox JE, Kuan L, Kuang X, Lecoq J, Lesnar P, Li Y, Luviano J, McConoughey S, Mortrud MT, Naeemi M, Ng L, Oh SW, Ouellette B, Shen E, Sorensen SA, Wakeman W, Wang Q, Wang Y, Williford A, Phillips JW, Jones AR, Koch C, Zeng H. 2019. Hierarchical organization of cortical and thalamic connectivity. *Nature*. 575:195–202.
- Harris KD, Hirase H, Leinekugel X, Henze DA, Buzsáki G. 2001. Temporal interaction between single spikes and complex spike bursts in hippocampal pyramidal cells. *Neuron*. 32:141–149.
- Harris KD, Mrsic-Flogel TD. 2013. Cortical connectivity and sensory coding. *Nature*. 503:51–58.
- Harris KD, Shepherd GMG. 2015. The neocortical circuit: themes and variations. *Nat Neurosci*. 18:170–181.
- Harrison MT, Geman S. 2009. A rate and history-preserving resampling algorithm for neural spike trains. *Neural Comput*. 21:1244–1258.
- Harvey CD, Coen P, Tank DW. 2012. Choice-specific sequences in parietal cortex during a virtual-navigation decision task. *Nature*. 484:62–68.
- Hattori R, Danskin B, Babic Z, Mlynaryk N, Komiyama T. 2019. Area-Specificity and Plasticity of History-Dependent Value Coding During Learning. *Cell*. 177:1858-1872.e15.
- Havenith MN, Zijderfeld PM, van Heukelum S, Abghari S, Glennon JC, Tiesinga P. 2018. The Virtual-Environment-Foraging Task enables rapid training and single-trial metrics of attention in head-fixed mice. *Sci Rep*. 8:17371.
- He M, Tucciarone J, Lee S, Nigro MJ, Kim Y, Levine JM, Kelly SM, Krugikov I, Wu P, Chen Y, Gong L, Hou Y, Osten P, Rudy B, Huang ZJ. 2016. Strategies and Tools for Combinatorial Targeting of GABAergic Neurons in Mouse Cerebral Cortex. *Neuron*. 91:1228–1243.
- Helmchen F, Gilad A, Chen JL. 2018. Neocortical Dynamics During Whisker-Based Sensory Discrimination in Head-Restrained Mice. *Neuroscience, Barrel Cortex Function*. 368:57–69.
- Hill DN, Mehta SB, Kleinfeld D. 2011. Quality Metrics to Accompany Spike Sorting of Extracellular Signals. *J Neurosci*. 31:8699–8705.

- Hintiryan H, Foster NN, Bowman I, Bay M, Song MY, Gou L, Yamashita S, Bienkowski MS, Zingg B, Zhu M, Yang XW, Shih JC, Toga AW, Dong H-W. 2016. The mouse cortico-striatal projectome. *Nat Neurosci.* 19:1100–1114.
- Hofer SB, Ko H, Pichler B, Vogelstein J, Ros H, Zeng H, Lein E, Lesica NA, Mrcic-Flogel TD. 2011. Differential connectivity and response dynamics of excitatory and inhibitory neurons in visual cortex. *Nat Neurosci.* 14:1045–1052.
- Hong YK, Lacefield CO, Rodgers CC, Bruno RM. 2018a. Sensation, movement and learning in the absence of barrel cortex. *Nature.* 561:542–546.
- Hu H, Gan J, Jonas P. 2014. Interneurons. Fast-spiking, parvalbumin⁺ GABAergic interneurons: from cellular design to microcircuit function. *Science.* 345:1255–1263.
- Huang ZJ. 2014. Toward a genetic dissection of cortical circuits in the mouse. *Neuron.* 83:1284–1302.
- Hubel DH, Wiesel TN. 1962. Receptive fields, binocular interaction and functional architecture in the cat's visual cortex. *J Physiol.* 160:106–154.2.
- Huber D, Petreanu L, Ghitani N, Ranade S, Hromádka T, Mainen Z, Svoboda K. 2008. Sparse optical microstimulation in barrel cortex drives learned behaviour in freely moving mice. *Nature.* 451:61–64.
- Huda R, Goard MJ, Pho GN, Sur M. 2019. Neural mechanisms of sensorimotor transformation and action selection. *Eur J Neurosci.* 49:1055–1060.
- Hunnicutt BJ, Jongbloets BC, Birdsong WT, Gertz KJ, Zhong H, Mao T. 2016. A comprehensive excitatory input map of the striatum reveals novel functional organization. *eLife.* 5.
- Huo Y, Chen H, Guo ZV. 2020. Mapping Functional Connectivity from the Dorsal Cortex to the Thalamus. *Neuron.* 107:1080–1094.e5.
- Hutson KA, Masterton RB. 1986. The sensory contribution of a single vibrissa's cortical barrel. *J Neurophysiol.* 56:1196–1223.
- Inagaki HK, Chen S, Ridder MC, Sah P, Li N, Yang Z, Hasanbegovic H, Gao Z, Gerfen CR, Svoboda K. 2022. A midbrain-thalamus-cortex circuit reorganizes cortical dynamics to initiate movement. *Cell.* 185:1065–1081.e23.
- Ingleby JD. 1967. Signal detection theory and psychophysics: by D. M. Green and J. A. Swets. New York: John Wiley & Sons Ltd, 1966. Cloth. 104s. *J Sound Vib.* 5:519–521.
- Isaacson JS, Scanziani M. 2011. How inhibition shapes cortical activity. *Neuron.* 72:231–243.
- Isett BR, Feasel SH, Lane MA, Feldman DE. 2018. Slip-Based Coding of Local Shape and Texture in Mouse S1. *Neuron.* 97:418–433.e5.
- Jaramillo S, Zador A. 2010. Auditory cortex mediates the perceptual effects of acoustic temporal expectation. *Nat Preced.* 1–1.
- Jun JJ, Steinmetz NA, Siegle JH, Denman DJ, Bauza M, Barbarits B, Lee AK, Anastassiou CA, Andrei A, Aydın Ç, Barbic M, Blanche TJ, Bonin V, Couto J, Dutta B, Gratiy SL, Gutnisky DA, Häusser M, Karsh B, Ledochowitsch P, Lopez CM, Mitelut C, Musa S, Okun M, Pachitariu M, Putzeys J, Rich PD, Rossant C, Sun W, Svoboda K, Carandini M, Harris KD, Koch C, O'Keefe J, Harris TD. 2017. Fully integrated silicon probes for high-density recording of neural activity. *Nature.* 551:232–236.
- Kawai R, Markman T, Poddar R, Ko R, Fantana AL, Dhawale AK, Kampff AR, Ölveczky BP. 2015. Motor cortex is required for learning but not for executing a motor skill. *Neuron.* 86:800–812.
- Keller GB, Bonhoeffer T, Hübener M. 2012. Sensorimotor Mismatch Signals in Primary Visual Cortex of the Behaving Mouse. *Neuron.* 74:809–815.
- Kerr JND, Kock CPJ de, Greenberg DS, Bruno RM, Sakmann B, Helmchen F. 2007. Spatial Organization of Neuronal Population Responses in Layer 2/3 of Rat Barrel Cortex. *J Neurosci.* 27:13316–13328.
- Kim E, Bari BA, Cohen JY. 2021a. Subthreshold basis for reward-predictive persistent activity in mouse prefrontal cortex. *Cell Rep.* 35:109082.
- Kim Y, Yang GR, Pradhan K, Venkataraju KU, Bota M, García Del Molino LC, Fitzgerald G, Ram K, He M, Levine JM, Mitra P, Huang ZJ, Wang X-J, Osten P. 2017. Brain-wide Maps Reveal Stereotyped

- Cell-Type-Based Cortical Architecture and Subcortical Sexual Dimorphism. *Cell*. 171:456–469.e22.
- Klein-Flügge MC, Bongioanni A, Rushworth MFS. 2022. Medial and orbital frontal cortex in decision-making and flexible behavior. *Neuron*. 110:2743–2770.
- Knutsen PM, Pietr M, Ahissar E. 2006. Haptic object localization in the vibrissal system: behavior and performance. *J Neurosci Off J Soc Neurosci*. 26:8451–8464.
- Komiyama T, Sato TR, O'Connor DH, Zhang Y-X, Huber D, Hooks BM, Gabitto M, Svoboda K. 2010a. Learning-related fine-scale specificity imaged in motor cortex circuits of behaving mice. *Nature*. 464:1182–1186.
- Kristan WB, Calabrese RL, Friesen WO. 2005a. Neuronal control of leech behavior. *Prog Neurobiol*. 76:279–327.
- Kuramoto E, Pan S, Furuta T, Tanaka YR, Iwai H, Yamanaka A, Ohno S, Kaneko T, Goto T, Hioki H. 2017. Individual mediodorsal thalamic neurons project to multiple areas of the rat prefrontal cortex: A single neuron-tracing study using virus vectors. *J Comp Neurol*. 525:166–185.
- Kvitsiani D, Ranade S, Hangya B, Taniguchi H, Huang JZ, Kepecs A. 2013. Distinct behavioural and network correlates of two interneuron types in prefrontal cortex. *Nature*. 498:363–366.
- Kwon SE, Yang H, Minamisawa G, O'Connor DH. 2016a. Sensory and decision-related activity propagate in a cortical feedback loop during touch perception. *Nat Neurosci*. 19:1243–1249.
- Kyriakatos A, Sadashivaiah V, Zhang Y, Motta A, Auffret M, Petersen CC. 2017a. Voltage-sensitive dye imaging of mouse neocortex during a whisker detection task. *Neurophotonics*. 4:031204.
- Lacefield CO, Pnevmatikakis EA, Paninski L, Bruno RM. 2019a. Reinforcement Learning Recruits Somata and Apical Dendrites across Layers of Primary Sensory Cortex. *Cell Rep*. 26:2000–2008.e2.
- Lak A, Arabzadeh E, Diamond ME. 2008. Enhanced Response of Neurons in Rat Somatosensory Cortex to Stimuli Containing Temporal Noise. *Cereb Cortex*. 18:1085–1093.
- Lak A, Okun M, Moss MM, Gurnani H, Farrell K, Wells MJ, Reddy CB, Kepecs A, Harris KD, Carandini M. 2020. Dopaminergic and Prefrontal Basis of Learning from Sensory Confidence and Reward Value. *Neuron*. 105:700–711.e6.
- Lazar JW. 2022. The early history of the knee-jerk reflex in neurology. *J Hist Neurosci*. 31:409–424.
- Le Merre P, Åhrlund-Richter S, Carlén M. 2021. The mouse prefrontal cortex: Unity in diversity. *Neuron*. 109:1925–1944.
- Le Merre P, Esmaeili V, Charrière E, Galan K, Salin P-A, Petersen CCH, Crochet S. 2018a. Reward-Based Learning Drives Rapid Sensory Signals in Medial Prefrontal Cortex and Dorsal Hippocampus Necessary for Goal-Directed Behavior. *Neuron*. 97:83–91.e5.
- Lee CCY, Kheradpezhohu E, Diamond ME, Arabzadeh E. 2020. State-dependent changes in perception and coding in the mouse somatosensory cortex. *Cell Rep*. 32:108197.
- Lee D, Seo H, Jung MW. 2012. Neural Basis of Reinforcement Learning and Decision Making. *Annu Rev Neurosci*. 35:287–308.
- Lee S, Kruglikov I, Huang ZJ, Fishell G, Rudy B. 2013. A disinhibitory circuit mediates motor integration in the somatosensory cortex. *Nat Neurosci*. 16:1662–1670.
- Lefort S, Tómm C, Floyd Sarria J-C, Petersen CCH. 2009. The Excitatory Neuronal Network of the C2 Barrel Column in Mouse Primary Somatosensory Cortex. *Neuron*. 61:301–316.
- Lein ES, Hawrylycz MJ, Ao N, Ayres M, Bensinger A, Bernard A, Boe AF, Boguski MS, Brockway KS, Byrnes EJ, Chen L, Chen L, Chen T-M, Chi Chin M, Chong J, Crook BE, Czaplinska A, Dang CN, Datta S, Dee NR, Desaki AL, Desta T, Diep E, Dolbeare TA, Donelan MJ, Dong H-W, Dougherty JG, Duncan BJ, Ebbert AJ, Eichele G, Estin LK, Faber C, Facer BA, Fields R, Fischer SR, Fliiss TP, Frensley C, Gates SN, Glattfelder KJ, Halverson KR, Hart MR, Hohmann JG, Howell MP, Jeung DP, Johnson RA, Karr PT, Kawal R, Kidney JM, Knapik RH, Kuan CL, Lake JH, Laramée AR, Larsen KD, Lau C, Lemon TA, Liang AJ, Liu Y, Luong LT, Michaels J, Morgan JJ, Morgan RJ, Mortrud MT, Mosqueda NF, Ng LL, Ng R, Orta GJ, Overly CC, Pak TH, Parry SE, Pathak SD, Pearson OC, Puchalski RB, Riley ZL, Rockett HR, Rowland SA, Royall JJ, Ruiz MJ, Sarno NR, Schaffnit K, Shapovalova NV, Sivisay T, Slaughterbeck CR, Smith SC, Smith KA, Smith BI, Sodt

- AJ, Stewart NN, Stumpf K-R, Sunkin SM, Sutram M, Tam A, Teemer CD, Thaller C, Thompson CL, Varnam LR, Visel A, Whitlock RM, Wohnoutka PE, Wolkey CK, Wong VY, Wood M, Yaylaoglu MB, Young RC, Youngstrom BL, Feng Yuan X, Zhang B, Zwingman TA, Jones AR. 2007. Genome-wide atlas of gene expression in the adult mouse brain. *Nature*. 445:168–176.
- Letzkus JJ, Wolff SBE, Meyer EMM, Tovote P, Courtin J, Herry C, Lüthi A. 2011. A disinhibitory microcircuit for associative fear learning in the auditory cortex. *Nature*. 480:331–335.
- Li N, Chen T-W, Guo ZV, Gerfen CR, Svoboda K. 2015. A motor cortex circuit for motor planning and movement. *Nature*. 519:51–56.
- Li N, Daie K, Svoboda K, Druckmann S. 2016. Robust neuronal dynamics in premotor cortex during motor planning. *Nature*. 532:459–464.
- Liu D, Deng J, Zhang Z, Zhang Z-Y, Sun Y-G, Yang T, Yao H. 2020. Orbitofrontal control of visual cortex gain promotes visual associative learning. *Nat Commun*. 11:2784.
- Liu D, Gu X, Zhu J, Zhang X, Han Z, Yan W, Cheng Q, Hao J, Fan H, Hou R, Chen Z, Chen Y, Li CT. 2014. Medial prefrontal activity during delay period contributes to learning of a working memory task. *Science*. 346:458–463.
- Liu Y, Foustoukos G, Crochet S, Petersen CCH. 2022. Axonal and Dendritic Morphology of Excitatory Neurons in Layer 2/3 Mouse Barrel Cortex Imaged Through Whole-Brain Two-Photon Tomography and Registered to a Digital Brain Atlas. *Front Neuroanat*. 15.
- Lohuis MNO, Pie JL, Marchesi P, Montijn JS, Kock CPJ de, Pennartz CMA, Olcese U. 2021. Task complexity temporally extends the causal requirement for visual cortex in perception.
- Lui JH, Nguyen ND, Grutzner SM, Darmanis S, Peixoto D, Wagner MJ, Allen WE, Kebschull JM, Richman EB, Ren J, Newsome WT, Quake SR, Luo L. 2021a. Differential encoding in prefrontal cortex projection neuron classes across cognitive tasks. *Cell*. 184:489-506.e26.
- Luo L, Callaway EM, Svoboda K. 2018. Genetic Dissection of Neural Circuits: A Decade of Progress. *Neuron*. 98:256–281.
- Luo P, Li A, Zheng Y, Han Y, Tian J, Xu Z, Gong H, Li X. 2019. Whole Brain Mapping of Long-Range Direct Input to Glutamatergic and GABAergic Neurons in Motor Cortex. *Front Neuroanat*. 13:44.
- MacDowell CJ, Buschman TJ. 2020. Low-Dimensional Spatiotemporal Dynamics Underlie Cortex-wide Neural Activity. *Curr Biol CB*. 30:2665-2680.e8.
- Macosko EZ, Basu A, Satija R, Nemesh J, Shekhar K, Goldman M, Tirosh I, Bialas AR, Kamitaki N, Martersteck EM, Trombetta JJ, Weitz DA, Sanes JR, Shalek AK, Regev A, McCarroll SA. 2015. Highly Parallel Genome-wide Expression Profiling of Individual Cells Using Nanoliter Droplets. *Cell*. 161:1202–1214.
- Madisen L, Mao T, Koch H, Zhuo J, Berenyi A, Fujisawa S, Hsu Y-WA, Garcia AJ 3rd, Gu X, Zanella S, Kidney J, Gu H, Mao Y, Hooks BM, Boyden ES, Buzsáki G, Ramirez JM, Jones AR, Svoboda K, Han X, Turner EE, Zeng H. 2012. A toolbox of Cre-dependent optogenetic transgenic mice for light-induced activation and silencing. *Nat Neurosci*. 15:793–802.
- Madisen L, Zwingman TA, Sunkin SM, Oh SW, Zariwala HA, Gu H, Ng LL, Palmiter RD, Hawrylycz MJ, Jones AR, Lein ES, Zeng H. 2010. A robust and high-throughput Cre reporting and characterization system for the whole mouse brain. *Nat Neurosci*. 13:133–140.
- Maimon G, Assad JA. 2006. A cognitive signal for the proactive timing of action in macaque LIP. *Nat Neurosci*. 9:948–955.
- Makino H, Ren C, Liu H, Kim AN, Kondapaneni N, Liu X, Kuzum D, Komiyama T. 2017. Transformation of Cortex-wide Emergent Properties during Motor Learning. *Neuron*. 94:880-890.e8.
- Manita S, Suzuki T, Homma C, Matsumoto T, Odagawa M, Yamada K, Ota K, Matsubara C, Inutsuka A, Sato M, Ohkura M, Yamanaka A, Yanagawa Y, Nakai J, Hayashi Y, Larkum ME, Murayama M. 2015. A Top-Down Cortical Circuit for Accurate Sensory Perception. *Neuron*. 86:1304–1316.
- Mante V, Sussillo D, Shenoy KV, Newsome WT. 2013. Context-dependent computation by recurrent dynamics in prefrontal cortex. *Nature*. 503:78–84.
- Mao T, Kusefoglu D, Hooks BM, Huber D, Petreanu L, Svoboda K. 2011a. Long-range neuronal circuits underlying the interaction between sensory and motor cortex. *Neuron*. 72:111–123.

- Mao T, Kusefoglu D, Hooks BM, Huber D, Petreanu L, Svoboda K. 2011b. Long-range neuronal circuits underlying the interaction between sensory and motor cortex. *Neuron*. 72:111–123.
- Maravall M, Petersen RS, Fairhall AL, Arabzadeh E, Diamond ME. 2007. Shifts in Coding Properties and Maintenance of Information Transmission during Adaptation in Barrel Cortex. *PLOS Biol*. 5:e19.
- Maravall M. 2019. Sensory Decision-Making: Rats Sleuth Evidence through Active Sensing. *Curr Biol*. 29:R317–R319.
- Marshall JH, Garrett ME, Nauhaus I, Callaway EM. 2011. Functional specialization of seven mouse visual cortical areas. *Neuron*. 72:1040–1054.
- Mateo C, Avermann M, Gentet LJ, Zhang F, Deisseroth K, Petersen CCH. 2011. In vivo optogenetic stimulation of neocortical excitatory neurons drives brain-state-dependent inhibition. *Curr Biol CB*. 21:1593–1602.
- Mathis A, Mamidanna P, Cury KM, Abe T, Murthy VN, Mathis MW, Bethge M. 2018. DeepLabCut: markerless pose estimation of user-defined body parts with deep learning. *Nat Neurosci*. 21:1281–1289.
- Mathis MW, Mathis A, Uchida N. 2017. Somatosensory Cortex Plays an Essential Role in Forelimb Motor Adaptation in Mice. *Neuron*. 93:1493–1503.e6.
- Matteucci G, Guyoton M, Mayrhofer JM, Auffret M, Foustoukos G, Petersen CCH, El-Boustani S. 2022. Cortical sensory processing across motivational states during goal-directed behavior. *Neuron*. S0896627322008984.
- Mátyás F, Lee J, Shin H-S, Acsády L. 2014. The fear circuit of the mouse forebrain: Connections between the mediodorsal thalamus, frontal cortices and basolateral amygdala. *Eur J Neurosci*. 39:1810–1823.
- Mayford M, Bach ME, Huang Y-Y, Wang L, Hawkins RD, Kandel ER. 1996. Control of Memory Formation Through Regulated Expression of a CaMKII Transgene. *Science*. 274:1678–1683.
- Mayrhofer JM, El-Boustani S, Foustoukos G, Auffret M, Tamura K, Petersen CCH. 2019a. Distinct Contributions of Whisker Sensory Cortex and Tongue-Jaw Motor Cortex in a Goal-Directed Sensorimotor Transformation. *Neuron*. 103:1034–1043.e5.
- McCormick DA, Connors BW, Lighthall JW, Prince DA. 1985. Comparative electrophysiology of pyramidal and sparsely spiny stellate neurons of the neocortex. *J Neurophysiol*. 54:782–806.
- Mehta SB, Whitmer D, Figueroa R, Williams BA, Kleinfeld D. 2007. Active spatial perception in the vibrissa scanning sensorimotor system. *PLoS Biol*. 5:e15.
- Miller EK. 2000. The prefrontal cortex and cognitive control. *Nat Rev Neurosci*. 1:59–65.
- Miller KJ, Botvinick MM, Brody CD. 2022. Value representations in the rodent orbitofrontal cortex drive learning, not choice. *eLife*. 11:e64575.
- Miyashita T, Feldman DE. 2013a. Behavioral Detection of Passive Whisker Stimuli Requires Somatosensory Cortex. *Cereb Cortex N Y NY*. 23:1655–1662.
- Moorman DE, Aston-Jones G. 2015a. Prefrontal neurons encode context-based response execution and inhibition in reward seeking and extinction. *Proc Natl Acad Sci U S A*. 112:9472–9477.
- Mori K, Manabe H, Narikiyo K, Onisawa N. 2013. Olfactory consciousness and gamma oscillation couplings across the olfactory bulb, olfactory cortex, and orbitofrontal cortex. *Front Psychol*. 4.
- Mountcastle V, Berman A, Davies P, others. 1955. Topographic organization and modality representation in first somatic area of cat's cerebral cortex by method of single unit analysis. *Am J Physiol*. 183.
- Mountcastle VB, Steinmetz MA, Romo R. 1990. Frequency discrimination in the sense of flutter: psychophysical measurements correlated with postcentral events in behaving monkeys. *J Neurosci*. 10:3032–3044.
- Musall S, Kaufman MT, Juavinett AL, Gluf S, Churchland AK. 2019a. Single-trial neural dynamics are dominated by richly varied movements. *Nat Neurosci*. 22:1677–1686.

- Musall S, von der Behrens W, Mayrhofer JM, Weber B, Helmchen F, Haiss F. 2014. Tactile frequency discrimination is enhanced by circumventing neocortical adaptation. *Nat Neurosci.* 17:1567–1573.
- Nakajima M, Schmitt LI, Halassa MM. 2019. Prefrontal cortex regulates sensory filtering through a basal ganglia-to-thalamus pathway. *Neuron.* 103:445–458.
- Nelder JA, Wedderburn RWM. 1972. Generalized Linear Models. *J R Stat Soc Ser Gen.* 135:370.
- Nelson A, Schneider DM, Takatoh J, Sakurai K, Wang F, Mooney R. 2013. A circuit for motor cortical modulation of auditory cortical activity. *J Neurosci.* 33:14342–14353.
- Newsome WT, Britten KH, Movshon JA. 1989. Neuronal correlates of a perceptual decision. *Nature.* 341:52–54.
- Nordhausen K. 2009. The Elements of Statistical Learning: Data Mining, Inference, and Prediction, Second Edition by Trevor Hastie, Robert Tibshirani, Jerome Friedman. *Int Stat Rev.* 77:482–482.
- O'Connor DH, Clack NG, Huber D, Komiyama T, Myers EW, Svoboda K. 2010. Vibrissa-based object localization in head-fixed mice. *J Neurosci.* 30:1947–1967.
- O'Connor DH, Peron SP, Huber D, Svoboda K. 2010a. Neural Activity in Barrel Cortex Underlying Vibrissa-Based Object Localization in Mice. *Neuron.* 67:1048–1061.
- O'Connor S, ChatGPT. 2023. Open artificial intelligence platforms in nursing education: Tools for academic progress or abuse? *Nurse Educ Pract.* 66:103537.
- Oh SW, Harris JA, Ng L, Winslow B, Cain N, Mihalas S, Wang Q, Lau C, Kuan L, Henry AM, Mortrud MT, Ouellette B, Nguyen TN, Sorensen SA, Slaughterbeck CR, Wakeman W, Li Y, Feng D, Ho A, Nicholas E, Hirokawa KE, Bohn P, Joines KM, Peng H, Hawrylycz MJ, Phillips JW, Hohmann JG, Wohnoutka P, Gerfen CR, Koch C, Bernard A, Dang C, Jones AR, Zeng H. 2014. A mesoscale connectome of the mouse brain. *Nature.* 508:207–214.
- Otchy TM, Wolff SBE, Rhee JY, Pehlevan C, Kawai R, Kempf A, Gobes SMH, Ölveczky BP. 2015. Acute off-target effects of neural circuit manipulations. *Nature.* 528:358–363.
- Otis JM, Namboodiri VM, Matan AM, Voets ES, Mohorn EP, Kosyk O, McHenry JA, Robinson JE, Resendez SL, Rossi MA, Stuber GD. 2017a. Prefrontal cortex output circuits guide reward seeking through divergent cue encoding. *Nature.* 543:103–107.
- Otis JM, Namboodiri VM, Matan AM, Voets ES, Mohorn EP, Kosyk O, McHenry JA, Robinson JE, Resendez SL, Rossi MA, Stuber GD. 2017b. Prefrontal cortex output circuits guide reward seeking through divergent cue encoding. *Nature.* 543:103–107.
- Pachitariu M, Sridhar S, Stringer C. 2023. Solving the spike sorting problem with Kilosort.
- Padoa-Schioppa C, Assad JA. 2006. Neurons in Orbitofrontal Cortex Encode Economic Value. *Nature.* 441:223–226.
- Padoa-Schioppa C, Conen KE. 2017. Orbitofrontal Cortex: A Neural Circuit for Economic Decisions. *Neuron.* 96:736–754.
- Pai S, Erlich J, Kopec C, Brody C. 2011. Minimal Impairment in a Rat Model of Duration Discrimination Following Excitotoxic Lesions of Primary Auditory and Prefrontal Cortices. *Front Syst Neurosci.* 5.
- Panzeri S, Harvey CD, Piasini E, Latham PE, Fellin T. 2017. Cracking the Neural Code for Sensory Perception by Combining Statistics, Intervention, and Behavior. *Neuron.* 93:491–507.
- Park IM, Meister MLR, Huk AC, Pillow JW. 2014. Encoding and decoding in parietal cortex during sensorimotor decision-making. *Nat Neurosci.* 17:1395–1403.
- Parker AJ, Newsome WT. 1998. SENSE AND THE SINGLE NEURON: Probing the Physiology of Perception. *Annu Rev Neurosci.* 21:227–277.
- Penfield W. 1953. A Consideration of the Neurophysiological Mechanisms of Speech and Some Educational Consequences. *Proc Am Acad Arts Sci.* 82:201.
- Pennartz CMA, Ito R, Verschure PFMJ, Battaglia FP, Robbins TW. 2011a. The hippocampal–striatal axis in learning, prediction and goal-directed behavior. *Trends Neurosci.* 34:548–559.
- Perkel DH, Gerstein GL, Moore GP. 1967. Neuronal spike trains and stochastic point processes. II. Simultaneous spike trains. *Biophys J.* 7:419–440.

- Peters AJ, Marica A-M, Fabre JMJ, Harris KD, Carandini M. 2022. Visuomotor learning promotes visually evoked activity in the medial prefrontal cortex. *Cell Rep.* 41:111487.
- Peters J, Kalivas PW, Quirk GJ. 2009. Extinction circuits for fear and addiction overlap in prefrontal cortex. *Learn Mem.* 16:279.
- Petersen CCH. 2007. The Functional Organization of the Barrel Cortex. *Neuron.* 56:339–355.
- Petersen CCH. 2019a. Sensorimotor processing in the rodent barrel cortex. *Nat Rev Neurosci.* 20:533–546.
- Petersen CCH, Crochet S. 2013. Synaptic Computation and Sensory Processing in Neocortical Layer 2/3. *Neuron.* 78:28–48.
- Petersen CCH, Grinvald A, Sakmann B. 2003. Spatiotemporal Dynamics of Sensory Responses in Layer 2/3 of Rat Barrel Cortex Measured In Vivo by Voltage-Sensitive Dye Imaging Combined with Whole-Cell Voltage Recordings and Neuron Reconstructions. *J Neurosci.* 23:1298–1309.
- Petersen CCH, Sakmann B. 2000. The Excitatory Neuronal Network of Rat Layer 4 Barrel Cortex. *J Neurosci.* 20:7579–7586.
- Pfeffer CK, Xue M, He M, Huang ZJ, Scanziani M. 2013. Inhibition of inhibition in visual cortex: the logic of connections between molecularly distinct interneurons. *Nat Neurosci.* 16:1068–1076.
- Pi H-J, Hangya B, Kvitsiani D, Sanders JI, Huang ZJ, Kepecs A. 2013. Cortical interneurons that specialize in disinhibitory control. *Nature.* 503:521–524.
- Pinto L, Dan Y. 2015a. Cell-Type-Specific Activity in Prefrontal Cortex during Goal-Directed Behavior. *Neuron.* 87:437–450.
- Pinto L, Rajan K, DePasquale B, Thiberge SY, Tank DW, Brody CD. 2019. Task-Dependent Changes in the Large-Scale Dynamics and Necessity of Cortical Regions. *Neuron.* 104:810-824.e9.
- Poort J, Wilmes KA, Blot A, Chadwick A, Sahani M, Clopath C, Mrcic-Flogel TD, Hofer SB, Khan AG. 2022. Learning and attention increase visual response selectivity through distinct mechanisms. *Neuron.* 110:686-697.e6.
- Popescu AT, Zhou MR, Poo M. 2016. Phasic dopamine release in the medial prefrontal cortex enhances stimulus discrimination. *Proc Natl Acad Sci.* 113:E3169–E3176.
- Poulet JFA, Crochet S. 2018. The cortical states of wakefulness. *Front Syst Neurosci.* 12:64.
- Poulet JFA, Petersen CCH. 2008. Internal brain state regulates membrane potential synchrony in barrel cortex of behaving mice. *Nature.* 454:881–885.
- Powell NJ, Redish AD. 2016. Representational changes of latent strategies in rat medial prefrontal cortex precede changes in behaviour. *Nat Commun.* 7:12830–12830.
- Ramesh RN, Burgess CR, Sugden AU, Gyetvan M, Andermann ML. 2018. Intermingled Ensembles in Visual Association Cortex Encode Stimulus Identity or Predicted Outcome. *Neuron.* 100:900-915.e9.
- Raposo D, Kaufman MT, Churchland AK. 2014. A category-free neural population supports evolving demands during decision-making. *Nat Neurosci.* 17:1784–1792.
- Recanzone GH, Jenkins WM, Hradek GT, Merzenich MM. 1991. A behavioral frequency discrimination paradigm for use in adult primates. *Behav Res Methods Instrum Comput.* 23:357–369.
- Reynolds JH, Heeger DJ. 2009. The Normalization Model of Attention. *Neuron.* 61:168–185.
- Riehle A, Requin J. 1989. Monkey primary motor and premotor cortex: single-cell activity related to prior information about direction and extent of an intended movement. *J Neurophysiol.* 61:534–549.
- Rikhye RV, Gilra A, Halassa MM. 2018. Thalamic regulation of switching between cortical representations enables cognitive flexibility. *Nat Neurosci.* 21:1753–1763.
- Rockland KS, Pandya DN. 1979. Laminar origins and terminations of cortical connections of the occipital lobe in the rhesus monkey. *Brain Res.* 179:3–20.
- Rodgers CC, Nogueira R, Pil BC, Greeman EA, Park JM, Hong YK, Fusi S, Bruno RM. 2021. Sensorimotor strategies and neuronal representations for shape discrimination. *Neuron.* 109:2308-2325.e10.

- Rodriguez-Moreno J, Porrero C, Rollenhagen A, Rubio-Teves M, Casas-Torremocha D, Alonso-Nanclares L, Yakoubi R, Santuy A, Merchan-Pérez A, DeFelipe J, Lübke JHR, Clasca F. 2020. Area-Specific Synapse Structure in Branched Posterior Nucleus Axons Reveals a New Level of Complexity in Thalamocortical Networks. *J Neurosci Off J Soc Neurosci*. 40:2663–2679.
- Roelfsema PR, Lamme VAF, Spekreijse H. 1998. Object-based attention in the primary visual cortex of the macaque monkey. *Nature*. 395:376–381.
- Roitman JD, Shadlen MN. 2002. Response of Neurons in the Lateral Intraparietal Area during a Combined Visual Discrimination Reaction Time Task. *J Neurosci*. 22:9475–9489.
- Rojas-Piloni G, Guest JM, Egger R, Johnson AS, Sakmann B, Oberlaender M. 2017. Relationships between structure, in vivo function and long-range axonal target of cortical pyramidal tract neurons. *Nat Commun*. 8:870.
- Romo R, de Lafuente V. 2013a. Conversion of sensory signals into perceptual decisions. *Prog Neurobiol*, Conversion of Sensory Signals into Perceptions, Memories and Decisions. 103:41–75.
- Romo R, Hernández A, Zainos A, Salinas E. 1998. Somatosensory discrimination based on cortical microstimulation. *Nature*. 392:387–390.
- Romo R, Salinas E. 2003. Flutter Discrimination: neural codes, perception, memory and decision making. *Nat Rev Neurosci*. 4:203–218.
- Rossant C, Kadir SN, Goodman DFM, Schulman J, Hunter MLD, Saleem AB, Grosmark A, Belluscio M, Denfield GH, Ecker AS, Tolias AS, Solomon S, Buzsaki G, Carandini M, Harris KD. 2016. Spike sorting for large, dense electrode arrays. *Nat Neurosci*. 19:634–641.
- Rossi MA, Li HE, Lu D, Kim IH, Bartholomew RA, Gaidis E, Barter JW, Kim N, Cai MT, Soderling SH, Yin HH. 2016. A GABAergic nigrotectal pathway for coordination of drinking behavior. *Nat Neurosci*. 19:742–748.
- Rossi-Pool R, Salinas E, Zainos A, Alvarez M, Vergara J, Parga N, Romo R. 2016. Emergence of an abstract categorical code enabling the discrimination of temporally structured tactile stimuli. *Proc Natl Acad Sci*. 113:E7966–E7975.
- Rybalko N, Šuta D, Nwabueze-Ogbo F, Syka J. 2006. Effect of auditory cortex lesions on the discrimination of frequency-modulated tones in rats. *Eur J Neurosci*. 23:1614–1622.
- Sachidhanandam S, Sermet BS, Petersen CC. 2016a. Parvalbumin-Expressing GABAergic Neurons in Mouse Barrel Cortex Contribute to Gating a Goal-Directed Sensorimotor Transformation. *Cell Rep*. 15:700–706.
- Sachidhanandam S, Sreenivasan V, Kyriakatos A, Kremer Y, Petersen CCH. 2013a. Membrane potential correlates of sensory perception in mouse barrel cortex. *Nat Neurosci*. 16:1671–1677.
- Saleem AB, Ayaz A, Jeffery KJ, Harris KD, Carandini M. 2013. Integration of visual motion and locomotion in mouse visual cortex. *Nat Neurosci*. 16:1864–1869.
- Sanders MD, Warrington ElizabethK, Marshall J, Wieskrantz L. 1974. “BLINDSIGHT”: VISION IN A FIELD DEFECT. *The Lancet*, Originally published as Volume 1, Issue 7860. 303:707–708.
- Sanzeni A, Akitake B, Goldbach HC, Leedy CE, Brunel N, Histed MH. 2020. Inhibition stabilization is a widespread property of cortical networks. *eLife*. 9:e54875.
- Schaeffer AA. 1917. Reactions of Ameba to Light and the Effect of Light on Feeding. *Biol Bull*. 32:45–74.
- Schlicht EJ, Schrater PR. 2007. Impact of Coordinate Transformation Uncertainty on Human Sensorimotor Control. *J Neurophysiol*. 97:4203–4214.
- Schmid MC, Mrowka SW, Turchi J, Saunders RC, Wilke M, Peters AJ, Ye FQ, Leopold DA. 2010. Blindsight depends on the lateral geniculate nucleus. *Nature*. 466:373–377.
- Schmitzer-Torbert N, Jackson J, Henze D, Harris K, Redish AD. 2005. Quantitative measures of cluster quality for use in extracellular recordings. *Neuroscience*. 131:1–11.
- Schoenbaum G, Roesch MR, Stalnaker TA, Takahashi YK. 2009. A new perspective on the role of the orbitofrontal cortex in adaptive behaviour. *Nat Rev Neurosci*. 10:885–892.

- Sermet BS, Truschow P, Feyerabend M, Mayrhofer JM, Oram TB, Yizhar O, Staiger JF, Petersen CC. 2019. Pathway-, layer- and cell-type-specific thalamic input to mouse barrel cortex. *eLife*. 8.
- Shadlen MN, Newsome WT. 2001. Neural Basis of a Perceptual Decision in the Parietal Cortex (Area LIP) of the Rhesus Monkey. *J Neurophysiol*. 86:1916–1936.
- Shamash P, Carandini M, Harris KD, Steinmetz NA. 2018. A tool for analyzing electrode tracks from slice histology. *Neuroscience*.
- Shepherd GMG, Pologruto TA, Svoboda K. 2003. Circuit Analysis of Experience-Dependent Plasticity in the Developing Rat Barrel Cortex. *Neuron*. 38:277–289.
- Shepherd GMG, Yamawaki N. 2021. Untangling the cortico-thalamo-cortical loop: cellular pieces of a knotty circuit puzzle. *Nat Rev Neurosci*. 22:389–406.
- Shuler MG, Bear MF. 2006. Reward Timing in the Primary Visual Cortex. *Science*.
- Siegel M, Buschman TJ, Miller EK. 2015. Cortical information flow during flexible sensorimotor decisions. *Science*. 348:1352–1355.
- Siegle JH, Jia X, Durand S, Gale S, Bennett C, Graddis N, Heller G, Ramirez TK, Choi H, Luviano JA, Groblewski PA, Ahmed R, Arkhipov A, Bernard A, Billeh YN, Brown D, Buice MA, Cain N, Caldejon S, Casal L, Cho A, Chvilicek M, Cox TC, Dai K, Denman DJ, de Vries SEJ, Dietzman R, Esposito L, Farrell C, Feng D, Galbraith J, Garrett M, Gelfand EC, Hancock N, Harris JA, Howard R, Hu B, Hytnen R, Iyer R, Jessett E, Johnson K, Kato I, Kiggins J, Lambert S, Lecoq J, Ledochowitsch P, Lee JH, Leon A, Li Y, Liang E, Long F, Mace K, Melchior J, Millman D, Mollenkopf T, Nayan C, Ng L, Ngo K, Nguyen T, Nicovich PR, North K, Ocker GK, Ollerenshaw D, Oliver M, Pachitariu M, Perkins J, Reding M, Reid D, Robertson M, Ronellenfitch K, Seid S, Slaughterbeck C, Stoecklin M, Sullivan D, Sutton B, Swapp J, Thompson C, Turner K, Wakeman W, Whitesell JD, Williams D, Williford A, Young R, Zeng H, Naylor S, Phillips JW, Reid RC, Mihalas S, Olsen SR, Koch C. 2021. Survey of spiking in the mouse visual system reveals functional hierarchy. *Nature*. 592:86–92.
- Simons DJ. 1978. Response properties of vibrissa units in rat SI somatosensory neocortex. *J Neurophysiol*. 41:798–820.
- Siniscalchi MJ, Phoumthippavong V, Ali F, Lozano M, Kwan AC. 2016. Fast and slow transitions in frontal ensemble activity during flexible sensorimotor behavior. *Nat Neurosci*. 19:1234–1242.
- Sippy T, Chaimowitz C, Crochet S, Petersen CCH. 2021. Cell Type-Specific Membrane Potential Changes in Dorsolateral Striatum Accompanying Reward-Based Sensorimotor Learning. *Function*. 2:zqab049.
- Sippy T, Lapray D, Crochet S, Petersen CC. 2015a. Cell-Type-Specific Sensorimotor Processing in Striatal Projection Neurons during Goal-Directed Behavior. *Neuron*. 88:298–305.
- Smith MA, Kohn A. 2008. Spatial and temporal scales of neuronal correlation in primary visual cortex. *J Neurosci Off J Soc Neurosci*. 28:12591–12603.
- Sohal VS, Rubenstein JLR. 2019. Excitation-inhibition balance as a framework for investigating mechanisms in neuropsychiatric disorders. *Mol Psychiatry*. 24:1248–1257.
- Soleimanzad H, Gurden H, Pain F. 2017. Optical properties of mice skull bone in the 455- to 705-nm range. *J Biomed Opt*. 22:010503.
- Song Y-H, Kim J-H, Jeong H-W, Choi I, Jeong D, Kim K, Lee S-H. 2017. A Neural Circuit for Auditory Dominance over Visual Perception. *Neuron*. 93:940-954.e6.
- Spellman T, Svei M, Kaminsky J, Manzano-Nieves G, Liston C. 2021. Prefrontal deep projection neurons enable cognitive flexibility via persistent feedback monitoring. *Cell*. 184:2750-2766.e17.
- Sreenivasan V, Esmaeili V, Kiritani T, Galan K, Crochet S, Petersen CC. 2016a. Movement Initiation Signals in Mouse Whisker Motor Cortex. *Neuron*. 92:1368–1382.
- Sreenivasan V, Kyriakatos A, Mateo C, Jaeger D, Petersen CCH. 2016. Parallel pathways from whisker and visual sensory cortices to distinct frontal regions of mouse neocortex. *Neurophotonics*. 4:031203.
- Staiger JF, Petersen CCH. 2021a. Neuronal Circuits in Barrel Cortex for Whisker Sensory Perception. *Physiol Rev*. 101:353–415.

- Staiger JF, Petersen CCH. 2021b. Neuronal Circuits in Barrel Cortex for Whisker Sensory Perception. *Physiol Rev.* 101:353–415.
- Stanek E IV, Cheng S, Takato H, Han B-X, Wang F. 2014. Monosynaptic premotor circuit tracing reveals neural substrates for oro-motor coordination. *eLife.* 3:e02511.
- Stanisor L, Van der Togt C, Pennartz C, Roelfsema P. 2013. A unified selection signal for attention and reward in primary visual cortex. *Proc Natl Acad Sci U S A.* 110.
- Steinmetz NA, Zatka-Haas P, Carandini M, Harris KD. 2019a. Distributed coding of choice, action and engagement across the mouse brain. *Nature.* 576:266–273.
- Stokel-Walker C. 2023. ChatGPT listed as author on research papers: many scientists disapprove. *Nature.* 613:620–621.
- Stringer C, Pachitariu M, Steinmetz N, Reddy CB, Carandini M, Harris KD. 2019. Spontaneous behaviors drive multidimensional, brainwide activity. *Science.* 364:eaav7893.
- Stüttgen M, Schwarz C, Jäkel F. 2011. Mapping Spikes to Sensations. *Front Neurosci.* 5.
- Stüttgen MC, Schwarz C. 2008. Psychophysical and neurometric detection performance under stimulus uncertainty. *Nat Neurosci.* 11:1091–1099.
- Stüttgen MC, Schwarz C. 2018. Barrel cortex: What is it good for? *Neuroscience.* 368:3–16.
- Sugrue LP, Corrado GS, Newsome WT. 2005. Choosing the greater of two goods: neural currencies for valuation and decision making. *Nat Rev Neurosci.* 6:363–375.
- Sun YJ, Wu GK, Liu B-H, Li P, Zhou M, Xiao Z, Tao HW, Zhang LI. 2010. Fine-tuning of pre-balanced excitation and inhibition during auditory cortical development. *Nature.* 465:927–931.
- Supér H, Spekreijse H, Lamme VAF. 2001. Two distinct modes of sensory processing observed in monkey primary visual cortex (V1). *Nat Neurosci.* 4:304–310.
- Svoboda K, Li N. 2018a. Neural mechanisms of movement planning: motor cortex and beyond. *Curr Opin Neurobiol.* 49:33–41.
- Sych Y, Fomins A, Novelli L, Helmchen F. 2022. Dynamic reorganization of the cortico-basal ganglia-thalamo-cortical network during task learning. *Cell Rep.* 40:111394.
- Takahashi N, Ebner C, Sigl-Glöckner J, Moberg S, Nierwetberg S, Larkum ME. 2020a. Active dendritic currents gate descending cortical outputs in perception. *Nat Neurosci.* 23:1277–1285.
- Takahashi N, Oertner TG, Hegemann P, Larkum ME. 2016a. Active cortical dendrites modulate perception. *Science.* 354:1587–1590.
- Talwar SK, Musial PG, Gerstein GL. 2001. Role of Mammalian Auditory Cortex in the Perception of Elementary Sound Properties. *J Neurophysiol.* 85:2350–2358.
- Tanaka M. 2007. Cognitive Signals in the Primate Motor Thalamus Predict Saccade Timing. *J Neurosci.* 27:12109–12118.
- Taniguchi H, He M, Wu P, Kim S, Paik R, Sugino K, Kvitsiani D, Fu Y, Lu J, Lin Y, Miyoshi G, Shima Y, Fishell G, Nelson SB, Huang ZJ. 2011. A resource of Cre driver lines for genetic targeting of GABAergic neurons in cerebral cortex. *Neuron.* 71:995–1013.
- Taniguchi H, He M, Wu P, Kim S, Paik R, Sugino K, Kvitsiani D, Kvitsani D, Fu Y, Lu J, Lin Y, Miyoshi G, Shima Y, Fishell G, Nelson SB, Huang ZJ. 2011. A resource of Cre driver lines for genetic targeting of GABAergic neurons in cerebral cortex. *Neuron.* 71:995–1013.
- Tanji J, Evarts EV. 1976. Anticipatory activity of motor cortex neurons in relation to direction of an intended movement. *J Neurophysiol.* 39:1062–1068.
- Tasic B, Yao Z, Graybiel LT, Smith KA, Nguyen TN, Bertagnolli D, Goldy J, Garren E, Economou MN, Viswanathan S, Penn O, Bakken T, Menon V, Miller J, Fong O, Hirokawa KE, Lathia K, Rimorin C, Tieu M, Larsen R, Casper T, Barkan E, Kroll M, Parry S, Shapovalova NV, Hirschstein D, Pendergraft J, Sullivan HA, Kim TK, Szafer A, Dee N, Groblewski P, Wickersham I, Cetin A, Harris JA, Levi BP, Sunkin SM, Madisen L, Daigle TL, Looger L, Bernard A, Phillips J, Lein E, Hawrylycz M, Svoboda K, Jones AR, Koch C, Zeng H. 2018. Shared and distinct transcriptomic cell types across neocortical areas. *Nature.* 563:72–78.
- Thorp HH. 2023. ChatGPT is fun, but not an author. *Science.* 379:313–313.
- Travers JB, Dinardo LA, Karimnamazi H. 1997. Motor and Premotor Mechanisms of Licking. *Neurosci Biobehav Rev.* 21:631–647.

- Tremblay L, Schultz W. 1999. Relative reward preference in primate orbitofrontal cortex. *Nature*. 398:704–708.
- Tremblay R, Lee S, Rudy B. 2016. GABAergic Interneurons in the Neocortex: From Cellular Properties to Circuits. *Neuron*. 91:260–292.
- Tyson AL, Vélez-Fort M, Rousseau CV, Cossell L, Tsitoura C, Lenzi SC, Obenhaus HA, Claudi F, Branco T, Margrie TW. 2022. Accurate determination of marker location within whole-brain microscopy images. *Sci Rep*. 12:867.
- Valyear KF. 2016. The hand that ‘sees’ to grasp. *eLife*. 5:e18887.
- Van Der Loos H. 1976. Barreloids in mouse somatosensory thalamus. *Neurosci Lett*. 2:1–6.
- Vanni MP, Chan AW, Balbi M, Silasi G, Murphy TH. 2017. Mesoscale Mapping of Mouse Cortex Reveals Frequency-Dependent Cycling between Distinct Macroscale Functional Modules. *J Neurosci Off J Soc Neurosci*. 37:7513–7533.
- Vavladeli A, Daigle T, Zeng H, Crochet S, Petersen CCH. 2020. Projection-specific activity of layer 2/3 neurons imaged in mouse primary somatosensory barrel cortex during a whisker detection task. *Function*. 1:zqaa008.
- Vincent SB. 1912. The function of the vibrissae in the behavior of the white rat. *Anim Behav Monogr*. 1, 5:84–84.
- Von Luxburg U. 2007. A tutorial on spectral clustering. *Stat Comput*. 17:395–416.
- Wallis JD, Miller EK. 2003. Neuronal activity in primate dorsolateral and orbital prefrontal cortex during performance of a reward preference task. *Eur J Neurosci*. 18:2069–2081.
- Wang Q, Burkhalter A. 2007. Area map of mouse visual cortex. *J Comp Neurol*. 502:339–357.
- Wang Q, Ding S-L, Li Y, Royall J, Feng D, Lesnar P, Graddis N, Naeemi M, Facer B, Ho A, Dolbeare T, Blanchard B, Dee N, Wakeman W, Hirokawa KE, Szafer A, Sunkin SM, Oh SW, Bernard A, Phillips JW, Hawrylycz M, Koch C, Zeng H, Harris JA, Ng L. 2020a. The Allen Mouse Brain Common Coordinate Framework: A 3D Reference Atlas. *Cell*. 181:936–953.e20.
- Whishaw IQ, Faraji J, Kuntz JR, Mirza Agha B, Metz GAS, Mohajerani MH. 2017. The syntactic organization of pasta-eating and the structure of reach movements in the head-fixed mouse. *Sci Rep*. 7:10987.
- Wills GD, Wesley AL, Moore FR, Sisemore DA. 1983. Social interactions among rodent conspecifics: a review of experimental paradigms. *Neurosci Biobehav Rev*. 7:315–323.
- Winkowski DE, Nagode DA, Donaldson KJ, Yin P, Shamma SA, Fritz JB, Kanold PO. 2018. Orbitofrontal Cortex Neurons Respond to Sound and Activate Primary Auditory Cortex Neurons. *Cereb Cortex*. 28:868–879.
- Woloszyn L, Sheinberg DL. 2012. Effects of long-term visual experience on responses of distinct classes of single units in inferior temporal cortex. *Neuron*. 74:193–205.
- Woodworth RS, Sherrington CS. 1904. A pseudoaffective reflex and its spinal path. *J Physiol*. 31:234–243.
- Woolsey TA, Van der Loos H. 1970. The structural organization of layer IV in the somatosensory region (S I) of mouse cerebral cortex: The description of a cortical field composed of discrete cytoarchitectonic units. *Brain Res*. 17:205–242.
- Xu D, Dong M, Chen Y, Delgado AM, Hughes NC, Zhang L, O’Connor DH. 2022. Cortical processing of flexible and context-dependent sensorimotor sequences. *Nature*. 603:464–469.
- Yamashita T, Pala A, Pedrido L, Kremer Y, Welker E, Petersen CCH. 2013. Membrane Potential Dynamics of Neocortical Projection Neurons Driving Target-Specific Signals. *Neuron*. 80:1477–1490.
- Yamashita T, Petersen CC. 2016a. Target-specific membrane potential dynamics of neocortical projection neurons during goal-directed behavior. *eLife*. 5:e15798.
- Yamashita T, Vavladeli A, Pala A, Galan K, Crochet S, Petersen SSA, Petersen CCH. 2018a. Diverse Long-Range Axonal Projections of Excitatory Layer 2/3 Neurons in Mouse Barrel Cortex. *Front Neuroanat*. 12:33–33.
- Yang H, Kwon SE, Severson KS, O’Connor DH. 2016a. Origins of choice-related activity in mouse somatosensory cortex. *Nat Neurosci*. 19:127–134.

References

- Yizhar O, Fenno LE, Prigge M, Schneider F, Davidson TJ, O'Shea DJ, Sohal VS, Goshen I, Finkelstein J, Paz JT, Stehfest K, Fudim R, Ramakrishnan C, Huguenard JR, Hegemann P, Deisseroth K. 2011. Neocortical excitation/inhibition balance in information processing and social dysfunction. *Nature*. 477:171–178.
- Yu J, Hu H, Agmon A, Svoboda K. 2019. Recruitment of GABAergic interneurons in the barrel cortex during active tactile behavior. *Neuron*. 104:412–427.
- Zareian B, Zhang Z, Zagha E. 2021. Cortical Localization of the Sensory-Motor Transformation in a Whisker Detection Task in Mice. *eNeuro*. 8:ENEURO.0004-21.2021.
- Zatka-Haas P, Steinmetz NA, Carandini M, Harris KD. 2021. Sensory coding and the causal impact of mouse cortex in a visual decision. *eLife*. 10:e63163.
- Zhang S, Xu M, Chang W-C, Ma C, Hoang Do JP, Jeong D, Lei T, Fan JL, Dan Y. 2016. Organization of long-range inputs and outputs of frontal cortex for top-down control. *Nat Neurosci*. 19:1733–1742.
- Zhao S, Ting JT, Atallah HE, Qiu L, Tan J, Gloss B, Augustine GJ, Deisseroth K, Luo M, Graybiel AM, Feng G. 2011a. Cell type-specific channelrhodopsin-2 transgenic mice for optogenetic dissection of neural circuitry function. *Nat Methods*. 8:745–752.
- Zuo Y, Diamond ME. 2019a. Texture Identification by Bounded Integration of Sensory Cortical Signals. *Curr Biol*. 29:1425-1435.e5.
- Zuo Y, Diamond ME. 2019b. Rats Generate Vibrissal Sensory Evidence until Boundary Crossing Triggers a Decision. *Curr Biol*. 29:1415-1424.e5.

List of abbreviations

AAV	adeno-associated virus	Hg	hyoglossus
ACB	nucleus accumbens	IAM	Interanteromedial thalamic nucleus
AD	anterodorsal thalamic nucleus	IL	infralimbic
AI	artificial intelligence	IOS	intrinsic optical imaging
ALM	anterior lateral motor cortex	L1	layer 1
AON	anterior olfactory nucleus	L2	layer 2
AUC	area under the curve	L2/3	layer 2/3
AUD	primary auditory cortex	L4	layer 4
BG	basal ganglia	L5	layer 5
BIC	bayesian information criterion	L6	layer 6
BLA	basolateral amygdalar nucleus	LHb	lateral habenula
c	central lateral thalamic nucleus	LIP	lateral intraparietal area
dCA1	CA1 region of the hippocampus	M1-p	wS1→M1 projecting neurons
CCF	common coordinate framework	MD	mediodorsal thalamic nucleus
ChR2	channelrhodopsin-2	Mo5	trigeminal motor nucleus
CLA	claustrum	Mos	secondary motor cortex
CM	central medial thalamic nucleus	mPFC	medial prefrontal cortex
CP	caudoputamen	MRN	median raphe nucleus
CPGs	central pattern generators	NA	nucleus accumbens
CR	correct rejection	P Lick	Probability of Lick
D1	day one	PAG	periaqueductal gray
DAPI	4',6-diamidino-2-phenylindole	PCA	principal component analysis
Dig	digastric	PERI	perirhinal cortex
DLS	dorsolateral striatum	PFC	prefrontal cortex
dmPFC	dorsomedial prefrontal cortex	PIR	piriform cortex
DRN	dorsal raphe nucleus	PL	prelimbic
dSPNs	direct pathway striatonigral projection neurons	PL2/3	prelimbic layer 2/3
ECT	ectorhinal cortex	PL5	prelimbic layer 5
EM	expected maximization	POm	thalamic medial posterior nucleus
ENTl	entorhinal cortex	POm-FO	first-order thalamic medial posterior nucleus
FA	false alarm	POm-HO	higher-order subdivision of POm
FDR	false-discovery rate	Pons	pons
fMRI	functional magnetic resonance imaging	PPC	posterior parietal cortex
FO	first-order	PPN	pedunclopontine nucleus
FSU	fast spiking units	Pr5	principal trigeminal brainstem nucleus
GABA	gamma-aminobutyric acid	PSTH	peristimulus time histogram
GLM	generalized linear model	PT	pyramidal tract
GMM	Gaussian mixture model	PtA	the parietal association area
GPT	generative pre-trained transformer	PV	parvalbumin
GU	gustatory cortex	PVT	paraventricular thalamic nucleus
Hg	hypoglossal motor nucleus	RE	reticular nucleus of the thalamus

RH	rhomboid nucleus of the thalamus
ROC	receiver operating characteristic
ROI	regions-of-interest
RSP	retrosplenial area
RSU	regular spiking neurons
S2-p	wS1→wS2 projecting neurons
SC	superior colliculus
SDT	signal detection theory
SEP	sensory-evoked potential
Sg	styloglossus
SI	selectivity index
SMT	Submedial thalamic nucleus
Sp5	spinal trigeminal nucleus
SSp	primary somatosensory areas
SSs	supplemental somatosensory areas
SST	somatostatin
TeA	temporal association cortex
Tem	temporalis
Tg	trigeminal ganglion
Th	thalamus
tjM1	tongue-jaw primary motor cortex
tjM2	tongue-jaw secondary motor cortex
tjS1	tongue-jaw primary somatosensory cortex
tjS2	tongue-jaw secondary somatosensory cortex
V1	primary visual cortex
VGAT	vesicular GABA transporter
VIP	vasoactive intestinal peptide
VIS	visual areas
VISC	visceral cortex
vIPFC	ventrolateral prefrontal cortex
Vm	membrane potential
vmPFC	ventromedial prefrontal cortex
VPM	thalamic ventral posterior medial nucleus
VPM-FO	first-order ventral posteromedial nucleus
vS1	primary visual cortex
VSD	voltage-sensitive dye imaging.
VTA	midbrain ventral tegmental area
wM2	whisker secondary motor cortex
wS1	whisker primary somatosensory cortex
wS2	whisker secondary somatosensory cortex
wS2	secondary somatosensory cortex
ZI	zona incerta

Curriculum vitae

ANASTASIIA ORYSHCHUK



ANASTASIIA ORYSHCHUK

anastasiia.oryshchuk@epfl.ch

n.oryshchuk@gmail.com

+41 78 247 00 44

Ch. des Perrettes 3,
Ecublens 1024, Switzerland

EDUCATION

Ph.D. in Neuroscience

2018 - 2023

Swiss Federal Institute of Technology (EPFL), Lausanne, Switzerland

Thesis: "Neuronal correlates of goal-directed sensorimotor transformation in sensory, motor and higher-order cortical areas"

Under the supervision of: Prof. Carl Petersen

- 🏆 Winner of the Jean Falk-Vairant presentation award, NeuroLéman Network meeting, Switzerland, 2022

Summer school in Neural Data Science

July 2019

Cold Spring Harbor Laboratory, New York, USA

- 🏆 Awarded Helmsley Scholarship

MSc in Neuroscience

2015 - 2018

University of Trieste, Trieste, Italy

Thesis conducted at EPFL: "Optogenetic and electrophysiological measurement of neuronal activity in mouse barrel cortex during psychometric analysis of a whisker-dependent tactile detection task"

Under the supervision of: Prof. Carl Petersen

- 🏆 Excellent grades for MSc degree 30 "Cum Laude"
- 🏆 "International Mobility Program Switzerland" scholarship

MSc in Genetics

2011 - 2013

Taras Shevchenko National University, Kyiv, Ukraine

Thesis: "Genetic monitoring of Hirundo Rustica on the radiation-contaminated areas"

Under supervision of: Prof. Katerina Afanasyeva

- 🏆 Scholarship for talented students "Cabinet of Ministers of Ukraine"

BSc in Molecular Biology

2007 - 2011

Taras Shevchenko National University, Kyiv, Ukraine

- 🏆 Scholarship for talented students "Cabinet of Ministers of Ukraine"

RECEARCH PROGETCS

Laboratory of Sensory Processing, Swiss Federal Institute of Technology (EPFL)

Supervisors: Prof. Carl Petersen and Dr. Sylvain Crochet

Research associate in neuroscience (Ph.D.) *May 2018- May 2023*

- Conceptualized and designed studies to investigate causal neural mechanisms of sensorimotor transformation during goal-directed behavior in mice.
- Applied large-scale electrophysiological and optogenetic techniques to record and manipulate brain activity in vivo in behaving animals.
- Developed automated electrophysiological and behavioral experiment setup for highly-synchronized neuronal and behavioral data acquisition.
- Designed analysis pipelines for pre-processing and integration of large-scale behavioral and electrophysiological data.
- Implemented machine learning, clustering algorithms and advanced statistical methods to extract, analyze and interpret neuronal activity patterns.

Research associate in neuroscience (MSc) *Feb. 2017-Jan. 2018*

- Developed and implemented a new psychophysical behavioral task for rodents.
- Performed brain stereotaxic microsurgeries, acute neural recordings, and optogenetic manipulations in rodents in vivo.
- Designed analysis pipelines for pre-processing of large-scale behavioral and electrophysiological data.

Tactile Perception and Learning Lab International School for Advanced Studies, Trieste, Italy

Supervisors: Prof. Mathew E. Diamond

Research associate in neuroscience *Sept. 2016-Jan. 2017*

- Investigated neural correlates of working memory.
- Applied an advanced linear model to correlate the behavioral choice of rats performing parametric working memory task.

laboratory of Molecular Biology and Genetics Taras Shevchenko National University, Kyiv, Ukraine

Supervisors: Prof. Katerina Afanasyeva

Research associate in genetics (MSc) *Sept. 2011-May 2013*

- Designed genetic monitoring frame of bird species in the radiation-contaminated area near Chernobyl Nuclear Power Plant.
- Performed screening of molecular markers for identification and quantification of population size, genetic diversity, hybridization, emergence, and spread of species.

Research associate in genetics (BSc) *Sept. 2010-Jul. 2011*

- Investigated mechanisms and kinetics of DNA exit during comet assay in single-cell electrophoresis.
- Investigated the influence of radiation on DNA-repairing mechanisms.

EXTRACURRICULAR ACTIVITIES

Treasurer and cocreator of “Association Culturelle Ukrainienne”,

EPFL, Lausanne, Switzerland

2022-Present

- Organized and planned the budget of the association
- Wrote several successful grants to finance cultural events

Teaching assistant, EPFL, Switzerland

2018-Present

- Co-supervised and trained 2 Master and Bachelor students.
- Taught two Neuroscience and “Experimental design” master courses

SELECTED TALKS AND PRESENTATIONS

“Experience-dependent representation of sensory-, motor-, and decision-related activity in primary sensory, motor, and medial prefrontal cortical areas”; FENS Forum 2022, Paris; Barrels meeting 2022 Lausanne; NeuroLéman Network meeting 2022, Les Diablerets.

“Neuronal correlates of goal-directed sensorimotor transformation in medial prefrontal cortex” Fens Forum 2000, Glasgow; Swisskors meeting 2000, Zurich.

“Contribution of S1 and mPFC cortical regions to sensorimotor transformation during goal-directed behavior in mice” Society for Neuroscience meeting 2019, Chicago.

PUBLICATIONS

Representation of sensory, motor and decision information in sensory, motor and medial prefrontal cortices of mice.

Anastasiia Oryshchuk, Christos Sourmpis, Reza Asri, Vahid Esmaeili, Wulfram Gerstner, Carl Petersen and Sylvain Crochet; in preparation.

Learning-related congruent and incongruent changes of excitation and inhibition in distinct cortical regions.

Vahid Esmaeili, Anastasiia Oryshchuk, Reza Asri, Keita Tamura, Georgios Foustoukos, Yanqi Liu, Romain Guet, Sylvain Crochet and Carl C.H. Petersen; Plosbiology 2022.

Rapid suppression and sustained activation of distinct cortical regions for a delayed sensory-triggered motor response.

Vahid Esmaeili*, Keita Tamura*, Samuel P. Muscinelli, Alireza Modirshanechi, Marta Boscaglia, Ashley B. Lee, Anastasiia Oryshchuk, Georgios Foustoukos, Yanqi Liu, Sylvain Crochet, Wulfram Gerstner and Carl C.H. Petersen; Neuron 2021.

Cortical circuits for transforming whisker sensation into goal-directed licking.

Vahid Esmaeili, Keita Tamura, Georgios Foustoukos, Anastasiia Oryshchuk, Sylvain Crochet, and Carl C.H. Petersen, Curr. Opin. Neurobiol. 2020.

COMPUTER SKILLS

MATLAB / Python / Unix / Git / Illustrator

LANGUAGES

English (C1) / French (B2) / Ukrainian (Native) / Russian (Native)

Ce document a été imprimé
au Centre d'impression EPFL,
imprimerie climatiquement
neutre, certifiée myClimate
depuis 2017



repro.epfl.ch